

**Multidentate phosphino-alkene ligands and
their late-transition metal complexes**

Amanda Gail Jarvis

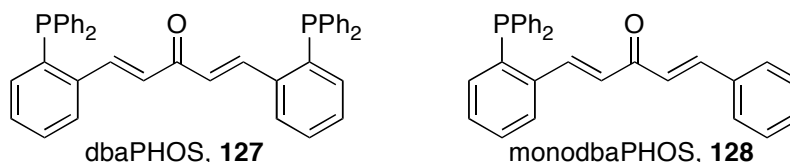
PhD

Chemistry

June 2011

Abstract

The synthesis and characterisation of a new class of multidentate conformationally flexible phosphino-alkene ligands, called dbaPHOS (**127**) and monodbaPHOS (**128**), are described in this PhD thesis. The related phosphine sulphide ligands, namely dbaTHIOPHOS (**137**) and monodbaTHIOPHOS (**149**), have also been prepared.



The coordination chemistry of the novel ligands was investigated with a variety of late-transition metals, including Cu, Rh, Pd and Pt. X-ray crystal structure determination of the complexes containing these ligands highlights the multiple coordination modes and versatility of each ligand system. The ability of the 1,4-dien-3-one backbone to adopt different conformational geometries around metal centers is of particular note. Dbaphos (**127**) was found to act as a *cis*- and *trans*-chelating bisphosphine in both square planar Pd^{II} and Pt^{II} complexes. The 1,4-dien-3-one motif is hemilabile; exchange between coordinated and non-coordinated alkenes is observed in both the Pd⁰ complex, **167**, and the related cationic Cu^I complex, **193**.

An investigation into the Cu^I complexes' activity in the cyclopropanation of styrene, as catalysts, showed that they are commensurate with other recently reported systems.

In addition to the coordination chemistry of the novel ligand systems, some interesting findings emerged in the ligand synthesis and characterisation studies. For example, monodbaTHIOPHOS (**149**) undergoes an interesting solid-state [2+2] intramolecular cycloaddition transformation, giving cycloadduct, **206**. Furthermore, 2-hydroperoxytetrahydrofuran was found to be an impurity in the microwave-assisted Horner-Wadsworth-Emmons reaction of 2-(diphenylthiophosphine)benzaldehyde (**136**) with 1,3-bis-(ethoxyphosphonato)-acetone (**130**) to give dbaTHIOPHOS (**137**) and an unexpected THF insertion product, **138**. The latter is explained by a side reaction involving the reduced compound, tetrahydrofuran-2-ol, derived from 2-hydroperoxytetrahydrofuran.

Abstract	i
Table of Contents	ii
Acknowledgments	vii
Declaration	viii
Abbreviations	ix
Key to Thesis	xiii

Table of Contents

Chapter 1: Introduction	1
1.1 Metal-heteroatom complexes	2
1.1.1 Nitrogen-containing ligands	2
1.1.2 Phosphorus containing ligands	3
1.1.3 Sulfur containing ligands	8
1.1.4 Oxygen containing ligands	9
1.2 Organometallic complexes	11
1.2.1 Alkenes	11
1.3 Alkene ligands in catalysis	14
1.3.1 Alkenes in precatalysts	14
1.3.2 Trisdibenzylidene acetone dipalladium(0)	15
1.3.2.1 <i>Dbp</i> effects on oxidative addition	15
1.3.2.2 <i>Supporting studies showing alkene effects on oxidative addition</i>	20
1.3.2.3 <i>Effect on reductive elimination and β-hydride elimination</i>	23
1.3.3 Mono- and polydentate alkene ligands in catalysis	28
1.3.3.1 <i>Palladium catalysis</i>	28
1.3.3.2 <i>Rhodium and iridium catalysis</i>	36
1.4 Heterobidentate alkene ligands	43
1.5 Heterobidentate ligands in catalysis	45

1.5.1	Phosphine alkene ligands in palladium catalysis	46
1.5.2	Phosphino-alkene ligands in rhodium and iridium catalysis	53
1.5.3	Nitrogen-alkene ligands in catalysis	59
1.6	Conclusion	60
1.7	Project Summary	61
1.8	References	63
Chapter 2: Synthesis of multidentate phosphino-alkene ligands		75
2.1	Design of ligands	75
2.2	Synthesis of ligands	75
2.2.1	Bisphosphine ligands	77
2.2.2	Microwave studies: An unexpected THF addition product	81
2.2.3	Monophosphine ligands	89
2.3	Reactivity of the ligands	90
2.4	Comparison of the structure of the ligands	93
2.5	Summary	98
2.6	Future work	99
2.6.1	Tuning the alkene electronics	99
2.6.2	Changing the phosphine substituents	100
2.6.3	Reduction of the double bond	102
2.7	Experimental	103
2.7.1	General information	103
2.7.2	Synthesis of ligands	104
2.7.3	Microwave studies	119
2.7.3.1	<i>General microwave method</i>	119
2.7.3.2	<i>Detailed microwave method</i>	119
2.7.4	Deprotection of phosphine sulfides	125
2.7.5	X-Ray diffraction Details	126

2.8 References	128
Chapter 3: Late-transition metal complexes of dbaPHOS and monodbaPHOS	133
3.1 Palladium and platinum complexes with dbaPHOS	133
3.1.1 Pt ^{II} and Pd ^{II} complexes	134
3.1.2 DFT studies on <i>cis</i> -[PtCl ₂ (dbaPHOS)]	142
3.1.3 Pd ⁰ and Pt ⁰ complexes	145
3.2 Platinum(II) and palladium(II) complexes of monodbaPHOS	154
3.2.1 X-ray crystallographic analysis	158
3.3 Rhodium complexes of dbaPHOS	163
3.4 Summary	167
3.5 Future work	168
3.6 Experimental	170
3.6.1 General information	170
3.6.2 Complex synthesis	172
3.6.2.1 <i>Pt and Pd with dbaPHOS</i>	172
3.6.2.2 <i>Pt^{II} and Pd^{II} with monodbaPHOS</i>	182
3.6.2.3 <i>Rh^I complexes with dbaPHOS</i>	188
3.6.3 P-P EXSY experiments	191
3.6.4 X-Ray diffraction data	192
3.7 References	194
Chapter 4: Copper(I) Complexes of the phosphine sulfide ligands	200
4.1 Introduction	200
4.1.1 Copper(I)-alkene complexes	202
4.1.2 Copper complexes with Phosphino-alkenyl ligands	205
4.1.3 Aims	207
4.2 Results and Discussion	207

4.2.1 Comparison of X-ray single crystal structures	209
4.2.2 NMR spectroscopic studies on complexes 193, 194 and 195	213
4.2.3 Interconversion of the complexes	217
4.2.4 Silver complexes of the phosphine sulfide ligands	220
4.2.4 Catalysis	223
4.3 Summary	225
4.3 Future work	225
4.4 Experimental	227
4.4.1 General information	227
4.4.2 Complex synthesis	228
4.4.3 NMR and UV spectroscopic experiments	234
4.4.4 Catalysis	235
4.4.5 X-ray diffraction data	237
4.5 References	239
 Chapter 5: The photochemistry of monodbaTHIOPHOS	 244
Introduction	244
5.1 Solid-state reactions	244
5.2 Photochemistry	245
5.2.1 <i>E/Z</i> isomerisation of C=C bonds	246
5.2.2 Cycloaddition	247
5.2.3 Photochemical solid-state reactions	248
5.3 Aims	252
5.4. Results and Discussion	253
5.4.1 Solution studies	255
5.4.2 Single crystal studies	256
5.4.3 Powder studies	264
5.5. Summary	272

5.6 Future work	273
5.7 Experimental	275
5.7.1 General information	275
5.7.2 Synthesis	275
5.7.3 Photochemical experiments	277
5.8 References	286
Chapter 6: Conclusions	290
Appendix 1 and 2: NMR spectra	(enclosed on CD)
Appendix 3: X-Ray crystal tables and cif files	(enclosed on CD)
Appendix 4: UV-visible spectra	(enclosed on CD)
Appendix 5: CSD database searches	(enclosed on CD)
Appendix 6: Simulated PXRD patterns	(enclosed on CD)
Appendix 7: ^{31}P-^{31}P EXSY data	(enclosed on CD)

Acknowledgements

Firstly, I would like to thank Ian for giving me the opportunity to work in his group and for his encouragement, guidance and support over the entire period of my PhD. It has been a great pleasure and a privilege to work for Ian.

This work would not have been possible without the collaboration of Professor Paul Raithby (Bath), Dr Hazel Sparkes (Durham) and Dr Martin Cockett for help on the photochemistry studies, Professor Lin and Dr Zhang for performing calculations, and Professor Simon Duckett, Dr David Williamson and John Clark for advanced NMR experiments. The time, effort and help you have given me has been greatly appreciated.

As with any chemistry thesis there have been plenty of people behind the scenes who make it possible, from the technical and workshop staff to the admin team. My heartfelt thanks goes out to all those that have helped everything run smoothly during my time here. I would particularly like to express my gratitude to Heather Fish, for taking the time to train me on the NMR instruments, and Dr Adrian Whitwood and Rob Thatcher for help with single crystal X-Ray diffraction, from running and solving my crystals to trying to teach me how to. I would also like to thank the Durham solid-state NMR service (Dr David Apperley) for spectra and advice on analysis.

I must also thank all the friends I have made during my time in York, in particular the past and present members of the Fairlamb group. A special mention goes to Mike Burns for mentoring me during my first weeks in the lab and reminding me how to do organic chemistry (but not so much for his wide fumehood stance)! And to Tom Storr for always being willing to talk me out of a rut when things didn't seem to be going so well, and being a constant drinking companion at symposia wine receptions. I would also like to thank Sara for letting me stay with her for the last days of writing up.

Finally, I would like to thank my family and Graeme for their love and support at every step on the way, and putting up with me during the last months whilst I was writing up.

Declaration

I declare that all the work presented in this thesis is my own, and that any material not my own is clearly referenced or acknowledged in the main body of the text. The work was conducted between October 2007 and May 2011.

Amanda Jarvis

June 2011

Abbreviations

Ac	Acetyl
AFM	Atomic Force Microscopy
anal.	Analytical
APC	Allylpalladiumchloride dimer
APCI	Atmospheric Pressure Chemical Ionisation
aq.	Aqueous
Ar	Aromatic group
ASIS	Aromatic Solvent Induced Shift
ba	Benzylideneacetone
BINAP	2,2'-Bis(diphenylphosphino)-1,1'-binaphthyl
biphep	<i>ortho</i> -(Diphenylphosphino)biphenyl
bipy	2,2'-Bipyridine
bmim	1-Butyl-3-methylimidazolium
Bn	Benzyl
bq	1,4-Benzoquinone
BSA	<i>N,O</i> -Bis(trimethylsilyl)acetamide
Bu	Butyl
c (prefix)	Cyclic
<i>ca.</i>	Circa
cat	Catalyst
C ₅ MPyrr	1-Pentyl-1-methylpyrrolidinium
cod	1,5-Cyclooctadiene
coe	Cyclooctene
conc.	Concentration
conv.	Conversion
coord.	Coordinated
COSY	Correlation Spectroscopy
Cp	Cyclopentadienyl
CPMAS	Cross Polarisation Magic Angle Spinning
Cy	Cyclohexyl
Cyp	Cyclopentyl
d (NMR)	Doublet

<i>d</i>	Deutero
dba	Dibenzylidene acetone
DCE	Dichloroethane
DCM	Dichloromethane
DEPT	Distortionless Enhancement by Polarisation Transfer
DFT	Density Functional Theory
DIBAL	<i>Di</i> isobutylaluminium hydride
DIPEA	<i>Di</i> isopropylethylamine
DMF	Dimethylformamide
DMSO	Dimethylsulfoxide
dmfu	Dimethyl fumarate
dppb	1,2-(Diphenylphosphino)benzene
dppe	1,2-(Diphenylphosphino)ethane
dppm	Diphenylphosphinomethane
dppm ⁻	Refers to dppm minus a proton
EDA	Ethyl diazoacetate
<i>ee</i>	Enantiomeric excess
eq.	Equivalent
ESI	Electrospray Ionisation
Et	Ethyl
EXSY	Exchange Spectroscopy
FAB	Fast Atom Bombardment
Fc	Ferrocene
fn	Fumaronitrile
HMBC	Heteronuclear Multiple Bond Coherence
HPYA	Pyridylacrylic acid
HRMS	High Resolution Mass Spectrometry
HSAB	Hard-Soft-Acid-Base
HSQC	Heteronuclear Single Quantum Coherence
<i>in vacuo</i>	Under reduced pressure
<i>i</i> (prefix)	Iso
IR	Infra-Red
<i>J</i>	Coupling constant
KDMO	Potassium 3,7-dimethyl-3-octylate
L	Ligand

LED	Light Emitting Diode
LIFDI	Liquid Injection Field Desorption Ionisation
LRMS	Low Resolution Mass Spectrometry
<i>m</i> (prefix)	Meta
<i>m</i> (IR)	Medium
<i>m</i> (NMR)	Multiplet
M	Transition Metal
M_n	Number average molar mass
M_w	Weight average molar mass
ma	Maleic anhydride
Me	Methyl
mol	Mole
MOP	Monophosphine ligands
<i>m/z</i>	Mass to charge ratio
M.p.	Melting Point
MS	Mass Spectrometry
<i>n</i> (prefix)	Normal
nbd	Norbornadiene
NHC	<i>N</i> -Heterocyclic carbene
NMR	Nuclear Magnetic Resonance
NOESY	Nuclear Overhauser Enhancement Spectroscopy
nq	Naphthoquinone
<i>o</i> (prefix)	Ortho
<i>p</i> (prefix)	Para
Ph	Phenyl
Pr	Propyl
phen	1,10-Phenathroline
PHT	Pyrrolidone hydrotribromide
POP (ligands)	Phosphine-ethers, phosphine-phosphites and other ligands that bind through P, O, P.
PXRD	Powder X-Ray Diffraction
<i>q</i> (NMR)	Quartet
R	Organic group
rt	Room Temperature (13-25 °C)

s (IR)	Strong
s (NMR)	Singlet
S	Solvent
Sol	Solvent
SCSC	Single-crystal, single-crystal
SIMes	1,3-Dimesityl-4,5-dihydroimidazol-2-ylidene
t (NMR)	Triplet
<i>t</i> (prefix)	Tertiary
tcne	Tetracyanoethylene
Tol	Methylphenyl
TBAF	Tetra- <i>n</i> -butylammonium fluoride
Tf	Trifluoromethyl sulfonyl
THF	Tetrahydrofuran
TLC	Thin Layer Chromatography (silica plates unless otherwise specified)
TMEDA	<i>N,N,N',N'</i> -Tetramethylethylenediamine
TMS	Trimethylsilane
Ts	<i>para</i> -Toluene sulfonyl
Tr	Triphenylmethyl
uncoord.	Uncoordinated
UV	Ultraviolet
v:v	Volume ratio
w (IR)	Weak
X	Halide
XantPhos	4,5-Bis(diphenylphosphino)-9,9-dimethylxanthene
XRD	X-ray Diffraction
Z	Aryl substituent

Key to thesis

Referencing: Each chapter is referenced individually starting at one with the references located at the end of the chapter.

Figures/Schemes: The figure numbering starts from one in each chapter and is thereafter sequential. The scheme numbering starts from one in each chapter and is thereafter sequential.

Numbering: Compounds that are referred to in the main body of text are numbered sequentially across all chapters. The main ligands described in this thesis are referred to by either abbreviated names (*e.g.* dbaPHOS) and/or by number. Complexes are referred to by either by number and/or by a formula.

Chapter 1: Introduction

Synthetic organic chemistry is concerned with the preparation of novel compounds and development of methodologies, particularly for the formation of C-C, C-O and C-N bonds. As a result the synthetic community is striving to increase the number of transformations available and the efficiency with which these transformations can be achieved. One common way of increasing efficacy (either in terms of increasing the yields and/or selectivities, the atom efficiency or the energy efficiency, *i.e.* reducing temperature) of a reaction is to use catalysis. There are two main areas in catalysis: heterogeneous catalysis and homogenous catalysis. The focus of this thesis is the design of ligands for homogenous catalysis using late-transition metals.

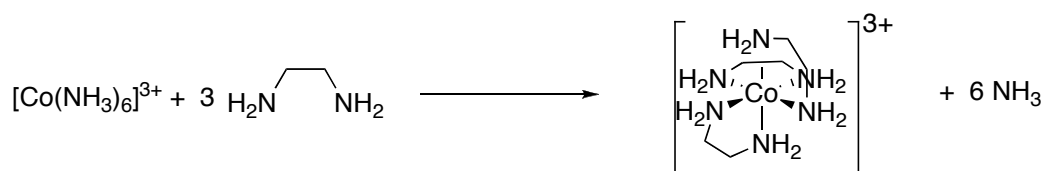
In homogenous transition metal catalysis, the active catalyst is usually a metal complex, which consists of a metal centre surrounded by a number of ligands dependent on the metal and reaction type. These ligands can range from simple molecules, such as triphenylphosphine, ethylenediamine and carbon monoxide (CO), to more complex compounds such as RNA and calixarenes.¹ There are numerous methods that have been used to classify ligands from systems that merely look at the number of coordination sites a ligand has (monodentate *vs.* polydentate) to those based on the electronic properties of the ligand. One common way to classify ligands is by the number of electrons they donate to the metal centre, *i.e.* L or X-type ligands.² L-type ligands are those that donate two electrons, whereas X-type ligands donate one electron. In cases where a ligand donates more than two electrons a mixture of L and X is used *e.g.* LX for three electrons and L₂ for four electrons. The main classes of two-electron donors are described below.

Metals and ligands can also be classified according to Pearson Hard-Soft Acid Base principle.³ The metals we are mostly interested in, Rh, Ir, Pd, Pt, Ag, are class B (or soft) metals and therefore prefer to bind to soft bases, *e.g.* P and S; whereas class A (hard) metals prefer N and O donors. Cu, Ni, Co and Fe are regarded as borderline metals. The hardness of a metal also depends on the oxidation state of the metal, for example Cu^I is considered soft, whilst Cu^{II} is considered borderline.

1.1 Metal-heteroatom complexes

1.1.1 Nitrogen-containing ligands

Complexes where the metal binds to a heteroatom have been known since the early 19th century and are often referred to as classical or Werner complexes.⁴ These complexes represent some of the simplest ligands and metal-ligand bonds. Perhaps the simplest of all complexes are those between a metal and either ammonia or water molecules e.g. $[\text{Co}(\text{NH}_3)_6]^{3+}$ and $[\text{Ni}(\text{OH}_2)_6]^{2+}$. It was with these types of complexes that coordination chemistry research began.⁴ Although amine ligands have been extensively studied in coordination chemistry they are not as common in organometallic chemistry. There are two main reasons for this: a) the N-H bond of the coordinated amine tends to be very reactive, and b) amines prefer class A metals and most organometallic chemistry focuses on class B metals which tend to only coordinate weakly. When amines do appear in organometallic chemistry it is most often with the borderline metals such as Cu^{I} as there is less of a hard/soft mismatch. The coordination can be strengthened by replacing monodentate amines with polydentate ligands such as ethylenediamine, due to the chelate effect. The chelate effect states, “chelating ligands are much less easily displaced from a complex than monodentate ligands of the same type”.⁵ This is due to the increase in entropy on displacing monodentate ligands as illustrated in Scheme 1.



Scheme 1: Increasing entropy on replacement of NH_3 with ethylenediamine.

Today, the nitrogen ligands available range from simple amines such as ethylenediamine, mentioned above, to pyridine ligands, such as 2,2'-bipyridine (bipy, **1**) and phenanthroline (phen, **2**), oxazolines (**4** and **5**), porphyrins, and imines (Figure 1). Pyridine, imine and oxazoline based ligands are more common in organometallic chemistry as they are softer than amines.⁶ In many cases the ligands are multidentate and include other heteroatoms such as phosphorus and oxygen. One famous class of N,O donor ligands are the salens (**3**), which have been used in both catalysis and coordination chemistry. They are prepared from the condensation of a salicylaldehyde

and a 1,2-diamine. The use of chiral amines leads to chiral salens suitable for asymmetric catalysis, *e.g.* the Jacobsen epoxidation.⁷

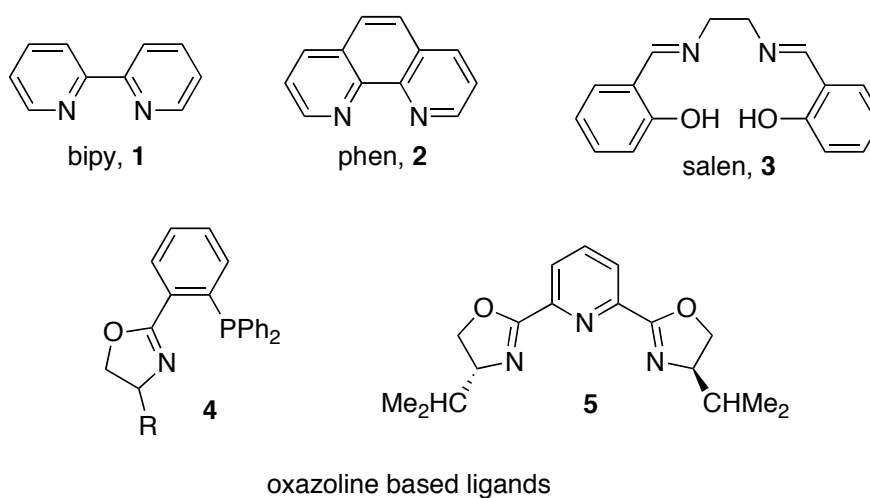


Figure 1: Examples of nitrogen-containing ligands.

1.1.2 Phosphorus containing ligands

The first phosphorus-metal complex, triethylphosphine platinum trichloride, was described by Hofmann in 1857.⁸ Since then phosphines (PR₃) have become a traditional and versatile ligand class for transition metal-catalysed reactions. Their steric and electronic properties can be altered in a systematic and predictable fashion by varying R (R = aryl, alkyl), allowing for a wide range of ligand reactivity profiles to be accessed.⁹ Tolman quantified the dependence of the phosphine's electronic properties on R in the 1970s, by looking at the changes in the A₁ C=O stretching frequency in [Ni(CO)₃(PR₃)] (Table 1).¹⁰ In this work one of the CO molecules was displaced from Ni(CO)₄ with the phosphine of interest, allowing the resulting shift in the C-O stretching frequency, to be assessed by IR spectroscopy. More electron-rich R-groups increase the electron density on the phosphorus, which in turn increases the back-bonding to the CO. This lengthens the C-O bond resulting in a decrease in the stretching frequency (see Figure 2). Ni(CO)₄ is very toxic, so other carbonyl complexes such as those of Rh and W have also been used.¹¹

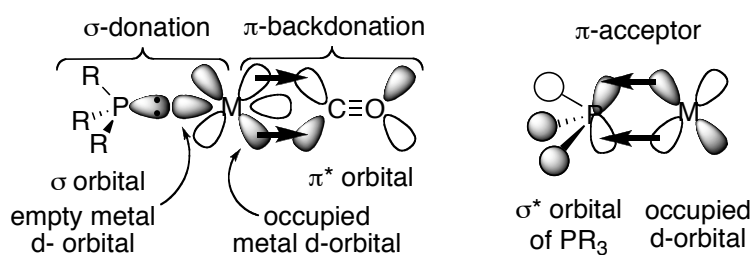


Figure 2: Phosphines as σ -donors and π -acceptors.

Table 1: CO stretching frequencies in $[\text{Ni}(\text{CO})_3(\text{PR}_3)]$ complexes.

Phosphine	$\nu_{\text{CO}} (A_1), \text{cm}^{-1}, \text{CH}_2\text{Cl}_2$
PtBu ₃	2056
PCy ₃	2056
PMe ₃	2064
PPh ₃	2069
P(OMe) ₃	2080
P(OPh) ₃	2085
P(C ₆ F ₅) ₃	2091
PF ₃	2111

One disadvantage of these carbonyl complexes is that although it works very well for the majority of phosphine ligands, $[\text{Ni}(\text{CO})_3\text{L}]$ complexes of other ligands such as pyridine and H_2O do not give rise to stable complexes. This means that it is difficult to compare other ligands to phosphines. Another method of measuring the electronic parameters was developed by Lever using the electrochemical E_0 value for the Ru(III)/Ru(II) redox couples in complexes with the ligands of interest.¹² A wider range of ligands were covered, however, the method is not as simple as using IR spectroscopy. More recently the advances in computational chemistry have made it possible to compute the values of the $A_1 \nu(\text{CO})$ vibration as an alternative.¹³ This allows the electronic parameters of almost any ligand to be approximated.

However, Gusev has shown that care needs to be taken when choosing the complexes to study.¹⁴ He showed that for phosphines and *N*-heterocyclic carbenes (hereafter referred

to as NHCs) the use of the calculated and experimental $\nu(\text{CO})$ of $[\text{Ni}(\text{CO})_3\text{L}]$ complexes gave good agreement as did the calculated $\nu(\text{CO})$ and C-O bond distance. Overall the order of the net donor power of phosphorus ligands was found to be in agreement with the Tolman parameters. For oxygen and nitrogen ligands the values were quite scattered, so a number of other complexes were explored. The results from $[\text{IrCl}(\text{CO})_2\text{L}]$ did not give good agreement, due to the averaging of the two carbonyl frequencies. Gusev also looked at the theoretical values from two more complexes, $[\text{IrCp}(\text{CO})\text{L}]$ and $[\text{IrCp}(\text{H}_2\text{C}=\text{CH}_2)\text{L}]$. A number of surprising results were obtained with these complexes. For example, water was found to give $\nu(\text{CO})$ and $d(\text{CO})$ values close to those of the best phosphorus donors in the $[\text{IrCp}(\text{CO})\text{L}]$ complex. In the $[\text{IrCp}(\text{CO})\text{L}]$ complexes NMe_3 is found to be the second best donor, outperformed only by the abnormal carbene 1,3-dimethylimidazol-4-ylidene. This is unexpected, as it is generally believed that they are worse donors than carbenes. The reason for the discrepancies is that the calculations only dealt with net donor properties. Amines and water are pure σ -donors and have no π -acceptor properties, whilst NHC's and phosphines do undergo some back donation reducing their net donation. Overall it is found that the order within the same ligand class is very reliable, however comparing different ligand classes is less reliable. Use of more than one parameter is best in these cases.

Phosphines are regarded as σ -donors due to the lone pair on phosphorus that can be donated to the metal. Increasing the electron density on phosphorus through the use of electron-donating substituents on R, increases the strength of σ -donation. They can also act as π -acceptors (sometimes referred to as π -acids), with the σ^* -orbital of the P-R bonds playing the role of acceptor (Figure 2). Alkyl phosphines are the weakest π -acceptors, followed by aryl phosphines, then phosphites, with PF_3 being similar to CO .¹⁵ Electron-withdrawing substituents on R favour π -back donation. It is difficult to separate out the σ -donor and π -acceptor properties of the phosphine by experimental methods; however, numerous computational methods have been applied.¹⁶ These studies confirm that phosphines are both σ -donors and π -acceptors, with σ -bonding primarily arising from the lone pair of phosphorus, and π -bonding arising from the donation of electron density from the metal into an empty orbital of the ligand exhibiting phosphorus $3p$ character.

Tolman also quantified the steric effects of phosphines by looking at their cone angles.^{10, 17} A bulkier phosphine (one with a larger cone angle as defined in Figure 3) tends to have a greater dissociation rate than a smaller phosphine. The cone angle also dictates the geometry of the complex. More recently another method has been developed to quantify the steric effects of ligands, known as the buried volume method.¹⁸ An advantage of this method is that it allows the determination of sterics in ligands where the cone angle is hard to determine, for example NHCs, and thus allows for greater comparison between ligand types.

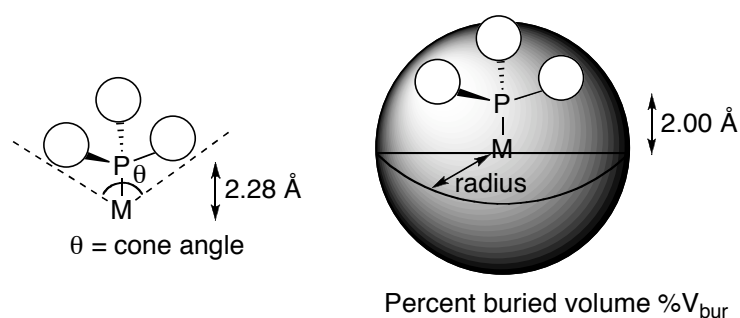


Figure 3: Steric parameters used for phosphines and other ligands.

Common phosphine ligands used in both commercial and research laboratories range from simple alkyl and aryl phosphines, PCy_3 and PPh_3 , to more complex phosphines, e.g. XantPHOS (**6**), and BINAP (**7**) (Figure 4).

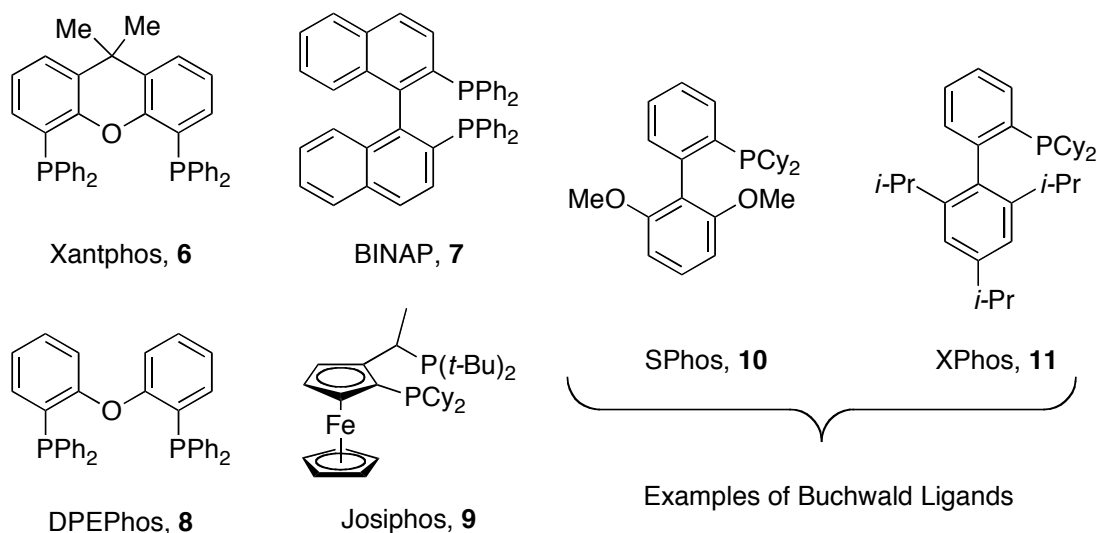


Figure 4: Commercially available phosphines.

Phosphine ligands have undergone continuous development since their introduction as successful ligands for transition metal ligands. A brief look at the history of the Buchwald-Hartwig amination reaction illustrates the development of phosphine ligands.¹⁹ Initially simple phosphines such as P(*t*-Bu)₃ and P(*o*-Tol)₃ were used. These were then superseded by chelating bisphosphines, such as BINAP (**7**). These defined the state-of-the-art until 1998 when Buchwald reported the synthesis and use of monophosphines containing a biphenyl backbone. Over the next few years the Buchwald group developed a large number of ligands based on this biaryl-framework, *e.g.* SPhos (**10**) and XPhos (**11**) (Figure 4). These increased the scope of the reaction allowing aryl chlorides and unactivated aryl halides to be aminated under very mild conditions. The ligands have also proved efficient in a number of C-C, and C-O bond formations.

Along with amination reactions, hydroformylations and Pd-catalysed cross-coupling reactions have driven forward the design of new ligands.²⁰ Many groups have been involved in further research. In the mid-1990s, van Leeuwen developed the bisphosphines XantPHOS (**6**) and DPEPhos (**8**) for use in Rh-catalysed hydroformylations reactions.²¹ They later showed that these ligands also showed high activity for coupling of aryl halides with a variety of nitrogen containing moieties.²² Interestingly, these bisphosphines can act in a *trans*-chelating mode,²³ due in part to their very wide bite angles.

Bite angle is used in place of cone angle for bisphosphines to give an approximation of their steric bulk. The bite angle of a particular ligand can vary quite a lot depending on the metal. The ligand's preferred bite angle will be dependant on the ligand backbone and the sterics around the phosphorous atoms, and the metal will have preferred geometries depending on the d-orbitals involved in bonding.²⁴ The "natural bite angle" of a ligand is calculated using a metal dummy atom and a fixed M-P distance typical for the metal in question. The flexibility range of a ligand can be calculated by forcing the P-M-P angle to deviate from the natural bite angle.²⁵ The bite angle of a ligand can have a large effect on catalyst.²⁶ For example, in Rh-catalysed hydroformylation reactions the bite angle plays a role in determining the reaction selectivity, large bite angles favour linear products.^{26d}

As well as phosphines numerous other phosphorus-based ligands have been studied and utilised in coordination and catalytic chemistry to enhance the electronic and steric properties of phosphorus ligands. These include phosphites, phosphinites and phosphoramidites.²⁷ Phosphites are considered to be electron-withdrawing compared to the majority of phosphines and hence have been used to great effect in promoting reductive elimination.^{27b}

1.1.3 Sulfur containing ligands

Sulfur containing ligands include thioethers, sulfoxides and phosphine sulfides.^{28,29} Thioethers are regarded as poorer σ -donors than phosphines but greater than amines; their π -acceptor properties are also between phosphines and amines. Like amines, due to the weak M-S bond they are often polydentate (**14**) and/or combined with other donors (**12**, **13**), for example phosphines (Figure 5).³⁰ Although the M-S bond of thioethers is weaker than a metal-phosphine bond, it is stronger than the M-O bond of ethers.³¹ Often this means that the M-S bond is not labile. Phosphine sulfides on the other hand are more labile than thioethers and therefore poorer ligands.³²

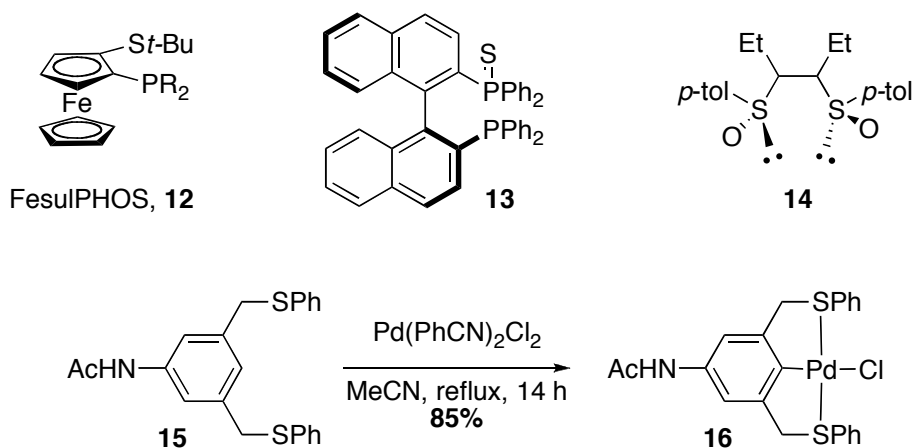
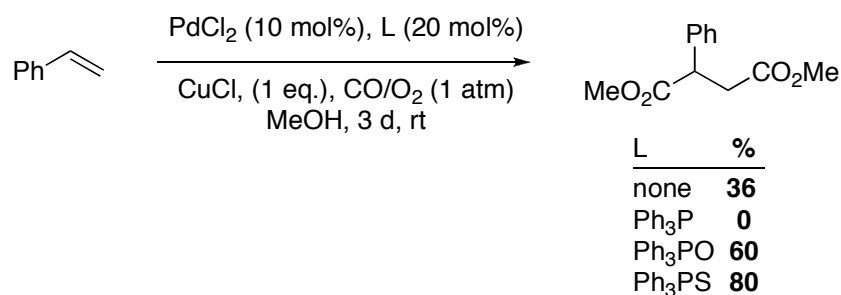


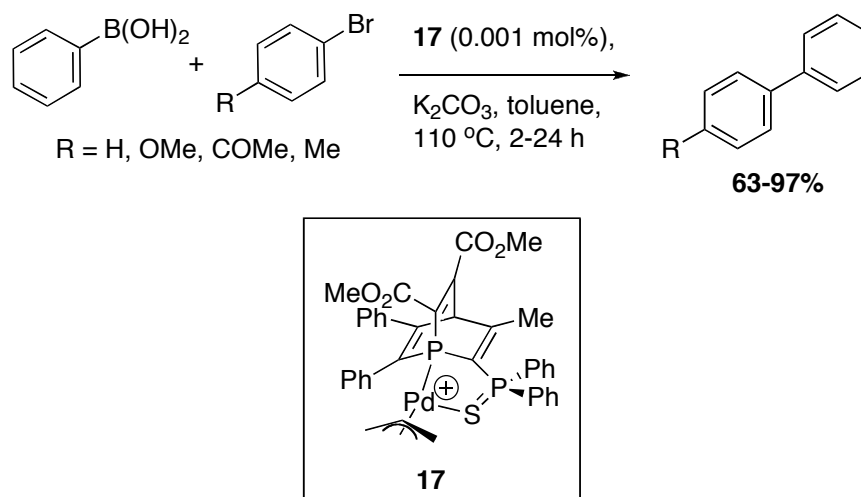
Figure 5: Examples of sulfur-containing ligands.

Whilst numerous late transition metal complexes of phosphine sulfides have been prepared,³³ their use in catalysis has been more limited. Triphenylphosphine sulfide was found to be a successful ligand in Pd-catalysed bisalkoxycarbonylation of alkenes.³⁴ Triphenylphosphine was found to inhibit the reaction with styrene, whilst both triphenylphosphine oxide and triphenylphosphine sulfide gave highly improved yields (Scheme 2). The authors propose that the lability of the ligand may play a central role.



Scheme 2: Pd-catalysed bisalkoxycarbonylation of styrene using triphenylphosphine sulfide.

The use of mixed phosphine/phosphine sulfide ligands has been explored in allylic amination,^{30b} carbonylation reactions,³⁵ and Suzuki cross-coupling reactions.³⁶ For example, le Floch and coworkers reported the use of 1-phosphabarrelene phosphine sulfide complexes in Suzuki cross-couplings.^{36a} Complex **17** was found to give high yields of cross-coupled product at low catalyst loadings (0.001-0.00001 mol%). The sulfide groups did not lead to catalyst poisoning.



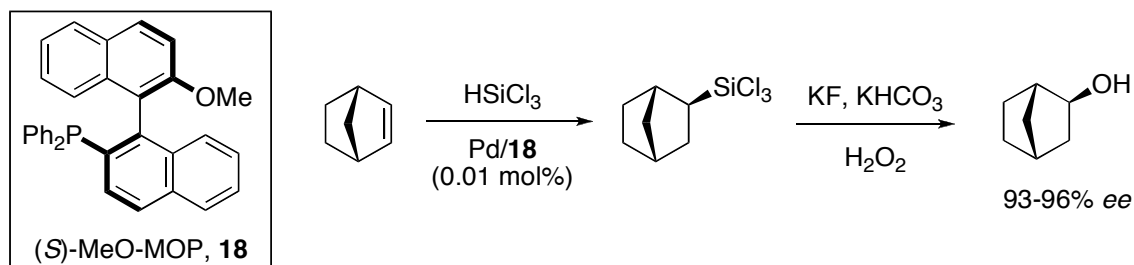
Scheme 3: Cross-coupling reactions of bromoarene and phenylboronic acid using a 1-phosphabarrelene phosphine sulfide Pd^{II} complex.

Coordination studies suggest that in mixed phosphine/ phosphine sulfide systems the ligands are hemilabile.³⁷ However, it is unclear if this plays a role in their catalytic activity.^{30b,35}

1.1.4 Oxygen containing ligands

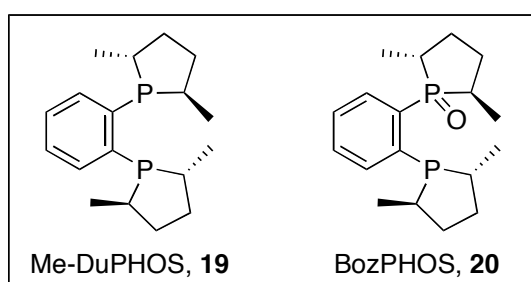
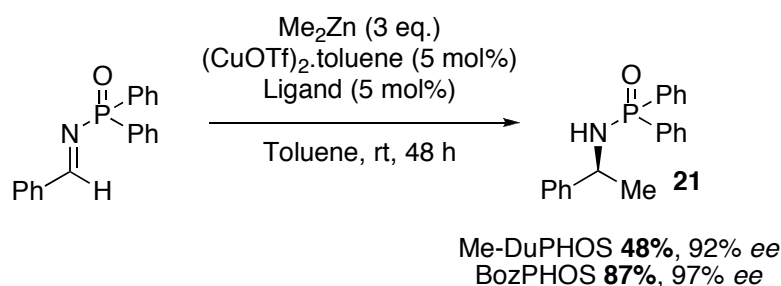
Common oxygen donor ligands include H₂O, MeOH, THF, acetone and phosphine oxides. The coordination between oxygen and the late-transition metals is weak as

oxygen is a hard donor. However, due to the prevalence of oxygen in common solvents it is often able to influence complex coordination and catalysis. Often the presence of these solvents can allow for the crystallisation of unstable intermediate complexes *via* trapping by the solvent, especially in the case of THF.³⁸



Scheme 4: An example of a MOP ligand in catalysis.

As seen with amines and sulfur ligands, oxygen ligands that have found the most use in organometallic chemistry are those combined with other donors such as phosphines.³⁹ One well-known class are the chiral monophosphine ligands (MOP ligands) such as **18**, which derive from BINOL a common asymmetric precursor (and bidentate oxygen ligand itself) and have been widely used in Pd-catalysed reactions (an example is shown in Scheme 4).⁴⁰



Scheme 5: Asymmetric catalysis with bidentate phosphine/phosphine oxide ligands.

Like phosphine sulfide ligands, phosphine/phosphine oxide ligands have also been explored to see if they will act as hemilabile ligands containing one soft and one hard

donor. Whilst studying the Cu-catalysed asymmetric synthesis of amines such as **21**, Charette and co-workers found that bidentate phosphines only gave good yields and enantioselectivities at high catalyst loadings.⁴¹ It was observed that hemilabile bidentate ligands accelerated the reaction. When the authors changed from Me-DuPHOS (**19**) to the monoxide ligand (**20**) the yields and enantioselectivities increased.

1.2 Organometallic complexes

Organometallic complexes are those with organic fragments bound *via* M-C bonds. Ligands that bind to the metal through carbon include alkyls (*e.g.* Me),⁴² Cp,⁴³ allyls, aromatics (*e.g.* C₆H₅), carbenes,⁴⁴ alkylidenes,⁴⁵ vinylidenes,⁴⁶ and alkenes.⁴⁷ Many of these ligands have been extensively studied and would require whole books to do them justice. A discussion of all these ligands is outside the remit of this project and a number of comprehensive reviews are available elsewhere,⁴⁸ hence only alkenes are discussed in this work.

1.2.3 Alkenes

The first reported alkene-metal complex was Zeise's salt, K[PtCl₃(C₂H₄)], in 1830, although its formula was not confirmed until 1861 by Griess and Martius.⁴⁹ It was almost another century before Dewar, Chatt and Duncanson proposed a reliable metal-alkene bonding model in the early 1950s.⁵⁰ According to this model a σ -bond is formed between the π orbital on the alkene and an empty hybrid orbital on the metal (L→M donation). This is complemented by the back-donation of electron density from a filled hybrid orbital on the metal to the π^* -orbital on the alkene (M→L back-donation). These two types of interactions are synergistic (Figure 6). The result is the weakening and lengthening of the C-C bond and the partial hybridisation of the coordinated carbon centre from sp² to sp³. The extent to which back-donation occurs depends on the metal and the alkene.

[(neocuproine)Pd⁰(alkene)] complexes is maleic anhydride (ma) \geq fumaronitrile (fn) > naphthoquinone (nq) \gg dimethyl fumarate.⁵² Complexes with tetracyanoethylene (tcne) are towards the extreme end of back-donation, indeed, [Pt(PPh₃)₂(tcne)] forms the metallocyclopropane structure.⁵³

The extent to which hybridisation occurs, and thus the degree of back-donation can be measured by the shift in NMR signal of the alkene carbon atoms coordination to the metal, $\Delta\delta = (\delta_{\text{complex}} - \delta_{\text{free ligand}})$. The stronger the back donation, the lower the frequency of the resonance of the complexed carbon atom and the greater $\Delta\delta$. One also expects a decrease in the C=C stretching frequencies upon coordination to a late transition metal centre.^{54,55} However, compared to carbonyl stretch in CO, the C=C stretching frequency is weak and overlaps with many other groups *e.g.* organic carbonyl stretches. This makes it a less reliable indicator of the strength of back-donation.

Theoretical calculations have been carried out to try and quantify the different orbital contributions to the metal-alkene bond.⁵⁶ In a series of theoretical studies, Lin and co-workers calculated the relative alkene dissociation energies and structures of [Pd(PH₃)₂(η^2 -CH₂CHX)], [Pd(PH₃)₂Cl(η^2 -CH₂CHX)]⁺ and *trans*-[Pd(PH₃)Cl₂(η^2 -CH₂CHX)] {X = CN, Cl, Br, Me, OMe, NMe₂} with B3LYP density functional theory.⁵⁷ They concluded that σ -donation is more important than π -back donation for interactions between alkenes and Pd^{II}. In the case of unsymmetrical alkenes this will lead to asymmetric coordination of the alkene, particularly with cationic Pd^{II} centres. For Pd⁰-alkene complexes π -back donation plays a dominant role, however, σ -donation also plays a role, leading to near symmetrical coordination. The authors also observed a trend between the alkene dissociation energies and the partial charges of the alkenes. The alkene dissociation energies for Pd^{II} are greater for electron donating substituents (*e.g.* OMe and NMe₂), and give a linear correlation with partial charge. Conversely, for Pd⁰-alkene complexes the alkene dissociation energies are greatest for alkenes with electron withdrawing substituents (*e.g.* CN), however a non-linear relationship is obtained indicating that more than one bonding interaction is occurring.

Steric effects also have a role to play in the strength of alkene binding: disubstituted alkene form stronger bonds than tri or tetra-substituted alkenes. There are also differences between *cis* and *trans* alkenes. No clear trend in coordination strength is

seen; it appears to be dependent on the alkene substituents and the other ligands around the metal centre.^{52,58}

1.3 Alkene ligands in catalysis

Numerous transition-metal catalysed reactions are now available to the synthetic chemist. These range from reactions done on an large scale such as hydroformylation, carbonylation and polymerisation to reactions such as the Pd-catalysed cross-couplings which are widely used in research laboratories and for smaller scale industrial applications such as fine chemical and pharmaceutical synthesis. Ligands such as phosphines and NHCs have been extensively investigated in these reactions.^{59,60} In comparison alkene ligands have received far less attention.⁶¹

Alkenes can be utilised in transition metal-mediated reactions in different ways; they can be part of the metal source, for example, the dibenzylideneacetone (dba) in $[\text{Pd}_2(\text{dba})_3]$, added as exogenous additives, used as the “working” ligand or as an ancillary ligand, or they can form part of the substrate (*e.g.* in the Heck reaction or in alkene metathesis). It is therefore useful to have an overview of how the alkene interacts with the metal centre and how it affects the catalytic cycle. Due to the comprehensive review by Rovis and Johnson in 2008,^{61b} the focus of the discussion below is the use of alkenes in metal precatalysts, in particular $[\text{Pd}_2(\text{dba})_3]$ (**24**), and alkenes as ligands.

1.3.1 Alkenes in precatalysts

Alkene coordination to metals has been studied extensively (see Section 1.2.1) and complexes of this type are often seen in transition metal catalysis as precatalysts. The use of these complexes as precatalysts assumes that the alkene takes no part in the catalytic cycle as they are more labile than the “working” ligands, *e.g.* phosphines or NHCs. The extent of lability is dependent on the strength of the metal-alkene bond. Electron rich alkenes will be more labile due to decreased back-donation, which will increase reactivity; however, this makes the compound less stable and harder to handle (practically). A balance of reactivity and stability needs to be reached for useful transition metal sources and catalysts. Most of the commercially available transition metal complexes contain dienes such as 1,5-cyclooctadiene (cod), norbornadiene (nbd)

and dicyclopentadiene (dcp) as they are more stable, although some mono-alkene metal complexes are available (Figure 9).

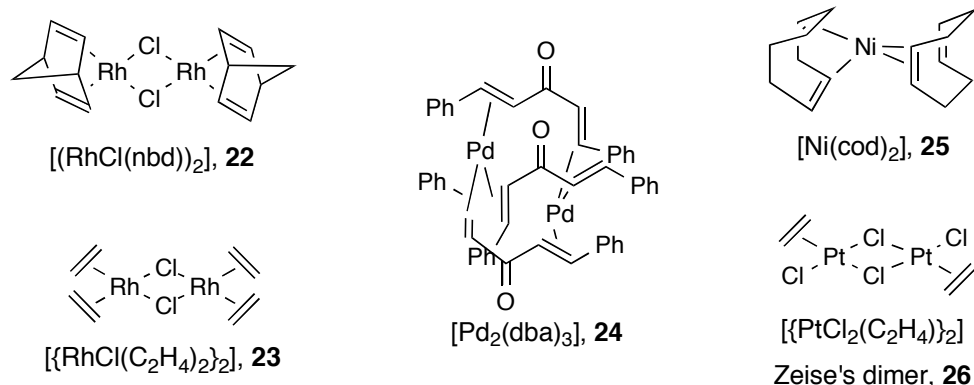


Figure 9: Common transition metal precursor complexes containing alkenes.

Since the 1990s a number of studies have come to light that challenge the notion that alkenes are more labile than phosphines.^{62,63} This immediately presents a problem to the catalytic chemist, as they can no longer assume that any alkene present in their system from precatalysts or substrates are innocent in the catalytic processes involving the metal centre. Studies have shown that the presence of alkenes, such as dba, can affect the rate of both oxidative addition and reductive elimination.^{62,64} β -Hydrogen elimination is also influenced by the presence of alkenes (*see below*).

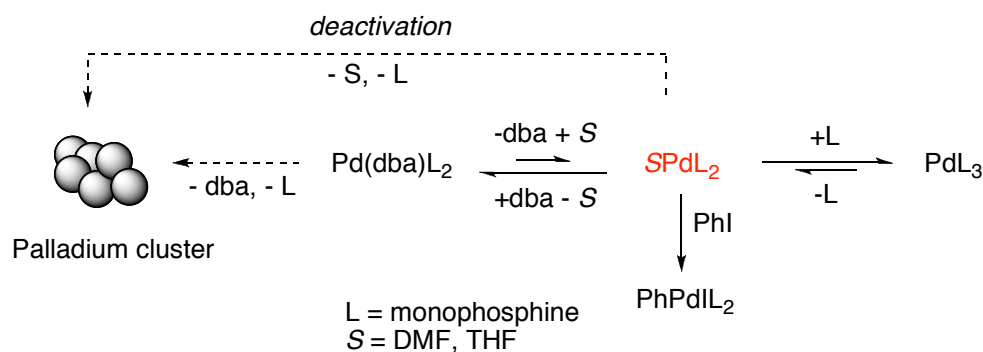
1.3.2 Trisdibenzylidene acetone dipalladium(0)

The most common Pd^0 -alkene precatalyst is $[\text{Pd}_2(\text{dba})_3]$, as it is easy to prepare and air and moisture stable. The dba ligand has been found to be non-innocent in catalysis as described below.

1.3.2.1 Dba effects on oxidative addition

Elegant studies by Jutand *et al.*⁶⁵ showed that in the case of $[\text{Pd}_2\text{dba}_3]$ the dba ligand was not as labile as previously thought and could need as much as 50 equivalents of PPh_3 to displace it entirely, *i.e.* dba has a higher affinity than PPh_3 for $[\text{Pd}(\text{PPh}_3)_2]$. As a result, the equilibrium shown in Scheme 6 is set up and means that dba reduces the rate of oxidative addition by reducing the amount of active catalyst “ $[\text{SPd}^0\text{L}_2]$ ”. Increasing the amount of dba or monophosphine will lead to a slower reaction as the $[\text{SPd}^0\text{L}_2]$ is diminished. By increasing the electron density of the phosphine the equilibrium is

pushed towards $[\text{Pd}^0(\text{dba})\text{L}_2]$, further decreasing the amount of active catalyst and thus influencing the rate of oxidative addition. Unfortunately, one often uses electron rich phosphines to promote oxidative addition as they will favour Pd^{II} over Pd^0 . Therefore, in these cases the behaviour of the dba can be considered to have a detrimental effect on the rate of oxidative addition.



Scheme 6: Oxidative addition equilibrium in the presence of dba.

In some cases the decrease in rate of oxidative addition is beneficial to the overall catalytic cycle, as it brings the rate of oxidative addition in line with the rest of the steps and improves the overall efficiency of the reaction.⁶⁶ The dba ligand may also help to prevent deactivation processes to Pd-black, improving catalyst longevity.⁶⁷ Therefore, it is too simplistic to argue that dba is detrimental to catalysis as Hartwig has done.⁶⁸ Indeed, Pd_2dba_3 has been widely used in numerous Pd-catalysed reactions, a fact that should not be easily dismissed.

The realisation that dba was not as labile as previously thought led Fairlamb and co-workers to study the effect of changing the electronic properties of dba in $[\text{Pd}_2(\text{dba})_3]$ on the rate of oxidative addition in a range of cross-coupling reactions.^{69a} By changing the aryl substituents (*Z*) on dba, they could influence the extent of back-donation between the palladium and the alkene. An electron withdrawing substituent would increase back-donation, whereas an electron donating substituent would destabilise back bonding.

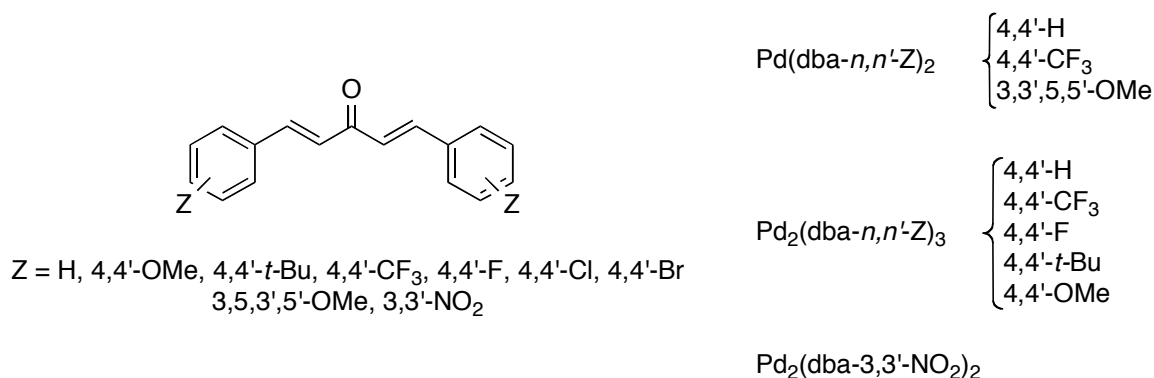
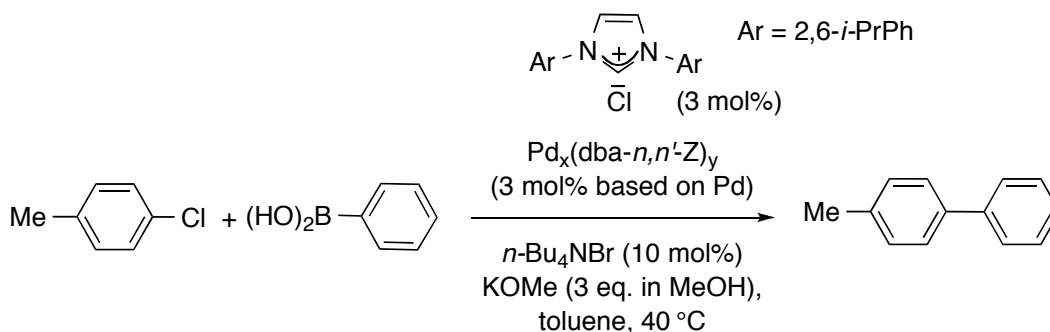


Figure 10: Substituted dba ligands and their Pd⁰ complexes.

A range of aryl-substituted dba ligands were synthesised and their Pd⁰ complexes prepared (Figure 10).⁶⁹ The complexes were studied in a Suzuki-Miyaura system utilising an *N*-heterocyclic carbene (NHC) as a ligand (Scheme 7), as well as under ligand free conditions.⁶⁹ The catalytic activity of the [Pd_x(dba-*n,n'*-Z)_y] complexes varied by an order of magnitude between the most electron-donating complex, [Pd(dba-3,5,3',5'-OMe)₂] (most active) and the most electron-withdrawing complex [Pd₂(dba-3,3'-NO₂)₂.H₂O] (least active). A linear correlation was observed between the observed rate constants and the Hammett parameter σ⁺ for the [Pd₂(dba-4,4'-Z)₃] complexes. The effect was independent of substrate and the presence of NHC donor ligands, suggesting that it is related to the relative strength of the Pd-η²-dba interaction.



Scheme 7: Benchmark Suzuki reaction for assessing the effect of Pd⁰ precursors containing dba-*n,n'*-Z ligands.

In collaboration with Jutand, Fairlamb reported kinetic studies on the oxidative addition of iodobenzene with Pd⁰ complexes generated from these precursors.⁷⁰ In all cases the addition of two equivalents of triphenylphosphine led to the formation of [Pd⁰(PPh₃)₂(dba)]. The kinetics of this complex in the presence of PhI was monitored by amperometry and showed the order of reactivity was Z = OMe > H > F. It was

shown that it is possible to increase the rate of oxidative addition by changing the substituents on the aryl rings in dba to more electron-donating moieties, which reduce the strength of the Pd⁰-alkene bond. Theoretical calculations undertaken with the Gaussian 3 software suite using the B3LYP functional and 6-311G(d,p) basis set support this conclusion. A good correlation between the observed rates and the calculated C=C Mulliken charges populations of the dba-4,4'-Z ligands was found (Figure 11).⁷¹ A similar correlation was found between the rate and the calculate C=O stretching frequency of the ligand, enabling future variants of these types of ligands to be evaluated *in-silico*.

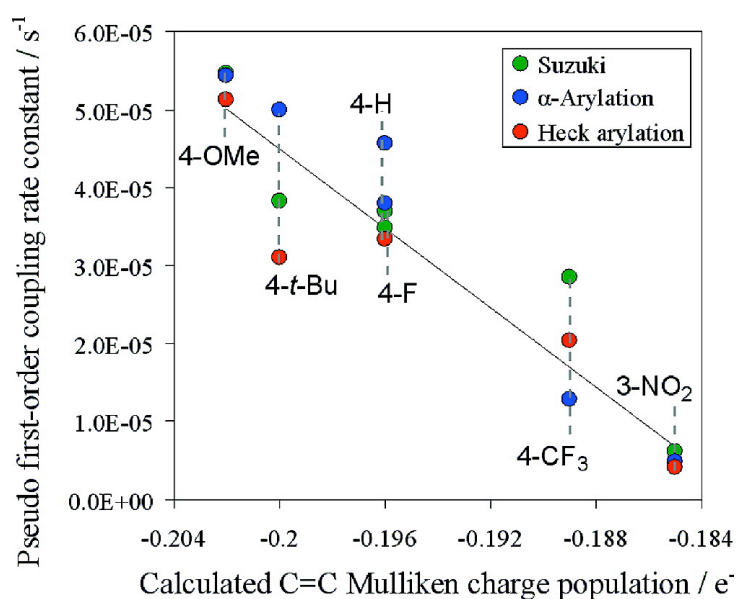
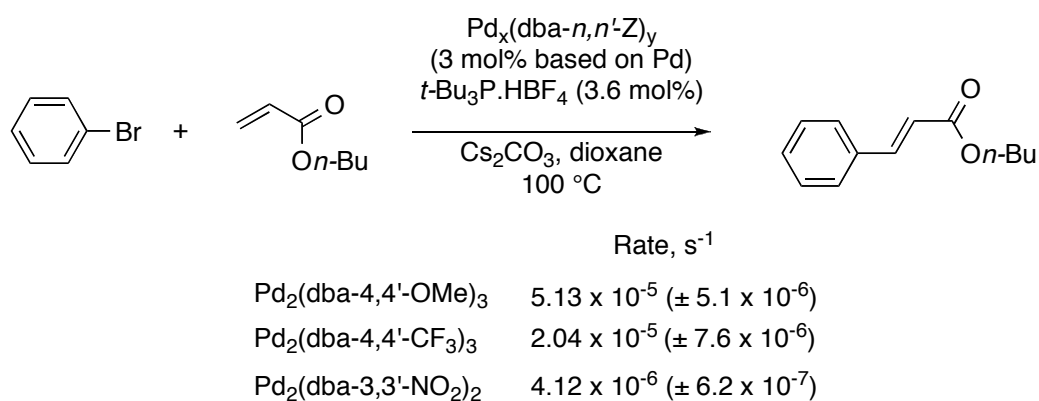
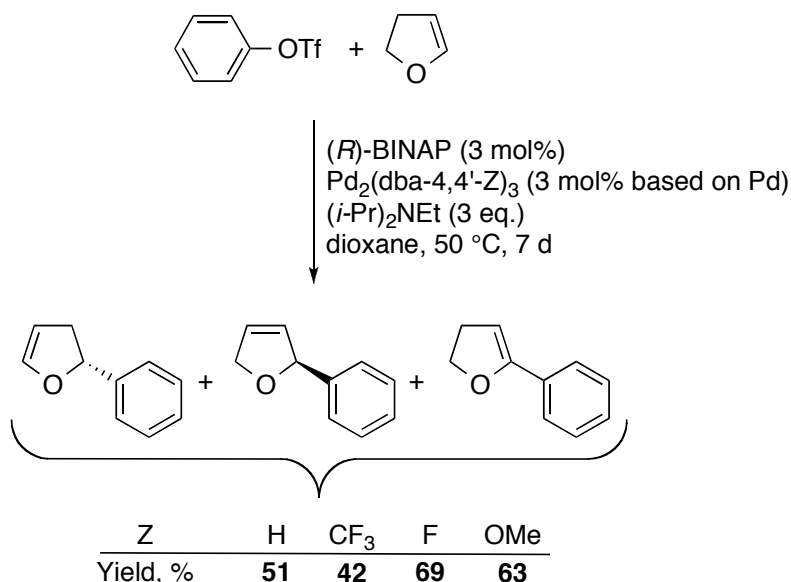


Figure 11: Linear correlation of the observed rate constants with the C=C Mulliken charge population for dba-4,4'-Z ligands.⁷¹



Scheme 8: Intermolecular Heck reaction (errors in bracket).

This phenomenon could be applied to a number of other catalytic reactions. In the α -arylation of esters and intermolecular Heck reaction (see Scheme 8) changing the aryl substituent of dba affected the rate of reaction.^{69a} The addition of electron-donating substituents led to an increase in the pseudo first order rate for the consumption of bromobenzene. Again there was an order of magnitude difference between the most active [Pd₂(dba-4,4'-OMe)₃] and the least active [Pd₂(dba-3,3'-NO₂)₂].

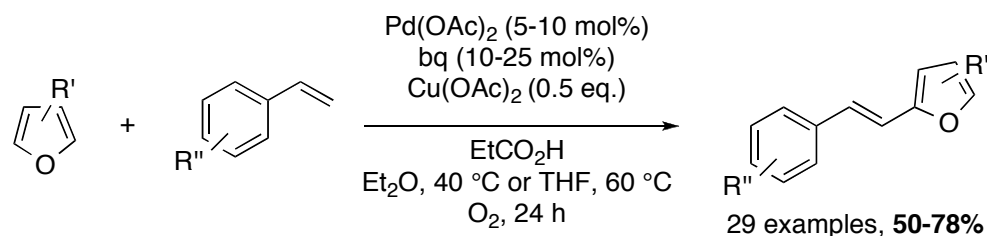


Scheme 9: Benchmark reaction for asymmetric Heck arylation.

Not all of the reactions studied by Fairlamb and co-workers had the same reactivity profile. On looking at an asymmetric intermolecular Heck reaction (Scheme 9) the fluorine substituted dba gave the greatest yield.^{69a} As the reaction time was long (7 d) it is believed the dba-4,4'-F plays a role in stabilising the Pd⁰ and prevents the formation of palladium black. No benefit was gained from using more electron donating substituents or more electron withdrawing substituents, showing a subtle balance is needed between stabilising the catalyst over time and still having an active catalyst. It can be argued that the 4-fluoro-substituent can undertake two roles electronically depending on whether inductive or mesomeric effects are taken into account. The best explanation is that the 4-fluoro-group will put most of the charge at the para-position (due to π -conjugation with the enone), and therefore act as an activating group.

Work by Bras and co-workers also supports the ability of alkenes to stabilise Pd⁰ species. Whilst investigating the dehydrogenative coupling of furans (Scheme 10), they

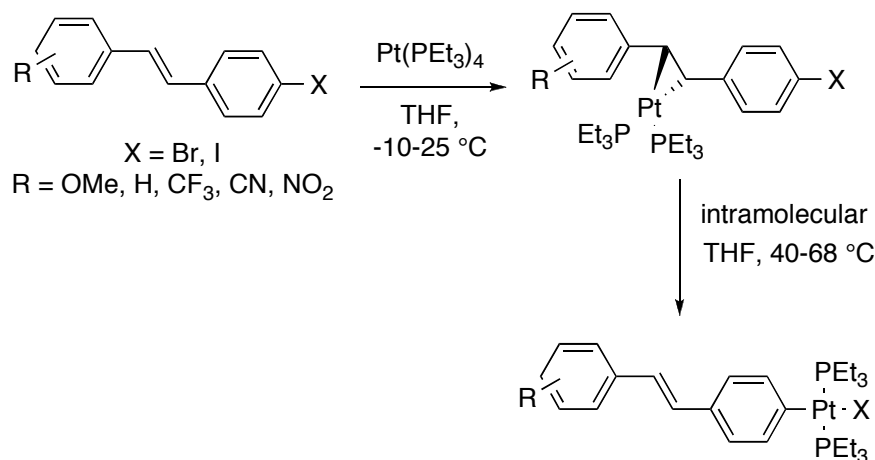
showed that in the presence of dba less Pd black formation was observed, and full conversion was obtained.⁷² This suggests that dba is aiding catalyst longevity. In some of the reactions, Pd black formation was not observed even in the absence of dba. The authors attribute this to the presence of an alkene in the products, which allows some of them to behave in a similar manner to dba. It should also be noted that benzoquinone (bq) is used as the oxidant, but can also act as an alkene ligand.



Scheme 10: Palladium catalysed dehydrogenative coupling of furans with styrenes.

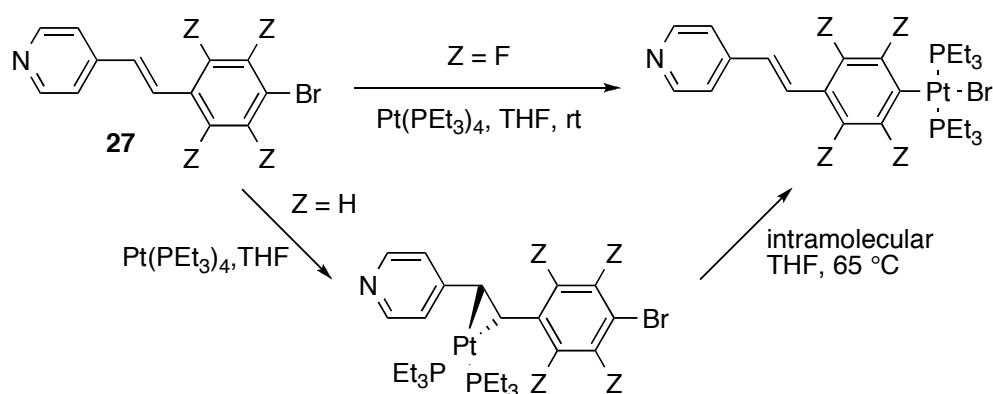
Overall it has been shown that the more electron-rich dba ligands can increase catalytic activity. This is rationalised in terms of the strength of the $\text{Pd-}\eta^2\text{-dba}$ interaction and its effect on oxidative addition. In longer reactions the ability to stabilise the Pd^0 catalyst from aggregation also becomes important. It should be noted that this effect is not always seen, in some examples, the dba appears to have no effect on oxidative addition and thus the dba can be regarded as innocent in these reactions, *e.g.* where it is chemically consumed.^{69a}

1.3.2.2 Supporting studies showing alkene effects on oxidative addition



Scheme 11: Kinetically favoured alkene coordination followed by oxidative addition.

Numerous studies on other alkenes support the observations of Jutand, Fairlamb and co-workers. In a series of elegant studies, van der Boom and co-workers showed that aryl halide substrates containing an alkene undergo η^2 -coordination to Pt before oxidative addition occurs (see Scheme 11).⁷³ Although the oxidative addition step is still rate-determining, as shown by aryl iodides reacting faster than aryl bromides, the order of alkene reactivity (OMe > H > CF₃ > CN > NO₂) is the opposite of that expected for substituted aryl halides indicating that it is controlled by alkene coordination. The rate of reaction increases with electron-donating substituents, which can be explained by weaker back-donation between the metal and the alkene, leading to a less stable intermediate that undergoes oxidative addition faster.

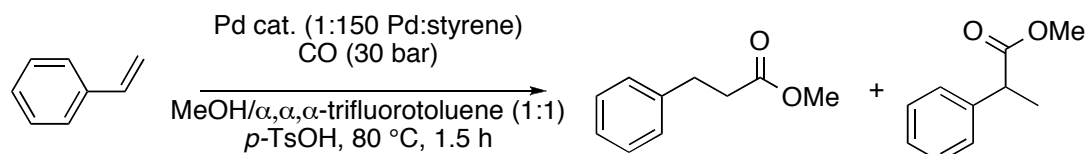


Scheme 12: 'Ring-walking' with stilbazoles.

Kinetic studies on a stilbazole substrate (**27**, Z = H) revealed that the rate-determining step was unimolecular and that the Pt “walks” along the ring prior to intramolecular insertion into the aryl-bromide bond (Scheme 12).⁷⁴ Fluorination of the aryl ring changes the kinetically favoured process from η^2 -coordination to oxidative addition.⁷⁵

A number of alkenes have been used to great effect in Pd-based catalytic studies. Alkenes such as dimethyl fumarate, fumaronitrile, and maleic anhydride have been used to create active Pd catalysts. Van Koten and co-workers studied how the electronic nature of the alkenes could influence the catalytic activity of Pd⁰-alkene bis(triarylphosphine) complexes in the methoxycarbonylation of styrene (Scheme 13).⁷⁶ The degree of conversion was seen to be dependent on the electronic nature of the alkene; the more electron deficient the alkene the lower the conversion. This matches the same trends observed by Fairlamb and co-workers (see above). The exception to

this was maleic anhydride, which has similar electron withdrawing properties to fumaronitrile, gave twice the conversion (Table 2).



Scheme 13: Methoxycarbonylation of styrene using Pd⁰-alkene complexes.

Table 2: Effect of different alkenes on the methoxycarbonylation of styrene

Entry	Complex	Conversion, %	branched:linear ratio
1	Pd(PPh ₃) ₂ (ma)	80	41:59
2	Pd(PPh ₃) ₂ (tcne)	2	42:58
3	Pd(PPh ₃) ₂ (fn)	40	40:60
4	Pd(PPh ₃) ₂ (bq)	27	41:59
5	Pd(PPh ₃) ₂ (C ₂ H ₄)	80	41:59

In all cases the linear vs. branched ratio of the products was the same suggesting the same active catalyst is generated each time. This is believed to be a Pd^{II} hydride species formed from the reaction of the Pd⁰ complex and acid. It is unclear which step is rate-determining and how the reaction is influenced by the alkenes, as no detailed kinetic studies have been carried out.

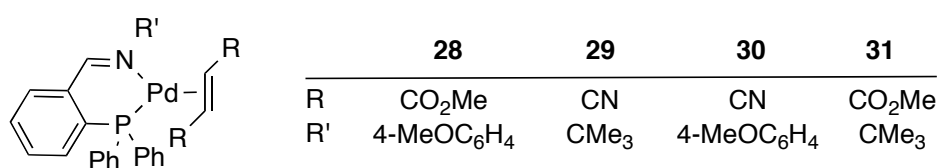


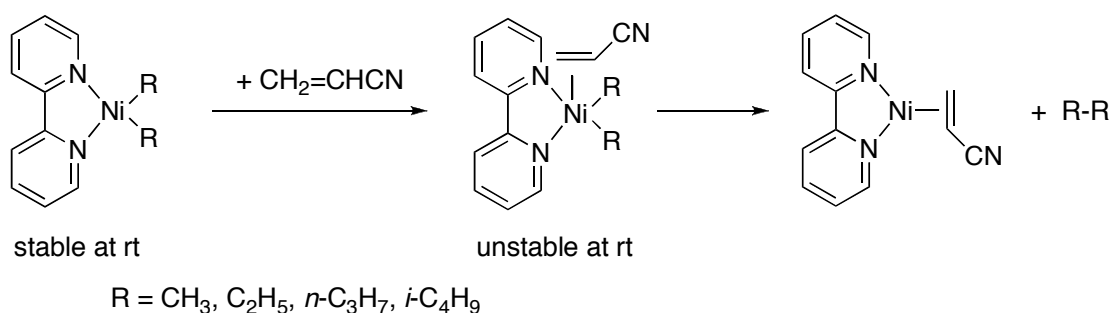
Figure 12: Iminophosphine-Pd⁰ complexes stabilised by alkene ligands.

Crociani and Antonaroli studied the reactivity of Pd⁰-iminophosphine complexes which were stabilised by activated alkenes such as dimethyl fumarate, 1,4-naphthoquinone, fumaronitrile and maleic anhydride (Figure 12).⁷⁷ Less π -accepting ligands such as methyl acrylate did not form stable complexes that could be isolated. They showed that

the dimethyl fumarate could be exchanged with the other ligands, following the accepted order of reactivity based on η^2 -coordination strength.⁵² In collaboration with Scrivanti, the authors went on to use the dimethyl fumarate complexes, **28** and **31**, as highly active catalysts in both the Stille and Suzuki coupling reactions.⁷⁸ Dimethyl fumarate has also been used as a stabilising ligand in Pd⁰ precatalysts for hydrogenation processes.⁷⁹

1.3.2.3 Effect on reductive elimination and β -hydride elimination

It has been known that electron-deficient alkenes can accelerate reductive elimination since the 1970's, when Yamamoto observed reductive elimination from Ni complexes following alkene coordination (Scheme 14).⁶⁴ The rate of reductive elimination from the Ni complexes is greatest when more electron deficient alkenes such as maleic anhydride are used. When unactivated alkenes such as ethene, norbornene or styrene are used, the reaction either happens slowly or not at all.



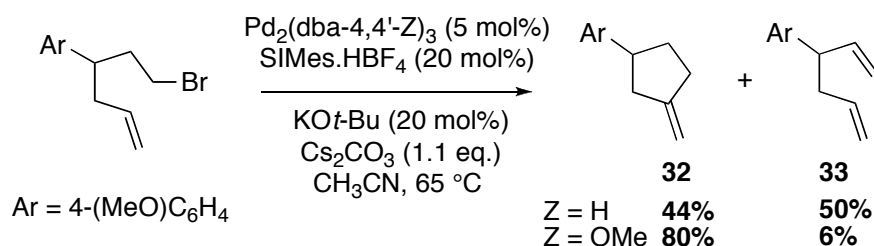
Scheme 14: Alkene effects on reductive elimination from Ni(bipy) complexes.

Alkene additives have also been shown to have an effect on the selectivity of many reactions, by interfering with isomerisation and β -H elimination pathways.^{61b}

The nature of the dba ligand can have an effect on β -H elimination and reductive elimination processes, as well as that seen above in oxidative addition. The studies on the effect of dba on these steps is not as extensive as those on oxidative addition, nevertheless the results are informative.

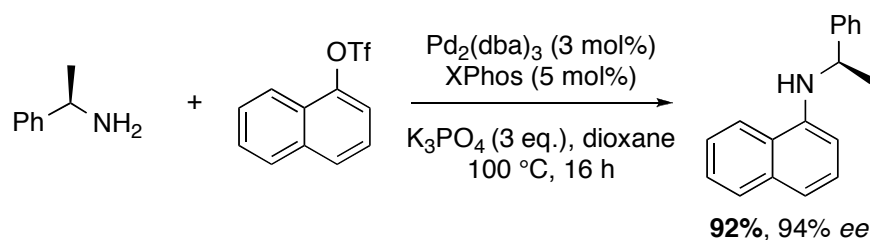
Firmansjah and Fu recently reported an intramolecular Heck reaction, which showed a remarkable dba-effect (Scheme 15).⁸⁰ There are two possible products from the reaction: 1) the cyclised product (**32**) where intramolecular insertion of the alkene

occurs before β -H elimination, and 2) the diene product (**33**) where β -H elimination is faster than alkene insertion.



Scheme 15: Intramolecular Heck reaction displaying a remarkable dba effect.

Using the Pd⁰ precursor [Pd₂(dba)₃] they got almost equal quantities of the cyclised and 1,5-diene products, whereas the use of [Pd₂(dba-4,4'-OMe)₃] resulted in cyclisation becoming the dominant pathway. It can be hypothesised that dba-4,4'-OMe slows down β -H elimination before alkene insertion, by coordinating to the Pd^{II} oxidative addition species, thus removing the vacant site needed. Dba-4,4'-OMe is more electron rich than dba-H, and so likely interacts more strongly with Pd^{II}.



Scheme 16: Chiral amination of aryl triflates.

Woodward and Meadows attributed the superior behaviour of [Pd₂(dba)₃] to [Pd(OAc)₂] as a precatalyst for the amination of aryl triflates and nonaflates, to the ability of dba to occupy a vacant site on the Pd thus stopping β -H elimination.⁸¹ When they used XPhos as a ligand no deprotection products were observed. The use of chiral amine substrates (Scheme 16) led to only small amounts of racemisation, in comparison to previous studies by Buchwald who saw racemisation when using a Pd/P(*o*-Tol)₃ system.⁸² Racemisation occurs via β -H elimination, which requires a vacant site on the palladium, *e.g.* in the monoligated Pd/P(*o*-Tol)₃ system. It is proposed that the XPhos binds through both the phosphine and the substituted aryl ring in an η^1 -interaction as shown in **34** (Figure 13). This removes the vacant site needed for β -H elimination, and this limits

the amount of racemisation that occurs. It is hypothesised that the dba can also fulfil this role *via* η^2 -binding of the alkene, **35**.

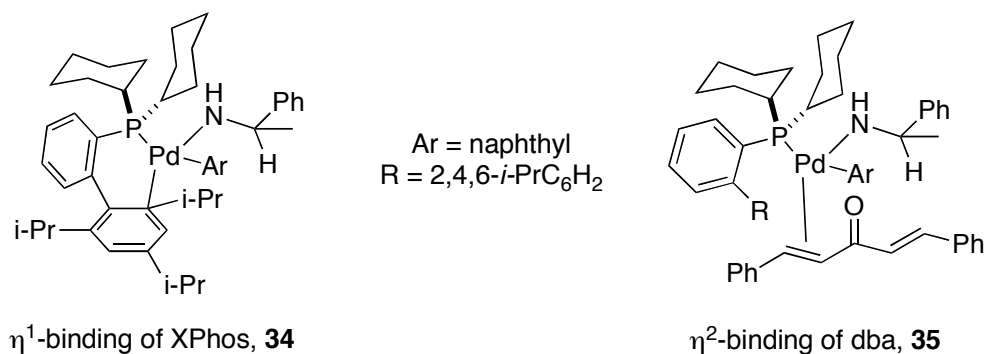
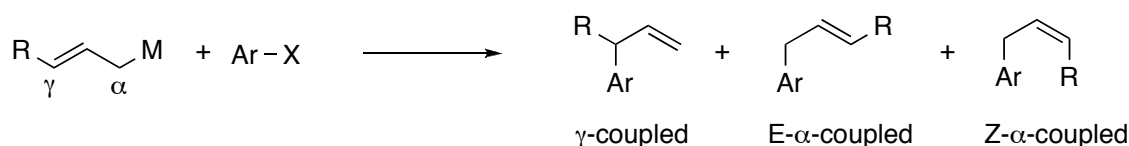


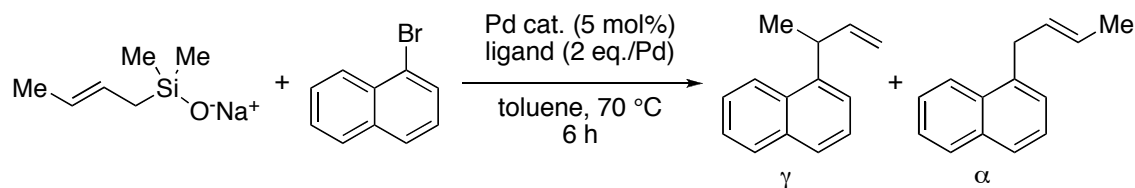
Figure 13: Removal of the vacant site by XPhos and dba.



Scheme 17: Possible products of cross-coupling between allylic partners and aryl halides.

Denmark and Werner found that alkenes had an effect on the site-selectivity of cross-coupling between aromatic bromides and allylic silanolate salts.⁸³ For unsymmetrically substituted allylic donors, the coupling can afford a mixture of products (Scheme 17) depending on the relative rates of reductive elimination and isomerisation/ β -H elimination. In the course of Denmark and Werner's investigation into fluoride free conditions, they observed that the presence of alkenes affected the site selectivity.

A comparison of [Pd₂(dba)₃] and [Pd(dba)₂] in the crotylation of 1-bromonaphthalene showed that an increase in dba concentration increased the γ -selectivity. Adding additional alkene ligands was also beneficial, leading to increased conversion and similar or better selectivities (Table 2, entries 4 and 5).

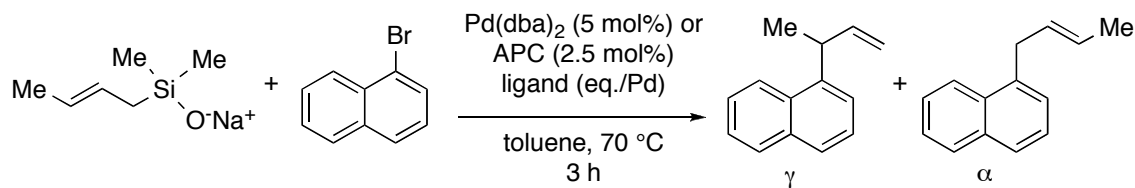
Table 3: Crotylation of 1-bromonaphthalene.

Entry	Pd source	Ligand	Conversion, %	γ : α
1	Pd ₂ (dba) ₃	PPh ₃	57	3.9:1
2	Pd(dba) ₂	PPh ₃	59	5.0:1
3	Pd(dba) ₂	None	47	10:1
4	Pd(dba) ₂	cod	90	9.5:1
5	Pd(dba) ₂	dba	77	16:1

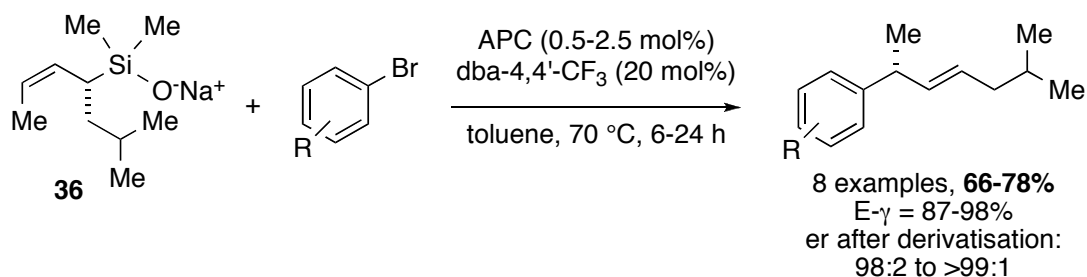
A range of different alkenes were investigated, and in general, the more electron deficient alkenes gave better γ -selectivity. This is consistent with previous studies on reductive elimination.⁶⁴ 1,4-Benzoquinone gives very high γ -selectivities but low yields (Table 4, entries 4 and 5), due to its ability to oxidise Pd⁰ to Pd^{II} which cannot re-enter the catalytic cycle under the reaction conditions. When allyl palladium(II) chloride dimer (APC) instead of [Pd(dba)₂] was used as the Pd source, only dba and dba-4,4'-CF₃ gave better than a 10:1 ratio, γ : α (Table 4, entries 7 and 9).

The alkene additives not only increase the γ : α ratio but they also increase the conversion of the reaction in some cases. In particular, the use of norbornadiene with APC led to high conversions but low site-selectivity. This suggests norbornadiene does not influence reductive elimination and the resulting product distribution in this reaction system. Two alternative roles it may play are: i) it increases the catalyst lifetime by stabilising the catalyst resting state, or ii) the electron rich norbornadiene increases the rate of oxidative addition.

Table 4: The effect of alkene ligands on the crotylation of 1-bromonaphthalene.



Entry	Pd source	Ligand	Eq./Pd	Conversion, %	γ : α
1		none	n/a	45	11:1
2		tetramethylethylene	4	41	6.5:1
3	Pd(dba) ₂	ma	6	41	10:1
4		bq	4	28	19:1
5		bq	8	13	61:1
6		dba	4	64	7.9:1
7		dba	10	85	18:1
8	APC	dba-4,4'-OMe	4	72	5.1:1
9		dba-4,4'-CF ₃	4	61	12:1
10		cod	4	80	1.3:1
11		nbd	1	92	2.0:1



Scheme 18: Preparative cross-coupling of chiral allylic silenolates to aryl bromides.

Denmark and Werner have taken on their findings to develop a protocol for the preparative cross-coupling of an enantioenriched allylic silenolate (**36**) with a variety of aryl bromides (Scheme 18).⁸⁴ The use of the electron-deficient dba ligand, dba-4,4'-CF₃, led to high selectivities and conversions. The reaction shows good substrate scope,

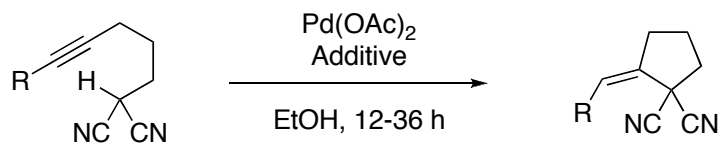
allowing both electron rich and electron poor aryl bromides to be used, along with *ortho*-substituted and heteroaromatic aryl bromides.

Despite less systematic studies into the role of dba in the later catalytic steps, it has been seen that dba (and other alkenes) can play a pivotal role in both β -H elimination and reductive elimination. As a result, improved product selectivity can be obtained via the use of a $[\text{Pd}_2(\text{dba-}n,n'\text{-Z})_3]$ precatalyst or the addition of dba-*n,n'*-Z ligand to an alternative Pd source.

1.3.3 Mono- and polydentate alkene ligands in catalysis

In all the above examples, apart from the ligand free Suzuki couplings and some of the hydrosilylation examples, alkenes have been used as auxiliary ligands in the presence of a “working” ligand, such as a phosphine, iminophosphine or carbene, to obtain the effective catalyst. There has been far less exploration of alkenes as “working” ligands in the literature, particularly in reference to Pd-catalysed reactions.⁸⁵

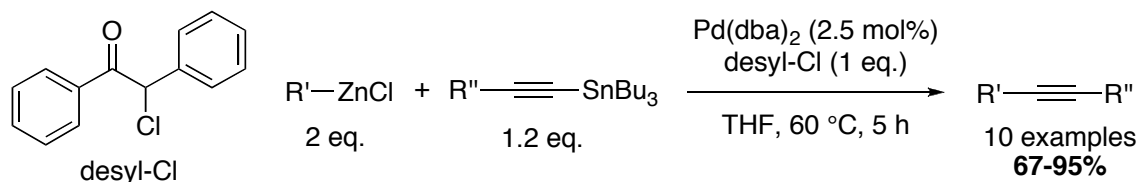
1.3.3.1 Palladium catalysis



Scheme 19: Intermolecular hydrocarbonation of ϵ -alkynyl malonitriles.

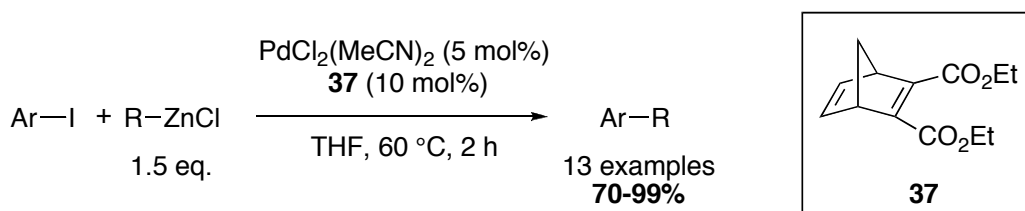
In the late 1990s Yamamoto and Tsukada published an example of intramolecular hydrocarbonation of ϵ -alkynyl malonitriles catalysed by Pd-alkene complexes (Scheme 19).⁸⁶ The addition of alkenes (1-octene and cod) to $[\text{Pd}(\text{OAc})_2]$ led to increased yields. In contrast, the addition of triphenylphosphine did not lead to an increase in yield. The use of cod allowed both the reaction temperature and catalyst loading to be reduced. When 1-octene was used Pd black formation was seen, which was not observed with cod. Presumably the Pd^0 -cod complex formed is more stable due to the chelating nature of cod, however no direct evidence of Pd^0 -cod complexes was obtained.

Lei and co-workers observed that dba facilitated reductive elimination in a $Csp-Csp^3$ system.⁸⁷ Using $[Pd(dba)_2]$ without added phosphines gave higher selectivities in the cross-coupling of alkylzinc and alkynylstannane reagents than other ligands (Scheme 20).



Scheme 20: Palladium catalysed oxidative cross-coupling.

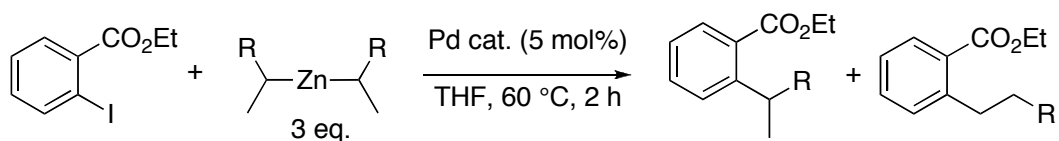
The use of alkyl zinc reagents leads to the possibility of β -H elimination and isomerisation side reactions after transmetallation, especially if the reductive elimination step is slow. Alkenes have been shown to increase the rate of reductive elimination, which should limit the amount of time for β -H elimination/isomerisation to occur. The authors designed ligand **37** to examine the possibility of increasing the rate of reductive elimination and to inhibit isomerisation pathways when alkyl organometallic reagents are used.⁸⁸



Scheme 21: Negishi reaction catalysed by diene 37.

Lei and co-workers showed that the electron deficient diene, **37**, could be added to $[PdCl_2(MeCN)_2]$ to efficiently catalyse Negishi reactions using Csp^3 -zinc reagents (Scheme 21).⁸⁸ Clear advantages were observed with ligand **37** when secondary alkyl zinc reagents were used. When just $[Pd(dba)_2]$ was used, inconsistent yields between different zinc reagents were observed, and isomerisation of secondary alkylzinc reagents was a problem. Using a dialkylzinc source and ligand **37** with either $[Pd(dba)_2]$ or $[PdCl_2(MeCN)]$ increased selectivity by inhibiting isomerisation (Table 5).

Table 5: Selectivity in Negishi couplings of secondary alkylzinc reagents in the presence of ligand **37.**



Entry	Pd cat.	R	Yield, %	Selectivity, %	
				linear	branched
1	Pd(dba) ₂	Me	90	26	74
2	Pd(dba) ₂ + 37	Me	87	91	9
3	PdCl ₂ (MeCN) ₂ / 37	Me	92	97	3
4	PdCl ₂ (MeCN) ₂ / 37	n-C ₂ H ₅	88	91	9

Attempts to synthesise the Pd⁰ complex of **37** using a similar method to that used to prepare [Pd(dba)₂] resulted in a black powder that gave similar results in catalysis but was hard to characterise, meaning the exact nature of the Pd catalyst (is it homogenous or heterogenous) and the precise role of ligand **37** is not known.

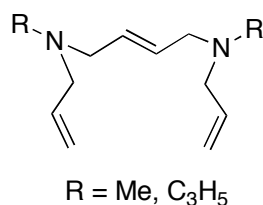


Figure 14: Pörschke's triene ligands.

[Pd₂(dba)₃] has three alkenes around each Pd atom, suggesting that trienes may be able to provide stable complexes. Both Pörschke and Moreno-Mañas have independently designed a variety of triene ligands that form stable Pd⁰ complexes. Pörschke and co-workers designed an open chain triene ligand, Figure 14, based on the premise that 'naked' Pd⁰ sources of the type [Pd⁰₂(1,6-diene)₃] were more stable than 1,5-diene based structures.⁸⁹ 'Naked' is used to mean a Pd⁰ complex without strongly coordinating ligands like phosphines, but instead the metal centre is stabilised by ligands that are easy to displace. The use of trienes would make the complexes much more stable than the corresponding tri-alkene complexes due to the chelate effect. In turn this makes

their description as naked more circumspect. These complexes were found to be more stable than the $[\text{Pd}_2(1,6\text{-diene})_3]$ complexes where 1,6-diene = 1,6-heptadiene and diallyl ether, but less stable than cyclic triene ligands.

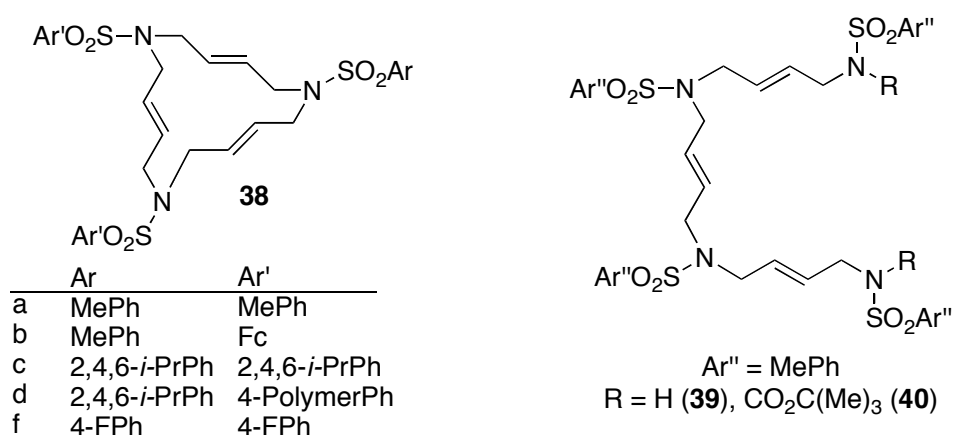
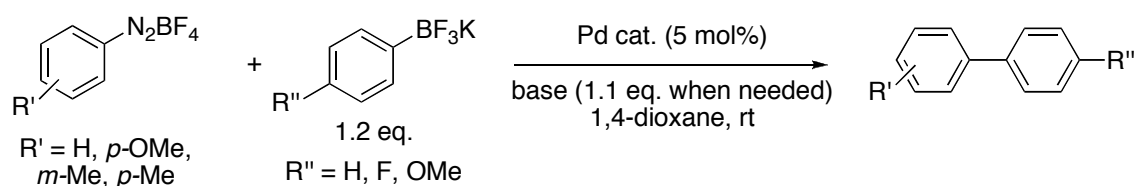


Figure 15: Macrocyclic and open-chain trienes designed by Moreno-Mañas.

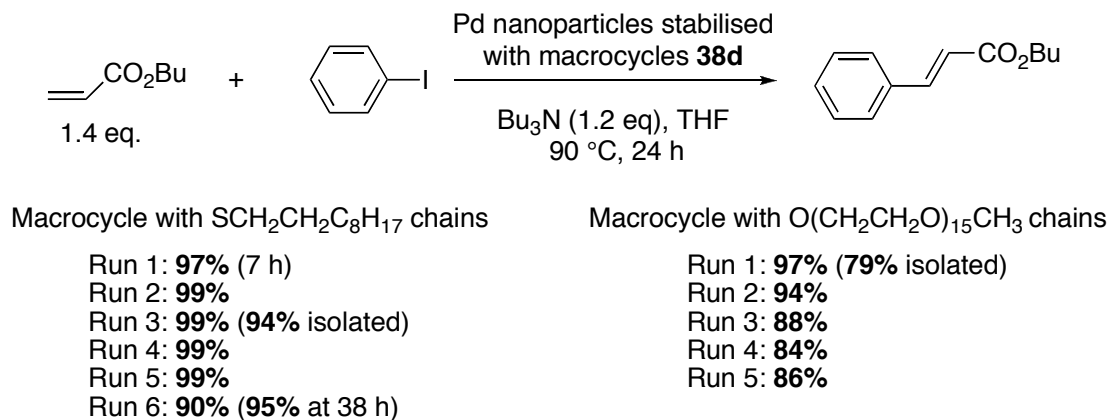
Moreno-Mañas and co-workers designed a series of macrocyclic ligands, with a 1,6-diene type motif and compared these to a number of open-chain trienes (Figure 15).⁹⁰ The Pd complexes of the macrocyclic ligands were found to be more stable than the open chain variants. Unexpectedly this does not appear to inhibit catalysis. A comparison of the open chain and macrocyclic ligands in a Suzuki-type reaction (Scheme 22) showed that in all cases the Pd⁰-macrocycle complex was fully recovered by column chromatography. Recovery of the open-chain Pd⁰-complexes was not possible when the sulfonamide nitrogens were left free (ligand 39), and base was required to enable the reaction. No trends were observed over the series of ligands and the yields were variable.



Scheme 22: Suzuki-type cross-coupling for comparison of macrocyclic vs. open chain ligands.

Pd complexes of the macrocyclic ligands have been found to act as catalysts for a number of processes including the Heck reaction and alkyne hydroarylation.^{90a,91} As mentioned above the palladium complexes can be recovered after the reaction by

chromatography. Solid-supported catalysts can be prepared by attaching a polymer (based on styrene and divinylbenzene) to one of the aryl groups (ligand **38d**). This enables the palladium complexes to be recovered by filtration alone and reused at least five times before any noticeable decrease in conversion.



Scheme 23: Mizorok-Heck reaction catalysed by Pd nanoparticles stabilised by macrocyclic ligands.

The activities of the Pd complexes with macrocyclic ligands were tested in ionic liquids as well as in conventional solvents. Ligand **38a** was found to effectively catalyse the hydroarylation of alkynes in [bmim]BF₄.^{90a} The ionic solution could be recycled up to six times before loss of activity occurred, whereas traditional Pd sources gave lower yields and recovery.

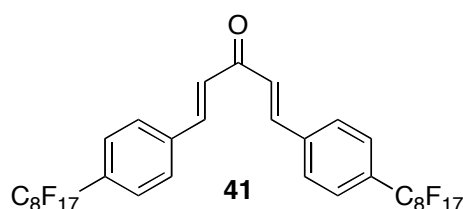


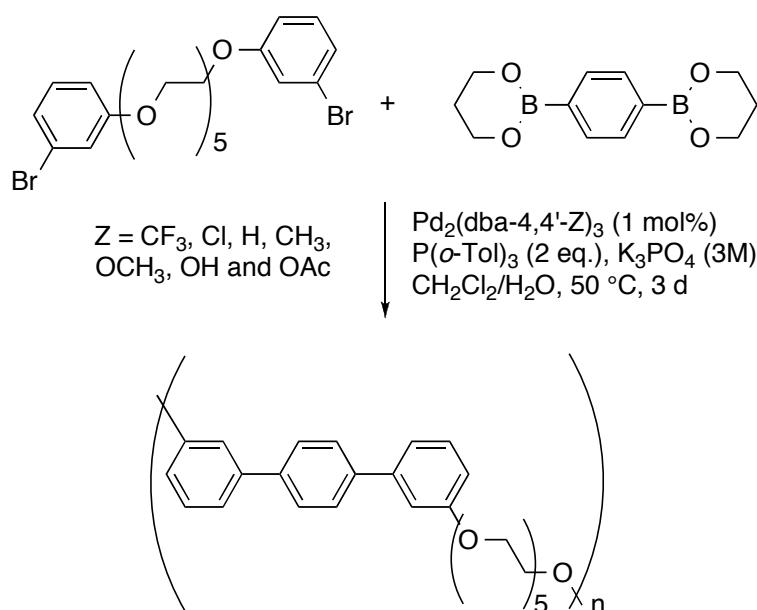
Figure 16: "Fluorous dba".

The introduction of fluororous chains or polyoxyethylenated chains onto the aryl rings of the macrocycles gave rise to ligands that were found to be excellent stabilisers of Pd nanoparticles.⁹² Nanoparticles stabilised with these macrocycles were found to give excellent conversion in a Mizoroki-Heck reaction, and could be recovered and reused (Scheme 23). The yield dropped after the fifth run; examination of the nanoparticles revealed they had agglomerated to particles sized ~100 nm – which is quite large

compared to other cross-couplings catalysed by Pd nanoparticles, where 2-5 nm nanoparticles are common.⁹³

Moreno-Mañas and co-workers also prepared Pd nanoparticles stabilised by “fluorous-dba” (**41**, Figure 16), which are 4-5 nm in diameter.⁹⁴ These were tested in both Mizoroki-Heck and Suzuki reactions in a biphasic fluorinated solvent system (perfluorooctylbromide/benzene). Once again the catalyst could be recovered and reused at least five times, whilst maintaining reasonable yields.

Table 6: Suzuki polycondensation reaction utilising Pd₂(dba-4,4'-Z)₃, including water soluble da ligands.



Entry	Z	P(<i>o</i> -Tol) ₃ , eq.	M _n , g/mol	M _w , g/mol	Yield, %
1	H	2	60 600	112 400	93
2	CF ₃	2	65 700	118 000	88
3	OMe	2	81 500	144 000	74
4	OH	2	131 000	290 000	94
5	OAc	2	104 000	244 000	96

Similarly, dba ligands substituted with OH or OAc have been prepared by Goodson and co-workers to probe ligand design in a biphasic aqueous system. Suzuki polycondensation reactions are carried out in biphasic medium. The traditional catalyst

is $[\text{Pd}(\text{P}(\text{o-Tol})_3)_2]$, which is not easy to handle *i.e.* is light, heat and oxygen sensitive.⁹⁵ The authors want to try and replace this catalyst with one that is easier to handle; unfortunately, the use of $[\text{Pd}_2(\text{dba-}n,n',n''\text{-Z})_3]$ had a detrimental effect on the polymer molecular weights (Table 6, entries 1-3), and $[\text{Pd}(\text{P}(\text{o-Tol})_3)_2]$ still gave the best molecular weights ($M_n = 188\,000$ g/mol, $M_w = 464\,000$ g/mol, Yield = 89%).

As these reactions are carried out under biphasic conditions, the authors reasoned that a water soluble dba ligand could be used which would give a stable precatalyst, but under the basic aqueous conditions transfer into the water phase so as not to play a role in any of the catalytic steps. To test their hypothesis they synthesised $[\text{Pd}_2(\text{dba-4,4'-OH})_3]$ and $[\text{Pd}_2(\text{dba-4,4'-OAc})_3]$. In both cases the polymer molecular weights were higher than with the other dba ligands tested (Table 6, entries 4 and 5), though still not matching the $[\text{Pd}(\text{P}(\text{o-Tol})_3)_2]$. The authors propose that designing dba ligands with more water solubilising groups could lead to more effective catalysts and once the ligands are completely solubilised one would have a system where the dba was truly innocent. At this point it would be possible to go back to optimising other parts of the system, *e.g.* the phosphine. However, it is not clear if this approach would work, particularly under the biphasic conditions. The phosphine is presumably in the organic layer, so increasing the water solubility of the Pd^0 precursor $[\text{Pd}_2(\text{dba-Z}_3)]$ could hinder the formation of $[\text{Pd}(\text{P}(\text{o-Tol})_3)_2]$, the active catalyst, as the Pd^0 may stay in the aqueous phase.

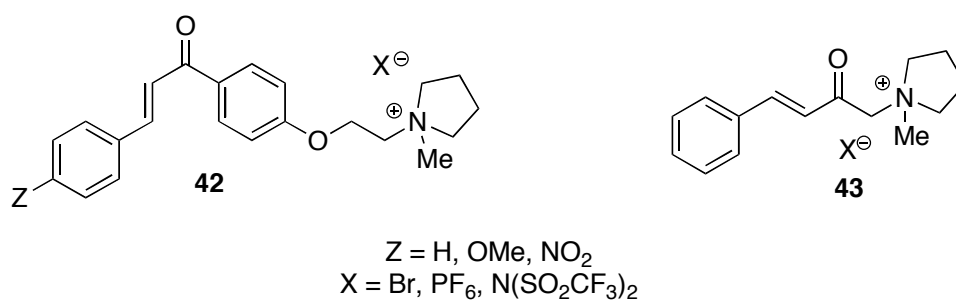


Figure 17: Novel ionic π -acidic alkene ligands.

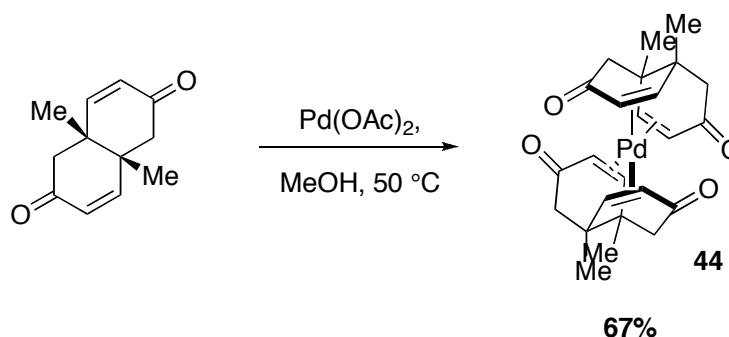
Fairlamb, Slattery and co-workers designed a range of ionic alkene ligands based on chalcones (**42**) and benzylidene acetone (**43**), Figure 17.⁹⁶ The authors were interested in addressing one of the drawbacks of using dba in catalysis: the complications in purification of products that are similar in polarity to dba. They identified a Hiyama-type cross coupling which had previously shown strong alkene effects and used this as a

benchmark for a coupling in ionic liquids (Scheme 24).⁹⁷ Using a neutral chalcone in THF gave similar conversions as the doped ionic liquids, confirming the effectiveness of the ligands in the reaction medium. No ligand contamination was observed in the products by ¹H NMR spectroscopy after extraction from the ionic liquids and filtration through a silica plug, indicating that the use of ionic alkene ligands in ionic liquid solvents can simplify and improve product recovery.

In all cases Pd nanoparticle formation was observed. The size of the nanoparticles formed depended on the aryl substituent on the ionic chalcone ligand; the nitro-substituted ligands gave larger nanoparticle sizes (10-15 nm) than the methoxy-substituted ligand (1-3 nm). This can be linked to the rate of reaction, which was faster for the methoxy ligand. Previously, it has been shown that nanoparticles that are <5 nm are optimal for related coupling processes.⁹³



Scheme 24: Benchmark Hiyama type coupling in ionic liquids.

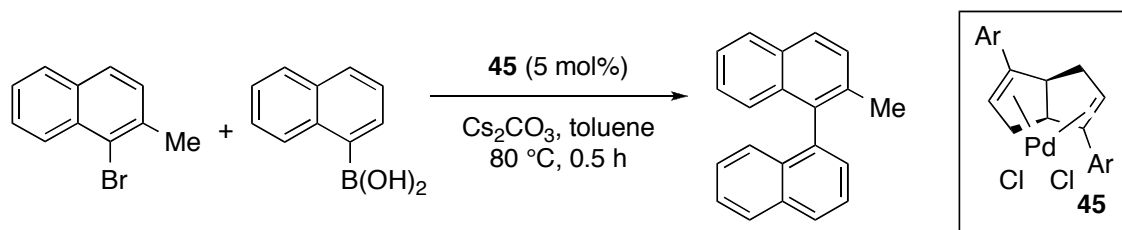


Scheme 25: Chiral Pd-diene complex.

The ligands described above have been achiral and only used in non-asymmetric processes. Very few chiral alkene ligands have been studied in Pd-catalysed reactions, despite their use in Rh and Ir-catalysed reactions (see below). Trauner and co-workers reported the synthesis of the chiral complex, **44** (Scheme 25), inspired by the unexpected observation of a Pd⁰ tetraalkene complex by Mulzer.⁹⁸ Complex **44** is a tetraalkene Pd⁰ complex, whose air and moisture stability is attributed to the increased back-donation caused by the electron-withdrawing carbonyl substituents. The complex

exhibited some activity in a Pd-catalysed 1,6-enyne cycloisomerisation, but no asymmetric induction was observed. No further studies have been carried out with this interesting chiral diene.

Recently, Lin and co-workers carried out the first asymmetric Suzuki-Miyaura coupling using Pd-diene complexes to give axially chiral biaryls (Scheme 26).⁹⁹

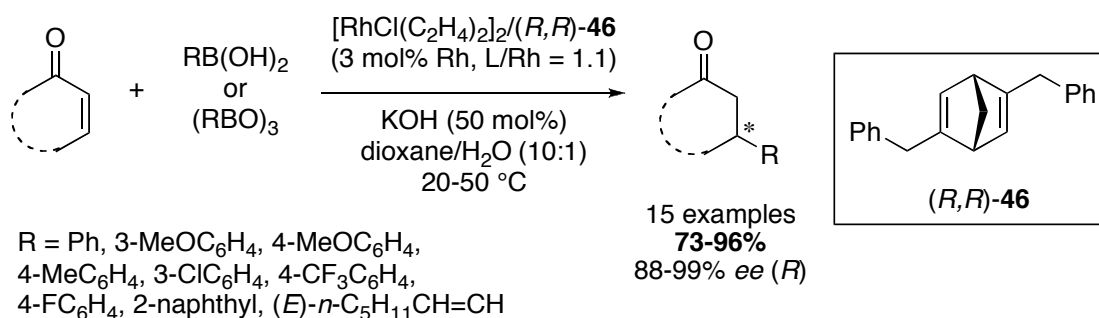


Scheme 26: Chiral diene catalysed Suzuki-Miyaura.

Similar yields were obtained regardless of the electronic nature of the diene, however, lower enantioselectivities were observed with bulkier ligands. Having determined that the best yields and selectivities were obtained when Ar = 3,5-(dimethyl)phenyl, further optimisation was carried out. The addition of the opposite enantiomer led to a racemic product, indicating that fast ligand exchange was occurring. They hypothesised that additional free ligand would be beneficial to catalyst turnover and asymmetric induction. The addition of 15 mol% free ligand enabled the temperature to be lowered to 25 °C, whilst seeing further improvements in yield and selectivity. The optimised reaction was effective for the formation of a variety of biaryls all in high yield (72-99%) and moderate to good enantioselectivity (48-90% *ee*).

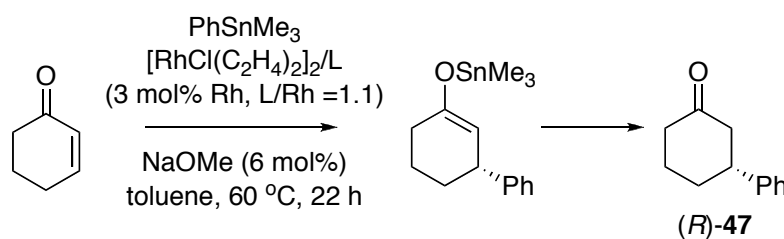
1.3.3.2 Rhodium and iridium catalysis

The use of chiral dienes in Rh and Ir catalysed processes has met with more success than in Pd-catalysed reactions. The metal-alkene bond strength depends on the metal. Alkenes bind more strongly to Rh and Ir and therefore provide a more definite steric environment. Hayashi and Carreira have made seminal contributions to the use of chiral dienes as ligands in Rh and Ir catalysis. In 2003, Hayashi and co-workers showed that chiral diene **46**, based on norbornadiene, could be successfully utilised as a chiral ligand in the Rh-catalysed 1,4-addition of organoboron reagents to enones.¹⁰⁰ High yields and enantioselectivities were obtained (Scheme 27).



Scheme 27: Rh-catalysed 1,4-addition of organoboron reagents to cyclic (5 and 6 membered rings) and acyclic enones.

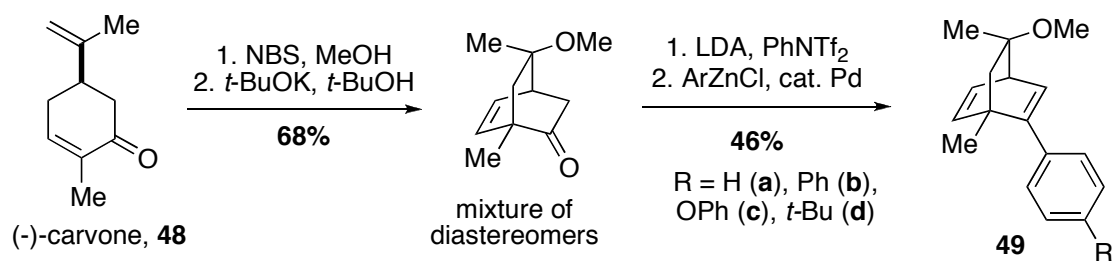
The high catalytic activity of the chiral diene, (*R,R*)-**46**, over chiral phosphines such as BINAP, has meant that less reactive transmetallation reagents can be used efficiently, *e.g.* the otherwise almost inert organostannane, PhSnMe₃ (Scheme 28).



Ligand	(<i>R</i>)- 47
(<i>R</i>)-BINAP	<10%
(<i>R,R</i>)- 46	80%, 95% <i>ee</i>

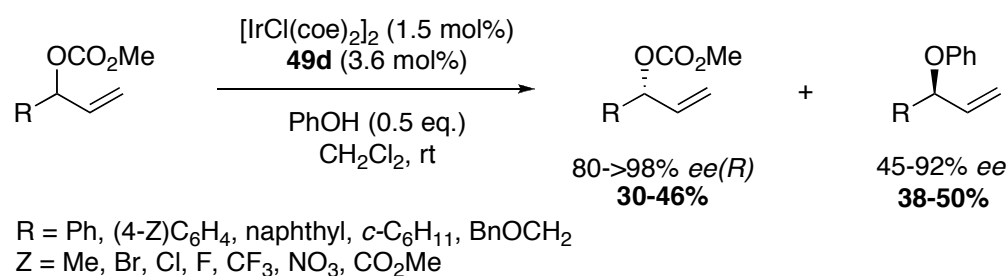
Scheme 28: Asymmetric conjugate addition to α,β -unsaturated carbonyl compounds.

Meanwhile, in early 2004, Carreira and co-workers published their studies into chiral dienes as ligands for Ir.¹⁰¹ Following their observation that [IrCl(cod)]₂ was active in allylic displacement reactions but [IrCl(coe)₂]₂ was inactive, they designed chiral dienes for the kinetic resolution of allyl carbonates. Starting from (*R*) or (*S*)-carvone (**48**) they were able to prepare a variety of chiral dienes (**49**) in 4 steps (Scheme 29).



Scheme 29: Synthesis of carvone-based diene ligands.

The kinetic resolution gave high enantioselectivities and good yields, for a broad range of aryl (electron-rich and electron poor) and alkyl-substituted allylic carbonates (Scheme 30).



Scheme 30: Kinetic resolution of allylic carbonates with Ir-diene complexes.

The authors also compared the reactivity of ligand **49d** with that of Hayashi's ligand **46** and found that **46** failed to form an Ir complex. This indicated that the small change in ligand backbone might favour different metals. In the Rh-catalysed 1,4-addition of PhB(OH)₂ to cyclohexanone they found that ligand **49d** was not as active as **46**, giving only 52% yield and 71% *ee*. This supports the observation that the slightly different ligand backbones may favour different metals.

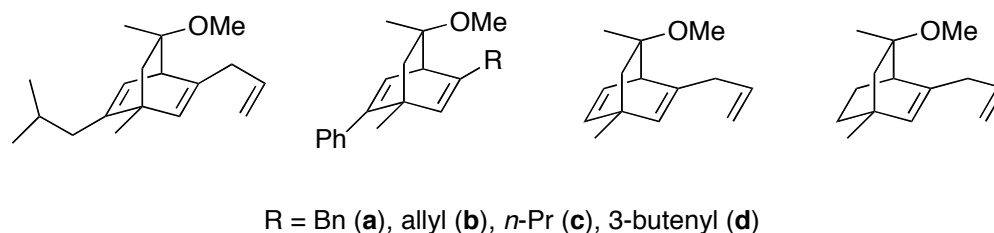
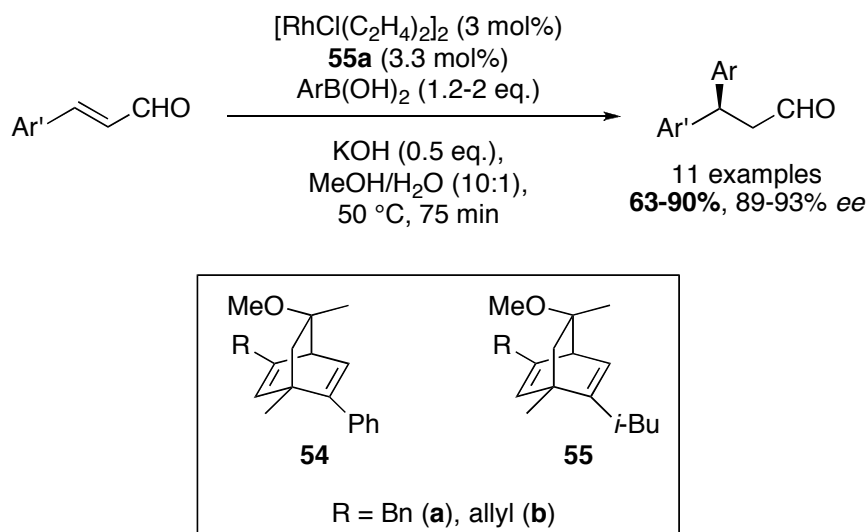


Figure 18: Bicyclo[2.2.2]octane Ligands for Rh-catalysed conjugate additions.

Further studies by Carreira assessed whether a [2.2.2]-bicyclooctadiene scaffold was intrinsically a disadvantage to the norbornadiene scaffold in Rh catalysis or if different

substitutes would afford more active catalysts. They found that changing the substituents on the alkenes led to an increase in yields and enantioselectivities for a variety of Rh-catalysed conjugate additions.¹⁰² A comparison of ligands **52** and **53** (Figure 18), in the addition of PhB(OH)₂ to cyclohexanone showed that the rigid diene core was essential for good conversions; with **53** less than 10% conversion was obtained compared to 93% with **52**. The enantioselectivities were greater with **50** and **51** over **52** (82-95% vs. 58%), presumably due to the increased steric congestion around the diene. Ligands **54** and **55** were studied in the conjugate addition of arylboronic acids to cinnamaldehyde derivatives (Scheme 31). Ligand **55a** gave high yields and enantioselectivities with both electron rich and electron poor organoboronic acids. The reaction was chemoselective with none or only minor amounts of 1,2-addition products observed.

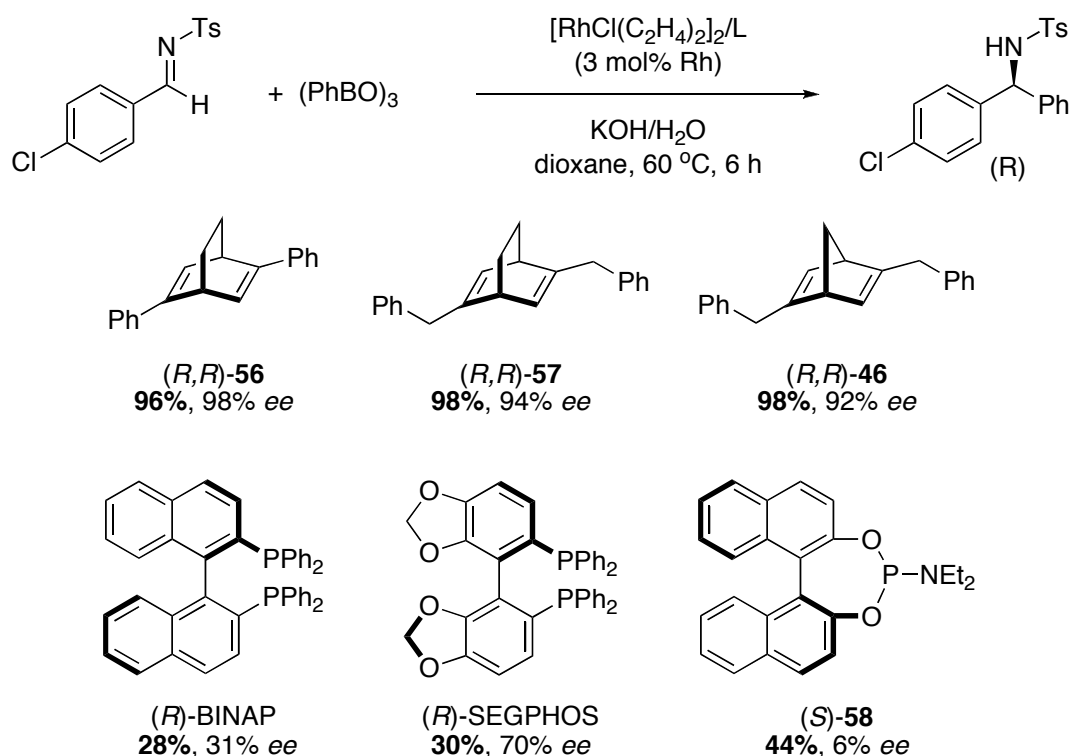


Scheme 31: Rh-catalysed synthesis of 3,3-diarylpropanals.

Following the initial use of chiral dienes in Rh-catalysed conjugate addition to α,β -unsaturated carbonyl compounds, the reaction scope has been expanded to include catalysed asymmetric 1,4-addition of arylboronic acids to maleimides,¹⁰³ arylative cyclisation of alkynes,¹⁰⁴ and the arylation of imines.¹⁰⁵ In many of the reactions studied, chiral dienes outperform phosphine ligands (Scheme 32).

As well as expanding the reaction scope, the development of other chiral dienes has continued (Figure 19); further variants of [2.2.2]-bicyclooctadiene scaffolds have been examined by Hayashi and Darses independently, **60**, **61**, and **67**,^{106,107} as well as [3.3.1]-

bicyclononadiene frameworks, **65**.¹⁰⁸ Separate investigations by Corey and Toste have examined the extension of norbornadiene-based frameworks, **62** and **66**,¹⁰⁹ Grützmacher has studied cyclooctene backbones,¹¹⁰ and Lin has studied dicyclopentadienes as ligands, **64**.¹¹¹ More complex ligand systems such as DNA-diene hybrid ligands, **59**, have also been developed.¹¹²



Scheme 32: A comparison of phosphines and dienes in the arylation of imines.

The majority of the ligands mentioned above have had bicyclic core structures, which impart rigidity to the ligand framework. This partially accounts for the high reactivities and enantioselectivities observed using these ligands. The rigid frameworks provide a very defined environment around the metal centre. The aryl group of the organoboronic acid coordinates first to the Rh complex, and will occupy the least sterically congested site. It has also been suggested that the aryl-Rh bond will form opposite the most electron deficient double bond. The imine or enone will then approach from the least hindered face minimising steric repulsion, leading to stereochemical control (**Error! Reference source not found.**). Disappointingly the studies cited do not attempt to distinguish between steric and electronic factors.

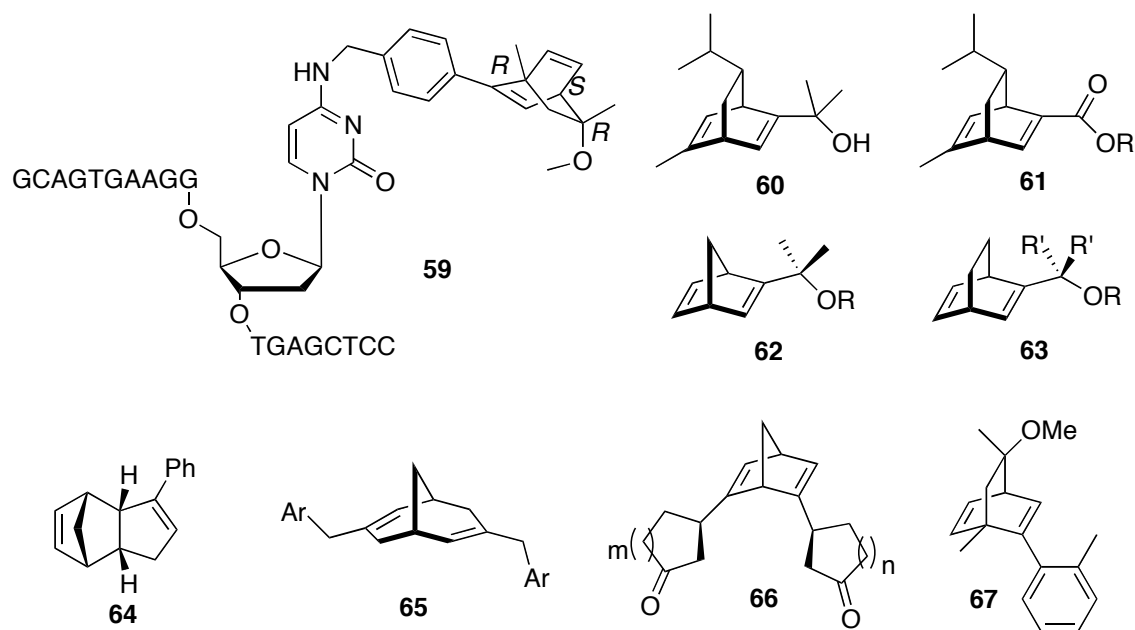
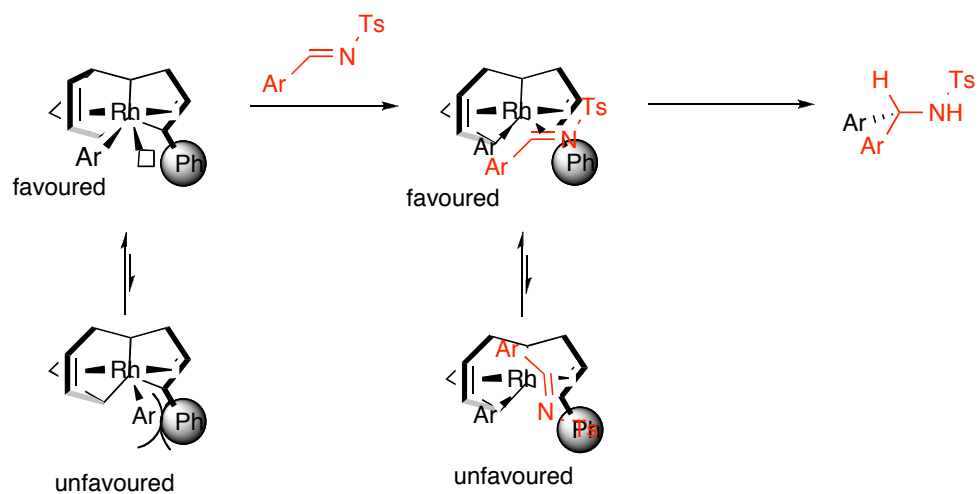
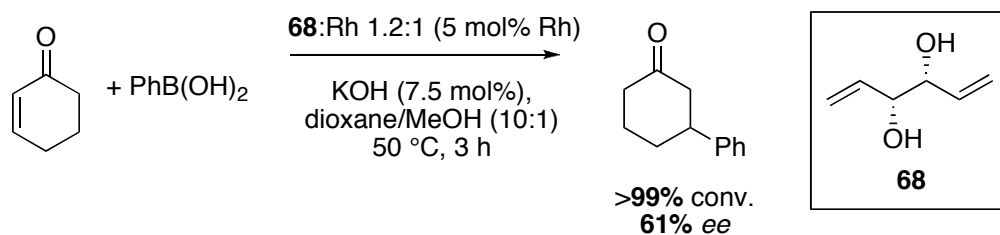


Figure 19: Selected examples of chiral dienes utilised as ligands.



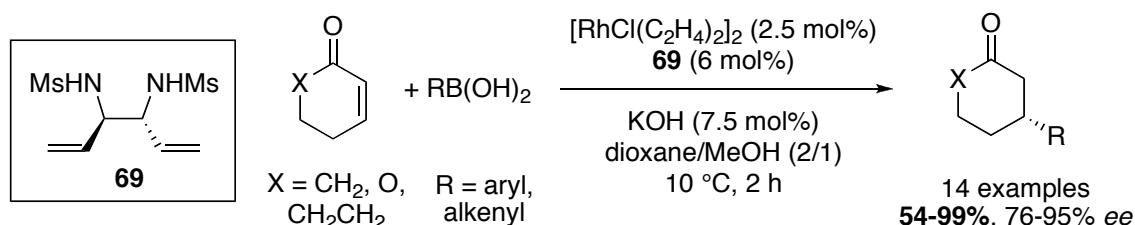
Scheme 33: Stereochemical control in the arylation of *N*-tosylarylimines by a Rh-dicyclopentadiene complex.

Du and co-workers tested the feasibility of chiral chain dienes in some simple Rh-catalysed conjugate additions (Scheme 34).¹¹³ Excellent yields and moderate to good enantioselectivities were obtained for a number of substrates, showing that ligand **68** was successful. As expected the enantioselectivities were not as high as those seen for dienes with a rigid ligand frameworks.



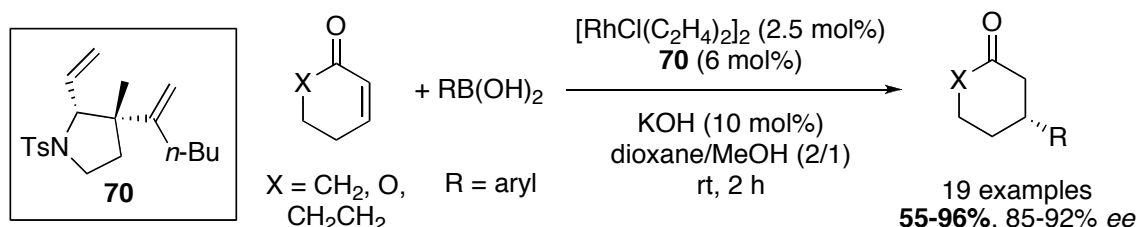
Scheme 34: Rh-catalysed conjugate addition with a chiral diene ligand.

Du and co-workers developed further acyclic dienes giving rise to increased enantioselectivities for conjugate additions. Surprisingly changing the hydroxyl groups (**68**) for protected amines (**69**) led to good to excellent enantioselectivities and yields (Scheme 35), suggesting that rigid frameworks are not essential.¹¹⁴



Scheme 35: Rh-catalysed conjugate addition with a chiral chain diene ligand containing protected amines.

Yu and co-workers recently reported that α,β -divinyl tetrahydropyrroles (*e.g.* **70**) can also act as effective acyclic chiral dienes in Rh-catalysed conjugate additions (Scheme 36).¹¹⁵ The reaction gave good yields and enantioselectivities for a range of substrates including *ortho*-substituents on the aryl boronic acid. However, a number of electron deficient aryl boronic acids gave low yields, as did acyclic α,β -unsaturated ketones and esters.



Scheme 36: The use of α,β -divinyl tetrahydropyrroles in Rh-catalysed conjugate additions.

Overall, a wide range of alkenes have been successfully utilised in transition metal catalysed reactions. In particular, alkenes have been widely applied in Pd-catalysed

cross-couplings to minimise unwanted side reactions such as isomerisation, and to facilitate the recovery of palladium from the reaction medium. In many cases where successful catalysis has been observed, dienes or polyene ligands have been used rather than mono-alkenes. The added alkene moieties increase the stability of the catalysts *via* the chelate effect.

Chiral alkenes, such as chiral dienes have not been widely utilised in Pd-catalysis. In contrast their use in Rh and Ir catalysis is well documented, especially for Rh-catalysed conjugate addition reactions to enones and imines with chiral dienes becoming the benchmark ligands in these reactions.

1.4 Heterobidentate alkene ligands

Alkenes have been shown to be beneficial in catalysis in a variety of different ways. However limitations do exist; the strength of the metal-alkene bond is dependant on the metal and its oxidation state, thus effective ligands with one metal often turn out to be unsuccessful ligands for other metals or oxidation states. As a result, a number of research groups have been interested in combining alkenes with other well studied ligands to gain access to more effective catalysts. Of particular interest has been combining alkenes with phosphorus donor groups, *e.g.* phosphines, to give bidentate ligands. The phosphine component ensures a strong binding to the transition metal, while the alkene provides both the opportunity to create a chiral environment in close proximity to the transition metal, or to provide another way to vary the electronic properties of the catalyst.

The first chelating phosphino-alkene ligand (**71**) was reported by Nyholm and co-workers in 1964, followed soon after by a number of further variants (**72**, **73**, and **74**; Figure 21).¹¹⁶ They observed that if the alkyl tether was less than $(\text{CH}_2)_2$, no metal-alkene interaction was observed. A number of groups have observed that a tether of $(\text{CH}_2)_2$ gives the best chelate ligands for Pd^{II} and Pt^{II} .¹¹⁷ However, there is some evidence from tungsten complexes that the alkene may coordinate in the solution phase when the tether is only CH_2 .¹¹⁸ Phosphino-alkene ligands can therefore be considered hemilabile.

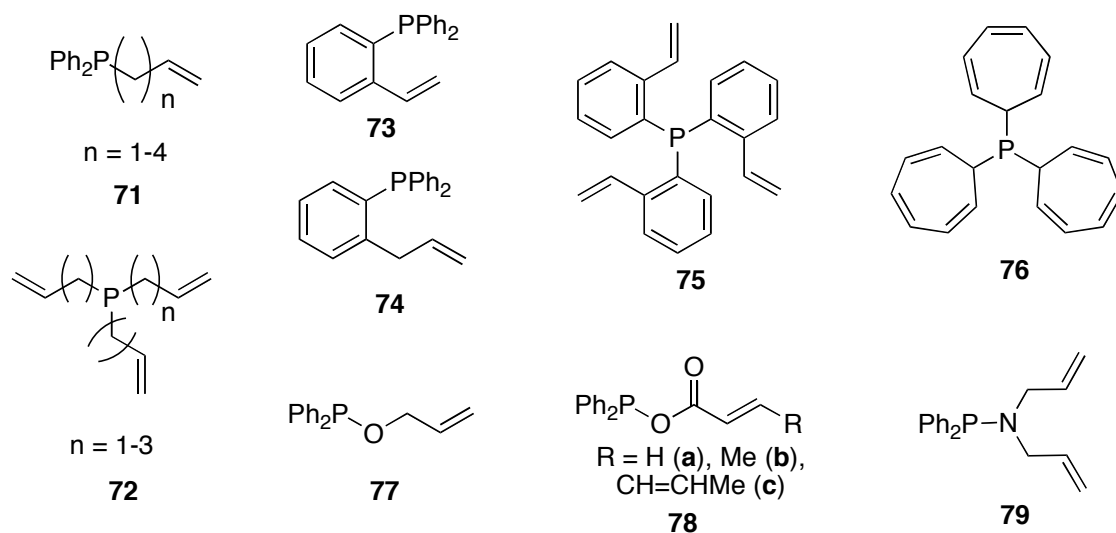


Figure 21: Phosphino-alkene ligands.

Since Nyholm's first publication the exploration of the coordination chemistry of phosphino-alkene ligands has continued, with many different transition metals being explored. The coordination of the alkene is dependant on the metal type. Metals such as Rh, Ir, Pt and Pd will generally coordinate to both the phosphine and alkene. The strength of alkene coordination in these complexes is in the order $\text{Ag}^{\text{I}} < \text{Cu}^{\text{I}} < \text{Pd}^{\text{II}} < \text{Pt}^{\text{II}} \approx \text{Rh}^{\text{I}} < \text{Ir}^{\text{I}}$, as shown by a decrease in $\nu_{\text{C}=\text{C}}$.^{117b,119} In general the free alkene $\text{C}=\text{C}$ stretching frequency is *ca.* 1640 cm^{-1} , on coordination this decreases by $100\text{-}150 \text{ cm}^{-1}$. Care must be taken as the assignment of the $\nu_{\text{C}=\text{C}}$ is not straight-forward, due to a number of reasons. The $\nu_{\text{C}=\text{C}}$ band may be weak in the starting ligand^{123a} or unclear due to overlapping bands with any carbonyl stretches present. In addition there is disagreement in the literature over which bands to assign to the $\text{C}=\text{C}$ stretching frequency.^{119d} In some cases bands at *ca.* 1500 cm^{-1} have been assigned as $\nu_{\text{C}=\text{C}}$,^{119a,116,120} in other cases bands at *ca.* 1250 cm^{-1} have been assigned as $\nu_{\text{C}=\text{C}}$,^{123a} whilst the band at 1500 cm^{-1} is assigned to the C-H bending mode.^{119c} In further cases it has been bands at both 1500 and 1250 cm^{-1} have been described as combinations of the $\text{C}=\text{C}$ stretching frequency and the CH_2 bend.^{119d,121} In more complex molecules it is likely that it will be even harder to assign the $\text{C}=\text{C}$ stretching frequency, and care must be taken with any comparisons made about the strength of the metal-alkene bond based on IR measurements.

The coinage metals are much less likely to coordinate to both the alkene and the phosphine, with often just the phosphine coordinated complexes being isolated,

particularly with Ag^I.^{119b} It was only in 2008 that the first Au^I phosphino-alkene complex was crystallised.¹²² W, Cr and Mo complexes of the internal alkene isomer of **74**, showed alkene coordination

Tripodal and tetradentate ligands such as **72**, **75**, and **76** have been synthesised.^{116, 117b, 119c, 123} In the Rh(L)X and Ir(L)X complexes (X= Br, Cl), the phosphine and all the alkenes were seen to coordinate leading to 5-coordinate complexes. In contrast with Pd^{II} and Pt^{II} the phosphine and only one of the alkenes would coordinate to give square planar M(L)X₂ complexes.

Ligands with other heteroatoms as well as phosphorus have also been synthesised, along with their metal complexes; Rh^I for ligand **78**,¹²⁴ and Pd^{II} and Pt^{II} for ligand **79**.¹²⁵ In the [RhCl(PPh₃)(**78b**)] complex fluxional behaviour of the alkene was observed. The double bond uncoordinates to give a 3-coordinate intermediate which can then either give the 4-coordinate complex with either the alkene *trans* to the Cl or to the PPh₃.

In the last 10 years, the focus of investigations into these ligands has moved from coordination chemistry to catalysis.

1.5 Heterobidentate ligands in catalysis

As shown above a number of phosphino-alkene ligands have been synthesised. More recently many more examples of phosphino-alkene ligands have followed from Grützmacher,¹²⁶ Carreira,¹²⁷ Hayashi,¹²⁸ Widhalm,¹²⁹ Ellmann¹³⁰ and Lei among others (Figure 22).¹³¹ The latter reported ligand **84** during the first months that the current project was started in York. These phosphino-alkene ligands have been utilised in a wide range of Pd, Rh and Ir catalysed reactions, as outlined below.

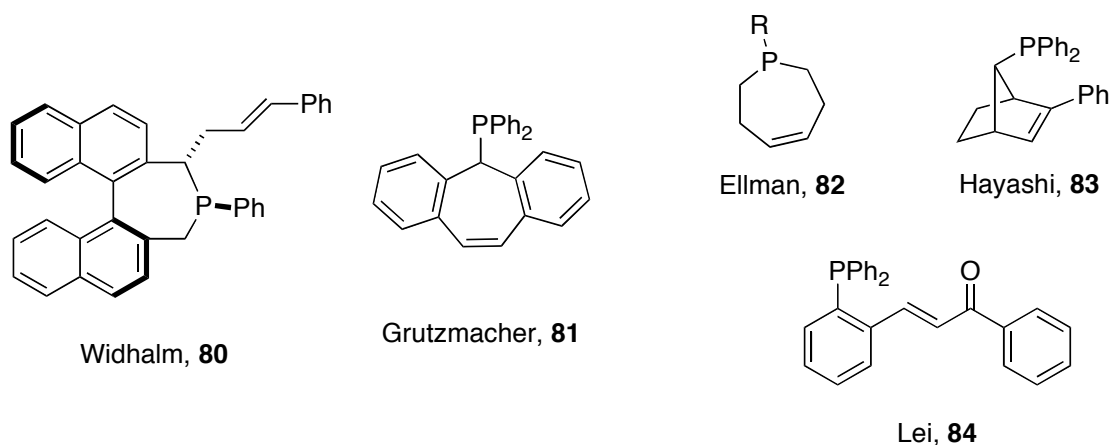
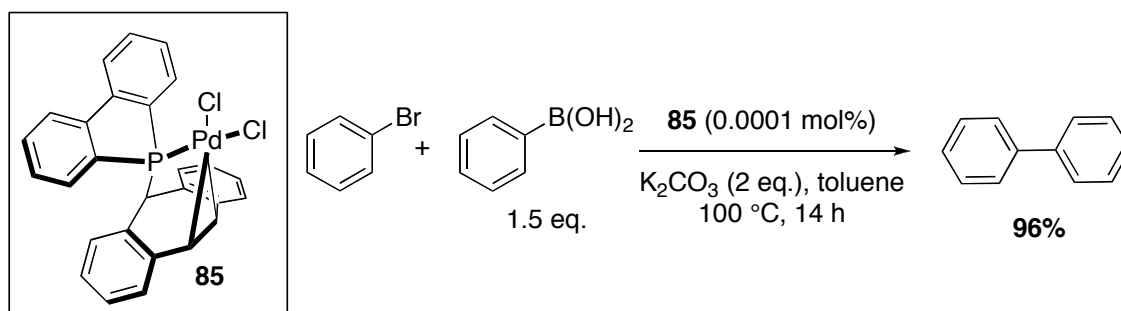


Figure 22: Further examples of phosphino-alkenyl ligands.

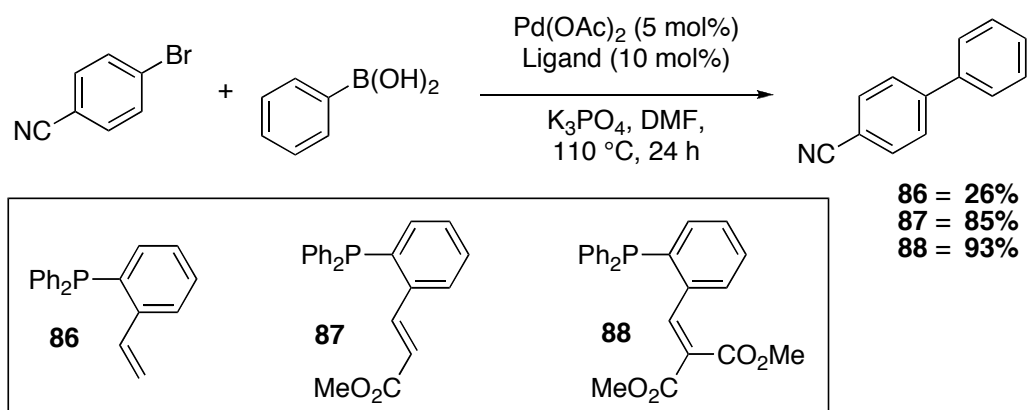
1.5.1 Phosphino-alkene ligands in palladium catalysis

Le Floch, Williams, and Lei have all independently investigated phosphino-alkene bidentate ligands in Pd-catalysed cross-couplings. Le Floch used a phosphole-based catalyst, **85**, to cross-couple bromoarenes with phenylboronic acid using very low catalyst loadings, 0.0001 mol% (Scheme 37).¹³² The catalyst was not active enough to be used for the less reactive chloroarenes.



Scheme 37: Suzuki coupling using a phosphole based Pd^{II} catalyst.

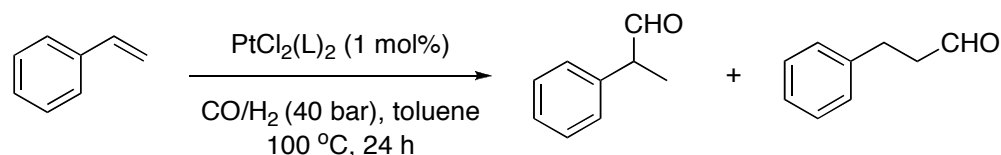
Williams and co-workers investigated a series of phosphino-alkene ligands in the Suzuki-Miyaura reaction (Scheme 38).¹³³ They found that the more electron-deficient and the more sterically hindered the alkene, the greater the yield and the stability of the catalyst. As complexes with just phosphine ligands are known to catalyse cross-couplings, control reactions with the saturated ligand were carried out to see if the alkene was necessary. A saturated version of ligand **87** gave poor yields, indicating that the alkene plays a role.



Scheme 38: A range of phosphine-alkene ligands studied in the Suzuki reaction.

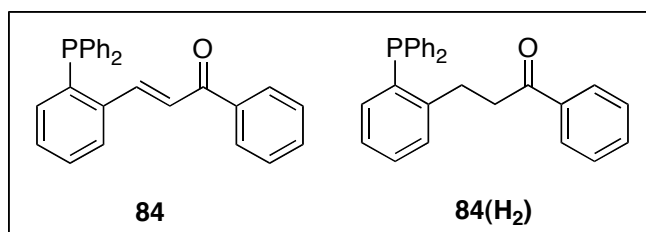
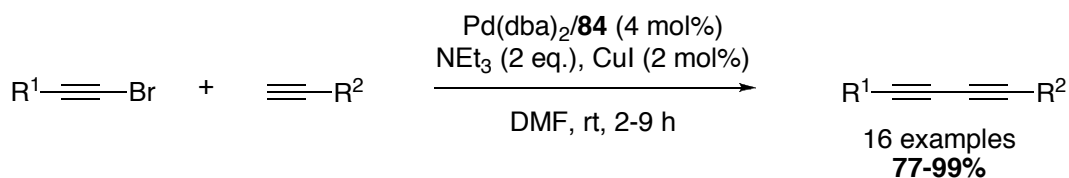
As seen in section 1.3.2.3, alkene ligands can accelerate reductive elimination and reduce β -H elimination. Although Williams and co-workers did not carry out detailed kinetic studies, they propose that in this case the rate-limiting step is one of the steps involving Pd^{II} species (*i.e.* transmetallation or reductive elimination), and not oxidative addition.

Williams and co-workers went on to investigate their ligands in the Pt-catalysed hydroformylation of styrene (Scheme 39).¹³⁴ They used the $[\text{PtCl}_2(\text{L})_2]$ complexes as the catalyst and found the best conversions were obtained with the ethyl and *i*-Pr ester versions of **88**. Although the ligands were active, the regioselectivity for the branched aldehyde was only between 50-55%.



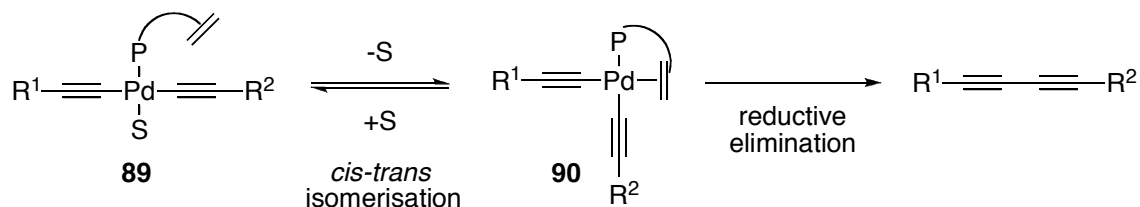
Scheme 39: Pt-catalysed hydroformylations with phosphino-alkene ligands.

For the platinum complexes there is no evidence for the alkene coordination apart from with ligand **87**. The elemental analysis is consistent with $[\text{PtCl}_2(\mathbf{87})_2]$, however, the alkene protons are at 2.3 and 4.6 ppm with decreased $^3J_{\text{HH}}$ values consistent with the alkene binding to Pt. The authors do not comment on this discrepancy. There is no indication if there is free phosphine in solution indicating that one ligand has been displaced by the alkene to give the square-planar complex.

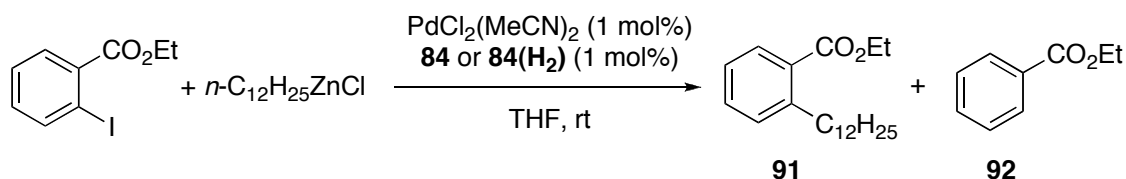


Scheme 40: Pd-catalysed C(sp)-C(sp) cross coupling employing a chalcone based phosphine-alkene ligand.

Lei and co-workers have carried out kinetic studies on a number of Pd-catalysed cross-coupling reactions using a chalcone based phosphino-alkene ligand, **84**. In a C(sp)-C(sp) cross-coupling (Scheme 40)¹³⁵ and a C(sp³)-C(sp²) Negishi cross-coupling, (Scheme 42),¹³⁶ it was observed that the phosphino-alkene ligand facilitated reductive elimination. In the former example the bidentate character of the ligand was held to be responsible for accelerating reductive elimination by promoting the isomerisation of **89** to **90** (see Scheme 41), which must occur before reductive elimination can take place.



Scheme 41: Cis-trans isomerisation before reductive elimination.

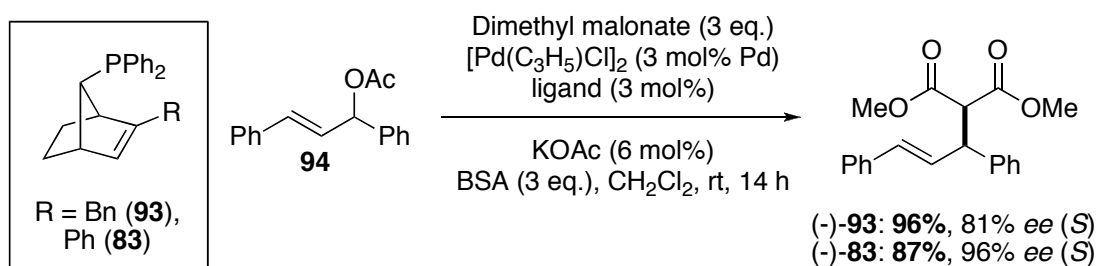


Scheme 42: Negishi cross-coupling employing a chalcone based phosphine-alkene ligand.

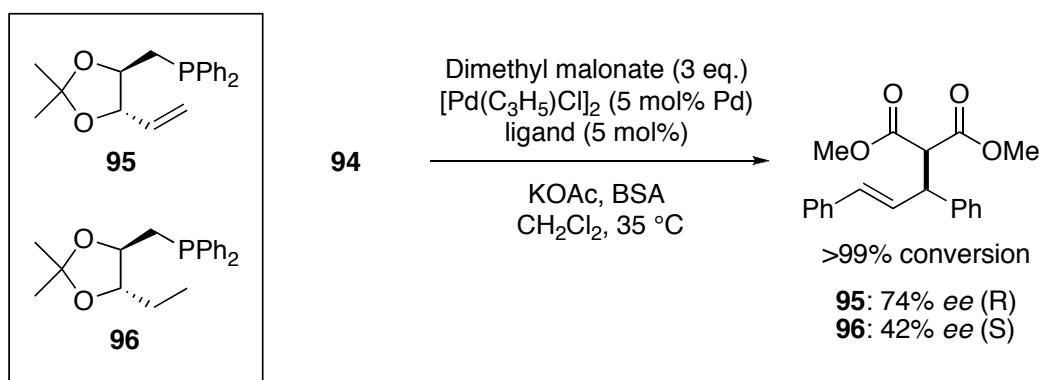
In the Negishi coupling, β -H elimination competes with reductive elimination; if the saturated version of ligand (**84(H₂)**) is used large amounts of ethyl benzoate (**92**) are observed along with product **91**, whereas ligand **84** has a very high selectivity for **91** (Scheme 42). This is credited to the reductive elimination being much faster than β -H

elimination in the presence of ligand **84**, as the hemilabile alkene blocks the coordination sites needed for β -H elimination. The authors used a variety of different kinetic regimes to analyse their data including a zero-order, first-order and a more complex regime. Regardless of which method was used, they observed the rate of reductive elimination to be much larger than those previously reported for other $C(sp^2)$ - $C(sp^3)$ systems.¹³⁷ It was also observed that the overall conversion decreased if **84(H₂)** was used, indicating that the alkene plays a crucial role in the reaction.

The above processes have all utilised achiral ligands. Another key objective of ligands in catalysis is to enable asymmetric transformations. It was observed that chiral dienes were able to coordinate strongly enough Rh or Ir to induce chirality. A number of groups that had been interested in chiral dienes went on to prepare chiral phosphine-alkene ligands, utilising the alkene as the source of chirality. Only one successful example of a chiral diene in Pd-catalysis has been observed, however, the phosphino-alkene ligands have met with more success. This is presumably due to the presence of the strongly coordinating phosphorus donor atom. Hayashi developed chiral phosphino-alkene ligands based on the norbornene framework (**83** and **93**) and demonstrated their use in a Pd-catalysed asymmetric allylic alkylation of **94** (Scheme 43).¹³⁸ The reaction proceeded in high yields and enantiomeric excess.

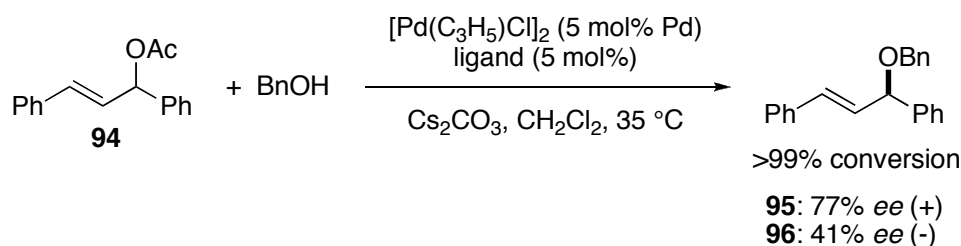


Scheme 43: Asymmetric allylic alkylation using a chiral P-alkene ligand based on norbornene.



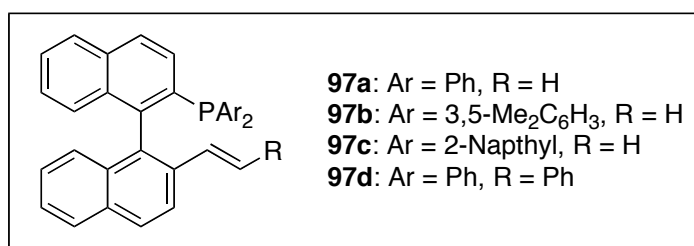
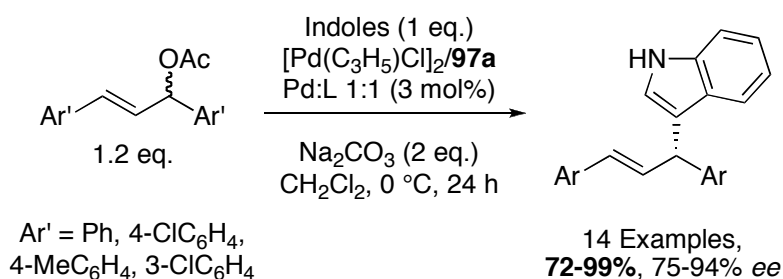
Scheme 44: Asymmetric allylic alkylation using phosphino-alkene ligands based on diethyl L-tartrate.

Du and co-workers previously synthesised acyclic chiral dienes for asymmetric catalysis. They found that the Rh complexes of their ligands were active in conjugate addition, however the enantioselectivities were often only moderate. They believe this was partially due to weak coordination between flexible dienes and the metal centre. To address this they developed a variety of chiral phosphino-alkene ligands based on diethyl L-tartrate, (see **95** in Scheme 44 as an example) which they hypothesised would bind more strongly to transition metal and thus provide a suitable chiral backbone. The ligands have been utilised in a number of palladium-catalysed reactions giving high yields and good enantioselectivity.¹³⁹ Interestingly, in both the asymmetric alkylation and etherification of **94** (Scheme 44 and Scheme 45 respectively), the use of the saturated ligand **96** led to products of the opposite configuration. This suggests that the active catalyst species is different between the two ligands, and that the terminal alkene plays an unidentified role in the asymmetric induction. The enantioselectivity of both reactions can be improved to >90% *ee* by reducing the temperature to -40 °C and changing the aryl groups on the phosphine to 3,5-Me₂C₆H₃. For the alkylation reactions the use of lithium acetate rather than potassium acetate improved the enantioselectivity and allowed lower catalyst loadings (0.5 mol%) to be used.



Scheme 45: Asymmetric etherification using P-alkene ligands based on diethyl L-tartrate.

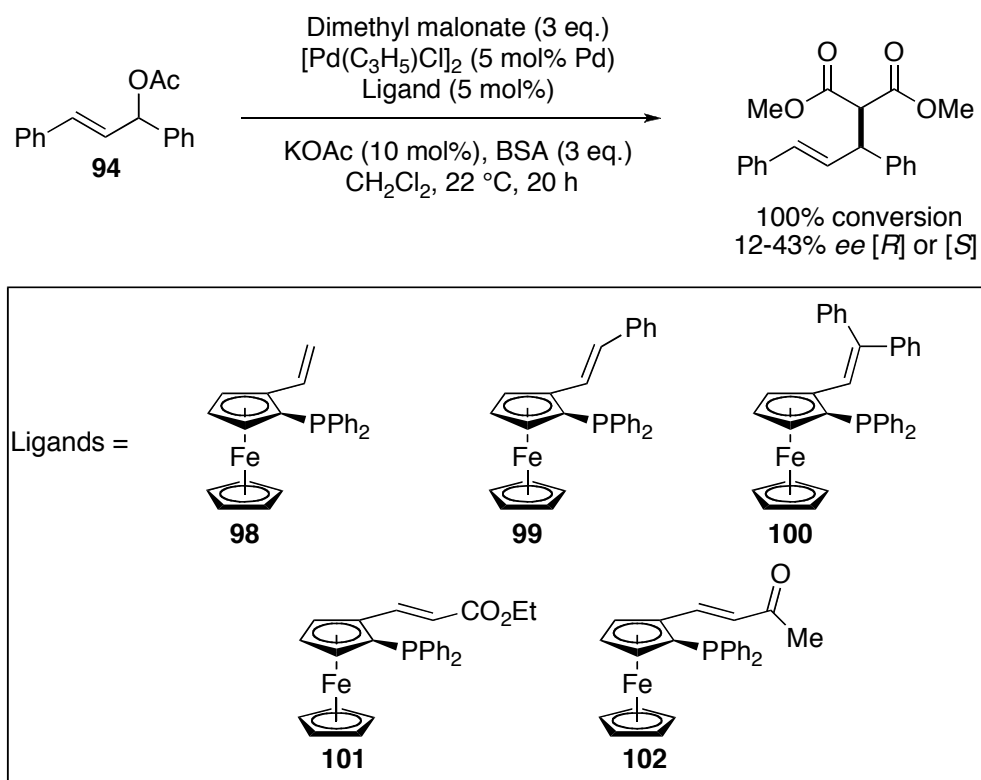
Ligand **95** was also shown to be an effective ligand for the asymmetric allylic substitution of **94** with morpholine.



Scheme 46: Pd-catalysed allylic alkylation of indoles using phosphino-alkene ligands based on binaphthyl.

Du has gone on to investigate another set of chiral phosphino-alkene ligands, utilising BINOL as the backbone.¹⁴⁰ Ligand **97a** was found to give the highest enantio- and regio-selectivities, in the allylic alkylation of indoles (Scheme 46). No product was observed when the saturated ligand or the related MOP ligand was utilised in the reaction, suggesting the vinyl group plays a crucial role not only in the enantioselectivity of the reaction but also the reactivity. Increasing the ratio of ligand to palladium had a detrimental effect on the reactivity (dropping from 95% conversion and 92% *ee* at Pd:L ratio 1:1 to 35% conversion and 64% *ee* at Pd:L ratio 1:2), presumably as the diphosphine complex is now formed and is unreactive. The authors also

demonstrated the allylic alkylation of pyrrole, although other N-heterocycles such as 1-methylpyrrole and benzimidazole were unreactive under these conditions.



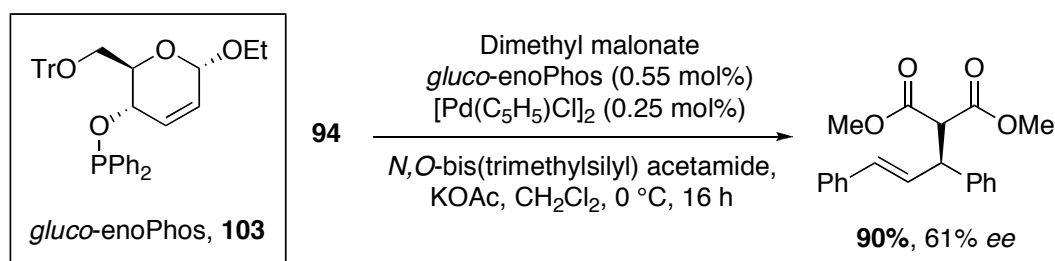
Scheme 47: Alkenylferrocene ligands.

Stepnicka and co-workers prepared a series of novel alkenylferrocene phosphines, **98-102** with planar chirality.¹⁴¹ The catalytic effectiveness of these ligands was probed in the Pd-catalysed asymmetric allylic alkylation of **94** (Scheme 47). In all cases the reaction went to completion, even in the saturated version of **98**, indicating that the double bond is not necessary for an active catalyst. However, the ligands appear to have an as yet unexplained effect on the enantioselectivity with some giving the (*S*)-enantiomer and some the (*R*)-enantiomer, in poor to moderate selectivity (see Table 7). The saturated ligand gave lower enantiomeric excess than the unsaturated version, which along with the unexplained selectivity suggests the double bond moiety does play an as yet undefined role.

Table 7: Enantioselectivities of allylic alkylation products using alkenylferrocene phosphine ligands.

Entry	Ligand	Conversion, %	ee, % (Config.)
1	(<i>S_P</i>)- 98	100	32 (<i>R</i>)
2	(<i>S_P</i>)- 99	100	22 (<i>S</i>)
3	(<i>S_P</i>)- 100	100	43 (<i>S</i>)
4	(<i>S_P</i>)- 102	100	26 (<i>S</i>)
5	(<i>S_P</i>)- 101	100	12 (<i>R</i>)
6	(<i>S_P</i>)- 98(H₂)	100	18 (<i>R</i>)

In the majority of phosphino-alkene ligands the phosphorus has been a simple phosphine. Other phosphorus environments commonly seen in ligands for metal catalysis include phosphites, phosphinites and phosphoramidates. A few examples of these environments in bidentate alkenyl ligands have surfaced. Boysen reported an alkene-phosphinite ligand based on D-glucose (**103**) and utilised it in Pd-catalysed asymmetric allylic alkylations (Scheme 48).¹⁴²

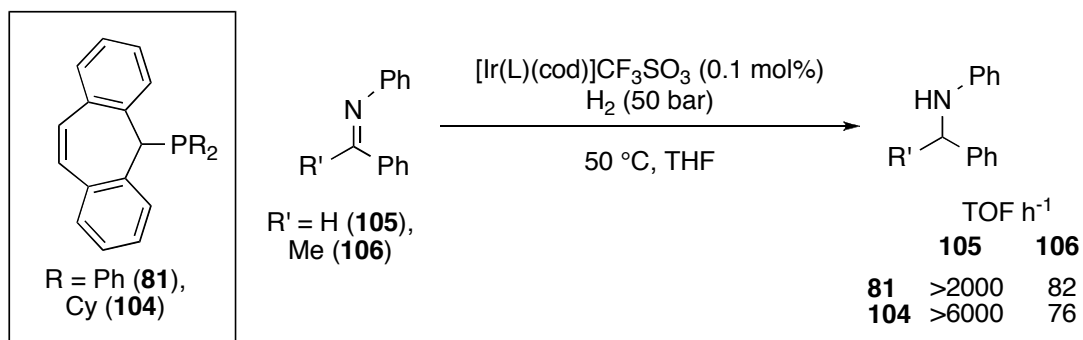


Scheme 48: Pd-catalysed asymmetric allylic alkylation using *gluco-enoPhos*.

1.5.2 Phosphino-alkene ligands in rhodium and iridium catalysis

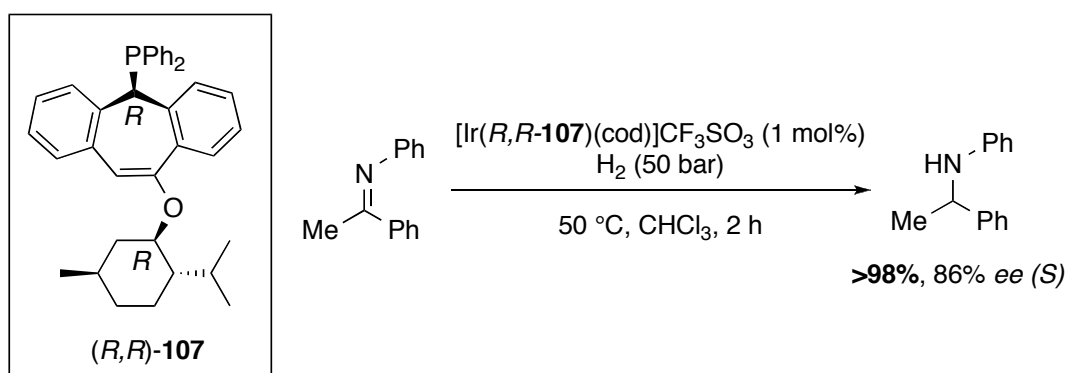
Chiral phosphino-alkene ligands have also been studied extensively in Rh and Ir-catalysed reactions, as a continuation of the success of chiral dienes in this area. Grützmacher and co-workers reported the first use of phosphino-alkene ligands in transition metal catalysis.¹⁴³ They were interested in the effect of alkenes in Ir-catalysed hydrogenations (Scheme 49). Initially they tested the Ir complexes of achiral ligands **81** and **104** in hydrogenation of benzylidene aniline, **105**, and the substituted amine **106**.

Excellent turnovers were observed for **105**, whereas lower activity was seen for **106** as expected.



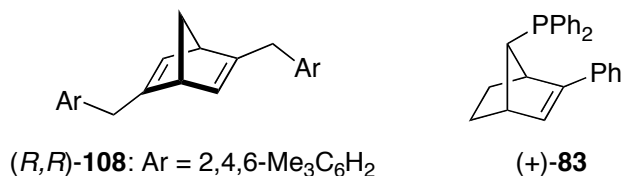
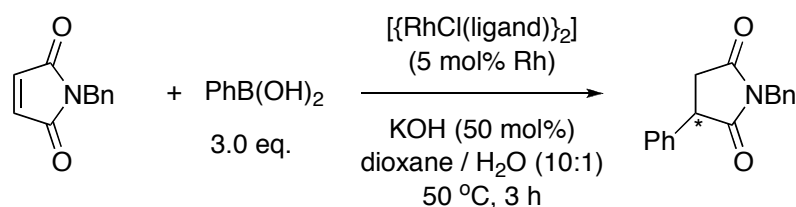
Scheme 49: Hydrogenation of imines using achiral phosphino-alkene Ir complexes.

The authors went on to prepare unsymmetrically substituted alkene variants of the ligands. The Ir complex of the (*R,R*)-**107** ligand gave high yields and good enantioselectivities in imine hydrogenation (Scheme 50). In comparison the Rh complex of (*S,R*)-**107** showed no catalytic activity.



Scheme 50: Asymmetric hydrogenation of imines using phosphino-alkene Ir complexes.

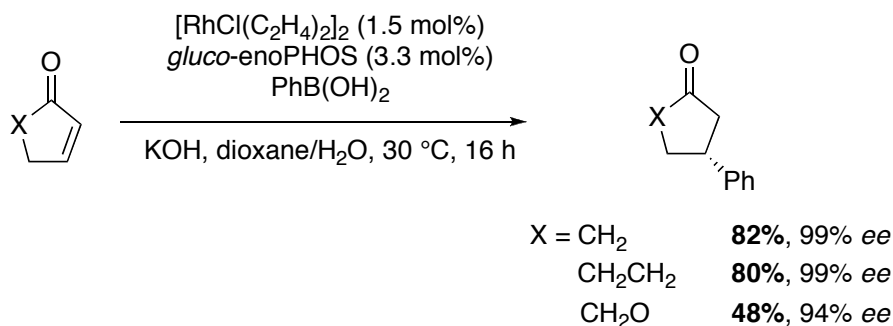
Almost concurrently, Hayashi and co-workers found that their phosphino-alkene ligand based on norbornadiene, **83**, exhibited higher activities and selectivities than diene ligand **108**, in a Rh-catalysed asymmetric 1,4-addition of arylboronic acids to maleimides (Scheme 51).¹⁴⁴ The chiral diene, which had outperformed phosphines, had been considered the benchmark ligand for a number of years. However, phosphine-alkenyl ligands increased the *ee* from 69 to 93%. The Rh complex of ligand **83**, was also found to be effective in the 1,4 addition to α,β -unsaturated carbonyl compounds.¹⁴⁵



Ligand	Yield, %	% ee
(<i>R</i>)-BINAP	70	58 (<i>R</i>)
(<i>R,R</i>)- 108	88	69 (<i>R</i>)
(+)- 83	98	93 (<i>S</i>)

Scheme 51: Asymmetric 1,4-addition of aryl boronic acids to malenides.

As a result, Rh-catalysed conjugate additions to enones have become benchmark reactions for new chiral phosphino-alkene ligands. Boysen and co-workers found that their ligand, *gluco*-enoPHOS (**103**) was active in Rh-catalysed addition of boronic acids to enones (Scheme 52), as well as Pd-alkylations.¹⁴² Good to moderate yields and excellent stereoselectivity was observed for cyclic enones and lactone.



Scheme 52: Rh-catalysed conjugate addition of boronic acids to enones using *gluco*-enoPHOS.

Widhalm and co-workers also tested their phosphine-alkene ligand (**80**) in the Rh-catalysed addition of phenylboronic acid to enones.¹²⁹ Good yields and excellent enantioselectivities were obtained for a variety of cyclic enones and lactones, and arylboronic acids.

Dorta and co-workers studied the use of chiral phosphoramidate-alkene ligands in Rh-catalysed conjugate additions.¹⁴⁶ They investigated a range of cationic and neutral Rh complexes. Overall they found that the cationic complex and the Rh-dimer complex of ligand **109**, gave the highest yields and enantioselectivities. They also looked at copper catalysed conjugate additions with these ligands.^{146b} However, in the copper complexes [CuI(L)₂] there was no evidence of alkene coordination (only the 1:2 Cu:Phosphine complex was observed by NMR or X-ray crystallography), and as a result there was either no stereinduction or only moderate induction. Again the cationic complex of ligand **109** gave the best enantioselectivities (39% *ee*) and excellent yields.

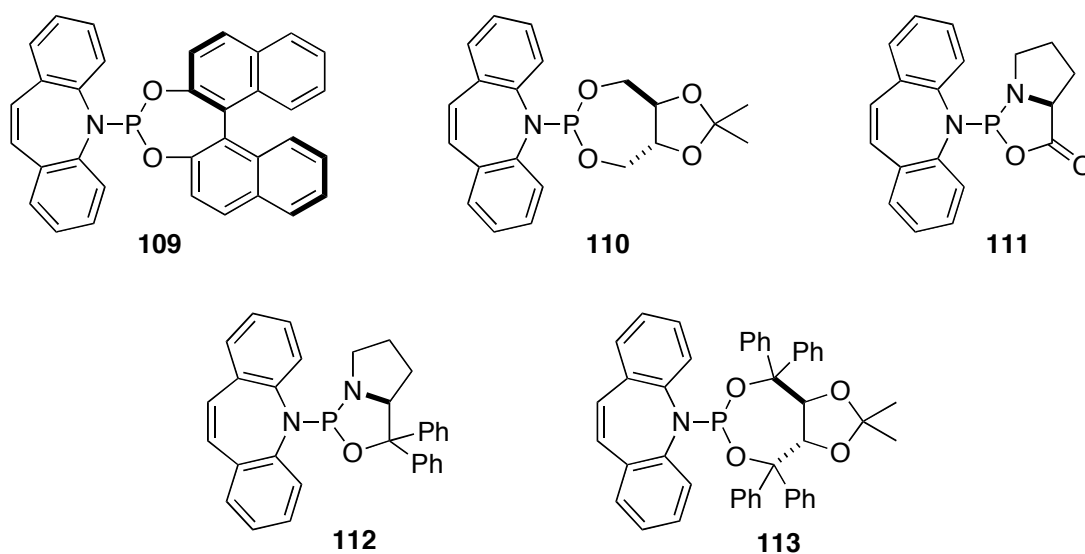
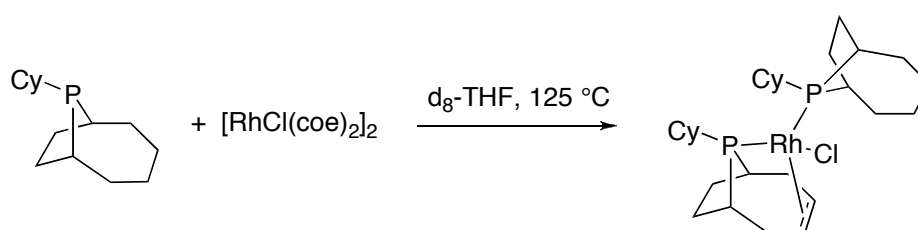


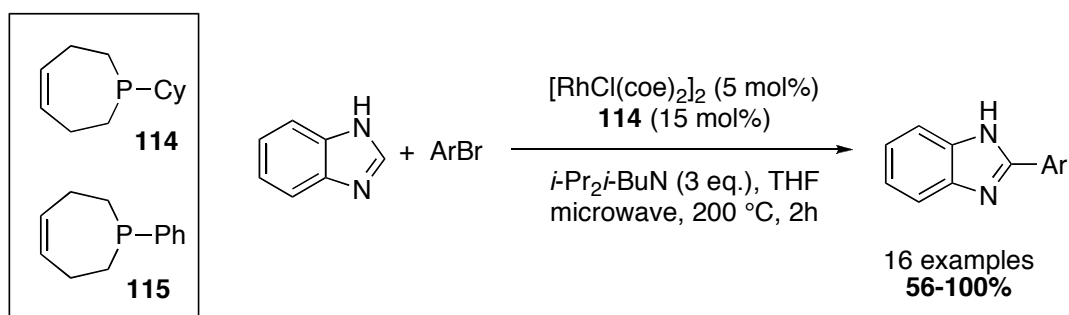
Figure 23: Phosphoramidite-alkene ligands.



Scheme 53: Dehydrogenation of cyclohexylphobane ligands in Rh complexes.

Ellman, Bergman and co-workers have used simple achiral phosphine alkene ligands in a very different Rh-catalysed reaction: the direct arylation of benzimidazoles.¹⁴⁷ They designed these ligands after the observation of the dehydrogenation of cyclohexylphobane ligands when reacted with [RhCl(coe)₂]₂ (Scheme 53). Ligand **114**

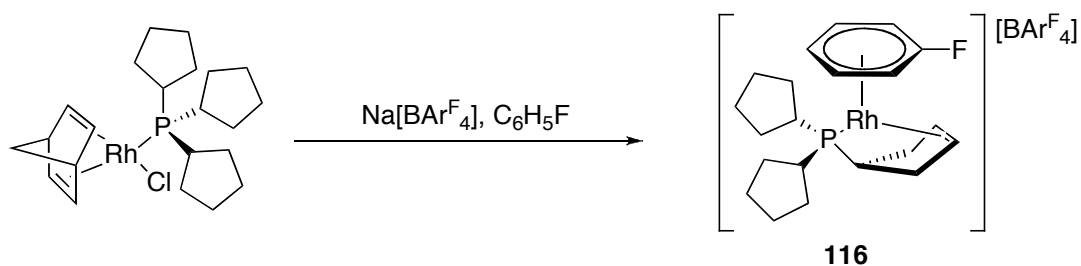
gave the best conversions, though ligand **115** had a faster initial rate, but moderate conversions were obtained due to catalyst inactivation.



Scheme 54: Direct arylation of benzimidazole with (Z)-2,3,6,7-tetrahydrophosphepine ligands.

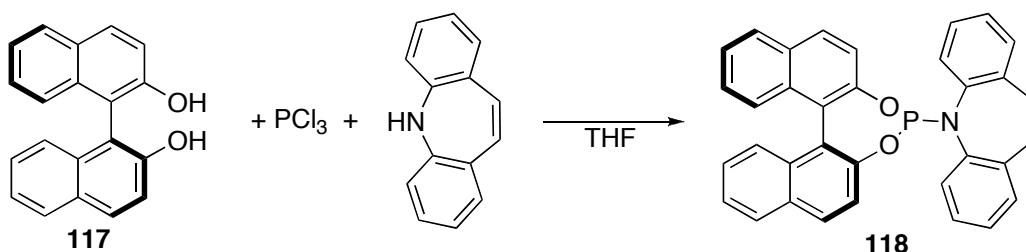
After optimising the reaction conditions with ligand **114** it was seen that the arylation of benzimidazole was compatible with a variety of aryl bromides in good to excellent yield (Scheme 54). A variety of functional groups were tolerated under the reaction conditions including free amine and hydroxyl groups. However, *ortho*-substitution was not tolerated. The conditions could also be applied to a number of different heterocycles including benzoxazole and benzothiazole in moderate yields. The reaction could be further optimised to avoid the need for using the glove box to prepare the reactions by utilising the HBF_4 salt of the phosphine and $[\text{RhCl}(\text{cod})]_2$. Once again a range of aryl bromides and heterocycles could be coupled with only modest decreases in product yield. Further optimisation of the solvent and catalyst loading improved the yields to similar levels as before. Despite the optimisation and the functional group tolerance it should be noted that the conditions are still quite harsh, requiring 2 h at 200 °C for the unprotected phosphine and 165 °C for the protected phosphine. As a result the methodology would be unsuitable for substrates containing more sensitive functional groups.

The success of any ligand, chiral or achiral, depends not only on its activity and selectivity but also on the ease of synthesis. Weller, Frost and co-workers developed a very simple route to phosphino-alkene ligands by the *in-situ* dehydrogenation of PCyp_3 (Cyp = cyclopentyl) when preparing cationic Rh complexes (Scheme 55).¹⁴⁸ Complex **116** was found to be an effective catalyst at low catalyst loadings (0.1 mol%) for the conjugate addition of PhZnCl to α,β -unsaturated carbonyl compounds.



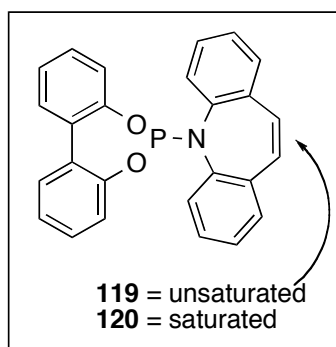
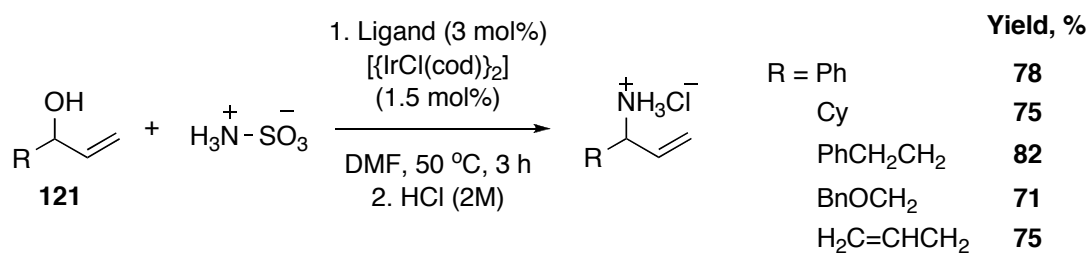
Scheme 55: *In-situ* preparation of phosphino-alkene ligands.

The synthesis of **118** is another simple example of P,alkene ligand synthesis; starting from the commercially available (*S*)-BINOL (**117**) the phosphoramidite ligand is obtained in just one step (Scheme 56).



Scheme 56: Synthesis of a phosphoramidite-alkenyl ligand by Carreira and co-workers.

Carreira and co-workers have successfully employed the chiral and achiral ligands **118** and **119**, respectively, in the iridium-catalysed synthesis of primary allylic amines from allylic alcohols (Scheme 57).¹²⁷ It is the first time that sulfamic acid ($\text{H}_2\text{NSO}_3\text{H}$) has been used in the direct transformation to amines from alcohols without the need for prior activation. When the saturated ligand **120** was used instead of **119**, only 20% conversion of alcohol **121** was achieved compared to >99% indicating that the alkene was key for the activity of the complex. Ligand **119** can also be used to enable stereospecific substitution of optically active allylic alcohols by sulfamic acid.¹⁴⁹ The addition of LiI and molecular sieves (4 Å) was found to be key to stereospecificity.



Scheme 57: Iridium-catalysed synthesis of primary allylic amines.

Ligand **118** was successfully utilised in the direct generation of a primary enantomerically enriched allylic amine from allylic alcohol, 1-cyclohexylprop-2-en-1-ol, using Ir catalysis. This is unusual as Ir is not normally a very good metal for kinetic resolution.

Overall, it can be seen that initial studies with phosphino-alkene ligands show they provide active catalysts in a variety of different transition metal-mediated transformations. In a number of cases, they have been shown to be more effective than either phosphines or alkene ligands alone, and have opened up new doors in the use of unactivated substrates. Other developments not mentioned above include the use of phosphino-alkene ligands as mechanistic probes in the Pauson Khand reaction.¹⁵⁰

1.5.3 Nitrogen-alkene ligands in catalysis

The focus of this project is on phosphino-alkene ligands, however alkenes have been combined with other donor atoms. Amino-alkene ligands have been developed (Figure 24) though not to the same extent as phosphino-alkene ligands.¹⁵¹ Grützmacher and co-workers have utilised ligands **124** and **125** in Rh-catalysed transfer hydrogenation reactions,^{151e,f} whereas Glorius and co-workers have tested their alkene-oxazoline ligands in the Rh-catalysed addition of boronic acids to cyclic enones.^{151c}

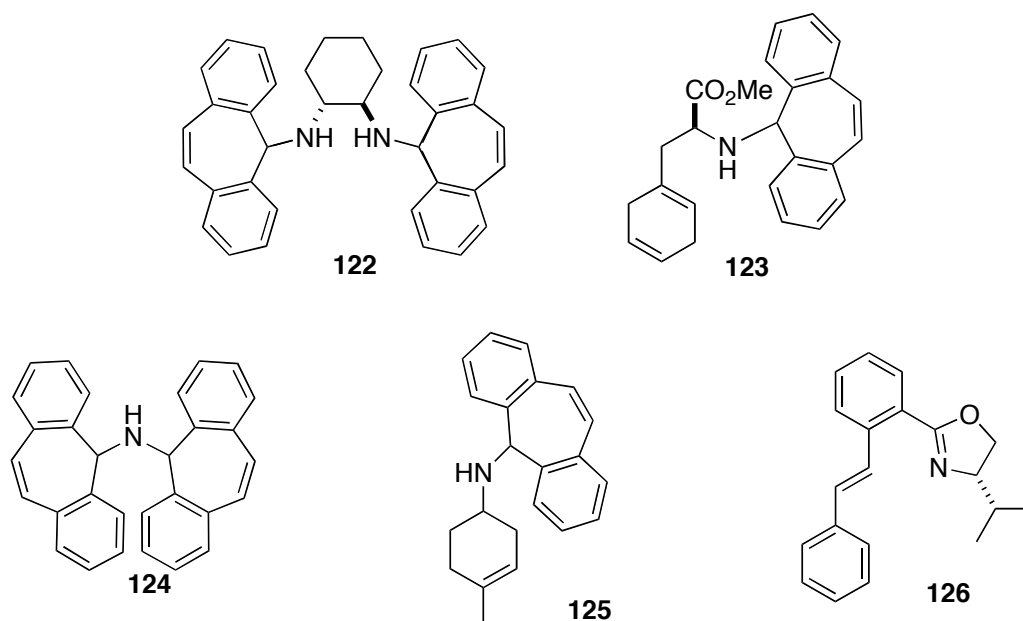


Figure 24: Amino-alkene ligands.

1.6 Conclusion

It has been shown that the addition of alkene ligands to transition metal catalysed reactions can benefit them in a number of ways: i) electron-rich alkenes can increase the rate of oxidative addition; ii) side reactions, such as isomerisation and β -H elimination, can be hindered by coordination of the alkene to the metal removing the vacant sites needed for these processes; iii) electron-deficient alkenes can increase the rate of reductive elimination. For Pd-catalysed reactions the focus of the studies has been on Suzuki-Miyaura, Mizoroki-Heck, Hiyama-type and Negishi cross-coupling reactions. Whilst studies continue to investigate the effect of alkenes on the fundamental steps in catalysis, research has broadened to designing alkene and alkene-containing ‘hemilabile’ ligands for catalysis. The initial results are promising and show that the field is ripe for exploitation. In particular, N-alkene, P-alkene and chiral alkene ligands have been underdeveloped for Pd catalysis compared to the explosion of interest in Rh and Ir catalysis with these types of ligands. Even fewer examples exist with other transition metals. For phosphino-alkene ligands the majority of studies have focused on the catalysis with little detailed investigation into the coordination chemistry and reactivity of the ligands themselves since the initial development of phosphino-alkene ligands in the 1960s. For the development of ligands for more challenging catalytic

reactions such as alkyl cross-coupling reactions and C-H functionalisation a greater understanding of possible coordination modes of phosphino-alkene ligands and their influence on important steps in catalytic cycles of late-transition metal mediated reactions will be needed.

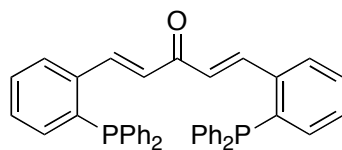
1.7 Project summary

The use of bidentate hemilabile ligands has been underexplored in transition metal catalysis, particularly in Pd-catalysed cross-coupling reactions. It has been shown that dba can be used as a tuneable ligand framework, and can influence all steps of a catalytic cycle. The addition of PR₂ in the *ortho*-position of dba would lead to a hemilabile bidentate class of phosphine ligands. This project provides an opportunity to investigate the coordination chemistry of multidentate phosphino-alkene ligands and their variants. The early studies on phosphino-alkene coordination were carried out in the 1960-70s. Often these studies relied on IR spectroscopy, and the occasional single X-ray crystal structure or ¹H NMR spectrum to determine the structure of the complexes. Since then, substantial developments in analytical chemistry have occurred. However, recent studies have chosen to focus on the catalytic properties of these ligands. Systematic studies of the structure of transition-metal complexes of these ligands are rare. We aim to use the wide variety of techniques now available to study the coordination chemistry and reactivity of dba-based phosphino-alkene ligands and their complexes. The insights gained will be utilised in the development of transition metal-catalysed reactions.

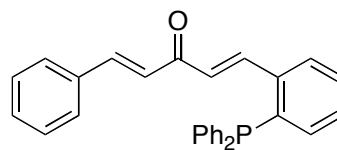
Phosphino-alkene ligands are not the only underutilised ligands; others include the phosphine sulfides. Phosphine sulfides have been found to act as successful ligands in a number of preliminary studies. One advantage of phosphine sulfides is unlike phosphines they are not susceptible to oxidation. Another aim of this project is to prepare the phosphine-sulfide variants of our ligands, to explore their coordination and catalytic chemistry further.

The overall aim for this project is to develop a diverse series of novel ligands based on the dba backbone and examining their coordination chemistry and catalytic properties. The specific objectives of this project are:

- To develop a rapid, efficient and simple methodology that allows access to the target phosphino-alkene ligands, dbaPHOS (**127**) and monodbaPHOS (**128**).



dbaPHOS, **127**



monodbaPHOS, **128**

- To apply solid-state and solution studies to elucidate the structures of the ligands and to probe their coordination chemistry with a variety of late transition metals.
- To synthesis variants of the target ligands. The phosphine sulfide variant will be prepared and its coordination chemistry investigated.
- To investigate the reactivity of the ligands.
- To screen any novel ligands in catalytic reactions.

1.8 References

-
- ¹ Seitz, J.; Maas, G. *Chem. Commun.* **2002**, 338-339.
- ² a) Green, M. L. H. *J. Organomet. Chem.* **1995**, *500*, 127-148. b) Hartwig, J. *Organotransition Metal Chemistry: From Bonding to Catalysis*; University Science Books: Sausalito, 2010, Chapters 1-2.
- ³ Pearson, R. G. *J. Am. Chem. Soc.* **1963**, *85*, 3533-3539.
- ⁴ Kauffman, G. B. In *Coordination Chemistry*; ACS Symposium Series 565; American Chemical Society: Washington, DC, 1994, p. 2-33.
- ⁵ Crabtree, R. H. *The Organometallic Chemistry of the Transition Metals*; John Wiley and Sons: Hoboken, 2005, p.1-28.
- ⁶ For a comprehensive review of nitrogen ligands in catalysis see: Fache, F.; Schulz, E.; Tommasino, M. L.; Lemaire, M. *Chem. Rev.* **2000**, *100*, 2159-2231. For oxazoline ligands see: McManus, H. A.; Guiry, P. J. *Chem. Rev.* **2004**, *104*, 4151-4202.
- ⁷ a) Baleizão, C.; Garcia, H. *Chem. Rev.* **2006**, *106*, 3987-4043. b) McGarrigle, E. M.; Gilheany, D. G. *Chem. Rev.* **2005**, *105*, 1563-1602.
- ⁸ a) Hofmann, A.W. *Ann. Chem. Pharm.* **1857**, *104*, 1-39. b) Malerbi, B. W. *Platinum Metal Rev.* **1965**, *9*, 47-50.
- ⁹ a) Jover, J.; Fey, N.; Harvey, J. N.; Lloyd-Jones, G. C.; Orpen, A. G.; Owen-Smith, G. J. J.; Murray, P.; Hose, D. R. J.; Osborne, R.; Purdie, M. *Organometallics* **2010**, *29*, 6245-6258. b) Fey, N.; Harvey, J. N.; Lloyd-Jones, G. C.; Murray, P.; Orpen, A. G.; Osborne, R.; Purdie, M. *Organometallics* **2008**, *27*, 1372-1383. c) Fey, N.; Tsipis, A. C.; Harris, S. E.; Harvey, J. N.; Orpen, A. G.; Mansson, R. A. *Chem. Eur. J.* **2005**, *12*, 291-302.
- ¹⁰ Tolman, C. A. *Chem. Rev.* **1977**, *77*, 313-348.
- ¹¹ a) Grim, S. O.; Wheatland, D. A.; McFarlane, W. *J. Am. Chem. Soc.* **1967**, *89*, 5573-5577. b) Vastag, S.; Heil, B.; Markó, L. *J. Mol. Cat.* **1979**, *5*, 189-195.
- ¹² Lever, A. B. P. *Inorg. Chem.* **1990**, *29*, 1271-1285.
- ¹³ Perrin, L.; Clot, E.; Eisenstein, O.; Loch, J.; Crabtree, R. H. *Inorg. Chem.* **2001**, *40*, 5806-5811.
- ¹⁴ Gusev, D. G. *Organometallics* **2009**, *28*, 763-770.

-
- ¹⁵ Crabtree, R. H. *The Organometallic Chemistry of the Transition Metals*, 2nd ed.; Wiley: New York, 1994, Chapter 4.
- ¹⁶ a) Mitoraj, M. P.; Michalak, A. *Inorg. Chem.* **2010**, *49*, 578-582. b) Woska, D.; Prock, A.; Giering, W. P. *Organometallics* **2000**, *19*, 4629-4638.
- ¹⁷ Brown, T. L.; Lee, K. J. *Coord. Chem. Rev.* **1993**, *128*, 89-116.
- ¹⁸ a) Clavier, H.; Nolan, S. P. *Chem. Commun.* **2010**, *46*, 841-861. b) Poater, A.; Cosenza, B.; Correa, A.; Giudice, S.; Ragone, F.; Scarano, V.; Cavallo, L. *Eur. J. Inorg. Chem.* **2009**, 1759-1766.
- ¹⁹ Schlummer, B.; Scholz, U. *Adv. Synth. Catal.* **2004**, *346*, 1599-1626.
- ²⁰ Bedford, R. B.; Cazin, C. S. J.; Holder, D. *Coord. Chem. Rev.* **2004**, *248*, 2283-2321.
- ²¹ Kranenburg, M.; van der Burgt, Y. E. M.; Kamer, P. C. J.; van Leeuwen, P. W. N. M. *Organometallics* **1995**, *14*, 3081-3089.
- ²² Kamer, P. C. J.; van Leeuwen, P. W. N. M.; Reek, J. N. H. *Acc. Chem. Res.* **2001**, *34*, 895-904.
- ²³ a) Yin, J.; Buchwald, S. L. *J. Am. Chem. Soc.* **2002**, *124*, 6043-6048. b) Bessel, C. A.; Aggarwal, P.; Marschilok, A. C.; Takeuchi, K. J. *Chem. Rev.* **2001**, *101*, 1031-1066. c) Freixa, Z.; van Leeuwen, P. W. N. M. *Coord. Chem. Rev.* **2008**, *252*, 1755-1786.
- ²⁴ Dierkes, P.; van Leeuwen, P. W. N. M. *J. Chem. Soc., Dalton Trans.* **1999**, 1519-1529.
- ²⁵ van Leeuwen, P. W. N. M.; Kamer, P. C. J.; Reek, J. N. H. *Pure Appl. Chem.* **1999**, *71*, 1443-1452.
- ²⁶ a) Mora, G.; Piechaczyk, O.; Houdard, R.; Mézailles, N.; Le Goff, X-F.; le Floch, P. *Chem. Eur. J.* **2008**, *14*, 10047-10057. b) Asano, Y.; Ito, H.; Hara, K.; Sawamura, M. *Organometallics* **2008**, *27*, 6495-6506. c) Kawabata, Y.; Hayashi, T.; Ogata, I. *J. Chem. Soc., Chem. Comm.* **1979**, 462-463. d) Kamer, P. C. J.; van Leeuwen, P. W. N. M.; Reek, J. N. H. *Acc. Chem. Res.* **2001**, *34*, 895-904. e) Birkholz, M-N.; Freixa, Z.; van Leeuwen, P. W. N. M. *Chem. Soc. Rev.* **2009**, *38*, 1099-1118. For discussions on the steric vs electronic nature of the bite angle see van Zeist, W-J.; Bickelhaupt, F. M. *Dalton Trans.* **2011**, *40*, 3028-3038; and Freixa, Z.; van Leeuwen, P. W. N. M. *Dalton Trans.* **2003**, 1890-1901.

-
- ²⁷ a) Fernández-Pérez, H.; Etayo, P.; Panossian, A.; Vidal-Ferran, A. *Chem. Rev.* **2011**, *111*, 2119-2176. b) van Leeuwen, P. W. N. M.; Kamer, P. C. J.; Claver, C.; Pàmies, O.; Diéguez, M. *Chem. Rev.* **2011**, *111*, 2077-2118.
- ²⁸ a) Mellah, M.; Voituriez, A.; Schulz, E. *Chem. Rev.* **2007**, *107*, 5133-5209. b) Bayón, J. C.; Claver, C.; Masdeu-Bultó, A. M. *Coord. Chem. Rev.* **1999**, *193-195*, 73-145. c) Masdeu-Bultó, A. M.; Diéguez, M.; Martin, E.; Gómez, M. *Coord. Chem. Rev.* **2003**, *242*, 159-201.
- ²⁹ Murray, S. G.; Hartley, F. R. *Chem. Rev.* **1981**, *81*, 365-414.
- ³⁰ a) Lam, F-L.; Kwong, F-Y.; Chan, A. S. C. *Chem. Commun.* **2010**, *46*, 4649-4667. b) Faller, J. W.; Wilt, J. C. *Org. Lett.* **2005**, *7*, 633-636. c) Bregbreiter, D. E.; Osburn, P. L.; Liu, Y-S. *J. Am. Chem. Soc.* **1999**, *121*, 9531-9538. d) Pettinari, C.; Pellei, M.; Cavicchio, G.; Crucianelli, M.; Panzeri, W.; Colpietro, M.; Cassetta, A. *Organometallics* **1999**, *18*, 555-563.
- ³¹ Slone, C. S.; Weinberger, D. A.; Mirkin, C. A. *Prog. Inorg. Chem.* **1999**, *48*, 233-350.
- ³² Genge, A. R. J.; Gibson, A. M.; Guymer, N. K.; Reid, G. *J. Chem. Soc., Dalton Trans.* **1996**, 4099-4107.
- ³³ a) Browning, J.; Bushnell, G. W.; Dixon, K. R.; Hilts, R. W. *J. Organomet. Chem.* **1992**, *434*, 241-252. b) Matrosov, E. I.; Starikova, Z. A.; Yanovsky, A. I.; Lobanov, D. I.; Alazhava, I. M.; Bykhovskaya, O. V.; Struchkov, Y. T.; Mastryukova, T. A.; Kabachnik, M. I. *J. Organomet. Chem.* **1997**, *535*, 121-127. c) Claver, C.; Ruiz, A.; Masdeu, A. M.; Viñas, J.; Saballs, T. *J. Organomet. Chem.* **1989**, *373*, 269-278. d) Talanova, G. G.; Yatsimeirskii, K. B.; Kuraeva, I. N.; Nazarenko, A. Y.; Aladzheva, I. M.; Bikhovskaya, O. V.; Leont'eva, I. V.; Kalyanova, R. M. *J. Coord. Chem.* **2000**, *51*, 21-32.
- ³⁴ Hayashi, M.; Takezaki, H.; Hashimoto, Y.; Takaoki, K.; Saigo, K. *Tetrahedron Lett.* **1998**, *39*, 7529-7532.
- ³⁵ Baker, M. J.; Giles, M. F.; Orpen, A. G.; Taylor, M. J.; Watt, R. J. *J. Chem. Soc., Chem. Commun.* **1995**, 197-198.
- ³⁶ a) Piechazyk, O.; Doux, M.; Ricard, L.; le Floch, P. *Organometallics* **2005**, *24*, 1204-1213. b) Dochnahl, M.; Doux, M.; Faillard, E.; Ricard, L.; le Floch, P. *Eur.*

-
- J. Inorg. Chem.* **2005**, 125-134. c) Aizawa, S-I.; Hase, T.; Wada, T. *J. Organomet. Chem.* **2007**, 692, 813-818.
- 37 Faller, J. W.; Milheiro, S. C.; Parr, J. *J. Organomet. Chem.* **2008**, 693, 1478-1493.
- 38 Jordan, R. F.; Bajgur, C. S.; Willett, R.; Scott, B. *J. Am. Chem. Soc.* **1986**, 108, 7410-7411.
- 39 Bader, A.; Lindner, E. *Coord. Chem. Rev.* **1991**, 108, 27-110.
- 40 Hayashi, T. *Acc. Chem. Res.* **2000**, 33, 354-362.
- 41 Boezio, A.A.; Pytkowicz, J.; Côté, A.; Charette, A. B. *J. Am. Chem. Soc.* **2003**, 125, 14260-14261.
- 42 Crabtree, R. H. *Chem. Rev.* **1985**, 85, 245-269.
- 43 Green, J. C. *Chem. Soc. Rev.* **1998**, 27, 263-272.
- 44 a) Cardin, D. J.; Cetinkaya, B.; Lappert, M. F. *Chem. Rev.* **1972**, 72, 545-574. Reviews on NHCs: b) Díez-González, S.; Marion, N.; Nolan, S. P. *Chem. Rev.* **2009**, 109, 3612-3676.
- 45 Schrock, R. R. *Chem. Rev.* **2009**, 109, 3211-3226.
- 46 A comprehensive text on vinylidenes: *Metal Vinylidenes and Allenylidenes in Catalysis: From Reactivity to Applications in Synthesis*, Bruneau, C.; Dixneuf, P. Eds.; Wiley-VCH: Weinheim, 2008.
- 47 Fairlamb, I. J. S. *Org. Biomol. Chem.* **2008**, 6, 3645-3656.
- 48 Reviews on carbenes in olefin metathesis: a) Vougioukalakis, G. C.; Grubbs, R. H. *Chem. Rev.* **2010**, 110, 1746-1787. b) Trnka, T. M.; Grubbs, R. H. *Acc. Chem. Res.* **2001**, 34, 18-29. c) Schrock, R. R. *Chem. Rev.* **2002**, 102, 145-180. d) Monsaert, S.; Vila, A. L.; Drozdak, R.; van der Voort, P.; Verpoort, F. *Chem. Soc. Rev.* **2009**, 38, 3360-3372.
- 49 Hunt, L. B. *Platinum Metals Rev.* **1984**, 28, 76-83.
- 50 a) Dewar, M. J. S. *Bull. Chem. Soc. Fr.* **1951**, 18, C71-C79. b) Chatt, J.; Duncanson, L. A. *J. Chem. Soc.* **1953**, 2939-2947.
- 51 a) Kurosawa, H.; Ikeda, I. *J. Organomet. Chem.* **1992**, 428, 289-301. b) Rubio, M.; Suárez, A.; del Río, D.; Galindo, A.; Álvarez, E.; Pizzano, A. *Organometallics* **2009**, 28, 57-560.
- 52 Canovese, L.; Visentin, F.; Santo, C.; Dolmella, A. *J. Organomet. Chem.* **2009**, 694, 411-419.

-
- ⁵³ a) Bombieri, G.; Forsellini, E.; Panattoni, C.; Graziani, R.; Bandoli, G. *J. Chem. Soc. A: Inorg. Phys. Theor.* **1970**, 1313-1318. b) Crayston, J. A.; Davidson, G. *Spectrochimica Acta, Part A.* **1986**, *42A*, 1385-1391.
- ⁵⁴ Ozawa, F.; Ito, T.; Nakamura, Y.; Tamamoto, A. *J. Organomet. Chem.* **1979**, *168*, 375-391.
- ⁵⁵ Nakamoto, K. *Infrared and Raman Spectra of Inorganic and Coordination Compounds, Part B: Applications in Coordination, Organometallic, and Bioinorganic Chemistry*; Wiley-Blackwell: Chichester, 2009.
- ⁵⁶ a) Dedieu, A.; *Chem. Rev.* **2000**, *100*, 543-600. b) Uddin, J.; Dapprich, S.; Frenking, G.; Yates, B. F. *Organometallics* **1999**, *18*, 457-465. c) Frenking, G.; Fröhlich, N. *Chem. Rev.* **2000**, *100*, 717-774.
- ⁵⁷ Zhao, H.; Ariaifard, A.; Lin, Z. *Inorg. Chim. Acta* **2006**, *359*, 3527-3534.
- ⁵⁸ a) Joy, J. R.; Orchin, M. *J. Am. Chem. Soc.* **1959**, *81*, 310-311. b) Tolman, C. A. *J. Am. Chem. Soc.* **1974**, *96*, 2780-2789.
- ⁵⁹ For recent reviews on phosphorus donor ligands see a) Gillespie, J. A.; Dodds, D. L.; Kamer, P. C. J. *Dalton Trans.* **2010**, *39*, 2751-2764. b) Fleckenstein, C. A.; Plenio, H. *Chem. Soc. Rev.* **2010**, *39*, 694-711.
- ⁶⁰ For a recent review on NHCs see, Kantchev, E. A. B.; O'Brien, C. J.; Organ, M. G. *Angew. Chem., Int. Ed.* **2007**, *46*, 2768-2813.
- ⁶¹ a) Glorius, F. *Angew. Chem., Int. Ed.* **2004**, *43*, 3364-3366. b) Johnson, J. B.; Rovis, T. *Angew. Chem., Int. Ed.* **2008**, *47*, 840-871. c) Defieber, C.; Grutzmacher, H.; Carreira, E. M. *Angew. Chem., Int. Ed.* **2008**, *47*, 4482-4502.
- ⁶² a) Amatore, C.; Jutand, A.; Meyer, G.; Atmani, H.; Khalil, F.; Ouazzani Chahdi, F. *Organometallics* **1998**, *17*, 2958-2964. b) Amatore, C.; Broeker, G.; Jutand, A.; Khalil, F. *J. Am. Chem. Soc.* **1997**, *119*, 5176-5185. c) Amatore, C.; Jutand, A.; Khalil, F.; M'Barki, M. A.; Mottier, L. *Organometallics* **1993**, *12*, 3168-3178.
- ⁶³ Amatore, C.; Jutand, A. *Coord. Chem. Rev.* **1998**, *178-180*, 511-528.
- ⁶⁴ a) Yamamoto, T.; Yamamoto, A.; Ikeda, S. *J. Am. Chem. Soc.* **1971**, *93*, 3350-3359. b) Kurosawa, H.; Emoto, M.; Urabe, A.; Miki, K.; Kasai, N. *J. Am. Chem. Soc.* **1985**, *107*, 8253-8254.
- ⁶⁵ a) Amatore, C.; Jutand, A.; Meyer, G.; Atmani, H.; Khalil, F.; Ouazzani Chahdi, F. *Organometallics* **1998**, *17*, 2958-2964. b) Amatore, C.; Jutand, A.; Khalil, F.; M'Barki, M. A.; Mottier, L. *Organometallics* **1993**, *12*, 3168-3178.

-
- ⁶⁶ Jutand, A. *Pure Appl. Chem.* **2004**, *76*, 565-576.
- ⁶⁷ In some cases the formation of Pd-nanoparticles is beneficial to catalysis a) de Vries, J. G. *Dalton Trans.* **2006**, 421-429 and references therein. b) Reetz, M. T.; Westermann, E. *Angew. Chem., Int. Ed.* **2000**, *39*, 165-168. c) Ellis, P. J.; Fairlamb, I. J. S.; Hackett, S. F. J.; Wilson, K.; Lee, A. F. *Angew. Chem., Int. Ed.* **2010**, *49*, 1820-1824.
- ⁶⁸ Hartwig, J. F. "Catalytic Organometallic Carbon-Heteroatom Bond Formation"; Oral presentation at BOSS XI, Ghent, 12th July 2008, and Hartwig, J. F. *RSC Joseph Chatt lecture "Catalytic Organometallic Carbon-Heteroatom Bond Formation"* York, 6th May 2009.
- ⁶⁹ a) Fairlamb, I. J. S.; Kapdi, A. R.; Lee, A. F.; McGlacken, G. P.; Weissburger, F.; de Vries, A. H. M.; Schmieder-van de Vondervoort, L. *Chem. Eur. J.* **2006**, *12*, 8750-8761. b) Fairlamb, I. J. S.; Kapdi, A. R.; Lee, A. F. *Org. Lett.* **2004**, *6*, 4435-4438.
- ⁷⁰ Macé, Y.; Kapdi, A. R.; Fairlamb, I. J. S.; Jutand, A. *Organometallics* **2006**, *25*, 1795-1800.
- ⁷¹ Fairlamb, I. J. S.; Lee, A. F. *Organometallics* **2007**, *26*, 4087-4089.
- ⁷² Aouf, C.; Thiery, E.; Le Bras, J.; Muzart, J. *Org. Lett.* **2009**, *11*, 4096-4099.
- ⁷³ Zenkina, O. V.; Karton, A.; Shimon, L. J. W.; Martin, J. M. L.; van der Boom, M. E. *Chem. Eur. J.* **2009**, *15*, 10025-10028.
- ⁷⁴ Strawser, D.; Karton, A.; Zenkina, O. V.; Iron, M. A.; Shimon, L. J. W.; Martin, J. M. L.; van der Boom, M. E. *J. Am. Chem. Soc.* **2005**, *127*, 9322-9323.
- ⁷⁵ Lucassen, A. C. B.; Shimon, L. J. W.; van der Boom, M. E. *Organometallics* **2006**, *25*, 3308-3310.
- ⁷⁶ de Pater, J. J. M.; Tromp, D. S.; Tooke, D. M.; Spek, A. L.; Deelman, B.-J.; van Koten, G.; Elsevier, C. J. *Organometallics*, **2005**, *24*, 6411-6419.
- ⁷⁷ Antonaroli, S.; Crociani, B. *J. Organomet. Chem.* **1998**, *560*, 137-146.
- ⁷⁸ a) Scrivanti, A.; Beghetto, V.; Matteoli, U.; Antonaroli, S.; Marini, A.; Mandoj, F.; Paolesse, R.; Crociani, B. *Tetrahedron Lett.* **2004**, *45*, 5861-5864. b) Scrivanti, A.; Matteoli, U.; Beghetto, V.; Antonaroli, S.; Crociani, B. *Tetrahedron* **2002**, *58*, 6881-6886. c) Crociani, B.; Antonaroli, S.; Beghetto, V.; Matteoli, U.; Scrivanti, A. *Dalton Trans.* **2003**, 2194-2202. d) Crociani, B.; Antonaroli, S.; Canovese, L.; Uguagliati, P.; Visentin, F. *Eur. J. Inorg. Chem.* **2004**, 732-742.

- 79 van Laren, M. W.; Duin, M. A.; Klerk, C.; Naglia, M.; Rogolino, D.; Pelagatti, P.;
Bacchi, A.; Pelizzi, C.; Elsevier, C. J. *Organometallics* **2002**, *21*, 1546-1553.
- 80 Firmansjah, L.; Fu, G. *J. Am. Chem. Soc.* **2007**, *129*, 11340-11341.
- 81 Meadows, R. E.; Woodward, S. *Tetrahedron* **2008**, *64*, 1218-1224.
- 82 Wagaw, S.; Rennels, R. A.; Buchwald, S. L. *J. Am. Chem. Soc.* **1997**, *119*, 8451-
8458.
- 83 Denmark, S. E.; Werner, N. S. *J. Am. Chem. Soc.* **2008**, *130*, 16382-16393.
- 84 Denmark, S. E.; Werner, N. S. *J. Am. Chem. Soc.* **2010**, *132*, 3612-3620.
- 85 Grützmacher and coworkers recently published a comprehensive review of chiral
dienes and their use in transition metal catalysis, reference 61c. The majority of
examples focused on Ir and Rh catalysed processes.
- 86 Tsukada, N.; Yamamoto, Y. *Angew. Chem., Int. Ed. Engl.* **1997**, *36*, 2477-2480.
- 87 Zhao, Y.; Wang, H.; Hou, X.; Hu, Y.; Lei, A.; Zhang, H.; Zhu, L. *J. Am. Chem.*
Soc. **2006**, *128*, 15048-15049.
- 88 Liu, Q.; Duan, H.; Luo, X.; Tang, Y.; Li, G.; Huang, R.; Lei, A. *Adv. Synth. Catal.*
2008, *350*, 1349-1354.
- 89 Blum, K.; Chernyshova, E. S.; Goddard, R.; Jonas, K.; Pörschke, K-R.
Organometallics, **2007**, *26*, 5174-5178.
- 90 a) Moreno-Mañas, M.; Plexiats, R.; Sebastián, R. M.; Vallribera, A.; Roglans, A.
J. Organomet. Chem. **2004**, *689*, 3669-3684 and references therein. b) Dachs, A.;
Masllorens, J.; Pla-Quintana, A.; Roglans, A.; Farjas, J.; Parella, T.
Organometallics **2008**, *27*, 5768-5776.
- 91 Cortès, J.; Moreno-Mañas, M.; Plexiats, R. *Eur. J. Org. Chem.* **2000**, 239-243.
- 92 Serra-Muns, A.; Soler, R.; Badetti, E.; de Mendoza, P.; Moreno-Mañas, M.;
Plexiats, R.; Sebastián, R. M.; Vallribera, A. *New J. Chem.* **2006**, *30*, 1584-1594.
- 93 Ellis, P. J.; Fairlamb, I. J. S.; Hackett, S. F. J.; Wilson, K.; Lee, A. F. *Angew.*
Chem., Int. Ed. **2010**, *49*, 1820-1824.
- 94 a) Moreno-Mañas, M.; Plexiats, R.; Villarroja, S. *Chem. Commun.* **2002**, 60-61.
b) Moreno-Mañas, M.; Plexiats, R.; Villarroja, S. *Organometallics* **2001**, *20*,
4524-4528. c) Tristany, M.; Courmarcel, J.; Dieudonné, P.; Moreno-Mañas, M.;
Plexiats, R.; Rimola, A.; Sodupe, M.; Villarroja, S. *Chem. Mater.* **2006**, *18*, 716-
722.

- ⁹⁵ Eddy, J. W.; Davey, E. A.; Malsom, R. D.; Ehle, A. R.; Kassel, S.; Goodson, F. E. *Macromolecules* **2009**, *42*, 8611-8614.
- ⁹⁶ Bäuerlein, P. S.; Fairlamb, I. J. S.; Jarvis, A. G.; Lee, A. F.; Müller, C.; Slattery, J. S.; Thatcher, R. J.; Vogt, D.; Whitwood, A. C. *Chem. Commun.* **2009**, 5734-5736.
- ⁹⁷ Shukla, K. H.; DeShong, P. *J. Org. Chem.* **2008**, *73*, 6283-6291.
- ⁹⁸ a) Grundl, M. A.; Kennedy-Smith, J. J.; Trauner, D. *Organometallics* **2005**, *24*, 2831-2833. b) Porth, S.; Bats, J. W.; Trauner, D.; Giester, G.; Mulzer, J. *Angew. Chem., Int. Ed.* **1999**, *38*, 2015-2016.
- ⁹⁹ Zhang, S-S.; Wang, Z-Q.; Xu, M-H.; Lin, G-Q. *Org. Lett.* **2010**, *12*, 5546-5549.
- ¹⁰⁰ Hayashi, T.; Ueyama, K.; Tokunaga, N.; Yoshida, K. *J. Am. Chem. Soc.* **2003**, *125*, 11508-11509.
- ¹⁰¹ Fischer, C.; Defieber, C.; Suzuki, T.; Carreira, E. M. *J. Am. Chem. Soc.* **2004**, *126*, 1628-1629.
- ¹⁰² a) Defieber, C.; Paquin, J-F.; Serna, S.; Carreira, E. M. *Org. Lett.* **2004**, *6*, 3873-3876. b) Paquin, J-F.; Defieber, C.; Stephenson, C. R.; Carreira, E. M. *J. Am. Chem. Soc.* **2005**, *127*, 10850-10851.
- ¹⁰³ Shintani, R.; Duan, W. L.; Nagano, T.; Okada, A.; Hayashi, T. *Angew. Chem., Int. Ed.* **2005**, *44*, 4611-4614.
- ¹⁰⁴ Shintani, R.; Okamoto, K.; Otomaru, Y.; Ueyama, K.; Hayashi, T. *J. Am. Chem. Soc.* **2005**, *127*, 54-55.
- ¹⁰⁵ a) Tokunaga, N.; Otomura, Y.; Okamoto, K.; Ueyama, K.; Shintani, R.; Hayashi, T. *J. Am. Chem. Soc.* **2004**, *126*, 13584-13585. b) Okamoto, K.; Hayashi, T.; Rawal, V. H. *Chem. Commun.* **2009**, *32*, 4815-4817. c) Shao, C.; Yu, H-J.; Wu, N-Y.; Feng, C-G.; Lin, G-Q. *Org. Lett.* **2010**, *12*, 3820-3823.
- ¹⁰⁶ a) Okamoto, K.; Hayashi, T.; Rawal, V. H. *Chem. Commun.* **2009**, 4815-4817. b) Okamoto, K.; Hayashi, T.; Rawal, V. H. *Org. Lett.* **2008**, *10*, 4387-4389. c) Nishimura, T.; Kumamoto, H.; Nagaosa, M.; Hayashi, T. *Chem. Commun.* **2009**, 5713-5715.
- ¹⁰⁷ Gendrineau, T.; Genet, J-P.; Darses, S. *Org. Lett.* **2010**, *12*, 308-310.
- ¹⁰⁸ Shintani, R.; Ichikawa, Y.; Takatsu, K.; Chen, F-X.; Hayashi, T. *J. Org. Chem.* **2009**, *74*, 869-873.

- ¹⁰⁹ a) Brown, M. K.; Corey, E. J. *Org. Lett.* **2010**, *12*, 172-175. b) Boyd, W. C.; Crimmin, M. R.; Rosebrugh, L. E.; Schomaker, J. M.; Bergman, R. G.; Toste, F. D. *J. Am. Chem. Soc.* **2010**, *132*, 16365-16367.
- ¹¹⁰ Läng, F.; Breher, F.; Stein, D.; Grützmacher, H. *Organometallics* **2005**, *24*, 2997-3007.
- ¹¹¹ Shao, C.; Yu, H-J.; Wu, N-Y.; Feng, C-G.; Lin, G-Q. *Org. Lett.* **2010**, *12*, 3820-3823.
- ¹¹² Fournier, P.; Fiammengo, R.; Jaschke, A. *Angew. Chem., Int. Ed.* **2009**, *48*, 4426-4429.
- ¹¹³ Hu, X.; Zhuang, M.; Cao, Z.; Du, H. *Org. Lett.* **2009**, *11*, 4744-4747.
- ¹¹⁴ Wang, Y.; Hu, X.; Du, H. *Org. Lett.* **2010**, *12*, 5482-5485.
- ¹¹⁵ Li, Q.; Dong, Z.; Yu, Z-X. *Org. Lett.* **2011**, *13*, 1122-1125.
- ¹¹⁶ Bennett, M. A.; Kouwenhoven, H. W.; Lewis, J.; Nyholm, R. S. *J. Chem. Soc.* **1964**, 4570-4577.
- ¹¹⁷ a) Haselzeldine, R. N.; Lund, R. J.; Parish, R. V. *J. Chem. Soc. A.* **1971**, 3705-3711. b) Clark, P. W.; Hartwell, G. E. *J. Organomet. Chem.* **1975**, *97*, 117-123.
- ¹¹⁸ Wang, I-H.; Werner, P. H.; Dobson, C. B.; Dobson, G. R. *Inorg. Chim. Acta* **1991**, *183*, 31-38.
- ¹¹⁹ a) Bennet, M. A.; Kneen, W. R.; Nyholm, R. S. *Inorg. Chem.* **1968**, *7*, 556-560. b) Bennet, M. A.; Kneen, W. R.; Nyholm, R. S. *Inorg. Chem.* **1968**, *7*, 552-556. c) Garrow, P. E.; Hartwell, G. E. *J. Organomet. Chem.* **1974**, *71*, 443-452. d) Hall, D. I.; Nyholm, R. S. *J. Chem. Soc. A.* **1970**, 1491-1493.
- ¹²⁰ a) Ryan, R. R.; Schaeffer, R.; Clark, P.; Hartwell, G. *Inorg. Chrm.* **1975**, *14*, 3039-3042. b) Interrante, L. V.; Bennett, M. A.; Nyholm, R. S. *Inorg. Chem.* **1966**, *5*, 2212-2217.
- ¹²¹ a) Aresta, M.; Nyholm, R. S. *Chem. Comm.* **1971**, 1459-1460. b) Hall, D. I.; Nyholm, R. S. *Chem. Comm.* **1970**, 488-489.
- ¹²² Shapiro, N. D.; Toste, F. D. *Proc. Natl. Acad. Sci. USA* **2008**, *105*, 2779-2782.
- ¹²³ a) Hall, D. I.; Nyholm, R. S. *J. Chem. Soc., Dalton Trans.* **1972**, 804-808. b) Clark, P. W.; Hartwell, G. E. *Inorg. Chem.* **1970**, *9*, 1948-1951. c) Herberhold, M.; Eibl, S.; Milius, W. *J. Organomet. Chem.* **2001**, *621*, 166-172. d) Herberhold, M.; Schmatz, T.; Milius, W.; Wracksneger, B. *Inorg. Chim. Acta* **2003**, *352*, 51-88.

- ¹²⁴ a) Irvine, D. J.; Glidewell, C.; Cole-Hamilton, D. J.; Barnes, J. C.; Howie, A. *J. Chem. Soc., Dalton Trans.* **1991**, 1765-1771. b) Borowski, A. F.; Iraqi, A.; Cupertino, D. C.; Irvine, D. J.; Cole-Hamilton, D. J. *J. Chem. Soc., Dalton Trans.* **1990**, 29-34. c) Irvine, D. J.; Borowski, A. F.; Cole-Hamilton, D. J. *J. Chem. Soc., Dalton Trans.* **1990**, 3549-3550.
- ¹²⁵ Slawin, A. M. Z.; Milton, H. L.; Wheatley, J.; Woolins, J. D. *Polyhedron* **2004**, *23*, 3125-3132.
- ¹²⁶ a) Maire, P.; Deblon, S.; Breher, F.; Geier, J.; Bohler, C.; Ruegger, H.; Schonberg, H.; Grutzmacher, H. *Chem. Eur. J.* **2004**, *10*, 4198-4205. b) Fischbach, U.; Ruegger, H.; Grutzmacher, H. *Eur. J. Inorg. Chem.* **2007**, 2654-2667.
- ¹²⁷ Defieber, C.; Ariger, M. A.; Moriel, P.; Carreira, E. M. *Angew. Chem., Int. Ed.* **2007**, *46*, 3139-3143.
- ¹²⁸ Tokunaga, N.; Otomaru, Y.; Okamoto, K.; Ueyama, K.; Shintani, R.; Hayashi, T. *J. Am. Chem. Soc.* **2004**, *126*, 13584-13585.
- ¹²⁹ Kasak, P.; Arion, V. B.; Widhalm, M. *Tetrahedron: Asymmetry* **2006**, *17*, 3084-3090.
- ¹³⁰ Lewis, J. C.; Berman, A. M.; Bergman, R. G.; Ellman, J. A. *J. Am. Chem. Soc.* **2008**, *130*, 2493-2500.
- ¹³¹ Luo, X.; Zhang, H.; Duan, H.; Liu, Q.; Zhu, L.; Zhang, T.; Lei, A. *Org. Lett.* **2007**, *6*, 4571-4574.
- ¹³² Thomazet, C.; Ricard, L.; Grützmacher, H.; Le Floch, P. *Chem. Commun.* **2005**, 1592-1594.
- ¹³³ Williams, D. B. G.; Shaw, M. L. *Tetrahedron* **2007**, *63*, 1624-1629.
- ¹³⁴ Pongrácz, P.; Petöcz, G.; Shaw, M.; Williams, D. B. G.; Kollár, L. *J. Organomet. Chem.* **2010**, *695*, 2381-2384.
- ¹³⁵ Shi, W.; Luo, Y.; Luo, X.; Chao, L.; Zhang, H.; Wang, J.; Lei, A. *J. Am. Chem. Soc.* **2008**, *130*, 14713-14720.
- ¹³⁶ a) Luo, X.; Zhang, H.; Duan, H.; Liu, Q.; Zhang, T.; Lei, A. *Org. Lett.* **2007**, *9*, 4571-4574. b) Zhang, H.; Luo, X.; Wongkhan, K.; Duan, H.; Li, Q.; Zhu, L.; Wang, J.; Batsanov, A. S.; Howard, J. A. K.; Marder, T. B.; Lei, A. *Chem. Eur. J.* **2009**, *15*, 3823-3829.
- ¹³⁷ a) Casares, J. A.; Espinet, P.; Fuentes, B.; Salas, G. *J. Am. Chem. Soc.* **2007**, *129*, 3508-3509. b) Culkin, D. A.; Hartwig, J. F. *Organometallics* **2004**, *23*, 3398-3416.

- ¹³⁸ Shintani, R.; Duan, W.-L.; Okamoto, K.; Hayashi, T. *Tetrahedron: Asymmetry* **2005**, *16*, 3400-3405.
- ¹³⁹ Liu, Z.; Du, H. *Org. Lett.* **2010**, *13*, 3054-3057.
- ¹⁴⁰ Cao, Z.; Liu, Y.; Liu, Z.; Feng, X.; Zhuang, M.; Du, H. *Org. Lett.* **2011**, *13*, 2164-2167.
- ¹⁴¹ Stepnicka, P.; Lamac, M.; Cisarova, I. *J. Organomet. Chem.* **2008**, *693*, 446-456.
- ¹⁴² Minuth, T.; Boysen, M. K. *Org. Lett.* **2009**, *11*, 4212-4215.
- ¹⁴³ Maire, P.; Deblon, S.; Breher, F.; Geier, J.; Böhler, C.; Rüeggör, H.; Schönberg, H.; Grützmacher, H. *Chem. Eur. J.* **2004**, *10*, 4198-4205.
- ¹⁴⁴ Shintani, R.; Duan, W. L.; Nagano, T.; Okada, A.; Hayashi, T. *Angew. Chem., Int. Ed.* **2005**, *44*, 4611-4614.
- ¹⁴⁵ Duan, W.-L.; Iwamura, A.; Shintani, R.; Hayashi, T. *J. Am. Chem. Soc.* **2007**, *129*, 2130-2138.
- ¹⁴⁶ a) Mariz, R.; Briceño, A.; Dorta, R.; Dorta, R. *Organometallics* **2008**, *27*, 6605-6613. b) Drinkel, E.; Briceño, A.; Dorta, R.; Dorta, R. *Organometallics* **2010**, *29*, 2503-2514.
- ¹⁴⁷ Lewis, J. C.; Berman, A. M.; Bergman, R. G.; Ellman, J. A. *J. Am. Chem. Soc.* **2008**, *130*, 2493-2500.
- ¹⁴⁸ Douglas, T. M.; Le Nôtre, J.; Brayshaw, S. K.; Frost, C. G.; Weller, A. S. *Chem. Commun.* **2006**, 3408-3410. For further investigation of the dehydrogenation of Rh(PCyp₃) complexes see: Douglas, T. M.; Brayshaw, S. K.; Dallanegra, R.; Kociok-Köhn, G.; Macgregor, S. A.; Moxham, G. L.; Weller, A. S.; Wondimagegn, T.; Vadivelu, P. *Chem. Eur. J.* **2008**, *14*, 1004-1022. The dehydrogenation of one of the cyclopentane units in PCyp₃ has also been seen in Ru complexes: Bolton, P. D.; Grellier, M.; Vautravers, N.; Vendier, L.; Sabo-Etienne, S. *Organometallics* **2008**, *27*, 5088-5093.
- ¹⁴⁹ Roggen, M.; Carriera, E. M. *J. Am. Chem. Soc.* **2010**, *132*, 11917-11919.
- ¹⁵⁰ Ferrer, C.; Benet-Buchholz, J.; Riera, A.; Verdaguer, X. *Chem. Eur. J.* **2010**, *16*, 8340-8346.
- ¹⁵¹ a) Maire, P.; Breher, F.; Schönberg, H.; Grützmacher, H. *Organometallics*, **2005**, *24*, 3207-3218. b) Grützmacher, H.; Buttner, T.; Maire, P.; Ramseier, M.; Scheschkewitz, D.; Zweifel, T. DE 102004027771, **2006**; EP 05011539.3. c) Hahn, B.; Tewes, F.; Fröhlich, R.; Glorius, F. *Angew. Chem., Int. Ed.* **2010**, *49*,

1143-1146. d) Fischbach, U.; Rüeggör, H.; Grützmacher, H. *Eur. J. Inorg. Chem.* **2007**, 2654-2667. e) Zweifel, T.; Naubron, J-V.; Büttner, T.; Ott, T.; Grützmacher, H. *Angew. Chem., Int. Ed.* **2008**, 47, 3245-3249. f) Zweifel, T.; Scheschkewitz, D.; Ott, T.; Vogt, M.; Grützmacher, H. *Eur. J. Inorg. Chem.* **2009**, 5561-5576.

Chapter 2: Synthesis of multidentate phosphino-alkene ligands

2.1 Design of ligands

The dba ligand has been shown to be a tuneable alkene framework (see Section 1.3.2).¹ The global aim of this project is to combine this framework with phosphine substituents, to provide access to tuneable phosphino-alkene ligands. A family of mono and bidentate phosphine ligands was envisioned, with alkene sites available for coordination in the ligand backbone (Figure 1). By changing the substituents on the aryl rings the electronic properties of the alkenes could be tuned in a manner similar to how Fairlamb and co-workers tuned dba-Z ligands.¹ The substituents on phosphorus could also be tuned depending on the electronic and steric properties desired.

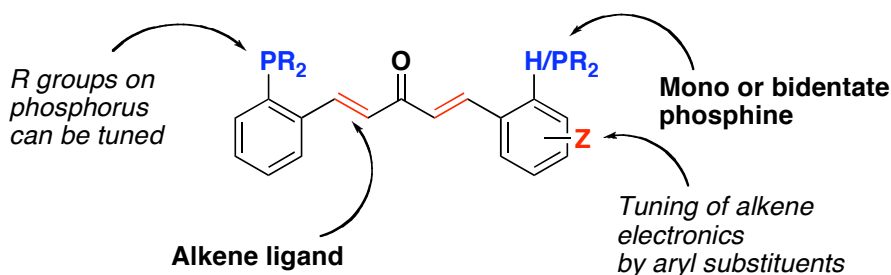


Figure 1: Design rationale of new multidentate phosphino-alkene ligands. Key:-Bold comments: mandatory requirements; italic comments: desirable properties.

The initial targets of the project were **127**, and **128**, shown in Figure 2.

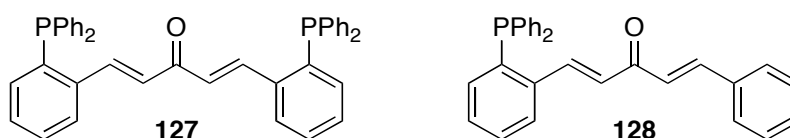


Figure 2: Initial ligand targets.

2.2 Synthesis of ligands

The two most obvious disconnections for the formation of the target ligands are the C=C bonds and C-P bonds (Figure 3).

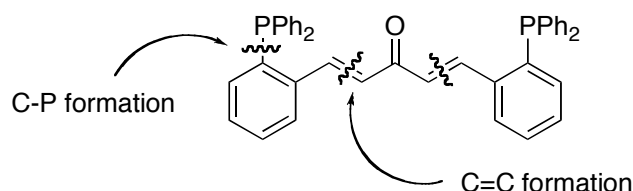
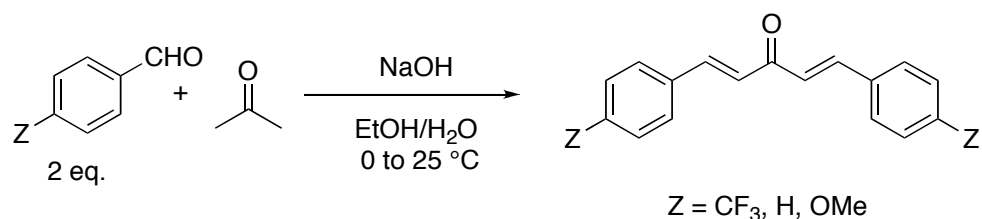


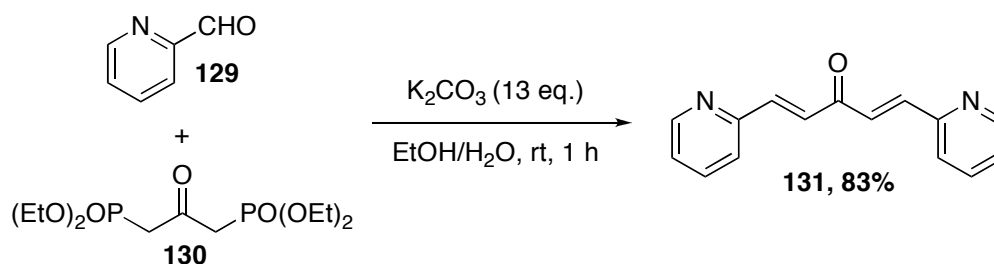
Figure 3: Ligand disconnections.

There are a wide variety of C=C bond formation methods known. The simplest reactions are the condensation reactions, such as the Claisen-Schmidt reaction, between the relevant aldehyde and acetone mediated by an appropriate base. This method works well for a number of symmetrically aryl-substituted dba ligands (Scheme 1).^{1,2} An adaptation of this synthetic route using benzylidene acetone facilitates the preparation of the unsymmetrical dba ligand systems.³



Scheme 1: Claisen-Schmidt condensation reaction.

In cases where the Claisen-Schmidt type reactions do not work, are very slow or susceptible to side-reactions, *e.g.* when using picolinaldehyde, **129** (see Scheme 2),^{3a} alternative C=C bond forming reactions can be used such as the Wittig,⁴ Horner-Wadsworth-Emmons^{4c,5} and Heck arylation reactions.⁶



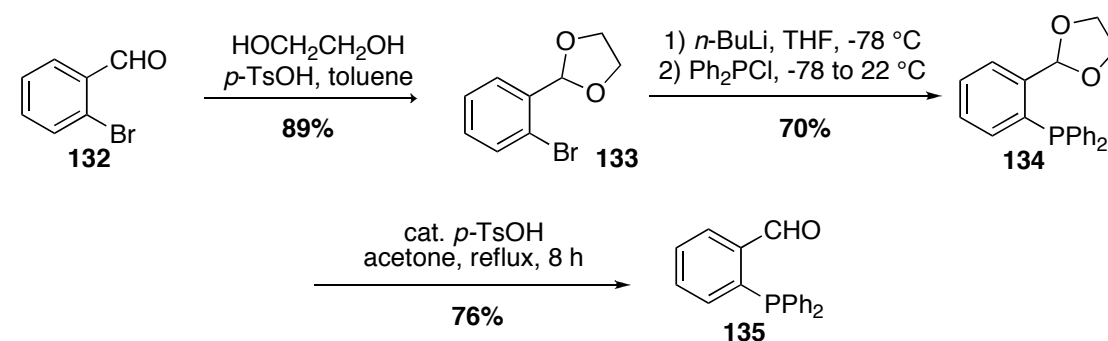
Scheme 2: Horner-Wadsworth-Emmons reaction for the synthesis of dba-based ligands.

There are many classical synthetic routes to tertiary phosphines: a) reaction of halophosphines with aryl Grignard reagents or organolithium reagents;⁷ b) addition of P-H compounds to unsaturated compounds;⁸ c) by reduction of either phosphine oxides

or phosphine sulfides;⁸ d) the cross-coupling of aryl halides (or pseudo halides) with diarylphosphines (H₂PAR₂), or phosphides (*e.g.* KPAR₂).⁹

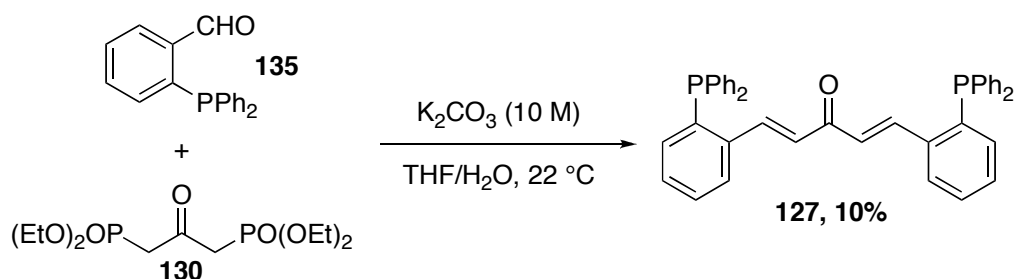
2.2.1 Bisphosphine ligands

The commercial availability of 2-(diphenylphosphino)benzaldehyde, **135** (£45.80/g, Aldrich, 2011) influenced the decision to explore C=C bond formation methodology, as it would allow efficient access to the ligands making them accessible to both the academic and industrial community. The aldehyde **135** can also be synthesised in-house on a large scale (15 grams) relatively simply from the 2-bromobenzaldehyde, via protection of the bromoaldehyde as the hemiacetal, **133**, followed by halogen-lithium exchange, trapping with chlorodiphenylphosphine and deprotection to reveal the aldehyde (Scheme 3).¹⁰



Scheme 3: Preparation of 2-(diphenylphosphino)benzaldehyde, **135**.

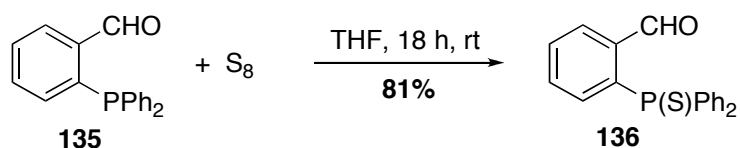
The initial attempt to synthesise **127** (referred to as dbaPHOS) *via* the Horner-Wadsworth-Emmons reaction followed similar conditions to those used in the synthesis of (1*E*,4*E*)-1,5-di(2-pyridinyl)penta-1,4-dien-3-one **131** (Scheme 2 and Scheme 4). The phosphonate ester, **130**, was prepared according to literature procedures.¹¹ Unfortunately, the ligand was obtained in low yields (*circa* 10%). Thin layer chromatography (TLC) revealed that no starting benzaldehyde remained. No other products were obtained by column chromatography suggesting that the remainder of the mass balance were polar side products, possibly the phosphine oxide derivative.



Scheme 4: Horner-Wadsworth-Emmons reaction in the synthesis of substituted dba ligands.

During attempts to optimise the reaction it was realised that the phosphine ligand was surprisingly air sensitive. As a result it was difficult to tell if any changes made to the reaction conditions were having a positive effect, as it is possible a considerable quantity of the ligand was oxidised during the purification. The phosphine oxides are more polar and so remained on the column, making quantification difficult. Attempts to prepare **127** and trap the phosphine as the borane adduct using $\text{BH}_3 \cdot \text{SMe}$ were also unsuccessful. Multiple phosphorus-containing products were observed by ^{31}P NMR spectroscopy. In addition, the ^1H NMR spectrum showed disappearance of the alkene bonds, and the appearance of peaks between 3 and 1 ppm. The IR spectrum has a number of weak bands between 2400 and 1900 cm^{-1} , indicating the presence of both terminal and bridging B-H bonds. The bands at 1654, 1614 and 1596 cm^{-1} attributed to the carbonyl and alkene stretches disappeared. Mass spectrometry (APCI) on the crude compound supports the observation of the removal of the carbonyl, and a peak at m/z 615.2 is attributed to $\text{C}_{41}\text{H}_{39}\text{P}_2\text{B}_2$. In contrast to the ^{31}P spectrum, the ^{13}C NMR spectrum was very simple showing 3 broad peaks in the aromatic region, 133, 131 and 130 ppm, and no evidence of a carbonyl peak.

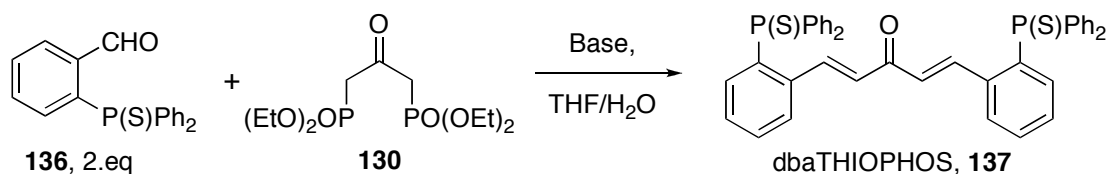
An alternative synthetic approach was pursued by protecting the dbaPHOS as a carbon disulfide adduct.¹² Interestingly, the product obtained was dbaPHOS, **127** as shown by the ^1H NMR spectrum, not the carbon disulfide adduct as expected. Crucially, almost no phosphine oxide was observed in the ^{31}P NMR spectrum. Inauspiciously, this reaction was found to be irreproducible. This coupled with the modest yields (10-45%) obtained suggested that an alternative synthetic route was necessary.



Scheme 5: Preparation of 2-(diphenylthiophosphino)benzaldehyde, 136.

Another synthetic method for the protection of phosphines is to prepare the phosphine sulfide and then reduce the P=S bond at a later stage. A number of synthetic methods exist for the reduction of P=S bonds, ranging from quite harsh conditions, such as Si₂Cl₆¹³ and Raney® Nickel,¹⁴ to milder conditions such as Schwartz's reagent,¹⁵ nickelocene,¹⁶ and a sacrificial phosphine.¹⁷ The 2-(diphenylphosphino)benzaldehyde (**135**) can easily be protected as the 2-(diphenylthiophosphino)benzaldehyde (**136**) by stirring overnight in THF in the presence of sulfur (Scheme 5), allowing access to **137** (hereafter referred to as dbaTHIOPHOS).¹⁸ DbaPHOS could then be obtained by reduction of the P=S bond. One possible drawback of this synthetic route is that a number of the deprotection methodologies could interfere with the conjugated 1,4-dien-3-one moiety of dbaTHIOPHOS, **137**. However, phosphine sulfides are also ligands in their own right (see Section 1.1.3) and have been utilised in a number of different catalytic reactions.¹⁹

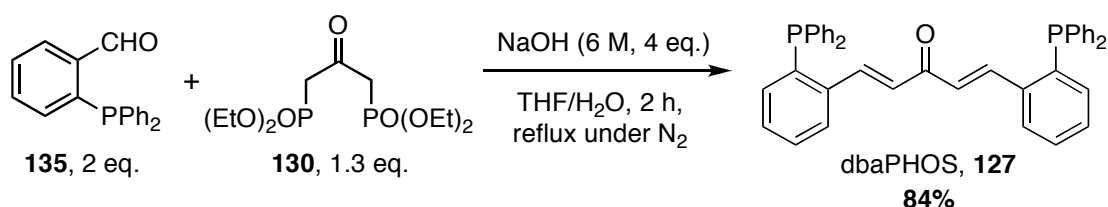
The synthesis of dbaTHIOPHOS, **137** was achieved via the Horner-Wadsworth-Emmons reaction with some optimisation. After screening several bases, sodium hydroxide was found to be the most effective (entries 1-3, Table 1). Increasing the reaction temperature by employing 1,4-dioxane (entry 5, Table 1) did not increase yields further. It was found that an excess of base was essential to push the reaction to completion (entries 3, 4, and 6, Table 1). By following the ³¹P signal of **136** by NMR spectroscopy it was determined that full conversion was reached under the conditions described in entry 6. If these conditions could be translated to the unprotected phosphinobenzaldehyde, **135** it would avoid the need for extensive purification, and potentially remove the need for phosphine protection and then deprotection.

Table 1: Optimisation of the Horner-Wadsworth-Emmons reaction.

Entry	Base	Eq.	Time	Temperature, °C	Yield of 137 , %
1	K ₂ CO ₃	13	6 d	25 to reflux	43
2	KDMO	2.5	6 d	25 to 50	30
3	NaOH	1	48 h	25 to reflux	15 ^a
4	NaOH	2	6 d	25 to reflux	63, 87 ^b
5	NaOH	2	5 d	reflux	68 ^c
6	NaOH	4	48 h	reflux	84

^a Conversion determined by ¹H NMR spectroscopy. ^b Repeat runs of this reaction. ^c 1,4-dioxane.

Using similar conditions to those described in entry 6 the reaction of 2-(diphenylphosphino)benzaldehyde, **135**, with **130** reached full conversion in 2 hours. Work-up by an aqueous wash (using degassed water), followed by extraction with degassed dichloromethane and removal of the solvent afforded dbaPHOS, **127** with >97% purity, as determined by ³¹P NMR spectroscopy. An excess of phosphonate ester was used to ensure no benzaldehyde remains, as column chromatography (on silica-gel) under N₂ is required to remove any remaining benzaldehyde. By contrast, the excess phosphonate ester is removed in the aqueous work-up. Recrystallisation conditions were also investigated, however dbaPHOS, **127** was found to be soluble in CH₂Cl₂, acetone, EtOH, toluene, MeCN, even dissolving to some extent in hexane and Et₂O.

**Scheme 6: Optimised synthesis of dbaPHOS (127).**

2.2.2 Microwave studies: An unexpected THF addition product

Table 2: Conventional vs. microwave conditions.

Entry	Base	Amount, eq.	Time, h	Temperature, °C	Yield of 137,
1	NaOH	4	48	reflux	84
2	NaOH	4	1.5	μ w, 110	67
3	NaOH	4	1	μ w, 110	80 ^a

^a 1.2 eq. 1,3-bis(ethoxyphosphonato)acetone.

The synthesis of dbaTHIOPHOS, **137** was considerably slower than that of dbaPHOS, **127**. The successful synthesis of dbaTHIOPHOS was achieved by conventional heating methods in a closed system (in a Schlenk flask) to give yields of 84% after 48 h at reflux (Table 2, entry 1). It was found that the reaction gave lower yields when an open system was used (*i.e.* round-bottomed flask and condenser). This indicated that an increased pressure under the closed system could have a positive effect on the reaction. Due to this effect and the extended reaction times at higher temperatures, the use of microwave technology was investigated. It was found that the reaction gave similar yields after 1 h if the amount of phosphonate ester was increased to 1.2-1.3 eq. (Table 2, entry 3 vs. entry 2). It is believed that the increase in temperature and pressure led to further ester decomposition.

However, on one attempt the yield was reduced substantially and a second product was formed (Scheme 7). The ¹H NMR spectrum of the second product revealed a distinctive set of alkyl protons that could not be accounted for from the starting materials (see Figure 4).

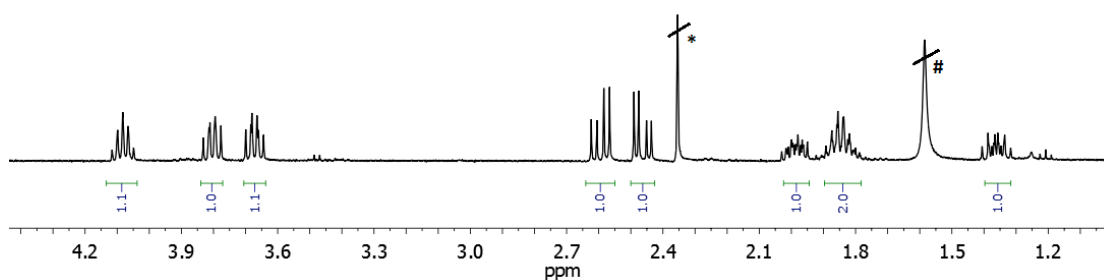
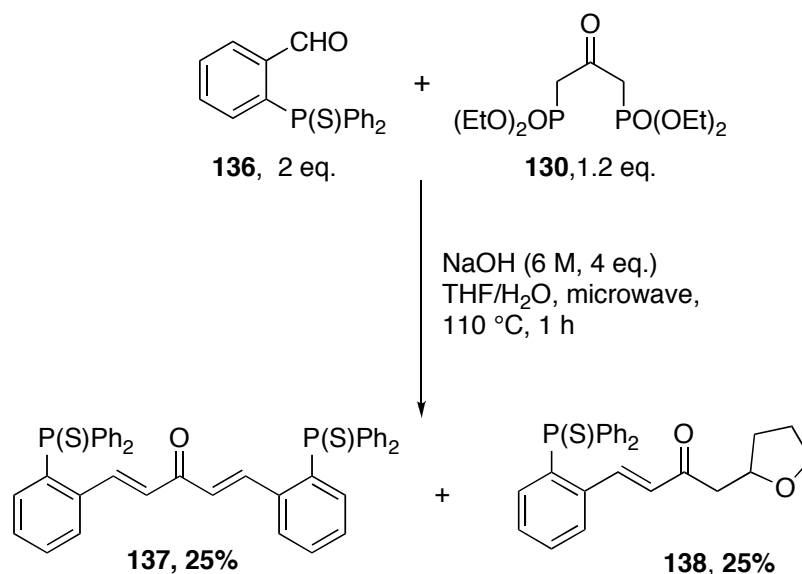


Figure 4: ¹H NMR spectrum detail of 138 (400 MHz, CDCl₃, * = toluene, # = H₂O).



Scheme 7: THF side product from microwave preparation of dbaTHIOPHOS.

The only remaining source of alkyl protons in the reaction was the solvent, THF. ESI mass spectrometry revealed that the side-product had a m/z 433.1380, which corresponds to $C_{26}H_{26}O_2PS$, giving $C_{26}H_{25}O_2PS$ as the formula of the side product. Two possible structures involving THF meet this mass, **138** and **139**. Inspection of reported 1H NMR spectra of compounds in the literature that contain either the THF or tetrahydropyran motif, revealed that the compound (2-tetrahydrofuryl)-propan-2-one was the best match for the alkyl portion of the side-product (see Table 3).²⁰ The diastereotopic protons between 2.7 and 2.4 ppm were especially distinctive, exhibiting roofing doublets of doublets with large coupling constants (~15 Hz). Single crystal X-ray diffraction analysis confirmed compound **138** as the side-product, (Figure 6).

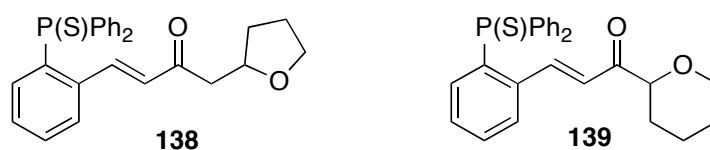
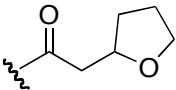
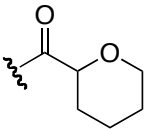


Figure 5: Possible structural isomers of the side product $C_{26}H_{25}O_2PS$.

Table 3: Comparison of the ¹H NMR spectroscopic data of tetrahydrofuran and tetrahydropyran motifs (selected peaks).

Compound	¹ H NMR, ppm
1-(2-tetrahydrofuran-2'-yl)propan-2-one ²⁰	4.26-4.17 (m, 1H), 3.90-3.82 (m, 1H), 3.76-3.67 (m, 1H), 2.74 (dd, J = 15.9, 7.2 Hz, 1H), 2.55 (dd, J = 15.9, 5.6 Hz, 1H), 2.15-2.04 (m, 1H), 1.97-1.83 (m, 2H), 1.52-1.40 (m, 1H).
	
2-acetyl tetrahydropyran ²¹	3.5 (m, 3H), 1.5 (m, 6H).
	
138	4.09 (quintet, J = 6.6 Hz, 1H), 3.80 (ddd, J = 8.2, 7.2, 6.3 Hz, 1H), 3.70-3.64 (m, 1H), 2.60 (dd, J = 15.6, 7.1 Hz, 1H), 2.46 (dd, J = 15.6, 6.0 Hz, 1H), 2.04-1.94 (m, 1H), 1.91-1.77 (m, 2H), 1.42-1.31 (m, 1H)

The unexpected introduction of a THF motif has previously been observed in the literature.²² The formation of these products has been attributed to either carbene or radical mechanisms. The deliberate synthesis of these compounds using both intermediates has also been described in the literature. The groups of Davies and Pérez have both described transition metal-catalysed carbene reactions,²³ whereas Zhang and co-workers have functionalised a variety of ring-containing ethers using radical methodology.²⁴ In our reaction, it is not immediately obvious by which mechanism **138** is being formed, as no transition metals or radical initiators were present. However, the reaction conditions could be considered ‘forcing’ for a microwave reaction (1 h at 110 °C), and **138** had never been observed in the conventionally-heated reaction.

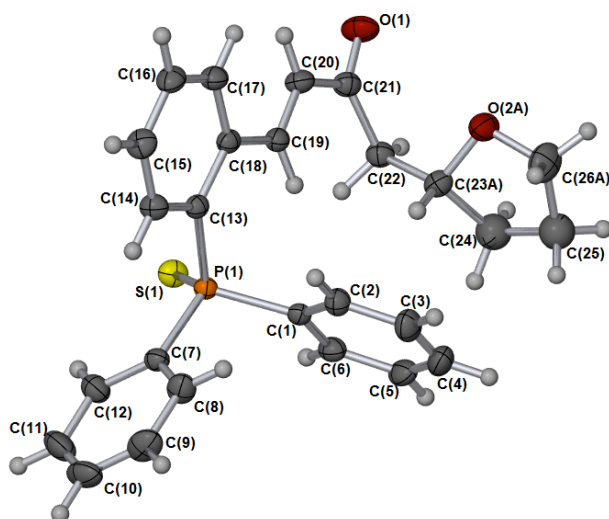
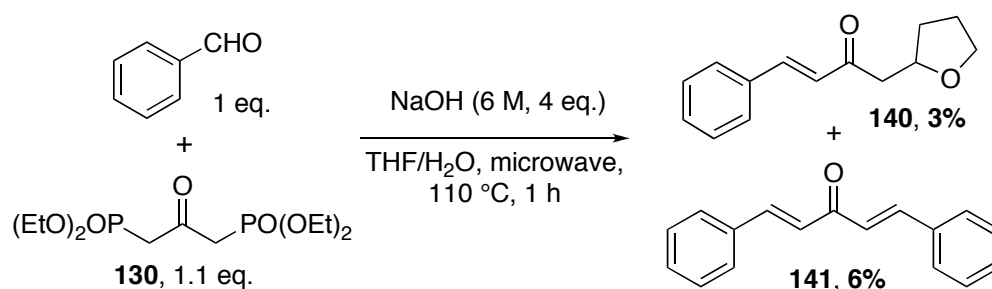


Figure 6: X-ray crystal structure of 138. Thermal ellipsoids shown at 50% probability; disorder is observed around the THF moiety. Selected bond angles (°): O(1)-C(21)-C(20) 119.69(13), C(18)-C(13)-P(1) 120.25(10).

A study was therefore conducted to explore the mechanism by which the **138** was being formed. It was carried out with the assistance of a second year undergraduate student, Ms Elizabeth Wells in the summer of 2010.

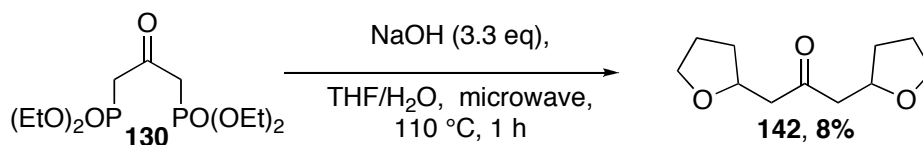
We also conducted reactions with benzaldehyde. Interestingly, in this example, only a small quantity of the THF product, **140**, was obtained (Scheme 8). Furthermore, dba (**141**) formation (the Horner-Wadsworth-Emmons product) was slow under these conditions suggesting that the benzaldehyde is surprisingly slow to react.



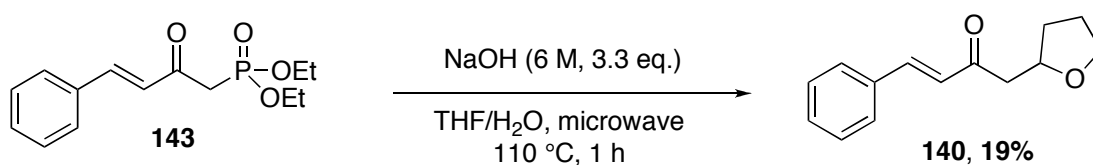
Scheme 8: THF addition product using benzaldehyde.

The reaction was also carried out in the absence of aldehyde (Scheme 9). Once again only small amounts of the THF addition product **142** were obtained. The benzyldiene acetone phosphonate ester (**143**), which was prepared *via* literature procedures,²⁵ was also tested under the reaction conditions (Scheme 10). An increase in yield for **140** was observed, although the conversion was still poor. One possibility was that the phosphonate ester needed to be hydrolysed before the side reaction took place, and if

the hydrolysis was slow and unfavourable then it may account for the poor yields. However, the related benzylidene acetone phosphonic acid did not give any of **140** ruling it out as a possible intermediate. This is perhaps unsurprising as hydrolysis is often difficult; the synthesis of phosphonic acids from the phosphonate esters requires TMSX (X= Br, I) to form the TMS esters prior to hydrolysis by acid.²⁶



Scheme 9: THF addition in the absence of benzaldehyde.

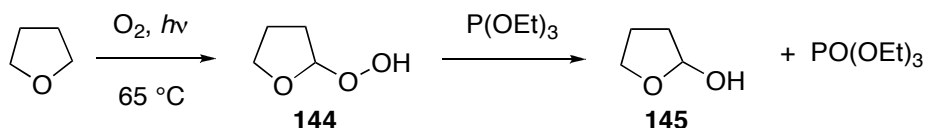


Scheme 10: THF addition using the benzylidene acetone based phosphonate ester.

Having shown that the THF addition occurred both in the presence and absence of the aldehydes, the reaction mechanism was investigated further. There are two plausible reaction mechanisms: either the formation of a carbene (possibly by an α -elimination process)²⁷ followed by C-H insertion, or a reaction involving THF radicals.²⁸ If carbene intermediates were present it was hypothesised they would partake in alkene cyclopropanation reactions. A variety of alkenes (cyclohexene, norbornene, 1,2-tetramethylethene; 5 eq.) were added to the above reactions as carbene traps. However, no evidence for cyclopropanation products was gathered by NMR spectroscopic or mass spectrometric analysis. It is possible that the THF was out competing the alkenes as it is in vast excess as it is the solvent. To eliminate this possibility, 1,4-dioxane was used as a solvent in place of THF. The addition of alkenes to these reactions still did not reveal any carbene intermediates.

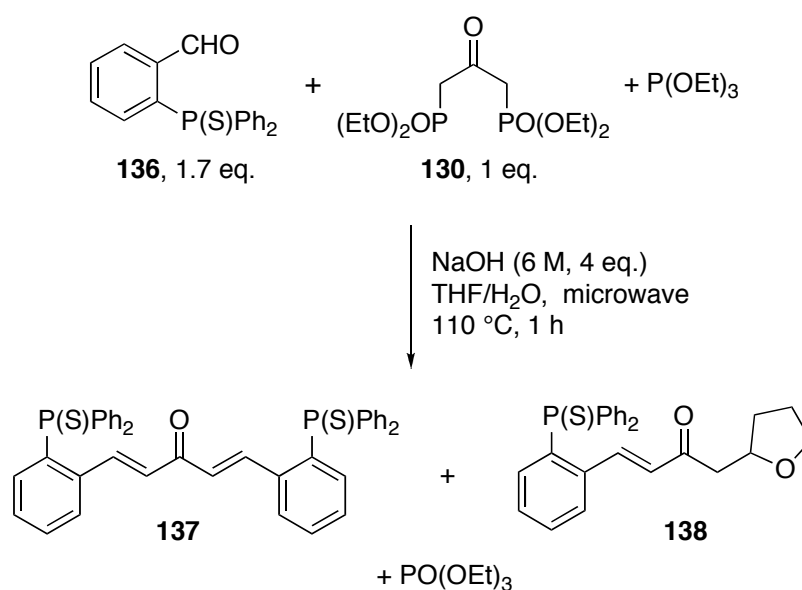
With no evidence for carbene intermediates, the possibility of a radical-based mechanism was explored. It is well known that ethers form radical products in the presence of oxygen and light, hence the requirement for separate ether waste bottles fitted with copper rods in the modern laboratory and regular testing of opened ethers by peroxidase test strips.²⁹ Several research groups have studied the preparation of 2-

hydroperoxytetrahydrofuran, **144**, from THF in the presence of light and oxygen.³⁰ Testing THF batches with peroxidase test strips prior to the reactions being undertaken revealed variable concentrations of peroxide, and thus the results were considered inconclusive that peroxides were responsible for the THF side products.



Scheme 11: Formation of hydroperoxide THF and subsequent detection by triethyl phosphite.

Table 4: Addition of triethyl phosphite.



Entry	P(OEt) ₃ , eq.	P(OEt) ₃ :PO(OEt) ₃ ratio by ³¹ P NMR	PO(OEt) ₃ , eq. formed	Peroxide conc., mM	Yield 138 (137), %
1	1	1:0.2	0.17	25	19 (33)
2	0.5	1:0.5	0.17	25	17 (22)

Another method for testing the presence of **144** is to add triethyl phosphite.³¹ The hydroperoxide will oxidise the reactive phosphite, giving the phosphate and tetrahydrofuran-2-ol, **145**, (Scheme 11). Upon addition of triethyl phosphite to the reaction with **136**, the formation of triethyl phosphate was observed by ³¹P NMR spectroscopy (Table 4). Regardless of the amount of phosphite added the same amount of triethyl phosphate (17 mol%) was observed (entries 1 and 2, Table 4), which matches the yields of **138** observed. A control reaction indicated that triethyl phosphite was not

oxidised under the reaction conditions, suggesting that **144** was present. From the extrapolation of the amount of PO(OEt)₃ formed, the concentration of peroxides present was found to be 25 mM. Another observation supporting the hypothesis of **144** as an intermediate was that when the reactions were performed under a N₂ atmosphere, using dry and degassed THF that had been kept in the dark, no THF addition products were formed.

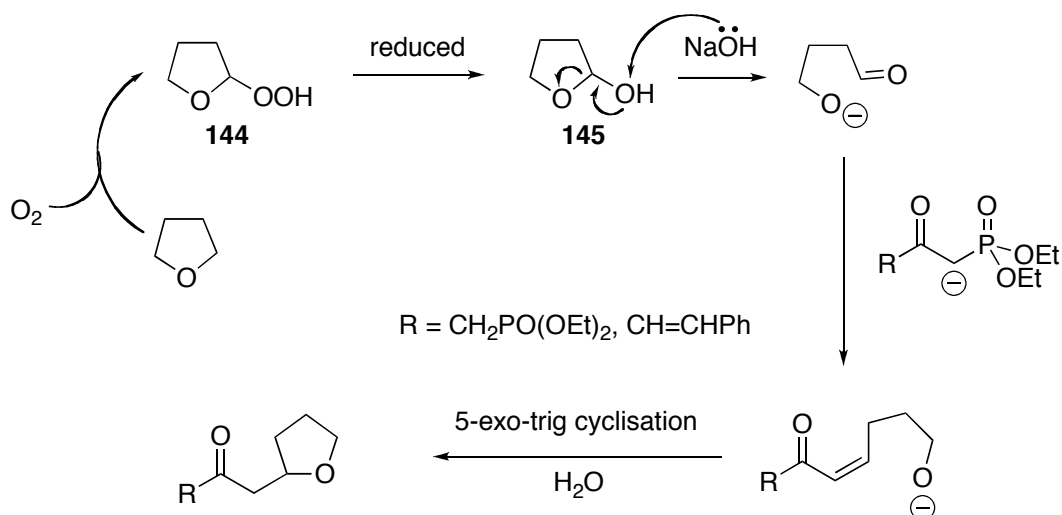
A base is necessary for this side-reaction, therefore the base stoichiometry was probed. It was found that lowering the amount of base improved the yield (Table 5). Studies on the conjugated phosphonate ester showed that no conversion was observed if NaOMe or NaOEt were used under anhydrous conditions (Table 5, entries 6 and 7), or if Et₃N was used (Table 5, entry 5).

Table 5: Effect of base on the formation of the THF addition products.

Entry	R	Base	Base, eq.	Yield, %
1	CH ₂ PO(OEt) ₂	NaOH	0	0
2	CH ₂ PO(OEt) ₂	NaOH	1.7	13
3	CH ₂ PO(OEt) ₂	NaOH	3.3	8
4	CH ₂ PO(OEt) ₂	NaOH	8	5
5	CH=CHPh	NEt ₃	3.3	0
6	CH=CHPh	NaOMe ^a	3.3	0
7	CH=CHPh	NaOEt ^a	3.3	0
8	CH=CHPh	NaOH	3.3	19
9	CH=CHPh	NaOMe ^b	3.3	21

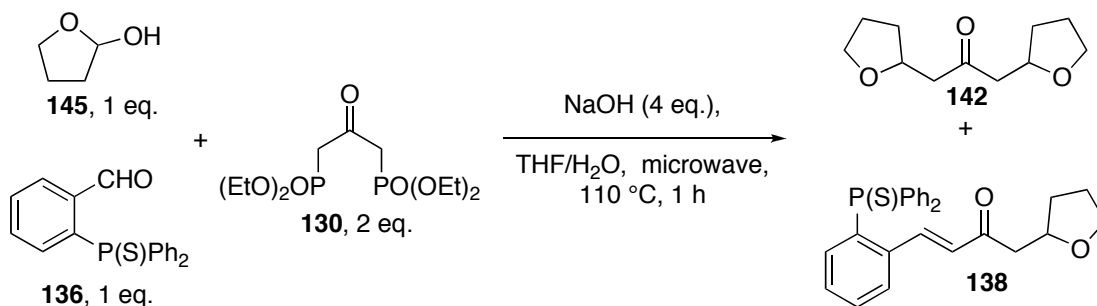
^a anhydrous conditions ^b “wet” conditions

From the evidence showing the presence of hydroperoxides and the necessity for base, it was hypothesised that under the microwave conditions **144** was being reduced to **145**, which can be regarded as a masked aldehyde. Compound **145** could act as a competing substrate in the Horner-Wadsworth-Emmons reaction. Following the formation of the C=C double bond, the alkoxide could undergo a 5-*exo*-trig cyclisation with the enone to reform the THF ring leading to the observed product (Scheme 12).



Scheme 12: Proposed mechanism for the formation of the THF addition products.

The reason for the differences observed between the conventionally heated reaction and the microwave reaction are not clear. Under the conventional conditions the reduction of **144** may not be occurring. On addition of one equivalent of triethyl phosphite to the conventionally heated reaction, the THF product **138** was now observed (17% yield), supporting the hypothesis that **145** is the reactive intermediate (*e.g.* under the conventionally heated reaction a reductant is needed). To test whether **145** acted as an effective substrate for the HWE reaction under the microwave conditions, the reaction was carried out using **145** obtained from the reduction of γ -butyrolactone with DIBAL.³² An increase in yield to 56% was recorded, demonstrating that **145** is a feasible substrate. Competition reactions with 1 equivalent of **136** and 1 equivalent of **145** show no evidence of dbaTHIOPHOS **137**, just the remaining **136**, and the products **138** and **142** (Scheme 13). This suggests that the **145** ‘masked aldehyde’ is the more activated electrophile.

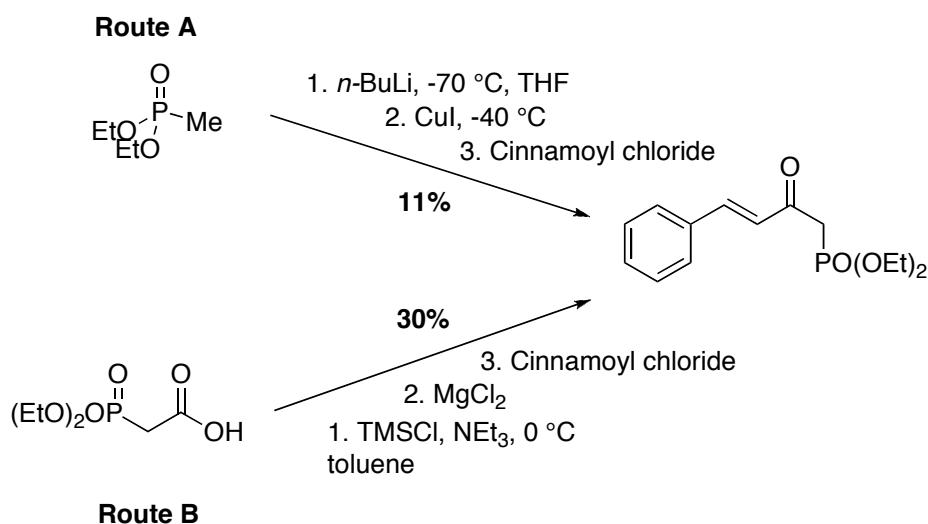


Scheme 13: Competition reaction between 145 and 136 in the HWE reaction.

In summary, the mechanistic studies suggest that hydroperoxides present in the THF as a result of storage conditions (light, oxygen) led to the formation of **144** initially, then reduction gave **145** under the microwave conditions. Compound **145** acted as a competing ‘masked’ aldehyde in the Horner-Wadsworth-Emmons reaction to give the THF addition products. In the conventionally heated reaction it is hypothesised that **145** is unable to form intermediate **144**, hence no THF addition products are observed.

2.2.3 Monophosphine ligands

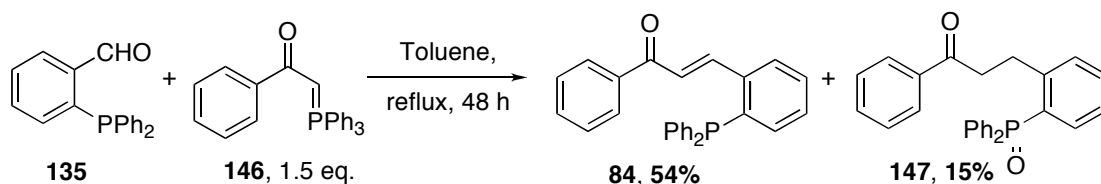
The other target ligand was monophosphine variant **128**. Attempts to synthesise the phosphonate ester, **143**, for the HWE reaction *via* two different literature procedures were found to be unsatisfactory, leading to poor yields (Scheme 14).^{25, 33} Using Route A, the crude NMR revealed *ca.* 40% of the starting phosphonate ester remained. After column chromatography, the majority of the material recovered was unidentified (~30% by weight). Using route B, 8% of the cinnamoyl chloride was recovered. The crude ¹H NMR for route B suggested that the majority of the material was the product, indicating that inefficient purification procedures gave rise to the low yields. It is possible that the polar product remained on the silica-gel during column chromatography. Attempts to purify the product by distillation gave mixed fractions at a range of temperatures.



Scheme 14: Attempted syntheses of the phosphonate ester.

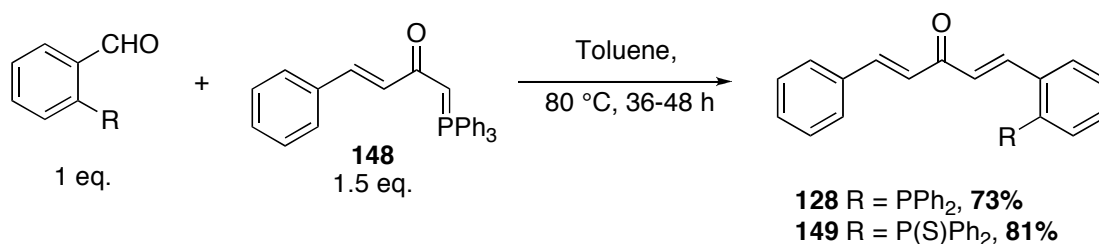
During the progress of this work, Lei and co-workers published the synthesis of the phosphine-chalcone ligand, **84** by using the Wittig reaction.³⁴ We were able to reproduce Lei’s results to give **84** in a moderate yield (54%). However, we also identified an unexpected side product, **147** – the phosphine oxide with the double bond

reduced (Scheme 15). This was confirmed by ^1H , ^{31}P , ^{13}C NMR, MS and IR. It is unclear how this product arises, though it is formally the addition of H_2O to **84**, which is presumably formed first.



Scheme 15: Synthesis of phosphine-chalcone ligand, 84.

Following literature procedures, it was possible to synthesise the ylide needed to prepare monodbaPHOS, **148**, in good yield.³⁵ The Wittig reaction to give monodbaPHOS was successful (Scheme 16). MonodbaPHOS **128** was found to be air sensitive, with phosphine oxide contaminating the product even after column chromatography on silica-gel. Column chromatography using a solvent eluent purged with N_2 gave pure monodbaPHOS (98% by ^{13}P NMR).



Scheme 16: MonodbaPHOS synthesis.

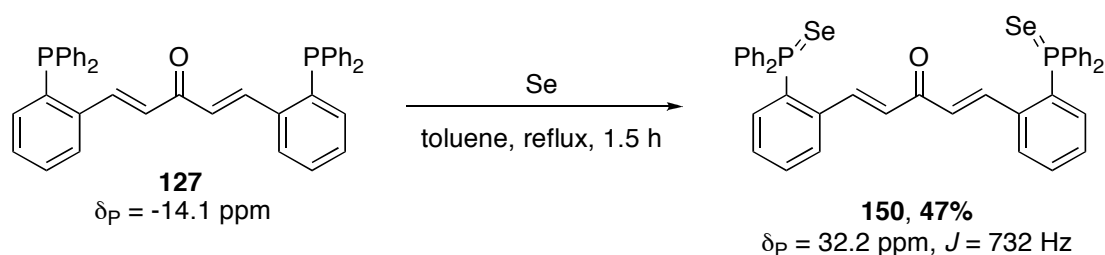
Compound **149** (monodbaTHIOPHOS) was synthesised from 2-(diphenylthiophosphino)benzaldehyde **136**. Similar reaction conditions were used as for monodbaPHOS **128**, though higher yields were recorded.

2.3 Reactivity of the ligands

As mentioned above the phosphine ligands were found to be more air sensitive than expected. The phosphorus is surrounded by two phenyl groups and one aryl group with an electron withdrawing substituent in the *ortho*-position, as a result the ligand was expected to behave in a similar fashion to PPh_3 .

To probe the electronics of the phosphine, the selenium variant of dbaPHOS, **127**, was synthesised. The Se-P coupling constant varies depending on the electronic nature of the ligand (see Table 6).³⁶ The more electron-withdrawing the groups on the phosphorus atom are the larger the J_{PSe} value. There is also a clear relationship between the phosphorus chemical shift of the phosphine and the phosphine selenides, for phosphines with carbon groups directly attached (Figure 7). The dbaPHOS ligand, **127**, falls within the area of the graph with phosphines that are more electron-poor than triphenylphosphine. This is to be expected, as the dba backbone is electron withdrawing.

For Se-dbaPHOS, **150**, $J_{PSe} = 732$ Hz, which is almost the same as triphenylphosphine selenide ($J_{PSe} = 733$ Hz), supporting the hypothesis that the ligand electronics of dbaPHOS, **127**, are similar to triphenylphosphine. Therefore, it is believed that the increase in air sensitivity is due to sterics and conformational preferences.



Scheme 17: Synthesis of Se-dbaPHOS, 150.

Table 6: Se-P Coupling constants as an electronic parameter for phosphines (CDCl₃).

No.	Phosphine	δ_P , ppm	Selenide	δ_P , ppm	$^1J_{PSe}$, Hz	$\Delta\delta_P$, ppm
1	PCy ₃	11.1	SePCy ₃	59.2	673 ³⁷	48.1
2	PMe ₃	-14.5 ^a	SePMe ₃	-	684 ³⁸	-
3	PPhCy ₂	5.0	SePPhCy ₂	55.9	701 ³⁷	50.9
4	PPh ₂ Cy	-1.3	SePPh ₂ Cy	46.3	725 ³⁷	47.6
5	PPh ₃	-5.3	SePPh ₃	36.8	729 ³⁷	42.1
6	P(4-FC ₆ H ₄) ₃	-8.3	SeP(4-FC ₆ H ₄) ₃	33.2	740 ³⁷	41.5
7	P(2-furyl) ₃	-76.9	SeP(2-furyl) ₃	-21.7	787 ³⁷	55.2

^a d_8 -toluene

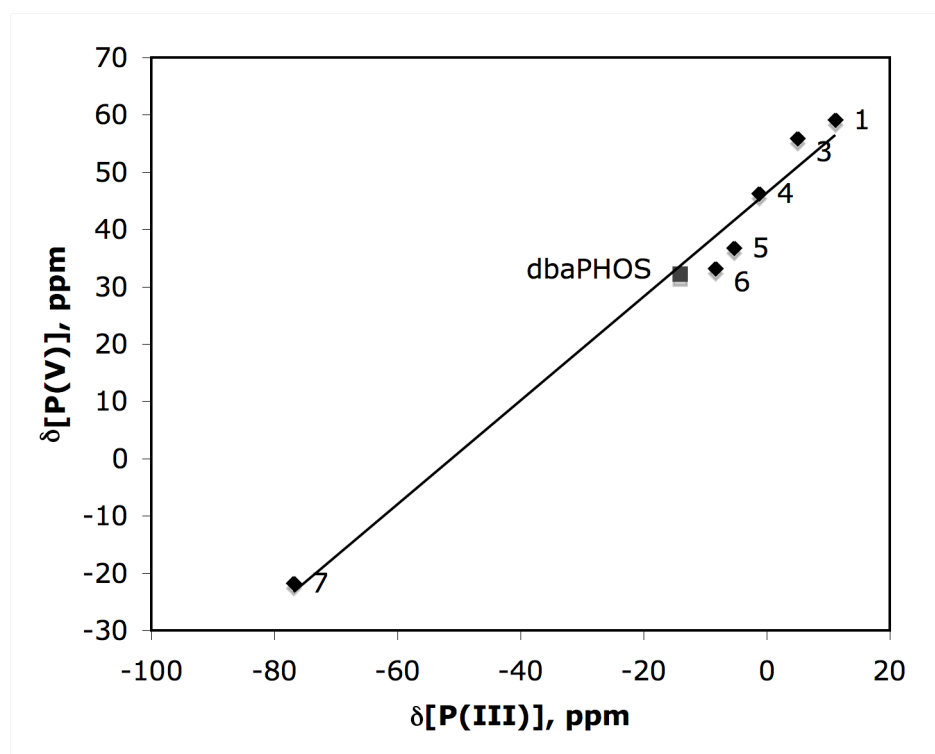


Figure 7: Graph showing the relationship between $\delta^{31}\text{P(III)}$ and $\delta^{31}\text{P(V)}$.

Conformational and steric constraints can have a large effect on the ease of oxidation as shown with Buchwald's ligands, which are more stable than expected due to the difficulty of the oxygen molecule in approaching the phosphine and then being attacked by another phosphine.³⁹ The opposite may be happening in the case of dbaPHOS, where once the oxygen molecule is close to one phosphorus the other phosphorus atom is correctly positioned to attack (Figure 8). If the compound has the *s-trans,s-trans* backbone geometry it can be seen that the oxygen will fit in very closely.

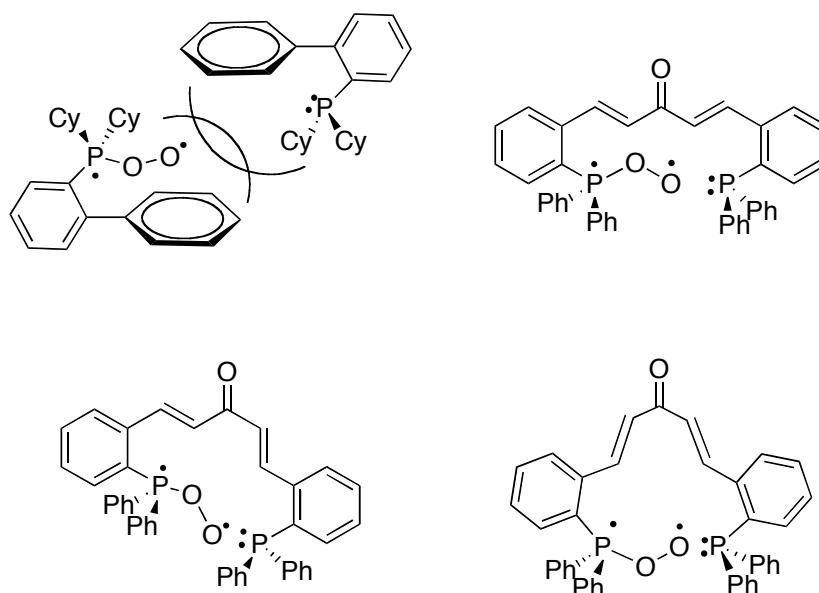


Figure 8: Steric influences on the ease of oxidation by O₂.

An initial X-ray crystal structure determination of monodbaTHIOPHOS revealed a [$\pi 2_s + \pi 2_s$] cycloaddition product, indicating that the ligands may also undergo photochemical reactions. This will be discussed in further detail in Chapter 5.

2.4 Comparison of the structure of the ligands

The single crystal X-ray structures were obtained for dbaPHOS, **127**, dbaTHIOPHOS, **137**, and monodbaTHIOPHOS, **149**, allowing comparisons to be made between them and dba-type compounds. Compound **138** could also be considered a ligand and has been included for comparison. Crystals of dbaPHOS, **127**, suitable for X-ray diffraction were obtained from hot acetonitrile.

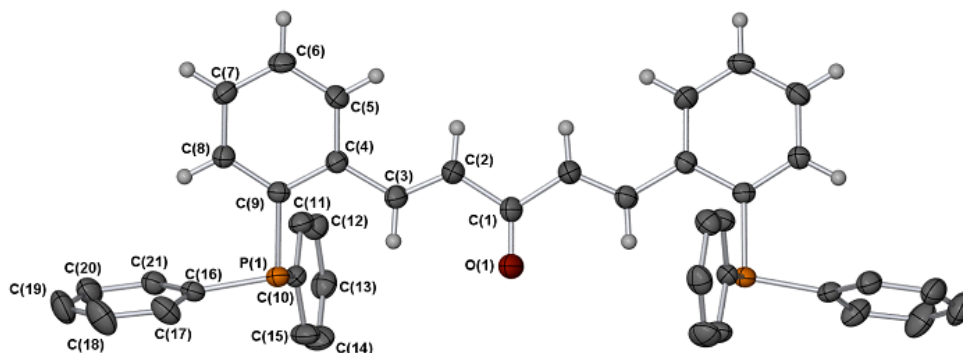


Figure 9: X-ray crystal structure of dbaPHOS, 127. Selected hydrogen atoms removed for clarity. Thermal ellipsoids shown at 50%. Selected Bond lengths (Å): C(2)-C(3) = 1.324(2), C(1)-O(1) = 1.214(3), P(1)-C(9) = 1.8438(14). Symmetry transformations: (A) $-x+1, y, -z+5/2$.

Crystals suitable for X-ray diffraction of dbaTHIOPHOS were obtained from dichloromethane layered with diethyl ether. The dichloromethane is present in the crystal structure as disordered solvent.

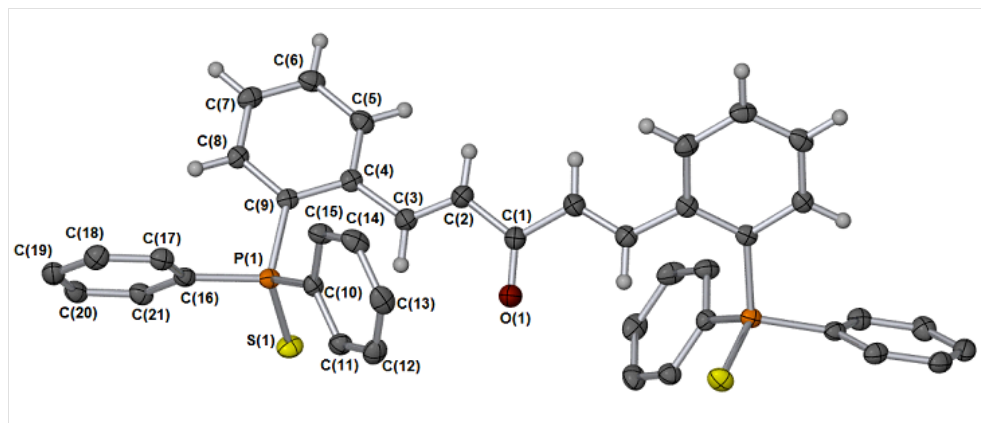


Figure 10: X-ray crystal structure of dbaTHIOPHOS, 137. Solvent and selected hydrogen atoms removed for clarity. Thermal ellipsoids shown at 50%. Selected Bond lengths (Å): C(2)-C(3) = 1.324(5), C(1)-O(1) = 1.221(6), P(1)-C(9) = 1.826(3), P(1)-S(1) = 1.9619(11). Symmetry transformations: (A) $-x, y, 1/2-z$.

Crystals suitable for X-ray diffraction of monodbaTHIOPHOS, 149, were obtained from a dichloromethane solution layered with diethyl ether (kept in the dark).

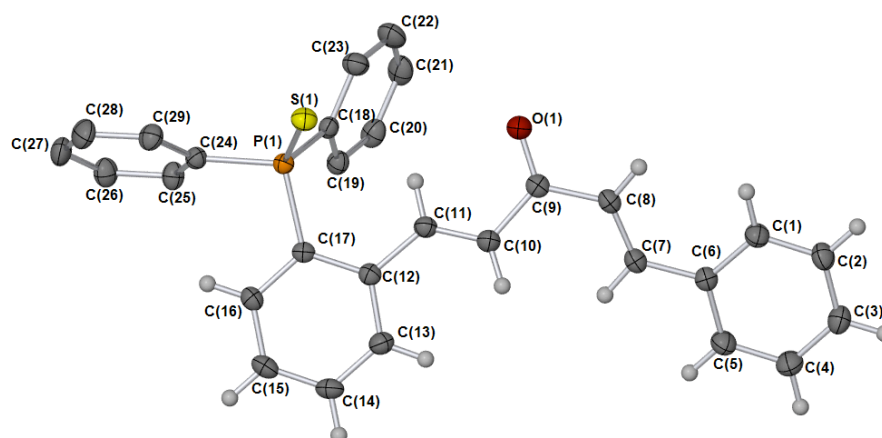
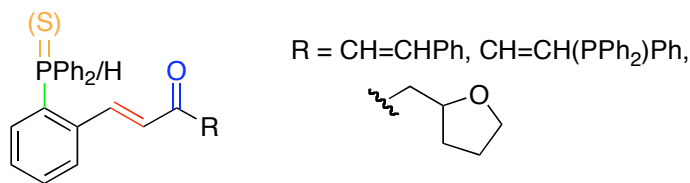


Figure 11: X-ray crystal structure of monodbaTHIOPHOS, 149. Selected hydrogen atoms removed for clarity. Thermal ellipsoids shown at 50%. Selected Bond lengths (Å): C(8)-C(7) = 1.3360(19), C(10)-C(11) = 1.3307(18), C(9)-O(1) = 1.2239(16), C(17)-P(1) = 1.8219(12), P(1)-S(1) = 1.9593(5).

Table 7: Comparison of bond lengths between dba-4,4'-Me and the different ligands.
Numbers in brackets estimated standard deviations (esd's).



Bond	Length, Å				
	Dba-4,4'- Me ⁴⁰	dbaPHOS	dbaTHIOPHOS	monodbaTHIOPHOS	138
C=C	1.329 (3)	1.324(2)	1.324(5)	1.3307(18) ^a 1.3360(18) ^b	1.3350(19)
C=O	1.211 (4)	1.214(3)	1.221(6)	1.2239(16)	1.2258(17)
C-P		1.8438(14)	1.826(3)	1.8219(12)	1.8242(13)
P=S			1.9619(11)	1.9593(5)	1.9504(5)

^a C(10)-C(11), ^b C(8)-C(7)

A comparison of the bond lengths of the different compounds shows that the bond lengths are broadly similar. The C=O bond lengths are the same within error* across all the compounds. DbaTHIOPHOS, **137**, and monodbaTHIOPHOS, **149**, have C-P and P=S bond lengths that are within error. The P=S bonds are all within the range you would expect for a P=S double bond (P-S = 2.00-2.15 Å).⁴¹ The C-P bond length is shorter in the phosphine sulfide ligands than in dbaPHOS, **127**. A comparison of Ph₃P, Ph₃PS and Ph₃PO show the same trend, with Ph₃P exhibiting longer C-P bonds than Ph₃PO, and Ph₃PS sits in the middle of this series. The addition of electronegative groups to the phosphine, such as oxygen, decreases the C-P length as electrons from the aromatic groups are attracted towards the more positive phosphorus.^{41b}

* Within error is used throughout this thesis to indicate the following conditions are met: In normally distributed data, 99% of measurements fall within ± 3 standard deviations of the mean. In crystallography bond distances and angles are only considered different if there is no overlap of the two measurements within ± 3 of their esd's. For further discussion on errors in crystallography see Haestier, J. *Crystallogr. Rev.* **2010**, *16*, 133-144.

Table 8: C-P bond length comparison.

	C-P bond length, Å	C-P-C bond angle, °
Ph₃P ⁴²	1.825(2) – 1.836(2)	102 - 103
Ph₃PS ⁴³	1.809(6) – 1.824(6)	103 - 107
Ph₃PO ⁴⁴	1.799(2) – 1.806(2)	106

The C=C bond lengths are all within error of each other. There is no difference between the C=C bond lengths in dbaPHOS, **127**, and dbaTHIOPHOS, **137**, indicating the difference between oxidation state on the phosphorus has little effect on the dba backbone in the solid-state. In solution there is very little difference in the chemical shifts of the alkene and carbonyl carbons between the compounds. However, there is an increase in the NMR chemical shift difference between the α - and β -protons on going from P(III) to P(V) (see Table 9), in both dbaPHOS, **127**, and monodbaPHOS, **128**. There is also an upfield shift in the α proton.

Table 9: Comparison of the dba backbones between P(III) and P(V) compounds.

Compound	δ , ppm (CD ₂ Cl ₂ , 400 MHz)					
	H $_{\alpha}$	H $_{\beta}$	$\Delta\delta_{\alpha\beta}$	C $_{\alpha}$	C $_{\beta}$	C=O
dbaPHOS (127)	6.78	8.30	1.52	127.2	141.4	188.7
dbaTHIOPHOS (137)	6.48	8.17	1.69	126.8	141.5	188.6
monodbaPHOS (128)	6.88	8.38	1.50	128.1	141.5	189.0
monodbaTHIOPHOS (149)	6.61	8.41	1.80	129.2	141.9	189.4

The phenyl ring on the dba backbone deviates from the plane of the enone by 30.9(5)° in dbaTHIOPHOS, **137**, in dba-4,4'-Me it only varies by 11.2(4)°, this increased non-planarity could be considered to result from the increase in steric bulk at the *ortho*-position of the aryl ring. However, in dbaPHOS, **127**, the backbone is only twisted by 9.5(2)°. This is surprising, as it also has increased steric bulk at the *ortho*-position of the phenyl ring in the dba backbone. In monodbaTHIOPHOS, **149**, the backbone is twisted by 6.9(2)°. In the solid-state, both dbaPHOS, **127**, and dbaTHIOPHOS, **137**, possess *s-cis,s-cis* geometry, whereas monodbaTHIOPHOS, **149**, crystallises in the *s-cis,s-trans* geometry, and **138** in the *s-trans* geometry.

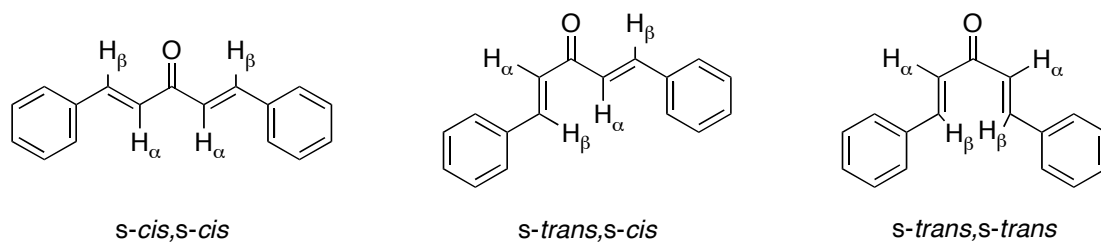


Figure 12: Dba backbone conformers.

The geometry of the basic dba backbone in solution can be determined from the ^1H NMR spectrum.⁴⁵ The *s-cis,s-cis* and *s-cis,s-trans* geometry will be favoured over the *s-trans,s-trans* to minimise the repulsion between the two β -alkene hydrogens. Kawazura and co-workers showed that the intramolecular shift $\Delta\delta_{\alpha\beta}$ can be viewed as a parameter of the conformation of an enone. Similar differences in the intramolecular shifts of 1,3-butadiene have been used to get conformational information.⁴⁶ Kawazura and co-workers looked at the change in $\Delta\delta_{\alpha\beta}$ over temperature. They observed a decrease in $\Delta\delta_{\alpha\beta}$ (tending towards 0.5 ppm) on decreasing the temperature. At lower temperatures the equilibrium will lie towards the *s-cis,s-cis* form. From comparing these results with the results from the ASIS effect (Aromatic Solvent Induced Shift) and the results from thermodynamic treatment the authors deduced that values of ~ 0.5 ppm are seen for the *s-cis* form, whereas values of 1.5 ppm are attributed to the *s-trans* form.

The alkene protons in monodbaPHOS could be said to illustrate this nicely. One set of doublets are 1.5 ppm apart indicating the *s-trans* geometry and the other pair are 0.5 ppm apart indicating *s-cis* geometry. Although we have been unable to obtain a crystal structure of monodbaPHOS, **128**, the crystal structure of monodbaTHIOPHOS, **149**, shows the backbone is *s-cis,s-trans*. However, in the crystal structure the bond nearest the phosphorus group is *s-cis*, whilst the conformer parameters obtained from the NMR spectroscopic data suggest this alkene is the *s-trans* alkene. It is well known that crystal structures do not always adequately reflect the solution structures, as crystal packing can influence the geometry of the compound.

Table 10: Conformation parameters of the ligands.

Compound	$\Delta\delta_{\alpha\beta}$, ppm (400 MHz)
dba, 141	0.66 ^a
monodbaPHOS, 128	1.50 ^b ~0.5
monodbaTHIOPHOS, 149	1.80 ^b not observed
dbaPHOS, 127	1.52 ^b
dbaTHIOPHOS, 137	1.69 ^b
Se-dbaPHOS, 150	1.72 ^a
THF addition product, 138	2.02 ^a

^aCDCl₃, ^bCD₂Cl₂.

Other inconsistencies are noticed with the observations for dba. In particular, much higher values of $\Delta\delta_{\alpha\beta}$ are observed, up to over 2 ppm for **138**. This could mean that the presence of substituents such as Ph₂P on the aryl rings leads to bigger chemical shift differences between the two alkene protons. As a result it is not clear what the limits would be: is 2 ppm now indicative of *s-trans* or can the difference be even larger? What is the difference for a fully *s-cis* alkene, 0.5, 1 or 1.5 ppm? Are we observing the average of the two conformers in these compounds? Further NMR investigations would be needed to find reliable parameters for substituted dba's, before any concrete conclusions can be made about the geometry in the dba backbone of these ligands, and indeed other new substituted dba compounds.

2.5 Summary

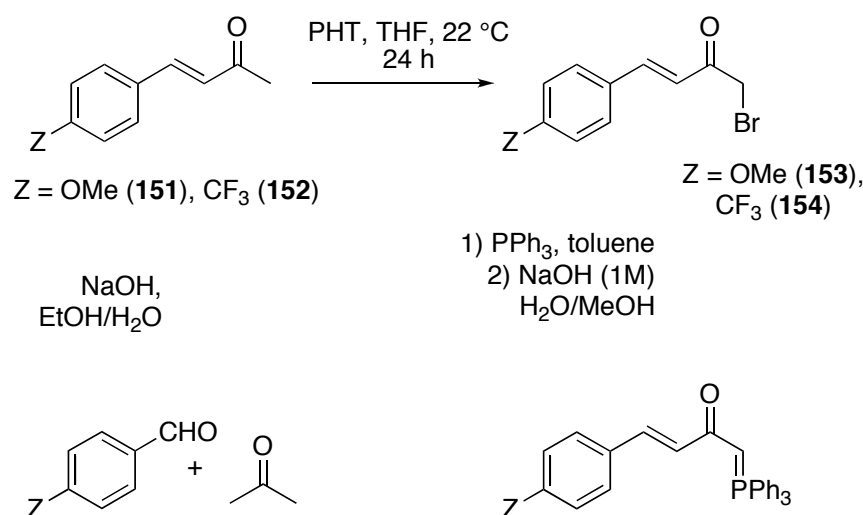
The target ligands, dbaPHOS, **127**, and monodbaPHOS, **128**, as well as their phosphine sulfide variants have been synthesised in good yields using a versatile synthetic methodology. The phosphine ligands were found to be more air sensitive than expected; an observation attributed to the conformational properties of the ligands. This interaction could be probed by the reaction of dbaPHOS with a 1:1 mixture of ¹⁶O₂ and ¹⁸O₂ and subsequent analysis by mass spectrometry. If only compounds with ¹⁶O₂ and ¹⁸O₂ isotopomers are observed than it would be evidence of an intramolecular process.⁴⁷ Low temperature ³¹P and ¹⁷O NMR spectroscopic studies could also be used to try and observe intermediates such as phosphadioxiranes.⁴⁸ Theoretical calculations could also be used elucidate viable intermediates and their relative energies. The formation of (*E*)-

4-(2-(diphenylphosphorothioyl)phenyl)-1-(tetrahydrofuran-2-yl)but-3-en-2-one, **138**, was observed on moving from conventional heating to microwave heating for the synthesis of dbaTHIOPHOS. An investigation into the mechanism explaining the formation of this side-product revealed that it most likely arose from the HWE reaction with tetrahydrofuran-2-ol, **145**, a ‘masked aldehyde’, formed *in situ* from 2-hydroperoxytetrahydrofuran, **144**, in the solvent. This compound could also be investigated as a ligand. The crystal structures of the ligands and **138** are mostly as expected. Both the *s-cis* and *s-trans* geometries around the 1,4-dien-3-one backbone were observed.

2.6 Future work

2.6.1 Tuning the alkene electronics

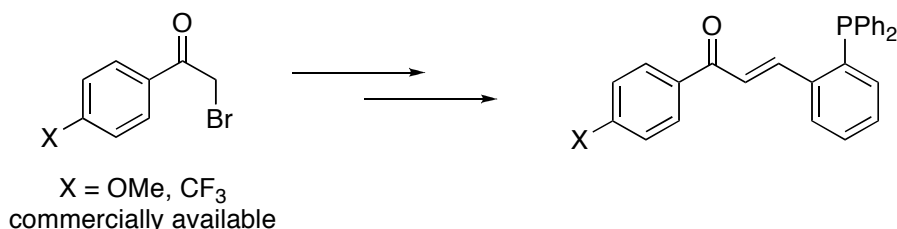
One of the main design features for these ligands was that the alkenes could go on to be tuned. For the monodbaPHOS ligands, it is easy to see that starting with a substituted benzylidene acetone you could potentially use the same methodology to make the phosphonium ylide and then the ligand. The substituted benzylidene acetones (**151**, **152**) are accessible from the relevant benzaldehyde and acetone, using the Claisen-Schmidt condensation reaction (Scheme 18).



Scheme 18: Synthesis of ylides for monodbaPHOS variants.

The benzylidene acetones would need to be α -halogenated. A preliminary study using the same method utilised for monodbaPHOS, gave a low yield in the case of **154**, and no product in the case of **153**. In the ¹H NMR spectrum of the product **153**, the alkenyl

protons signal had shifted from 7-8 ppm to ~5 ppm indicating that the bromine atoms had added to the double bond carbons as well as the α -carbon. As a result alternative halogenation methods need to be found to make this synthetic route viable. Different bromination agents could be tried, *e.g.* 2-bromo-2-cyano-*N,N*-dimethylacetamide,⁴⁹ or the α -lithiation of the benzylidene acetone, followed by trapping with chlorine.⁵⁰

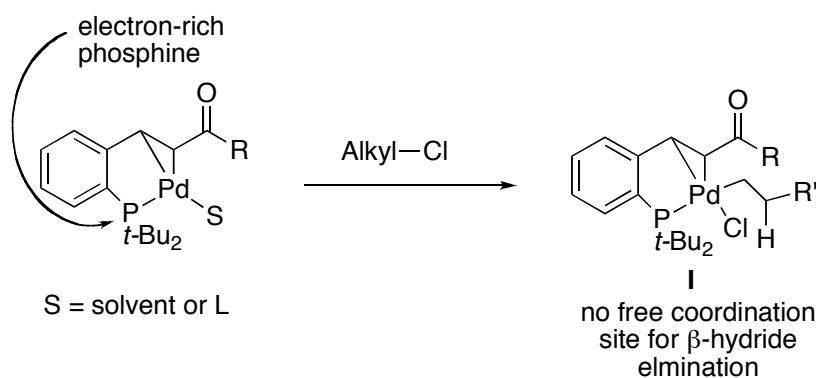


Scheme 19: Ligands based on **84 for the investigation of electronic effects on alkene coordination.**

The ligand **84**, developed by Lei, could also be tuned in a similar way and used for comparison. This route would be less labour intensive, as the substituted starting materials are commercially available (Aldrich, 2011).

2.6.2 Changing the phosphine substituents

Electron-rich phosphines and NHCs have shown great potential in the Pd-catalysed cross-coupling of alkyl halides. For example, in the intermolecular Heck reaction Fu used an NHC whilst also finding benefits in tuning the Pd-alkene precursor. Electron-rich phosphines such as P(*t*-Bu)₃ have been used to cross-couple aryl chlorides.⁵¹ As a result, ligands containing electron-rich phosphines and an alkene could be beneficial in thwarting β -H elimination from the σ -alkyl-palladium(II) species following oxidative addition (Scheme 20), whilst also being reactive enough to successfully undergo oxidative addition with a wide variety of halides.



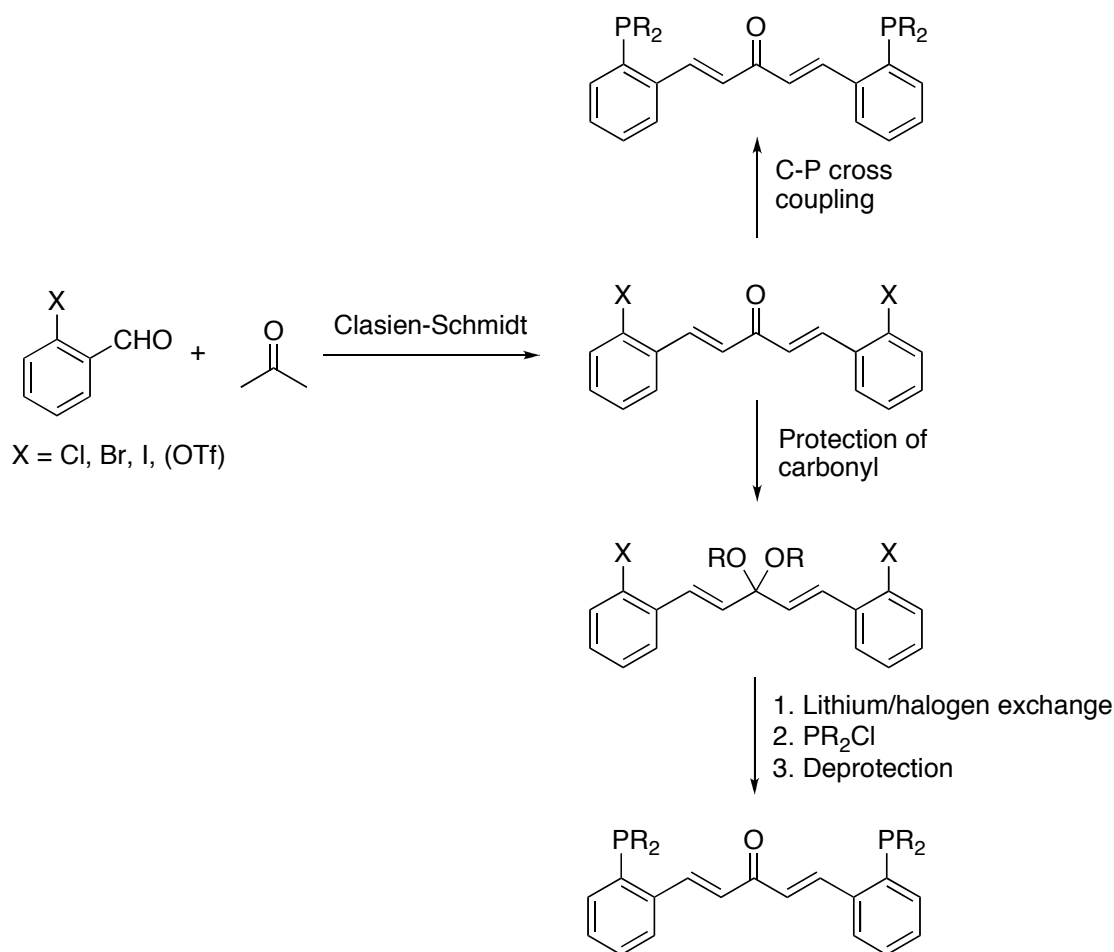
Scheme 20: Utilising phosphino-alkene ligands in catalysis.

So far this project has not focused on investigating different phosphine substituents, but it is likely that a ligand with a different phosphine would ultimately be needed for some catalytic reactions. The successful preparation of the ligands was made using the 2-(diphenylphosphino)benzaldehyde, **135**. This means that the phosphine is introduced early on in the synthesis, making changes to the phosphine quite time-consuming. Another drawback is that the more electron-rich phosphines are more air sensitive and thus would either need to be protected (introducing further protection/deprotection steps) or kept under an inert atmosphere, potentially complicating the purification of the intermediates.

It has been shown that protection as borane adducts does not give a clean product and reactions occur with the double bond. In contrast, the protection of the phosphines with sulfur has been successful and also allows access to the phosphine sulfide ligands. Preliminary studies into the removal of the sulfur have been conducted. We were unable to reduce triphenylphosphine sulfide with HSiCl_3 in a test reaction. By contrast, using Raney Ni with dbaTHIOPHOS, **137**, did appear to give the free phosphine, however, the crude ^1H NMR spectrum did not match that of dbaPHOS, **127**, as the alkene protons were no longer visible, but a number of multiplets were identified between 3.2 and 2.5 ppm, with HSQC showing the carbons related to them came around 45 and 30 ppm. MS analysis provided further evidence of the reduction of the double bond. It is unclear how the double bonds were reduced as no obvious hydrogen donor was in the reaction mixture with the exception of THF. Schwartz's reagent was partially successful at reducing triphenylphosphine sulfide (94% yield, $\text{PPh}_3:\text{SPPh}_3$, 3:2). Another approach not attempted is the protection of the phosphine as the salt using HBF_4 .⁵²

A different approach is to change the methodology, so that the phosphine is introduced nearer the end of the synthesis of the ligands. Two alternative synthetic methods are proposed (see Scheme 21). The advantage of the cross-coupling route is that it is short, and includes the possibility of creating a stereogenic phosphorus atom if an asymmetric protocol is followed. One disadvantage could be that the product acts as a ligand to the metal, possibly deactivating the catalyst. An advantage of the lithiation route is that the methodology introducing the phosphorus substituent is well understood and can be

carried out to give high conversions minimising any purification needed. The deprotection should also give a quantitative yield.



Scheme 21: Possible alternate synthetic strategies for the preparation of dbaPHOS with different phosphine substituents.

2.6.3 Reduction of the alkene double bond

To understand the role of the alkene in any catalysis, the reaction would need to be compared to the same reaction without the alkene bonds present. As a result, the synthesis of the reduced dbaPHOS would be desirable. The alkenes in dba can be reduced selectively with a range of reagents *e.g.* Pd/C,⁵³ or zinc-copper couple.⁵⁴ Lei and co-workers successfully reduced the double bond in their chalcone ligand using InCl_3 and NaBH_4 , however, no experimental details or references were provided.⁵⁵

2.7 Experimental

2.7.1 General information

NMR spectra were obtained in the solvent indicated, using a JEOL ECX400 or JEOL ECS400 spectrometer (400MHz for ^1H , 100 MHz for ^{13}C and 162 MHz for ^{31}P), or a Bruker 500 (500 MHz, 126 MHz and 202 MHz for ^1H , ^{13}C and ^{31}P respectively). Chemical shifts are reported in parts per million and were referenced to the residual undeuterated solvent of the deuterated solvent used (CHCl_3 $\delta = 7.26$ and 77.16 , CDHCl_2 $\delta = 5.31$ and 53.80 , $(\text{CHD}_2)\text{SO}(\text{CD}_3)$, $\delta 2.50$ and 39.52 , ^1H and ^{13}C respectively). All ^{13}C NMR spectra were obtained with ^1H decoupling. ^{31}P NMR were externally referenced to H_3PO_4 , and obtained with ^1H decoupling. NMR spectra were processed using MestrNova software. For ^{13}C NMR spectra the coupling constants are quoted to ± 1 Hz. For the ^1H NMR spectra the resolution varies from ± 0.15 to ± 0.5 Hz; the coupling constants have been quoted to ± 0.5 Hz in all cases for consistency.

Melting points were recorded using a Stuart digital SMP3 machine. IR spectroscopy was undertaken using a Jasco/MIRacle FT/IR-4100typeA spectrometer using an ATR attachment on solid and liquid compounds; solution and KBr IR spectra were obtained on a Nicolet Avatar 370 FT-IR spectrometer. The relative intensities of the peaks are denoted by (s) = strong, (m) = medium and (w) = weak, whilst (br) is used to describe broad peaks. MS spectra were measured using a Bruker Daltronics micrOTOF MS, Agilent series 1200LC with electrospray ionisation (ESI and APCI) or on a Thermo LCQ using electrospray ionisation, with < 5 ppm error recorded for all HRMS samples. LIFDI mass spectrometry was carried out using a Waters GCT Premier MS Agilent 7890A GC. Mass spectral data is quoted as the m/z ratio along with the relative peak height in brackets (base peak = 100). UV-visible spectra were recorded using a JASCO V-560 instrument with quartz cells (1 cm path length). Elemental analysis was carried out on an Exeter Analytical CE-440 Elemental Analyser.

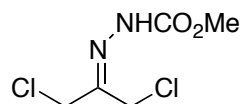
TLC analysis was carried out on Merck TLC aluminium sheets (silica gel 60 F254) and visualised with UV light (254 nm), iodine vapour or an aqueous solution of potassium permanganate. All column chromatography was run on silica gel 60 using the solvent systems specified in the text. The fraction of petroleum ether used was 40-60.

Dry and degassed toluene, CH₂Cl₂ and hexane were obtained from a Pure Solv MD-7 solvent purification system. THF and Et₂O were either obtained from a Pure Solv MD-7 solvent purification system and degassed by the freeze-pump-thaw method or purged with N₂ under sonication, or dried over sodium-benzophenone ketyl and collected by distillation. Benzene was dried over sodium-benzophenone ketyl, EtOH was dried and distilled from magnesium-iodine, and triethylamine was dried over KOH. All air sensitive procedures were carried out using Schlenk techniques. Nitrogen gas was oxygen free and was dried immediately prior to use by passage through a column containing sodium hydroxide pellets and silica. Room temperature was between 13-25 °C. Commercial chemicals were purchased from Sigma-Aldrich and Alfa Aesar and used directly unless stated in the text. Brine refers to a saturated aqueous solution of NaCl.

Microwave reactions were carried out using a CEM Discover S-class instrument (maximum limits set for Power = 150 W and Pressure = 250 psi).

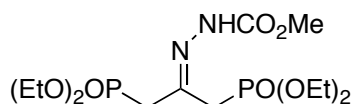
2.7.2 Synthesis of ligands

Methyl 2-[2-chloro-1-(chloromethyl)ethylidene]-1-hydrazinecarboxylate,¹¹ 155



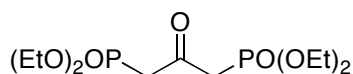
To a solution of methyl 1-hydrazinecarboxylate (4.90 g, 1 eq., 0.054 mol) in MeOH (100 mL) was added 1,3-dichloroacetone (6.97 g, 0.055 mol) in two parts. The reaction was stirred at 23 °C for 4 h and then left in the fridge overnight. The solvent was removed *in vacuo* until ~20 mL remained and the white product had precipitated. The known product was isolated by filtration and washed with ether to afford a white powder (5.80 g, 54%). No further purification was carried out, before taking on in the following experiment. ¹H NMR (400 MHz, CDCl₃) δ 8.37 (s, 1H), 4.32 (s, 2H), 4.18 (s, 2H), 3.88 (s, 3H); HRMS (ESI) *m/z* 220.9854 [*MNa*]⁺ (calculated for C₅H₈Cl₂N₂NaO₂ = 220.9854).

Methyl 2-2-(diethoxyphosphoryl)-1-[(diethoxyphosphoryl)methyl]ethylidene-1-hydrazinecarboxylate,¹¹ **155**



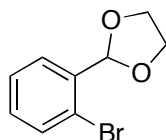
To a suspension of the hydrazinecarboxylate, **155** (5.8 g, 1 eq., 0.029 mol) in toluene (50 mL), triethylphosphite (11.15 mL, 2.2 eq., 0.064 mol) was added portion wise. The resulting mixture was refluxed for 18 h. The toluene was removed *in vacuo*, and the residue taken up in H₂O (40 mL) and extracted with EtOAc (3x 20 mL). Solvent and excess triethylphosphite were removed *in vacuo* to give the crude known product (12.8 g, >95% pure by ³¹P NMR). No further purification was carried out. ¹H NMR (400 MHz, CDCl₃) δ 9.48 (s, 1H), 4.20-4.07 (m, 9H), 3.80 (s, 3H), 3.15 (dd, ²J_{HP} = 22.5 Hz, ⁴J_{HH} = 2.5 Hz, 2H), 3.00 (dd, ²J_{PH} = 21.5 Hz, ⁴J_{HH} = 2.5 Hz, 2H), 1.33 (td, J_{HH} = 7.0, 3.0 Hz, 13H); ³¹P NMR (162 MHz, CDCl₃) δ 23.86-23.58 (m, br), 23.50 (d, ⁴J_{PP} = 11.0 Hz); HRMS (ESI) m/z 425.1225 [MNa]⁺ (calculated for C₁₃H₂₈N₂NaO₈P₂ = 425.1213).

[3-(Diethoxy-phosphoryl)-2-oxo-propyl]-phosphonic acid diethyl ester, (1,3-Bis(diethoxy-phosphonato)-acetone),¹¹ **130**



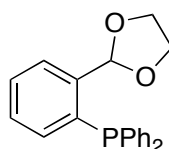
To a solution of the crude product, **156** (12.8 g) in acetone (20 mL) was added 3M HCl (20 mL). The reaction mixture was stirred at 23 °C for 5 h. H₂O (40 mL) was added and the acetone removed. Extraction with CHCl₃ (3x 20 mL), followed by drying over Na₂SO₄, filtration and removal of the solvent *in vacuo*, gave the known product as yellow oil (10.15 g, 94% purity by ¹H NMR, 99% yield). B.p. 200 °C, 1.5 mbar, (*Lit.*¹¹ 185 °C, 0.03 mbar); ¹H NMR (400 MHz, CDCl₃) δ 4.18-4.04 (m, 8H), 3.31 (dd, ²J_{HP} = 23.0 Hz, ⁵J_{HH} = 1.0 Hz, 4H), 1.31 (td, ³J_{HH} = 7.0 Hz, ⁵J_{HH} = 1.0 Hz, 12H); ¹³C NMR (100 MHz, CDCl₃) δ 193.9, 62.9-62.7 (m), 43.3 (d, ¹J_{CP} = 126.6 Hz), 16.5-16.2 (m); ³¹P NMR (162 MHz, CDCl₃) δ 19.48 (s); HRMS (ESI) m/z 331.1076 [MH]⁺ (calculated for C₁₁H₂₅O₇P₂ = 331.1070).

2-(*o*-Bromophenyl)-1,3-dioxolane,^{10a} **133**



2-Bromobenzaldehyde (15.0 g, 1 eq., 0.08 mol), ethylene glycol (6.7 ml, 1.33 eq., 0.12 mol) and *para*-toluenesulfonic acid (63 mg) were dissolved in toluene (100 mL) and refluxed while the evolved water was collected in a Dean-Stark trap (*ca.* 2 mL, theoretically 1.5 mL). After water is no longer evolved (*ca.* 24 h) the solution is cooled and washed with a saturated solution of NaHCO₃ (40 mL), followed by a saturated solution of NaCl (20 mL). The solution is dried over MgSO₄, filtered, concentrated on a rotary evaporator and distilled at 100 °C, 0.5 mmHg, (*Lit.*^{10a} 135-137 °C, 4 mmHg), to give the known title compound as a colourless oil (16.33 g, 89%). ¹H NMR (400 MHz, CDCl₃) δ 7.60 (dd, *J*_{HH} = 8.0, 2.0 Hz, 1H), 7.56 (dd, *J*_{HH} = 8.0, 1.5 Hz, 1H), 7.34 (ddd, *J*_{HH} = 7.5, 7.5, 1.5 Hz, 1H), 7.22 (ddd, *J*_{HH} = 7.5, 8.0, 2.0 Hz, 1H), 6.10 (s, 1H), 4.20-4.03 (m, 4H). ¹³C NMR (100 MHz, CDCl₃) δ: 136.7, 133.1, 130.7, 127.9, 127.5, 123.0, 102.7, 65.6; HRMS (ESI) *m/z* 228.9859 [*MH*]⁺ (calculated for C₉H₁₀BrO₂ = 228.99); IR (ATR, ν cm⁻¹): 2955 (w, br), 2886 (m, br), 1730 (w), 1592 (w), 1571 (w), 1472 (w), 1443 (w), 1387 (m), 1270 (w), 1211 (m), 1124 (m), 1084 (s, br), 1042 (m), 1021 (m), 969 (m), 941 (m), 754 (s).

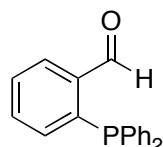
2-(*o*-Diphenylphosphinophenyl)-1,3-dioxolane,^{10b} **134**



A solution of compound **133** (20.95 g, 1 eq., 91 mmol) in dry THF (220 mL) was cooled to -78 °C and kept under an inert atmosphere. *n*-BuLi in hexanes (40 mL, 1.03eq, 93 mmol) was added by syringe pump at a rate of 30 cm³ h⁻¹. After stirring for 2 h at -78 °C, diphenylphosphine chloride (16.3 mL, 1 eq., 91 mmol) was added by syringe pump at a rate of 40 cm³ h⁻¹. The reaction was allowed to warm up to 24 °C overnight, before the addition of H₂O (240 mL). The organic phase was extracted with Et₂O, dried over anhydrous Na₂SO₄, decanted and the solvent removed. The resulting oily liquid was purified by recrystallisation from hot EtOH and cooled to -25 °C, to afford the known title compound as a waxy white solid (21.24 g, 70%). M.p. 94-95 °C, (*Lit.*^{10b} 96 °C); ¹H NMR (400 MHz, CDCl₃) δ 7.7 (dddd, *J* = 8.0, 4.0, 1.5, 0.5 Hz, 1H),

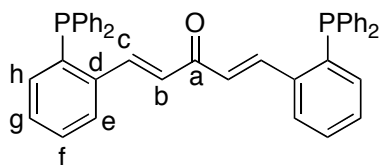
7.4 (ddd, $J = 7.5, 7.5, 1.5$ Hz, 1H), 7.35-7.30 (m, 6H), 7.30-7.22 (m, 5H), 6.96 (ddd, $J = 7.5, 4.5, 1.5$ Hz, 1H), 6.43 (d, $J = 5.0$ Hz, 1H), 4.14-3.92 (m, 4H); ^{13}C NMR (100MHz, CDCl_3) δ 142.1 (d, $J_{\text{CP}} = 22$ Hz), 137.1 (d, $J_{\text{CP}} = 10$ Hz), 136.0 (d, $J_{\text{CP}} = 19$ Hz), 134.2 (d, $J_{\text{CP}} = 1$ Hz), 134.0, 133.8, 129.4 (d, $J_{\text{CP}} = 18$ Hz), 128.7, 128.6 (d, $J_{\text{CP}} = 7$ Hz), 126.6 (d, $J_{\text{CP}} = 6$ Hz), 101.8 (d, $J_{\text{CP}} = 24$ Hz), 65.5; ^{31}P NMR (162 MHz, CDCl_3) δ -15.86 (s); LRMS (ESI) m/z (rel.%) 291.1 [$M\text{-C}_2\text{H}_4\text{O}$] $^+$ (100), 273.1 (26), 261.1 (3), 242.1 (5), 213.0 (8).

2-(Diphenylphosphino)benzaldehyde,^{10a} **135**



Compound **134** (21.24 g, 1 eq., 64 mmol) and *para*-toluenesulfonic acid (0.45 g) were dissolved in acetone (450 mL) and refluxed for 8 h. Whilst still warm, H_2O (100 mL) was added and the volume reduced to ~125 mL by solvent evaporation. The resulting mixture was cooled to -25 °C overnight, and the precipitate filtered and dried *in vacuo* to afford the known title compound as a bright yellow powder (15.88 g, 85%). M.p. $114\text{-}117$ °C, (*Lit.*^{10a} $118\text{-}119$ °C); ^1H NMR (400 MHz, CDCl_3) δ 10.50 (d, $J = 5.5$ Hz, 1H), 8.00-7.95 (m, 1H), 7.53-7.44 (m, 2H), 7.38-7.26 (m, 10H), 6.99-6.94 (m, 1H); ^{13}C NMR (100 MHz, CDCl_3) δ 191.9 (d, $J_{\text{CP}} = 19$ Hz), 141.4, 136.2 (d, $J_{\text{CP}} = 10$ Hz), 134.3, 134.1, 134.0, 133.8, 130.9 (d, $J_{\text{CP}} = 4$ Hz), 129.3, 129.0, 128.9 (d, $J_{\text{CP}} = 7$ Hz); ^{31}P NMR (162 MHz, CDCl_3) δ -11.03 (s); HRMS (ESI) m/z 291.0944 [$M\text{H}$] $^+$ (calculated for $\text{C}_{19}\text{H}_{16}\text{OP}$: 291.1016); IR (ATR, ν cm^{-1}): 3057 (w, br), 2851 (w), 1696 (m), 1672 (m), 1583 (w), 1432 (m), 1198 (m), 843 (m), 751 (s), 744 (s), 696 (s), 670 (s).

(1E,4E)-1,4-di[2-(1,1-diphenylphosphino)phenyl]-1,4-pentadien-3-one, Dbaphos,
127



Dry and degassed THF (17 mL) was added by cannula to an N₂-flushed Schlenk containing **135** (2.09 g, 2 eq., 7.2 mmol). 1,3-bis(diethoxy-phosphonato)-acetone (**130**) (1.55 g, 1.2 eq., 4.7 mmol) was added dropwise and a yellow solution formed on stirring. A solution of NaOH (576 mg, 4 eq., 14.4 mmol) in degassed water (2.2 mL) was added dropwise. The resulting mixture was stirred vigorously for 2-3 h at 80 °C (the reaction could be followed by ³¹P NMR spectroscopy and extra 1,3-bis(diethoxy-phosphonato)-acetone (**130**) added if needed). Saturated N₂-purged NH₄Cl (5 mL) was added to the mixture, followed by degassed H₂O (5 mL) and the aqueous layer extracted with dry and degassed CH₂Cl₂ (3x 10 mL until the CH₂Cl₂ layer remained colourless) and the organic layer transferred by cannula to a Schlenk containing dry Na₂SO₄. After filtration under N₂, the solvent was removed *in vacuo*, to give a yellow oily solid which turned to green oil overnight. The green oil was redissolved in dry and degassed Et₂O, washed with degassed H₂O, transferred to a Schlenk containing dry Na₂SO₄, filtered by cannula under N₂ and the solvent removed to give the product as a green[†] solid (1.81 g, 84%, >96% pure by ³¹P NMR).[‡] Mp. 67 °C_(dec); ¹H NMR (400 MHz, CD₂Cl₂) δ 8.30 (dd, ³J_{HH} = 16.0 Hz, ⁴J_{HP} = 5.0 Hz, 2H, H_c), 7.69 (dddd, *J* = 8.0, 4.5, 1.5, 0.5 Hz, 2H, H_h), 7.44-7.39 (m, 2H, H_g), 7.37-7.21 (m, 22H, H_f and Ar), 6.96 (ddd, *J* = 7.5, 4.5, 1.5 Hz, 2H, H_e), 6.78 (dd, ³J_{HH} = 16.0 Hz, ⁵J_{HP} 1.5 Hz, 2H, H_b); ¹³C NMR (100 MHz, CD₂Cl₂) δ 188.7 (C_a), 141.4 (d, ³J_{CP} = 26 Hz, C_c), 139.7 (d, ¹J_{CP} = 22 Hz, *ipso*-C), 138.8 (d, ¹J_{CP} = 16 Hz, *ipso*-C), 136.3 (d, ²J_{CP} = 10 Hz, C_d), 134.3 (d, *J*_{CP} = 20 Hz, Ar), 134.0 (C_e), 130.3 (d, ³J_{CP} = 1 Hz, C_g), 129.5 (C_f), 129.3 (*p*-C), 129.0 (d, *J*_{CP} = 7 Hz, Ar), 127.2 (d, ⁴J_{CP} = 3 Hz, C_b), 127.0 (d, ²J_{CP} = 4 Hz, C_h); ³¹P NMR (162 MHz, CD₂Cl₂) δ -14.09 (s); HRMS (ESI) *m/z* 603.1993 [*MH*]⁺ (calculated for C₄₁H₃₃OP₂: 603.2001); IR (ATR, ν cm⁻¹): 3051 (w), 2962 (w), 1654 (w), 1614 (w), 1596 (w), 1457 (w), 1434 (w), 1325

[†] On repeat synthesis the product colour varied to give yellow and red products.

[‡] If the benzaldehyde still remains, column chromatography on silica gel eluting with Et₂O:hexane (20:80 v/v) under N₂ can be used to purify the product. The benzaldehyde is the first yellow band, the second bright yellow band is the product.

(br, w), 1260 (w), 1182 (w), 1093 (m), 1026 (w), 975 (w), 799 (br, w), 741 (s), 694 (s); Anal. Calcd. for C₄₁H₃₂OP₂ (602) C 81.71, H 5.36; Observed C 80.82, H 5.40. It is possible that the compound is being oxidised during the elemental analysis. The calculated results for 20% oxidation match those observed; Anal. Calcd. for 20% phosphine oxide C 80.86, H 5.30.

Crystals suitable for X-Ray diffraction were recrystallised from hot MeCN.

Attempted protection of dbaPHOS, 127 as the CS₂ adduct:

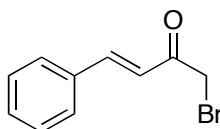
Dry and degassed THF (4 mL) was added to an N₂-flushed Schlenk containing **135** (500 mg, 2 eq., 1.72 mmol). 1,3-bis(diethoxy-phosphonato)-acetone (**130**) (360 mg, 1.2 eq., 0.95 mmol) was added dropwise and a yellow solution formed on stirring. A solution of K₂CO₃ (10M, 1 mL) was added dropwise. The resulting mixture was stirred vigorously for 86 h at 25 °C. The product was extracted with dry THF (5 x 5 mL) under an inert N₂ atmosphere, dried over MgSO₄ and filtered. The solvent was removed and degassed CS₂ (0.5 mL) added and the mixture stirred for 1 h at r.t.. Upon addition of dry EtOH (5 mL) the solution turned red and was then cooled to -10 °C and stirred for 45 min. The yellow precipitate formed was isolated by filtration and dried *in vacuo* to afford dbaPHOS as the product (216 mg, 45%).

Attempted protection of dbaPHOS, 127 as the borane adduct:⁵⁶

To a solution of dbaPHOS (50 mg, 1 eq., 0.08 mmol) in dry and degassed CH₂Cl₂ (1 mL) was added BH₃•SMe (0.8 mL, 20 eq., 1.6 mmol) dropwise at 0 °C. The mixture was stirred at r.t. for 24 h, during which time the solution changed from yellow to colourless. Saturated NH₄Cl_{aq} solution (3 mL) was then added portionwise to the reaction mixture and left for 1 h, before pouring into H₂O (30 mL) and extracting with CH₂Cl₂ (3 x 30 mL). The combined organic phases were washed with saturated NaHCO₃ solution (30 mL), dried over MgSO₄, filtered and concentrated *in vacuo*. The residue was then dissolved in CH₂Cl₂ (5 mL) and filtered through a silica plug, eluting with CH₂Cl₂ (50 mL). The solvent was removed to give a mixture of products as a white solid (22 mg). ¹H NMR (400 MHz, CDCl₃, crude) δ 7.84-6.61 (m, 31H), 3.07-2.06 (m, 4H), 1.95-0.96 (m, 11H, -BH₃), 0.94-0.78 (m, 1.4H); ¹³C NMR (100 MHz, CDCl₃) δ 133.3 (br), 131.2 (br), 128.9 (br); ³¹P NMR δ 25.1 (br, m, 1P), 20.5 (br, s, 15P), 16.6 (br, m, 1.7 P), 7.1 (br, s, 2.5P); ¹¹B NMR δ -37.0 (br, s); LRMS (APCI) m/z

(rel%) 615.2 [C₄₁H₃₉P₂B₂]⁺ (78) {isotope pattern 614 (46), 615 (100), 616 (43); calculated 49, 100, 44}, 605.2 (100); IR (ATR, ν cm⁻¹): 2962 (w), 2372 (br, w), 2161 (br, w), 2036 (br, w), 1980 (br, w), 1482 (w), 1436 (m), 1259 (m), 1069 (br, m), 1014 (br, s), 906 (w), 868 (w), 795 (s), 738 (m), 693 (s); LRMS (ESI) m/z (rel%) 779, 758, 741, 684, 657, 635, 621, 610, 536, 519.

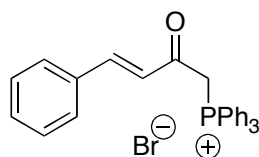
(E)-1-Bromo-4-phenyl-3-buten-2-one, (Bromomethylstyryl ketone),⁵⁷ **157**



Pyrrolidone hydrotribromide (20.3 g, 1.2 eq., 40.9 mmol) in THF (80 ml) was added dropwise over 45 min to a solution of benzylidene acetone (5 g, 1 eq., 34.2 mmol) in dry, degassed THF (120 mL) under an inert N₂ atmosphere. The mixture was stirred at 23 °C for 24 h. The solid was removed by filtration, and the filtrate concentrated *in vacuo* to dryness. The residue was dissolved in Et₂O, washed with brine and dried over Na₂SO₄. Filtration followed by removal of the solvent *in vacuo* afforded a crude product that was purified by column chromatography on silica gel eluting with Et₂O:petroleum ether (5:95 v/v) to give the known title compound as a colourless solid (5.2 g, 68%). Mp 48-49 °C, (*Lit.*⁵⁸ 44-45 °C); ¹H NMR (400 MHz, CDCl₃) δ 7.68 (d, ³J_{HH} = 16.0 Hz, 1H), 7.59-7.54 (m, 2H), 7.44-7.36 (m, 3H), 6.93 (d, ³J_{HH} = 16.0 Hz, 1H), 4.08 (s, 2H); ¹³C NMR (100 MHz, CDCl₃) δ 191.0, 145.3, 133.9, 131.1, 129.1, 128.7, 122.2, 33.3; HRMS (ESI) m/z 224.9916 [MH]⁺ (calculated for C₁₀H₁₀BrO: 224.9910); LRMS (ESI) m/z (rel.%) 249 [M⁸¹BrNa]⁺ (40%), 247 [M⁷⁹BrNa]⁺ (41%), 227 [M⁸¹BrH]⁺ (100%), 225 [M⁷⁹BrH]⁺ (99%), 145 [M-Br]⁺ (12%), 117 (17%).[§]

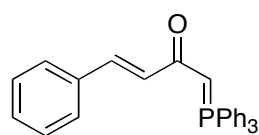
[§] In some instances over bromination was observed to give the dibrominated product LRMS (ESI) m/z (rel.%) 329 [M⁸¹Br₂Na]⁺ (30%), 327 [M⁸¹Br⁷⁹BrNa]⁺ (61%), 325 [M⁷⁹Br₂Na]⁺ (30%), 307 [M⁸¹Br₂H]⁺ (49%), 305 [M⁸¹Br⁷⁹BrH]⁺ (100%), 303 [M⁷⁹Br₂H]⁺ (51%).

[(E)-2-oxo-4-phenyl-3-butenyl](triphenyl)phosphonium bromide, (Cinnamoyl methylenetriphenylphosphonium bromide),^{35a} **158**



A solution of **157** (2.644 g, 1 eq., 11.8 mmol) in toluene (12 mL) was added dropwise to a solution of triphenylphosphine (3.096 g, 1eq., 11.8 mmol) in toluene (12 mL) under N₂. The mixture was stirred overnight at 23 °C. The toluene was removed *in vacuo* to afford the title compound as a colourless solid (5.091 g, 88%), which was carried forward without further purification. M.p. 242-246 °C, (*Lit.*^{35a} 245-247 °C); ¹H NMR (400 MHz, CDCl₃) δ 8.44 (d, ³J_{HH} = 16.5 Hz, 1H), 7.95-7.86 (m, 6H), 7.80-7.72 (m, 5H), 7.70-7.62 (m, 6H), 7.41-7.34 (m, 3H), 7.10 (dd, ³J_{HH} = 16.5 Hz, ⁴J_{HP} = 2.5 Hz, 1H), 5.96 (d, ²J_{HP} = 12.5 Hz, 2H); ¹³C NMR (100 MHz, CDCl₃) δ 191.6 (d, J_{CP} = 6 Hz), 149.5 (d, J_{CP} = 2 Hz), 134.9 (d, J_{CP} = 3 Hz), 134.1 (d, J_{CP} = 11 Hz), 134.1, 131.5, 130.3 (d, J_{CP} = 13 Hz), 129.7, 129.0, 125.3 (d, J_{CP} = 6 Hz), 119.0 (d, ¹J_{CP} = 89 Hz), 38.6 (d, ¹J_{CP} = 60 Hz); ³¹P NMR (162 MHz, CDCl₃) δ 22.22 (s); HRMS (ESI) m/z 407.1558 [*M*]⁺ (calculated for C₂₈H₂₄OP: 407.1559); IR (ATR, ν cm⁻¹): 2928 (w), 1627 (s), 1436 (s), 1331 (m), 1171 (s), 1110 (s), 977 (m), 764 (m), 750 (s), 718 (s), 686 (s).

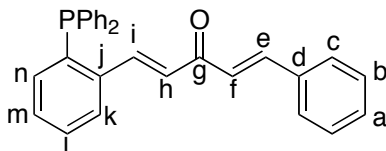
(E)-4-Phenyl-1-(1,1,1-triphenyl-λ⁵-phosphanylidene-3-buten-2-one, (Cinnamoyl methylenetriphenylphosphorane),^{35a} **148**



Compound **158** (4 g, 1 eq., 8.23 mmol) was suspended in a H₂O/MeOH mix (150 mL each), and stirred for 3 h. Aqueous NaOH solution (1 M) was added until pH 7 (monitored using pH indicator paper), and the mixture stirred for 2 h. The resulting solid was filtered off, washed with H₂O (20 mL), followed by Et₂O (20 mL), and dried to give the known title compound as a colourless solid (3.02 g, 90%). M.p. 149-150 °C, (*Lit.*^{35a} 147-149 °C); ¹H NMR (400 MHz, CDCl₃) δ 7.74-7.66 (m, 6H), 7.60-7.54 (m, 3H), 7.53-7.45 (m, 8H), 7.41 (d, ³J_{HH} = 15.5 Hz, 1H), 7.33-7.28 (m, 2H), 7.26-7.21 (m, 1H), 6.90 (dd, ³J_{HH} = 15.5 Hz, ⁴J_{HP} = 0.5 Hz, 1H), 4.02 (d, ²J_{HP} = 25.0 Hz, 1H); ¹³C NMR (100 MHz, CDCl₃) δ 183.0 (d, J_{CP} = 3 Hz), 136.9 (d, J_{CP} = 1 Hz), 134.0 (d, J_{CP} =

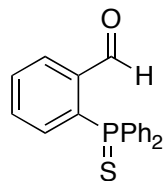
3 Hz), 133.2 (d, $J_{CP} = 10$ Hz), 132.3 (d, $J_{CP} = 3$ Hz), 129.6 (d, $J_{CP} = 19$ Hz), 129.1 (d, $J_{CP} = 12$ Hz), 128.6, 128.2, 127.6, 126.8 (d, $^1J_{CP} = 91$ Hz), 56.6 (d, $^1J_{CP} = 109$ Hz); ^{31}P NMR (162 MHz, CDCl_3) δ 16.30 (s); HRMS (ESI) m/z 407.1570 [$M\text{H}]^+$ (calculated for $\text{C}_{28}\text{H}_{24}\text{OP}$: 407.1559); IR (ATR, ν cm^{-1}): 1634 (w), 1514 (s), 1482 (m), 1435 (m), 1384 (s, br), 1103 (s), 972 (m), 883 (s), 754 (s), 727 (s), 688 (s).

(1E,4E)-1-[2-(1,1-diphenylphosphino)phenyl]-5-phenyl-1,4-pentadiene-3-one, MonodbaPHOS, 128



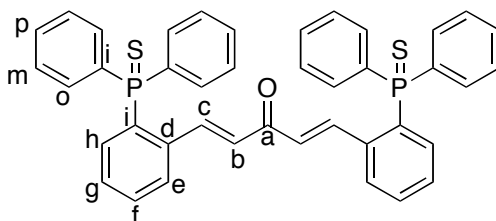
To a Schlenk containing **135** (0.500 g, 1 eq., 1.7 mmol) and **148** (1.05 g, 1.5 eq., 2.6 mmol) under an inert atmosphere was added dry, degassed toluene (30 mL). The mixture was stirred at 50 °C for 16 h, before increasing the temperature to 80 °C for 24 h. After the toluene was removed *in vacuo*, purification by column chromatography on silica gel eluting with EtOAc:petroleum ether (4:96 to 8:92 v/v) afforded the title compound as a solid (0.518 g, 73%, 10% phosphine oxide by ^{31}P NMR). M.p. 107-109 °C; ^1H NMR (400 MHz, CD_2Cl_2) δ 8.38 (dd, $^3J_{\text{HH}} = 16.0$ Hz, $^4J_{\text{HP}} = 5.0$ Hz, 1H, H_i), 7.77 (d, $J = 8.0, 4.0$ Hz 1H, H_{Ar}), 7.63-7.54 (m, doublet peaks visible, $^3J_{\text{HH}} = 16.0$ Hz, 3H, H_{Ar} and H_e), 7.46-7.26 (m, 15H, H_{Ar}), 7.00-6.93 (m, doublet peaks visible, $^3J_{\text{HH}} = 16.0$ Hz, 2H, H_{Ar} and H_f), 6.88 (d, $^3J_{\text{HH}} = 16.0$ Hz, 1H, H_h); ^{13}C NMR (100 MHz, CD_2Cl_2) δ 189.0 (C=O), 143.2 (C_e), 141.5 (d, $^3J_{CP} = 26$ Hz, C_i), 139.7 (d, $^1J_{CP} = 22$ Hz, *ipso*-C), 138.8 (d, $^1J_{CP} = 16$ Hz, *ipso*-C), 136.3 (d, $^2J_{CP} = 10$ Hz, C_j), 135.2 (C_d), 134.4 (d, $^2J_{CP} = 20$ Hz, *o*-C), 134.1 (Ar), 130.7 (Ar), 130.4 (d, $J_{CP} = 1$ Hz, Ar), 129.6 (C_a), 129.4 (*p*-C), 129.3 (C_c), 129.0 (d, $^3J_{CP} = 7$ Hz, *m*-C), 128.7 (C_b), 128.1 (d, $^4J_{CP} = 3$ Hz, C_h), 127.1 (d, $J_{CP} = 4$ Hz, Ar), 125.1 (C_f); ^{31}P NMR (162 MHz, CD_2Cl_2) δ -13.75 (s) and 30.43 (s, "P=O" impurity); HRMS (ESI) m/z 419.1568 (calculated for $\text{C}_{29}\text{H}_{24}\text{OP} = 419.1566$); IR (CH_2Cl_2 , ν cm^{-1}): 3061 (w), 3045 (w), 2963 (w), 1656 (s), 1619 (s), 1600 (s), 1577 (m), 1460 (w), 1450 (w), 1433 (m), 1336 (m), 1187 (s), 1099 (s). Anal. Calcd. for $\text{C}_{41}\text{H}_{32}\text{OP}_2$ (418) C 83.24, H 5.54; Observed C 82.66, H 5.68. It is possible that the compound is being oxidised during the elemental analysis. The calculated results for 20% oxidation match those observed; Anal. Calcd. for 20% phosphine oxide C 82.60, H 5.50.

2-(Diphenylphosphorothioyl)benzaldehyde,¹⁸ **136**



2-(Diphenylphosphino)benzaldehyde, **135** (1.48 g, 1 eq., 5 mmol) and S₈ (1.31 g, 1 eq., 5 mmol) were stirred in THF (60 mL) overnight at rt. The resulting mixture was centrifuged (3000 rpm, 3 min) to remove the solid sulfur, and the solvent removed *in vacuo*. Purification by column chromatography on silica gel eluting with petroleum ether to remove the remaining sulfur, and then Et₂O:pentane (1:4 to 3:7 v/v), afforded the title compound as a cream powder (1.31 g, 81%). M.p. 136-137 °C, (*Lit.*⁵⁹ 131-132 °C); ¹H NMR (400 MHz, CDCl₃) δ 10.71 (s, 1H), 8.12 (ddd, *J* = 8.0, 4.0, 1.0 Hz, 1H), 7.85-7.77 (m, 4H), 7.66-7.61 (m, 1H), 7.60-7.44 (m, 7H), 7.03 (ddd, *J*_{HP} = 14.5 Hz, *J*_{HH} = 8.0, 1.0 Hz, 1H); ¹³C NMR (100 MHz, CDCl₃) δ 190.3 (d, *J*_{CP} = 8 Hz), 138.0 (d, *J*_{CP} = 7 Hz), 137.9 (d, ¹*J*_{CP} = 79 Hz), 132.8 (d, *J*_{CP} = 12 Hz), 132.7 (d, *J*_{CP} = 10 Hz), 132.5 (d, *J*_{CP} = 11 Hz), 132.3 (d, *J*_{CP} = 3 Hz), 132.17 (d, *J*_{CP} = 3 Hz), 132.13 (d, ¹*J*_{CP} = 85 Hz), 129.9 (d, *J*_{CP} = 9 Hz), 129.0 (d, *J*_{CP} = 13 Hz); ³¹P NMR (162 MHz, CDCl₃) δ 40.74 (s); HRMS (ESI) *m/z* 345.0478 [MNa]⁺ (calculated for C₁₉H₁₅NaOPS: 345.0473); IR (ATR, ν cm⁻¹): 1685 (s), 1580 (w), 1435 (m), 1199 (m), 1099 (s), 822 (w), 749 (m), 711 (s), 691 (s), 640 (s), 633 (s), 613 (m).

(1*E*,4*E*)-1,5-bis(2-diphenylphosphorothioyl)phenyl)pentan-1,4-dien-3-one, DbaTHIOPHOS (**137**)

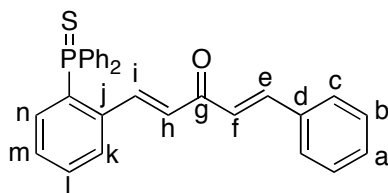


1,3-Bis(phosphonato)acetone (**130**) (256 mg, 1 eq., 0.776 mmol) was added to a magnetically stirred solution of compound **136** (500 mg, 2 eq., 1.56 mmol) in THF (3 mL). To this was added dropwise NaOH (124 mg, 4 eq., 3.11 mmol) dissolved in H₂O (0.5 mL) and THF (1 mL). The mixture was refluxed for 48 h. After cooling, the

solution was washed with saturated $\text{NH}_4\text{Cl}_{(\text{aq})}$ (5 mL), extracted with EtOAc (5 x 5 mL), dried over Na_2SO_3 and filtered. After removing the solvent *in vacuo* the product was recrystallised from CH_2Cl_2 :hexane (1:3 v/v) to afford the title compound as a yellow solid (435 mg, 84%). M.p. 133-138 °C_{dec}; ^1H NMR (400 MHz, CD_2Cl_2) δ 8.17 (d, $^3J_{\text{HH}} = 16.0$ Hz, 2H, H_c), 7.84-7.69 (m, 10H, H_e and *o*-Ar), 7.64-7.57 (m, 2H, H_f), 7.56-7.49 (m, 4H, *p*-Ar), 7.49-7.41 (m, 8H, *m*-Ar), 7.34 (tdd, $J = 7.5, 2.5, 1.5$ Hz, 2H, H_g), 7.09 (ddd, $^3J_{\text{HP}} = 14.5$ Hz, $J_{\text{HH}} = 8.0, 1.0$ Hz, 2H, H_h), 6.48 (d, $^3J_{\text{HH}} = 16.0$ Hz, 2H, H_b); ^{13}C NMR (100 MHz, CD_2Cl_2) δ 188.6 (C=O), 141.5 (d, $^3J_{\text{CP}} = 8$ Hz, C_c), 138.9 (d, $^2J_{\text{CP}} = 7$ Hz, C_d), 133.9 (d, $^1J_{\text{CP}} = 83$ Hz, *ipso*-C), 133.4 (d, $^2J_{\text{CP}} = 11$ Hz, C_h), 132.7 (d, $^2J_{\text{CP}} = 11$ Hz, *o*-Ar), 132.5 (d, $^1J_{\text{CP}} = 85$ Hz, *ipso*-C), 132.4 (d, $^4J_{\text{CP}} = 3$ Hz, C_f), 132.2 (d, $^4J_{\text{CP}} = 3$ Hz, *p*-Ar), 129.6 (d, $^3J_{\text{CP}} = 12$ Hz, C_g), 129.0 (d, $^3J_{\text{CP}} = 13$ Hz, *m*-Ar), 128.8 (d, $^3J_{\text{CP}} = 10$ Hz, C_e), 126.8 (C_b); ^{31}P NMR (162 MHz, CDCl_3) δ 42.07 (s); HRMS (ESI) m/z [$M\text{Na}]^+$ 689.1266 (calculated for $\text{C}_{41}\text{H}_{32}\text{NaOP}_2\text{S}_2$: 689.1262); LRMS (ESI) m/z (rel.%) 689.1 [$M\text{Na}]^+$ (100), 667.1 [$M\text{H}]^+$ (3); IR (ATR, ν cm^{-1}): 3053 (w), 1656 (w), 1619 (w), 1602 (w), 1460 (w), 1436 (m), 1184 (w), 1098 (m), 753 (m), 711 (s), 692 (s), 636 (s), 614 (m), 575 (m); UV-vis (CH_2Cl_2) λ_{max} nm: 318 ($\epsilon = 19513$ $\text{mol}^{-1}\text{dm}^3\text{cm}^{-1}$); Anal. Calcd. for $\text{C}_{41}\text{H}_{32}\text{OP}_2\text{S}_2 \cdot 1/10\text{CH}_2\text{Cl}_2$ (675) C 73.10, H 4.81; Observed C 73.32, H 4.83. Elemental analysis conducted with crystals used for XRD analysis.

Crystals suitable for X-ray crystallography were grown from a solution of **X** in CH_2Cl_2 layered with Et_2O .

(1E,4E)-1-(2-(diphenylphosphorothioyl)phenyl)-5-phenylpentan-1,4-dien-3-one, MonodbaTHIOPHOS, 149

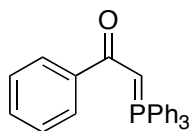


2-(Diphenylthiophosphino)benzaldehyde, **136** (0.75 g, 1 eq., 2.3 mmol) and cinammoyl methylenetriphenylphosphorane, **148** (1.42 g, 1.5 eq., 3.4 mmol) were dissolved in toluene (35 mL) and heated to 80 °C for 48 h. The toluene was removed *in vacuo*. Purification by column chromatography on silica gel eluting with EtOAc:toluene (3:97 v/v) gave the product as a yellow solid (0.84 g, 81 %). M.p. 199-200 °C. ^1H NMR (400

MHz, CD₂Cl₂) δ 8.41 (dd, ³J_{HH} = 16.0 Hz, ¹J_{IP} = 1.0 Hz, 1H, H_i), 7.89-7.77 (m, 5H, H_k and *o*-Ph), 7.64-7.39 (m, 13H, Ar), 7.33 (apparent tdd, *J* = 7.5, 2.5, 1.0 Hz, 1H, H_m), 7.06 (dddd, *J* = 14.5, 8.0, 1.5, 0.5 Hz, 1H, H_n), 6.90 (d, ³J_{HH} = 16.0 Hz, 1H, H_f), 6.61 (d, ³J_{HH} = 16.0 Hz, 1H, H_h); ¹³C NMR (100 MHz, CD₂Cl₂) δ 189.4 (C_g), 143.0 (C_e), 141.9 (d, ³J_{CP} = 8 Hz, C_i), 138.8 (d, ²J_{CP} = 8 Hz, C_j), 135.3 (C_d), 134.0 (d, ¹J_{CP} = 83 Hz, *ipso*-C), 133.4 (d, ²J_{CP} = 11 Hz, H_n), 132.7 (d, ²J_{CP} = 11 Hz, *o*-Ph), 132.4 (d, ⁴J_{CP} = 3 Hz, H_l), 132.3 (d, ¹J_{CP} = 85 Hz, *ipso*-C), 132.2 (d, ⁴J_{CP} = 3 Hz, *p*-Ph), 130.7 (C_a), 129.7 (d, ³J_{CP} = 12 Hz, H_m), 129.2 (Ar), 129.2 (C_h), 129.0 (d, ³J_{CP} = 13 Hz, *m*-Ph), 128.8 (d, ³J_{CP} = 9 Hz, H_k), 128.7 (Ar), 123.4 (C_f); ³¹P NMR (162 MHz, CD₂Cl₂) δ 42.14 (s); HRMS (ESI) *m/z* 451.1285 [*MH*]⁺ (calculated for C₂₉H₂₄OPS: 451.1280); LRMS (ESI) *m/z* (rel.%) 473 [*MNa*]⁺ (20), 451 [*MH*]⁺ (100), 346 (7); IR (ATR, ν cm⁻¹): 3057 (w), 1653 (m), 1593 (m), 1436 (m), 1331 (br, m), 1182 (br, m), 1096 (s), 984 (m), 764 (s), 749 (m), 708 (s), 689 (s), 636 (s). UV-vis (DCM) λ_{max} nm: 306 (ε = 4218 mol⁻¹dm³cm⁻¹); UV-Vis (solid) λ_{max} nm: 289, (br shoulder to 450); Anal. Calcd. for C₂₉H₂₃OPS (450) C 77.31, H 5.15; Observed C 77.10, H 5.14.

Crystals suitable for X-ray crystallography were grown from a solution of **4** in CH₂Cl₂ layered with Et₂O.

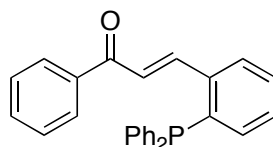
2-Phenyl(triphenylphosphoranylidene)ethan-2-one, (*α*-triphenylphosphoranylideneacetophenone,) 146



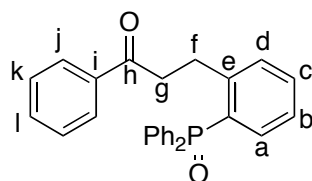
A solution of *α*-bromoacetophenone (2 g, 1 eq., 10 mmol) in dry and degassed toluene (8 mL) was added dropwise to a solution of triphenylphosphine (2.63 g, 1 eq., 10 mmol) in dry and degassed toluene (8 mL) under a N₂ atmosphere. The mixture was stirred overnight and the resulting phosphonium salt was suspended in a mixture of H₂O (100 mL) and MeOH (100 mL). After stirring for 1 h, aqueous NaOH (1 M) was added dropwise until pH 7 was reached. The mixture was then stirred vigorously for 1 h. The white phosphorane precipitate was filtered, washed with H₂O and dried. Purification by recrystallisation from EtOAc afforded the known title compound as an off white solid (2.36 g, 68%). M.p. 185-186 °C, (*Lit.*⁶⁰ 175 °C); ¹H NMR (400 MHz, CDCl₃) δ 7.99-7.92 (m, 2H), 7.75-7.65 (m, 6H), 7.57-7.50 (m, 3H), 7.50-7.44 (m, 6H), 7.36-7.30 (m,

3H), 4.42 (d, $^2J_{\text{PH}} = 25$ Hz, 1H). ^{13}C NMR (400 MHz, CDCl_3) δ 185.0 (d, $J_{\text{CP}} = 3$ Hz), 141.3 (d, $J_{\text{CP}} = 15$ Hz), 133.2 (d, $J_{\text{CP}} = 10$ Hz), 132.1 (d, $J_{\text{CP}} = 3$ Hz), 129.4, 129.0 (d, $J_{\text{CP}} = 12$ Hz), 127.5, 127.1 (d, $^1J_{\text{CP}} = 91$ Hz), 127.0, 51.0 (d, $^1J_{\text{CP}} = 112$ Hz); ^{31}P NMR (162 MHz, CDCl_3) δ 17.23 (s). HRMS (ESI) m/z $[\text{MH}]^+$ 381.1403 (calculated for $\text{C}_{26}\text{H}_{22}\text{OP}$: 381.1403). IR (ATR, ν cm^{-1}): 1586 (m), 1511 (s), 1482 (m), 1435 (s), 1385 (s), 1104 (s), 871 (m), 747 (m), 707 (s), 688 (s).

(E)-3-(2-(Diphenylphosphino)phenyl)-1-phenylprop-2-en-1-one,³⁴ 84



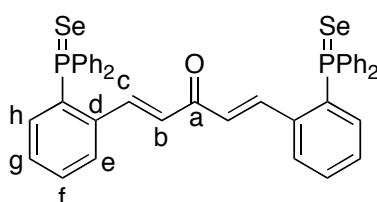
Compounds **135** (0.25 g, 1 eq., 0.86 mmol) and **146** (0.46 g, 1.5 eq., 1.2 mmol) were added to an oven dried Schlenk flask charged with degassed toluene (7 mL) under an inert N_2 atmosphere. The resulting mixture was heated to reflux for 48 h. After the toluene was removed *in vacuo*, purification by column chromatography on silica gel eluting with EtOAc:petroleum ether (10:90 v/v) afforded the known title compound as a cream solid (0.285 g, 54%). M.p. 91-94 $^\circ\text{C}$ (no reported M.p.); ^1H NMR (400 MHz, CDCl_3) δ 8.35 (dd, $^3J_{\text{HH}} = 16.0$ Hz, $^4J_{\text{HP}} = 4.5$ Hz, 1H), 7.75-7.71 (m, 3H), 7.55-7.51 (m, 1H), 7.42-7.25 (m, 14H), 7.18 (dd, $^3J_{\text{HH}} = 16.0$ Hz, $^5J_{\text{HP}} = 1.0$ Hz, 1H), 6.94 (ddd, $J = 7.5, 4.5, 1.0$ Hz, 1H). ^{13}C NMR (100 MHz, CDCl_3) δ 192.1, 143.7 (d, $J_{\text{CP}} = 25$ Hz), 139.8 (d, $J_{\text{CP}} = 22$ Hz), 138.5 (d, $J_{\text{CP}} = 16$ Hz), 138.0, 136.0 (d, $J_{\text{CP}} = 10$ Hz), 134.2 (d, $J_{\text{CP}} = 20$ Hz), 133.8, 132.6, 130.1, 129.3, 129.1, 128.81, 128.76, 128.7 (d, $J_{\text{CP}} = 24$ Hz), 127.1 (d, $J_{\text{CP}} = 4$ Hz), 125.7 (d, $J_{\text{CP}} = 3$ Hz); ^{31}P NMR (162 MHz, CDCl_3) δ -13.32 (s); HRMS (ESI) m/z $[\text{MH}]^+$ 393.1405 (calculated for $\text{C}_{27}\text{H}_{22}\text{OP}$: 393.1403); IR (ATR, ν cm^{-1}): 1667 (s), 1605 (s), 1432 (s), 1309 (m), 1214 (m), 1011 (m), 744 (s), 694 (s).



Further elution with EtOAc:petroleum ether (1:1 v/v) gave a side product as an off-white solid, **147** (52 mg, 15%). M.p. 129-131 $^\circ\text{C}$; ^1H (400 MHz, CDCl_3) δ 7.96-7.83 (m, 2H, Ar), 7.69-7.60 (m, 4H, Ar), 7.57-7.35 (m, 11H, Ar), 7.16 (tdd, $J = 7.0, 2.5, 1.5$ Hz, 1H, H_b), 7.09 (ddd, $^3J_{\text{HP}} = 14.0$ Hz, $J_{\text{HH}} = 8.0, 1.0$ Hz, H_a), 3.34-3.14 (m, 4H, H_f and H_g); ^{13}C NMR (100 MHz, CDCl_3) δ 199.6 (C_h), 147.1 (d, $^2J_{\text{CP}} = 8$ Hz, C_e), 136.8 (C_i),

133.8 (d, $J_{CP} = 13$ Hz), 133.1 (d, $^1J_{CP} = 103$ Hz, *ipso*-C), 133.0 (C_l), 132.5 (d, $^4J_{CP} = 3$ Hz, C_c), 132.0 (d, $^2J_{CP} = 10$ Hz, *o*-Ar), 132.0 (d, $^4J_{CP} = 3$ Hz, *p*-Ar), 131.9 (d, $J_{CP} = 10$ Hz), 131.1 (d, $^1J_{CP} = 103$ Hz, *ipso*-C), 128.7 (d, $^3J_{CP} = 12$ Hz, *m*-Ar), 128.5 (C_k or C_j), 128.4 (C_k or C_j), 125.8 (d, $J_{CP} = 13$ Hz), 41.1 (C_g), 29.7 (d, $^3J_{CP} = 5$ Hz, C_f); ^{31}P NMR (162 MHz, CDCl_3) δ 32.0; HRMS (ESI) m/z 433.1322 [MNa] $^+$ (calculated for $\text{C}_{27}\text{H}_{23}\text{NaO}_2\text{P} = 433.1328$), 411.1504 [MH] $^+$ (calculated for $\text{C}_{27}\text{H}_{24}\text{O}_2\text{P} = 411.1508$); IR (ATR, ν cm^{-1}): 1680 (m), 1437 (m), 1288 (w), 1207 (w), 1178 (m), 1119 (m), 1000 (w), 982 (w), 750 (m), 722 (m), 706 (m), 692 (m).

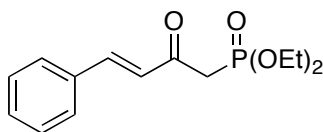
(1E,4E)-1,5-Bis(2-diphenylphosphoroselenoyl)phenyl)pentan-1,4-dien-3-one, 150



A mixture of dbaPHOS, **127** (100 mg, 1 eq. 0.016 mmol) and selenium (31.6 mg, 2.5 eq., 0.04 mmol) in degassed toluene (2.5 ml) was heated at reflux for 1.5 h under N_2 . After cooling, the excess selenium was removed via filtration. Column chromatography on silica gel eluting with toluene gave the product as a yellow solid (58 mg, 47%). M.p. 147-152 $^\circ\text{C}$; ^1H NMR (400 MHz, CDCl_3) δ 8.23 (d, $^3J_{\text{HH}} = 16.0$ Hz, 2H, H_c), 7.85 (dd, $^3J_{\text{HP}} = 13.5$ Hz, $^3J_{\text{HH}} = 8.0$ Hz, 8H, Ar), 7.72 (dd, $J = 8.0, 4.5$ Hz, 2H, H_e), 7.56 (apparent t, $^3J_{\text{HH}} = 8.0$ Hz, 2H, H_f), 7.52-7.40 (m, 12H, Ar), 7.33 (apparent t, $^3J_{\text{HH}} = 7.5$ Hz, 2H, H_g), 7.13 (dd, $^3J_{\text{HP}} = 15.0$ Hz, $^3J_{\text{HH}} = 8.0$ Hz, 2H, H_h), 6.51 (d, $^3J_{\text{HH}} = 16.0$ Hz, 2H, H_b); ^{31}P NMR (162 MHz, CD_2Cl_2) δ 32.17 ($^1J_{\text{PSe}} = 732$ Hz); ^{13}C NMR (100 MHz, CDCl_3) ** δ 188.8 (C_a), 141.3 (d, $^3J_{CP} = 8$ Hz, C_c), 138.8 (d, $^2J_{CP} = 8$ Hz, C_d), 133.2, 133.1 (d, $J_{CP} = 11$ Hz, Ar), 132.3 (d, $^1J_{CP} = 74$ Hz, *ipso*-C), 132.2 (d, $J_{CP} = 3$ Hz), 132.0 (d, $^4J_{CP} = 3$ Hz, *p*-Ar), 130.6 (d, $^1J_{CP} = 76$ Hz, *ipso*-C), 129.3 (d, $J_{CP} = 12$ Hz), 128.9, 128.8 (d, $J_{CP} = 13$ Hz, Ar), 126.44 (C_b); HRMS (ESI) m/z 785.0160 [MNa] $^+$ (calculated for $\text{C}_{41}\text{H}_{32}\text{NaOP}_2\text{Se}_2 = 785.0160$), 763.0370 [MH] $^+$ (calculated for $\text{C}_{41}\text{H}_{33}\text{OP}_2\text{Se}_2 = 763.0340$); IR (ATR, ν cm^{-1}): 1654 (w), 1601 (br, w), 1478 (w), 1458 (w), 1435 (m), 1312 (br, w), 1183 (w), 1119 (w), 1093 (m), 997 (w), 968 (w), 745 (m), 687 (m); Anal. Calcd. for $\text{C}_{41}\text{H}_{32}\text{OP}_2\text{Se}_2$ (762) C 64.75, H 4.24; Observed C 64.10, H 4.29.

** Some signals underlying others, therefore not all doublets reported.

(E)-diethyl 2-oxo-4-phenylbut-3-enylphosphonate, (β -ketophosphonate), 143



Method 1:²⁵

To a solution of diethylphosphonoacetic acid (3.21 mL, 1 eq. 20 mmol) in dry toluene (50 mL) at 0 °C was added triethylamine (11.2 mL, 4 eq. 80 mmol, dried and distilled before use) and TMSCl (3.8 mL, 1.5 eq. 30 mmol). The solution was stirred at r.t. for 1 h, before the addition of more toluene (15 mL) and MgCl₂ (1.9 g, 1 eq. 20 mmol). After a further 1 h stirring at r.t., cinnamoyl chloride (3.99 g, 1.2 eq. 24 mmol) in dry toluene (10 mL) was added dropwise. After stirring at r.t. for 6 h, NH₄Cl (30 mL) was added, followed by extraction of the organics using Et₂O (3 x 50 mL). The combined organic phases were dried over MgSO₄, the mixture filtered and the solvent removed *in vacuo* to give the crude product. Column chromatography on silica gel using EtOAc:petroleum ether (60:40 v/v) as the eluent afforded the known product as a colourless oil (1.72 g, 30%). ¹H NMR (400 MHz, CDCl₃) δ 7.64 (d, ³J_{HH} = 16.0 Hz, 1H), 7.60-7.54 (m, 2H), 7.40 (m, 3H), 6.89 (d, ³J_{HH} = 16.0 Hz, 1H), 4.23-4.06 (m, 4H), 3.32 (d, ²J_{HP} = 22.5 Hz, 2H), 1.33 (t, ³J_{HH} = 7.0 Hz, 6H); ³¹P NMR (162 MHz, CDCl₃) δ 20.87 (s); HRMS (ESI) m/z [MH]⁺ 283.1094 (calculated for C₁₄H₂₀O₄P = 283.1094).

Method 2:³³

A solution of nBuLi in hexanes (2.5 M, 4.4 mL, 1.1 eq., 11 mmol) in dry and degassed THF (10 mL) under a N₂ atmosphere was cooled to -60 °C. To this was added a solution of diethylmethylphosphinate (1.46 mL, 1 eq., 10 mmol) in dry and degassed THF (5 mL) dropwise, and stirred for 10 min. CuI (2.09 g, 1.1 eq., 11 mmol) was added portion-wise to the solution making sure the temperature did not exceed -30 °C, and stirred for 1 h at -30 °C. The mixture was then cooled down to -45 °C, and the cinnamoyl chloride (1.75 g, 1.05 eq., 10.5 mmol) added as a solution in Et₂O (8 mL). The reaction was then left for a further 3 h at -30 °C, before being allowed to warm up to ambient temperature overnight. To the mixture was added water (10 mL) before filtration through CeliteTM and washed with CH₂Cl₂ (30 mL). The organic phases were dried with MgSO₄, filtered and solvent removed *in vacuo*. Column chromatography on

silica gel eluting with EtOAc:petroleum ether (60:40 v/v) gave the known product as an oil (307 mg, 11%).^{††}

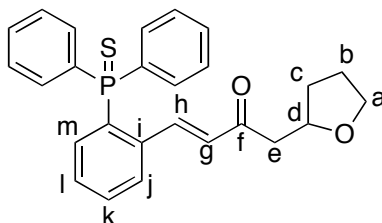
2.7.3 Microwave studies

2.7.3.1 General microwave method

The relevant phosphonate ester (0.65 mmol) was added to a stirring solution of the benzaldehyde, if using, in THF (3 mL). (Triethylphosphite was added at this point when used.) To this was added dropwise NaOH dissolved in H₂O (2.174 mmol in 0.35 mL to give a 6M solution). The mixture was heated in a microwave for 1 h at 110 °C in a 10 mL microwave tube. After cooling to ambient temperature the solution was washed with saturated NH₄Cl_(aq) (5 mL) and extracted with EtOAc (5 x 5 mL). The combined organic phases were dried over Na₂SO₃ and filtered. Purification was carried out by column chromatography on silica gel to give the organic product(s).

2.7.3.2 Detailed microwave experimental

(E)-4-(2-(diphenylphosphorothioyl)phenyl)-1-(tetrahydrofuran-2-yl)but-3-en-2-one, 138



1,3-Bis(phosphonato)acetone (**130**) (215 mg, 1.2 eq., 0.65 mmol) was added to a stirring solution of compound **136** (350 mg, 2 eq., 1.09 mmol) in THF (3 mL). To this NaOH (87 mg, 4 eq., 2.17 mmol) dissolved in H₂O (0.35 mL) was added dropwise. The mixture was heated in a microwave for 1 h at 110 °C. After cooling, the solution was washed with saturated NH₄Cl_(aq) (5 mL) and extracted with EtOAc (5x 5 mL). The organic phases were combined and then dried over Na₂SO₃ and filtered. After removing the solvent *in vacuo* the product was purified by column chromatography on silica gel eluting with EtOAc:toluene (5:95 v/v) to afford dbaTHIOPHOS, **137** (88 mg, 25%) and the title compound as an off-white solid (71 mg, 25%). M.p. 152-154 °C; ¹H

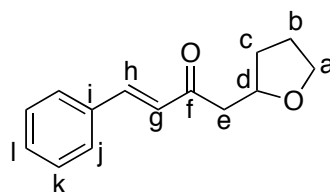
^{††} Distillation using a Kugelrohr was attempted, but this led to mixed fractions being obtained.

NMR (400 MHz, CDCl₃) δ 8.36 (d, $^3J_{\text{HH}} = 16.5$ Hz, 1H, H_h), 7.87-7.78 (m, 4H, Ar), 7.73-7.68 (m, 1H, H_j), 7.57-7.43 (m, 7H, H_k, *p*-H and Ar), 7.29 (apparent tdd, $J = 7.5, 2.5, 1.5$ Hz, 1H, H_i), 7.03 (ddd, $^3J_{\text{HP}} = 14.5$ Hz, $J_{\text{HH}} = 8.0, 1.5$ Hz, 1H, H_m), 6.34 (d, $^3J_{\text{HH}} = 16.5$ Hz, 1H, H_g), 4.09 (apparent quintet, $^3J_{\text{HH}} = 6.5$ Hz, 1H, H_d), 3.80 (ddd, $J_{\text{HH}} = 8.0, 7.0, 6.5$ Hz, 1H, H_a), 3.70-3.64 (m, 1H, H_a), 2.60 (dd, $^2J_{\text{HH}} = 15.5$ Hz, $^3J_{\text{HH}} = 7.0$ Hz, 1H, H_e), 2.46 (dd, $^2J_{\text{HH}} = 15.5$ Hz, $^3J_{\text{HH}} = 6.0$ Hz, 1H, H_e), 2.04-1.94 (m, 1H, H_c), 1.91-1.77 (m, 2H, H_b), 1.42-1.31 (m, 1H, H_c); ^{31}P NMR (162 MHz, CDCl₃) δ 42.23 (s); ^{13}C NMR (100 MHz, CDCl₃) δ 199.5 (C_f), 143.3 (d, $^3J_{\text{CP}} = 8$ Hz, H_h), 138.5 (d, $^2J_{\text{CP}} = 8$ Hz, C_i), 133.6 (d, $^1J_{\text{CP}} = 83$ Hz, *ipso*-C), 133.1 (d, $^2J_{\text{CP}} = 11$ Hz, C_m), 132.60 (d, $J_{\text{CP}} = 11$ Hz, Ar), 132.56 (d, $J_{\text{CP}} = 11$ Hz, Ar), 132.2 (d, $^4J_{\text{CP}} = 3$ Hz, C_k), 132.2 (d, $^1J_{\text{CP}} = 84$ Hz, *ipso*-C), 132.1 (d, $^1J_{\text{CP}} = 85$ Hz, *ipso*-C), 132.1 (d, $^4J_{\text{CP}} = 3$ Hz, *p*-Ar), 132.0 (d, $^4J_{\text{CP}} = 3$ Hz, *p*-Ar), 131.7 (d, $^2J_{\text{CP}} = 10$ Hz, C_i), 129.6 (C_g), 129.4 (d, $J_{\text{CP}} = 12$ Hz), 128.9 (d, $J_{\text{CP}} = 13$ Hz, Ar), 128.8 (d, $J_{\text{CP}} = 13$ Hz, Ar), 128.6 (d, $^3J_{\text{CP}} = 9$ Hz, C_j), 75.3 (C_d), 67.9 (C_a), 44.4 (C_e), 31.6 (C_b), 25.7 (C_c); HRMS (ESI) m/z 433.1380 [MH]⁺ (calculated for C₂₆H₂₆OPS = 433.1386); LRMS (ESI) m/z (rel.%) 455 [MNa]⁺ (80), 433 [MH]⁺ (100), 401 (4), 301 (4), 236 (7); IR (ATR, ν cm⁻¹): 2966 (w), 2861 (w), 1658 (br, m), 1583 (w), 1478(w), 1457 (w), 1435 (m), 1387 (w), 1311 (w), 1260 (w), 1184 (w), 1162 (m), 1120 (w), 1097 (m), 1059 (m), 1027 (m), 998 (m), 970 (m), 798 (br, m), 755 (m), 709 (s), 690 (s).

Crystals suitable for X-ray diffraction were grown by slow evaporation from 1,4-dioxane.

(*E*)-4-phenyl-1-(tetrahydrofuran-2-yl)but-3-en-2-one, 140

From (*E*)-diethyl 2-oxo-4-phenylbut-3-enylphosphonate, **143**:



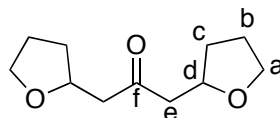
The reaction was carried out following the general procedure in section 2.7.3.1. Purification by column chromatography on silica-gel eluting with EtOAc:petroleum ether (20:80 v/v) gave the title compound as a yellow oil (26 mg, 19%). ^1H NMR (400 MHz, CDCl₃) δ 7.59-7.52 (m with underlying d, $^3J_{\text{HH}} = 16.0$ Hz, 3H, H_h and Ar), 7.43-7.32 (m, 3H, H_l and Ar), 6.77 (d, $^3J_{\text{HH}} = 16.0$ Hz, 1H, H_g), 4.33 (apparent dq, $J_{\text{HH}} = 13.0, 6.5$ Hz, 1H, H_d), 3.89 (apparent dt, $J_{\text{HH}} = 8.5, 7.0$ Hz, 1H, H_a), 3.80-3.70 (m, 1H,

H_a), 3.05 (dd, $^2J_{\text{HH}} = 15.5$ Hz, $^3J_{\text{HH}} = 6.5$ Hz, 1H, H_e), 2.78 (dd, $^2J_{\text{HH}} = 15.5$ Hz, $^3J_{\text{HH}} = 6.0$ Hz, 1H, H_e), 2.21-2.09 (m, 1H, H_c), 1.98-1.88 (m, 2H, H_b), 1.61-1.47 (m, 1H, H_c); ^{13}C NMR (100 MHz, CDCl₃) δ 198.6 (C_f), 143.2 (C_h), 134.6 (C_i), 130.6 (C_l), 129.1 (Ar), 128.5 (Ar), 126.6 (C_g), 75.6 (C_d), 68.0 (C_a), 46.9 (C_e), 31.7 (CH₂), 25.7 (CH₂); HRMS (ESI) m/z 239.1035 [$M\text{Na}$]⁺ (calculated for C₁₄H₁₆NaO₂ = 239.1043), 217.1213 [$M\text{H}$]⁺ (calculated for C₁₄H₁₇O₂ = 217.1223); IR (ATR, ν cm⁻¹): 2929 (w), 2865 (w), 1685 (m), 1653 (m), 1607 (m), 1576 (w), 1495 (w), 1448 (m), 1380 (w), 1332 (w), 1180 (br, m), 1128 (w), 1046 (br, s), 977 (m), 918 (w), 748 (s), 690 (s).

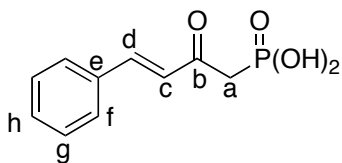
From 1,3-Bis(diethoxy-phosphonato)-acetone, **130**:

The reaction was carried out following the general procedure (section 2.7.3.1) using benzaldehyde (0.056 mL, 1 eq., 0.544 mmol), 1,3-Bis(diethoxy-phosphonato)-acetone, **130** (197 mg, 1.1 eq., 0.598 mmol) and NaOH (87 mg, 4 eq., 2.17 mmol). Both *E,E*-dibenzylidene acetone (7 mg, 6%) and the title compound (3 mg, 3%) were obtained after column chromatography on silica-gel eluting with EtOAc:petroleum ether (10:90 v/v). Characterisation was as above.

1,3-Bis(tetrahydrofuran-2-yl)propan-2-one, **142**



The reaction was carried out following the general procedure described above in section 2.7.3.1. Purification by column chromatography on silica-gel eluting with EtOAc gave the title compound as a clear oil (11 mg, 8%, 1:1 mixture of diastereoisomers). ^1H NMR (400 MHz, CDCl₃) δ 4.22 (apparent tdd, $J_{\text{HH}} = 10.5, 7.0, 3.5$ Hz, 2H, H_d), 3.88-3.81 (m, 2H, H_a), 3.76-3.63 (m, 2H, H_a), 2.77 (ddd, $^2J_{\text{HH}} = 16.0$ Hz, $J_{\text{HH}} = 7.0, 2.5$ Hz, 2H, H_e), 2.58 (ddd, $^2J_{\text{HH}} = 16.0$ Hz, $J_{\text{HH}} = 5.5, 1.0$ Hz, 2H, H_e), 2.15-2.04 (m, 2H, H_c), 1.93-1.82 (m, 4H, H_b), 1.46 (ddd, $J_{\text{HH}} = 16.0, 12.0, 8.0$ Hz, 2H, H_c). ^{13}C NMR (100 MHz, CDCl₃) δ 207.9 (C_f), 207.8 (C_f), 75.04 (C_d), 75.02 (C_d), 67.95 (C_a), 67.95 (C_a), 49.5 (C_e), 49.4 (C_e), 31.6 (CH₂), 25.7 (CH₂); HRMS (ESI) m/z 221.1148 (calculated C₁₁H₁₈NaO₃ = 221.1148); IR (ATR, ν cm⁻¹): 2952 (br, w), 2877 (br, w), 1709 (br, m), 1458 (br, w), 1383 (br, w), 1240 (br, w), 1163 (br, w), 1029 (br, s), 982 (br, m), 855 (br, w).

(E)-2-oxo-4-phenylbut-3-enylphosphonic acid, 159

To a solution of **143** (300 mg, 1 eq., 1.06 mmol) in dry and degassed CH₂Cl₂ (10 mL) at 0 °C was added trimethylsilyliodide, TMSI (0.3 mL, 2 eq., 2.12 mmol). The solution was stirred overnight at r.t. MeOH (10 mL) was added and the solution stirred, before removal of the solvents *in vacuo*. This was repeated two further times. The resultant oily solid was stirred with CHCl₃; filtration afforded a pale brown solid, which was dried *in vacuo* (234 mg, 98%). M.p. 139-145 °C; ¹H NMR (400 MHz, DMSO-*d*₆) δ 7.68 (dd, *J*_{HH} = 6.5, 3.0 Hz, 2H, H_f), 7.60 (d, ³*J*_{HH} = 16.0 Hz, 1H, H_d), 7.47-7.41 (m, 3H, H_g and H_h), 6.94 (d, ³*J*_{HH} = 16.0 Hz, 1H, H_c), 6.59 (br s, OH), 3.21 (d, ²*J*_{HP} = 22.5 Hz, 2H, H_a); ¹³C NMR (100 MHz, DMSO-*d*₆) δ 192.8 (d, ²*J*_{CP} = 5 Hz, C_b), 142.92, 134.40, 130.57, 129.03, 128.45, 126.69, 43.4 (d, ¹*J*_{CP} = 122 Hz, C_a); ³¹P NMR (162 MHz, DMSO-*d*₆) δ 15.6 (s); HRMS (ESI) *m/z* 227.0463 [*MH*]⁺ (calculated for C₁₀H₁₂O₄P = 227.0468); IR (KBr, ν cm⁻¹): 3300-3000 (br, s), 2942 (s), 2905 (s), 2500 (br, m), 2256 (br, m), 1700 (w), 1621 (s, br), 1599 (s), 1576 (s), 1494 (w), 1450 (m), 1370 (w), 1344 (br, s), 1305 (w), 1265 (m), 1200 (br, s), 1153 (br, s), 976 (br, s), 949 (br, s), 885 (m), 866 (m), 822 (m), 750 (s), 686 (s), 655 (m), 525 (s).

Alkene additions:

The following reactions were carried out following the general procedure described in section 2.7.3.1, using between 0.54 and 0.59 mmol of benzaldehyde (1 eq.), with the addition of alkenes (5 eq.). Analysis of the crude reactions mixtures was carried out using ¹H NMR spectroscopy and mass spectrometry.

Entry	Benzaldehyde	Phosphonate	Eq.	NaOH, Eq.	Alkene
1	136	130	1	4	Cyclohexene
2	Benzaldehyde	130	1.1	4	Cyclohexene
3 ^a	Benzaldehyde	130	1.1	4	Cyclohexene
4	Benzaldehyde	130	1.1	4	Norbornene
5	None	130	1 (0.652 mmol)	3.3	2,3-dimethylbut-2-ene
6 ^b	None	143	1 (0.652 mmol)	3.3	Cis-cyclooctene

^a Solvent: dioxane, ^b alkene used as the solvent.

Changing the base

The following reactions were carried out following the general procedure (described in section 2.7.3.1), using the phosphonate esters stated in the table below (1 eq., 0.65 mmol). Purification of the products was carried out by column chromatography on silica-gel eluting with EtOAc for **130**, and EtOAc:petroleum ether (20:80 v/v) for **143**.

R	Base	Base, Eq.	Yield, %
130	NaOH	0	0
130	NaOH	1.7	13
130	NaOH	3.3	8
130	NaOH	8	5
143	NEt ₃	3.3	0
143	NaOMe ^a	3.3	0
143	NaOEt ^a	3.3	0
143	NaOH	3.3	19
143	NaOMe	3.3	21

^a anhydrous conditions using dry and N₂ purged THF.

Triethyl phosphite reactions

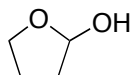
Triethyl phosphite and NaOH (6M) in dioxane was subject to microwave irradiation at 110 °C. After 1 h, ³¹P NMR spectroscopic analysis of the crude mixture revealed that none of the triethyl phosphite had been oxidised under the reaction condition. ³¹P NMR (Dioxane, 400 MHz) δ 137.88.

The following reactions were carried out following the general procedure described in section 2.7.3.1, using 2-(diphenylthiophosphino)benzaldehyde, **136** (1.67 eq., 0.37 mmol) and 1,3-bis(diethoxy-phosphonato)-acetone, **130** (1.0 eq.).

Entry	P(OEt) ₃ , Eq.	P(OEt) ₃ :PO(OEt) ₃ ratio by ³¹ P NMR	Yield 138 (137), %
1	1	1:0.2	19 (33)
2	0.50	1:0.5	17 (22)
3	1	-	14 (17) ^a

^a conventionally heated reaction, reflux, 48 h, using 0.65 mmol **130**.

Tetrahydrofuran-2-ol,⁶¹ 145



To a stirred solution of γ -butyrolactone (0.45 mL, 1 eq., 5.8 mmol) in dry Et₂O (6 mL) at -78 °C, was added a solution of DIBAL (6.5 mL, 1.12 eq., 6.5 mmol) under N₂. The resulting solution was stirred at -78 °C for 3 h, and then quenched with MeOH (1.2 mL). After warming to 0 °C, brine solution (3 mL) was added. The precipitate was removed by filtration through CeliteTM and the filtrate dried with Na₂SO₄, filtered and the solvent removed *in vacuo*. The crude known product (58%, ~90% pure by ¹H NMR spectroscopy) was used without further purification. B.p. 75 °C (35 mbar), (*Lit.*⁶¹ 63-65 °C (15 mbar)); ¹H NMR (400 MHz, CDCl₃) δ 5.51 (s, 1H), 4.06-3.91 (m, 2H), 3.86-3.75 (m, 1H), 2.10-1.77 (m, 4H); ¹³C NMR (400 MHz, CDCl₃) δ 98.4, 67.4, 33.2, 23.5; IR (ATR, ν cm⁻¹): 3369 (br, m), 2955 (w), 2892 (w), 1713 (w), 1646 (br, w), 1442 (br, w), 1366 (w), 1342 (w), 1280 (w), 1184 (m), 1116 (m), 1052 (m), 1032 (s), 984 (s), 918 (m), 843 (m).

Formation of 1,3-Bis(tetrahydrofuran-2-yl)propan-2-one, 142 using 2-hydroxytetrahydrofuran 145.

1,3-Bis(phosphonato)acetone (**130**) (215 mg, 1.2 eq., 0.652 mmol) was added to a stirring solution of tetrahydrofuran-2-ol, **145** (96 mg, 2 eq., 1.09 mmol) in THF (3 mL). To this was added dropwise NaOH (87 mg, 4 eq., 2.17 mmol) dissolved in H₂O (0.35 mL). The mixture was heated in a microwave for 1 h at 110 °C. After cooling, the solution was washed with saturated NH₄Cl_(aq) (5 mL), extracted with EtOAc (5 x 5 mL), dried over Na₂SO₃ and filtered. After removal of the solvent *in vacuo* the product was purified by column chromatography on silica gel eluting with EtOAc to afford the title compound as a clear oil (60 mg, 56%). The product exhibited identical characterisation data as that given in section 2.6.3.2.

Competition reaction between 2-(diphenylthiophosphino)benzaldehyde, 136 and tetrahydrofuran-2-ol, 145.

Tetrahydrofuran-2-ol, **145** (22 mg, 90% pure, 1 eq., 0.224 mmol) and 2-(diphenylthiophosphino)benzaldehyde, **136** (72 mg, 1 eq., 0.244 mmol) were added to a solution of 1,3-bis(ethoxyphosphonato)acetone, **130** (74 mg, 1 eq., 0.224 mmol) in THF (1.5 mL). A NaOH solution (30 mg in 0.12 mL H₂O, 6M) was added dropwise. The

mixture was then heated in a microwave for 1 h at 110 °C. After cooling, the solution was washed with saturated $\text{NH}_4\text{Cl}_{(\text{aq})}$ (5 mL), extracted with EtOAc (5 x 5 mL), dried over Na_2SO_3 and filtered. After removal of the solvent *in vacuo* the crude product was analysed by ^1H NMR spectroscopy and mass spectrometry. No dbaTHIOPHOS or phosphonate ester was observed. 1,3-Bis(tetrahydrofuran-2-yl)propan-2-one, **142**, (*E*)-4-(2-(diphenylphosphorothioyl)phenyl)-1-(tetrahydrofuran-2-yl)but-3-en-2-one, **138** and the 2-(diphenylthiophosphino)benzaldehyde, **136** were observed in a 0.18:0.30:0.53 ratio respectively.

2.7.4 Deprotection of phosphine sulfides

Deprotection of triphenylphosphine sulfide using silanes

To a solution of triphenylphosphine sulfide (118 mg, 1 eq., 0.4 mmol) in dry toluene (15 mL) was added SiCl_3H (0.2 mL, 5 eq., 2 mmol) and the resulting solution heated to 80 °C for 2.25 h under a N_2 atmosphere. The solution was then cooled to 0 °C, and a solution of NaOH (15 mL, 30% w/w) added dropwise. The solution was heated at 50 °C until the organic and aqueous layers became clear (*ca.* 30 min). The solution was extracted with toluene (60 mL), the combined organic phases washed with NaOH solution (30 mL), dried over MgSO_4 and filtered. Following removal of the solvent *in vacuo* the starting material was returned; ^{31}P NMR (162 MHz, CDCl_3) δ 43.97 ($\text{Ph}_3\text{P}=\text{S}$).

Deprotection of triphenylphosphine sulfide using Schwartz's reagent¹⁵

Schwartz reagent (Cp_2ZrHCl) (175 mg, 2 eq., 0.66 mmol) and triphenylphosphine sulfide (100 mg, 1 eq., 0.33 mmol) were placed under a N_2 atmosphere. Dry and degassed THF (4 mL) was added to the reaction and the solution stirred for 3 h at 60 °C. The solution turned from white to yellow to green. The solvent was removed *in vacuo*, the residue dissolved in a hexane:EtOAc mixture (5:1 v/v, 13 mL) and passed through a silica plug. Removal of the solvent gave a white solid (82 mg, 3:2 PPh_3 : SPPH_3 as shown by ^{31}P NMR spectroscopic analysis). ^{31}P NMR (162 MHz, CDCl_3) δ 43.97 ($\text{Ph}_3\text{P}=\text{S}$), -4.80 (PPh_3).

Deprotection¹⁴ of dbaTHIOPHOS using Raney® Nickel

A N₂ flushed Schlenk tube was charged with Raney nickel (3.3 g) and washed sequentially with MeOH (3 x 10 mL), dry Et₂O (3 x 10 mL), and dry THF (3 x 10 mL). A solution of dbaTHIOPHOS, **137** (163 mg, 1 eq., 0.25 mmol) in dry and degassed THF (10 mL) was transferred to the flask and the reaction mixture stirred under a N₂ atmosphere over three days. The mixture was filtered through CeliteTM under N₂, and washed with dry and degassed THF (30 mL). Removal of the solvent *in vacuo* gave the crude product. This was not purified further as at the product was clearly not dbaPHOS. ¹H NMR (400 MHz, CDCl₃) δ 7.67-7.00 (m, 21H), 6.89-6.83 (m, 1H), 3.16-2.43 (m, 8H); ³¹P NMR (162 MHz, CDCl₂) δ -15.00 (s); HRMS (ESI) m/z 639.2212 [oxidisedMH]⁺ (calculated for C₄₁H₃₇O₃P₂ = 639.2212), 623.2266 [oxidisedMH-O]⁺ (calculated for C₄₁H₃₇O₂P₂ = 623.2269), 607.2304 [MH]⁺ (calculated for C₄₁H₃₇OP₂ = 607.2314); LRMS (ESI) m/z (rel%) 661 [oxidisedMNa]⁺ (100), 639 [oxidisedMH]⁺ (23), 623 [oxidisedMH-O]⁺ (67), 607 [MH]⁺ (25), 541 (23), 461 (52), 423 [MH-PPh₂]⁺ (23); IR (ATR, ν cm⁻¹): 2919 (m), 2851 (m), 1706 (w), 1436 (m), 1366 (w), 1178 (m), 1116 (m), 1028 (w), 747 (m), 720 (m), 694 (s).

2.7.5 X-Ray Diffraction details

Single X-ray diffraction data were collected at 110 K in the dark on an Oxford diffractometer or on a Bruker Smart Apex diffractometer with Mo-Kα radiation (λ = 0.71073 Å) using a SMART CCD camera unless otherwise stated. Diffractometer control, data collection and initial unit cell determination was performed using “SMART”.⁶² Frame integration and unit-cell refinement software was carried out with “SAINT+”.⁶³ Absorption corrections were applied by SADABS (v2.10, Sheldrick). Structures were solved by direct methods using SHELXS-97⁶⁴ and refined by full-matrix least squares using SHELXL-97. All non-hydrogen atoms were refined anisotropically. Hydrogen atoms were placed using a “riding model” and included in the refinement at calculated positions.

Table 11: Single Crystal data

Compound reference	ijf0821m, 137	ijf0904a, 127	ijf0909m, 149	ijf1013m, 138
Chemical formula	C ₄₁ H ₃₂ OP ₂ S ₂ •2(CH ₂ Cl ₂)	C ₄₁ H ₃₂ OP ₂	C ₂₉ H ₂₃ OPS	C ₂₆ H ₂₅ O ₂ PS
Formula Mass	836.58	602.61	450.50	432.49
Crystal system	Monoclinic	Monoclinic	Monoclinic	Triclinic
<i>a</i> /Å	24.539(3)	19.718(2)	9.4829(7)	8.7345(14)
<i>b</i> /Å	9.8002(10)	17.231(2)	17.0177(13)	9.0917(15)
<i>c</i> /Å	17.1991(17)	9.9214(13)	14.5741(11)	14.239(2)
α /°	90.00	90.00	90.00	99.344(3)
β /°	90.768(2)	109.031(4)	101.8810(10)	91.734(3)
γ /°	90.00	90.00	90.00	99.613(3)
Unit cell volume/Å ³	4135.8(8)	3186.6(7)	2301.5(3)	1098.2(3)
Temperature/K	110(2)	110(2)	110(2)	130(2)
Space group	<i>C2/c</i>	<i>C2/c</i>	<i>P2(1)/n</i>	<i>P</i> $\bar{1}$
No. of formula units per unit cell, <i>Z</i>	4	4	4	2
No. of reflections measured	15724	13353	23431	11375
No. of independent reflections	3666	4562	5718	5415
<i>R</i> _{int}	0.0302	0.0273	0.0248	0.0169
Final <i>R</i> _I values (<i>I</i> > 2σ(<i>I</i>))	0.0569	0.0458	0.0360	0.0367
Final <i>wR</i> (<i>F</i> ²) values (<i>I</i> > 2σ(<i>I</i>))	0.1612	0.1165	0.0940	0.0949
Final <i>R</i> _I values (all data)	0.0679	0.0611	0.0425	0.0439
Final <i>wR</i> (<i>F</i> ²) values (all data)	0.1732	0.1272	0.0991	0.1002

For ijf1013m (**138**) the structure contained a mixture of compounds which differed in the stereochemistry of the THF attached to C22. The two forms which were modelled had a refined occupancy of 54:46.

For ijf0821m (dbaTHIOPHOS, **137**) considerable solvent disorder was observed. Two CH₂Cl₂ molecules modelled as disordered, each over two positions refined to relative occupancies 74:26 and 52:48 respectively. Atoms C14a and C14b were constrained to the same position and same ADP. Atoms C11a and C11b were constrained to the same position and same ADP, as were atoms C12a and C12b, and C13a and C13b. Atoms C23a and C23b were restrained as approximately isotropic. Further solvent disorder was evident but could not be modelled satisfactorily.

2.8 References

- ¹ a) Fairlamb, I. J. S.; Kapdi, A. R.; Lee, A. F.; McGlacken, G. P.; Weissburger, F.; de Vries, A. H. M.; Schmieder-van de Vondervoort, L. *Chem. Eur. J.* **2006**, *12*, 8750-8761. b) Fairlamb, I. J. S.; Kapdi, A. R.; Lee, A. F. *Org. Lett.* **2004**, *6*, 4435-4438.
- ² Conard, C. R.; Dolliver, M. A. *Org. Synth.* **1943**, *2*, 167.
- ³ a) Sehnal, P.; Taghzouti, H.; Fairlamb, I. J. S.; Jutand, A.; Lee, A. F.; Whitwood, A. C. *Organometallics* **2009**, *28*, 824-829. b) Rosamilia, A. E.; Giarrusso, M. A.; Scott, J. L.; Strauss, C. R. *Green Chem.* **2006**, *8*, 1042-1050.
- ⁴ a) Denney, D. B.; Song, J. *J. Org. Chem.* **1964**, *29*, 495-496. b) Hercouet, A.; Le Corre, M. *Tetrahedron* **1977**, *33*, 33-37. c) Maryanoff, B. E.; Reitz, A. B. *Chem. Rev.* **1989**, *89*, 863-927.
- ⁵ a) Wadsworth, W. S.; Emmons, W. D. *J. Am. Chem. Soc.* **1961**, *83*, 1733-1738. b) Boutagy, J.; Thomas, R. *Chem. Rev.* **1974**, *74*, 87-99.
- ⁶ Lemhadri, M.; Doucet, H.; Santelli, M. *Synlett* **2006**, *18*, 2935-2940.
- ⁷ a) Sasaki, S.; Yoshifuji, M. *Curr. Org. Chem.* **2007**, *11*, 17-31. b) Kyba, E. P.; Kerby, M. C.; Rines, S. P. *Organometallics* **1986**, *5*, 1189-1194. c) Langer, F.; Puntener, K.; Sturner, R.; Knochel, D. *Tetrahedron: Asymmetry* **1997**, *8*, 715-738.
- ⁸ Allen, D. W. *Organophosphorus Chemistry* **2002**, *25*, 1-62.
- ⁹ a) Tunney, S. E.; Stille, J. K. *J. Org. Chem.* **1987**, *52*, 748-753. b) Ager, D. J.; East, M. B.; Eisenstadt, A.; Laneman, S. A. *Chem. Commun.* **1997**, 2359-2360. c) McCarthy, M.; Goddard, R.; Guiry, P. J. *Tetrahedron: Asymmetry* **1999**, *10*, 2797-2807.
- ¹⁰ a) Hoots, J. E.; Rauchfuss, T. B.; Wroblewski, D. A. *Inorg. Synth.* **1982**, *21*, 175-179. b) Ahlmann, M.; Walter, O. *J. Organomet. Chem.* **2004**, *689*, 3117-3131.
- ¹¹ Corbel, B.; Medinger, L.; Haelters, J. P.; Strutz, G. *Synthesis* **1985**, 1048-1051.
- ¹² De Souza, R. F.; Thiele, D.; Monteiro, A. L. *J. Catal.* **2006**, *241*, 232-234.
- ¹³ Zon, G.; DeBruin, K. E.; Naumann, K.; Mislow, K. *J. Am. Chem. Soc.* **1969**, *25*, 7023.
- ¹⁴ Tang, W.; Wang, W.; Zhang, X. *Angew. Chem., Int. Ed.* **2003**, *42*, 943-946.
- ¹⁵ Zablocka, M.; Delest, B.; Igua, A.; Skowronska, A.; Majoral, J. P. *Tetrahedron Lett.* **1997**, *38*, 5997-6000.

-
- ¹⁶ a) Mathey, F.; Mercier, F. *J. Organomet. Chem.* **1979**, *177*, 255-263. b) Mathey, F. *J. Organomet. Chem.* **1975**, *87*, 371-377. c) Mathey, F.; Sennyey, G. *J. Organomet. Chem.* **1976**, *105*, 73-84.
- ¹⁷ Wu, H-C.; Yu, J-Q.; Spencer, J. B. *Org. Lett.* **2004**, *25*, 4675-4678.
- ¹⁸ Maraval, A.; Magro, G.; Maraval, V.; Vendier, L.; Caminde, A. M.; Majoral, J-P. *J. Organomet. Chem.*, 2006, **691**, 1333-1340.
- ¹⁹ a) Faller, J. W.; Milheiro, S. C.; Parr, J. *J. Organomet. Chem.* **2008**, *693*, 1478-1493. b) Faller, J. W.; Wilt, J. C. *Org. Lett.* **2005**, *7*, 633-636.
- ²⁰ Jung, H. H.; Floreancig, P. E. *Org. Lett.* **2006**, *8*, 1949-1951.
- ²¹ Gauthier, R.; Axiotis, G. P.; Chastrette, M. *J. Organomet. Chem.* **1977**, *140*, 245-255.
- ²² Mahlokozera, T.; Goods, J. B.; Childs, A. M.; Thamattoor, D. M. *Org. Lett.* **2009**, *11*, 5095-5097. For a related reference on unexpected reactions of THF see Wang, X-S.; Zhou, J.; Yang, Ke.; Li, Y-L. *Tetrahedron Lett.* **2011**, *52*, 612-614.
- ²³ a) Davies, H. M. L.; Hansen, T.; Churchil, M. R. *J. Am. Chem. Soc.* **2000**, *122*, 3063-3070. b) Diaz-Requejo, M. M.; Belderrain, T. R.; Nicasio, M. C.; Trofimenko, S.; Pérez, P. J. *J. Am. Chem. Soc.* 2002, **124**, 896-897.
- ²⁴ K. Cheng, L. Huang and Y. Zhang, *Org. Lett.* **2009**, *11*, 2908-2911.
- ²⁵ Kim, D. Y.; Kong, M. S.; Lee, K. *J. Chem. Soc., Perkin Trans. 1* **1997**, 1361-1363.
- ²⁶ a) Kumar, G. D. K.; Saenz, D.; Lokesh, G. L.; Natarajan, A. *Tetrahedron Lett.* **2006**, *47*, 6281-6284. b) Xu, Y.; Qian, L.; Prestwich, G. D. *Org. Lett.* **2003**, *5*, 2267-2270. c) Hawkins, M. J.; Powell, E. T.; Leo, G. C.; Gauthier, D. A.; Greco, M. N.; Maryanoff, B. *Org. Lett.* **2006**, *8*, 3429-3431.
- ²⁷ a) Moody, C. J.; Whitham, G. H. *Reactive Intermediates*; OUP: Oxford, 2006. b) Anslyn, E. V.; Dougherty, D. A. *Modern Physical Organic Chemistry*; University Science Books: Sausalito, 2006, Chapter 10. c) Doyle, M. P.; Duffy, R.; Ratnikov, M.; Zhou, L. *Chem. Rev.* **2010**, *110*, 704-724.
- ²⁸ a) Hill, D. J. T.; Shao, L. Y.; Pomery, P. J.; Whittaker, A. K. *Polymer* **2001**, *42*, 4791-4802. b) Parsons, A. E. *An Introduction to Free Radical Chemistry*; Blackwell Science: Oxford, 2000. c) Troisi, L.; Granito, C.; Ronzini, L.; Rosato, F.; Videtta, V. *Tetrahedron Lett.* **2010**, *51*, 5980-5983.

-
- 29 a) Armarego, W. L. F.; Li Lin Chai, C. *Purification of Laboratory Chemicals*, 6th Ed.; Elsevier: Oxford, 2009, pp. 73. b) Hill, R. H.; Finster, D. *Laboratory Safety for Chemistry Students*; Wiley: Hoboken, 2010, pp. 5-56.
- 30 a) Robertson, A. *Nature* **1948**, *162*, 153. b) Nikishin, G. I.; Glukhovtsev, V. G.; Peikova, M. A.; Ignatenko, A. V. *Russ. Chem. Bull.* **1972**, *20*, 2202-2204. c) Kharasch, M. S.; Mosher, R. A.; Bengelsdorf, I. S. *Organophosphorus Chemistry* **1960**, *25*, 1000. d) Butters, M.; Harvey, J. N.; Jovver, J.; Lennox, A. J. J.; Lloyd-Jones, G. C.; Murray, P. M. *Angew. Chem., Int. Ed.* **2010**, *49*, 5156-5160.
- 31 Tsuji, S.; Kondo, M.; Ishiguro, K.; Sawaki, Y. *J. Org. Chem.* **1993**, *58*, 5055-5059.
- 32 Takagi, M.; Takikawa, H.; Mori, K. *Biosci. Biotechnol. Biochem.* **2001**, *65*, 2065-2069.
- 33 Mathey, F.; Savignac, P. *Tetrahedron* **1978**, *34*, 649-654.
- 34 Luo, X.; Zhang, H.; Duan, H.; Liu, Q.; Zhu, L.; Zhang, T.; Lei, A. *Org. Lett.* **2007**, *9*, 4571-4574.
- 35 a) Clemo, N. G.; Gedge, D. R.; Pattenden, G. *J. Chem. Soc., Perkin Trans. 1* **1981**, 1448-1453. b) Awang, D. V. C.; Wolfe, S. *Can. J. Chem.* **1969**, *47*, 706. c) Li, X.-C.; Ferreira, D.; Jacob, M. R.; Zhang, Q.; Khan, S. I.; Elsohly, H. N.; Nagle, D. G.; Smillie, T. J.; Khan, I. A.; Walker, L. A.; Clark, A. M. *J. Am. Chem. Soc.* **2004**, *126*, 6872-6873. Related procedures: Denney, D. B.; Song, J. *J. Org. Chem.* **1964**, *29*, 495-496.
- 36 a) Bungu, P. N.; Otto, S. *J. Organomet. Chem.* **2007**, *692*, 3370-3379. b) Allen, D. W.; Taylor, B. F. *J. Chem. Soc., Dalton Trans.* **1982**, 51-54.
- 37 Muller, A.; Otto, S.; Roodt, A. *Dalton Trans.* **2008**, 650-657.
- 38 Cogne, A.; Grand, A.; Laugier, J.; Robert, J. B.; Wisenfeld, L. *J. Am. Chem. Soc.* **1980**, *102*, 2238-2242.
- 39 a) Barder, T. E.; Buchwald, S. L. *J. Am. Chem. Soc.* **2007**, *129*, 5096-5101. b) Zhang, D.; Celeja, J. A.; Agua, A.; Doan, C.; Stewart, T.; Baú, R.; Selke, M. *Org. Lett.* **2010**, *12*, 3100-3103.
- 40 Arshad, M. N.; Tahir, M. N.; Asghar, M. N.; Khan, I. U.; Ashfaq, M. *Acta Crystallogr. Sect. E* **2008**, *64*, o1413.
- 41 a) Corbridge, D. E.C. *Phosphorus: An Outline of its Chemistry, Biochemistry and Technology*, 4th Ed; Elsevier: New York, 1990. b) Cameron, T. S.; Dahlèn, B. *J.*

-
- Chem. Soc., Perkin Trans. II* **1975**, 1737-1751. c) Schmidt, M. W.; Gordon, M. S. *J. Am. Chem. Soc.* **1985**, *107*, 1922-1930. d) Gilheany, D. G. *Chem. Rev.* **1994**, *94*, 1339-1374.
- 42 Ziemer, B.; Rabis, A.; Steinberger, H.-U. *Acta Crystallogr., Sect. C: Cryst. Struct. Commun.* **2000**, *56*, e-58-e59.
- 43 Gao, W.; Lin, J.; Akermark, B.; Sun, L. *J. Organomet. Chem.* **2007**, *692*, 1579-1583.
- 44 I-Farhan, K. A. *J. Cryst. Spectrosc.* **1992**, *22*, 687-689.
- 45 Tanaka, H.; Yamada, K-i.; Kawazura, H. *J. Chem. Soc., Perkin Trans. II* **1978**, 231-235.
- 46 Lipnick, R. L.; Garbisch, E. W., Jr. *J. Am. Chem. Soc.* **1973**, *95*, 6370-6375.
- 47 Porcel, S.; Bouhadir, G.; Saffon, N.; Marpn, L.; Bourissou, D. *Angew. Chem., Int. Ed.* **2010**, *49*, 6186-6189.
- 48 Ho, D. G.; Gao, R.; Celaje, J.; Chung, H-Y.; Selke, M. *Science* **2003**, *302*, 259-262.
- 49 Sekiya, M.; Ito, K.; Suzuki, K. *Tetrahedron* **1975**, *31*, 231-233
- 50 a) Vaz, A. D. N.; Schoellmann, G. *J. Org. Chem.* **1984**, *49*, 1286-1288. b) Guy, A.; Lemaire, M.; Guetté, J-P. *Synthesis* **1982**, 1018-1020.
- 51 a) Fu, G. C. *Acc. Chem. Res.* 2008, *41*, 1555-1564. b) Littke, A. F.; Fu, G. C. *Angew. Chem., Int. Ed.* **1998**, *37*, 3387-3388.
- 52 Netherton, M. R.; Fu, G. C. *Org. Lett.* **2001**, *3*, 4295-4298.
- 53 Altava, B.; Burgueta, M. I.; García-Verdugo E.; Luis, S. V.; Miravet, J. F.; Vicent, M. J. *Tetrahedron: Asymmetry* **2000**, *11*, 4885-4893.
- 54 Sondengam, B. L.; Fomum, Z. T.; Charles, G.; Akam, T. M. *J. Chem. Soc., Perkin Trans. I* **1983**, 1219-1221.
- 55 Zhang, H.; Luo, X.; Wongkhan, K.; Duan, H.; Li, Q.; Zhu, L.; Wang, J.; Batsanov, A. S.; Howard, J. A. K.; Marder, T. B.; Lei, A. *Chem. Eur. J.* **2009**, *15*, 3823-3829.
- 56 Van Overschelde, M.; Vervecken, E.; Modha, S. G.; Cogen, S.; Van der Eycken, E.; Van der Eycken, J. *Tetrahedron* **2009**, *65*, 6410-6415.
- 57 Li, X-C.; Ferreira, D.; Jacob, M. R.; Zhang, Q.; Khan, S. I.; ElSohly, H. N.; Nagle, D. G.; Smillie, T. J.; Khan, I. A.; Walker, L. A.; Clark, A. M. *J. Am. Chem. Soc.* **2004**, *126*, 6872-6873.

-
- ⁵⁸ Kuse, M.; Isobe, M. *Tetrahedron* **2000**, *56*, 2629-2639.
- ⁵⁹ Schiemenz, G. P.; Kaack, H. *Justus Liebigs Ann. Chem.* **1973**, *9*, 1480-1482.
- ⁶⁰ Blank, B.; DiTullio, N. W.; Deviney, L.; Roberts, J. T.; Saunders, H. L. *J. Med. Chem.* **1975**, *18*, 952-954.
- ⁶¹ Takagi, M.; Takikawa, H.; Mori, K. *Biosci. Biotechnol. Biochem.* **2001**, *65*, 2065-2069.
- ⁶² Smart diffractometer control software (v5,625), Bruker-AXS, Bruker AXS GmbH, Karlsruhe, Germany.
- ⁶³ Saint+ (v6.22) Bruker AXS, Bruker AXS GmbH, Karlsruhe, Germany.
- ⁶⁴ Sheldrick, G. M. SHELXS-97, Program for solution of crystal structures, University of Göttingen, Germany, 1997.

Chapter 3: Late-transition metal complexes of dbaPHOS and monodbaPHOS

The target ligands, dbaPHOS, **127**, and monodbaPHOS, **128**, can be regarded as multidentate ligands. They are able to bind through the phosphine, alkene and possibly even the carbonyl group. As shown in the introduction chapter, phosphino-alkene ligands have been utilised in both Pd- and Rh-catalysed reactions successfully. In this chapter coordination studies involving Pd and Rh are described. These allow one to obtain a greater understanding of the ligand environment created around the metal centre, which could be used to inform any catalytic studies. The platinum complexes were also studied, as the NMR active platinum nuclei can provide confirmation of structural analysis, *e.g.* *cis* versus *trans* coordination of phosphines.

3.1 Palladium and platinum complexes with dbaPHOS

The target ligand dbaPHOS, **127**, has five possible coordination sites. Alkenes are often considered as hemilabile moieties compared to phosphines (although the extent of hemilability depends on the metal centre).¹ It was anticipated that the coordination of the alkene would depend on the metal centre and its oxidation state. The dba compound itself is seen to either coordinate through the carbonyl with Lewis acids and uranium (**160**),² or through its alkenes with late-transition metals such as Pd (**162** and **24**), Pt and Rh (**161**) (Figure 1).³ In the $[\text{Pd}_2\text{dba}_3]$ complex the dba ligand acts as a bridging ligand between two Pd centres with the alkenes bound to different Pd atoms.⁴ If another ligand is on the Pd, such as bipy in $[\text{Pd}(\text{bipy})(\text{dba})]$, only one alkene of the dba coordinates.⁵ In $[\text{RhCp}^*(\eta^4\text{-dba})]$ both alkenes are bound to one η Rh atom.⁶ All possible geometries are observed: *s-cis,s-cis*, *s-cis,s-trans*, *s-trans,s-trans*.

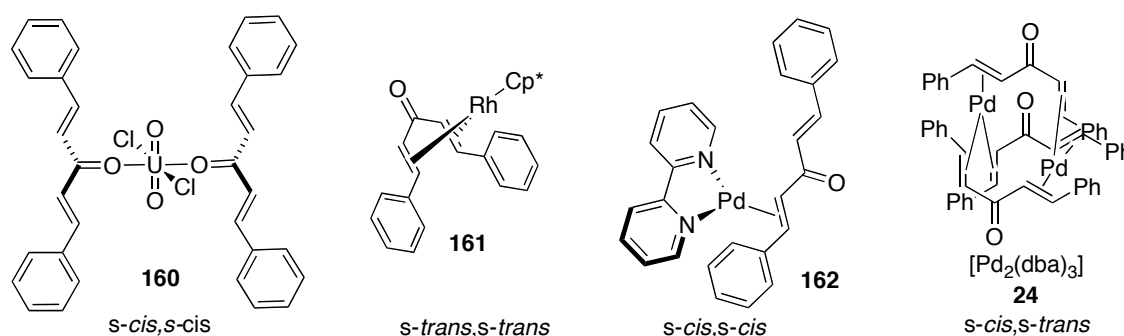
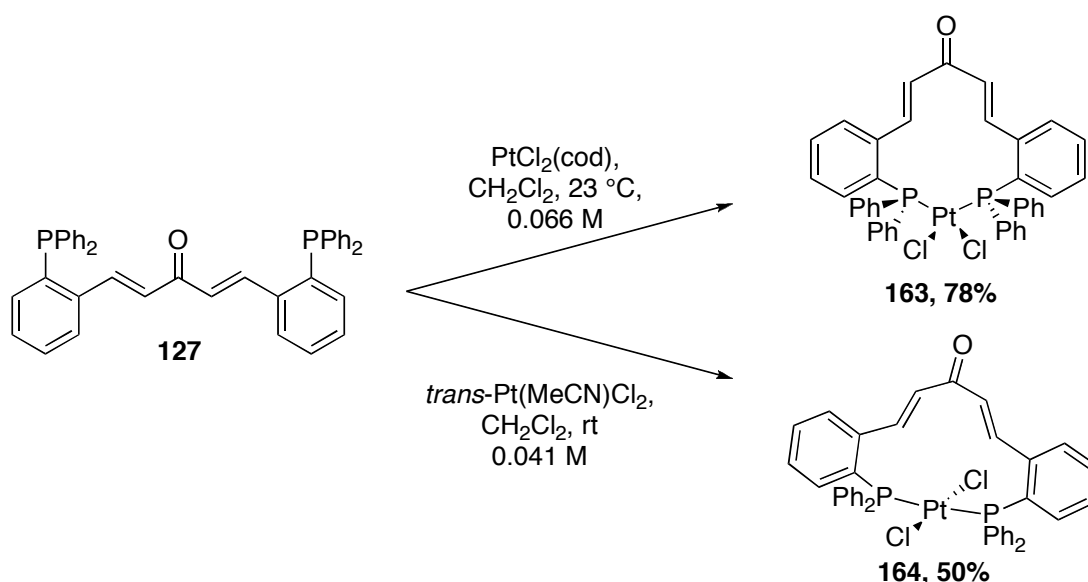


Figure 1: Coordination of dba to metal centres.

In our ligands, the phosphines would be expected to be the most strongly coordinating moiety to late transition metals. The coordination of the alkenes and/or the carbonyl will depend on the oxidation state (e.g. Pt⁰/Pd⁰ are expected to be more likely to coordinate the alkene than Pt^{II}/Pd^{II}), the other ligands around the metal, the coordination number of the complex and the geometry of the ligand backbone as compared to the rest of the complex.

3.1.1 Pt^{II} and Pd^{II} complexes

Platinum(II) and Palladium(II) complexes are mostly square-planar.⁷ Common starting materials to these complexes include [MCl₂(cod)] and [MCl₂(MeCN)₂], where upon addition of dbaPHOS, **127**, one would expect the phosphines to displace the labile cod or MeCN ligands to give the corresponding [MCl₂(P-P)] complexes.



Scheme 1: Platinum(II) complexes of dbaPHOS.

Platinum(II) complexes of dbaPHOS were prepared from both [PtCl₂(cod)] and [PtCl₂(MeCN)₂] (Scheme 1). Initial attempts using [PtCl₂(cod)] gave an insoluble material which was possibly polymeric; on reducing the reaction concentration to ~0.07 M a product partially soluble in CH₂Cl₂ (~2 mg in 1 mL) was formed. The single peak in the ³¹P NMR spectrum indicated that the two phosphorus centres were in the same environment and therefore the ligand acts as a symmetrical bidentate phosphine ligand. The ¹J_{PtP} coupling value can be used to identify *cis* vs. *trans* coordination of the two phosphines in a square planar complex. Typically, if the phosphines in [PtCl₂(PR₃)₂]

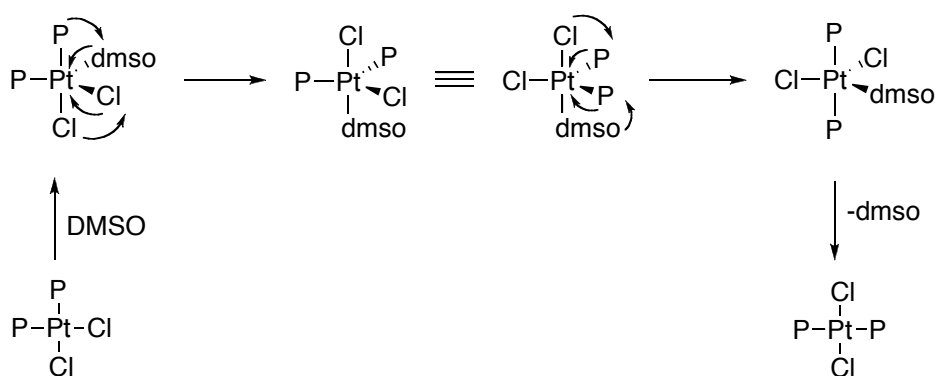
are *trans* a coupling constant of 1500-3000 Hz would be expected, whereas the coupling constant for a *cis* complex would be higher, >3500 Hz in most cases (see Table 1).⁸

Table 1: ³¹P chemical shifts and ¹J_{PtP} values of common *cis* and *trans*-PtCl₂(PR₃)₂ and PtCl₂(P-P) complexes.

Complex	δ _P , ppm, (CDCl ₃)	¹ J _{PtP} , Hz
<i>cis</i> -[PtCl ₂ (PEt ₃) ₂] ⁹	9.6	3520
<i>trans</i> -[PtCl ₂ (PEt ₃) ₂] ¹⁰	13.1	2490
<i>cis</i> -[PtCl ₂ (PPh ₃) ₂] ⁹	14.3	3673
<i>trans</i> -[PtCl ₂ (PPh ₃) ₂] ⁹	19.8	2637
<i>cis</i> -[PtCl ₂ (dppm)] ¹¹	-64.2	3084
<i>cis</i> -[PtCl ₂ (dppe)] ¹¹	40.8	3616
<i>cis</i> -[PtCl ₂ (biphep)] ¹²	7.9 ^a	3610
<i>cis</i> -[PtCl ₂ (DPEPhos)] ¹³	19.7 ^b	3796
<i>cis</i> -[PtCl ₂ (XantPHOS)] ¹⁴	7.1	3693
<i>trans</i> -[Pt(¹³ CN) ₂ (XantPHOS)] ¹⁴	5.5 (t, J _{PC} = 14.1 Hz)	2612

^a CD₂Cl₂, ^b CHCl₃

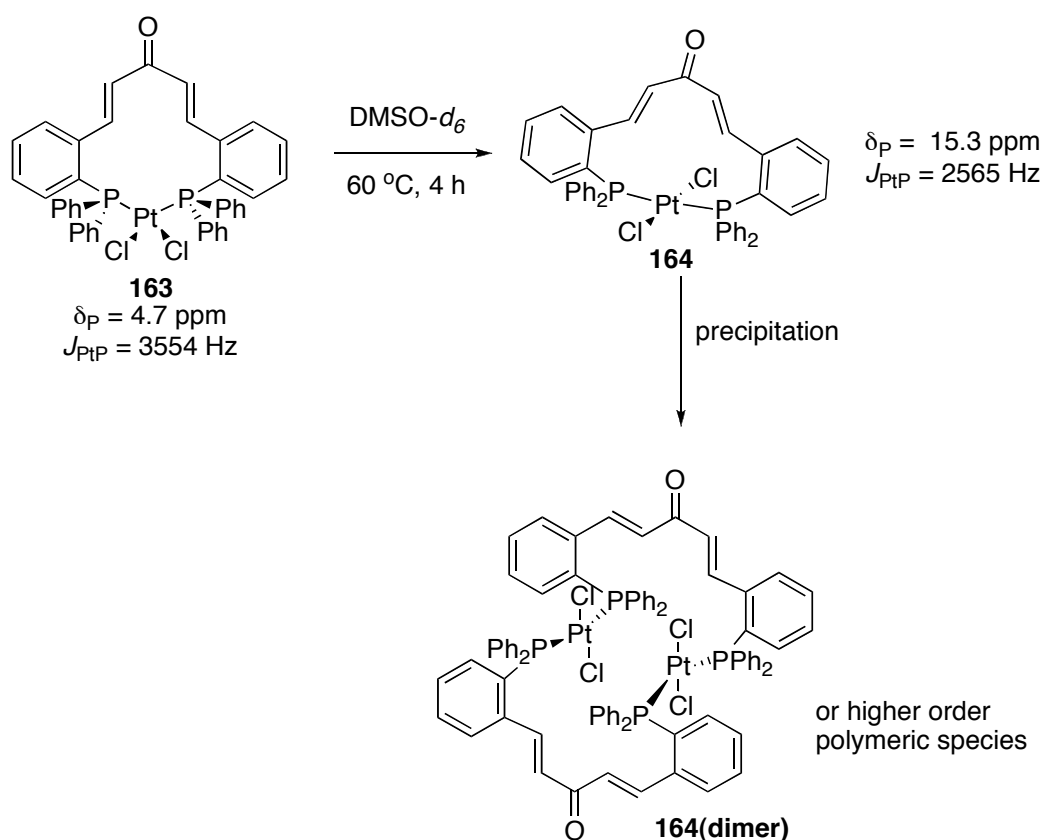
In CD₂Cl₂, the ¹J_{PtP} coupling constant of the complex from [PtCl₂(cod)] (complex **163**) is 3553 Hz indicating that the phosphines are *cis* to each other (as shown in Scheme 1). The crystal structure of **163** supports this (Figure 4). If **163** is dissolved in *d*₆-DMSO it quickly starts to isomerise to a *trans* complex with a J_{PtP} value of 2565 Hz. On heating to 60 °C for 4 h **163** completely isomerises to the *trans* complex (**164**).



Scheme 2: Berry pseudorotation in the isomerisation of square-planar complexes.

Extensive investigations into the mechanism of *cis-trans* isomerisation in square-planar platinum complexes have been reported in the literature.¹⁵ The most commonly observed mechanism proceeds by an associative path, especially when coordinating

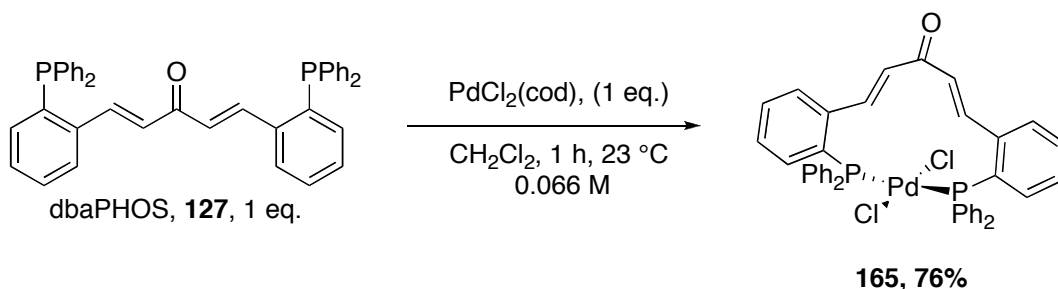
solvents are present (see Scheme 2). In light of these studies it is proposed that the DMSO coordinates to the platinum(II). The resulting five-coordinate complex can then undergo Berry pseudorotation¹⁶ to give the phosphines *trans* to each other, followed by dissociation of the DMSO. No free phosphine or intermediate complexes are observed by ³¹P NMR spectroscopy, suggesting this process is faster than the NMR timescale. After the formation of the soluble *trans*-monomeric complex, a precipitate is seen to form. It is proposed that this is a dimeric (such as **164(dimer)**) or higher order polymeric species (Scheme 3).



Scheme 3: Isomerisation of *cis*-[PtCl₂(dbaPHOS)] in DMSO.

Complex **164** could also be synthesised directly from *trans*-[PtCl₂(MeCN)₂] to give a product with $^1J_{PtP} = 2577 \text{ Hz}$ indicating the phosphines are *trans* to each other. From the NMR evidence it is unclear whether complex **164** is a monomeric or dimeric platinum complex in the bulk material. From the ¹H NMR spectrum the ligand is still observed as being symmetrical, suggesting that the dba backbone must either be in the *s-cis,s-cis* or *s-trans,s-trans* geometry. Due to its insolubility in DMSO compared with the *cis*-[PtCl₂(dbaPHOS)] complex, and the observation of a precipitate following the formation of *trans*-[PtCl₂(dbaPHOS)], we believe it is more likely to be the binuclear

complex in the bulk insoluble material. The species in the ^1H NMR spectrum is still most likely the mononuclear complex from the evidence available. Comparison of the melting points of the bulk material of **163** and **164** also supports this conclusion, **164** melts (decomposes) at 230 °C whilst **163** melts (decomposes) at a substantially lower temperature, 140 °C. This is a larger difference than you would expect if they were just the *cis*- and *trans*-isomers.



Scheme 4: Synthesis of [PdCl₂(dbaPHOS)].

Complex **165** was prepared from [PdCl₂(cod)] in the same manner as the platinum complexes. The ^{31}P NMR spectrum shows a singlet at 19.45 ppm, showing that the phosphorus environments are the same. Compared to Pt complexes it is harder to determine if the complex is *cis* or *trans*. The ^{31}P NMR chemical shift is nearer that of complex **164** (14.89 ppm) than complex **163** (4.72 ppm), suggesting it is the *trans* complex. The ^1H NMR spectra are also very similar to the *trans* complex obtained from *trans*-[PtCl₂(MeCN)₂] (spectra b and c in Figure 2). The solid-state ^{31}P NMR spectrum shows a slightly distorted “solution” AB multiplet with $J_{\text{PP}} = 540 \text{ Hz}$. Crucially, the large size of the PP spin-spin coupling constant is indicative of a *trans*-chelating phosphine.¹⁷

Once again it is not possible to tell from the NMR spectroscopic analysis if **165** is the monomeric complex as shown in Scheme 4, or a dimeric/polymeric species. The melting point is higher than that of complex **164**, once again possibly indicating that it is a dimeric compound. The ^1H NMR spectra of **163**, **164** and **165** indicate that the highest resonating alkene protons have shifted downfield on coordination to M^{II} . In complex **163** the alkene protons (H(7) and H(11) in the crystal structure) have shifted by +1.52 ppm compared to the free phosphine (9.82 vs. 8.30 ppm), whereas in complex **164** and **165** the shifts are only +0.6 and +0.4 ppm, respectively. This could be evidence of a proton-metal interaction, in particular in **163**.

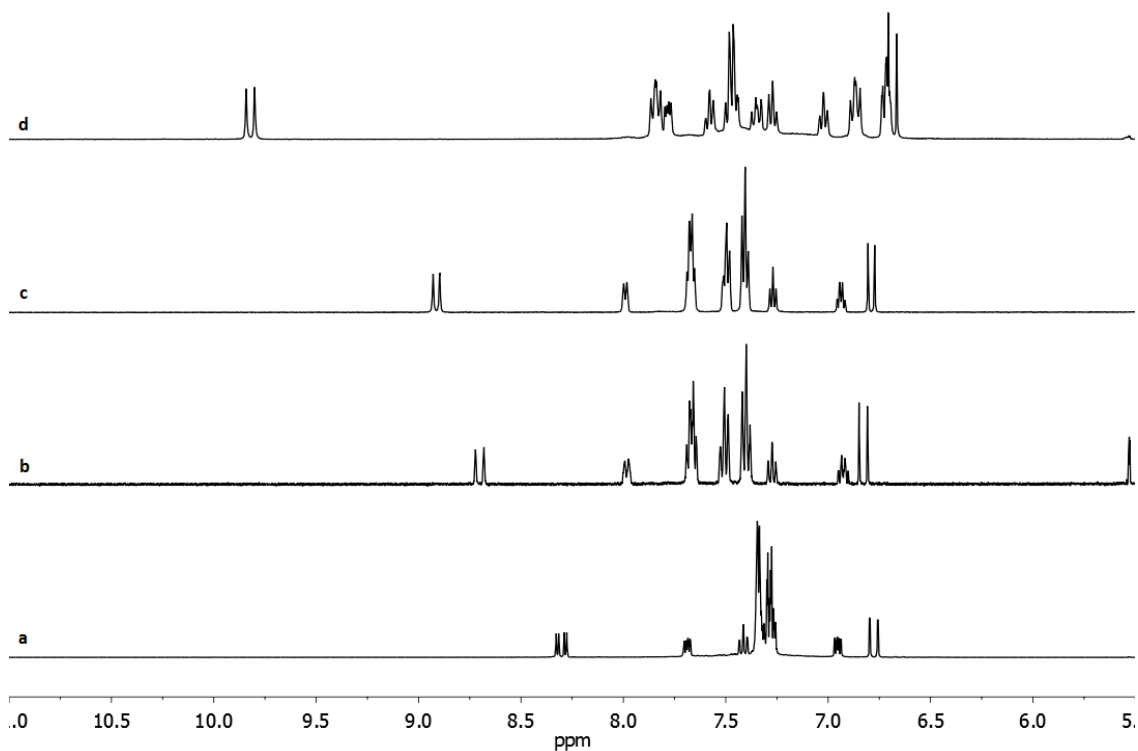


Figure 2: (a) dbaPHOS (400 MHz, CD₂Cl₂), (b) [PdCl₂(dbaPHOS)] (400 MHz, CD₂Cl₂), (c) *trans*-[PtCl₂(dbaPHOS)] (500 MHz, CD₂Cl₂), (d) *cis*-[PtCl₂(dbaPHOS)] (400 MHz, CD₂Cl₂).

In all cases the complexes were not soluble enough in CH₂Cl₂ or DMSO to get fully resolved ¹³C NMR spectra. The ¹³C NMR spectrum of **163** showed numerous multiplet signals, which appeared to be triplets or overlapping doublets; however, due to the low signal-noise ratio this could not be confirmed. Triplet-like multiplets have been reported in ¹³C NMR of Ni and Pt phosphine complexes previously, and are attributed to the magnetic inequivalence of chemically equivalent ¹³C environments.¹⁸ The solid-state ¹³C NMR spectra were obtained for complexes **163** and **165**. As expected the majority of the carbons are within the aromatic region, with only the carbonyl signal distinct. In complex **163** the carbonyl was observed at 192.2 ppm, and in **165** at 194.3 ppm, where you would expect carbonyl shifts (the ¹³C chemical shift of the carbonyl of dbaPHOS in CD₂Cl₂ is 188.7 ppm).

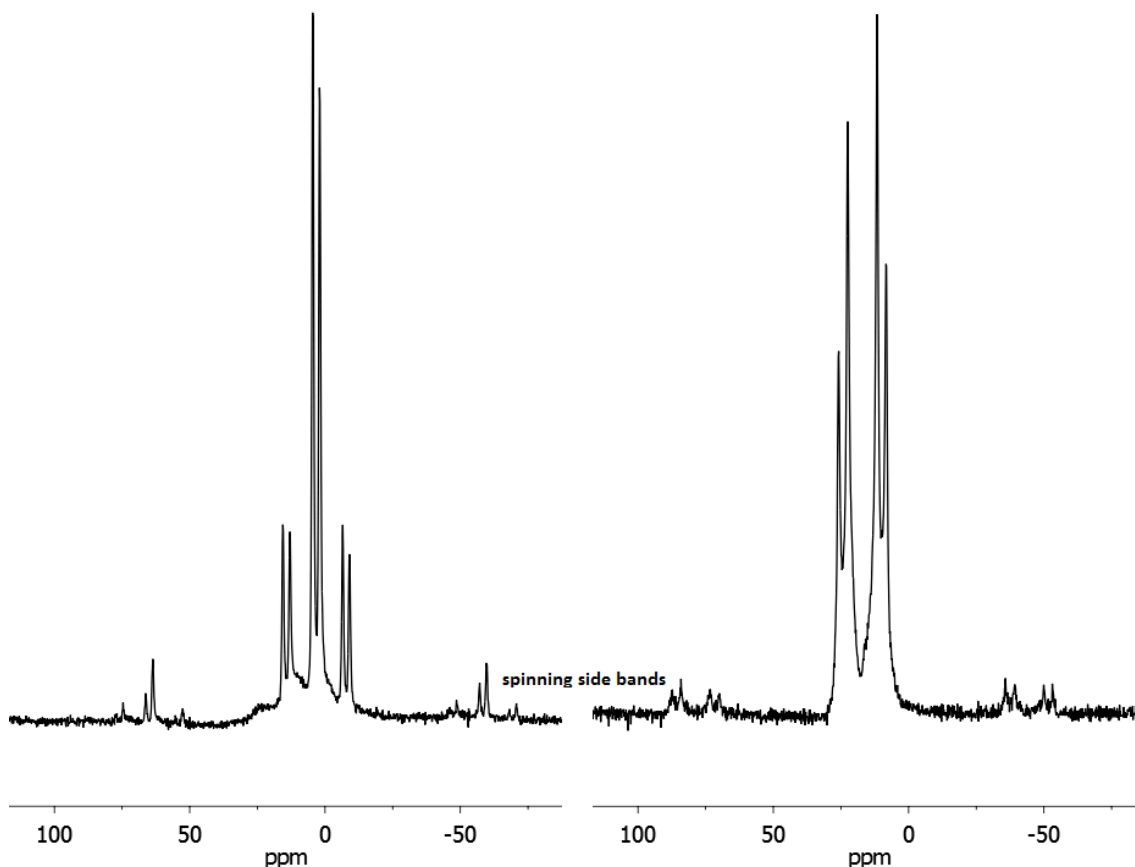


Figure 3: Solid-state ^{31}P CPMAS-NMR spectroscopic analysis of *cis*-[PtCl₂(dbaPHOS)], **163** (left) and *trans*-[PdCl₂(dbaPHOS)], **165** (right).

The elemental analysis of these metal complexes was always too low on carbon. Along with their insolubility it was possible that we had a mix of monomers, dimers and polymeric material. Solid-state ^{31}P NMR spectroscopic analysis was carried out on the material to see if there was any indication of polymeric material such as extra phosphorus signals for end of chain versus middle chain phosphorus atoms, or broad signals indicating a lack of long range order. In the case of complex **163** two slightly different signals with Pt satellites were observed (1.9 and 4.4 ppm, $^1J_{\text{PtP}} = 3590$ Hz, 1:4:1 pattern), and a broad signal centred ~ 10 ppm. The singlets are assigned to the two phosphorus atoms that are in slightly different environments in the solid-state (see the X-ray crystal structure in Figure 4), whilst the broad signal could be due to polymeric side products of varying composition. This would explain the lack of consistency with the elemental analysis. In the solid-state ^{31}P NMR spectroscopic analysis of complex **165** there was no evidence for polymeric material. As a result a different explanation for the lack of agreement with the elemental analysis is needed. The ^1H NMR spectrum (solution-state) clearly shows there are no organic impurities; other possibilities include

that there are inorganic impurities, *e.g.* PdCl₂, the compounds are hygroscopic (H₂O was observed in IR spectra) or the complexes are not combusting well.

Crystals of complex **163** suitable for X-ray diffraction were obtained by slow evaporation from a solution of **163** in CD₂Cl₂ (Figure 4). The ligand acts as a wide bite angle bidentate phosphine. The P-Pt-P bite angle is fairly large (105.9°), which is similar in size to the bite angles quoted for other wide bite angle ligands such as Xantphos, DPEPhos, Trost ligand, and POP ligands (107-112° calculated for Pt(allyl) complexes).¹³ A comparison of the bite angle of Xantphos, **6**, and dbaPHOS, **127**, on PtCl₂ shows that dbaPHOS has the larger bite angle by 5° (Table 2). A search of CSD for [PtCl₂(P)(P)] gave 549 hits (638 observations),¹⁹ the majority of P-Pt-P angles were in the region associated with *cis*-coordination modes (68-115°). It shows that the dbaPHOS bite angle on PtCl₂ is one of the largest *cis*-coordinating bidentate phosphines, with only six other crystal structures recorded with bidentate phosphine bite angles the same size or larger.²⁰

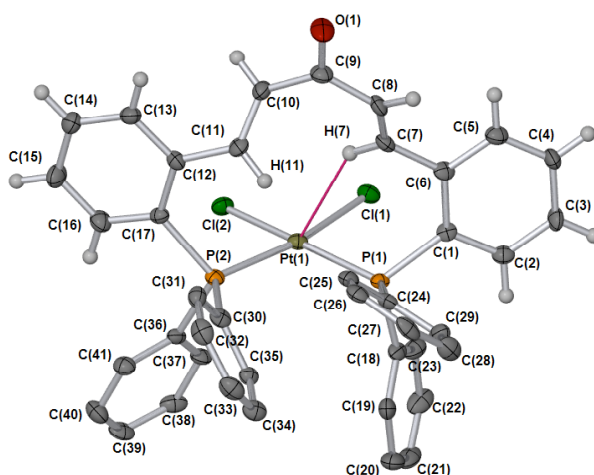
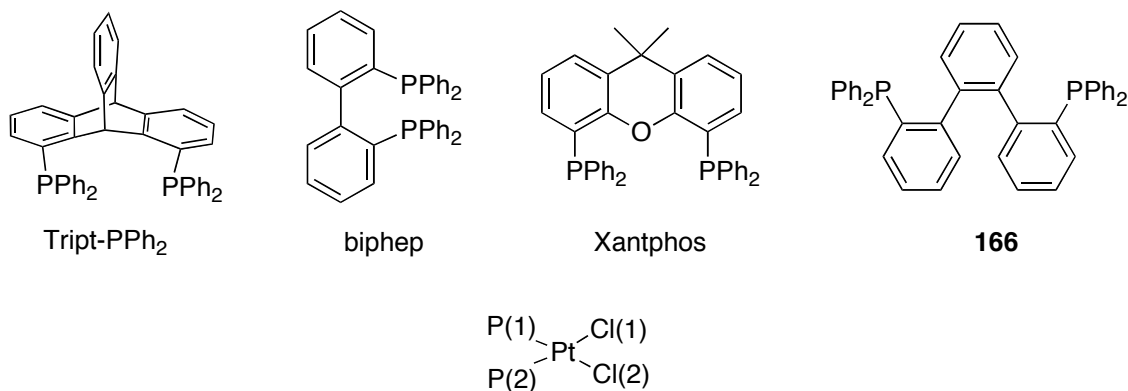


Figure 4: X-ray crystal structure of *cis*-PtCl₂(dbaPHOS) (163**). Selected hydrogen atoms removed for clarity.** Thermal ellipsoids shown at 50%. Selected angles (°) include: P(2)-Pt(1)-P(1) = 105.89(5), P(2)-Pt(1)-Cl(2) = 81.18(5), P(1)-Pt(1)-Cl(2) = 169.71(4), P(2)-Pt(1)-Cl(1) = 167.60(4), P(1)-Pt(1)-Cl(1) = 86.49(5), Cl(2)-Pt(1)-Cl(1) = 86.45(5).

Other angles of interest in the crystal structure of **163** include the dihedral angle of the (P, P, Pt, Cl, Cl) plane and (P, P, C=O) plane, which is 83.2° showing that overall the ligand backbone is almost perpendicular to the square-planar Pt. In *cis*-[PtCl₂(XantPHOS)] the backbone is almost perpendicular to the (P, P, Pt, Cl, Cl) plane, the dihedral angle between the (P, P, Pt, Cl, Cl) plane and (P, P, C2, C12) plane is 86.8°. If the same two planes are used for **163** ((P, P, Pt, Cl, Cl) and (P1, P2, C1, C17)) the dihedral angle is now calculated to be 61.0°. The difference in the two dihedral

angles for **163** shows that there is considerable twist in the ligand backbone. This is also supported by the large dihedral angle of C7-C8-C10-C11, 47.01°, which brings about a twist of the alkenes around the 1,4-dien-3-one.

Table 2: Table showing the bond lengths around the metal for *cis*-PtCl₂(dbaPHOS) and comparing it to other phosphine complexes.



<i>Cis</i> -Complex	Bond Lengths, Å				Bond Angle
	P(1)-Pt	P(2)-Pt	Cl(1)-Pt	Cl(2)-Pt	P(1)-Pt-P(2)
PtCl ₂ (dbaPHOS), 163	2.2802(13)	2.2534(14)	2.3592(13)	2.3395(12)	105.89(5)
PtCl ₂ (PPh ₃) ₂ ²¹	2.2713(9)	2.2515(8)	2.3632(8)	2.3294(9)	99.12(3)
PtCl ₂ (dppe) ²²	2.208(6)	2.208(6)	2.341(6)	2.355(6)	86.3
PtCl ₂ (biphep) ²³	2.248(2)	2.236(2)	2.345(2)	2.354(2)	93.40(6)
PtCl ₂ (Xantphos) ²⁴	2.253(3)	2.264(2)	2.354(2)	2.348(2)	100.87(8)
PtCl ₂ (166) ²⁵	2.2576(10)	2.2638(10)	2.3577(11)	2.3522(11)	105.82(4)
PtCl ₂ (Tript-PPh ₂) ²⁶	2.2392(12)	2.2391(12)	2.3339(13)	2.3339(13)	107.54(6)

The X-ray crystal structure shows that the dbaPHOS, **127**, is not symmetrical around the Pt as shown by the difference of 0.0268(19) Å in the two P-Pt bond lengths. The longest P-Pt bond is *trans* to the shortest Pt-Cl bond, and *vice versa*. The P-Pt bonds are on the longer side of the P-Pt lengths seen in platinum chloride phosphine complexes. A search of the CSD reveals that the mean P-Pt distance in *cis* complexes is 2.233 Å (see Appendix 5), which is shorter than both the distances seen in [PtCl₂(dbaPHOS)]. The Pt-Cl distances are within the majority of observed distances (LQ = 2.333 Å, HQ = 2.374 Å, see Appendix 5).

It can be seen that the C-C double bonds in the ligand backbone are within error of each other, although compared to the free ligand one of the alkene bonds is the same whilst the other is now longer. The shorter alkene (C7-C8) also displays a fairly short Pt-H interaction, 2.642 Å. This provides further evidence of a metal-proton interaction in these complexes.

Table 3: Comparison of the bond lengths in dbaPHOS, 127, and complex 163.

Bond	dbaPHOS, 127	<i>cis</i> -PtCl ₂ (dbaPHOS), 163
C=O	1.214(3)	1.230(6)
C=C	1.324(2)	1.329(7), 1.348(7)
C-P	1.8438(14)	1.823(5), 1.845(5)

3.1.2 DFT studies on *cis*-Pt(dbaPHOS)Cl₂

Interactions between N-H and C-H bonds and transition metals have been well recognised.²⁷ Two different types of interactions have been clearly identified, agostic and anagostic interactions.²⁸ Agostic interactions refer to 3-center-2-electron interactions and are characterised by small M---H bond lengths (ca. 1.8-2.3 Å), small C-H-M bond angles (ca. 90-140°), and an upfield shift in δ_{H} of the CH upon coordination, along with low $^1J_{\text{CH}}$ values. Agostic interactions require the metal centre to be coordinately unsaturated, with an empty orbital available for σ -donation from the C-H bond. The term “anagostic” was used by Lippard and co-workers to describe any C-H---M interactions that were not agostic.²⁹ Other terms such as “pregostic” have been used, and anagostic interactions also cover those described by hydrogen bonding. Anagostic interactions are characterised by larger M---H distances (ca. 2.3-2.9 Å), larger C-H-M angles (ca. 110-170°) and by a downfield shift in δ_{H} of the CH upon coordination (a general feature of hydrogen bonds). Anagostic interactions do not need an empty orbital and therefore can involve 18 electron metal centres. For d₈ square planar complexes either agostic or anagostic interactions are able to occur. While the N-H---M(d⁸) interactions can be confidently described with a 3-center-4-electron bond (hydrogen bond), the C-H---M(d⁸) interactions are believed to be much more complicated. It has been proposed that a weak hydrogen bond is involved.^{27a}

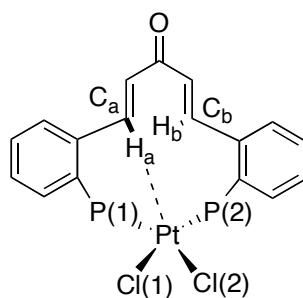
The experimental data for complex **163** shows a Pt-H interaction of 2.642 Å in the crystal structure, and a downfield shift of the H(7) and H(11) protons in the ^1H NMR spectrum, suggesting an anagostic interaction of some sort is present. Using theoretical calculations we wished to gain a greater understanding of this interesting interaction. It was also clear from the ^1H NMR spectrum that the exchange of the H(7) and H(11) protons was rapid, as the spectrum was sharp and with only one signal observed for these protons. DFT calculations were performed in collaboration with Zhang and Lin (HKUST, Hong Kong) with no simplification of complex **163**, to gain an insight into the nature of the short platinum-proton interaction and the exchange process shown in Scheme 5.



Scheme 5: Rapid exchange of Pt---Ha/b.

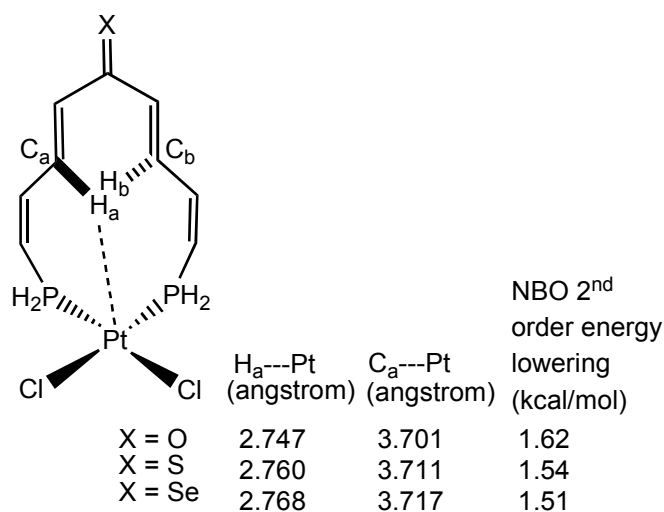
Density functional theory calculations at the MPW1PW91 level were carried out to optimize all of the complexes studied.³⁰ This level of theory plus the basis set described below has been confirmed to give good results regarding C-H---M(d^8) interactions.^{27b} The intrinsic reaction coordinate (IRC)³¹ analysis was also carried out to confirm that all stationary points are smoothly connected to each other. Gibbs free energy at 298.15 K was obtained on the basis of the frequency calculations. The SDD basis set with the Stuttgart relativistic effective core potentials was used in the calculations.^{30a} An additional d polarization shell was added for Cl, P, S and Se, with exponents of 0.640, 0.387, 0.503 and 0.364, respectively. All calculations were performed with Gaussian 03 packages.³²

The structure of complex **163** was optimised. The calculated structural values agree with the experimental ones (Table 4). The largest deviation was seen between the calculated and experimental C-H_a---Pt distances. This might be expected as the hydrogen atoms were placed using a “riding model”. As the calculated C_a---Pt and C_b---Pt distances were in good agreement with the experimental it is believed that the calculated C-H---Pt is more realistic than the experimental value.

Table 4: Comparison of experimental and calculated bond lengths in complex 163.

Bond	Experimental	Calculated	Difference
Pt---H _a	2.642	2.543	0.099
Pt---C _a	3.425	3.450	-0.025
Pt---C _b	3.485	3.480	0.005
Pt-P(1)	2.2802(13)	2.353	-0.0728
Pt-P(2)	2.2534(14)	2.347	-0.0936
Pt-Cl(1)	2.3592(13)	2.406	-0.0468
Pt-Cl(2)	2.3395(12)	2.401	-0.0615

The barrier for the exchange was calculated to be 1.04 kcalmol⁻¹ in electronic energy and 1.16 kcalmol⁻¹ in free energy, which is consistent with the experimental observation that the exchange is very rapid. It is also consistent with a previously reported theoretical estimates of a C-H---Pd(II) interaction of 0.8 kcalmol⁻¹.³³

**Figure 5: NBO results for a simplified model.**

In order to understand the nature of the C-H---Pt interactions, natural bond orbital (NBO) analyses³⁴ were carried out on the basis of the electronic structures calculated for the complex **163**. No appreciable Wiberg bond index³⁵ (a measure of bond strength)

was seen for the close C-H---Pt contact. However, an appreciable second order perturbation energy related to the donor-acceptor interaction of $\text{Pt}(\text{dz}^2)\rightarrow\text{C}_a\text{-H}_a(\sigma^*)$ (where, z is defined as the axis perpendicular to the square plane of the complex studied)³⁴ was found. This second order energy lowering was calculated to be 1.59 kcalmol^{-1} , which points to the involvement of a weak hydrogen bond. The second order energy lowering is a measure of the donor-acceptor interaction.³⁶ To further support the notion of a weak hydrogen bond, the C-H---Pt contact distances for the simplified model complexes shown in Figure 5 were calculated and the relevant NBO analysis performed. The results indicate that the less electronegative X is ($X = \text{O}, \text{S}$ and Se), the longer the C-H---Pt contacts are and a smaller second order energy lowering is observed. The changes along the series of different X are only marginal suggesting the C-H---Pt interactions are weak.

The results from the NBO analysis are consistent with both the small energies calculated from DFT for the exchange and with the experimental observations. A deshielded proton resonance for H_a/H_b is seen in the ^1H NMR spectrum of **163** with respect to the free ligand. In light of the calculations, the deshielding effect in **163** can be attributed to a weak hydrogen bond resulting from the $\text{Pt}(\text{dz}^2)\rightarrow\text{C}_a\text{-H}_a(\sigma^*)$ interaction.

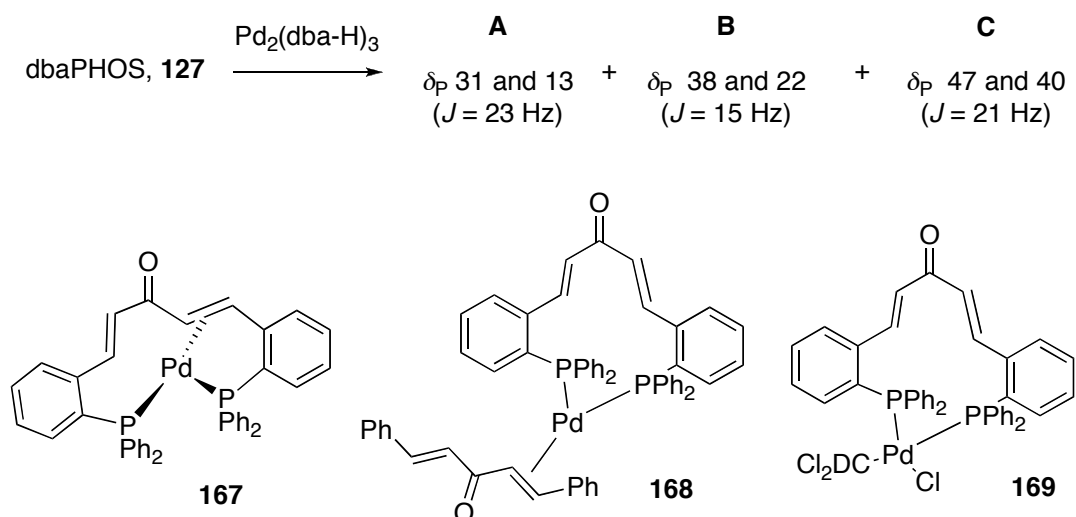
3.1.3 Pd^0 and Pt^0 complexes

As expected no coordination of the alkene was observed in the square-planar Pt^{II} and Pd^{II} complexes of dbaPHOS, **127**. It was anticipated that by changing to Pt^0 and Pd^0 , alkene coordination would be observed.

Initially, NMR scale experiments with dbaPHOS, **127** and $[\text{Pd}_2\text{dba}_3]$ were carried out in a number of solvents (at 20-55 mM conc.). In all cases a mixture of different phosphorus signals were observed, including broad peaks at 30 and -15 ppm (Scheme 6). In THF/ CD_2Cl_2 the peaks attributed to **A** and **B** were clearly seen. On changing the solvent to THF/acetone- d_6 only the peaks of **A** were clearly seen. As a result **A** and **B** were initially assigned as **168** and **169**, respectively. However, the independent preparation of **167** (see below) showed that **A** corresponded to **167**. The addition of dba to **167** led to the peaks attributed to **B**, meaning that **B** corresponds to **168**, not **169** as initially thought. However, there is a substantial difference in the chemical shifts of **168**

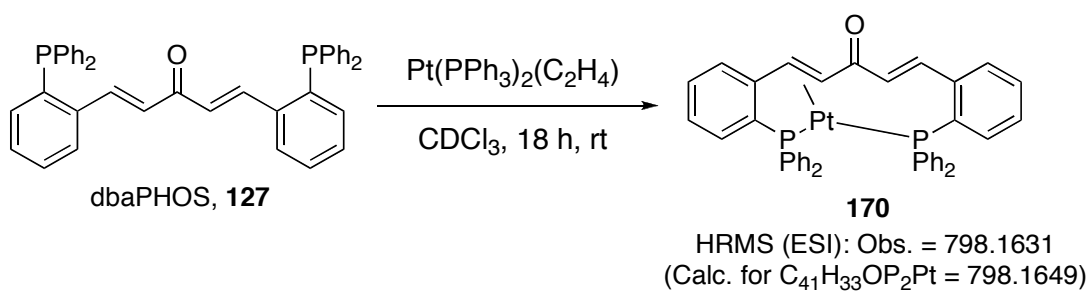
(B) compared to $[\text{Pd}(\eta^2\text{-dba})(\text{PPh}_3)_2]$ (unresolved doublets at 28.2 and 26.0 in d_8 -toluene).³⁷

On leaving a sample of **167** in CDCl_3 the peaks corresponding to **C** were observed, it was thought these could correspond complex **169**. However, similar peaks were also observed in the reaction of Pd_2dba_3 and dbaPHOS in benzene. On heating the complex **167** in CD_2Cl_2 to 55 °C for 48 h, similar peaks to those of **C** were observed at 47 and 40 ppm ($J = 22$ Hz) as well as peaks corresponding to another complex at 39 and 22 ppm ($J = 21$ Hz). It is therefore unclear what complex the peaks for **C** might correspond to, as similar peaks have been observed both in the presence and absence of chlorinated solvent.



Scheme 6: NMR study on dbaPHOS and $\text{Pd}_2(\text{dba-H})_3$.

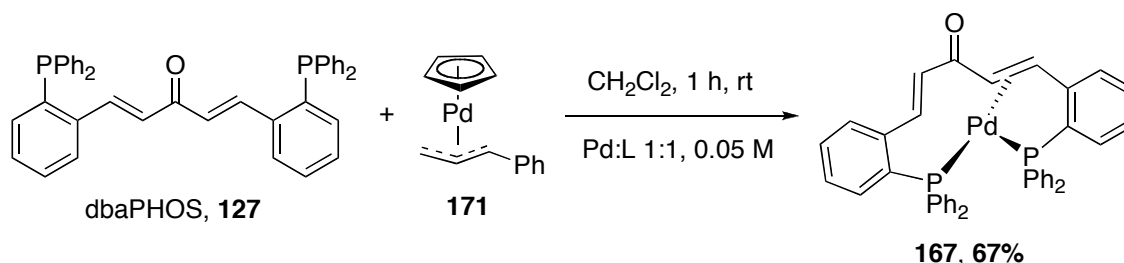
Using Pt_2dba_3 in benzene with dbaPHOS also leads to a mixture of products. Regardless of M:L ratio, free ligand was always observed, suggesting incomplete solvation of the metal complex or that the metal complex was contaminated by nanoparticles. A number of new peaks were observed in the ^{31}P NMR spectrum including a peak at 21.2 ppm with Pt satellites ($J_{\text{Pt-P}} = 3127$ Hz), and a new peak at -15 ppm without any satellites.



Scheme 7: Complexation study of dbaPHOS with Pt^0 .

The use of $\text{Pt(PPh}_3)_2(\text{C}_2\text{H}_4)$ as the metal precursor also led to a mixture of products. The ^1H NMR spectrum was very unclear due to the large number of aromatic protons from the triphenylphosphine and the ligand **127**. The ^{31}P NMR spectrum showed a number of peaks; only one had any evidence of possible Pt satellites indicating binding to the metal. This was a very broad peak at ~ 20 ppm. There was also free triphenylphosphine observed indicating that some of the triphenylphosphine had been exchanged. The HRMS results provide evidence for one of the products being **170** (Scheme 7). No further attempts were made to prepare Pt^0 complexes of dbaPHOS.

The results so far indicated that a better metal precursor was needed, which would not contain ligands that would compete with dbaPHOS, **127**. Baird and co-workers recently described the use of $[\text{Pd}(\eta^5\text{-C}_5\text{H}_5)(\eta^3\text{-1-PhC}_3\text{H}_4)]$ (**171**) as a ‘stable precursor’ for Pd^0 complexes.³⁸ Upon addition of two equivalents of phosphine the allyl fragment and the Cp undergo reductive elimination to give the $\text{Pd}^0(\text{Phosphine})_2$ complexes. In our hands, only moderate yields of **171** were obtained ($\sim 30\%$, *Lit.* 73%) and the work-up needed to be conducted under an inert atmosphere to reduce the degradation of the product. The complex was also temperature sensitive, suggesting that the description of the complex as a ‘stable precursor’ may be an overstatement. The addition of dbaPHOS to **171** gave $\text{Pd}^0(\text{dbaPHOS})$ (**167**) in good yields (Scheme 8).



Scheme 8: Synthesis of $[\text{Pd}^0(\text{dbaPHOS})]$ **167.**

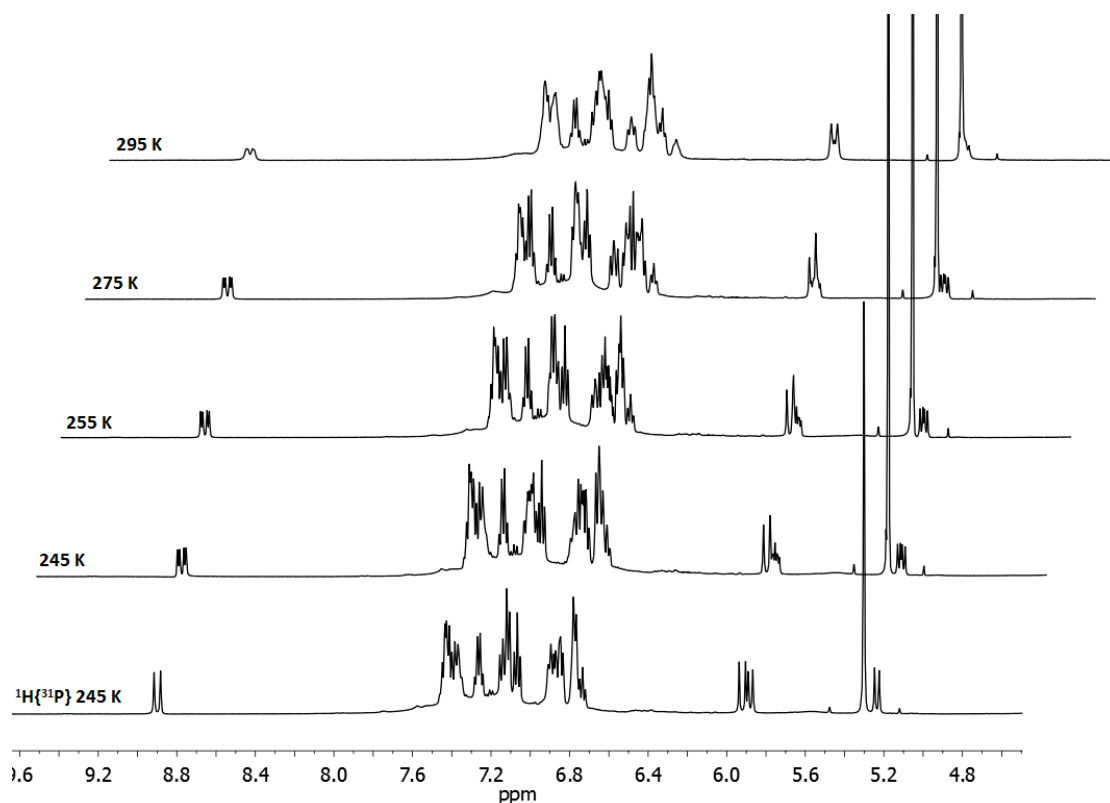


Figure 6: Variable temperature ^1H NMR spectra of $[\text{Pd}^0(\text{dbaPHOS})]$ (500 MHz, CD_2Cl_2).

The ^{31}P NMR spectrum indicated there were two phosphorus environments, suggesting that one of the alkenes was bound to the Pd centre. More concrete evidence was provided by the ^1H NMR spectrum (Figure 6), which showed two alkene environments shifted upfield at 5.28 and 5.95 ppm. On cooling the sample it was clear that signal due to H_α of the coordinated alkene exhibits a much greater coupling to phosphorus $J_{\text{HP}} = 8.0$ Hz (as shown by the $^1\text{H}\{^{31}\text{P}\}$ spectrum), than is observed in the free alkene $J_{\text{HP}} = 1.5$ Hz). The H_β signal at 5.9 ppm (245 K) is coupling to two different phosphorus nuclei $J_{\text{HP}} = 6.5$ and 4 Hz. This provides further evidence of the alkene coordination as in the free ligand only coupling to one phosphorous nuclei is observed for H_β , $J_{\text{HP}} = 4.5$ Hz. Conclusive evidence was provided by the ^{13}C NMR and HSQC spectra, which showed the alkene carbons associated with the upfield alkene protons had shifted upfield to give broad signals at 83 and 69 ppm. The H_β signal (83 ppm) was well enough resolved to show a doublet with $J_{\text{CP}} = 21$ Hz, which is similar to the value for the free ligand, $J_{\text{CP}} = 26$ Hz.

The UV-visible spectrum also supports the presence of a M-alkene bond as an absorption band due to MLCT is seen at 454 nm, $\epsilon = 7088 \text{ mol}^{-1} \text{ dm}^3 \text{ cm}^{-1}$ (CH_2Cl_2). This is between the values seen for $\text{Pd}(\eta^2\text{-dba})(\text{PPh}_3)_2$, (396 nm, DMF, 405 nm

MeOH)^{39,40} and Pd₂dba₃ (530 nm, MeOH).⁴⁰ The IR spectrum (CH₂Cl₂) also supports the presence of a M-alkene bond. The bands at 1654 and 1616 cm⁻¹ have moved to 1627 and 1567 cm⁻¹, along with new shoulders appearing to the left of the bands at 1480 and 1454 cm⁻¹ (Figure 7).

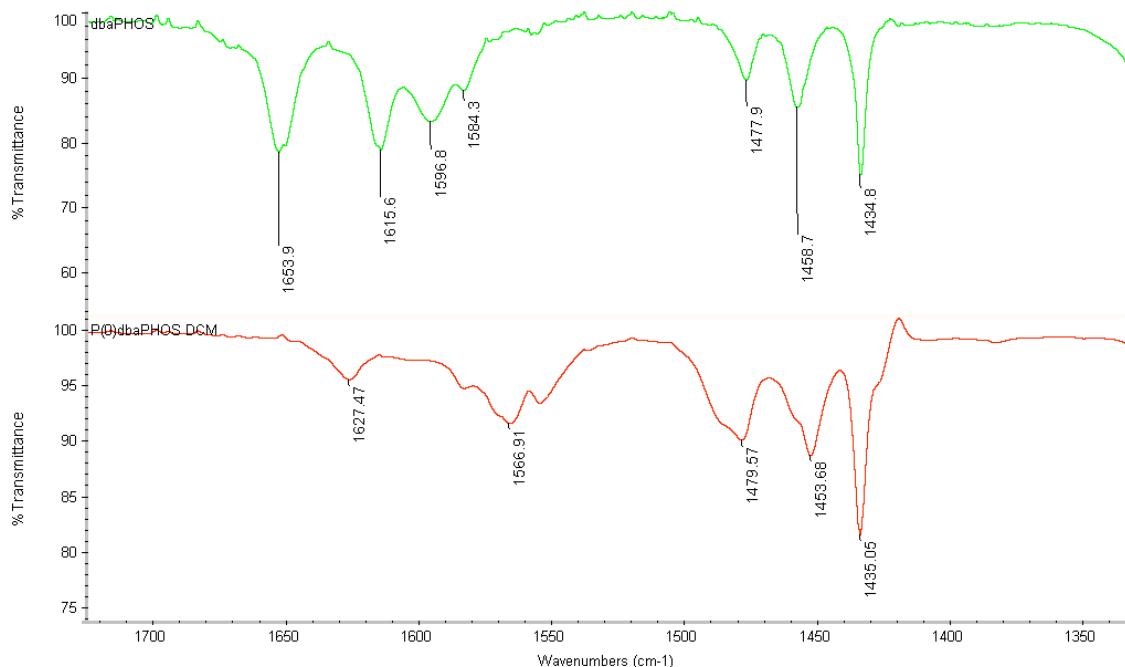


Figure 7: IR spectra of dbaPHOS (top) and [Pd⁰(dbaPHOS)] (bottom) in CH₂Cl₂.

In Chapter 2 the use of the chemical shift difference of the H_α and H_β protons as an indication of the dba backbone geometry was discussed. For dba, *s-cis* geometry is determined by a minimum $\Delta\delta_{\alpha\beta}$ of 0.5 ppm, whilst the *s-trans* form must have a maximum $\Delta\delta_{\alpha\beta}$ value of 1.5 ppm. For Pd₂dba₃ a similar trend in the $\Delta\delta_{\alpha\beta}$ value was seen, values less than 0.2 ppm were attributed to alkenes in the *s-cis* form and values higher than 0.6 ppm were observed for the *s-trans* alkenes.⁴¹ In [Pd⁰(dbaPHOS)] the $\Delta\delta_{\alpha\beta}$ value of the unbound proton is much larger than the $\Delta\delta_{\alpha\beta}$ value of the bound alkene (2.98 vs. 0.64 ppm). This could indicate that the bound alkene is in the *s-cis* form, and the unbound alkene in the *s-trans* form. However, these values are just a guide and it is not clear if they can be considered accurate for substituted dba ligands (see discussion in Chapter 2.3 and Section 3.2.1). Definitive evidence for the complex having an *s-cis,s-trans* backbone is given by the ¹H-¹H ROESY experiment, which shows a nOe contact between H_β of the unbound alkene and H_α of the bound proton

(Figure 10).^{*} For the other dba conformations the only nOe's expected are those between both α -protons (*s-cis,s-cis*) or both β -protons (*s-trans,s-trans*) (Figure 8).

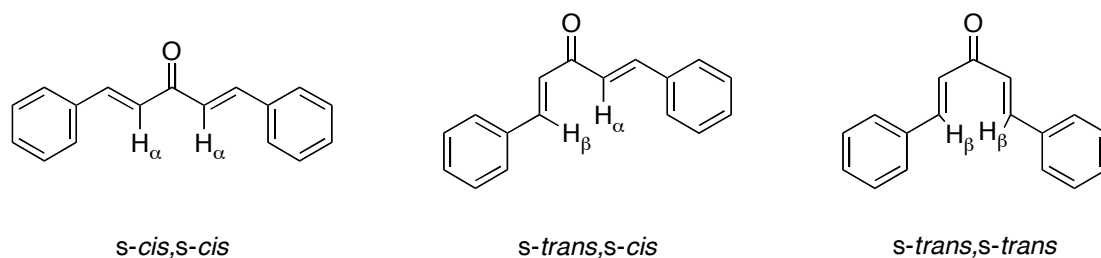
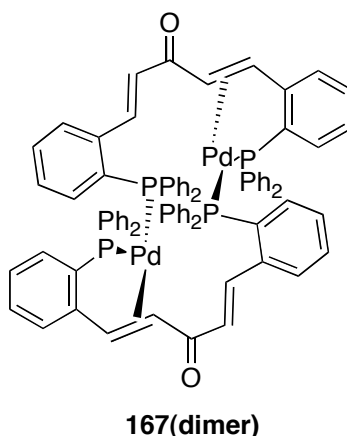


Figure 8: Protons which would show nOe's in the different dba backbone geometries.



167(dimer)
Figure 9: Dimer of [Pd⁰(dbaPHOS)].

X-ray crystallographic analysis on a poor quality crystal allowed us to unambiguously define the connectivities of the atoms in **167**. However, the data set obtained was not adequate enough to refine the structure with acceptable *R*-values for accurate structure determination ($R_1 = 12\%$). The crystal structure confirmed the *s-cis,s-trans* backbone geometry (Figure 9). However, it was clear that the crystal was a binuclear complex, not the monomer so far proposed. It is unclear if this is the case in solution. A similar complex was obtained with Cu^I and dbaTHIOPHOS (see Chapter 4 for a full analysis and discussion), in this case the ¹H NMR spectrum at 298 K was very broad. This is not the case with complex **167**, which has a comparatively sharp spectrum in contrast. Further information is needed to confirm if the complex is a monomer or not, such as DOSY experiments or freezing point depression. For the remainder of this chapter, the complex has been depicted as the monomer for clarity.

^{*} The assumption is made that the H_α will always be the furthest upfield proton of the alkene, which is consistent with enones in general and related dba structures.

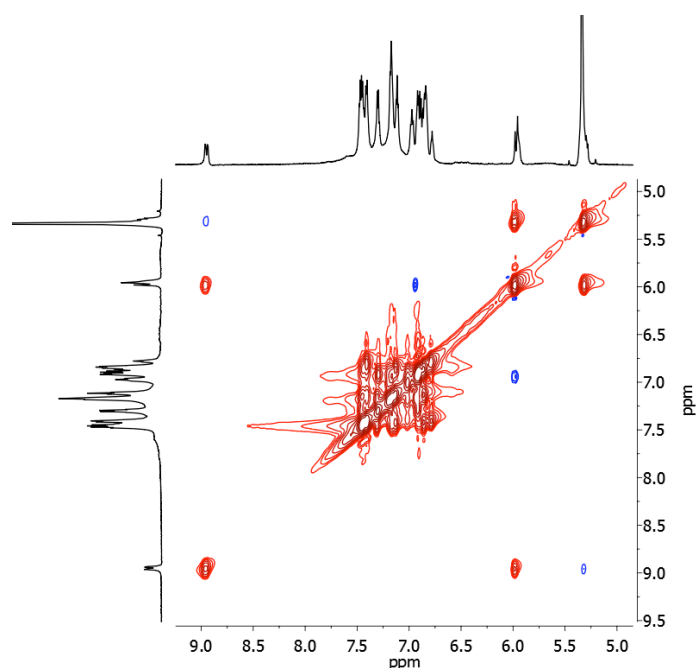


Figure 10: ^1H - ^1H ROESY NMR spectrum of $[\text{Pd}^0(\text{dbaPHOS})]$, 167 (700 MHz, CD_2Cl_2).

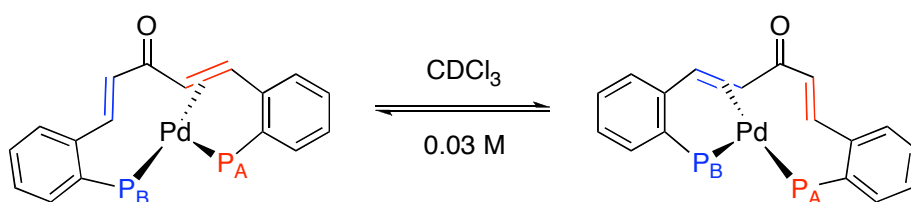


Figure 11: Alkene exchange in $[\text{Pd}^0(\text{dbaPHOS})]$, 167, phenyl groups not shown for clarity.

The broad alkene environments and the ROESY experiment showed that the alkenes were exchanging (Figure 10 and 11). ^{31}P - ^{31}P EXSY experiments can be used to obtain rate constants for this process by varying the mixing time (d8) at different temperatures.⁴² As EXSY experiments are the same as NOESY experiments we wanted to be sure that the exchange seen in the 1D EXSY spectrum at 298 K was indeed exchange and not a nOe. The exchange processes will be affected by temperature to a greater extent than nOe processes, and therefore it should be possible to freeze out the exchange. We were pleased to find that at 268 K in CD_2Cl_2 that no cross-peaks were observed on irradiating at 31.2 ppm, showing that there is not a nOe between the two phosphorus atoms. As a result we are confident that we are only observing exchange processes. To enable a sufficient number of temperature points to be obtained for an Arrhenius plot the ^{31}P - ^{31}P EXSY were carried out in CDCl_3 .

Table 5: Rate constant data for the alkene exchange in [Pd⁰(dbaPHOS)] (0.03 M, CDCl₃), 167.

Temperature, K	293	298	303	308	313	318
k_{obs} , s ⁻¹ †	0.58	0.85	1.42	2.23	3.34	5.09
	(± 0.03)	(± 0.05)	(± 0.05)	(± 0.17)	(± 0.14)	(± 0.27)

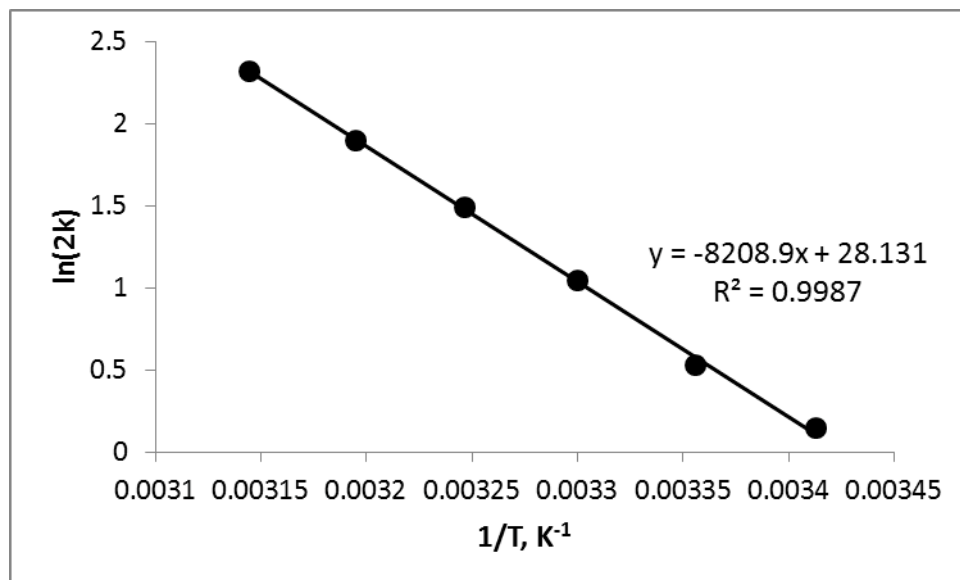
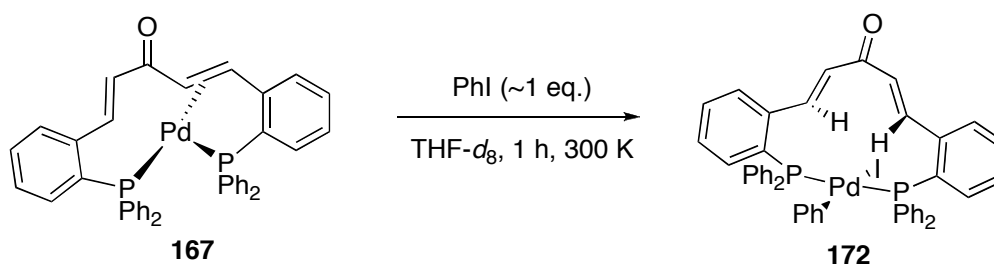


Figure 12: Arrhenius plot for the alkene exchange in [Pd⁰(dbaPHOS)] in CDCl₃.

An Arrhenius plot of $1/T$ against $\ln 2k$ gives a straight line with slope $-E_a/R$, allowing the activation energy to be estimated (68.2 kJ mol⁻¹) and the pre-exponential factor to be determined (1.65×10^{-12} s⁻¹) (Figure 12). Using the Eyring equation, a plot of $\ln(2k/T)$ against $1/T$ gives a straight line ($R^2 = 0.9989$) from which the enthalpy and entropy of activation can be calculated; $\Delta H^\ddagger = 65.7 (\pm 3.4)$ kJ mol⁻¹ and $\Delta S^\ddagger = -19.5 (\pm 11.1)$ J mol⁻¹ K⁻¹. The small value for ΔS^\ddagger is in keeping with the exchange being intramolecular, and with most of the barrier to exchange being explained by enthalpic differences. The free energy of activation (ΔG^\ddagger) at 298 K is 71.5 (± 4.7) kJ mol⁻¹.

† The errors correspond to the difference between rate constants calculated with the maximum and minimum integral values obtained from the EXSY experiment using MestreNova™. The values of k_{obs} given are for the average integrals (each integral was measured at least 5 times). These average k_{obs} values were then used to plot the Arrhenius and Eyring equations. The error values given for ΔH^\ddagger and ΔS^\ddagger were obtained by linear regression analysis of these plots and does not include any contribution from the error values on k_{obs} .



Scheme 9: Stoichiometric oxidative addition of PhI to complex 167.

One of the aims of this project was to develop ligands for use in transition metal catalysed reactions, such as cross-coupling reactions. The stoichiometric oxidative addition reaction, the first committed step in cross-coupling, with PhI was carried out (Scheme 9). The reaction of Pd⁰(dbaPHOS), **167**, and PhI (1 eq.)[‡] in THF-*d*₈ was followed by NMR spectroscopy. The oxidative addition took 1 h to go to completion at 300 K. Surprisingly the ³¹P NMR spectrum of this reaction showed just a single peak ($\delta_{\text{P}} = 16.83$ ppm) indicating that the ligand was acting as a *trans*-spanning ligand, as shown in **172**. Four of the protons from the PhI also appeared to be further upfield than expected occurring between 5.9 and 6.4 ppm (Figure 13). This is due to shielding from the phenyl rings of the phosphine.⁴³

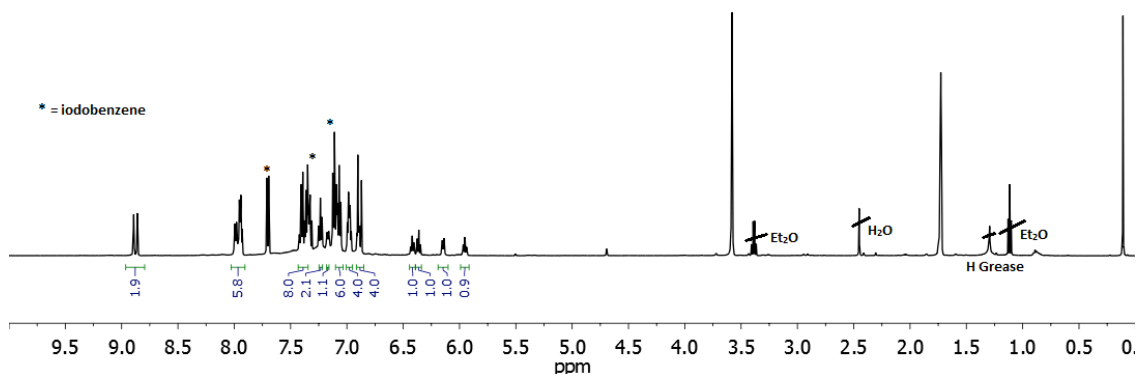


Figure 13: ¹H NMR spectrum of 172 (THF-*d*₈, 300 K, 500 MHz).

Cooling the sample to 18 °C provided crystals of **172** suitable for X-ray diffraction, which provides further evidence of the *trans* nature of the ligand (Figure 14). The bite angle of the ligand in this complex is 172.37(3)°. The C(7)-H(7) bond points towards the Pd centre, the distance between the M and H is longer than in the *cis*-[PtCl₂(dbaPHOS)], **163**, complex, 2.90 vs. 2.64 Å. The other ligand bond distances (C=O, C=C and C-P) are within error of those in the *cis*-[PtCl₂(dbaPHOS)], **163**, complex. This is expected, as Pt^{II} and Pd^{II} are quite similar. The P-Pd distances are

[‡] The [Pd⁰(dbaPHOS)], **167**, was not fully dissolved, further details provided in the experimental (Section 3.6.2.1).

longer than the P-Pt^{II} distances, presumably due to the *trans*-nature of the ligand defining the sterics. As in **163** the ligand backbone is almost perpendicular to the (P,P,C,I) plane, and a considerable twist is observed around the 1,4-dien-3-one backbone. The dihedral angle between C(16), C(17), C(14), and C(13) is -49.0°.

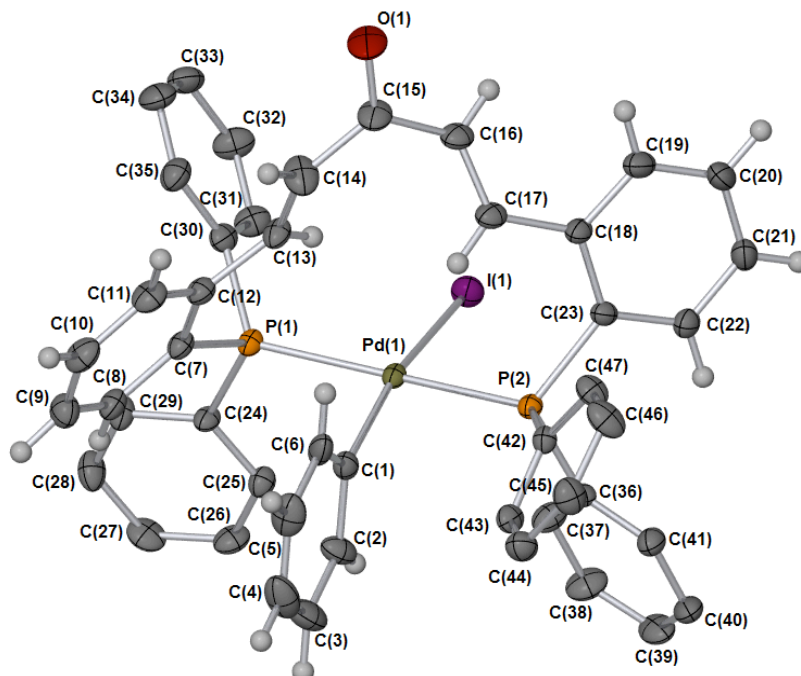


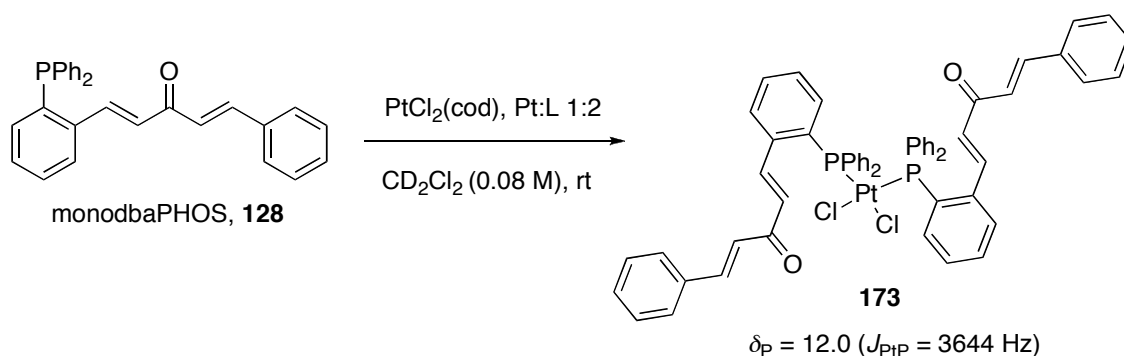
Figure 14: Single crystal X-ray structure of 172. Disordered solvent molecules (THF) and selected hydrogen atoms removed for clarity. Thermal ellipsoids shown at 50%. Selected bond lengths (Å) and bond angles (°): C(15)-O(1) = 1.226(5), C(16)-C(17) = 1.342(5), C(14)-C(13) = 1.335(5), P(1)-C(7) = 1.827(4), P(2)-C(23) = 1.831(4), P(2)-Pd = 2.3181(10), P(1)-Pd = 2.3459(10), Pd-I = 2.6810(5), Pd-C(1) = 2.028(4); P(1)-Pd-P(2) = 172.37(3).

3.2 Platinum(II) and palladium(II) complexes of monodbaPHOS

The dbaPHOS ligand **127** was found to act as bidentate phosphine with Pd^{II} and Pt^{II}, whilst in the Pd⁰ complexes alkene coordination was also observed. In a number of cases dimers were observed and it is possible that higher polymers were also formed. In monodbaPHOS, **128**, only one phosphine is present. It is therefore more likely that alkene coordination will be observed with Pd^{II} and Pt^{II} if the right stoichiometries are used (*i.e.* 1:1, M:L).

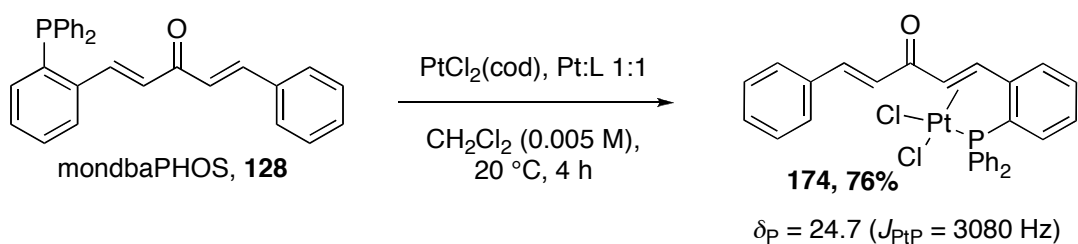
Solution NMR spectroscopic studies were carried out with monodbaPHOS, **128**, and [PdCl₂(cod)] and [PtCl₂(cod)] in both metal:ligand ratios of 1:1 and 1:2. The Pd^{II} complexes crashed out of solution almost instantaneously, to give a product that was insoluble in benzene, DMSO, CH₂Cl₂ and CHCl₃. The Pt^{II} complexes stayed in solution

longer, allowing NMR spectroscopic data to be obtained. In the 1:2 case, one phosphorus signal was observed at 12.0 ppm with ($J_{\text{PtP}} = 3644$ Hz) indicating that the monodbaPHOS is acting as a monodentate ligand and the two ligands are *cis* to each other (*i.e.* complex **173** in Scheme 10). No evidence for alkene coordination was observed in the ^1H NMR spectrum.



Scheme 10: Preparation of $[\text{PtCl}_2(\text{monodbaPHOS})_2]$.

The ^{31}P NMR spectrum of the 1:1 Pt:L experiment showed two different chemical shifts, 24.8 and 12.0 ppm, indicating two complexes in solution, *e.g.* $[\text{PtCl}_2(\text{monodbaPHOS})]$ (**174**) and $[\text{PtCl}_2(\text{monodbaPHOS})_2]$ (**173**), respectively. The ^1H NMR spectrum shows that $[\text{PtCl}_2(\text{cod})]$ still remains, along with **174** and **173**. A larger scale reaction (0.1 mmol) at higher dilution (5 mM) gave **174** in a 76% yield (Scheme 11). The ^1H NMR spectrum gives clear evidence of the coordination of the alkene as two of the alkene protons have shifted upfield to 6.3 and 5.1 ppm and have Pt satellites ($J_{\text{PtP}} = 28$ and 37, respectively) (Figure 15). The ^{13}C NMR spectrum also gave clear evidence of coordination of the alkene as evidence by the upfield shift of the alkenyl carbons to 81 and 87 ppm. Compared to the free ligand the P-C coupling constants have decreased substantially from $J_{\text{CP}} = 26$ and 3 Hz (C_β and C_α respectively) to $J_{\text{CP}} = 4$ and 0 Hz). The CH carbons of the phenyl rings exhibit slightly different shifts in the ^{13}C NMR spectrum, showing that the two phenyl rings of the PPh_2 are in different chemical environments.



Scheme 11: Synthesis of [PtCl₂(monodbaPHOS)] 174.

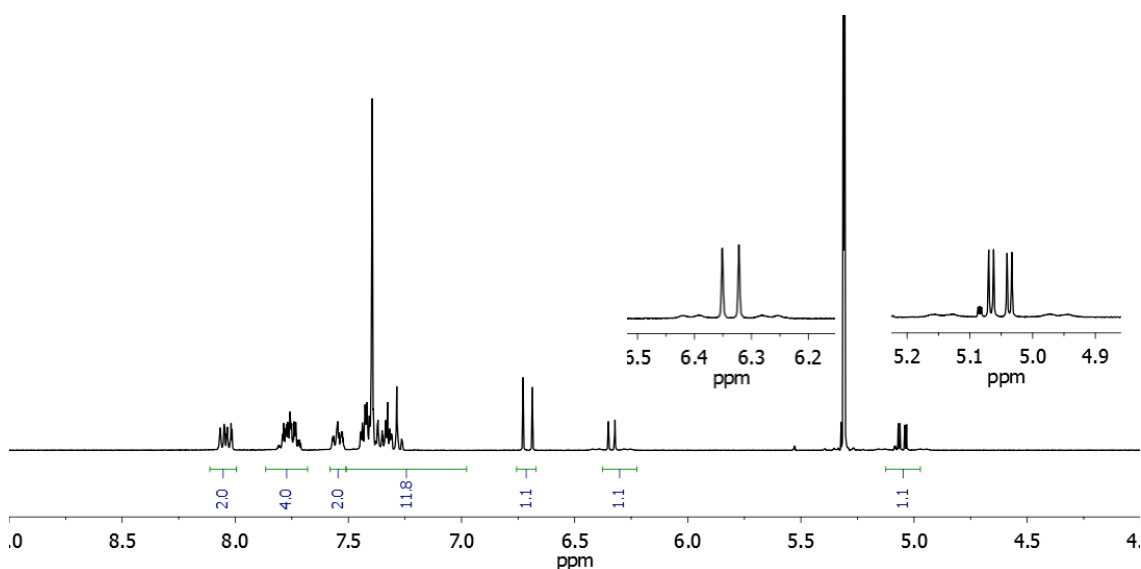


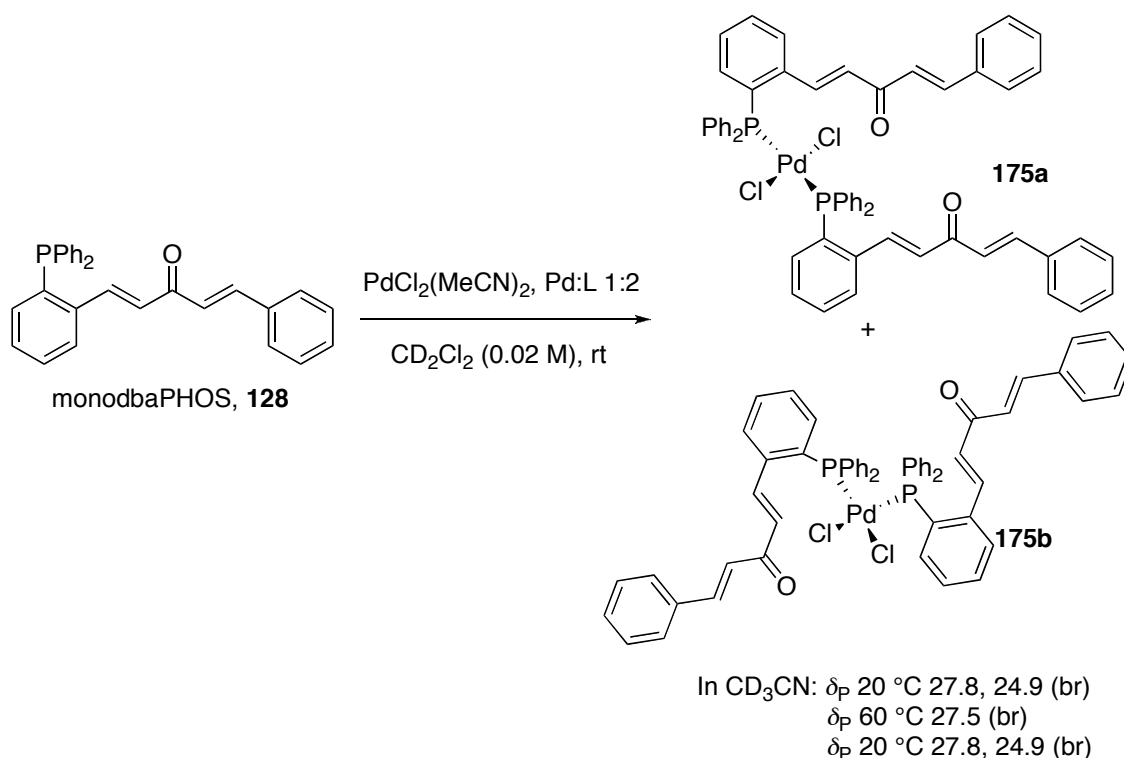
Figure 15: ¹H NMR spectrum of [PtCl₂(monodbaPHOS)] 174 (400 MHz, CD₂Cl₂).

Crystals suitable for study by X-ray diffraction were grown from solutions of the compounds in CH₂Cl₂. Surprisingly, X-ray diffraction analysis showed that from both the experiments (1:1 and 1:2 Pt:L ratios) a 1:1 Pt:L complex crystallises. This evidence, together with the mixture of complexes observed by NMR spectroscopy when a 1:1 Pt:L ratio is used, could suggest that complex **173** is the kinetic product, whereas **174** is the thermodynamic product. Alternatively, **174** could crystallise more easily in the solvent systems used.

Complexation experiments were also carried out with [PtCl₂(MeCN)₂] (30-60 mM), and [PdCl₂(MeCN)₂] (~40 mM). In this case the platinum complexes were now found to be completely insoluble suggesting polymeric complexes had formed. The IR spectra (KBr) of the complexes from experiments run at both 1:1 and 1:2 Pt:L stoichiometries were the same and showed that no [PtCl₂(MeCN)₂] remained. The elemental analysis of the compounds was inconclusive, suggesting either mixtures of products, polymers or the presence of inorganic impurities. The solid-state ³¹P NMR spectra of the material

from the 1:2 reaction showed a mixture of products, all with Pt-P couplings of ~2550 Hz suggesting that the phosphines were *trans* to each other.

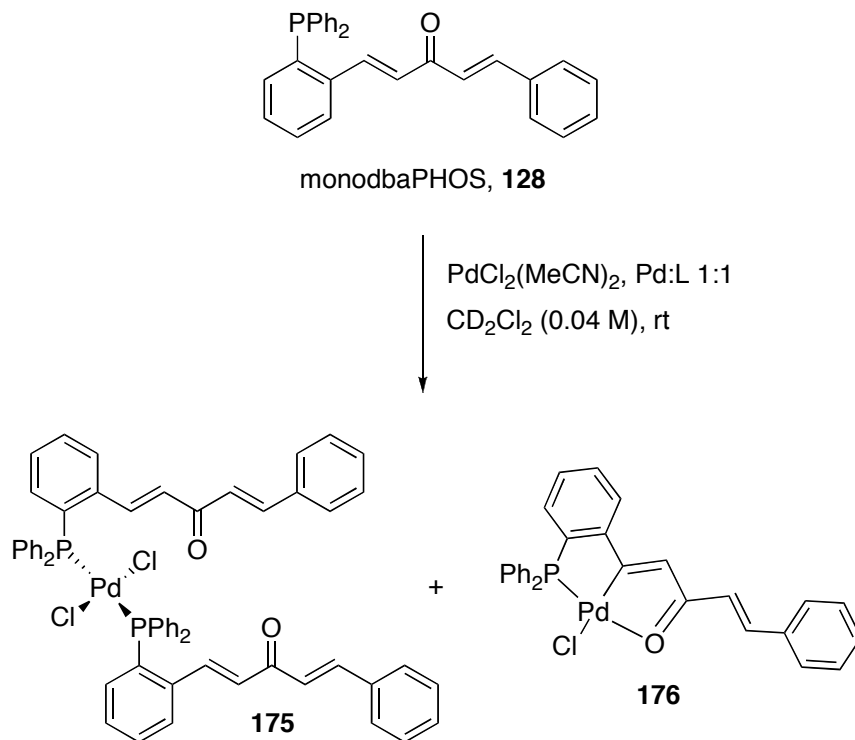
The material from the palladium complexations with $[\text{PdCl}_2(\text{MeCN})_2]$ was now found to be completely soluble in MeCN and CH_2Cl_2 unlike the material from the $[\text{PdCl}_2(\text{cod})]$ complexations. However, with both 1:1 and 1:2 Pd:L stoichiometries a mixture of complexes was obtained. Attempts to separate the complexes by crystallisation proved unsuccessful. The material from the 1:2 reaction in CD_3CN showed two phosphorus signals in the ^{31}P NMR spectrum. Heating the sample to 60 °C, the two phosphorus signals became one and on cooling returned to the original two signals. This could indicate that the backbone of the ligand is changing conformation (as shown in **175a** vs. **175b** Scheme 12) or some other type of isomerisation-like process is occurring. The ^1H NMR spectrum shows a signal shifted downfield to 9.2 ppm. This could indicate a C-H---Pd interaction similar to that seen in complexes **163** and **165**.



Scheme 12: Reaction between monodbaPHOS (2 eq.) and $[\text{PdCl}_2(\text{MeCN})_2]$ (1 eq.).

The material from the 1:1 Pd:L reaction also showed two phosphorus signals in the ^{31}P NMR spectrum this time at 27.1 and 54.0 ppm. The one at 27.1 ppm may correspond to a complex with a 1:2 Pd:L stoichiometry (**175**), and a similar downfield shift to 8.8 ppm

is seen in the ^1H NMR spectrum. It is unclear from the ^1H NMR spectrum whether the alkene is coordinated. Pd^{II} -alkene interactions are weaker than Pt^{II} -alkene interactions⁴⁴ and therefore coordinated alkene protons will not exhibit such strong upfield shifts in the ^1H NMR spectrum. Crystals suitable for X-ray diffraction were obtained from the NMR sample of the 1:1 reaction, and found to be **176**. NMR spectroscopic analysis of the crystals obtained, showed that **176** had a δ_{P} of 54.6 ppm.



Scheme 13: Reaction between monodbaPHOS, **128** (1 eq.) and $[\text{PdCl}_2(\text{MeCN})_2]$ (1 eq.).

3.2.1 X-ray crystallographic analysis

As mentioned above crystals suitable for X-ray crystallography were obtained from both the 1:1 and 1:2 Pt:L reactions with $[\text{PtCl}_2(\text{cod})]$, both crystals had the same stoichiometry (1:1 Pt:L). The X-ray structures show that monodbaPHOS acts as a chelating bidentate ligand binding through both the phosphorus and the alkene in each complex. The complexes are both square planar, which is expected for Pt^{II} as it is d^8 . However, in the crystal from the 1:1 complexation reaction the coordinated C=C bond was *E* as it is in the free ligand (**174**), whilst in the crystal from the 1:2 complexation reaction the coordinated C=C bond is *Z* (**177**). Subtle differences in the enone conformer were also observed. For example, in **174** the backbone had the *s-cis,s-cis* geometry (Figure 16) and in **177** it was *s-cis,s-trans* (Figure 17).

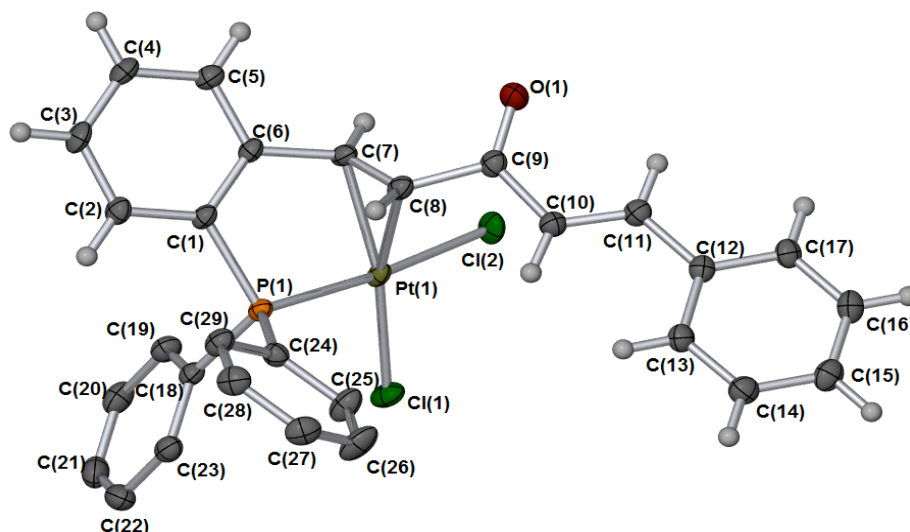


Figure 16: X-ray crystal structure of *s-cis,s-cis*[Pt(*E,E*-monodbaPHOS)Cl₂], 174. Hydrogen atoms removed for clarity. Thermal ellipsoids shown at 50 %. Selected bond angles (°): C(8)-Pt(1)-P(1) = 88.51(9), C(7)-Pt(1)-P(1) = 84.89(9), P(1)-Pt(1)-Cl(1) = 91.88(3), C(8)-Pt(1)-Cl(2) = 92.15(9), C(7)-Pt(1)-Cl(2) = 91.29(9), P(1)-Pt(1)-Cl(2) = 172.89(3), Cl(1)-Pt(1)-Cl(2) = 90.20(3).

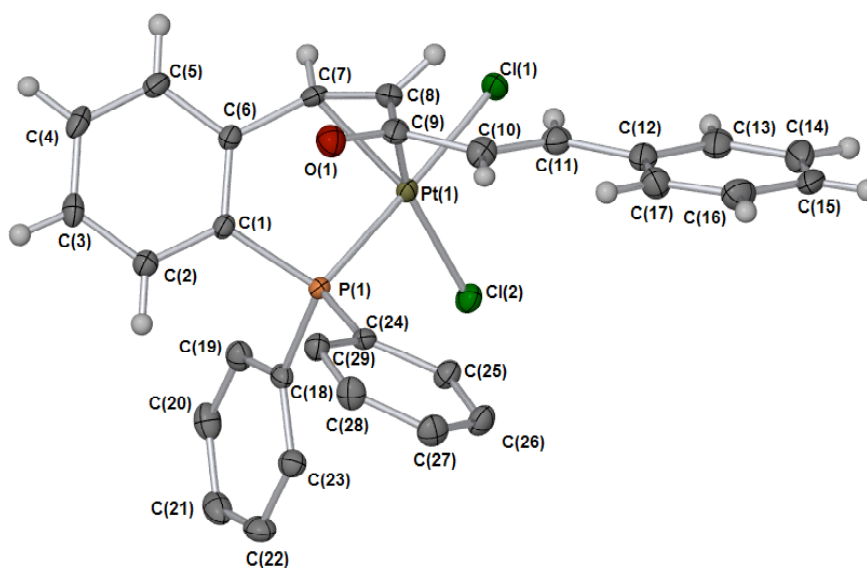
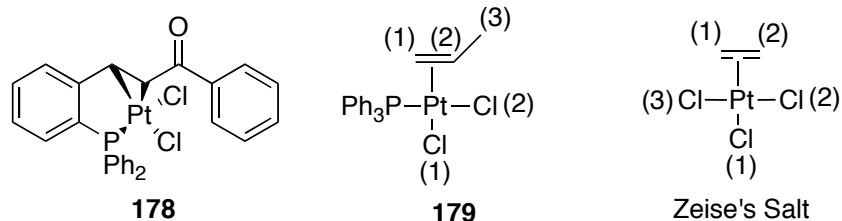


Figure 17: X-ray crystal structure of *s-cis,s-trans*[Pt(*Z,E*-monodbaPHOS)Cl₂], 177. Hydrogen atoms and solvent removed for clarity. Thermal ellipsoids shown at 50 %. Selected bond angles (°): C(20)-Pt(1)-P(1) = 93.67(8), C(19)-Pt(1)-P(1) = 84.29(8), P(1)-Pt(1)-Cl(2) = 90.72(3), C(20)-Pt(1)-Cl(1) = 86.38(8), C(19)-Pt(1)-Cl(1) = 94.47(8), P(1)-Pt(1)-Cl(1) = 177.90(2), Cl(2)-Pt(1)-Cl(1) = 89.90(3).

Table 6: Bond lengths in [PtCl₂(monodbaPHOS)] **174(*E,E*) and **177**(*Z,E*) and comparison with other alkene complexes (esd's in brackets). Pt-Cl(*trans*) = *trans* to alkene, Pt-Cl(*cis*) = *cis* to alkene.**



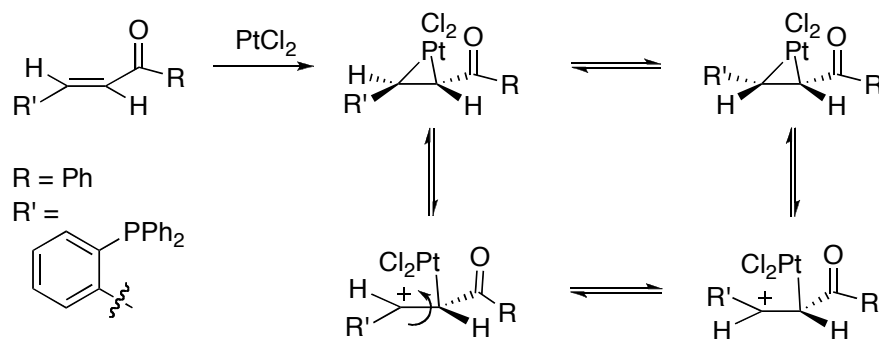
Bond Lengths, Å	174	177	178 ⁴⁵	179 ⁴⁶	Ziese's Salt ⁴⁷
Pt(1)-P(1)	2.2363 (8)	2.2409 (7)	2.2452 (8)	2.2610 (7)	
Pt(1)-Cl(<i>cis</i>)	2.3429 (8)	2.3545 (7)	2.3579 (8)	2.3623 (8)	2.302 (2) 2.302(2)
Pt(1)-Cl(<i>trans</i>)	2.2995 (8)	2.3043 (7)	2.2924 (8)	2.3195 (8)	2.340 (2)
Pt(1)-C(<i>nearest C=O</i>)	2.132 (3)	2.138 (3)	2.152 (3)	2.146 (3)	2.128 (3)
Pt(1)-C	2.175 (3)	2.173 (3)	2.161 (3)	2.188 (3)	2.135 (3)
C=C <i>coord</i>	1.399 (5)	1.413 (4)	1.402 (5)	1.394 (5)	1.375 (4)
C=C <i>uncoord</i>	1.341 (5)	1.334 (4)			
C=O	1.215 (4)	1.219 (4)	1.214 (4)		
Angles, °					
Cl-Pt-Cl	90.20 (3)	89.90 (3)	88.85 (3)		
P(1)-Pt(1)-Cl(<i>cis</i>)	172.89 (3)	177.90 (2)	177.84 (3)		
P(1)-Pt(1)-Cl (<i>trans</i>)	91.88 (3)	90.72 (3)	91.76 (3)		

The C-C bond length for ethane is 1.54 Å, which shortens to 1.33 Å in ethene. The non-complexed double bond in the two [Pt(mono-dbaPHOS)Cl₂] complexes is similar to ethene, 1.334 Å. The complexed double bond has lengthened by *ca.* 0.6-0.8 Å, indicating an increase in sp³-character on complexation. For both **174** and **177** the alkene bond lengths (both bonded and non-bonded) and carbonyl bond lengths are within error of each other, suggesting that the change from *E* to *Z* does not affect the alkene coordination strength. The alkene and carbonyl bond lengths in **178** are also similar. The coordinated C=C bond in phosphine-alkene ligands are longer than the double bond in Zeise's salt indicating that there is either more σ-donation from alkene-Pt or more back-donation, leading to greater sp³ character. It is impossible to tell from the experimental data as both result in the lengthening of the C=C bond.

The coordinated double bonds in all the complexes compared are perpendicular to the PtCl₂P plane. This is expected for neutral Pt^{II} square planar complexes, and suggests that σ-donation is the dominating alkene-metal interaction, as the π-bond of the alkene will overlap with the empty dx²-y² orbital of the Pt. Analysis of both crystal structures

show that the Pt-C bonds are unsymmetrical, with the Pt-C(8) bond shorter than the Pt-C(7) bond. This is also seen in complex **179**, whereas Zeises's salt and **178** both have symmetrical coordination. The unsymmetrical coordination of the alkene can be explained electronically, as the α -carbon is δ -negative and thus will exhibit greater σ -donation. This also supports σ -donation as the major interaction.

To explain the *trans-cis* alkene isomerisation at Pt^{II} one needs to consider nucleophilic attack on Pt-coordinated alkenes. Markovnikov regioselectivity is usually observed, with the more hindered carbon (most stable carbocation) being attacked.⁴⁸ During the reaction the η^2 -coordination of the alkene to Pt^{II} slips towards η^1 -coordination. In a number of alkene complexes where this slippage towards the η^1 -coordinated complex is observed, the ground state complexes show unsymmetrical bonding of the alkene.⁴⁸ In **174** it is possible that an equilibrium exists between the two extremes allowing isomerisation to occur, as shown in Scheme 14. The β -carbon would be the most stabilised carbocation, leading to η^1 -coordination to the α -carbon. The Pt-P bond of the bound alkene must be broken for rotation to occur. It is possible the presence of excess phosphine favours this process as it can stabilise the η^1 -intermediate (at Pt^{II}).



Scheme 14: Proposed mechanism of alkene isomerisation in the Pt^{II} complexes of monodbaPHOS.

The Pt-P bond length in **178** are within error of one of the monodbaPHOS complexes (*s-trans*), but not the other. All the phosphino-alkene complexes have shorter Pt-P distances than in **179**. This is presumably determined by the chelating nature of the ligand.

In all cases the Pt-Cl bond *trans* to the phosphine was longer than that *trans* to the alkene. All the Pt-Cl bonds *trans* to the phosphine exhibit similar bond lengths; independent of the ligand, presumably as in all cases the phosphine is very similar

electronically. The difference between the Pt-Cl lengths can be understood by the *trans influence*. Phosphines have a greater *trans influence* than alkenes (the *trans influence* is dominated by σ -donation) and hence will lengthen the bond opposite them more than an alkene would. Similar differences are seen in other phosphino-alkene complexes both when they are bidentate and separate.

The phosphino-alkene complexes all show only very slight deviations from square planar geometry. Complex **174** has a smaller P(1)-Pt(1)-Cl(cis) angle (172.9°) than **177** (177.9°). The monodbaPHOS complexes both have the largest Cl-Pt-Cl angle at almost exactly 90° .

In the two crystal structures two different backbone geometries are observed *s-cis,s-cis* and *s-trans,s-cis*, with the difference in the uncoordinated alkene. In Chapter 2 the use of the chemical shift difference of the H_α and H_β protons as an indication of the dba backbone geometry was discussed. For dba, the *s-cis* geometry is determined by a minimum $\Delta\delta_{\alpha\beta}$ of 0.5 ppm, whilst *s-trans* form must have a maximum $\Delta\delta_{\alpha\beta}$ value of 1.5 ppm. Studies were also carried out on $[Pt_2dba_3]$ and $[Pd_2dba_3]$, where similar trends were found with the *s-cis* form of the alkene always having a lower $\Delta\delta_{\alpha\beta}$ value than the *s-trans*.^{49,41} These trends were also observed in the Pd^0 complex of dbaPHOS above and in the Cu^I complexes of dbaTHIOPHOS (Chapter 4). In both these cases the conclusions from the 1H NMR spectroscopic analysis are supported by further NMR evidence such as NOESY spectra and X-ray diffraction analysis.

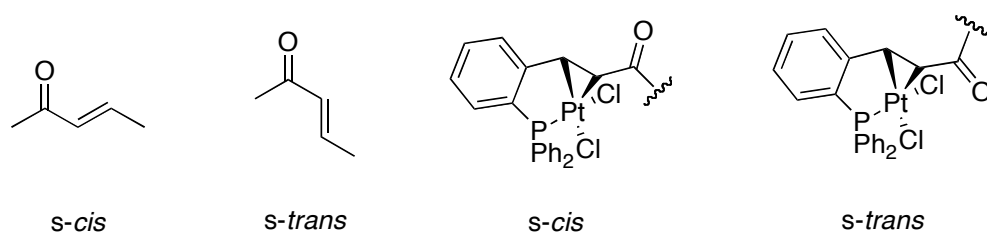


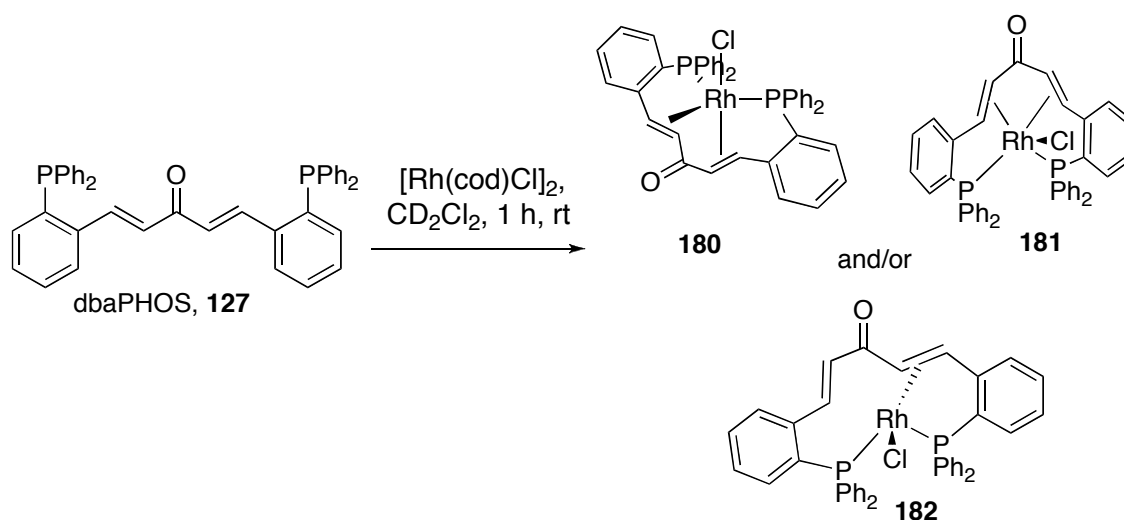
Figure 18: Ligand backbone conformations.

In the case of complex **174**, the NMR spectroscopic data and the crystallographic data seem to give different interpretations. In both crystal structures the coordinated alkene is *s-cis*, however, the $\Delta\delta_{\alpha\beta}$ value of this alkene is 1.29 ppm, whilst the $\Delta\delta_{\alpha\beta}$ value of the uncoordinated alkene is ~ 0.6 ppm. This would imply that the coordinated alkene is actually *s-trans* in solution, and the uncoordinated alkene is *s-cis* if the same rules as for dba are followed. Analysis of the $\Delta\delta_{\alpha\beta}$ values of the ligands themselves (see Chapter

2.3), requires some caution to be exerted in using these parameters to discern the geometrical preferences of the ligands and the related metal complexes. Firstly, as with the ligands it is unclear what the limits of the $\Delta\delta_{\alpha\beta}$ values are for each geometric form, and whether or not we are observing an average of the two conformers. It is possible that future studies using NMR spectroscopic techniques at various temperatures could address this. Secondly, one needs to consider the influence of the strained-bicyclic structure of the P,alkene chelate at Pt^{II} (shown in Figure 18). It is possible that this plays a far greater role in determining the ¹H chemical shifts than the backbone conformation. Thirdly, the alkene is unsymmetrically bound to the platinum. Overall, the evidence suggests that $\Delta\delta_{\alpha\beta}$ values are not a conclusive parameter for the determination of the 1,4-dien-3-one backbone geometry in our ligands.

3.3 Rhodium complexes of dbaPHOS

In contrast to Pt^{II} and Pd^{II}, which both usually give square-planar complexes; Rh^I can give rise to trigonal-bipyramidal complexes as well as square planar complexes. In some cases, geometries closer to square-pyramidal are also observed. In the early work on the coordination of phosphino-alkene ligands a number of Rh complexes were prepared and the alkenes were always found to coordinate as long as there were free coordination sites. It is therefore predicted that the alkenes in dbaPHOS, **127**, will coordinate. However, it is not immediately obvious whether both alkenes will coordinate to give a five-coordinate geometry or just one alkene will coordinate to give the square-planar complexes.



Scheme 15: Rhodium(I) complexation of dbaPHOS (possibilities).

Initial NMR scale studies (*ca.* 0.02 mmol, 20 mM) on Rh^I complexes of dbaPHOS reveal two products, the ³¹P NMR spectrum after 1 h (Figure 19) shows a major product (95%) possessing two phosphorus environments indicating that at least one of the alkenes is bound, possible structures are **180** or **182** (Scheme 15). The broad peaks suggest that the alkene is labile. In the minor product (5%) only one phosphorus environment is present suggesting that the ligand is symmetrically bound through both phosphines, a suggested structure is **181**. The minor product is always present in amounts of 5% or less. After leaving overnight a number of smaller peaks appeared in the ³¹P NMR spectrum. Rhodium(I) complexes are known to activate CH₂Cl₂ so it is possible that this could have been the cause,⁵⁰ or that complexes containing COD are being formed.

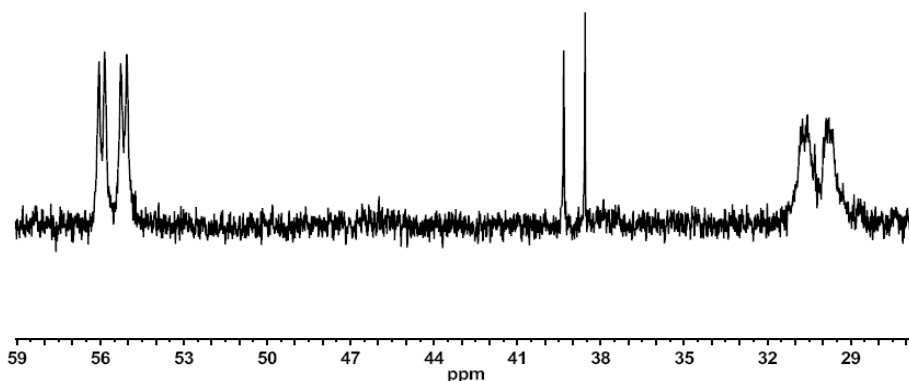
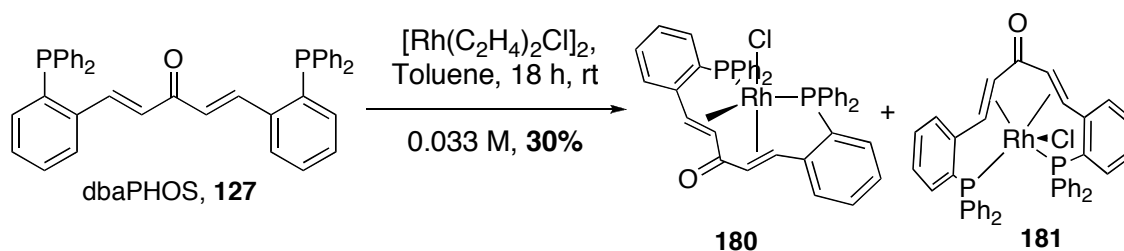


Figure 19: ³¹P NMR spectrum of Rh^I complexation after one hour in CD₂Cl₂. Major product: δ 55.52 ($J_{\text{Rh-P}} = 127$ Hz, $J_{\text{P-P}} = 36$ Hz), 29.97 ($J_{\text{Rh-P}} = 141$ Hz, $J_{\text{P-P}} = 36$ Hz). Minor product: δ 38.93 ($J = 127$ Hz) (5%).

The experiment was repeated in *d*₆-benzene. Once again the two products were observed, along with some smaller peaks possibly due to cod containing complexes. After leaving, for a few weeks an orange precipitate appeared. Isolation of the precipitate revealed it was the same mixture of the two products (**180** and **181**, 93:7 ratio by ³¹P and ¹H NMR) as initially seen. However, no further peaks were seen if the precipitate was dissolved in CH₂Cl₂ and left overnight. The 1,5-cyclooctadiene (cod) had been removed by filtration. This suggests that the original degradation of the complexes was due to free cod, or small amounts of starting material, not activation of CH₂Cl₂. Unfortunately, scaled up reactions (0.2 mmol) proved unsuccessful.

The cod ligand appears to be acting as a competing ligand. To eliminate any side products due to this, the reaction was tried using $[\text{Rh}_2(\text{C}_2\text{H}_4)_4\text{Cl}_2]$ as a precursor. On stirring the Rh precursor and dbaPHOS, **127**, together in toluene overnight the reaction turned from red to brown and gave a brown precipitate, with the same ^1H and ^{31}P NMR spectrum as before. Once again it is the same mixture of complexes, **180** and **181** (10:1 ratio by ^1H NMR at 255K). The mixture is only sparingly soluble in benzene, CH_2Cl_2 , THF, and MeNO_2 .



Scheme 16: Large-scale synthesis of Rh complexes of dbaPHOS.

Both the ^1H and ^{31}P NMR spectra appeared quite broad at 295 K due to exchange processes, such as Berry pseudorotation, occurring. Cooling the sample down sharpened the spectra up and revealed the multiplicities on the alkene protons (Figure 20). The two alkene protons at 3.6 and 2.6 ppm show a COSY correlation indicating that they are one of the alkenes. The large upfield shifts from the free ligand alkene protons (4.7 and 4.2 ppm) are evidence for the alkene binding to the rhodium centre. In comparison the other alkene has only shifted by 2.7 and 1.2 ppm. The alkene coupling constants have decreased in both cases from 15.8 to 13.3 and ~ 7 Hz, again an indication of M-alkene binding. Coupling to the phosphorus nuclei is observed on both protons of the upfield alkene and the furthest downfield of proton of the other alkene. All the above data points to both alkene moieties coordinating to the Rh^{I} centre, meaning that a 5-coordinate complex is formed, as chloride is not often observed as a non-coordinated anion.

Previous work with phosphino-alkene ligands has shown that in 5-coordinate trigonal bipyramidal Rh^{I} complexes the alkenes will preferentially bind in the equatorial plane.⁵¹ From the P-P spin-spin coupling constant of 36 Hz it is clear that the phosphines are not *trans* to each other, as much larger coupling constants are observed in those cases (~ 300 Hz).⁵² As alkenes prefer the equatorial plane it makes sense to place one phosphine and the chloride in the axial positions and one phosphine in the equatorial plane. However, there is a large difference in the chemical shifts of the two alkenes indicating that they

are in very different positions. Based on the evidence available it is more likely that the alkene shifted furthest upfield is the most strongly bound and therefore is in the equatorial plane, whilst the other alkene has swapped positions with chloride (to give an unsymmetrical 1,4-dien-3-one system, **180**).

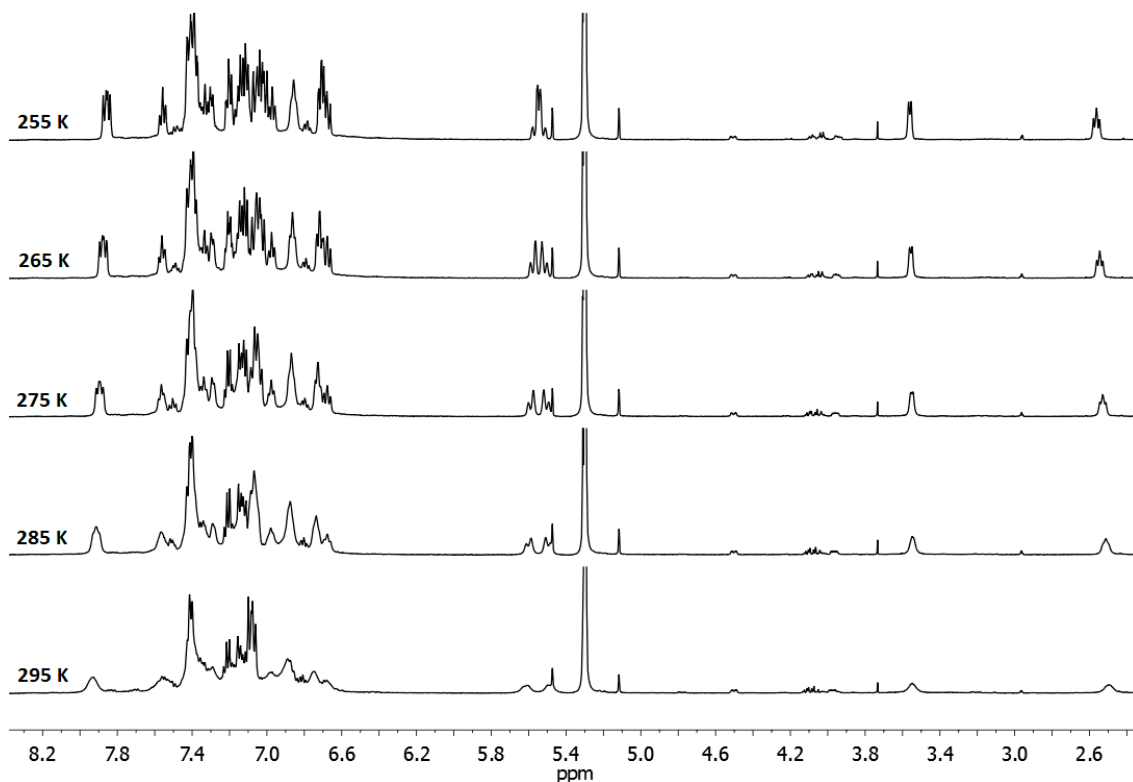
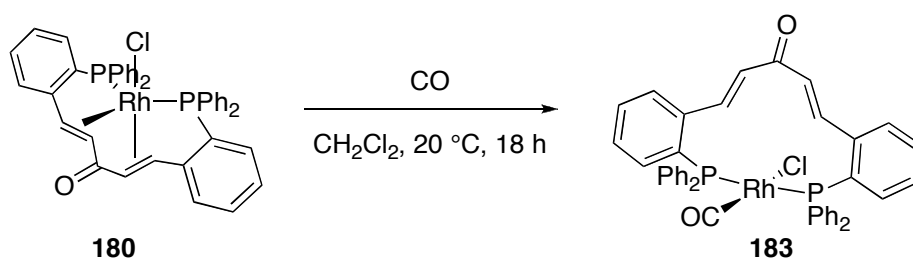


Figure 20: Variable temperature ^1H NMR spectra (500 MHz, CD_2Cl_2).

NOESY and ROESY experiments were attempted to give an indication of the ligand backbone geometry. At 265 K only exchange processes were observed between the two α -protons and the two β -protons, and no nOe processes were observed. Cooling the temperature down further to 225 K stopped the exchange processes, and an nOe was observed between the proton at 2.6 ppm (H_α) and one of the protons at 5.6 ppm. However, the signals at 5.6 ppm were not sufficiently resolved to differentiate which proton the nOe contact related to. Therefore, both *s-cis,s-cis* and *s-cis,s-trans* geometries are possible, (if it were *s-trans,s-trans* the β -proton of the lowest alkene should show the nOe).

In an attempt to try and obtain more information about the Rh^{I} complexes formed, the material was stirred in CH_2Cl_2 under a CO atmosphere. It was proposed that the CO would displace the alkenes to give square planar bisphosphine complex, **183** (Scheme 17). ^1H NMR spectroscopic analysis shows that the alkenes are still shifted upfield

indicating that they are bound to Rh. The material is also still a mixture of at least two species. The CH₂Cl₂ solution IR spectrum shows two bands in the metal-carbonyl region; a weak band at 2083 cm⁻¹ and a strong band at 2001 cm⁻¹. Both stretches correspond to terminal metal-carbonyls, the weak band is presumably due to the minor species, and the strong band for the major species. Unfortunately this has not helped determine what the original Rh^I species was.



Scheme 17: Reaction of the Rh^I complex with CO (one possible outcome).

3.4 Summary

The phosphino-alkene ligands coordinate in a variety of modes depending on the metal and its oxidation state. DbaPHOS, **127**, acted as a bidentate phosphine ligand to give square planar complexes with Pt^{II} and Pd^{II}. It is a wide bite angle ligand and both *cis* and *trans* chelation was observed. There is also evidence that dbaPHOS acts as a bridging ligand to form dimers and possibly higher order aggregates. In contrast, with Pd⁰ both phosphine and alkene coordination are observed, to give the complex, [Pd⁰dbaPHOS], **167**. This complex undergoes slow oxidative addition with PhI to give *trans*-[Pd(dbaPHOS)I(Ph)], **172**, confirmed by a X-ray single crystal structure. The observation that dbaPHOS can act as a *trans*-spanning ligand is exciting as *trans*-spanning bisphosphines are still quite rare.⁵³ Both phosphine and alkene coordination is observed for the Rh^I complexes of **127**.

MonodbaPHOS, **128**, can act as a monodentate phosphine or a P,alkene chelate with Pt^{II} depending on the stoichiometry of the reagents used. We were unable to obtain crystals of complex **173**, instead obtaining P,alkene-chelate complexes (**174** and **177**) from both reaction stoichiometries used. The results with Pd^{II} were less conclusive, it is clear that the phosphine is coordinated to the metal centre but less clear what the role of the alkene is. The isolation of complex **176** suggests that the alkene will coordinate to the metal but that it is reactive, and liable to undergo C-H insertion. This potentially reduces the use of monodbaPHOS as a potential ligand for catalysis involving Pd. A

common problem identified with the Pt^{II} and Pd^{II} complexes was that they were often very insoluble. Again, this could cause problems in catalysis, and suggests that initial catalytic attempts may be best conducted with the Pd⁰ complexes, which are far more soluble.

In a number of the complexes downfield shifts of the β -alkenyl proton are observed. The most dramatic shift occurs in the Pt^{II} complex of dbaPHOS, **163**, where a shift of +1.52 ppm (from the free ligand) was seen. The experimental data indicates an anagostic interaction between the hydrogen and the Pt^{II}. Theoretical calculations support the conclusion of a weak hydrogen bond in this complex.

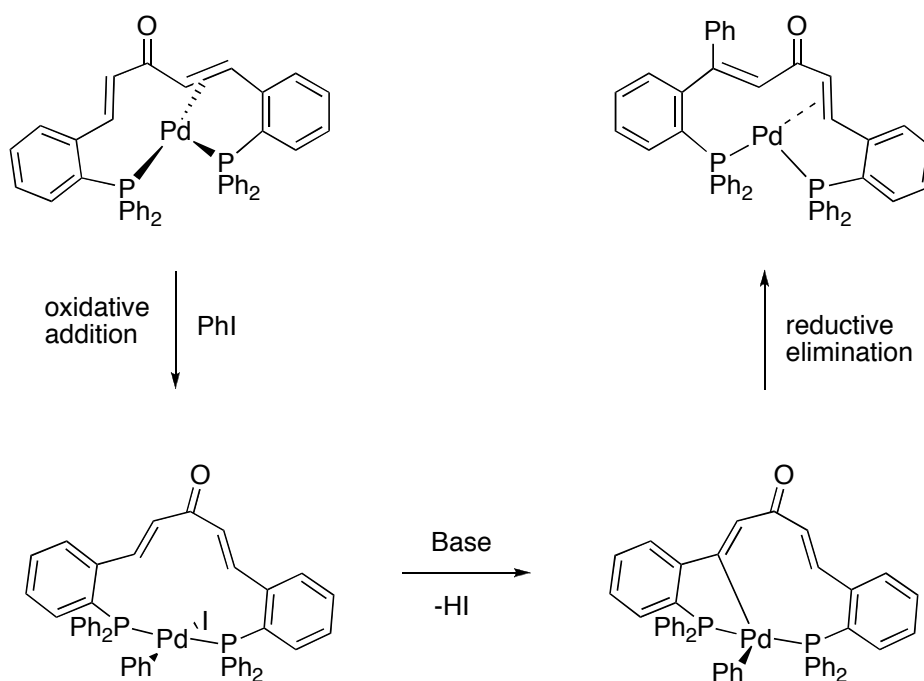
The X-ray crystal structures obtained show the dba '1,4-dien-3-one' backbone in all three different geometries: *s-cis,s-cis*, *s-cis,s-trans*, and *s-trans,s-trans*. Kawazura and co-workers have previously used the $\Delta\delta_{\alpha\beta}$ values in dba and complexes of dba to elucidate the solution geometries of the alkenes. In general they observed larger $\Delta\delta_{\alpha\beta}$ values for *s-trans* alkenes than *s-cis*. When comparing the solution ¹H NMR spectroscopic data and the crystal structures, we observed discrepancies with these trends. As a result, we feel that the use of $\Delta\delta_{\alpha\beta}$ values as a parameter for alkene geometry determination in dba-like backbones must be used with caution, and in conjunction with other techniques.

3.5 Future Work

The aims of this project were to design ligands for use in transition-metal catalysis. Having successfully synthesised the ligands we then studied their coordination modes to several transition metals. This has led to a number of observations including the wide bite angle nature of dbaPHOS, **127**, and its ability to be a *cis*- or *trans*-chelating bidentate phosphine. Future work with these ligands will need to concentrate on their applications in catalysis. The success of the catalytic studies depends on the identification of reactions that will benefit from the properties of the ligands. In light of the coordination studies a number of possibilities present themselves. Firstly, dbaPHOS could be tested in reactions previously known to benefit from wide-bite angle ligands, such as hydroformylation.⁵⁴ Secondly, dbaPHOS could be tested in reactions that work well with bidentate phosphines able to undergo *cis-trans* isomerism and where *trans*-chelating phosphines have shown good activity, such as amidation reactions.⁵⁵ Thirdly,

as alkene coordination was observed for both dbaPHOS, **127**, and monodbaPHOS, **128**, they could be tested in reactions such as the Negishi coupling and C(sp)-C(sp) cross-coupling reactions where other phosphino-alkene ligands have been seen to be successful.⁵⁶ Other more ambitious catalytic reactions to study are alkyl Heck reactions,⁵⁷ with both alkyl halides and alkenes. This would test whether the presence of an alkene in the phosphine backbone reduces unwanted β -hydride elimination, as hypothesised in the introduction.

One of the possible problems with some of these reactions, for instance hydroformylation, is that they use alkenes as substrates. It is therefore possible that the alkene backbone will be chemically modified under the catalytic conditions. The reactivity of the backbone could also be exploited to detect catalytic intermediates in reactions involving alkenes as substrates, such as the Heck reaction. Both dbaPHOS, **127**, and monodbaPHOS, **128**, can be regarded as phosphines with tethered alkenes. The presence of the phosphine could be utilised as a NMR active mechanistic probe (Scheme 18). Phosphino-alkene ligands have previously been used in this way to study the mechanism of the Pauson-Khand reaction.⁵⁸



Scheme 18: Phosphine-alkene, 127 as a tethered alkene substrate for potential intermediate detection in catalysis.

3.6 Experimental

3.6.1 General Information

NMR spectra were obtained in the solvent indicated, using a JEOL ECX400 or JEOL ECS400 spectrometer (400MHz for ^1H , 100 MHz for ^{13}C and 162 MHz for ^{31}P), a Bruker 500 (500 MHz, 126 MHz and 202 MHz for ^1H , ^{13}C and ^{31}P respectively) or on a Bruker AV700 (700 MHz and 283 MHz for ^1H and ^{31}P respectively). Chemical shifts were referenced to the residual undeuterated solvent of the deuterated solvent used (see Table 7). All ^{13}C NMR spectra were obtained with ^1H decoupling. ^{31}P NMR were externally referenced to H_3PO_4 , and obtained with ^1H decoupling. For ^{13}C NMR spectra the coupling constants are quoted to ± 1 Hz. For the ^1H NMR spectra the resolution varies from ± 0.15 to ± 0.5 Hz; the coupling constants have been quoted to ± 0.5 Hz in all cases for consistency. For ^{31}P NMR spectra the coupling constants have been quoted to either ± 0.5 or ± 1 Hz. NMR spectra were processed using Mestronova software.

Solid-state NMR spectroscopy was carried out by the National Solid-State Service in Durham. The spectra were obtained on a Varian VNMRS spectrometer operating at 161.87 MHz (spin rate = 10000 Hz) for ^{31}P and 100.56 MHz (spin rate = 6800 Hz) for ^{13}C . A 4 mm probe was used for the ^{31}P measurements and a 6 mm probe for the ^{13}C . In the ^{13}C measurements the conditions used put a sideband over the ketone signal, so a TOSS sideband suppression experiment was used to reveal the ketone signal. Spectral referencing is with respect to 85% H_3PO_4 or neat tetramethylsilane.

Table 7: Chemical shifts of the residual undeuterated solvent of the deuterated solvents used for NMR spectroscopic analysis.

Solvent	δ_{H} , ppm	δ_{C} , ppm
CHCl_3	7.26	77.16
CDHCl_2	5.31	53.80
$\text{C}_6\text{D}_5\text{H}$	7.16	n/a
THF	3.58	n/a
CD_2HCN	1.94	n/a
Acetone	2.05	n/a
DMSO	2.50	n/a

Melting points were recorded using a Stuart digital SMP3 machine. IR spectroscopy was undertaken using a Jasco/MIRacle FT/IR-4100typeA spectrometer with an ATR attachment on solid and liquid compounds; KBr and solution IR spectra were obtained on a Nicolet Avatar 370 FT-IR spectrometer as stated. The relative intensities of the

peaks are denoted by (s) = strong, (m) = medium and (w) = weak, whilst (br) is used to describe broad peaks. MS spectra were measured using a Bruker Daltonics micrOTOF machine with electrospray ionisation (ESI) or on a Thermo LCQ using electrospray ionisation, with <5 ppm error recorded for all HRMS samples. LIFDI mass spectrometry was carried out using a Waters GCT Premier MS Agilent 7890A GC, with <15 ppm error recorded for all HRMS. Mass spectral data is quoted as the m/z ratio along with the relative peak height in brackets (base peak = 100). UV-visible spectra were recorded using a JASCO V-560 instrument in quartz cells (1 cm path length). Elemental analysis was carried out on an Exeter Analytical CE-440 Elemental Analyser.

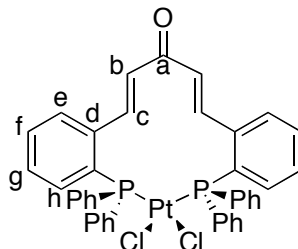
TLC analysis was carried out on Merck TLC aluminium sheets (silica gel 60 F254) and visualised with UV light (254 nm) and iodine vapour. All column chromatography was run on silica gel 60 using the solvent systems specified in the text. The fraction of petroleum ether used was 40-60.

Dry and degassed toluene, CH_2Cl_2 and hexane were obtained from a Pure Solv MD-7 solvent purification system. THF and Et_2O were either obtained from a Pure Solv MD-7 solvent purification system and degassed by the freeze-pump-thaw method or purged with N_2 under sonication; or dried over sodium-benzophenone ketyl and collected by distillation. Benzene was dried over sodium-benzophenone ketyl, and ethanol was dried and distilled from magnesium-iodine. All air-sensitive reactions were carried out using Schlenk techniques or in a MBraun MG-20-G with TP170b glove-box with an N_2 atmosphere. Nitrogen gas was oxygen free and was dried immediately prior to use by passage through a column containing sodium hydroxide pellets and silica. Room temperature was between 13-25 °C. Commercial chemicals were purchased from Sigma-Aldrich or Alfa Aesar. PdCl_2 and RhCl_3 were obtained from Precious Metals Online.⁵⁹

3.6.2 Complex Synthesis

3.6.2.1 Pt and Pd with dbaPHOS

Cis-[PtCl₂(dbaPHOS)], 163



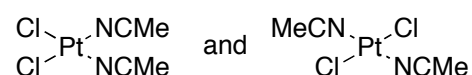
To a solution of dbaPHOS, **127** (200 mg, 1 eq., 0.33 mmol) in dry and degassed CH₂Cl₂ (5 mL) was added [PtCl₂(cod)] (125 mg, 1 eq., 0.33 mmol). The solution was stirred for 1 h under N₂ at rt. A pale yellow precipitate formed. Et₂O (2 mL) was added and the mixture filtered through a funnel with a sintered glass frit and washed with Et₂O (15 mL) to afford the product as a pale yellow powder (224 mg, 78 %). M.p. 140 °C_(dec.); ¹H NMR (400 MHz, CD₂Cl₂) δ 9.82 (d, ³J_{HH} = 16.5 Hz, 2H, H_c), 7.88-7.81 (m, 4H, *o*-Ph), 7.78 (dd, *J* = 8.0, 4.0 Hz, 2H, Ar), 7.61-7.55 (m, 2H, *p*-Ph), 7.52-7.43 (m, 8H, *m*-Ph and Ar), 7.38-7.23 (m, 2H, Ar), 7.05-6.98 (m, 2H, *p*-Ph), 6.91-6.82 (m, 4H, *o*-Ph), 6.74-6.65 (m, 6H, H_b and *m*-Ph); ³¹P NMR (162 MHz, CD₂Cl₂) δ 4.72 (s, ¹J_{PtP} = 3562 Hz); HRMS (ESI) *m/z* 868.1046 [*MH*]⁺ (calculated for C₄₁H₃₃Cl₂OP₂Pt = 868.1026), 833.1235 [*M*-Cl]⁺ (calculated for C₄₁H₃₂ClOP₂Pt = 832.1259), 796.1467 [*M*-HCl₂]⁺ (calculated for C₄₁H₃₁OP₂Pt = 796.1492); IR (KBr, ν cm⁻¹): 3680-3300 (w, br, H₂O), 3055 (m), 3020 (w), 1635 (s), 1616 (s), 1586 (w), 1481 (m), 1461 (m), 1434 (s), 1313 (w), 1293 (m), 1271 (m), 1199 (w), 1188 (w), 1121 (w), 1096 (s), 998 (w), 968 (m), 904 (w), 886 (w), 876 (w), 846 (w), 760 (s), 745 (s), 693 (s), 570 (m), 548 (s), 517 (s), 475 (w); Anal. Calcd. for C₄₁H₃₂OP₂PtCl₂·H₂O (868) C 55.54, H 3.87, Observed C 55.70, H 3.62. Water is observed in the IR spectrum.

Solid-state CPMAS-NMR: ³¹P NMR (162 MHz) δ 4.4 (¹J_{PtP} = 3590 Hz), 1.9 (¹J_{PtP} = 3590 Hz); ¹³C NMR (101 MHz) δ 192.2, 145.2, 141.5, 139.3, 138.3, 135.8, 134.0, 132.9, 129.6, 125.6.

In DMSO-*d*₆ ³¹P NMR (162 MHz, DMSO-*d*₆) δ 15.33 (¹J_{PtP} = 2565 Hz, *trans*-[PtCl₂(dbaPHOS)]), 4.68 (¹J_{PtP} = 3554 Hz, *cis*-[PtCl₂(dbaPHOS)]). After heating at 60 °C for 4 h only the *trans*-[PtCl₂(dbaPHOS)] is now observed: ¹H NMR (400 MHz,

DMSO- d_6) δ 8.81 (d, $^3J_{\text{HH}} = 16.5$ Hz, 2H), 8.20 (d, $J = 8.0$ Hz, 2H), 7.98-7.27 (m, 22H), 7.14-7.04 (m, 2H), 6.97 (d, $^3J_{\text{HH}} = 16.5$ Hz, 2H), 6.87-6.78 (m, 2H); ^{31}P NMR (162 MHz, DMSO- d_6) δ 15.33 ($^1J_{\text{PtP}} = 2565$ Hz). A minor product was also observed in the ^{31}P NMR spectrum δ 43.04 (d, $^2J_{\text{PP}} = 12.0$ Hz), 20.32 (d, $^2J_{\text{PP}} = 12.0$ Hz); no Pt satellites were observed.

***Trans* and *cis*-[PtCl₂(MeCN)₂]⁶⁰**



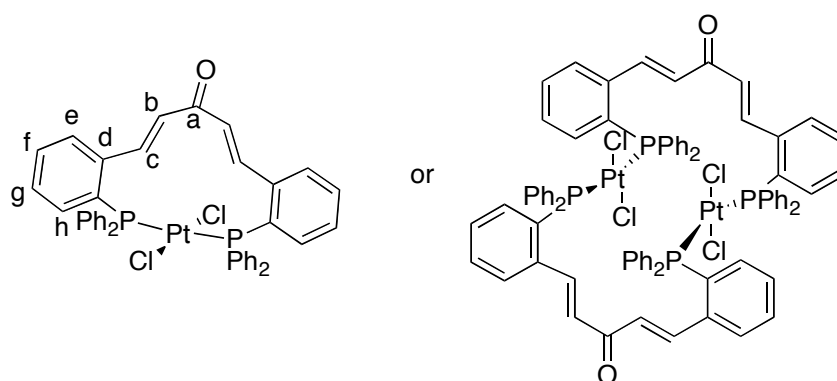
A solution of K₂[PtCl₄] (500 mg, 1 eq., 1.2 mmol) and MeCN (1 mL, 16 eq., 19 mmol) in water (10 mL) was stirred at 25 °C for 7 days. The pale yellow precipitate was filtered and washed with water (20 mL) and dried in air. The *cis* and *trans* isomers were separated by column chromatography on silica gel eluting with acetone:CH₂Cl₂ (v/v 1:9), (the products could be visualized on TLC plates by iodine vapour). A better separation would be achieved by using a less polar elutant.

Trans-[PtCl₂(MeCN)₂] (36 mg, 9%); R_f = 0.58 (White/grey spot in I₂); ^1H NMR (400 MHz, Acetone- d_6) δ 2.77 (s).

Cis-[PtCl₂(MeCN)₂] (33 mg, 8%); R_f = 0.26 (Black spot in I₂); ^1H NMR (400 MHz, Acetone- d_6) δ 2.67 (s).

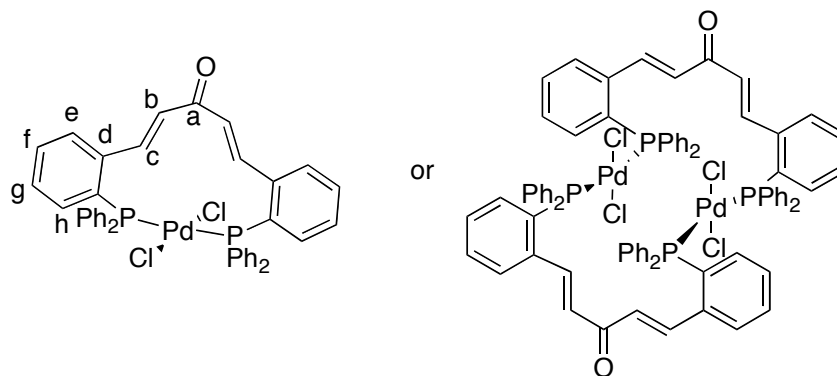
Mixed isomeric fractions (227 mg, 54 %). IR (KBr, ν cm⁻¹): 2969 (m), 2922 (m), 2332 (m), 2302 (w), 1408 (m), 1355 (w), 1030 (m); Anal. Calcd. For C₄H₆Cl₂N₂Pt (348) C 13.80 H 1.74, N 8.05, Observed C 13.93, H 1.69, N 7.68.

***Trans*-[PtCl₂(μ -dbaPHOS)], 164**



To *trans*-[PtCl₂(MeCN)₂] (12 mg, 1 eq., 0.033 mmol) was added a solution of dbaPHOS, **127** (20 mg, 1 eq., 0.033 mmol) in dry and degassed CD₂Cl₂ (0.8 mL) in a glove-box. The reaction was monitored by ¹H and ³¹P NMR spectroscopy. A pale yellow precipitate formed. After 3 h the precipitate was collected by filtration, washed with Et₂O (5 mL) and dried *in vacuo* to give a pale yellow solid (14 mg, 50%). M.p. >230 °C_(dec.); ¹H NMR (500 MHz, CD₂Cl₂) δ 8.90 (d, ³J_{HH} = 16.5 Hz, 2H, H_c), 7.98 (d, ³J_{HH} = 8.0 Hz, 2H, Ar), 7.71-7.62 (m, 8H, Ph), 7.51-7.46 (m, 6H, *p*-Ph and Ar), 7.43-7.36 (m, 8H, Ph), 7.30-7.23 (m, 2H, Ar), 6.93 (dtd, *J* = 7.0, 5.5, 1.0 Hz, 2H, Ar), 6.78 (d, ³J_{HH} = 16.5 Hz, 2H, H_b); ³¹P NMR (202 MHz, CD₂Cl₂) δ 14.89 (¹J_{PtP} = 2577 Hz); HRMS (ESI) *m/z* 796.1470 [*M*-HCl₂]⁺ (calculated for C₄₁H₃₂OP₂Pt = 796.1496); LRMS (LIFDI) *m/z* (rel%) 868.05 [*M*]⁺ (28), 832.02 [*M*-Cl]⁺ (12), 795.11 [*M*-HCl₂]⁺ (100); IR (KBr, ν cm⁻¹): 3680-350 (w, br, H₂O), 3053 (m), 1634 (s), 1560 (w), 1478 (w), 1462 (m), 1432 (s), 1301 (m), 1274 (w), 1202 (m), 1122 (w), 1095 (m), 970 (m), 770 (w), 750 (m), 740 (w), 705 (m), 692 (s), 570 (w), 514 (s), 485 (w). Not enough material was available for elemental analysis.

Trans-[PdCl₂(μ-dbaPHOS)], 165



To a solution of dbaPHOS, **127** (100 mg, 1 eq., 0.17 mmol) in dry and degassed CH₂Cl₂ (2.5 ml) was added [PdCl₂(cod)] (48 mg, 1 eq., 0.17 mmol). The solution was stirred for 1.25 h under N₂ at rt. A pale yellow precipitate had formed. Et₂O (2 mL) was added and the mixture stirred for 10 min. The precipitate was filtered through a funnel with a sintered glass frit and washed with Et₂O to afford the product as a pale yellow powder (98 mg, 76 %). M.p. 252-255 °C_(dec.); ¹H NMR (400 MHz, CD₂Cl₂) δ 8.70 (d, ³J_{HH} = 16.5 Hz, 2H, H_c), 8.01-7.95 (m, 2H, H_e), 7.71-7.63 (m, 8H, *o*-Ph), 7.54-7.47 (m, 6H, *p*-Ph and H_f), 7.43-7.37 (m, 8H, *m*-Ph), 7.30-7.25 (m, 2H, H_g), 6.96-6.89 (m, 2H, H_h), 6.83 (d, ³J_{HH} = 16.5 Hz, 2H, H_b); ³¹P NMR (162 MHz, CD₂Cl₂) δ 19.45 (s); HRMS (ESI) m/z 784.0906 [MMeCN-Cl]⁺ (calculated for C₄₃H₃₅ClNOP₂Pd = 784.0924), 743.0649 [M-Cl]⁺ (calculated for C₄₁H₃₂ClOP₂Pd = 743.0658); LRMS (ESI) m/z (rel%) 784.1 [MMeCN-Cl]⁺ (100), 743.1 [M-Cl]⁺ (77), 707.1 [M-HCl₂]⁺ (86); IR (KBr, cm⁻¹): 3660-3200 (v.w, br H₂O), 3053 (m), 3004 (w), 1633 (s, shoulder at 1616), 1560 (w), 1482 (m), 1462 (m), 1432 (s), 1301 (m), 1274 (m), 1202 (m), 1168 (w), 1121 (w), 1093 (m), 1027 (w), 999 (w), 972 (m), 907 (w), 872 (w), 853 (w), 770 (m), 749 (m), 692 (s), 668 (w), 570 (m), 551 (w), 511 (s), 482 (m); Anal. Calcd. for C₄₁H₃₂OP₂PdCl₂·2H₂O (815) C 60.35, H 4.45, Observed C 60.30, H 3.78. Water was observed in the IR spectrum.

Solid-state CPMAS-NMR: ³¹P NMR (162 MHz) δ 24.0 (d, ²J_{PP} = 540 Hz), 9.9 (d, ²J_{PP} = 540 Hz); ¹³C NMR (101 MHz) δ 194.3, 139.4, 137.0, 135.0, 133.3, 132.2, 129.9, 129.1, 127.1.

[Pd₂(dba)₃] experiments

Experiment 1:

Reaction conducted by I. J. S. Fairlamb

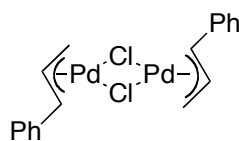
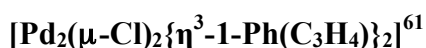
In a glove box, [Pd₂(dba)₃] (10 mg, 0.5 eq., 0.011 mmol) and dbaPHOS **127** (13.4 mg, 1 eq., 0.022 mmol) were desolved in dry CD₂Cl₂/*d*₈-THF (1:1, 1 mL). The mixture was left to stir for 2 h and then an aliquot (0.7 mL) was removed and filtered (glass wool pipette), and then analysed by ³¹P NMR spectroscopy, which revealed two major complexes in a ratio of ~1:1. ³¹P NMR (202 MHz, CD₂Cl₂/*d*₈-THF) δ 37.7 (d, *J*_{PP} = 15.5, 1P), 30.9 (d, *J*_{PP} = 21.5, 1P), 29.2 (d, *J*_{PP} = 15.5, 1P), 12.9 (d, *J*_{PP} = 21.5, 1P). Three other minor phosphorus signals were observed at 27.5, 28.3 and 28.6 ppm as singlets. ¹H NMR spectroscopy showed a mixture of species, in addition to considerable amounts of free dba ligand.

Experiment 2:

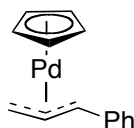
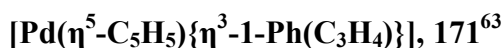
In a glove box, [Pd₂(dba)₃] (16 mg, 0.5 eq., 0.018 mmol) and dbaPHOS **127** (22 mg, 1 eq., 0.036 mmol) were dissolved in dry and degassed THF (0.7 mL). Acetone-*d*₆ (10%) was added to facilitate analysis by ³¹P NMR spectroscopy. The ³¹P NMR spectrum showed broad signals around 35-29 ppm and the two doublets at 31.4 and 13.1 ppm (*J*_{PP} = 25 Hz). On heating the sample to 50 °C, further signals appeared at 27.8, 26.7, and 16.6 (d, *J*_{PP} = 21 Hz).

Experiment 3:

The reaction above was also conducted in C₆D₆. The ³¹P NMR spectrum showed broad signals around 32-26 ppm and -12—16 ppm. Five other phosphorus signals were observed at 0.1, -11.2, -14.0, -16.3 and -17.9 ppm as singlets. ¹H NMR spectroscopy showed a considerable amount of free dba. On heating the sample to 60 °C two distinct doublets were observed in a ratio of 10:1. ³¹P NMR (162 MHz, C₆D₆) δ 46.9 (d, *J*_{PP} = 20.0 Hz, 1P), 39.7 (d, *J*_{PP} = 20.0 Hz, 1P), 37.9 (d, *J*_{PP} = 20.0 Hz, 0.1P), 22.2 (d, *J*_{PP} = 20.0 Hz, 0.1P). Six other other phosphorus signals were observed at 29.0, 28.5, 28.3, 26.9, 0.6, -13.6 ppm as singlets, the latter one broad. A broad peak was still observed between 33-27 ppm. No product signals could be clearly observed in the ¹H NMR spectrum due to considerable amounts of free dba.



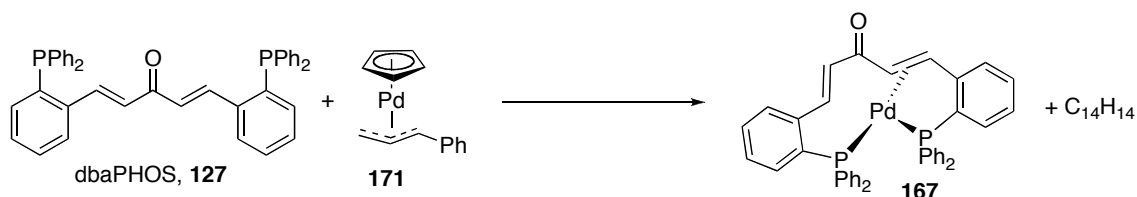
Under air, PdCl₂ (0.5 g, 1 eq., 2.8 mmol) and LiCl (0.5 g, 4.2 eq., 11.8 mmol) were added to a large Schlenk. H₂O (0.7 mL) was added and the mixture heated to 70 °C for 20 min. Once the mixture had cooled to rt, a solution of cinnamyl chloride (1.6 mL, 3.9 eq., 10.9 mmol) in EtOH (5.6 mL) was added whilst stirring. The Schlenk was then placed under a CO atmosphere after a freeze-pump-thaw cycle, and stirred at rt. After 2.5 h the Schlenk was filled again with CO and stirred overnight. Yellow precipitate appeared, and the mixture was cooled to 0 °C, the precipitate collected by filtration and washed with MeOH (10 mL). The yellow solid was recrystallized from CHCl₃ (50 mL) and Et₂O (150 mL) at 4 °C, and the bright yellow known product collected by filtration (632 mg, 87%). M.p. 188 °C_(dec.), (*Lit.*⁶² 218-220 °C); ¹H NMR (400 MHz, CDCl₃) δ 7.50 (d, ³J_{HH} = 7.5 Hz, 2H), 7.35 (t, ³J_{HH} = 7.5 Hz, 1H), 7.27 (t, ³J_{HH} = 7.5 Hz, 2H), 5.80 (ddd, ³J_{HH} = 12.0, 11.5, 7.0 Hz, 1H), 4.62 (d, ³J_{HH} = 11.5 Hz, 1H), 3.97 (d, ³J_{HH} = 7.0 Hz, 1H), 3.04 (d, ³J_{HH} = 12.0 Hz, 1H); Anal. Calcd. for C₁₈H₁₈Cl₂Pd₂ (517) C 41.73, H 3.50, Observed C 41.52, H 3.46.



To a suspension of [Pd₂(μ-Cl)₂{η³-1-Ph(C₃H₄)}₂] (250 mg, 1 eq., 0.48 mmol) in dry and N₂ purged THF (20 mL), was added 2M NaCp solution (0.5 mL, 2 eq., 1 mmol) in extra THF (4.5 mL). The mixture was stirred for 35 min, before removing the solvent *in vacuo*. The residue was extracted using dry and degassed hexane (20 mL), the volume of solvent was reduced *in vacuo* to ~6 mL and the solution cooled to -40 °C. The resulting red/purple precipitate was collected by cannula filtration to give the known product (103 mg, 37%). M.p. 51.2-52.9 °C, (*Lit.*⁶³ 50 °C); ¹H NMR (400 MHz, C₆D₆) δ 7.37-7.21 (m, 2H), 7.07-6.95 (m, 3H), 5.68 (s, 5H), 5.16 (ddd, ³J_{HH} = 10.5, 10.0, 6.0 Hz, 1H), 3.87 (dd, ³J_{HH} = 10.0 Hz, ²J_{HH} = 0.5 Hz, 1H), 3.35 (d, ³J_{HH} = 6.0 Hz, 1H), 2.17 (dd, ³J_{HH} = 10.5 Hz, ²J_{HH} = 0.5 Hz, 1H); Anal. Calcd. for C₁₄H₁₄Pd (288) C 58.25, H 4.89, Observed C 58.47, H 4.98.

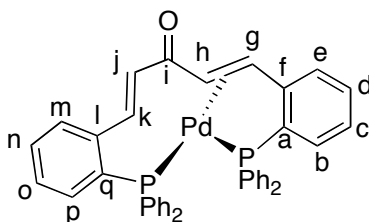
[Pd⁰(dbaPHOS)], **167**

NMR experiment



In a glove-box, a solution of **171** (10 mg, 1 eq., 0.034 mmol) in dry and degassed CD₂Cl₂ (0.65 mL) was added to dbaPHOS, **127** (20.5 mg, 1 eq. 0.034 mmol). The reaction mixture was analysed directly. A ³¹P NMR spectrum was obtained: δ 31.74 (d, ²J_{PP} = 20.5 Hz), 13.79 (d, ²J_{PP} = 20.5 Hz). The solvent was removed and the resulting purple residue washed with dry and degassed Et₂O to remove the organic side products, to give the product as a purple solid (7.5 mg, 31%). HRMS (ESI) m/z 707.0884 [*M*-H]⁺ (calculated for C₄₁H₃₁OP₂Pd = 707.0894).

Preparative synthesis of [Pd⁰(dbaPHOS)], **167**



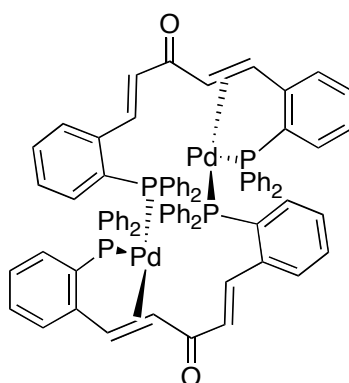
To a Schlenk containing dbaPHOS, **127** (100 mg, 1 eq., 0.17 mmol) and [Pd(η^5 -C₅H₅){ η^3 -1-Ph(C₃H₄)}], **171** (47 mg, 1 eq., 0.17 mmol) was added dry and degassed CH₂Cl₂ (3.5 ml), which was stirred at rt. for 2 h. The solvent was then removed *in vacuo* to give a red solid. Dry and degassed Et₂O (8 ml) was added and the mixture stirred to dissolve any remaining organics. Filtration by cannula, followed by drying the solid *in vacuo* gave the product as a red/purple solid[§] (79 mg, 66%). M.p. 188 °C_(dec.); ¹H NMR (500 MHz, CD₂Cl₂, 295 K) 8.92 (dd, ³J_{HH} = 16.5 Hz, ³J_{HP} = 4.5 Hz, 1H, H_k), 7.47-6.67 (m, 28H, Ar), 5.95 (m with underlying d, ³J_{HH} = 16.5 Hz, 2H, H_j and H_g), 5.28 (dd, ³J_{HH} = 11.5 Hz, ²J_{HP} = 8.0 Hz, 1H, H_h); ³¹P NMR (202 MHz, CD₂Cl₂) δ 31.15 (d, ²J_{PP} = 20.5 Hz), 13.19 (d, ²J_{PP} = 20.5 Hz); ¹³C NMR (126 MHz, CD₂Cl₂)^{**} δ 185.7 (C_i), 134.6 (d, J_{CP} = 17 Hz), 133.9 (d, J_{CP} = 16 Hz), 133.1, 132.6 (d, J_{CP} = 13 Hz, C_k), 131.2 (C_j), 130.6, 129.9, 129.6, 129.3, 128.9 (d, J_{CP} = 9 Hz), 128.7-128.5 (m),

[§] The product varied from purple to brick red depending on the batch - no differences were observed by UV-vis spectroscopy.

^{**} Observed signals given, doublets given when observed.

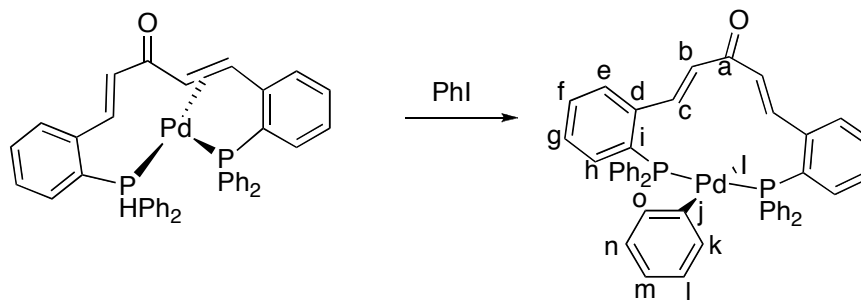
128.2 (d, $J_{CP} = 10$ Hz), 127.7 (d, $J_{CP} = 5$ Hz), 82.9 (d, $J_{CP} = 21$ Hz, C_g), 69.5-69.2 (m, C_h); HRMS (LIFIDI) m/z 708.0887 $[M]^+$ (calculated for $C_{41}H_{32}OP_2Pd = 708.0963$); IR (KBr, ν cm^{-1}): 3050 (w), 1653 (m), 1588(m), 1478 (m), 1457 (m), 1433 (s), 1298 (m), 1209 (w), 1180 (w), 1118 (w), 1093 (m), 1026 (w), 998 (w), 968 (w), 830 (w), 742 (m), 693 (s), 574 (w), 505 (m); UV-vis (CH_2Cl_2) λ_{max} nm: 454 ($\epsilon = 7088$ $mol^{-1}dm^3cm^{-1}$), 284 ($\epsilon = 18951$ $mol^{-1}dm^3cm^{-1}$); Anal. Calcd. for $C_{41}H_{32}OP_2Pd$ (708) C 69.45 H 4.55, Observed C 69.32 H 4.55.

Crystals of $[Pd_2(\mu\text{-dbaPHOS})_2]$, **167(dimer)**, were obtained from CD_2Cl_2 layered with Et_2O (1:1 $CD_2Cl_2:Et_2O$). The crystals were of low quality ($R_I = 0.09$) due to disorder and twinning, so no bond lengths *etc.* could be determined. However, it was clear that the complex existed as a dinuclear complex with the dbaPHOS acting as a bridging ligand. The 1,4-dien-3-one backbone geometry was found to be *s-cis,s-trans*. Unit cell details: $a = 16.3500(4)$ Å, $b = 17.7477(4)$ Å, $c = 25.4143(10)$ Å; $\alpha = 78.161(3)^\circ$, $\beta = 89.978(3)^\circ$, $\gamma = 89.9313(18)^\circ$.



A solution of $[Pd^0(\text{dbaPHOS})]$, **167**, in CD_2Cl_2 was heated at 55 °C for 48 h. ^{31}P NMR (162 MHz, CD_2Cl_2) δ 47.10 (d, $^2J_{PP} = 22.0$ Hz, 1P), 39.53 (d, $^2J_{PP} = 22.0$ Hz, 1P), 38.54 (d, $^2J_{PP} = 20.5$ Hz, 0.4P), 31.74 (d, $^2J_{PP} = 20.5$ Hz, 1.5P), 21.95 (d, $^2J_{PP} = 20.5$ Hz, 0.4P), 13.79 (d, $^2J_{PP} = 20.5$ Hz, 1.1P). 1H NMR (400 MHz, CD_2Cl_2) δ 8.91 (d, $J = 11.0$ Hz, 0.8H), 8.0-5.9 (m, 66H), 5.98-5.87 (m, 1H), 5.29-5.23 (m, 1H), 4.21-4.11 (m, 0.7H), 4.03-3.90 (m, 0.4H), 3.32-3.19 (m, 0.5H), 3.08-2.83 (m, 1.6H).

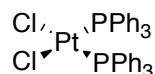
[Pd⁰(dbaPHOS)] + iodobenzene, **172**



To a solution of [Pd⁰(dbaPHOS)], **167** (11.6 mg, 1 eq., 0.015 mmol)^{††} in THF-*d*₈ (0.8 mL) in a Youngs tap NMR tube was added iodobenzene (1.8 μL, measured as 1 eq.) under a flow of Ar. The reaction was monitored by ¹H and ³¹P NMR spectroscopy. After 1 h the oxidative addition was complete (100% conversion by ³¹P NMR spectroscopy). ¹H NMR (500 MHz, THF-*d*₈) δ 8.88 (d, ³J_{HH} = 16.5 Hz, 2H, H_c), 8.02-7.91 (m, 6H, Ar), 7.41-7.30 (m, 8H, Ar), 7.24 (apparent t, ³J_{HH} = 7.5 Hz, 2H, Ar), 7.17 (d, ³J_{HH} = 7.5 Hz, 1H, H_o), 7.09-7.04 (m, 6H, Ar), 7.01-6.95 (m, 4H, Ar), 6.93-6.84 (m, underlying d, ³J_{HH} = 16.5 Hz, 4H, H_b and Ar), 6.42 (apparent t, ³J_{HH} = 7.5 Hz, 1H, H_n), 6.36 (apparent t, ³J_{HH} = 7.5 Hz, 1H, H_m), 6.15 (apparent d, ³J_{HH} = 7.5 Hz, 1H, H_k), 5.95 (apparent t, ³J_{HH} = 7.5 Hz, 1H, H_i); ³¹P NMR (202 MHz, THF-*d*₈) δ 16.83 (s); LRMS (LIFDI) m/z (rel%) 911.06 [*M*]⁺ (8) {isotope pattern 908.99 (24), 910.12 (47), 911.10 (86), 912.01 (40), 913.08 (100), 914.07 (25), 915.08 (21)}, 784.14 [*M*-I]⁺ (100) {isotope pattern: 782.14 (17), 783.15 (58), 784.14 (100), 786.13 (67), 788.14 (25), 789.45 (8)}, 706.09 (31), 679.26 (44); HRMS (LIFDI) m/z 784.1377 [*M*-I]⁺ (calculated for C₄₇H₃₆OP₂Pd = 784.1276).

Crystals of **172** suitable for X-Ray diffraction were grown by cooling the reaction mixture to -18 °C (*d*₈-THF). Not enough material was recovered for elemental analysis.

[PtCl₂(PPh₃)₂]⁶⁴

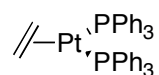


A solution of K₂[PtCl₄] (250 mg, 1 eq. 0.6 mmol), and triphenylphosphine (474 mg, 3 eq. 1.8 mmol) in *p*-xylene (5 mL) was heated to 140 °C for 6.5 h, and then left to stir overnight at rt. The precipitate was then filtered and washed with EtOH (3 x 5 mL),

^{††} Not all the material dissolved, only the solution was transferred to the Youngs tap NMR tube, therefore the iodobenzene was actually in excess, estimated from the NMR spectra to be 2.5 eq.

H₂O (3 x 5 mL), EtOH (5 mL) and Et₂O (3 x 5 mL). The product was then dried *in vacuo* to give the known product (404 mg, 85%). M.p. 301-303 °C, (*Lit.*⁶⁵ 193-195 °C_(dec.)); ¹H NMR (400 MHz, CDCl₃) δ 7.55-7.44 (m, 12H), 7.37-7.29 (m, 6H), 7.17 (td, *J* = 8.0, 2.0 Hz, 12H); ³¹P NMR (400 MHz, CDCl₃) δ 14.93 (s, ¹*J*_{PtP} = 3680 Hz); Anal. Calcd. for C₃₆H₃₀Cl₂P₂Pt (790) C 54.69, H 3.83, Observed C 54.57, H 3.75.

[Pt(C₂H₄)(PPh₃)₂]⁶⁶



Dry and degassed CH₂Cl₂ (5 mL) and EtOH (5 mL) were put into a three-necked flask. [PtCl₂(PPh₃)₂] (300 mg, 1 eq., 0.38 mmol) was added and the mixture stirred. After three freeze-pump-thaw cycles the mixture was placed under a C₂H₄ atmosphere, NaBH₄ (72 mg, 5 eq., 1.9 mmol) was added in small amounts under a stream of C₂H₄. The resulting mixture was stirred for 30 min under a C₂H₄ atmosphere. EtOH (20 mL) was added, stirring continued for 5 min. The C₂H₄ atmosphere was removed and the precipitate filtered by Büchner filtration and washed with H₂O (20 mL), EtOH (20 mL) and pentane (20 mL). After air drying the known product was obtained (217 mg, 77%, 80% purity by ³¹P NMR spectroscopy). Mp. 124 °C_(dec) (*Lit.* >65 °C_(dec)); ¹H NMR (400 MHz, CDCl₃) δ 7.62-7.43 (br m, 12H), 7.03-6.88 (br m, 18H), 2.75 (s, ²*J*_{PtH} = 60 Hz, 2H), 2.74 (s, ²*J*_{PtH} = 60 Hz, 2H); ³¹P NMR (400 MHz, CDCl₃) δ 35.16 (s, ¹*J*_{PtP} = 3739 Hz).

Pt⁰ complexation of dbaPHOS:

Using [Pt₂(dba)₃]:

To [Pt₂(dba)₃] (11 mg, 1 eq., 0.01 mmol), was added a solution of dbaPHOS (12 mg, 2 eq., 0.02 mmol) in dry and degassed C₆D₆ (0.7 mL). The ³¹P and ¹H NMR spectra were recorded. ³¹P NMR (500 MHz, C₆D₆) δ 21.23 (¹*J*_{PtP} = 3128 Hz), 20.39 (d, ²*J*_{PP} = 14.6 Hz, Pt(dbaPHOS)(dba)?), 19.18 (d, ²*J*_{PP} = 14.6 Hz, Pt(dbaPHOS)(dba)?), and other signals at 0.10, -11.24, -13.98, -14.52, -14.92; ¹H NMR (500 MHz, C₆D₆) δ 8.78 (dd, ³*J*_{HH} = 16.0 Hz, ⁴*J*_{HP} = 4.5 Hz, 1.5H, uncoordinated C=C from dbaPHOS), 8.67 (dd, ³*J*_{HH} = 15.5 Hz, ⁴*J*_{HP} = 4.0 Hz, 1H, uncoordinated C=C from dbaPHOS), 7.86 (d, ³*J*_{HH} = 16.0 Hz, 6H), 7.38 (td, *J* = 7.5, 2.0 Hz, 10H), 7.33-7.28 (m, 18H), 7.13-7.09 (m, 20H), 7.09-7.03 (m, 24H), 7.02-6.88 (m with underlying d, ³*J*_{HH} = 16.0 Hz, 25H), 6.85 (t, ³*J*_{HH} = 7.5 Hz, 3H), 6.79 (d, ³*J*_{HH} = 16.0 Hz, 2H), 6.75 (t, ³*J*_{HH} = 7.5 Hz, 1H), 6.51-6.36 (m, 1H), 5.31-5.17 (m, 1H), 4.64 (d, ³*J*_{HH} = 9.5 Hz, ²*J*_{PtH} = 34 Hz, 1H, bound C=C).

Nothing distinctive occurred on leaving for 48 h, and a very similar ^{31}P NMR spectrum was obtained for a Pt:L ratio of 1:2.

Using $[\text{Pt}(\text{C}_2\text{H}_4)(\text{PPh}_3)_2]$ as a precursor:

To a yellow solution of dbaPHOS, **127** (13.6 mg, 1 eq. 0.026 mmol) in degassed CDCl_3 (1 mL) was added $[\text{Pt}(\text{C}_2\text{H}_4)(\text{PPh}_3)_2]$ (16.8 mg, 1 eq. 0.026 mmol). The reaction mixture turned red immediately. After stirring for 10 min the mixture was left to stand overnight, before characterisation ^1H and ^{31}P NMR spectroscopy. ^1H NMR (400 MHz, CDCl_3) δ 8.12-5.32 (br m, 40H), 5.02-3.41 (br m, 1H); ^{31}P NMR (400 MHz, CDCl_3) δ 20.46 (br, 0.9P), -4.83 (br, PPh_3 1P), -14.33 (br, 0.14P), -14.45 (br, 0.14P); HRMS (ESI) m/z 798.1631 $[\text{MH}]^+$ (calculated for $\text{C}_{41}\text{H}_{33}\text{OP}_2\text{Pt} = 798.1649$).

3.6.2.2 Pt^{II} and Pd^{II} complexes of monodbaPHOS

From $\text{M}(\text{COD})\text{Cl}_2$

NMR scale reactions:

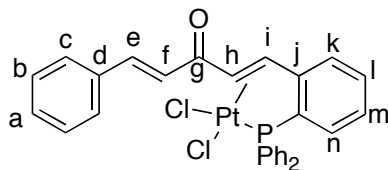
Pd:monodbaPHOS 1:1 ($[\text{PdCl}_2(\text{monodbaPHOS})]$)

To monodbaPHOS, **128** (22 mg, 1 eq. of free phosphine if take as 90% pure, 0.046 mmol) was added a solution of $[\text{PdCl}_2(\text{cod})]$ (13 mg, 1 eq., 0.046 mmol) in dry and degassed CD_2Cl_2 (0.7 mL). The monodbaPHOS dissolved and almost immediately precipitate started to form. The reaction mixture was analysed directly. ^{31}P NMR (162 MHz, CD_2Cl_2) δ 30.56 (s, "P=O" impurity, 1P), 21.26 (s, 0.3P). In the ^1H NMR spectrum (400 MHz, CD_2Cl_2) only one peak was assignable to the product δ 6.33 (d, $^3J_{\text{HH}} = 16.2$ Hz, C=C, 0.06H). Free COD δ 5.54 (s, 1H), 2.34 (s, 2H). Coordinated COD δ 6.27-6.20 (m, 1.2H), 2.94-2.80 (m, 1.2H), 2.61-2.48 (m, 1.2H).

Pd:monodbaPHOS 1:2 ($[\text{PdCl}_2(\text{monodbaPHOS})_2]$)

To monodbaPHOS, **128** (43 mg, 2 eq. of free phosphine if take as 90% pure, 0.089 mmol) was added a solution of $[\text{PdCl}_2(\text{cod})]$ (13 mg, 1 eq., 0.045 mmol) in dry and degassed CD_2Cl_2 (0.7 mL). The dbaPHOS dissolved and almost immediately precipitate started to form, and only the phosphine oxide is observed in the ^{31}P NMR.

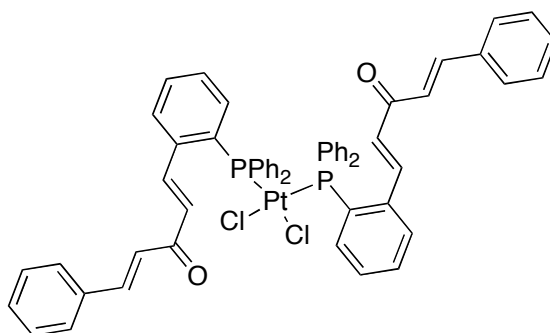
[PtCl₂{s-cis,s-cis(*E,E*monodbaPHOS)}], 174



To monodbaPHOS, **128** (27 mg, 1 eq. of free phosphine if taken as 90% pure, 0.055 mmol) was added a solution of [PtCl₂(cod)] (21 mg, 1 eq., 0.055 mmol) in dry and degassed CD₂Cl₂ (0.7 mL). The reaction mixture was analysed directly and shown to give a 1:1 ratio of products. ³¹P NMR (162 MHz, CD₂Cl₂) δ 30.47 (s, “P=O” impurity), 24.75 (s, ¹J_{PtP} = 3080 Hz, 1:1 product), 11.96 (s, ¹J_{PtP} = 3644 Hz, 1:2 product); Independent observed signals for Pt(monodbaPHOS)Cl₂: ¹H NMR (400 MHz, CD₂Cl₂) δ 8.11-8.00 (m, 2H), 7.80-7.71 (m, 4H), 7.36-7.31 (m, 2H), 6.72 (d, ³J_{HH} = 16.5 Hz, 1H, H_f), 6.35 (d, ³J_{HH} = 11.5 Hz, ²J_{PH} ~ 30 Hz, 1H, H_i), 5.06 (dd, ³J_{HH} = 11.5 Hz, ²J_{HP} = 3.0 Hz, ²J_{PH} = 35 Hz, 1H, H_h); LRMS (ESI) m/z (rel%) 1329 (9), 891 (26), 725 [M+MeCN]⁺ (10), 703 [M+H₂O]⁺ (14), 649 [M-Cl]⁺ (100), 612 (12), 567 (19), 499 (16), 457 [monodbaPHOS oxideNa]⁺ (47).

Crystals of **[PtCl₂{s-cis,s-cis(*E,E*-monodbaPHOS)}], 174**, suitable for X-Ray diffraction were obtained by layering a CH₂Cl₂ solution with Et₂O (ijf0826m).

[PtCl₂(monodbaPHOS)₂], 173



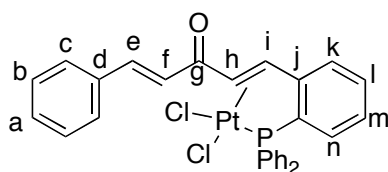
To a solution of monodbaPHOS, **128** (25 mg, 2 eq. of free phosphine if taken as 90% pure, 0.0518 mmol) in dry and degassed CD₂Cl₂ (0.7 mL) was added [PtCl₂(cod)] (9.7 mg, 1 eq., 0.0258 mmol). The reaction mixture was analysed directly. No bound COD was observed by ¹H NMR spectroscopy. ³¹P NMR (162 MHz, CD₂Cl₂) δ 30.44 (s, “P=O” impurity, 1P), 11.96 (s, ¹J_{PtP} = 3647 Hz, 8P); ¹H NMR (400 MHz, CD₂Cl₂) δ 7.90 (d, ³J_{HH} = 16.0 Hz, 2H), 7.53 (d, *J* = 11.5 Hz, 8H), 7.51-7.33 (m, 20H), 7.28 (t, *J* = 7.5 Hz, 4H), 7.09 (t, *J* = 7.0 Hz, 8H), 6.82 (d, ³J_{HH} = 16.0 Hz, 2H), 6.28 (d, ³J_{HH} = 16.0

Hz, 2H); LRMS (ESI) m/z (rel%) 1341 (8), 1325 (30), 1151 (10), 1125 $[MNa]^+$ (10), 1062 (49), 1031 $[M-Cl_2]^+$ (9), 891 (100), 457 $monodbaPHOSoxideNa]^+$ (34).

Crystals of $[PtCl_2\{s-cis,s-trans-(Z,E-monodbaPHOS)\}]$, **177**, suitable for X-Ray diffraction were obtained on layering a CH_2Cl_2 solution with hexane (ijf0839m).

Preparative scale reactions:

$[PtCl_2\{s-cis,s-cis(E,E-monodbaPHOS)\}]$, **174**



To a solution of $[PtCl_2(cod)]$ (37 mg, 1 eq., 0.1 mmol) in dry and degassed CH_2Cl_2 (20 mL, 0.005 M) was added monodbaPHOS, **128** (42 mg, 1 eq., 0.1 mmol). The mixture was stirred at 20 °C for 4 h. The solvent was removed under reduced pressure and the residue redissolved in CH_2Cl_2 (~5 mL) and Et_2O (15 mL) added. After leaving in the fridge overnight a pale yellow precipitate was observed. The solid was collected by vacuum filtration using a sintered glass frit and washed with Et_2O (5 mL). The solid was dried to give the title compound (52 mg, 76 %). M.p. 170 °C_(dec.); 1H NMR (400 MHz, CD_2Cl_2) δ 8.10-7.98 (m, 2H, Ar), 7.86-7.68 (m, 4H, Ar), 7.59-7.50 (m, 2H, Ar), 7.48-7.15 (m, 12H, H_e, H_a, H_b, H_c and Ar), 6.71 (d, $^3J_{HH} = 16.5$ Hz, 1H, H_f), 6.34 (d, $^3J_{HH} = 11.5$ Hz, $^2J_{PH} = 28$ Hz, 1H, H_i), 5.05 (dd, $^3J_{HH} = 11.5$ Hz, $^2J_{HP} = 3.0$ Hz, $^2J_{PH} = 37$ Hz, 1H, H_h). ^{31}P NMR (162 MHz, CD_2Cl_2) δ 24.72 (s, $^1J_{PtP} = 3080$ Hz); ^{13}C NMR (100 MHz, CD_2Cl_2) δ 188.0 (C_g), 150.2 (d, $^2J_{CP} = 16$ Hz, C_j), 144.7 (s, C_e), 134.7 (d, $J_{CP} = 3$ Hz), 134.6 (C_d), 134.0 (d, $J_{CP} = 11$ Hz, Ar), 133.6 (d, $J_{CP} = 3$ Hz, Ar), 133.5 (d, $J_{CP} = 3$ Hz, Ar), 133.3 (d, $J_{CP} = 11$ Hz, Ar), 132.8 (d, $J_{CP} = 3$ Hz, Ar), 131.2 (C_a), 130.5 (d, $J_{CP} = 12$ Hz, Ar), 130.4 (d, $J_{CP} = 9$ Hz, Ar), 129.2 (Ar), 129.0 (d, $J_{CP} = 13$ Hz, Ar), 128.7 (Ar), 127.7 (d, $J_{CP} = 13$ Hz, Ar), 127.4 (C_f), 126.2 (d, $^1J_{CP} = 74$ Hz, *ipso*-C), 125.2 (d, $^1J_{CP} = 62$ Hz, *ipso*-C), 86.6 (d, $^3J_{CP} = 4$ Hz, C_i), 80.7 (C_h); HRMS (ESI) m/z 648.0828 $[M-Cl]^+$ (calculated for $C_{29}H_{23}ClOPPt = 648.0820$); IR (KBr, ν cm^{-1}): 3030 (m), 1683 (s), 1658 (m), 1607 (s), 1576 (m), 1495 (w), 1481 (m), 1436 (s), 1330 (m), 1315 (m), 1231 (w), 1176 (m), 1135 (w), 1090 (s), 1071 (m), 1026 (w), 998 (m), 975 (m), 764 (s), 753 (m), 710 (s), 691 (s), 570 (m), 558 (s), 542 (s), 513 (m), 502 (m), 474 (m); Anal. Calcd. for $C_{29}H_{23}Cl_2PPt$ (613) C 50.89, H 3.39, Observed C 50.63, H 3.38.

From M(MeCN)₂Cl₂

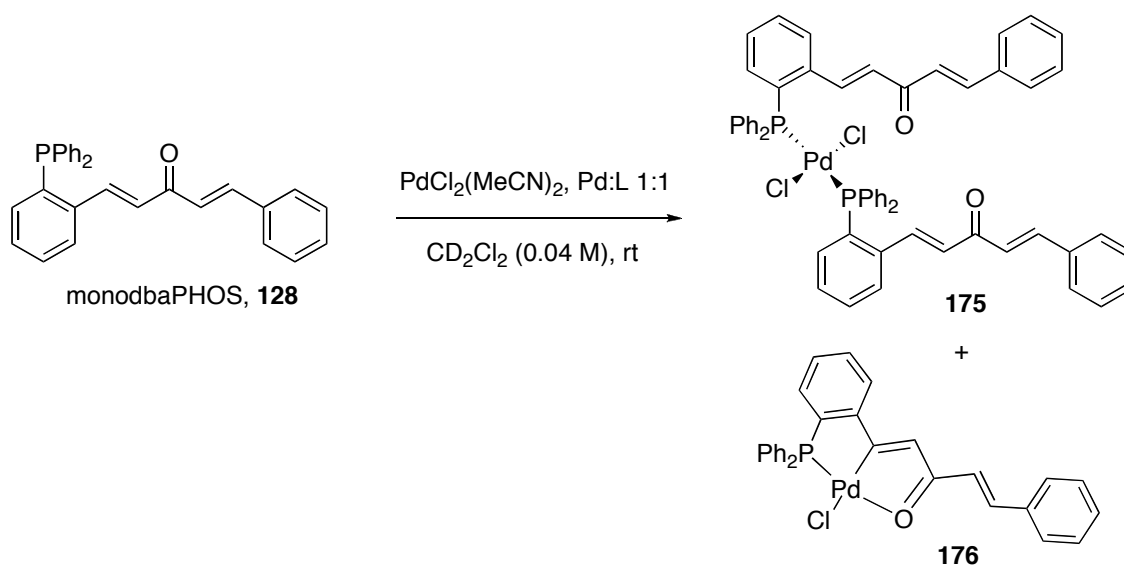
Pt:monodbaPHOS 1:1 (*[PtCl₂(monodbaPHOS)]*)

To a suspension of *cis*-[PtCl₂(MeCN)₂] (33 mg, 1 eq., 0.095 mmol) in dry and degassed CH₂Cl₂ (3 mL) was added monodbaPHOS, **128** (40 mg, 1 eq., 0.095 mmol) and the mixture stirred for 16 h. Et₂O was added and the precipitate collected by filtration, washed with Et₂O (10 mL), and acetone (25 mL) and then dried to give a pale yellow solid (44 mg, 68 %) insoluble in CH₂Cl₂, CHCl₃, acetone, DMSO, MeCN. Mp 240-244 °C_(dec.); IR (KBr, ν cm⁻¹): 3057 (w), 1655 (s), 1617 (m), 1600 (s), 1574 (m), 1495 (w), 1481 (w), 1460 (m), 1434 (s), 1329 (s), 1282 (w), 1187 (s), 1168 (m), 1124 (m), 1097 (s), 1028 (w), 1000 (w), 976 (m), 950 (m), 873 (w), 847 (w), 771 (m), 750 (m), 710 (m), 692 (s), 668 (w), 560 (m), 524 (s), 510 (s), 477 (m), 452 (m); LRMS (LIFDI) m/z (rel%) 648.05 [*M*-HCl]⁺ (100) {isotope pattern 646.04 (40), 647.05 (63), 648.05 (100), 649.06 (29), 650.05 (21)}; LRMS (ESI) m/z (rel%) 719 (100), 684 [*MH*]⁺ (10), 610 (31), 522 (42), 481 (21), 419 [monodbaPHOS+H]⁺ (85), 371 (45), 330 (35), 289 (24), 208 (28).

Pt:monodbaPHOS 1:2 (*[PtCl₂(monodbaPHOS)₂]*)

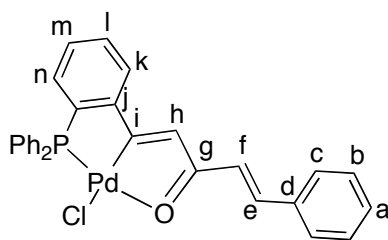
To a suspension [PtCl₂(MeCN)₂] (41 mg, 1 eq., 0.12 mmol) in dry and degassed CH₂Cl₂ (4 mL) was added monodbaPHOS, **128** (100 mg, 2 eq., 0.24 mmol). The solution was left to stir for 2 h, during which time a pale yellow precipitate formed. Et₂O (5 mL) was added and the resulting solid collected by filtration, washed with Et₂O (10 mL) and dried to give a pale yellow solid (112 mg, 85 %) insoluble in CH₂Cl₂, CHCl₃, acetone, DMSO, MeCN. Mp 244-245 °C_(dec.); IR (KBr, ν cm⁻¹): 3660-3300 (w, br, H₂O), 3058 (w), 3032 (w), 1655 (s), 1624 (m), 1599 (s), 1495 (w), 1481 (m), 1459 (m), 1437 (s), 1329 (s), 1282 (w), 1187 (s), 1167 (m), 1097 (m), 1028 (w), 1000 (w), 977 (m), 950 (w), 874 (w), 850 (w), 763 (m), 749 (m), 707 (m), 692 (s), 560 (w), 525 (s), 514 (s), 491 (w), 476 (w); LRMS (ESI) m/z (rel%) 1125 [*MNa*]⁺ (4), 899 (26), 758 (9), 684 (22), 610 (54), 536 (30), 481 (100); Anal. Calcd. for C₅₈H₆₄Cl₂O₂P₂ Pt.3H₂O (1156) C 60.21 H 4.53, Observed C 60.66, H 4.15. Water was observed in the IR spectrum.

Pd:monodbaPHOS 1:1 (176)



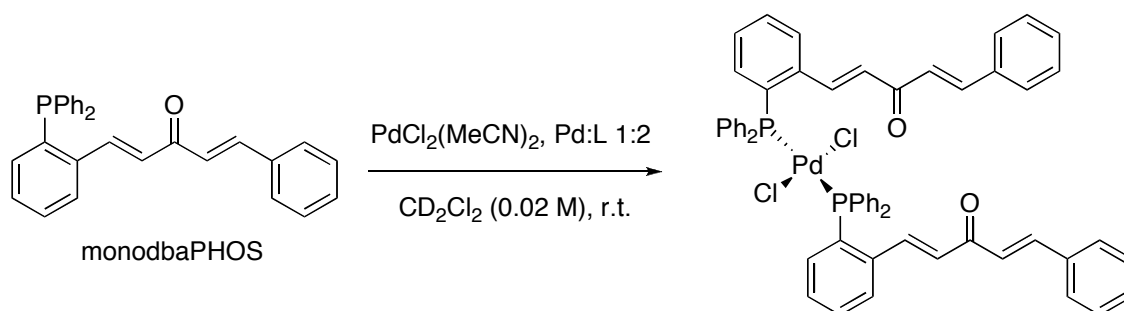
A solution of monodbaPHOS, **128** (~90% pure, 80 mg, 1.15 eq., 0.19 mmol) in dry and degassed CH_2Cl_2 (4 mL) was added to $[\text{PdCl}_2(\text{MeCN})_2]$ (43 mg, 1 eq., 0.166 mmol). After stirring for 16 h at rt a yellow precipitate appeared. The mixture was left to stand and the precipitate obtained by filtration. The precipitate was found to be a mixture of two products by ^{31}P NMR spectroscopy. ^{31}P NMR (162 MHz, CD_3CN) δ 53.98 (s, 1P), 27.14 (s, 2.2P); ^1H NMR (400 MHz, CD_3CN) δ 8.79 (d, $^3J_{\text{HH}} = 15.0$ Hz, 1H), 8.14-8.06 (m, 1H), 7.91-7.86 (m, 1H), 7.86-7.75 (m, 9H), 7.72 (br s, 2H), 7.70-7.40 (m, 26H), 7.36 (t, $J = 7.5$ Hz, 2H), 7.29 (d, $^3J_{\text{HH}} = 15.5$ Hz, 1H), 7.19 (d, $^3J_{\text{HH}} = 16.0$ Hz, 1H), 7.13 (dd, $J = 12.5, 8.0$ Hz, 1H), 6.83 (d, $^3J_{\text{HH}} = 15.5$ Hz, 1H).

Redissolving the precipitate and the filtrate together gave the bulk material, which was shown to be the same mixture of two products (δ 54:27 ratio 1:0.55 by ^{31}P NMR spectroscopy). IR (KBr, ν cm^{-1}): 3053 (w), 2961 (w), 2922 (w), 1653 (w), 1617 (m), 1576 (w), 1545 (s), 1456 (m), 1436 (m), 1363 (w), 1334 (w), 1261 (w), 1186 (w), 1145 (w), 1099 (m), 1026 (w), 999 (w), 803 (w), 768 (w), 748 (w), 692 (m), 668 (m), 538 (w), 513 (w); LRMS (LIFDI) m/z (rel%) 559.97 $[\text{M}-\text{Cl}]^+$ (100), 522.98 (10), 435.10 $[\text{monodbaPHOSNH}_4]^+$ (13), 417.10 $[\text{monodbaPHOS}-\text{H}]^+$ (17), 309.11 (10); LRMS (ESI) m/z 1519, 1074, 968, 891, 837, 684, 610, 564 $[\text{MH}_4-\text{Cl}]^+$, 457, 435.



Crystals of **176** were obtained from CD_3CN . Subsequent characterisation was carried out on the crystals: ^1H NMR (400 MHz, CD_3CN) 8.12-8.06 (m, 2H, H_e), 7.8417.75 (m, 6H, *o*-Ph and Ar), 7.71-7.57 (m, 6H, *p*-Ph and Ar), 7.557.48 (m, 7H, *m*-Ph and Ar), 7.19 (dd, $^3J_{\text{HH}} = 16.0$ Hz, $J = 0.5$ Hz, 1H, H_f); ^{31}P NMR (162 MHz, CD_3CN) δ 54.58 (s); HRMS (LIFDI) m/z 558.0140 $[\text{M}]^+$ (calculated for $\text{C}_{29}\text{H}_{22}\text{OPd} = 558.0132$); LRMS (LIFDI) m/z (rel%) 560.00 $[\text{M}]^+$ (100) {isotope pattern 555.99 (26), 557.00 (59), 558.00 (99), 559.00 (43), 560.00 (100), 561.00 (23), 562.00(50), 562.99 (10), 563.99 (8)}, 522.99 (42), 451.09 (38). Not enough material remained for further characterisation.

$[\text{PdCl}_2(\text{monodbaPHOS})_2]$, **175**



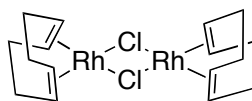
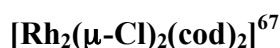
To a solution of monodbaPHOS, **128** (~90% pure, 80 mg, 2.3 eq., 0.19 mmol) in dry and degassed CH_2Cl_2 (4 mL) was added $[\text{PdCl}_2(\text{MeCN})_2]$ (21.5 mg, 1 eq., 0.083 mmol) and the solution stirred at r.t. for 35 min. During this time precipitate started to appear. After leaving overnight in the 4°C the precipitate was collected by filtration to give a yellow solid (5.6 mg). ^{31}P NMR spectroscopy showed the material was a mixture of products. ^1H NMR (400 MHz, C_6D_6) δ 9.20 (d, $^3J_{\text{HH}} = 16.0$ Hz, 1H), 9.08-8.92 (m, 1H), 7.93-7.86 (m, 3H), 7.80-7.65 (m 5H), 7.51-7.32 (m, 6H), 7.07-6.57 (m, 23H); ^{31}P NMR (162 MHz, C_6D_6) δ 29.10 (br, 1P), 28.69 (s, 0.8P), 21.73 (s, 0.8P).

In MeCN one of the signals disappeared. It was felt that the remaining two products may be isomers of some sort, so the ^1H and ^{31}P NMR spectra were recorded at 20°C , 60°C and then at 20°C again. ^{31}P NMR (162 MHz, CD_3CN , 20°C) δ 27.79 (s, 1P), 24.91 (br s, 0.3P); ^{31}P NMR (162 MHz, CD_3CN , 60°C) δ 27.47 (br); ^1H NMR (400 MHz,

CD₃CN, 60 °C) δ 8.92-8.70 (br m, 1H), 7.92-7.80 (m underlying d, ³J_{HH} = 16.0 Hz, 5H), 7.78-7.70 (m, 2H), 7.70-7.48 (m, 5H), 7.50-7.41 (m, 6H), 7.36 (ddd, J = 7.5, 4.5, 1.5 Hz, 2H), 7.18 (dd, J = 12.0, 8.0 Hz, 1H), 6.77 (br d, ³J_{HH} = 15.0 Hz, 1H). The sample gave the original spectra when cooled down to 20 °C again.

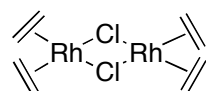
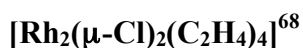
The filtrate and the yellow solid were recombined, and the solvent removed *in vacuo* to give the bulk material (30 mg). ³¹P NMR (162 MHz, CD₃CN) δ 30.08 (br, “P=O” impurity?, 1P), 27.79 (s, 3P); IR (KBr, ν cm⁻¹): 3054 (w), 2962 (w), 1675 (w), 1652 (m), 1617 (m), 1594 (m), 1574 (m), 1494 (w), 1481 (w), 1448 (w), 1436 (m), 1333 (w), 1262 (s), 1186 (m), 1097 (s), 1026 (m), 801 (m), 765 (w), 750 (w), 692 (m), 538 (m), 509 (m); LRMS (LIFDI) m/z (rel%) 1127 (9), 1082 (4), 957 (100), 868 (29), 795 (33), 560 (36), 434 (29), 417 (52), 340 (31); LRMS (ESI) m/z 1074, 943, 891, 853. No evidence for dimers or polymers was observed in the MS.

3.6.2.3 Rh^I complexes with dbaPHOS



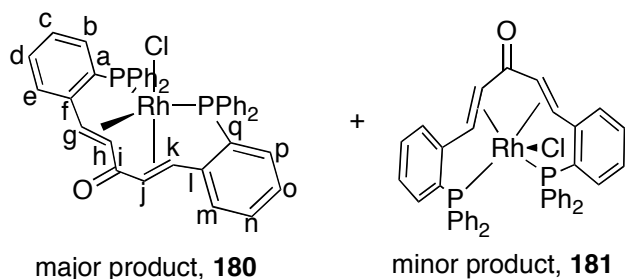
An EtOH:H₂O (5:1, 5 mL) mixture was deoxygenated by bubbling N₂ whilst under sonication. A Schlenk containing RhCl₃ (500 mg, 1 eq., 1.9 mmol) and Na₂CO₃ (210 mg, 1.05 eq., 2 mmol) was evacuated and refilled with N₂ three times. To this was transferred the solvent mixture and COD (0.75 mL, 3.2 eq., 6.1 mmol). The solution was heated at 95 °C for 15.5 h. After cooling the precipitate was collected by filtration, washed with pentane (10 mL) and then a MeOH:H₂O mix (1:5) until no more chloride was observed in the filtrate by the addition of AgNO₃ solution. The olive green^{††} air stable known product was dried *in vacuo* (422 mg, 90%). ¹H NMR (400 MHz, CDCl₃) δ 4.23 (br s, 4H), 2.57-2.41 (m, 4H), 1.75 (apparent br q, J = 7.0 Hz, 4H). ¹³C NMR (100 MHz, CDCl₃) δ 78.9 (d, ¹J_{CRh} = 14 Hz), 31.0; IR (ATR, ν cm⁻¹): 2936, 2873, 2827, 1468, 1423, 1322, 1300, 1172, 995, 960, 868, 815; Anal. Calcd. for RhC₈H₁₂Cl (493) C 38.97 H 4.91, Observed C 38.77, H 4.82.

^{††} Other colours are reported in the literature.



RhCl_3 (575 mg, 1 eq., 2.18 mmol) was dissolved in H_2O (1 mL) at 50 °C. MeOH (12 mL) was added when the solution cooled to rt. The mixture was then freeze-pump-thawed twice, and placed under a C_2H_4 atmosphere and stirred for 30 min. More C_2H_4 was added and then the mixture left to stir overnight. The orange precipitate was filtrated to give the known product (303 mg, 71%). IR (ATR, ν cm^{-1}): 1430, 1217, 999, 710; Anal. Calcd. for $\text{Rh}_2\text{C}_8\text{H}_{16}\text{Cl}_2$ (493) C 24.71 H 4.18, Observed C 21.59, H 3.80.

Rh^{I} complexation, **180** and **181**:



1. A yellow solution of dbaPHOS (20 mg, 2 eq. 0.033 mmol) in dry and degassed CD_2Cl_2 (0.5 mL) was added to a solution of $[\text{Rh}_2(\mu\text{-Cl})_2(\text{cod})_2]$ (8.2 mg, 1 eq. 0.017 mmol) in CD_2Cl_2 (0.5 mL). The solution went red immediately. The reaction was followed by ^{31}P NMR spectroscopy.

- Immediately (~10min): δ 68.73-62.48 (series of br small peaks, 3.7P), 55.62 (dd, $^1J_{\text{RhP}} = 120$, $^2J_{\text{PP}} = 36$ Hz, 4P), 38.96 (d, $^1J_{\text{RhP}} = 124$ Hz, 1P), 30.36 (br m, 9.7P).
- After 1h: major product, **180** (95%): ^{31}P NMR (162 MHz, CD_2Cl_2) δ 55.52 (dd, $^1J_{\text{RhP}} = 127$, $^2J_{\text{PP}} = 36$ Hz), 29.97 (dd, $^1J_{\text{RhP}} = 141$, $^2J_{\text{PP}} = 36$ Hz); minor product, **181** (5%): ^{31}P NMR (162 MHz, CD_2Cl_2) δ 38.95 (d, $^1J_{\text{RhP}} = 124$ Hz); ^1H NMR (400 MHz, CD_2Cl_2) δ 8.52-6.50 (m, 38H), 5.6 (br s, 1.2H), 5.53 (br s, cod, 4H), 4.5 (br m, 0.4H), 4.0 (br, s, 0.4H(minor product)), 3.6 (br s, 1.2H), 2.51 (br s, 1.2H), 2.34 (s, cod,

8H); HRMS (ESI) m/z 705.0948 (calculated for $C_{41}H_{32}OP_2Rh = 705.0978$).

- After more time the number of peaks in the ^{31}P NMR spectrum increased, including peaks at δ 54.9, 54.1, 44.5, 19.3 (dd, $J = 72, 15$ Hz).

2. A yellow solution of dbaPHOS (20 mg, 2 eq. 0.033 mmol) in dry and degassed C_6D_6 (0.5 mL) was added to a solution of $[Rh_2(\mu-Cl)_2(cod)_2]$ (8.2 mg, 1 eq. 0.017 mmol) in C_6D_6 (0.5 mL). The solution went red immediately. The initial ^{31}P NMR showed a more complicated spectrum: δ 65.68 (br d, $J = 200.0$ Hz), 55.48 (dd, $^1J_{RhP} = 128.0, ^2J_{PP} = 35$ Hz), 39.61 (d, $^1J_{RhP} = 126.0$ Hz), 29.08 (dd, $^1J_{RhP} = 140.0, ^2J_{PP} = 35$ Hz).

A solid precipitated and this was dissolved in CD_2Cl_2 to give the two products in a ratio of 93:7 (**180**:**181**): 1H NMR (500 MHz, CD_2Cl_2) δ 7.94 (br s, 2H), 7.67-7.04 (m, 25H), 7.04-6.53 (m, 10H), 5.60 (br s, 1H), 5.50 (br s, 1H), 4.51 (dd, $J = 10.0, 3.0$ Hz, 0.2H), 3.98 (ddd, $J = 10.5, 6.5, 1.5$ Hz, 0.2H), 3.54 (br s, 1H), 2.50 (br s, 1H). ^{31}P NMR (162 MHz, CD_2Cl_2) δ 55.51 (dd, $^1J_{RhP} = 131, ^2J_{PP} = 36$ Hz), 38.94 (d, $^1J_{RhP} = 124$ Hz), 29.96 (dd, $^1J_{RhP} = 141, ^2J_{PP} = 36$ Hz).

3. $[Rh_2(\mu-Cl)_2(C_2H_4)_4]$ (32 mg, 0.5 eq., 0.083 mmol) was placed in a Schlenk flask and the flask evacuated and refilled with N_2 three times, under a flow of N_2 dbaPHOS (100 mg, 1 eq., 0.166 mmol) was added. Then dry and degassed toluene (5 mL) was added and the reaction mixture stirred. The reaction mixture goes from red to brown. After leaving overnight a brown precipitate was collected by cannula filtration, (37 mg, 30%). This gave virtually identical spectra as before. M.p. 222-240 $^{\circ}C_{(dec)}$; 1H NMR (500 MHz, CD_2Cl_2 , 255 K) major product (**180**) δ :^{§§} 7.86 (dd, $J = 11.0, 7.5$ Hz, 2H, Ar), 7.56 (t, $J = 8.0$ Hz, 2H, Ar), 7.45-7.28 (m, 10H, Ar), 7.24-6.94 (m, 13H, Ar), 6.86 (t, $J = 6.5$ Hz, 2H, Ar), 6.75-6.65 (m, 3H, Ar), 5.57 (dd, $^3J_{HH} = 13.5$ Hz, $J = 2.5$ Hz, 1H, H_j), 5.52 (d, $^3J_{HH} = 13.5$ Hz, 1H, H_k), 3.56 (d, $J = 6.5$ Hz, 1H, H_g), 2.56 (dd, $J = 8.5, 7.5$ Hz, 1H, H_h); minor product (**181**) visible peaks δ : 7.51-7.45 (m, 1H), 6.83-6.75 (m, 1H), 4.51 (dd, $J = 10.5, 3.0$ Hz, 0.2H), 3.94 (dd, $J = 10.0, 5.5$ Hz, 0.2 Hz); ^{31}P NMR (202 MHz, CD_2Cl_2 , 255 K) δ 55.32 (dd, $^1J_{RhP} = 128.0, ^2J_{PP} = 35.5$ Hz, 0.97P), 38.27 (d, $^1J_{RhP} = 124.0$ Hz, 0.03P), 30.04 (dd, $^1J_{RhP} = 143.5,$

^{§§} Four extra protons are observed due to underlying protons from the minor product.

$^2J_{PP} = 35.5$ Hz, 0.97P); IR (KBr, ν cm^{-1}): 3051 (w), 1628 (w, br), 1554 (m), 1482 (m), 1454 (m), 1434 (s), 1419 (s), 1354 (w), 1291 (w), 1273 (w), 1246 (w), 1209 (m), 1187 (w), 1156 (w), 1120 (w), 1093 (9m), 1068 (w), 1028 (w), 999 (w), 980 (w), 877 (w), 868 (w), 829 (w), 753 (m), 740 (m), 705 (m), 694 (s), 657 (w), 626 (w), 592 (w), 534 (m), 517 (m), 505 (s), 464 (w). HRMS (ESI) m/z 705.0948 $[M-\text{Cl}]^+$ (calculated for $\text{C}_{41}\text{H}_{32}\text{OP}_2\text{Rh} = 705.0978$).

UV-vis of a 1.35×10^{-4} M solution in CH_2Cl_2 showed no distinctive peaks. The baseline started going up at ~ 400 nm to give a broad shoulder to the solvent cut off.

Rh complex + CO

A solution of the Rh complexes, **180** and **181** (28 mg) in CH_2Cl_2 (20 mL) was stirred under an atmosphere of CO for 18h at 20 °C. The solvent was removed *in vacuo* and the residue redissolved in CD_2Cl_2 (1 mL). ^1H NMR (400 MHz, CD_2Cl_2) δ 7.91-6.75 (m, 48H), 6.65 (ddd, $J = 11.0, 8.5, 1.0$ Hz, 2.4H), 6.56 (d, $J = 12.5$ Hz, 1 H), 6.09 (br, 0.6H), 5.62 (br d, $J = 12.5$ Hz, 0.5H), 4.69 (br, 0.5H), 3.86 (br, 1H), 3.39 (br, 1H), 2.55 (br, 0.5H); ^{31}P NMR (162 MHz, CD_2Cl_2) δ 56.03 (dd, $^1J_{\text{RhP}} = 128.0$, $^2J_{\text{PP}} = 34.5$ Hz, 0.6P), 53.65 (d, $^1J_{\text{RhP}} = 116.7$ Hz, 0.1P), 48.39 (dd, $^1J_{\text{RhP}} = 131.6$, $^2J_{\text{PP}} = 19.7$ Hz, 1P), 44.79 (dd, $^1J_{\text{RhP}} = 88.1$, $^2J_{\text{PP}} = 19.7$ Hz, 1P), 34.57 (br d, $^1J_{\text{RhP}} = 199.4$ Hz, 0.6P), 24.66 (d, $^1J_{\text{RhP}} = 122.6$ Hz, 0.1P); HRMS (ESI) m/z 1465.1748 (calculated for $\text{C}_{84}\text{H}_{63}\text{O}_4\text{P}_4\text{Rh}_2 = 1465.1781$) 705.0985 (calculated for $\text{C}_{41}\text{H}_{32}\text{OP}_2\text{Rh} = 705.0978$); LRMS (LIFDI) m/z (rel%) 732.12 $[\text{Rh}(\text{dbaPHOS})\text{CO}]^+$ (100); IR (CD_2Cl_2 , ν cm^{-1}): 3060 (w), 2083 (w), 2001 (s), 1629 (s), 1563 (w), 1482 (m), 1467 (w), 1436 (s), 1263 (w), 1094 (m), 1028 (w).

3.6.3 ^{31}P - ^{31}P EXSY experiments

To monitor the alkene exchange in $\text{Pd}(0)\text{dbaPHOS}$ a series of 1D ^{31}P - ^{31}P EXSY spectra were recorded. In a typical run, data were collected for a series of mixing times (usually $d8 = 0.02, 0.05, 0.1, 0.2, 0.3, 0.4, 0.5, 0.7, 1.0, 1.2$ s) at selected temperatures (293, 298, 303, 308, 313 and 318 K). The sum of the integrals of the irradiated (31 ppm) and cross-peak (13 ppm) were normalised to 100%. The rate of alkene exchange was then determined by stimulation; the change in intensity of the signal at 31 ppm (100 when $d8 = 0$) was modelled as a function of mixing time. This was carried out using

Microsoft Excel. The peak intensities were calculated for 0.01 s intervals from 0.01 to 40 s, and those were then compared with the experimental values via a minimised linear least-squares difference analysis. The associated rate constants were varied until the sum of the squares of the difference between the measured and stimulated points was minimised. Rate constants obtained in this way were denoted as k_{obs} . For further thermodynamic analysis the rate constants were multiplied by a factor of 2 to take into account the analysis method.⁶⁹ The kinetic model used assumed an $A \rightarrow B$ reaction following first-order kinetics.

3.6.4 X-Ray Diffraction Data

Diffraction data for **163**, **174** and **177** were collected at 110 K on a Bruker Smart Apex diffractometer with Mo- K_{α} radiation ($\lambda = 0.71073 \text{ \AA}$) using a SMART CCD camera. Diffractometer control, data collection and initial unit cell determination was performed using “SMART”.⁷⁰ Frame integration and unit-cell refinement was carried out with “SAINT+”.⁷¹ Absorption corrections were applied by SADABS.⁷² Structures were solved by “direct methods” using SHELXS-97 (Sheldrick, 1997)⁷³ and refined by full-matrix least squares using SHELXL-97 (Sheldrick, 1997).⁷⁴ All non-hydrogen atoms were refined anisotropically. Hydrogen atoms were placed using a “riding model” and included in the refinement at calculated positions. Exceptions to this were the placement of the hydrogen atoms of the coordinated alkene in **174** and **177**, which were placed using the difference map and allowed to refine.

Diffraction data for **176** (ijsf1104) were collected at 110 K on an Oxford Diffraction SuperNova diffractometer with Mo- K_{α} radiation ($\lambda = 0.71073 \text{ \AA}$) using a EOS CCD camera. The crystal was cooled with an Oxford Instruments Cryojet. Diffractometer control, data collection, initial unit cell determination, frame integration and unit-cell refinement was carried out with “Crysalis”.⁷⁵ Face-indexed absorption corrections were applied using spherical harmonics, implemented in SCALE3 ABSPACK scaling algorithm.⁷⁶ OLEX2⁷⁷ was used for overall structure solution, refinement and preparation of computer graphics and publication data. Within OLEX2, the algorithms used for structure solution were “direct methods”, using the “A short history of SHELX (Sheldrick, 2007)/Bruker”. Refinement by full-matrix least-squares used the SHELXL-97⁷⁴ algorithm within OLEX2.⁷⁸ All non-hydrogen atoms were refined anisotropically. Hydrogen atoms were placed using a “riding model” and included in the refinement at

calculated positions. The H8 atom in ijsf1104 was located by difference map after all other atoms had been located.

Table 8: Single Crystal X-Ray Details

Compound reference	ijf0803, 163	ijsf1102, 172	ijf0826m, 174	ijf0839m, 177	ijsf1104, 176
Chemical formula	C ₄₁ H ₃₂ Cl ₂ OP ₂ Pt	C ₅₇ H ₅₇ IO _{3.50} P ₂ Pd	C ₂₉ H ₂₃ Cl ₂ OPPt	C ₂₉ H ₂₃ Cl ₂ OPPt•CH ₂ Cl ₂	C ₂₉ H ₂₂ ClOPOPd
Formula Mass	868.60	1093.27	684.43	769.36	559.29
Crystal system	Triclinic	Triclinic	Triclinic	Triclinic	Monoclinic
<i>a</i> /Å	10.9691(5)	12.4868(17)	9.6208(6)	10.1809(11)	8.8974(3)
<i>b</i> /Å	11.9562(7)	14.079(3)	10.1270(7)	11.0444(12)	22.4140(6)
<i>c</i> /Å	14.2851(8)	14.7391(15)	13.3171(9)	14.1359(16)	12.5622(4)
<i>α</i> /°	80.970(3)	86.400(11)	101.8980(10)	103.095(2)	90.00
<i>β</i> /°	85.202(4)	89.126(10)	96.0040(10)	93.769(2)	110.563(4)
<i>γ</i> /°	69.949(4)	67.573(15)	93.7290(10)	112.847(2)	90.00
Unit cell volume/Å ³	1737.21(16)	2390.3(6)	1257.63(14)	1405.6(3)	2345.61(14)
Temperature/K	120(2)	110(2)	110(2)	110(2)	110.0
Space group	<i>P</i> $\bar{1}$	<i>P</i> $\bar{1}$	<i>P</i> $\bar{1}$	<i>P</i> $\bar{1}$	<i>P</i> 121/ <i>c</i> 1
No. of formula units per unit cell, <i>Z</i>	2	2	2	2	4
No. of reflections measured	35786	17216	14195	14631	17699
No. of independent reflections	7957	11935	7061	6938	7467
<i>R</i> _{int}	0.0903	0.0203	0.0181	0.0143	0.0271
Final <i>R</i> _{<i>I</i>} values (<i>I</i> > 2σ(<i>I</i>))	0.0432	0.0443	0.0282	0.0217	0.0274
Final <i>wR</i> (<i>F</i> ²) values (<i>I</i> > 2σ(<i>I</i>))	0.0791	0.1063	0.0669	0.0534	0.0589
Final <i>R</i> _{<i>I</i>} values (all data)	0.0745	0.0603	0.0320	0.0231	0.0334
Final <i>wR</i> (<i>F</i> ²) values (all data)	0.0876	0.1199	0.0687	0.0541	0.0616

3.7 References

- ¹ a) Slone, C. S.; Weinburger, D. A.; Mirkin, C. A. *Prog. Inorg. Chem.* **1999**, *48*, 233-350. b) Braunstein, P.; Naud, F. *Angew. Chem., Int. Ed.* **2001**, *40*, 680-699.
- ² Alcock, N. W.; Herron, N.; Kemp, T. J. *J. Chem. Soc., Chem. Comm.* **1975**, 785-786.
- ³ Rubezhov, A. Z. *Russ. Chem. Rev.* **1988**, *57*, 1194-1207.
- ⁴ a) Pierpont, C. G.; Mazza, M. C. *Inorg. Chem.* **1974**, *13*, 1891-1895. b) Mazza, M. C.; Pierpont, C. G. *J. Chem. Soc., Chem. Comm.* **1973**, 207-208.
- ⁵ Pierpont, C. G.; Buchanan, R. M.; Downs, H. H. *J. Organomet. Chem.* **1977**, *124*, 103-112.
- ⁶ Ibers, J. A. *J. Organomet. Chem.* **1974**, *73*, 389-400.
- ⁷ a) Cotton, F. A.; Wilkinson, G. *Advanced Inorganic Chemistry: A Comprehensive Text*, 2nd Ed.; Interscience: New York, 1966. b) Five-coordinate compounds have been observed for alkene complexes with N,N-donor ligands: Albano, V. G.; Natile, G.; Panunzi, A. *Coord. Chem. Rev.* **1994**, *133*, 67-114.
- ⁸ Al-Najjar, I. M. *Inorg. Chim. Acta* **1987**, *128*, 93-104.
- ⁹ Bemis, L.; Clark, H. C.; Davies, J. A.; Fyfe, C. A.; Wasylisten, R. E. *J. Am. Chem. Soc.* **1982**, *104*, 438-445.
- ¹⁰ Garcia, J. J.; Mann, B. E.; Adams, H.; Bailey, N. A.; Maitlis, P. M. *J. Am. Chem. Soc.* **1995**, *117*, 2179-2186.
- ¹¹ Anderson, G. K.; Clark, H. C.; Davies, J. A. *Inorg. Chem.* **1981**, *20*, 3607-3611.
- ¹² Tudor, M. D.; Becker, J. J.; White, P. S.; Gagné, M. R. *Organometallics* **2000**, *19*, 4376-4384.
- ¹³ Ohshima, T.; Miyamoto, Y.; Ipposhi, J.; Nakahura, Y.; Utsunomiya, M.; Mashima, K. *J. Am. Chem. Soc.* **2009**, *131*, 14317-14328.
- ¹⁴ Petöcz, G.; Berente, Z.; Kégl, T.; Kollár, L. *J. Organometallic Chem.* **2004**, *689*, 1188-1193.
- ¹⁵ a) Hartwig, J. *Organotransition Metal Chemistry: From Bonding to Catalysis* **2010**, University Science Books: Sausalito. b) Cross, R. J. *Chem. Soc. Rev.* **1985**, 197-223.
- ¹⁶ a) Berry, R. S. *J. Chem. Phys.* **1960**, *32*, 933-938. b) Anderson, G. K.; Cross, R. J. *Chem. Soc. Rev.* **1980**, *9*, 185-215.
- ¹⁷ Krevor, J. V. Z.; Simonis, U.; Richter II, J. A. *Inorg. Chem.* **1992**, *31*, 2409-2414.

-
- 18 a) Boeré, R. T.; Montgomery, C. D.; Payne, N. C.; Willis, C. J. *Inorg. Chem.* **1985**, *24*, 3680-3687. b) Pregosin, P. S.; Kunz, R. *Helv. Chim. Acta* **1975**, *58*, 423-431.
- 19 CSD searched on the 24th April 2011.
- 20 CCDC deposition numbers and refcodes: AYOQIO (241666), MAWHUO (275889), NISBAT (673332), TEWSIY (613524), INICOX (220613), XOJFIM (687181).
- 21 Fun, H-K.; Chantrapromma, S.; Liu, Y-C.; Chen, Z-F.; Liang, H. *Acta Crystallogr. Section E*, **2006**, *E26*, m1252-m1254.
- 22 Farrar, D. H.; Ferguson, G. *J. Crystallogr. Spectrosc. Res.* **1982**, *12*, 465.
- 23 Mikami, K.; Kakuno, H.; Aikawa, K. *Angew. Chem., Int. Ed.* **2005**, *44*, 7257 - 7260.
- 24 Niksch, T.; Görls, H.; Friedrich, M.; Oilunkaniemi, R.; Laitinen, R.; Weigand, W. *Eur. J. Inorg. Chem.* **2010**, 74-94.
- 25 van der Vlugt, J. I.; van Duren, R.; Batema, G. D.; den Heeten, R.; Meetsma, A.; Fraanje, J.; Goubitz, K.; Kamer, P. C. J.; van Leeuwen, P. W. N. M.; Vogt, D. *Organometallics* **2005**, *24*, 5377-5382.
- 26 Bini, L.; Müller, C.; Wilting, J.; von Chrzanowski, L.; Spek, A. L.; Vogt, D. *J. Am. Chem. Soc.* **2007**, *129*, 12622-12623.
- 27 a) Yao, W.; Eisenstein, O.; Crabtree, R. H. *Inorg. Chim. Acta.* **1997**, *254*, 105-111. b) Zhang, Y.; Lewis, J. C.; Bergman, R. G.; Ellman, J. A.; Oldfield, E. *Organometallics* **2006**, *25*, 3515-3519. c) Mukhopadhyay, A.; Pal, S. *Eur. J. Inorg. Chem.* **2006**, 4879-4887 and references therein.
- 28 a) Brammer, L. *Dalton Trans.* **2003**, 3145-3157. b) Brookhart, M.; Green, M. L. H.; Parkin, G. *Proc. Natl. Acad. Sci.* **2007**, *104*, 6908-6914. c) Thakur, T. S.; Desiraju, G. R. *J. Mol. Struct. Theochem* **2007**, *810*, 143-154. The main review of agostic interactions: Brookhart, M.; Green, M. L. H. *J. Organomet. Chem.* **1983**, *250*, 395-408.
- 29 Sundquist, W. I.; Bancroft, D. P.; Lippard, S. J. *J. Am. Chem. Soc.* **1990**, *112*, 1590-1596.
- 30 a) Leininger, T.; Nicklass, A.; Stoll, H.; Dolg, M.; Schwerdtfeger, P. *J. Chem. Phys.* **1996**, *105*, 1052. b) Adamo, C.; Barone, V. *J. Chem. Phys.* **1998**, *108*, 664.
- 31 a) Fukui, K. *J. Phys. Chem.* **1970**, *74*, 4161. b) Fukui, K. *Acc. Chem. Res.* **1981**, *14*, 363.

- ³² Frisch, M. J.; Trucks, G. W.; Schlegel, H. B.; Scuseria, G. E.; Robb, M. A.; Cheeseman, J. R.; Zakrzewski, V. G.; Montgomery, J. A., Jr.; Stratmann, R. E.; Burant, J. C.; Dapprich, S.; Millam, J. M.; Daniels, A. D.; Kudin, K. N.; Strain, M. C.; Farkas, O.; Tomasi, J.; Barone, V.; Cossi, M.; Cammi, R.; Mennucci, B.; Pomelli, C.; Adamo, C.; Clifford, S.; Ochterski, J.; Petersson, G. A.; Ayala, P. Y.; Cui, Q.; Morokuma, K.; Malick, D. K.; Rabuck, A. D.; Raghavachari, K.; Foresman, J. B.; Cioslowski, J.; Ortiz, J. V.; Stefanov, B. B.; Liu, G.; Liashenko, A.; Piskorz, P.; Komaromi, I.; Gomperts, R.; Martin, R. L.; Fox, D. J.; Keith, T.; Al-Laham, M. A.; Peng, C. Y.; Nanayakkara, A.; Gonzalez, C.; Challacombe, M.; Gill, P. m. W.; Johnson, B.; Chen, W.; Wong, M. W.; Andres, J. L.; Gonzalez, C.; Head-Gordon, M.; Replogle, E. S.; Pople, J. A. Gaussian 03, Revision B.05; Gaussian, Inc.: Pittsburgh, PA, 2003.
- ³³ Peganova, T. A.; Valyaeva, A. V.; Kalsin, A. M.; Petrovskii, P. V.; Borissova, A. O.; Lyssenko, K. A.; Ustynyuk, N. A. *Organometallics* **2009**, *28*, 3021-3028.
- ³⁴ Reed, A.; Curtiss, L. A.; Weinhold, F. *Chem. Rev.* **1988**, *88*, 899.
- ³⁵ Wiberg, K. B. *Tetrahedron*, **1968**, *24*, 1083.
- ³⁶ Reed, A.; Curtiss, L. A.; Weinhold, F. *Chem. Rev.* **1988**, *88*, 899.
- ³⁷ Herrmann, W. A.; Thiel, W. R.; Broßmer, C.; Öfele, K.; Priermeier, T.; Scherer, W. *J. Organomet. Chem.* **1993**, *461*, 51-60.
- ³⁸ Norton, D. M.; Mitchell, E. A.; Botros, N. R.; Jessop, P. G.; Baird, M. C. *J. Org. Chem.* **2009**, *74*, 6674-6680.
- ³⁹ Amatore, C.; Jutand, A.; Meyer, G. *Inorg. Chim. Acta.* **1998**, *273*, 76-84.
- ⁴⁰ Snelders, D. J. M.; van der Burg, C.; Lutz, M.; Spek, A. L.; van Koten, G.; Gebbink, R. J. M. K. *Chem. Cat. Chem.* **2010**, *2*, 1425-1437.
- ⁴¹ Kawazura, H.; Tanaka, H.; Yamada, K.; Takahashi, T.; Ishii, Y. *Bull. Chem. Soc. Japan* **1978**, *51*, 3466-3470.
- ⁴² Green, M. L. H.; Wong, L-L; Sella, A. *Organometallics* **1992**, *11*, 2660-2668.
- ⁴³ a) Mei, X.; Wolf, C. *J. Org. Chem.* **2005**, *70*, 2299-2305. b) Ting, Y.; Lai, Y-H. *J. Am. Chem. Soc.* **2004**, *126*, 909-914. c) Bosch, E.; Barnes, C. L.; Brennan, N. L.; Eakins, G. L.; Breyfogle, B. E. *J. Org. Chem.* **2008**, *73*, 3931-3934.
- ⁴⁴ Strömberg, S.; Svensson, M.; Zetterberg, K. *Organometallics* **1997**, *16*, 3165-3168.
- ⁴⁵ Data included with kind permission from Ms Somia Bajwa. Bajwa, S.; Fairlamb, I. J. S.; Whitwood, A. C. *Unpublished Results*.

- ⁴⁶ Pryadun, R.; Sukumaran, D.; Bogadi, R.; Atwood, J. D. *J. Am. Chem. Soc.* **2004**, *126*, 12414-12420.
- ⁴⁷ Love, R. A.; Koetzle, T. F.; Williams, G. J. B.; Andrews, L. C.; Bau, R. *Inorg. Chem.* **1975**, *14*, 2653-2657.
- ⁴⁸ Chianese, A. R.; Lee, S. J.; Gagné, M. R. *Angew. Chem., Int. Ed.* **2007**, *46*, 4042-4059.
- ⁴⁹ Tanaka, H.; Kawazura, H. *Bull. Chem. Soc. Jap.* **1979**, *52*, 2815-2818.
- ⁵⁰ a) Brunet, J.-J.; Couillens, X.; Daran, J.-C.; Diallo, O.; Lepetit, C.; Neibecker, D.; *Eur. J. Inorg. Chem.* **1998**, 349-353. b) Marder, T. B.; Fultz, W. C.; Calabrese, J. C.; Harlow, R. L.; Milstein, D. *J. Chem. Soc. Chem. Commun.* **1987**, 1543-1545. c) Cowley, M. J.; Lynam, J. M. *Unpublished Results*.
- ⁵¹ Clark, P. W.; Hartwell, G. E. *Inorg. Chem.* **1970**, *9*, 1948-1951.
- ⁵² a) Tau, K. D.; Meek, D. W.; Sorrell, T.; Ibers, J. A. *Inorg. Chem.* **1978**, *17*, 3454-3460. b) Douglas, T. M.; Le Nôtre, J.; Brayshaw, S. K.; Frost, C. G.; Weller, A. S. *Chem. Commun.* **2006**, 3408-3410.
- ⁵³ Freixa, Z.; van Leeuwen, P. W. N. M. *Coord. Chem. Rev.* **2008**, *252*, 1755-1786.
- ⁵⁴ a) van Leeuwen, P. W. N. M.; Kamer, P. C. J.; Reek, J. N. H. *Pure Appl. Chem.* **1999**, *71*, 1443-1452. b) Birkholz (née Gensow), M.-N.; Freixa, Z.; van Leeuwen, P. W. N. M. *Chem. Soc. Rev.* **2009**, *38*, 1099-1118. c) Freixa Z.; van Leeuwen, P. W. N. M. *Dalton Trans.* **2003**, 1890-1901. d) Kawabata, Y.; Hayashi, T.; Ogata, I. *J. Chem. Soc., Chem. Comm.* **1979**, 462. Further examples: e) Tschan, M. J.-L.; López-Valbuena, J.-M.; Freixa, Z.; Launay, H.; Hagen, H.; Benet-Buchholz, J.; van Leeuwen, P. W. N. M. *Organometallics* **2011**, *30*, 792-799. Using Xantphos and DPEphos: f) Yang, B. H.; Buchwald, S. L. *Org. Lett.* **1999**, *1*, 35-37. g) Sadighi, J. P.; Harris, M. C.; Buchwald, S. L. *Tetrahedron Lett.* **1998**, *39*, 5327-5330. h) Katagiri, T.; Tsurugi, H.; Satoh, T.; Miura, M. *Chem. Commun.* **2008**, 3405-3407. i) Mora, G.; Piechaczyk, O.; Houdard, R.; Mézailles, N.; Le Goff, X.-F.; le Floch, P. *Chem. Eur. J.* **2008**, *14*, 10047-10057. j) Lavén, G.; Stawinski, J. *Synlett* **2009**, 225-228. k) Martinelli, J. R.; Watson, D. A.; Frechmann, D. M. M.; Barder, T. E.; Buchwald, S. L. *J. Org. Chem.* **2008**, *73*, 7102-7107.
- ⁵⁵ a) Fujita, K.; Yamashita, M.; Puschmann, F.; Alvares-Falcon, M. M.; Incarvito, C. D.; Hartwig, J. F. *J. Am. Chem. Soc.* **2006**, *128*, 9044-9045. b) Yin, J.; Buchwald, S. L. *J. Am. Chem. Soc.* **2002**, *124*, 6043-6048.

56 a) Shi, W.; Luo, Y.; Luo, X.; Chao, L.; Zhang, H.; Wang, J.; Lei, A. *J. Am. Chem. Soc.* **2008**, *130*, 14713-14720. b) Luo, X.; Zhang, H.; Duan, H.; Liu, Q.; Zhang, T.; Lei, A. *Org. Lett.* **2007**, *9*, 4571-4574. For other examples see references from Chapter 1.5

57 Firmansjah, L.; Fu, G. *J. Am. Chem. Soc.* **2007**, *129*, 11340-11341

58 Roggen, M.; Carriera, E. M. *J. Am. Chem. Soc.* **2010**, *132*, 11917-11919.

59 <http://precmnet.com.au>

60 Fanizzi, F. P.; Intini, F. P.; Maresca, L.; Natile, G. *J. Chem. Soc., Dalton Trans.* **1990**, 199-202.

61 Auburn, P. R.; Mackenzie, P. B.; Bosnich, B. *J. Am. Chem. Soc.* **1985**, *107*, 2033-2046.

62 <http://www.sigmaaldrich.com> accessed on 27th April 2011.

63 Murrall, N. W.; Welch, A. *J. Organomet. Chem.* **1986**, *301*, 109-130.

64 Hsu, C-Y.; Leshner, B. T.; Orchin, M. *Inorg. Synth.* **1979**, *19*, 114-116.

65 Balema, V. P.; Wiench, J. W.; Pruski, M.; Pecharsky, V. K. *Chem. Commun.* **2002**, 1606-1607.

66 Head, R. A. *Inorg. Synth.* **1990**, *28*, 132-135

67 Giordano, G.; Crabtree, R. H. *Inorg. Synth.* **1990**, *28*, 88-89.

68 Cramer, R. *Inorg. Synth.* **1990**, *28*, 86-88.

69 Green, M. L. H.; Wong, L-L.; Sella, A. *Organometallics* **1992**, *11*, 2660-2668.

70 "SMART" - control software Bruker SMART Apex X-ray Diffractometer. v5.625, Bruker-AXS GMBH, Karlsruhe, Germany.

71 "SAINT+" - integration software for Bruker SMART detectors. v6.45, Bruker-AXS GMBH, Karlsruhe, Germany.

72 "SADABS" - program for absorption correction. v2.10. Sheldrick, G. M. Bruker AXS Inc., Madison, Wisconsin, USA, 2007.

73 "SHELXS-97" - program for structure solution. Sheldrick, G. M. University of Göttingen, Göttingen, Germany, 1997.

74 "SHELXL-97" - program for the Refinement of Crystal Structures. Sheldrick, G. M. University of Göttingen, Göttingen, Germany, 1997.

75 CrysAlisPro, Oxford Diffraction Ltd. Version 1.171.34.40

76 Empirical absorption correction using spherical harmonics, implemented in SCALE3 ABSPACK scaling algorithm within CrysAlisPro software, Oxford Diffraction Ltd. Version 1.171.34.40

-
- ⁷⁷ Dolomanov, O.V.; Bourhis, L. J.; Gildea, R. J.; Howard, J. A. K.; Puschmann, H. OLEX2: a complete structure solution, refinement and analysis program. *J. Appl. Cryst.* **2009**, *42*, 339-341, using "SHELXS-97" - program for structure solution. Sheldrick, G. M. University of Göttingen, Göttingen, Germany, 1997.
- ⁷⁸ "smtbx-flip" plug-in module to "Olex2" crystallography software, *J. Appl. Cryst.* **2009**, *42*, 339–341.

Chapter 4: Copper(I) Complexes of the phosphine sulfide ligands

The work detailed in this chapter resulted in the following publication: A. G. Jarvis, A. C. Whitwood, and I. J. S. Fairlamb: “Cu^I complexes containing a multidentate and conformationally flexible dibenzylidene acetone ligand (dbathiophos): Application in catalytic alkene cyclopropanation” *Dalton Trans.* **2011**, 40, 3695-3702.

4.1 Introduction

Copper(I) complexes have been of interest to inorganic and organometallic chemists due to their varied coordination chemistry and the resulting properties. In recent years, synthetic research has focused on the use of copper in catalytic reactions as both the main metal centre (*e.g.* conjugate addition to α,β -unsaturated carbonyl compounds,¹ *N*-arylation,² hydroboration of styrenes³ and cyclopropanation reactions⁴) and as a co-catalyst (*e.g.* direct C-H functionalisation of arenes and heteroarenes⁵). Research has also focused on the physical properties of copper(I) complexes (such as in fluorescence⁶ and ferroelectric applications⁷) and on their cluster and supramolecular chemistry.⁸

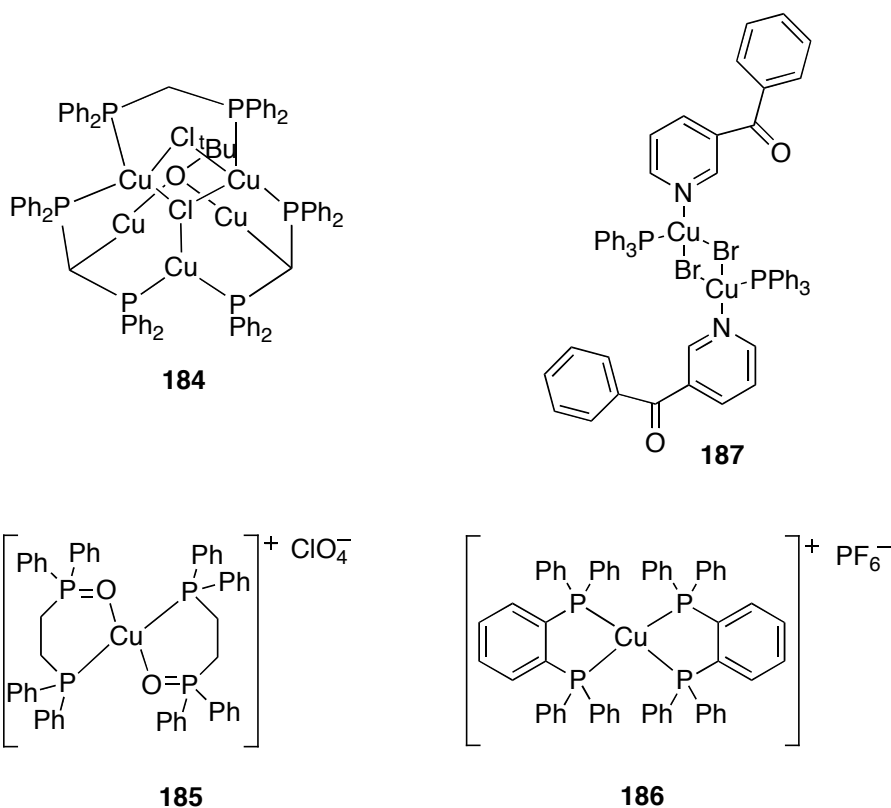


Figure 1: Selected examples of Copper(I) phosphine complexes from the literature.

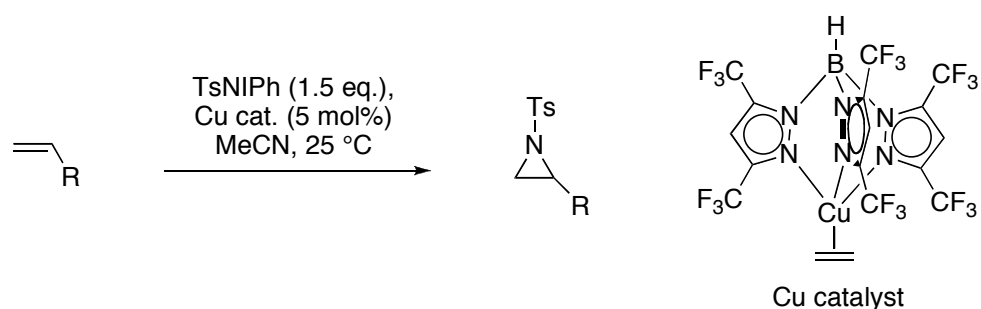
Traditionally, copper(I) is regarded as a metal ion with soft Lewis acid character,⁹ and therefore it will form covalent bonds with soft ligands (*e.g.* with S or P as the donor atom). An indication of the soft character of copper(I) is evidenced by the number of examples of copper clusters stabilised by ligands containing group 16 elements (in particular S and Se) in the literature.¹⁰ A number of phosphorus ligands, such as diphenylphosphine benzene, diphenylphosphine methane and $\text{Ph}_2\text{P}(\text{CH}_2)_2\text{P}(\text{O})\text{Ph}_2$, have also been successfully coordinated to copper(I) centres (see complexes **184-186**, Figure 1).^{6c,8a,11}

Contrary to this are the large number of stable copper(I) complexes known in which Cu coordinates to nitrogen ligands (N is regarded as a hard donor).^{8a} It has been observed that the stability of copper(I) complexes is increased by a mixture of hard and soft ligands rather than by all soft ligands, as would be expected if copper(I) was a classic soft acid.¹² Indeed, ligands such as triphenylphosphine are often used as ancillary ligands to help stabilise complexes with hard donors (Complex **187**, Figure 1). Experimental and theoretical studies have shown that copper(I) is an exception to Pearson's Hard-Soft Acid-Base (HSAB) principle.^{11,12,9}

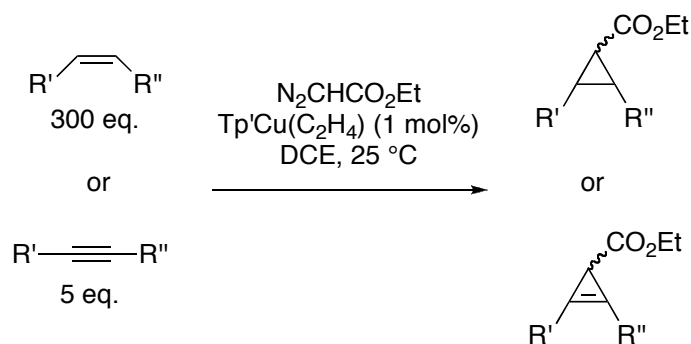
Another feature of copper(I)'s coordination chemistry is its ability to form close $\text{Cu}\cdots\text{Cu}$ contacts of less than twice the van der Waals radius of Cu (2.8 Å), referred to as "cuprophilicity".¹³ This metal-metal interaction was originally observed in gold complexes.¹⁴ The precise nature of short $\text{Cu}\cdots\text{Cu}$ interactions, and whether they can be considered as bonds at all is controversial.¹⁵ In many cases it is hard to determine if the short distances are due to M-M bonding (either ionic or covalent) or due to the ligands 'fixing' the copper centres close to each other. As copper(I) is a d^{10} metal one would expect repulsion between the metal centres. However, Pyykko has determined that attractive dispersion forces (*e.g.* van der Waals type interactions) are able to overcome this repulsion to give interactions with strengths roughly comparable to hydrogen bonds ($\text{Au}\cdots\text{Au}$ interactions are stronger due to relativistic effects).¹⁶

4.1.1 Copper(I)-alkene complexes

Copper(I) complexes are catalytically active in a wide range of reactions, particularly those involving alkenes, for example cyclopropanation. At some point during the catalytic cycles of these reactions it is likely that copper-alkene coordination occurs. Intermediate copper(I)-alkene complexes have been observed in conjugate addition to α,β -unsaturated carbonyls.¹⁷ Copper(I)-alkene complexes also catalyse aziridine formation (Scheme 1)¹⁸ and the conversion of alkynes and alkenes to cyclopropenes and cyclopropanes, respectively (Scheme 2).¹⁹



Scheme 1: Aziridination of alkenes using a Cu^I complex containing a fluorinated tris(pyrazolyl)borate ligand and ethene.¹⁸



Scheme 2: Cyclopropanation and cyclopropenation of alkenes and alkynes (Tp' = hydrotris(3,5-dimethyl-1-pyrazolyl)borate).

The ability of copper(I) to bind alkenes has allowed it to be used in the separation of alkenes from alkanes or aqueous media,²⁰ and the resolution of racemic allylic alcohols.²¹ Copper(I)-alkene polymers and complexes have also been shown to be useful in the resolution of alcohols²² and as sensitizers in alkene photoreactions, including rearrangements and cycloadditions of cyclooctadiene and norbornadiene.²³ Copper(I)-alkene complexes have also been used in materials chemistry,²⁴ and in

biological chemistry. For the latter, it is well known that ethene is the smallest plant hormone and plays a key role in fruit development. The ethene receptor ETR 1 contains Cu and research suggests it acts as a co-factor in the active site and binds to ethene.²⁵

The first copper(I)-alkene complex was reported by Manchot and Brandt when they reacted ethene with CuCl to give an unstable compound.²⁶ Since then many ethene copper(I) complexes have been reported and studied. However, the exact structures of these complexes remained unknown until the 1960's when van den Hende and Baird reported the X-ray crystal structure of di- μ -chlorido-tetraethenedicopper.²⁷ Other structures quickly followed including those with cyclooctatetraene²⁸ and norbornadiene.²⁹ In 1983 Thompson and co-workers demonstrated that stable ethene-copper(I) complexes could be synthesised and were consistent with the tight ethene binding to copper(I) observed in the ethene receptor site.³⁰ Since the mid-1980's the number of copper(I)-alkene crystal structures reported has steadily increased.²⁴ Recent work has focused on the use of bidentate and tridentate N-donors ligands to stabilise copper(I)-alkene complexes.³¹ Walton and co-workers observed that in $[\text{CuL}(\text{C}_2\text{H}_4)]\text{PF}_6$ ($\text{L} = N,N'$ -bis(2,4,6-trimethylbenzylidene)-1,2-diaminocyclohexane) the binding of ethene was reversible in MeCN.³² The binding could be followed by UV-visible spectroscopy as the ethene bound complex is colourless, whereas $[\text{CuL}(\text{NCCH}_3)]^+$ is yellow.

One of the reasons for the interest in copper(I) complexes and their properties is due to the large number of possible coordination geometries they possess. Copper(I)-alkene structures are no exception and exhibit a wide variety of coordination modes (see Figure 2).²⁴ Often a four coordinate copper(I) centre is observed with a distorted tetrahedral arrangement. When bulky ligands are present, steric constraints dictate that a three coordinate copper(I) centre is formed with a trigonal planar geometry. Cationic complexes of copper(I) are also known. In the case of $[\text{Cu}(\text{norbornene})_3][\text{SbF}_6]$, a three coordinate spoke wheel complex was obtained.³³

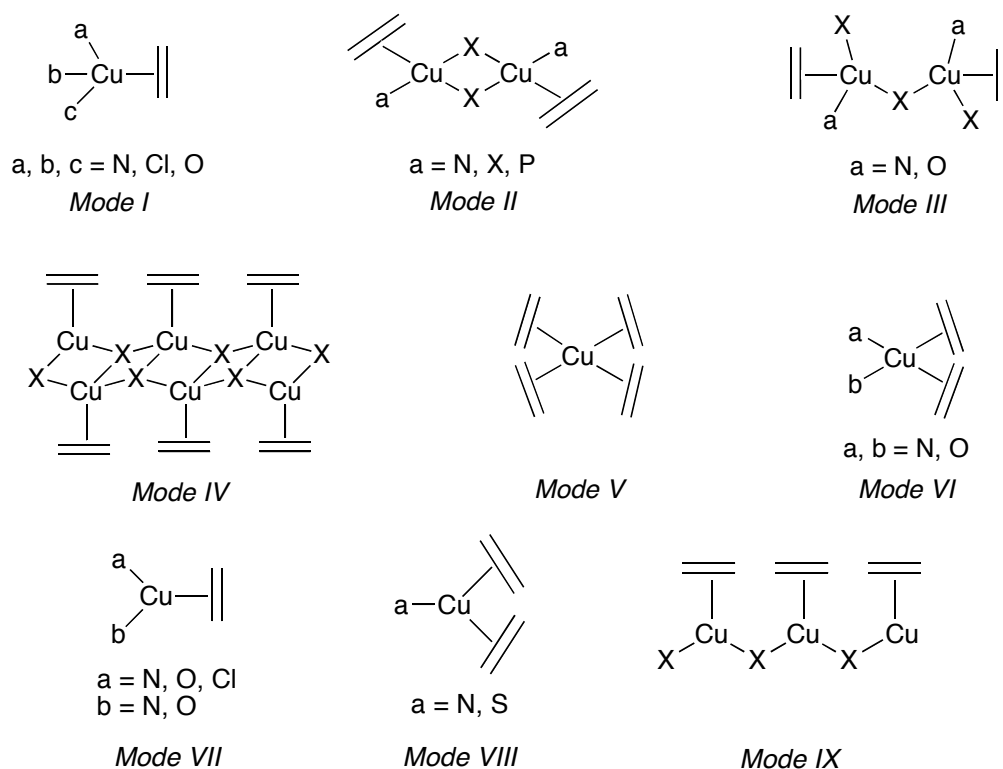
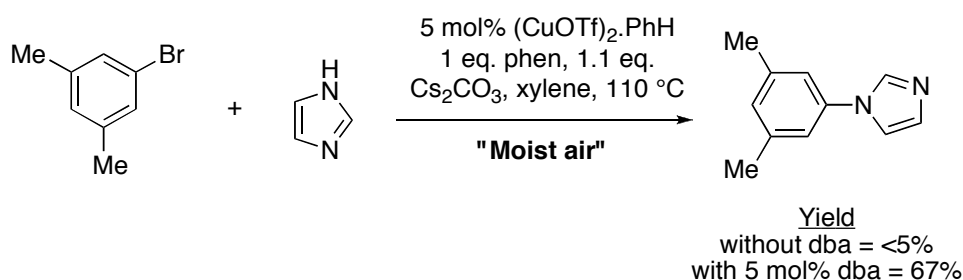


Figure 2: Coordination modes exhibited in copper(I)-alkene complexes (counter-ions not indicated).²⁴

Considering the increasing interest in alkene complexes, copper(I) complexes of dienes, polyenes and other conjugated alkenes are relatively rare. The copper(I) complexes of simple dienes such as isoprene were only structurally determined in the early 1990's.³⁴ In these complexes the dienes act as an η^2, η^2 -donor ligand bridging two copper(I) centres, rather than as an η^4 -donor to one Cu atom.³⁵ Often just one alkene of a diene will coordinate.³⁶ There are only a handful of complexes where crystallographic evidence shows a single Cu centre is bound to two or more alkenes in the same polyene.³⁷ The polyenes used in these studies were 1,5-cyclooctadiene, 1,2,5,6,9,10-tribenzocyclododeca-1,5,9-triene-3,7,11-triynes and cyclododecatriene. There are a number of coordination polymers that make use of copper(I)-alkene binding to stabilise large supramolecular networks.³⁸ Xiong used 4-HPYA (4-pyridylacrylic acid) and 3-HPYA to make a series of 1D and 2D copper(I)-alkene coordination polymers with high thermal stability.³⁹

To the best of our knowledge, compounds such as benzylidene acetone and dibenzylidene acetone have not been explored as ligands for copper(I).⁴⁰ In 1999 Buchwald reported the use of dba as an additive in a copper-catalysed C-N bond

formation (Scheme 3).⁴¹ In the presence of dba the reaction could be carried out in air with high yield; whereas in the absence of dba an inert environment was needed. This result suggests that the dba is stabilising the copper(I), presumably by coordinating to copper(I). However, no information was given on role played by the dba ligand in this chemistry.



Scheme 3: Buchwald amination using dba.

4.1.2 Copper complexes with phosphino-alkenyl ligands

A number of simple phosphino-alkenyl ligands have been coordinated to copper(I) centres. Kelly and co-workers reported the synthesis of diphenylvinyl-phosphine and diphenyl- α -styrenyl-phosphine complexes of copper(I), **189** and **188**, respectively.⁴² In both cases only the phosphine was bound to the copper(I) centre, with the alkene left non-coordinated. By contrast the allenylphenyl-phosphine did show evidence for alkene coordination in complex **190**.⁴³ In the free ligand the IR stretch of the alkene occurs at 1640 cm⁻¹. On coordination to copper(I) this disappears and a weak band at 1560 cm⁻¹ appears, which the authors attributed to the Cu-bound alkene. Silver(I) complexes were also studied, with no evidence found for alkene coordination. This led to the conclusion that the Cu^I-alkene bond is more stable than the Ag^I-alkene bond. It is worth noting that gold(I) complexes of phosphino-alkenes are also known.⁴⁴

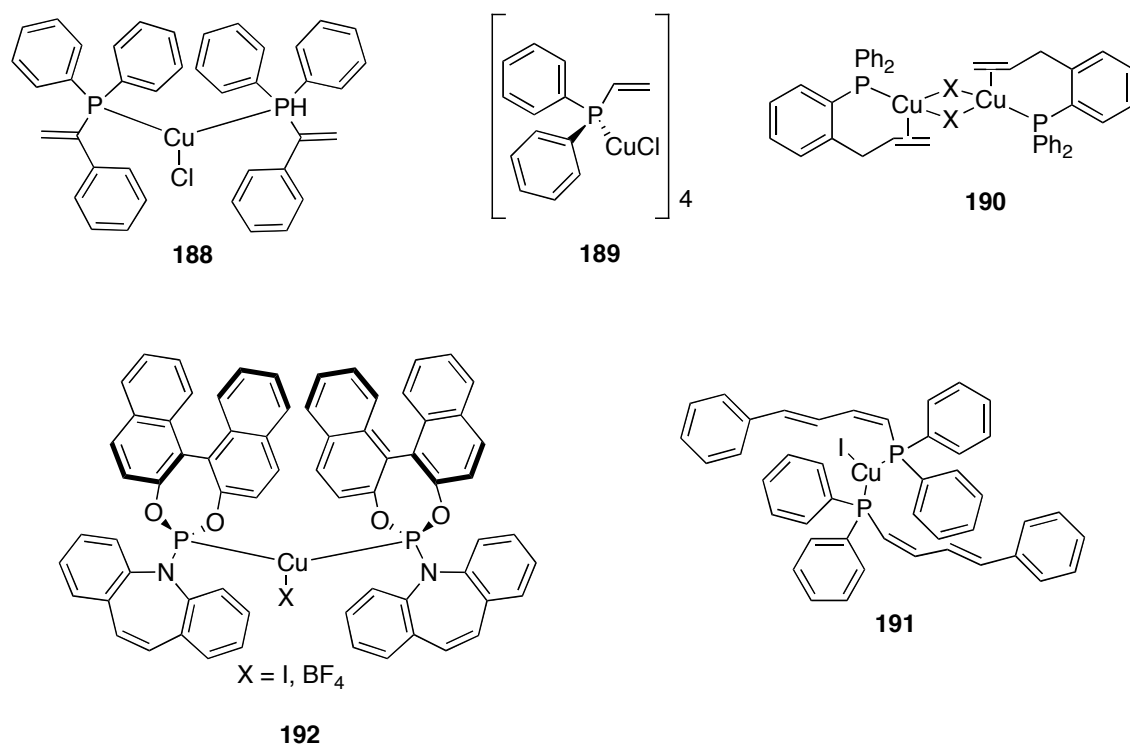
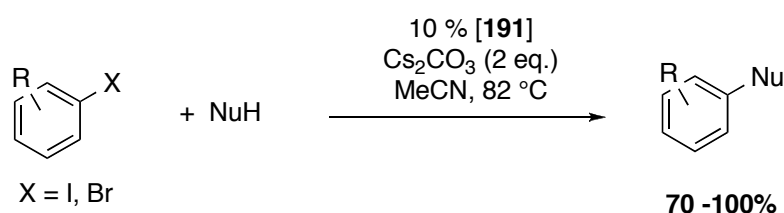


Figure 3: Copper(I) complexes with phosphino-alkenyl ligands.



Scheme 4: Copper-catalysed arylation of nucleophiles using butadienyldi-phosphine ligands.

Taillefre and co-workers used 4-phenyl-1,3-butadienyldi-phosphine as a ligand for the copper-catalysed arylation of nucleophiles such as pyrazoles and phenols.⁴⁵ In their work they isolated copper(I) complex **191**, which gave the same results in the arylation reactions as using CuI and two equivalents of ligand. Once again only the phosphine was found coordinated to the metal centre, in keeping with Kelly's studies,⁴² leaving the diene moiety non-coordinated. Dorta and co-workers also evaluated the use of phosphoramidate based phosphino-alkene ligands in Cu-catalysis.⁴⁶ Interestingly, in the rhodium complexes of these ligands alkene coordination was observed. However, on moving to the copper(I) complexes no evidence for such interactions was found. Instead, complexes of the type **192** shown in Figure 3 were obtained. These complexes were evaluated in a catalytic 1,4-addition of organoaluminum reagents to conjugated enones. The neutral copper(I) complexes did not catalyse the reaction; indeed, they stopped the reaction completely. This is noteworthy as the 'control' reaction gives a

64% yield with no Cu catalyst present! By contrast, the cationic copper(I) complexes gave excellent yields, though only with moderate enantioselectivities.

Searches of online chemical databases such as SciFinder and the CCDC reveal that Cu complexes containing alkenes and phosphine sulfide ligands are very rare.⁴⁷

4.1.3 Aims

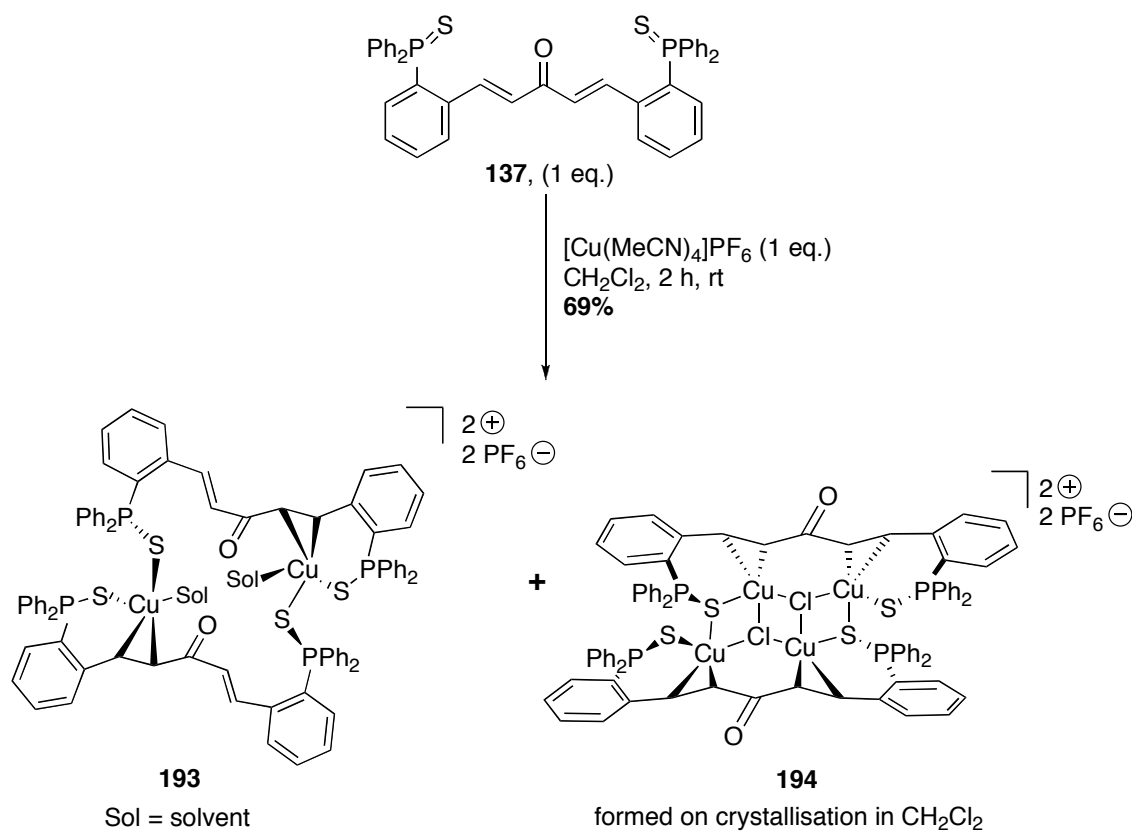
Relatively little work has been carried out on copper(I) complexes containing conjugated alkene ligands. Extending this to phosphino-alkenyl ligands reveals only a few previous investigations. In Chapter 2, the development of phosphino-alkenyl ligands and their corresponding phosphine sulfide derivatives was described. The aim for this part of the project is to investigate copper(I) complexes of these ligands, and their activity in benchmark catalytic reactions. We choose to concentrate on the phosphine sulfide ligands.

4.2 Results and Discussion

An initial copper(I) complex was formed by the reaction of dbaTHIOPHOS **137** with tetrakis(acetonitrile)copper(I) hexafluorophosphate in CH₂Cl₂ at room temperature.⁴⁸ A new product was observed which shows very broad signals in the ¹H NMR spectrum (see Figure 8). Crystallisation of the solid material from CH₂Cl₂ layered with Et₂O gave both pale yellow (the majority) and bright yellow crystals suitable for study by X-ray diffraction. A pale yellow crystal was identified as dinuclear copper(I) complex **193**, whereas a bright yellow crystal was found to be tetranuclear copper(I) complex **194** (see Scheme 5).

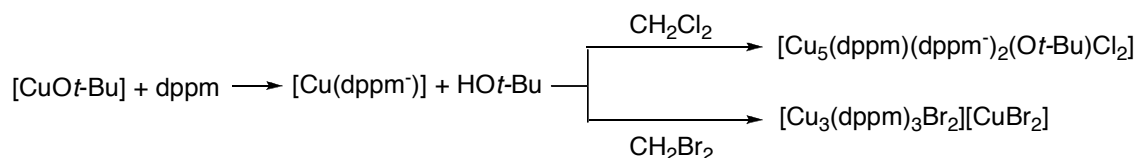
Complex **194** includes chloride ions, which are not present in the reactants. Elemental analysis of the tetrakis(acetonitrile)copper(I) hexafluorophosphate confirmed that it was not contaminated with chloride. Mass spectrometry (LIFDI) of the product before crystallisation showed the presence of one ion (*m/z* 729) which is [Cu^I(dbaTHIOPHOS)]⁺. The ESI-MS showed the same peak along with a number of others including a peak at *m/z* 1397 attributed to [Cu(dbaTHIOPHOS)₂]⁺, and one at *m/z* 829 attributed to [Cu₂Cl(dbaTHIOPHOS)]⁺. It is believed that the presence of chloride in the MS spectrum is due to the mass spectrometry conditions as the peak at *m/z* 829

also appears in the product from the reaction conducted in THF (*i.e.* no chloride present at all). It is therefore believed that **193** is the product from the reaction, and that **194** was formed under the crystallisation conditions.



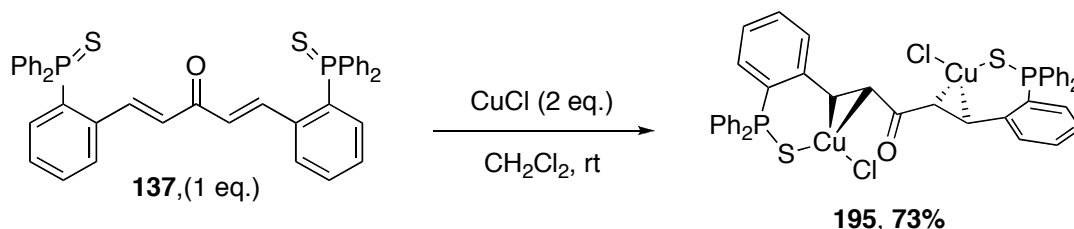
Scheme 5: Reaction between dbaTHIOPHOS (137) and copper(I).

The chloride ions in **194** are believed to have originated from the crystallisation solvent, either by halide abstraction from a molecule of CH₂Cl₂ or from trace quantities of HCl formed by photolysis of CH₂Cl₂. Halide abstraction from CH₂Cl₂ by copper(I) complexes is known in the literature. For example, Rothenberger reported the abstraction of halides from both CH₂Cl₂ and CH₂Br₂ by [Cu(dppm⁻)] (see Scheme 6).⁴⁹ The reactions were performed under the exclusion of light to avoid potential photolysis of the solvent. Under these reported reaction conditions *t*-BuOH was present and assumed to play a role in the abstraction of halide or HX from the solvent.



Scheme 6: Extraction of halides by a copper(I)-phosphine complex.

Lui reported a series of copper(I) complexes with dithiophosphates and bis(diphenylphosphino)alkanes as ligands.⁵⁰ In a series of complexes, Cu clusters formed with the abstraction of chloride from CH_2Cl_2 or CHCl_3 . The halide abstraction was found to be dependent on the ligand-to-metal ratio. This observation, along with the reasonable yields, suggest that the mechanism was indeed abstraction of chloride from the solvent molecules, but no control reactions were carried out in the dark to eliminate photolysis of the solvents to give HCl. Due to the conditions used for our crystallisation, we were unable to rule out either mechanism. However, as no changes are observed after long periods of time in dry and degassed CD_2Cl_2 solutions, it is reasonable to conclude that C-H activation is unlikely to be occurring, and the chloride comes from trace HCl in the solvent used for the crystallisation.



Scheme 7: Neutral copper(I) complex formation.

The reaction of dbaTHIOPHOS with CuCl in CH_2Cl_2 at room temperature gave the neutral complex **195** in good yield (see Scheme 7). Complex **195** was crystallised from CH_2Cl_2 solutions layered with pentane, to give crystals suitable for analysis by X-ray diffraction (Figure 7).

4.2.1 Comparison of X-ray single crystal structures

In both the cationic complexes the Cu is tetracoordinate (see Figure 4 and Figure 6). In complex **A**, the copper is in a distorted tetrahedral arrangement; the sulfur atoms and alkene form an almost planar triangle with the water sitting perpendicular to this.

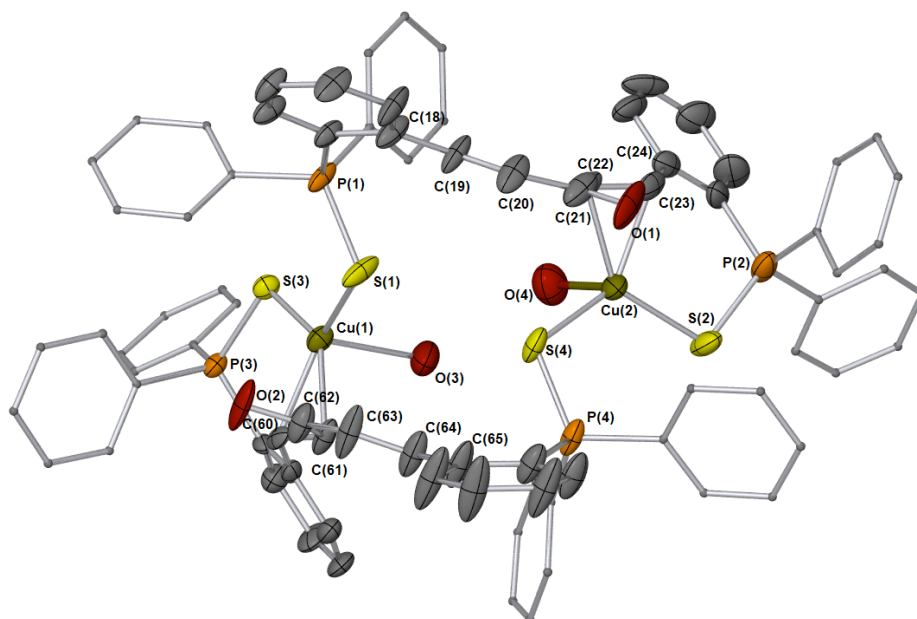


Figure 4: X-ray crystal structure of 193. Hydrogen and counter ion atoms have been removed for clarity. Thermal ellipsoids shown at 50%. Selected bond angles ($^{\circ}$): S(3)-Cu(1)-S(1) = 117.91(6), C(60)-Cu(1)-O(3) = 99.81(19), C(61)-Cu(1)-O(3) = 92.0(2), S(3)-Cu(1)-O(3) = 96.37(14), S(1)-Cu(1)-O(3) = 98.68(13), S(4)-Cu(2)-S(2) = 119.86(7), C(23)-Cu(2)-O(4) = 98.3(2), C(22)-Cu(2)-O(4) = 93.8(2), S(4)-Cu(2)-O(4) = 96.28(14), S(2)-Cu(2)-O(4) = 95.78(15).

The coordination geometry of the copper in **194** is similar to that described as Mode IV by Xiong and co-workers (see Figure 2).²⁴ The same ‘pleated ladder’ polymeric core is observed; the central step is a rhombus whereas the two outside steps all have different angles leading to a twisted system. The two dbaTHIOPHOS ligands bridge two copper(I) atoms each side of the ladder with the phosphine sulfides capping the ends. Two chloride ions fill the remaining coordination sites.

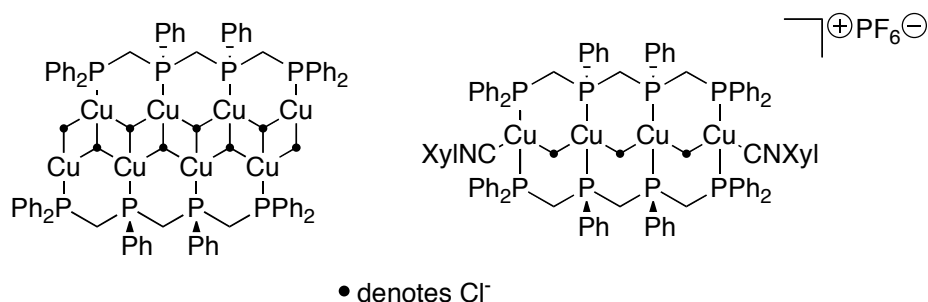


Figure 5: Examples of related copper chloride ladder complexes.

Note the presence of the chloride anions in **194** is only supported by X-Ray diffraction analysis. To confirm that chlorides were present, a comparison with literature Cu-Cl

bond lengths in related complexes were carried out. The Cu-Cl bond lengths of similar complexes (see Figure 5) were found to be between 2.3 and 2.8 Å,⁵¹ which matches our data, 2.3-2.6 Å. This is a closer match than other anions such as hydroxides, which have Cu-OH bonds distances in ladder complexes of 1.9-2.3 Å.⁵² The copper environment in **194** is nearer a classic tetrahedral arrangement than in complex **193**, but still distorted. Complex **195** on the other hand exhibits trigonal planar geometry around the copper(I) centres. The Cu-Cl bond distances in **195** are considerably shorter than those in **194**.

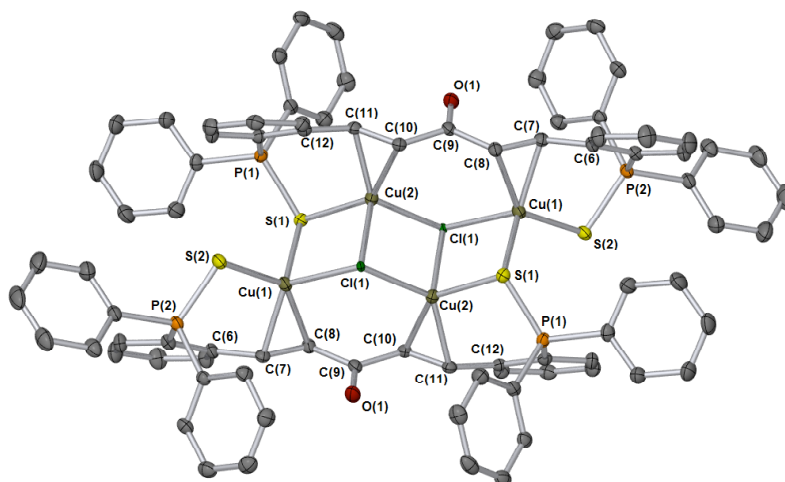


Figure 6: X-ray crystal structure of 194. Hydrogen, solvent and counter ion atoms have been removed for clarity. Thermal ellipsoids shown at 50%. Selected bond angles (°): C(7)-Cu(1)-S(2) = 102.24(8), C(8)-Cu(1)-S(2) = 139.68(8), C(7)-Cu(1)-Cl(1) = 125.06(8), C(8)-Cu(1)-Cl(1) = 102.56(8), S(2)-Cu(1)-Cl(1) = 104.95(3), C(7)-Cu(1)-S(1) = 115.78(8), C(8)-Cu(1)-S(1) = 93.14(8), S(2)-Cu(1)-S(1) = 112.26(3), Cl(1)-Cu(1)-S(1) = 96.37(2).

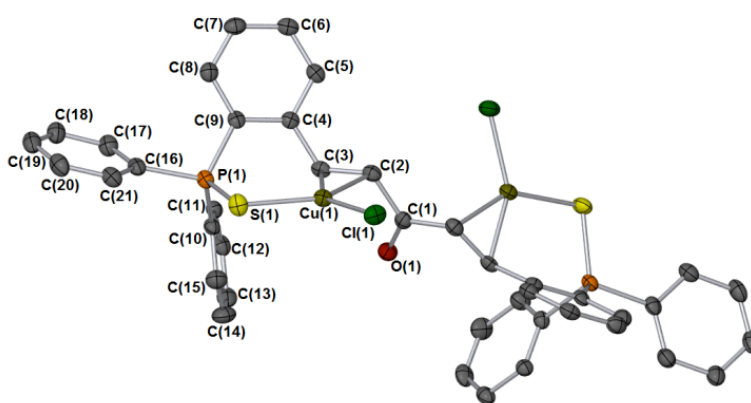


Figure 7: X-ray structure of 195. Thermal ellipsoids shown at 50% probability; Selected bond angles (°): C(3)-C(2)-Cu(1) 70.22(18), C(1)-C(2)-Cu(1) 105.11(17), P(1)-S(1)-Cu(1) 98.81(4), C(3)-Cu(1)-S(1) 104.51(9), C(2)-Cu(1)-S(1) 143.46(10), Cl(1)-Cu(1)-S(1), 111.34(4).

In all the copper(I) complexes the C=C and P=S bonds have lengthened on

coordination, as you might expect, due to the removal of electron density and the increase in sp^3 character. In **193** all the P=S bonds are identical (within error).^{*} By contrast in **194** the P=S distances in different environments are different; the P=S bond capping the ladder structure, *i.e.* coordinated to two Cu atoms, are longer than those coordinated to just one Cu atom. This is also matched by a difference in the Cu-S bond lengths; the Cu-S bond outside of the ladder is the shortest (2.2767(8) Å), whilst the Cu-S distances within the ladder are longer (2.2948(8) and 2.4872(8) Å). The Cu-S distances in **195** are even shorter (2.2546(9) Å) and are consistent with those in a reported neutral copper(I) complex containing phosphine sulfide ligands.⁵³ The Cu-Cl bond distances are also consistent.

Table 1: Comparison of bond lengths (Å) in dbaTHIOPHOS, 137, and complexes 193-195.

Cpd.	Key bonds and lengths (Å)					
	C=C	C=O	P=S	Cu-S	Cu-C	Cu-Cl
137	C(2)-C(3) 1.324(5)	C(1)-O(1) 1.221(6)	P(1)-S(1) 1.9619(11)	-	-	-
193	C(22)-C(23) 1.360(9)	C(21)-O(1) 1.224(7)	P(1)-S(1) 1.993(2)	Cu(1)-S(1) 2.2826(18)	Cu(1)-C(60) 2.091(6)	-
	C(19)-C(20) 1.346(8)	C(62)-O(2) 1.225(7)	P(2)-S(2) 1.987(3)	Cu(1)-S(3) 2.2488(16)	Cu(1)-C(61) 2.125(6)	
	C(60)-C(61) 1.384(8)		P(3)-S(3) 2.002(2)	Cu(2)-S(2) 2.2619(18)	Cu(2)-C(22) 2.089(6)	
	C(63)-C(64) 1.319(8)		P(4)-S(4) 1.995(2)	Cu(2)-S(4) 2.2585(18)	Cu(2)-C(23) 2.087(7)	
194	C(8)-C(7) 1.373(4)	C(9)-O(1) 1.224(4)	P(1)-S(1) 2.0221(10)	Cu(1)-S(1) 2.4872(8)	C(7)-Cu(1) 2.112(3)	Cu(1)-Cl(1) 2.4155(7)
	C(10)-C(11) 1.373(4)		P(2)-S(2) 1.9936(10)	Cu(1)-S(2) 2.2767(8)	C(8)-Cu(1) 2.164(3)	Cu(2)-Cl(1) 2.3330(7)
				Cu(2)-S(1) 2.2948(8)	C(10)-Cu(2) 2.108(3)	Cu(2)#1-Cl(1) 2.5906(7)
					C(11)-Cu(2) 2.089(3)	Cu(2)-Cl(1)#1 2.5907(7)
195	C(2)-C(3) 1.375(4)	C(1)-O(1) 1.228(5)	P(1)-S(1) 2.0072(12)	Cu(1)-S(1) 2.2546(9)	C(2)-Cu(1) 2.060(3)	Cu(1)-Cl(1) 2.1908(9)
					C(3)-Cu(1) 2.053(3)	

* Within error is used throughout this thesis to indicate the following conditions are met: In normally distributed data, 99% of measurements fall within ± 3 standard deviations of the mean. In crystallography bond distances and angles are only considered different if there is no overlap of the two measurements within ± 3 of their esd's. For further discussion on errors in crystallography see Haestier, J. *Crystallogr. Rev.* **2010**, *16*, 133-144.

The Cu-C bond lengths also vary between the complexes. The shortest Cu-C bond lengths are seen in **195** and the longest seen in **194**. In complex **194**, the Cu-C bonds are unsymmetrical with the Cu-C bonds α to the carbonyl longer than those in the β position. In all cases the coordinated alkenes adopt the *s-cis* conformation. This leads to complex **193** having an *s-cis,s-trans* backbone, whilst both **194** and **195** are in the *s-cis,s-cis* conformation. The *s-cis,s-trans* geometry was also observed in the palladium(0) complex of dbaPHOS (see Section 3.1.3). The carbonyl bond length is the same (within error) in both the ligand and the complexes.

4.2.2 NMR spectroscopic studies on complexes **193**, **194** and **195**

The ^1H NMR spectrum of **193** in CD_2Cl_2 exhibits very broad peaks at 300 K (Figure 8). It was suspected that the broadness was due to free and coordinated alkenes exchanging on the NMR timescale (Scheme 8). The ^{31}P NMR spectrum exhibits two broad singlets (δ 46.4 and 40.6), plus a septet at -143.8 ppm from the PF_6 anion. This indicates that the two phosphorous environments of the ligand are different. This would be the case if only one alkene was coordinated to copper(I). A variable temperature ^1H NMR experiment confirmed that at low temperatures this fluxional behaviour could be frozen out to reveal the free and coordinated alkenes separately (Figure 8). At 230 K, the proton chemical shifts of the coordinated alkene (δ 5.94 and 5.99) possess a coupling constant of 13.3 Hz, whereas the non-coordinated alkene (δ 6.60 and 7.82), have a coupling constant of 16.4 Hz, which is supported by a low temperature 2D ^1H - ^1H COSY experiment (see Figure 9). The reduction of the coupling constant and the shift upfield is consistent with coordination to a metal. The two broad singlets in the ^{31}P NMR spectrum sharpen on lowering the temperature to 230K. A 2D ^1H - ^{31}P HMQC experiment shows that the ^{31}P signal at δ 40.6 couples with the proton at δ 5.94, whereas the ^{31}P signal at δ 46.4 couples with the proton at δ 7.82.

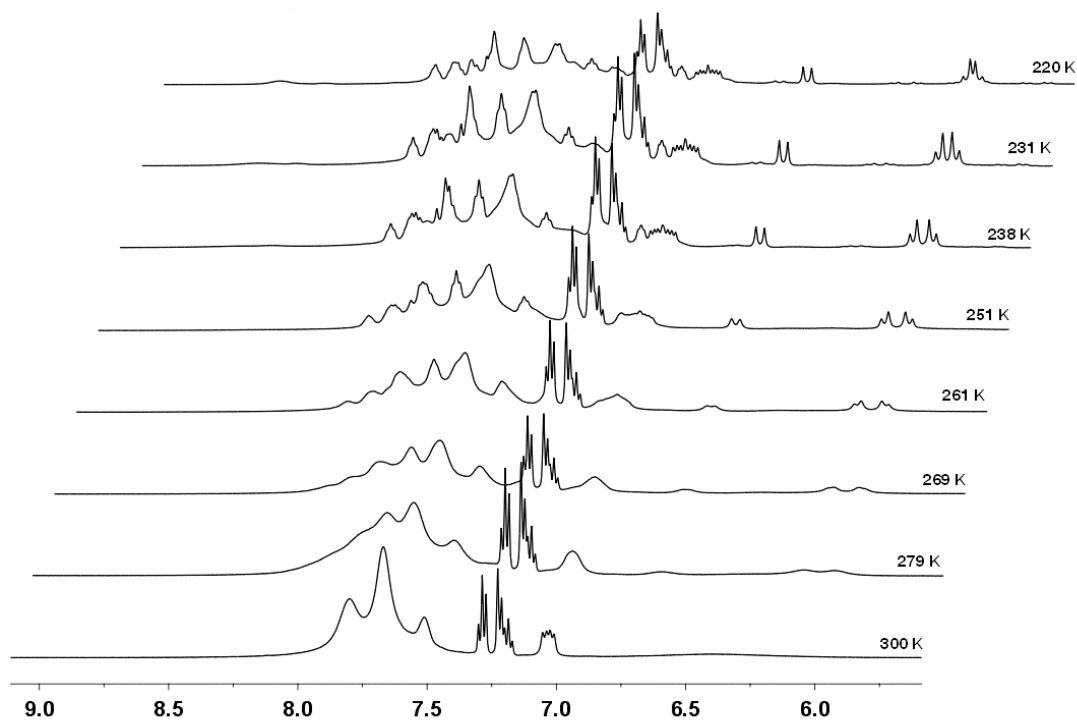


Figure 8: Variable temperature ^1H NMR spectra of 193 (CD_2Cl_2 , 500 MHz).

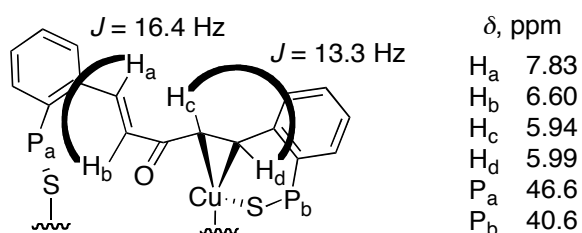
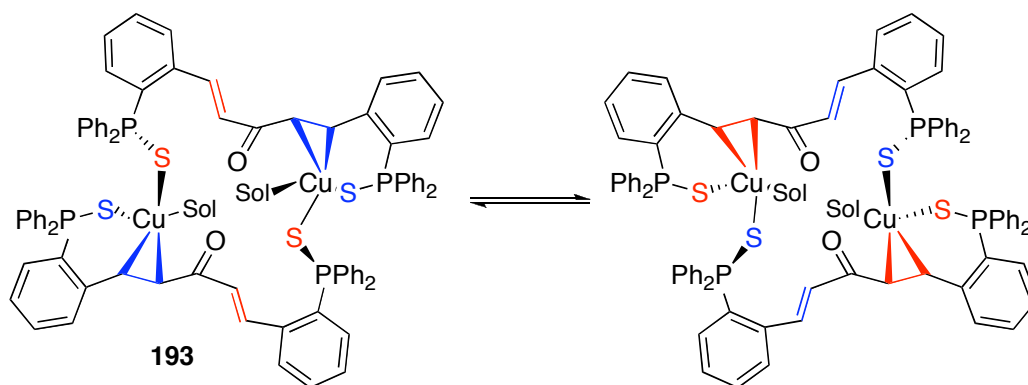


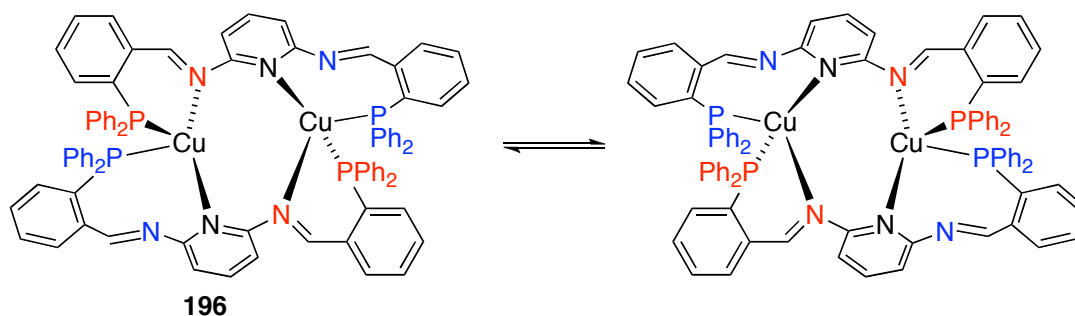
Figure 9: ^1H and ^{31}P NMR assignment of alkene protons.

Using *gNMR* software,⁵⁴ it was possible to simulate the line shape of the experimentally observed spectra to calculate the rate constants for the exchange process at a number of temperatures. An Arrhenius plot of $1/T$ against $\ln k$ gives a straight line with slope $-E_a/R$, allowing the activation energy to be estimated ($58.23 \text{ kJ mol}^{-1}$). In addition, an Eyring plot of $\ln(k/T)$ against $1/T$ afforded a linear plot from which the enthalpy, $\Delta H^\ddagger = 56.0 \pm 6.4 \text{ kJ mol}^{-1}$, and entropy, $\Delta S^\ddagger = 0.43 \pm 6.9 \text{ J mol}^{-1}\text{K}^{-1}$, of activation were determined. The small ΔS^\ddagger value is in keeping with exchange being intramolecular and therefore independent of water dissociation. The ΔH^\ddagger value indicates that the barrier to rotation is mostly enthalpic. The free energy of activation (ΔG^\ddagger) at 300 K is $55.9 \pm 9.7 \text{ kJ mol}^{-1}$ ($13.4 \pm 2.3 \text{ kcal mol}^{-1}$).



Scheme 8: Alkene exchange in 193.

Interestingly, a related cationic copper(I) complex, $[\text{Cu}_2(2,6\text{-}(\text{Ph}_2\text{P}(o\text{-C}_6\text{H}_4)\text{CH}=\text{N})_2\text{C}_5\text{H}_3\text{N})_2][\text{BF}_4]_2$ (**196**) was reported by Yeh and Chen⁵⁵ recently. They noted dynamic exchange between the coordinated and the non-coordinated imine groups in solution $\{\Delta G^\ddagger = 8.8 \text{ kcal mol}^{-1}$ (36.8 kJ mol^{-1}), estimated} (Scheme 9).



Scheme 9: Imine exchange in 196.

Complex **167** ($[\text{Pd}^0(\text{dbaPHOS})]$) reported in Chapter 3 also undergoes alkene exchange. The exchange parameters were determined by P-P EXSY experiments: $\Delta S^\ddagger = -19.5$ (± 11.1) $\text{J mol}^{-1} \text{K}^{-1}$ and $\Delta H^\ddagger = 65.7$ (± 3.4) kJ mol^{-1} . It can be seen that once again the barrier is mostly enthalpic. The free energy of activation (ΔG^\ddagger) at 300 K is 71.6 kJ mol^{-1} ($17.1 \text{ kcal mol}^{-1}$). In both our complexes the free energy of activation is almost double that of the imine exchange in **196**.

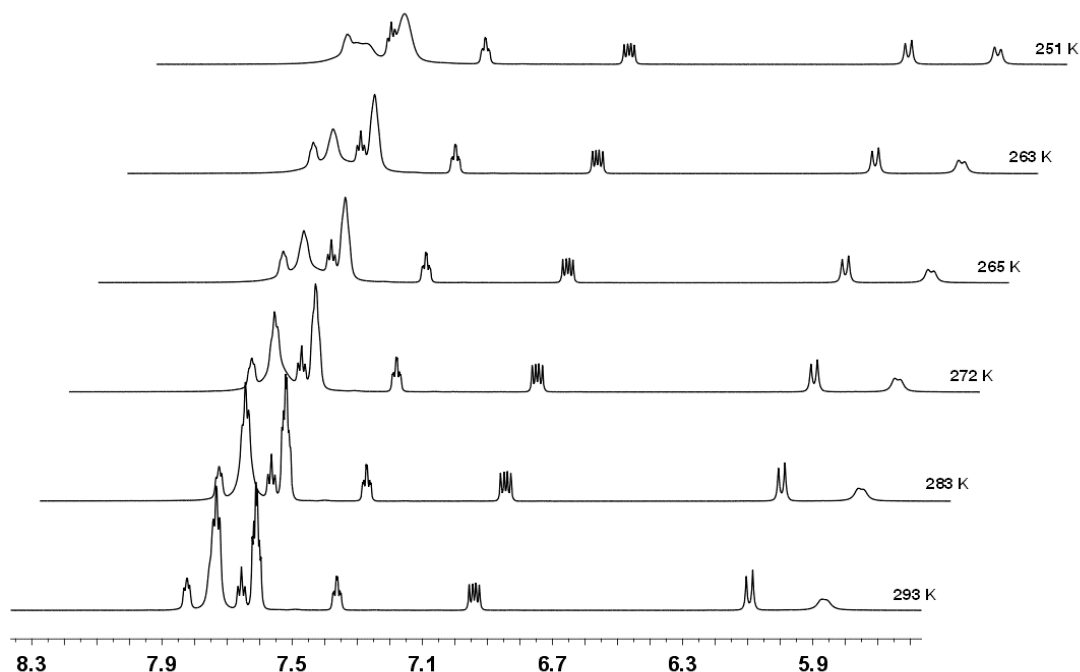


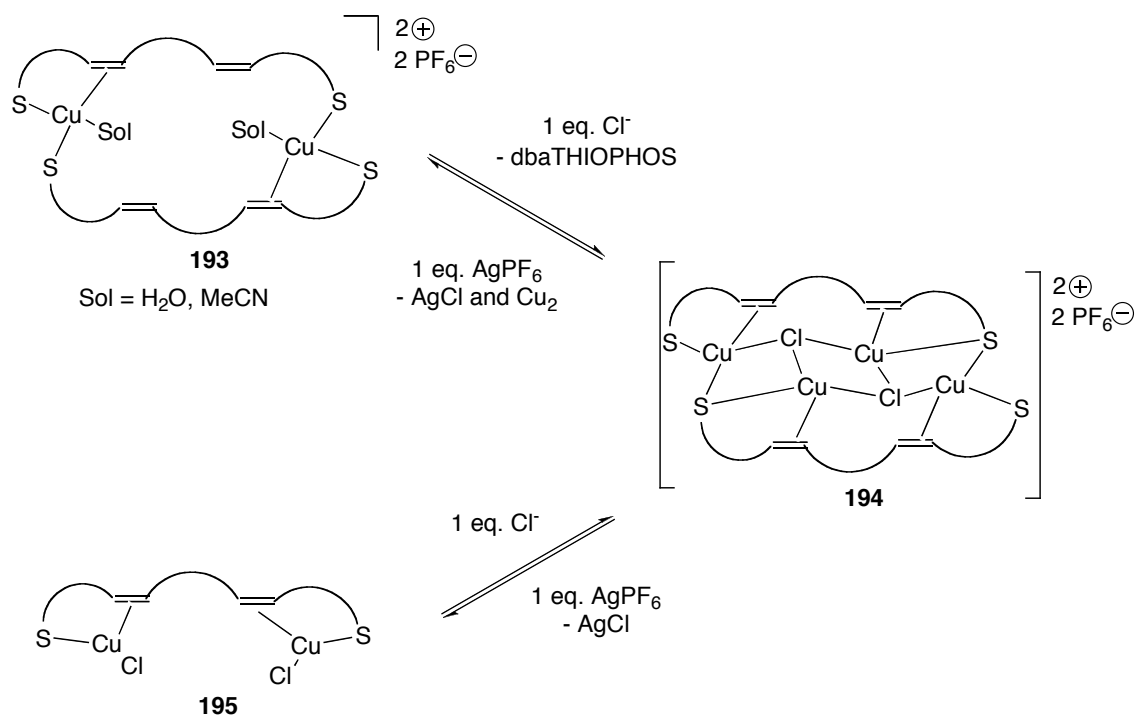
Figure 10: Variable temperature ^1H NMR spectra of **195 in CD_2Cl_2 (700 MHz).**

The ^{31}P NMR spectrum of **195** shows one phosphorous singlet at 40.8 ppm, confirming that the both phosphorus environments are the same. The ^1H NMR spectrum of complex **195** is as expected, with the alkenyl protons shifted upfield to 6.07 and 5.83 ppm, indicating coordination to copper(I). The ^{13}C NMR spectrum of **195** is also as expected, with the alkenyl carbons shifted upfield as broad peaks at 95.3 and 94.4 ppm. However, at 293 K, one of the alkene protons appears broad in the ^1H NMR spectrum (see Figure 10). A variable temperature ^1H NMR experiment shows that the alkene sharpens on cooling to give a doublet with the same coupling constant (13.9 Hz) as the other alkenyl proton. A ^1H - ^1H COSY experiment also confirms that both peaks are associated with the alkene. If the alkenes were exchanging with each other by breaking their coordination with the Cu, then both alkene proton environments would be expected to appear broad. As the other alkene proton peak is sharp another explanation is required. Possible explanations could include that one side of the alkene is much closer to the Cu or that exchange and/or rotational processes are occurring which only affect one end of the alkene. The former suggestion is unlikely as the crystal structure shows the two C-Cu bond lengths are the same within error. The broadness of the α -proton is therefore tentatively attributed to a partially restricted rotation about the C-C single bonds connecting the carbonyl moiety.

4.2.3 Interconversion of the complexes

Using dbaTHIOPHOS **137**, three different copper(I) complexes have been isolated, each with different Cu:Cl ratios. It was hypothesised that it may be possible to interconvert between the different complexes by chloride addition (**193**→**194**→**195**) or chloride abstraction using silver salts (**195**→**194**→**193**) (Scheme 10). It was proposed that this would enable further characterisation of **194**. The forward conversion was assessed by the addition of aliquots of a *n*-Bu₄NCl solution in CD₂Cl₂ to a solution of complex **193** in CD₂Cl₂. The ¹H and ³¹P spectra were recorded after the addition of each aliquot. Unfortunately, after the addition of ~0.5 eq. of chloride no clear intermediate complex was observed. The addition of further equivalents of chloride leads to sharpening of the aromatic peaks and appearance of broad alkene protons between 6.2 and 6.4 ppm. On addition of more than 3 eq. chloride only the free ligand was observed (spectra k and l in Figure 11) and not complex **195**.

In a separate NMR spectroscopic study, crystals suitable for X-ray diffraction were obtained after the addition of 0.5 eq *n*-Bu₄NCl. They were found to be complex **195**, thus possessing a 1:1 Cu:Cl ratio rather than the expected 1:0.5 ratio. The unexpected stoichiometry suggests that either a mixture of products is formed on addition of chloride or the species formed with a 1:0.5 Cu:Cl ratio is unstable and decomposes to give **195** and free ligand. The crystal structure was similar to the previous structure of **195**, with the exception that the unit cell contained disordered dichloromethane molecules (see Appendix 3).



Scheme 10: Interconversion of the copper(I) complexes by addition or abstraction of chloride anions.

The addition of chloride was also monitored by UV-visible spectroscopy, which revealed a number of Cu species in solution. It appears to show an initial product forming up to the addition of 0.4 eq. of chloride and then a new product forming on addition of up to 1 eq. of chloride. However, together with the NMR spectroscopic data no clear conclusions can be drawn.

A similar NMR spectroscopic study was carried out for the reverse reaction - the abstraction of chloride by silver salts. The reactions of complex **195** with varying amounts of AgPF₆ were carried out in CD₂Cl₂, and the ¹H and ³¹P NMR spectra recorded. The addition of 2 eq. AgPF₆ gave a similar ¹H NMR spectrum to complex **193**. When the reaction was repeated with *ca.* 2.5 eq. AgPF₆, again a similar spectrum was obtained at 298 K, and on cooling the proton signals did not sharpen up as seen in complex **193**. It was proposed that silver(I) coordination could be occurring. Indeed, silver(I) complexes of dbaTHIOPHOS have been synthesised (see Section 4.2.4). It is therefore likely that silver(I) complexation is competing with copper(I), which would account for the differences observed.

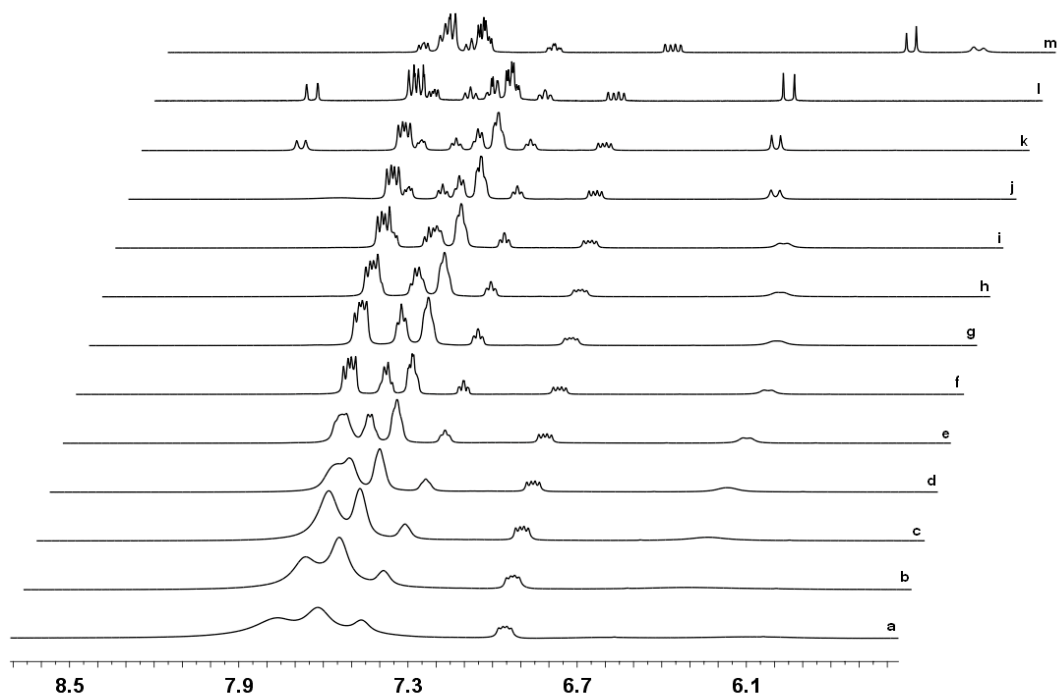


Figure 11: ^1H NMR spectroscopic study of the addition of chloride anions to 193 (500 MHz, CD_2Cl_2 , 295 K): a) 193; b) 0.3 eq. Cl^- ; c) 0.6 eq.; d) 0.9 eq.; e) 1.2 eq.; f) 1.5 eq.; g) 1.8 eq.; h) 2.1 eq.; i) 2.4 eq.; j) 3 eq.; k) 3.6 eq.; l) dbaTHIOPHOS (137); m) 195.

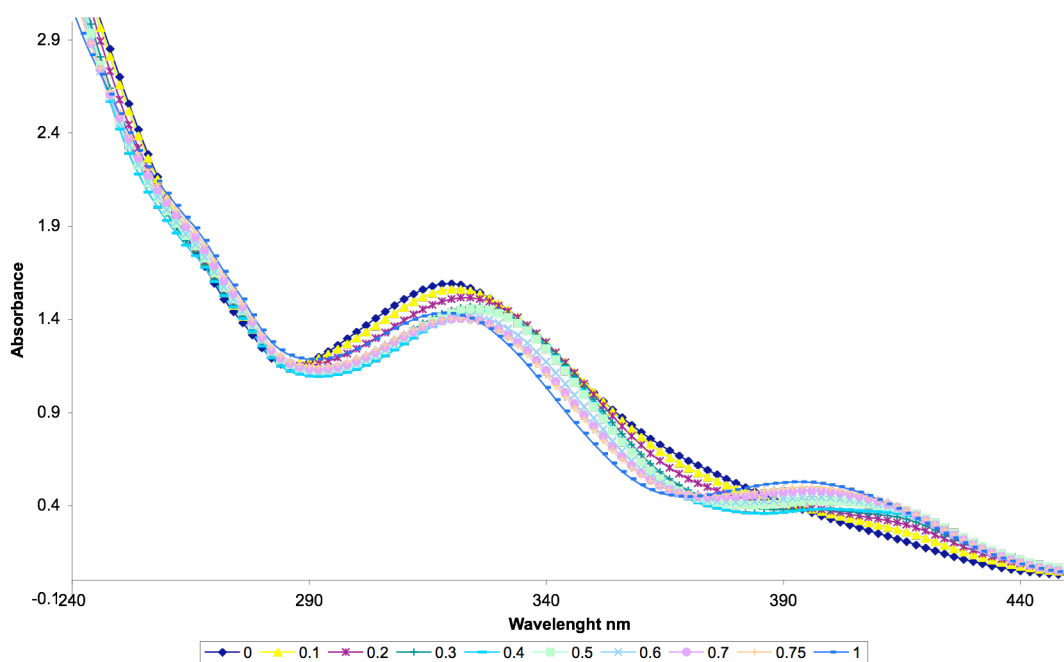


Figure 12: UV-visible spectroscopic analysis on addition of varying equivalents of chloride to a solution of 193 in CH_2Cl_2 (5.7×10^{-5} M). The legend depicts the number of equivalents of chloride relative to Cu.

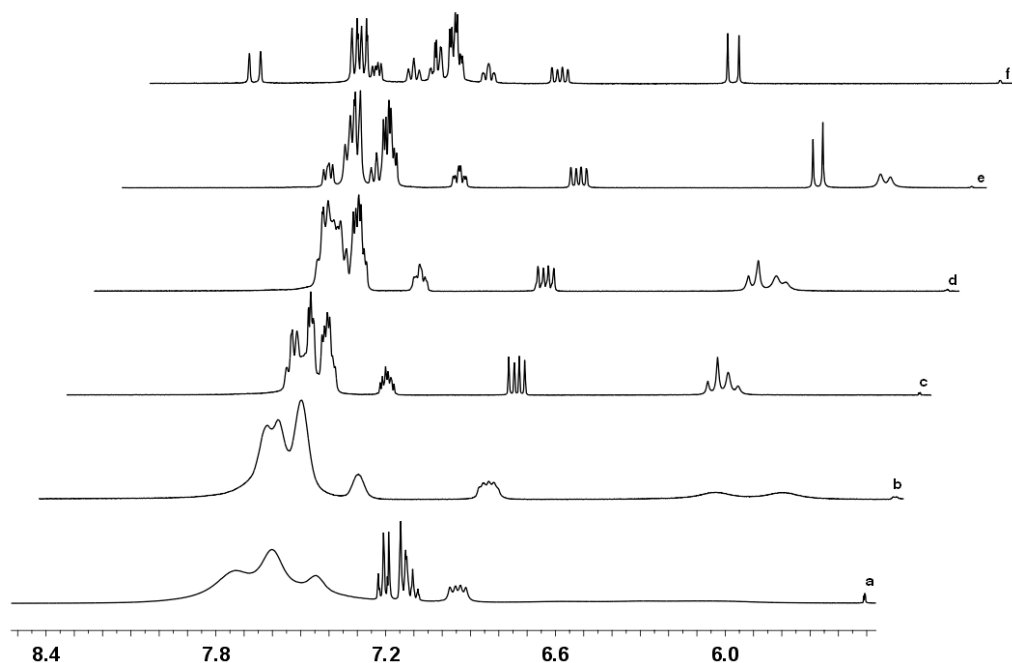
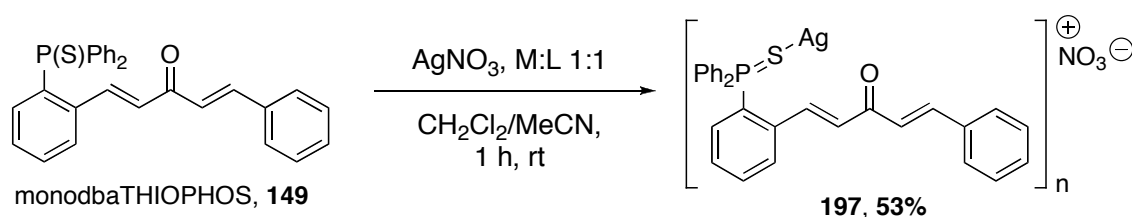


Figure 13: ^1H NMR spectroscopic analysis of the addition of silver(I) salts to **195** (400 MHz, CD_2Cl_2 , 298 K): a) **193** (contains trace toluene); b) 2 eq. AgPF_6 ; c) 1 eq. AgPF_6 ; d) 0.5 eq. AgPF_6 ; e) **195**; f) **dbaTHIOPHOS**, (**137**).

4.2.4: Silver complexes of the phosphine sulfide ligands

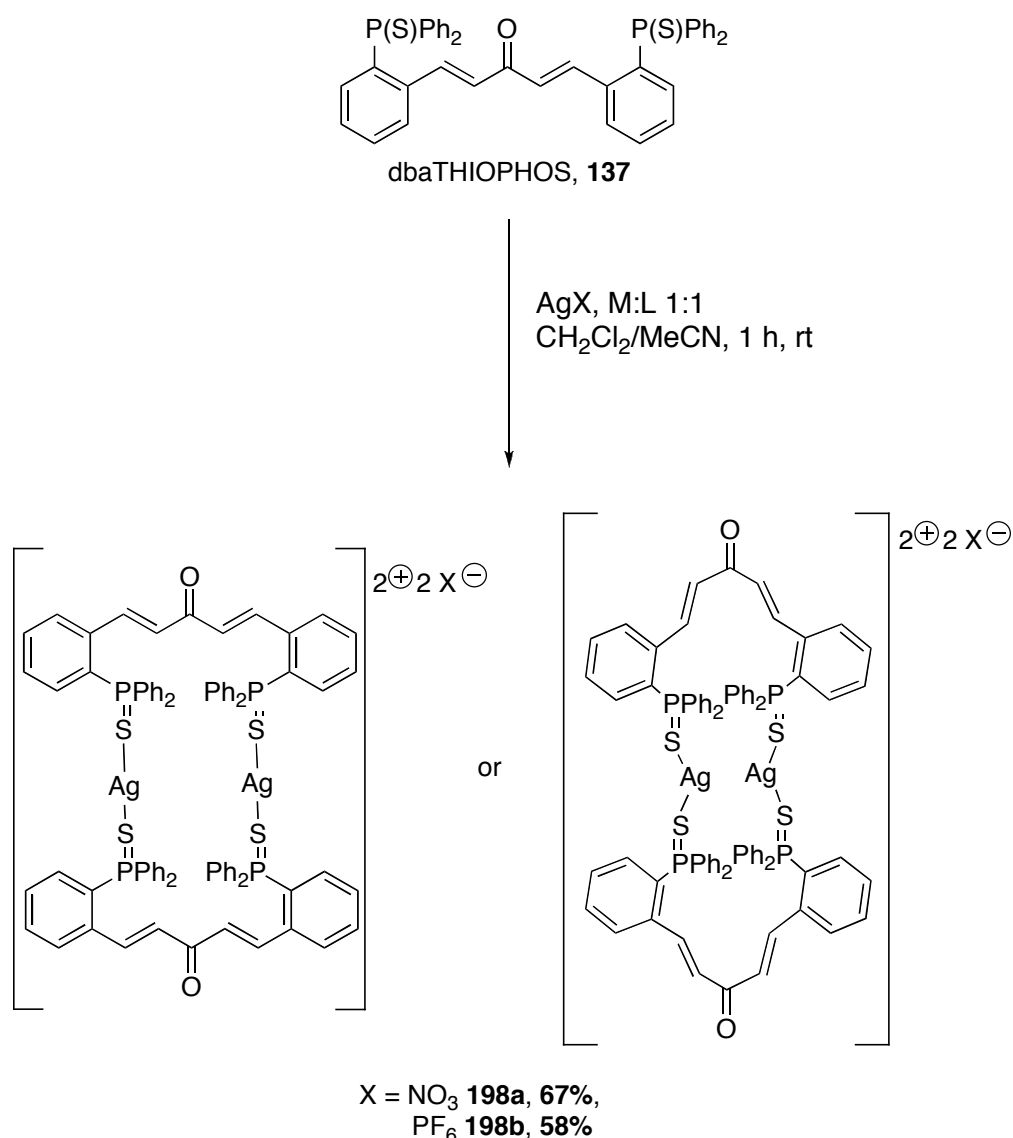
The silver(I) complexes of both **dbaTHIOPHOS**, **137**, and **monodbaTHIOPHOS**, **149**, have been synthesised in good yield (Scheme 11 and 12).



Scheme 11: Silver(I) complex of monodbaTHIOPHOS.

For the nitrate complexes, a small shift is observed in the ^{31}P NMR spectrum from 42.07 ppm in the free ligand to 44.54 ppm in the **198a**, and from 42.14 ppm to 45.52 ppm, **197**. The alkene proton shifts have moved closer together: $\Delta\delta_{\alpha\beta} = 1.69$ in **dbaTHIOPHOS**, **137**, and $\Delta\delta_{\alpha\beta} = 1.39$ in **198b** (Figure 14). The proton shift is mostly due to the shift in the β -proton from 8.2 to 7.9 ppm on complexation. The NMR spectroscopic data gives no indication that the alkene moieties are coordinated to

silver(I). As a result, **197** and **198** have been proposed as the structures of the complexes.



Scheme 12: Synthesis of silver(I) complex of dbaTHIOPHOS.

Unfortunately single crystals suitable for X-ray diffraction were not obtained, so we are unable to confirm these structures. As mentioned in previous chapters, NMR spectroscopic data can be used to give an indication of the backbone geometry of the ligand in the complex.⁵⁶ Only two alkenyl protons are observed for **198** indicating the alkenes are in the same environments. As a result both the *s-cis,s-cis* and *s-trans,s-trans* backbone geometries could be envisaged (Scheme 12). The $\Delta\delta_{\alpha\beta}$ value is quite large (1.39 ppm) which may indicate that the geometry is *s-trans*. However, care must be taken with these values as they were described for dba and no rigorous assessment of their use in related compounds has been carried out (see Section 2.4, Chapter 2).

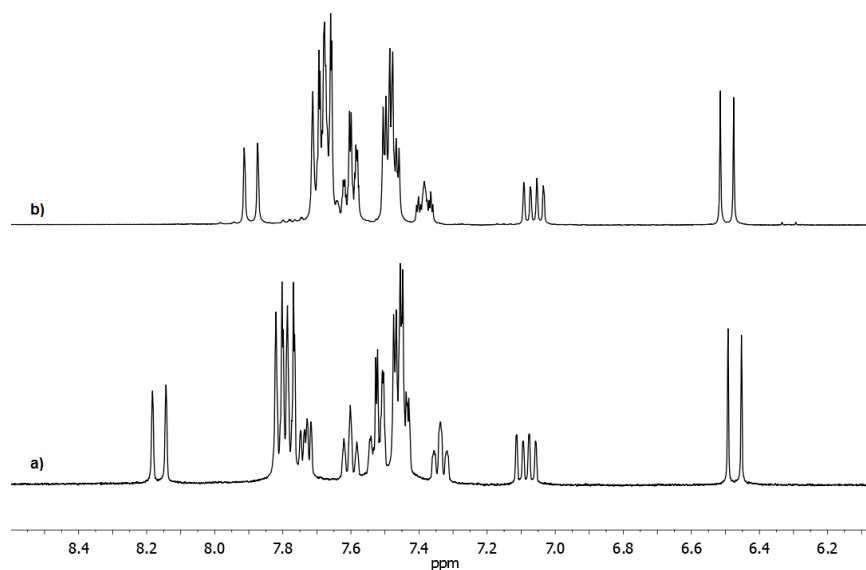


Figure 14: ^1H NMR spectra of a) dbaTHIOPHOS, **137**, b) **198a** (400 MHz, CD_2Cl_2). Alkene protons in dbaTHIOPHOS, **137**: 8.16 and 6.47 ppm; in **198**: 7.89 and 6.50 ppm.

Mass spectrometric analysis (ESI) of **198** showed the presence of two ions (m/z 1439 and 773). The highest weight molecular ion could suggest the presence of a complex with Ag:L ratio 1:2 (**199**). To confirm that this was not the species present a NMR scale reaction between AgPF_6 and dbaTHIOPHOS, **137**, (2 eq.) in CD_2Cl_2 was conducted (Scheme 13). The resulting ^1H and ^{31}P NMR spectra were different from those for **198b** (^1H NMR spectrum shown in Figure 15). The δ_{P} for **198b** is 44.5 and for **199** is 43.1 ppm.

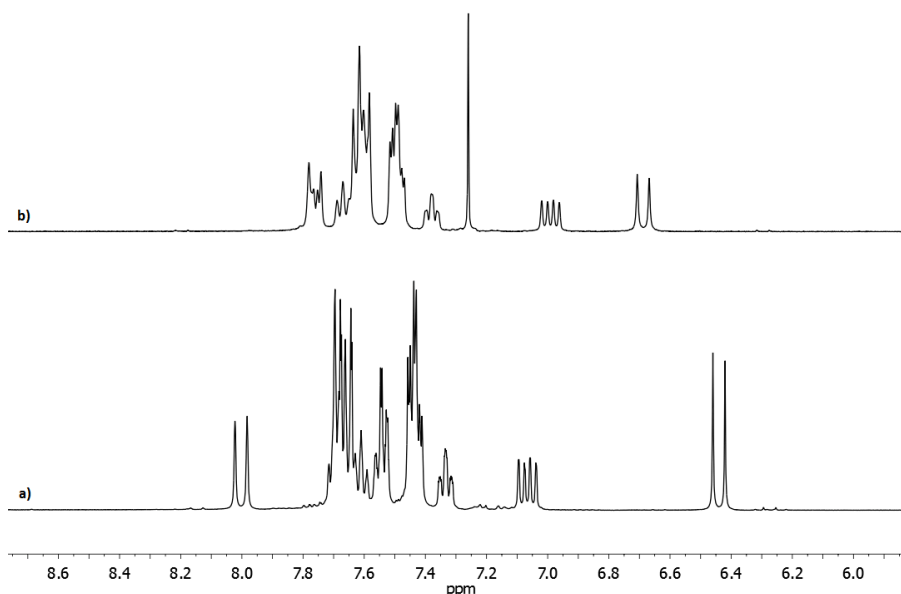
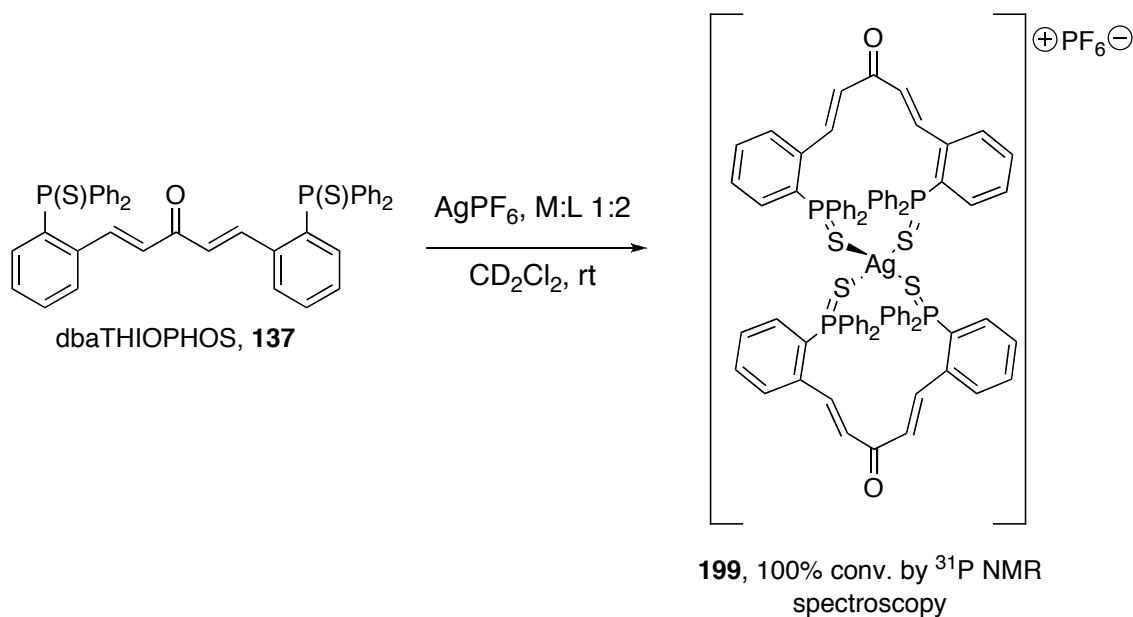


Figure 15: ^1H NMR spectra of a) **198b**, b) **199** (400MHz, CD_2Cl_2 and CDCl_3).



Scheme 13: Proposed synthesis of 199 (NMR scale).

4.2.4 Catalysis

Cyclopropanation of alkenes is a common benchmark reaction for Cu^{I} complexes.⁵⁷ The cyclopropanation of styrene with EDA does not occur in the absence of copper(I) (Table 2, entry 1). Our complexes were tested in this reaction; both **193** and **195** were found to be more active than CuBr (Table 2, entries 3 and 5 vs. entry 2). The diastereomeric ratios were moderate, but similar to those achieved with a recently reported copper(I)/copper(III) complex, **200** (Figure 16).⁵⁸ Complex **195** was a slightly superior catalyst to **193** for this reaction. Reducing the temperature had a detrimental effect on both the conversion and diastereomeric ratio achieved (Table 2, entry 4). The minor side products of the reaction, diethyl maleate and diethyl fumarate, are formed by well-established competing pathways.⁵⁹

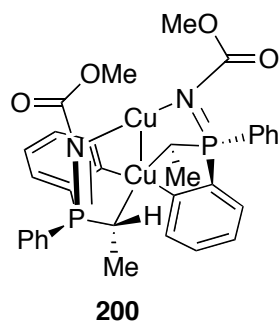
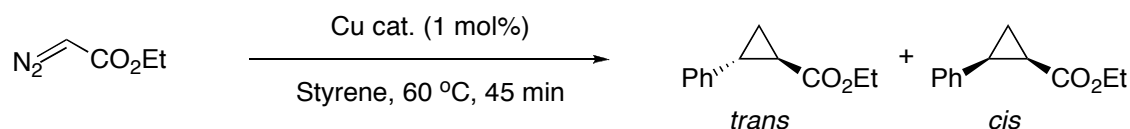


Figure 16: Copper(I)/copper(III) complex, 200.

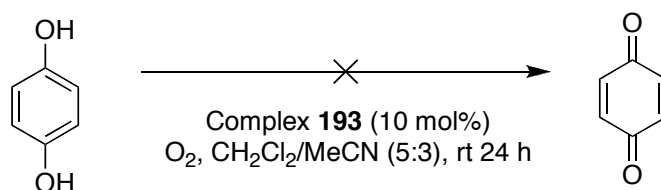
Table 2: Comparison of Cu^I complexes in the cyclopropanation of styrene.

Entry	Complex	Conversion, % ^a	<i>cis:trans</i> ratio ^c
1	None	0	-
2	CuBr	24	40:60
3	193	85	32:68
4	193	18 ^b	50:50
5	195	91	30:70

^a % conversion to cyclopropane products determined by ¹H NMR spectroscopy (by-products include diethyl maleate and diethyl fumarate) ^b 40 °C, 90 min. ^c determined by ¹H NMR spectroscopy.

One potential concern for these complexes is the presence of alkene moieties in the ligand backbone, which are susceptible to cyclopropanation. However, no cyclopropanation of the ligand has been observed by mass spectrometric analysis. In a stoichiometric reaction of **193** with ethyl diazoacetate (EDA) (Cu:EDA, 1:1) at ambient temperature in CD₂Cl₂ no observable formation of diethyl maleate or diethyl fumarate was observed after 1 h. After 24 h small quantities of diethyl maleate and diethyl fumarate were observed. In the ³¹P NMR spectrum two new phosphorus signals appeared at 42.2 and 41.6 ppm. But, the majority of the material was still the starting complex. The ¹H NMR spectrum showed a number of small peaks below 4 ppm, but nothing that could be clearly identified. Under ‘catalytic’ conditions, in the absence of styrene (**193**:EDA, 1:100), conversion to diethyl maleate and diethyl fumarate was observed (ratio 60:40, 80% conversion) by ¹H NMR spectroscopic analysis.

Oxidation reactions are also catalysed by copper(I) complexes.⁶⁰ One example is the oxidation of hydroquinone to quinone (Scheme 14).⁵⁸ However, complex **193** showed no activity in this oxidation reaction under these conditions.

**Scheme 14: Copper(I) catalysed oxidation of hydroquinone.**

4.3 Summary

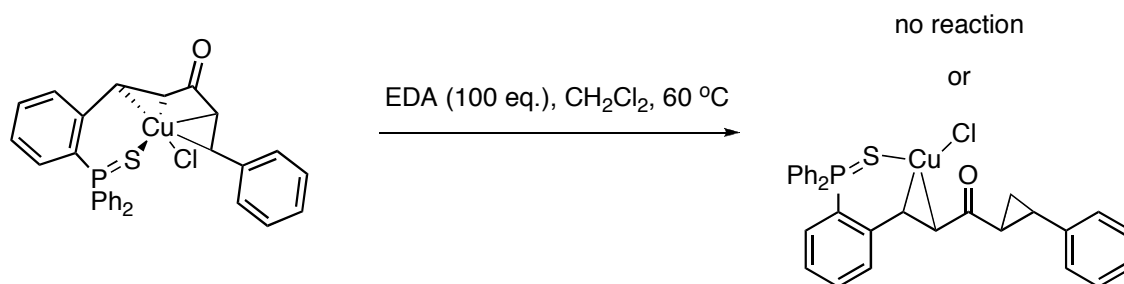
The coordination chemistry of dbaTHIOPHOS **137** with copper(I) has been studied in detail, where the ligand was found to be multidentate and hemilabile. X-ray single crystal structures have been obtained for three unique copper(I)-alkene complexes, all with different Cu:Cl stoichiometries. In all the complexes the coordinated alkenes were found to adopt the *s-cis* conformer of the enone whilst the free alkenes were *s-trans*. Complex **193** was found to be dynamic in solution. Low temperature NMR studies allowed further characterisation of the complex and the determination of the rate constants for the alkene exchange. The activation parameters of this exchange were determined ($\Delta S^\ddagger = 0.43 \pm 6.9 \text{ J mol}^{-1} \text{ K}^{-1}$, $\Delta H^\ddagger = 56.0 \pm 6.4 \text{ kJ mol}^{-1}$ and $\Delta G^\ddagger = 55.9 \pm 9.7 \text{ kJ mol}^{-1}$ at 300 K), showing the exchange barrier is primarily enthalpic.

Attempts to interconvert between the complexes, by addition of chloride or halide abstraction with silver salts were unsuccessful. Independent investigations show silver(I) coordinates to both dbaTHIOPHOS and monodbaTHIOPHOS through the sulfur atom of the phosphine sulfide (complexes **197-199**). No evidence for alkene coordination was observed, unlike in the copper(I) complexes.

Complexes **193** and **195** were found to be catalytically active in the cyclopropanation of styrene at low catalyst loadings (1 mol%). High conversions were obtained (85-91%) and moderate diastereotopic ratios (*cis:trans* 30:70).

4.4 Future work

No studies so far have been carried out with monodbaTHIOPHOS (**149**) and copper(I). In particular it would be interesting to see if the second alkene would be able to coordinate as well to the copper(I). A comparison of the resulting complexes in the cyclopropanation reaction could be carried out. If the second alkene did coordinate it would be interesting to see if this slowed down/stopped the decomposition of EDA to diethyl maleate and diethyl fumarate, or if the alkene was cyclopropanated.



Scheme 15: Possibilities for copper(I) complexes of monodbaTHIOPHOS.

The substrate scope of the cyclopropanation reaction could be expanded, to examine the stereoselectivity, *e.g.* is there retention of stereoselectivity when *cis/trans* alkenes are used. Further work could evaluate the use of chiral variants of the ligands (*e.g.* chiral at phosphorus) in an asymmetric variant. A related reaction to transition metal-catalysed cyclopropanation of alkenes, is the azridination of alkenes,⁶¹ which could also be tested.

It would also be interesting to study the copper(I) coordination chemistry of the phosphine selenide variants of the ligands.

In our studies on the coordination chemistry of monodbaPHOS and palladium(II), we observed the coordination of the oxygen from the carbonyl group, (complex **176**). Further work could investigate whether similar observations are observed with the copper(I) complex of monodbaTHIOPHOS, and what effect changing the oxygen for sulfur or selenium would have. One could envisage that the C=S variant may act similarly to S,C,S pincer ligands.⁶²

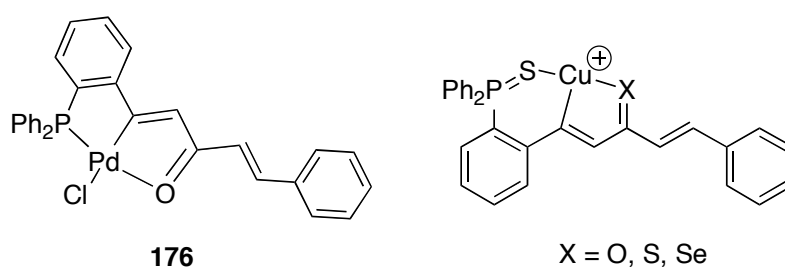


Figure 17: Carbonyl (C=X) coordination.

4.5 Experimental

4.5.1 General information

NMR spectra were obtained in the solvent indicated, using a JEOL ECX400 or JEOL ECS400 spectrometer (400MHz for ^1H , 100 MHz for ^{13}C and 162 MHz for ^{31}P , respectively), a Bruker 500 (500 MHz, 126 MHz and 202 MHz for ^1H , ^{13}C and ^{31}P , respectively) and low temperature NMR studies were carried out on a Bruker AV700 (700 MHz and 283 MHz for ^1H and ^{31}P , respectively). Chemical shifts were referenced to the residual solvent of the deuterated solvent used (CHCl_3 $\delta = 7.26$ and 77.16 , CDHCl_2 $\delta = 5.31$ and 53.80 , ^1H and ^{13}C respectively). All ^{13}C NMR spectra were obtained with ^1H decoupling. ^{31}P NMR spectra were externally referenced to 85% H_3PO_4 , and obtained with ^1H decoupling. For ^{13}C NMR spectra the coupling constants are quoted to ± 1 Hz. For the ^1H NMR spectra the resolution varies from ± 0.15 to ± 0.5 Hz; the coupling constants have been quoted to ± 0.5 Hz in all cases for consistency. For ^{31}P NMR spectra the coupling constants have been quoted to either ± 0.5 or ± 1 Hz. NMR spectra were processed using MestreNova software.

Melting points were recorded using a Stuart digital SMP3 machine. IR spectroscopy was undertaken using a Jasco/MIRacle FT/IR-4100 type A spectrometer with an ATR attachment on solid compounds; or solution IR spectra were obtained on a Nicolet Avatar 370 FT-IR spectrometer in the solvent stated. The relative intensities of the peaks are denoted by (s) = strong, (m) = medium and (w) = weak, whilst (br) is used to describe broad peaks. MS spectra were measured using a Bruker Daltronics micrOTOF machine with electrospray ionisation (ESI) or on a Thermo LCQ using electrospray ionisation, with < 5 ppm error recorded for all HRMS samples. LIFDI mass spectrometry was carried out using a Waters GCT Premier MS Agilent 7890A GC. UV-visible spectra were recorded using a JASCO V-560 instrument in quartz cells (1 cm path length). Elemental analysis was carried out on an Exeter Analytical CE-440 Elemental Analyser.

Dry and degassed toluene, CH_2Cl_2 , hexane and acetonitrile were obtained from a Pure Solv MD-7 solvent purification system. THF and Et_2O were either obtained from a Pure Solv MD-7 solvent purification system and degassed by the freeze-pump-thaw

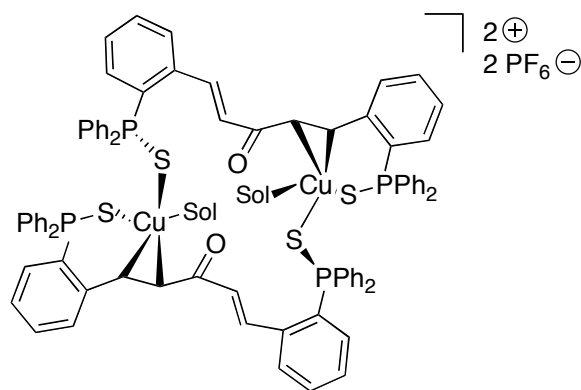
method or purged with N₂ under sonication; or dried over sodium-benzophenone ketyl and collected by distillation. Benzene was dried over sodium-benzophenone ketyl, and EtOH was dried and distilled from magnesium-iodine. All air-sensitive reactions were carried out using Schlenk techniques or in a MBraun MB-20-G with TP170b glove-box under a N₂ atmosphere. Nitrogen gas was oxygen free and was dried immediately prior to use by passage through a column containing sodium hydroxide pellets and silica. Commercial chemicals were purchased from Sigma-Aldrich or Alfa Aesar.

4.5.2 Complex synthesis

Tetrakis(acetonitrile)copper(I) hexafluorophosphate⁶³

To a stirred suspension of Cu₂O (1 g, 7 mmol) in MeCN (20 mL) was added 60 % HPF₆ (2.5 mL) in 0.5 mL portions. Heat is released, which helps dissolve the white solid formed. The hot solution was stirred for 3 min and filtered through a funnel with a sintered glass frit; any remaining white solid was washed through with a small amount of acetonitrile. The solution was cooled to -20 °C for 3 h and the resulting precipitate collected by filtration and washed with ether. The precipitate was then redissolved in acetonitrile (25 mL), filtered through a funnel with a sintered glass frit, ether (25 mL) added and cooled to -20 °C overnight. The white precipitate was filtered, washed with ether, dried *in vacuo* to afford the title compound as a white solid (4.17 g, 80%). The solid was stored in a glove-box. M.p. 147-152 °C, (*Lit.*⁶⁴ 160 °C_(dec.)); ¹H NMR (400 MHz, CD₂Cl₂) δ 2.18 (s); ¹³C NMR (100 MHz, CD₂Cl₂) δ 117.0, 2.53; IR (ATR, ν cm⁻¹): 1419 (w, br), 1037 (w), 833 (s, br); Anal. Calcd. for C₈H₁₂CuF₆N₄P (372.72) C 25.78, H 3.25, N 15.03; Observed C 25.77, H 3.20, N 14.80.

[Cu₂(μ-dbaTHIOPHOS)₂][(PF₆)₂].(solvent), 193

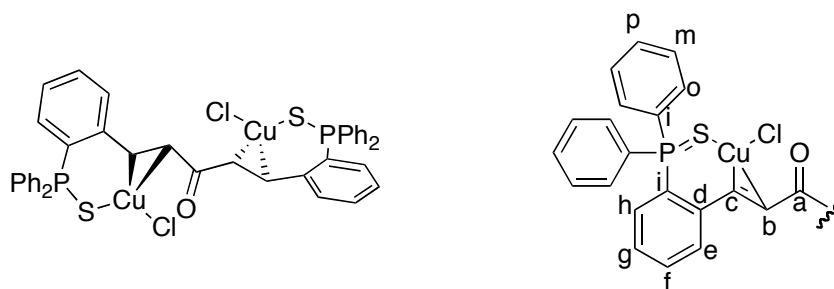


A solution of Cu(MeCN)₄PF₆ (168 mg, 1 eq., 0.45 mmol) in dry, degassed CH₂Cl₂ (5 mL) was added by cannula to a solution of dbaTHIOPHOS, (**137**), (300 mg, 1 eq., 0.45 mmol) in dry, degassed CH₂Cl₂ (10 mL).[†] The resulting solution was stirred for 2 h at 20 °C. CH₂Cl₂ was removed *in vacuo* to give a concentrated solution (4 mL) and layered with dry, degassed toluene (5 mL) to afford yellow crystals (270 mg, 69 %) separated by filtration. M.p. 200 °C_(dec.); ¹H NMR (400 MHz, CD₂Cl₂) δ 8.20-7.26 (br m, ~56H), 6.98 (dd, *J* = 15.0, 7.5 Hz, 4H), 6.52 (br s, 2H), 6.21 (br s, 2H); ³¹P NMR (162 MHz, CD₂Cl₂) δ 46.43 (br s), 40.59 (br s), -143.80 (hept, ¹*J*_{PF} = 711 Hz); ¹³C NMR (126 MHz, CD₂Cl₂) δ 137.8 (d, *J*_{CP} = 8 Hz), 136.4, 136.1, 134.8-134.3 (m), 134.0-132.1 (m), 131.1 (d, *J*_{CP} = 14 Hz), 131.0-130.8 (m), 130.6-129.9 (m); HRMS (ESI) *m/z* 729.0708 (calculated for C₄₁H₃₂OP₂S₂Cu: 729.0660); LRMS (ESI) *m/z* (rel%) 1397.2 [Cu(dbaTHIOPHOS)₂]⁺ (74), 829.0 [Cu₂(dbaTHIOPHOS)+Cl]⁺ (6), 729.1 [Cu(dbaTHIOPHOS)]⁺ (100), 667.1 [dbaTHIOPHOS+H]⁺ (33); LRMS (LIFDI) *m/z* (rel%) 729.27 [Cu(dbaTHIOPHOS)]⁺ (100); IR (ATR, ν cm⁻¹): 1652 (m), 1457 (m), 1438 (m), 1312 (w), 1170 (w), 1103 (m), 836 (s), 691 (s); UV-vis (CH₂Cl₂) λ_{max} nm: 320 (ε = 18345 mol⁻¹dm³cm⁻¹); Anal. Calcd. for C₈₂H₆₄Cu₄F₁₂P₆ (Cu₂(dbaTHIOPHOS)₂PF₆) C 56.26, H 3.69, N 0.00; Observed C 56.61, H 4.02, N 0.20.

Crystals of [Cu₂(μ-dbaTHIOPHOS)₂(H₂O)₂][(PF₆)₂] suitable for XRD were obtained by layering CH₂Cl₂ with Et₂O, along with crystals of [Cu₄(μ-Cl)₂(μ-dbaTHIOPHOS)₂][(PF₆)₂] (**194**) presumably formed by halide abstraction from HCl or CH₂Cl₂.

[†] The reaction was also carried out in THF. The product precipitated overnight and the resulting yellow crystals were collected by filtration (48%).

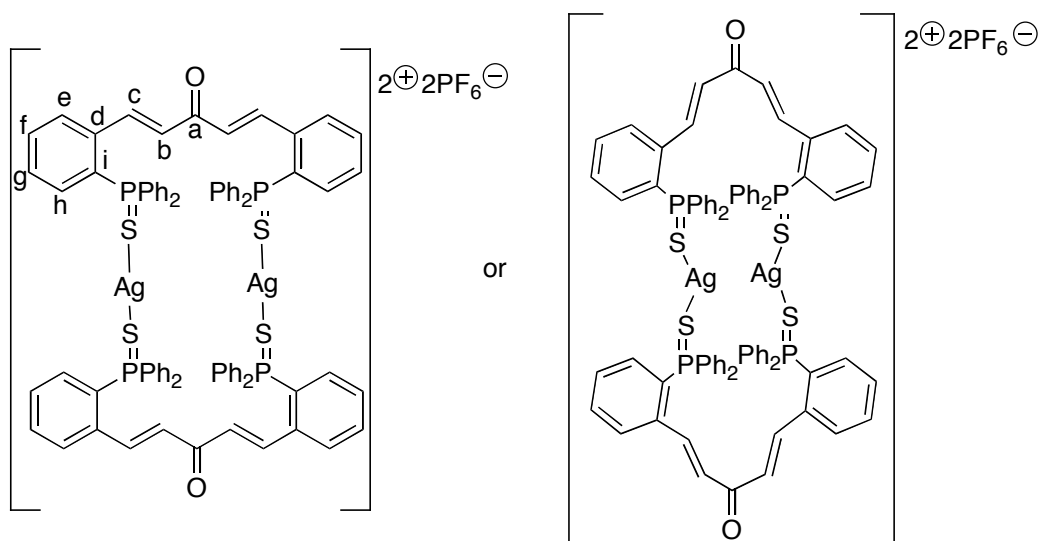
[Cu₂Cl₂(μ-dbaTHIOPHOS)], **195**



In a glovebox, dbaTHIOPHOS, (**137**), (125 mg, 1 eq., 0.188 mmol) was dissolved in dry, degassed CH₂Cl₂ (7 mL) and CuCl (37 mg, 2 eq., 0.375 mmol) was added. After stirring for 1 h at 23 °C, more CH₂Cl₂ (2 mL) was added to dissolve the last traces of CuCl and the reaction stirred overnight, until no solid remained. Half the solvent was removed *in vacuo*, and the concentrated solution left overnight. The precipitate was filtered, washed with pentane and dried *in vacuo* to give a yellow crystalline product (119 mg, 73%). The solid was stored in a glove-box. M.p. 223 °C_(dec.); ¹H NMR (400 MHz, CD₂Cl₂) δ 7.83-7.79 (m, 2H, H_e), 7.79-7.67 (m, 12H, Ar), 7.66-7.54 (m, 10H, H_f and Ar), 7.37-7.31 (m, 2H, H_g), 6.92 (ddd, *J* = 14.5, 7.5, 1.0 Hz, 2H, H_h), 6.07 (d, ³*J*_{HH} = 14.0 Hz, 2H, H_c), 5.83 (d (br), ³*J*_{HH} = 14.0 Hz, 2H, H_b); ¹³C NMR (100 MHz, CD₂Cl₂) δ 184.2 (C=O), 139.8 (d, ²*J*_{CP} = 8 Hz, C_d), 134.4 (d, ⁴*J*_{CP} = 2 Hz, C_f), 133.9 (d, ⁴*J*_{CP} = 3 Hz, *p*-Ar), 133.1 (d, *J*_{CP} = 11 Hz, Ar), 132.9 (d, ²*J*_{CP} = 11 Hz, C_h), 131.8 (d, ¹*J*_{CP} = 85 Hz, *ipso*-C), 131.6 (d, ³*J*_{CP} = 9 Hz, C_e), 129.6 (d, *J*_{CP} = 13 Hz, Ar), 128.6 (d, ³*J*_{CP} = 13 Hz, C_g), 127.2 (d, ¹*J*_{CP} = 86 Hz, *ipso*-C), 95.3 (br, C=C), 94.4 (br, C=C); ³¹P NMR (162 MHz, CD₂Cl₂) δ 40.78 (s); LRMS (LIFDI) *m/z* (rel.%) 829 [*M*-Cl]⁺ (100), 729 [*M*-CuCl₂]⁺ (27), 667 [dbaTHIOPHOS+H]⁺ (8); HRMS (ESI) *m/z* 826.9623 (calculated for C₄₁H₃₂ClCu₂OP₂S₂ = 826.9645); IR (ATR, ν cm⁻¹): 1653 (w), 1537 (w), 1455 (w), 1433 (m), 1312 (m), 1247 (w), 1103 (m), 1084 (m), 1064 (m), 967 (m), 756 (s), 691 (s); IR (CH₂Cl₂, ν cm⁻¹): 3046 (w), 1653 (w), 1539 (w), 1457 (w), 1439 (m), 1314 (w), 1271 (m), 1265 (m), 1261 (m), 1106 (w); UV-vis (CH₂Cl₂) λ_{max} nm: 396 (ε = 12199 mol⁻¹dm³cm⁻¹) shoulders at 326 (ε = 10213 mol⁻¹dm³cm⁻¹) and 258 (ε = 34000 mol⁻¹dm³cm⁻¹); Anal. Calcd. for C₄₁Cl₂Cu₂H₃₂OP₂S₂·CH₂Cl₂ (949) C 53.12, H 3.61; Observed C 53.17, H 3.58.

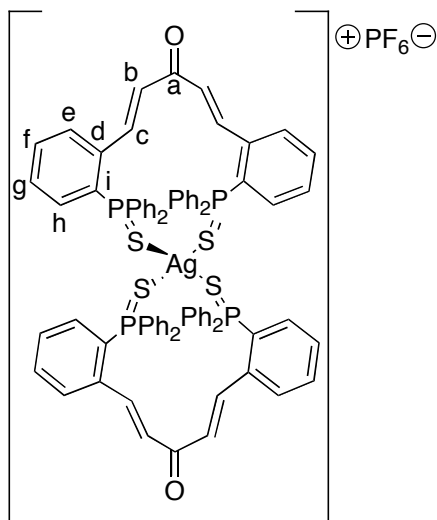
Crystals of [Cu₂Cl₂(dbaTHIOPHOS)], **195**, suitable for XRD were obtained by from a solution of CH₂Cl₂ in an atmosphere of Et₂O.

[Ag₂(μ-dbaTHIOPHOS)₂][(PF₆)₂], 198b



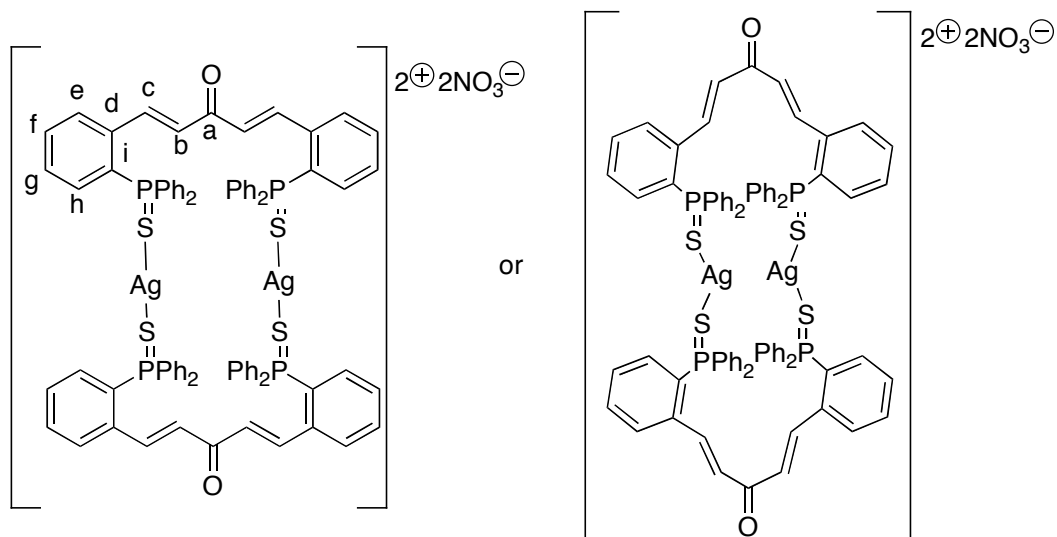
To a solution of dbaTHIOPHOS, **137** (100 mg, 1.25 eq., 0.15 mmol) in dry and degassed CH₂Cl₂ (6 mL) in the dark was added a solution of silver hexafluorophosphate (31.2 mg, 1 eq., 0.12 mmol) in dry and degassed CH₃CN (1.5 mL). The yellow solution was stirred for 1 h, and then the solvent removed *in vacuo*. The solid was then dissolved in CH₂Cl₂ (1 mL) and layered with Et₂O (5 mL). The resulting pale yellow solid was filtered (64 mg, 58%). The solid was stored in the dark under N₂. M.p. 150 °C_(dec); ¹H NMR (400 MHz, CDCl₃) δ 7.82 (d, ³J_{HH} = 15.5 Hz, 2H, H_c), 7.74-7.57 (m, 16H, H_e, H_f and Ph), 7.54-7.45 (m, 8H, Ph), 7.43-7.36 (m, 2H, H_g), 7.03 (dd, ²J_{HP} = 15.5 Hz, ³J_{HH} = 8.0 Hz, 2H, H_h), 6.58 (d, ³J_{HH} = 15.5 Hz, 2H, H_b); ³¹P NMR (162 MHz, CDCl₃) δ 44.76 (s), -143.55 (hept, ¹J_{PF} = 708 Hz); ¹³C NMR (100 MHz, CD₂Cl₂) δ 188.3 (C_a), 139.4 (d, ³J_{CP} = 6 Hz, C_c), 138.0 (d, ²J_{CP} = 8 Hz, C_d), 134.1 (d, ⁴J_{CP} = 2 Hz, C_f), 133.9 (d, ²J_{CP} = 12 Hz, C_h), 133.6 (d, ⁴J_{CP} = 3 Hz, *p*-Ph), 132.5 (d, ²J_{CP} = 11 Hz, *o*-Ph), 130.5 (d, ³J_{CP} = 9 Hz, C_g), 130.6 (d, ¹J_{CP} = 82 Hz, ipso-C), 130.1 (d, ³J_{CP} = 9 Hz, C_e), 129.7 (d, ³J_{CP} = 13 Hz, *m*-Ph), 128.7 (d, ¹J_{CP} = 86 Hz, ipso-C), 126.9 (C_b); LRMS (ESI) *m/z* (rel.%) 1441.2 [Ag(dbaTHIOPHOS)₂]⁺ (38), 775.0 [Ag(dbaTHIOPHOS)]⁺ (100), 729.1 (21), 667.1 [dbaTHIOPHOS+H]⁺ (58); IR (ATR, ν cm⁻¹): 1653 (w), 1617 (w), 1580 (w), 1480 (w), 1457 (w), 1473 (m), 1327 (w), 1267 (w), 1185 (w), 1098 (m), 977 (w), 971 (w), 875 (w) and 834 (s);

NMR experiment: Preparation of $[\text{Ag}(\text{dbaTHIOPHOS})_2][\text{PF}_6]$, 199



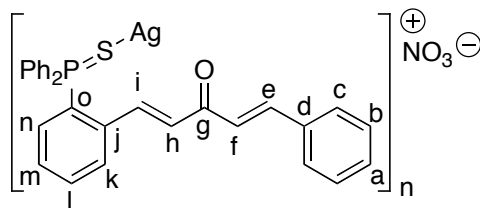
A solution of dbaTHIOPHOS, **137** (20 mg, 2 eq., 0.03 mmol) in dry and degassed CD_2Cl_2 (0.5 mL) was added to AgPF_6 (3.8 mg, 1 eq., 0.015 mmol) in the dark. NMR spectroscopic analysis was carried out directly on the reaction mixture. ^1H NMR (400 MHz, CD_2Cl_2) δ 8.01 (d, $^3J_{\text{HH}} = 16.0$ Hz, 4H, H_c), 7.75-7.59 (m, 24H, Ar), 7.59-7.50 (m, 8H, Ar), 7.50-7.39 (m, 16H, Ar), 7.38-7.31 (m, 4H, Ar), 7.08 (ddd, $^3J_{\text{HP}} = 15.0$ Hz, $J_{\text{HH}} = 8.0, 1.0$ Hz, 4H, H_h), 6.45 (d, $^3J_{\text{HH}} = 16.0$ Hz, 4H, H_b); ^{31}P NMR (162 MHz, CD_2Cl_2) δ 43.14 (s), -143.88 (hept, $^1J_{\text{PF}} = 708$ Hz); ^{13}C NMR (100 MHz, CD_2Cl_2) δ 189.0 (C_a), 141.5 (d, $^3J_{\text{CP}} = 8$ Hz, C_c), 138.9 (d, $^2J_{\text{CP}} = 8$ Hz, C_d), 134.0 (d, $J_{\text{CP}} = 11$ Hz), 133.2 (d, $J_{\text{CP}} = 3$ Hz), 132.9 (d, $^4J_{\text{CP}} = 3$ Hz, *p*-Ph), 132.7 (d, $J_{\text{CP}} = 11$ Hz, Ph), 131.9 (d, $^1J_{\text{CP}} = 83$ Hz, *ipso*-C), 130.9 (d, $^1J_{\text{CP}} = 85$ Hz, *ipso*-C), 130.0 (d, $J_{\text{CP}} = 13$ Hz), 129.3 (d, $J_{\text{CP}} = 13$ Hz, Ph), 129.2 (C_f), 127.5 (C_b).

[Ag₂(dbaTHIOPHOS)₂][(NO₃)₂], 198a



In the dark, dbaTHIOPHOS, **137** (100 mg, 1 eq., 0.15 mmol) was dissolved in CH₂Cl₂ (6 mL) and a solution of silver nitrate (26 mg, 1 eq., 0.15 mmol) in acetonitrile (1.5 mL) was added. The mixture was stirred for 1 h at 23 °C. The solvent was removed, the crude product dissolved in CH₂Cl₂ (1.5 mL) and precipitated with ether (5 mL). An off-white powder was obtained (84 mg, 67%). Mp. 145 °C_(dec.); ¹H NMR (400 MHz, CD₂Cl₂) δ 7.89 (dd, ³J_{HH} = 15.5 Hz, *J* = 1.0 Hz, 2H, H_c), 7.74-7.63 (m, 12H, H_e, H_f and *o*-Ph), 7.62-7.56 (m, 4H, *p*-Ph), 7.53-7.43 (m, 8H, *m*-Ph), 7.43-7.33 (m, 2H, H_g), 7.06 (ddd, *J* = 9.0, 7.5, 1.0 Hz, 2H, H_h), 6.50 (d, ³J_{HH} = 15.5 Hz, 2H, H_b); ³¹P NMR (162 MHz, CD₂Cl₂) δ 44.54 (s); ¹³C NMR (100 MHz, CD₂Cl₂) δ 189.4 (C=O), 141.4 (d, ³J_{CP} = 8 Hz, C_c), 138.9 (d, ²J_{CP} = 11 Hz, C_d), 134.2 (d, ²J_{CP} = 11 Hz, C_h), 133.8 (d, ⁴J_{CP} = 3 Hz, C_f), 133.3 (d, ⁴J_{CP} = 3 Hz, *p*-Ph), 132.8 (d, ²J_{CP} = 11 Hz, *o*-Ph), 130.4 (d, ¹J_{CP} = 83 Hz, *ipso*-C), 130.2 (d, ³J_{CP} = 13 Hz, C_g or C_e), 126.7 (d, ³J_{CP} = 10 Hz, C_e or C_g), 129.54 (d, ³J_{CP} = 13 Hz, *m*-Ph), 129.45 (d, ¹J_{CP} = 86 Hz, *ipso*-C), 127.8 (C_b); HRMS (ESI) *m/z* 1439.1820 [Ag(dbaTHIOPHOS)₂]⁺ (calculated for C₈₂H₆₄AgO₂P₄S₄ = 1439.1785) and 773.0414 [Ag(dbaTHIOPHOS)]⁺ (calculated for C₄₁H₃₂AgOP₂S₂ = 773.0415); IR (ATR, ν cm⁻¹): 1653 (w), 1617 (w), 1458 (w), 1437 (m), 1311 (m, br), 1186 (w), 1000 (s), 998 (w), 972 (w), 745 (m), 689 (s).

[Ag(monodbaTHIOPHOS)]_n[NO₃]_n, **197**



In the dark, monodbaTHIOPHOS, **149** (68 mg mg, 1 eq., 0.15 mmol) was dissolved in CH₂Cl₂ (6 mL) and a solution of silver nitrate (26 mg, 1 eq., 0.15 mmol) in acetonitrile (1.5 mL) was added. The mixture was stirred for 1 h at 23 °C. The solvent was removed, the crude product dissolved in CH₂Cl₂ (1.5 mL) and precipitated with ether (5 mL). An off-white powder was obtained (49 mg, 53%). Mp. 97 °C_(dec.); ¹H NMR (400 MHz, CD₂Cl₂) δ 7.89 (d, ³J_{HH} = 15.5 Hz, 1H, H_i), 7.86-7.82 (m, 1H, H_k), 7.82-7.75 (m, 4H, *o*-Ph), 7.72-7.66 (m, 1H, H_l), 7.65-7.60 (m, 3H, Ar), 7.56-7.49 (m, 6H, *m*-Ph and Ar), 7.46-7.37 (m, 4H, H_m and Ar), 7.27 (ddd, ³J_{HP} = 15.5 Hz, J_{HH} = 8.0, 1.0 Hz, 1H, H_n), 6.83 (d, ³J_{HH} = 15.5 Hz, 1H, H_h), 6.79 (d, ³J_{HH} = 16.0 Hz, 1H, H_f); ³¹P NMR (162 MHz, CD₂Cl₂) δ 45.52; ¹³C NMR (100 MHz, CD₂Cl₂) δ 188.4 (C_g), 144.1 (C_e), 139.4 (d, ³J_{CP} = 7 Hz, C_i), 138.8 (d, ²J_{CP} = 8 Hz, C_j), 135.0 (C_d), 134.4 (d, J_{CP} = 12 Hz), 134.2 (d, J_{CP} = 3 Hz), 133.8 (d, ⁴J_{CP} = 3 Hz, *p*-Ph), 132.8 (d, ²J_{CP} = 11 Hz, *o*-Ph), 131.0 (C_a), 130.4 (d, J_{CP} = 13 Hz), 129.9 (d, ¹J_{CP} = 83 Hz, *ipso*-C), 129.84 (d, ³J_{CP} = 13 Hz, *m*-Ph), 129.77 (d, J_{CP} = 9 Hz), 129.3 (Ar), 128.8 (Ar), 128.7 (d, ¹J_{CP} = 86 Hz, *ipso*-C), 128.6 (C=C), 124.6 (C=C); HRMS (ESI) m/z 557.0266 [*M*-NO₃]⁺ (calculated for C₂₉H₂₃AgOPS = 557.0253. LRMS (ESI) m/z (rel%) 1458.2 [Ag(monodbaTHIOPHOS)₃]⁺ (16), 1009.1 [Ag(monodbaTHIOPHOS)₂]⁺ (48), 557.0 [*M*-NO₃]⁺ (100); IR (ATR, ν cm⁻¹): 1648 (w), 1617 (w), 1437 (m), 1332 (m), 1184 ~ (w), 1100 (m), 977 (w), 765 (m), 686 (s); Anal. Calcd. for C₂₉H₂₃AgNO₄PS (620) C 56.14, H 3.74, N 2.26, Observed C 56.54, H 3.77, N 2.03.

4.5.3 NMR and UV spectroscopic experiments

Chloride doping of **193**

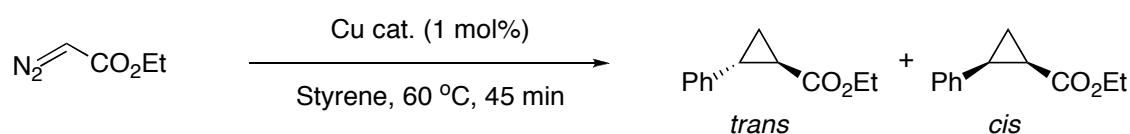
UV-vis: Aliquots of nBu₄NCl in CH₂Cl₂ (0.1 mL, 1.47 x10⁻³ M) were added to a solution of **193** (5.76 x10⁻⁵ M) in CH₂Cl₂. The UV-visible absorption spectrum was measured after the addition of each aliquot until 2 eq. had been added.

NMR spectroscopic analysis: To a solution of the **193** (15 mg, 0.01 mmol, 0.015 M) in CD₂Cl₂ was added aliquots of a solution of *n*Bu₄NCl (0.01 ml, 0.3 eq., 0.25M) in CD₂Cl₂. The ¹H and ³¹P NMR spectra were recorded after each aliquot was added.

Addition of AgPF₆ to 195: To solutions of **195** (9.5 mg, 0.011 mmol) in dry and degassed CD₂Cl₂ (0.8 ml) was added AgPF₆, (0.5 eq., 1 eq. and 2 eq. respectively). The ¹H and ³¹P NMR spectra were recorded for each.

4.5.4 Catalysis

Cyclopropanation of styrene⁵⁸



To a solution of **193** (9.2 mg, 1 mol%, 0.0053 mmol) in distilled styrene (1 mL) at 60 °C was added ethyldiazoacetate, EDA, (55 μ l, 0.53 mmol) in three portions over 20 min. The reaction was stirred for a further 25 min at 60 °C. The reaction was left to cool and an aliquot (40 μ l) measured into CDCl₃ (0.5 mL). ¹H NMR spectroscopic analysis determined that the product was formed in 85% conversion (not isolated) with a *cis:trans* ratio of 32:68 (*Figure 1*).

Control experiments were performed using CuBr and without the presence of Cu. When no Cu is present the reaction does not occur. When CuBr is used, after 45 min there is still EDA remaining, shown by the broad singlet at 4.7 ppm. ¹H NMR spectroscopy determined that the product was formed in 24% conversion (not isolated) with a *cis:trans* ratio of 40:60. Using **193**, a small amount of product (18% conversion) was observed by ¹H NMR spectroscopy after 90 min if the temperature was lowered to 40 °C with a *cis:trans* ratio of 50:50.

The reaction was also carried out with complex **195** using the same procedure as above. ¹H NMR determined that the product was formed in 91% conversion (not isolated) with a *cis:trans* ratio of 30:70.

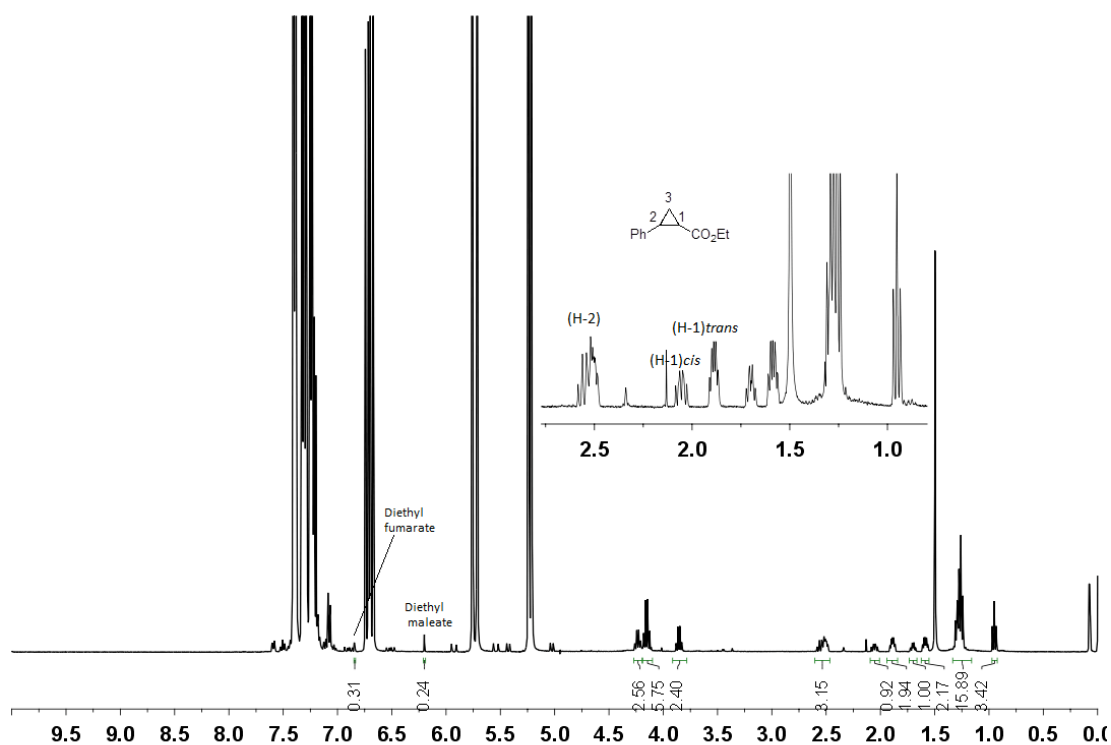


Figure 18: ^1H NMR spectrum (400 MHz, CDCl_3 , referenced to TMS) of the crude reaction mixture of the cyclopropanation with **193**.

Reaction of **193** plus EDA (catalytic amounts of Cu)

Complex **193** (4.6 mg, 1 mol%, 0.0026 mmol) was dissolved in CD_2Cl_2 (0.5 mL). EDA (28 μL , 1 eq., 0.26 mmol) was added and the reaction monitored by ^1H NMR spectroscopy at room temperature. After ~ 1 h at room temperature over 80% conversion of the EDA to diethyl maleate and diethyl fumarate had occurred. After 24 h all the EDA had been converted.

Reaction of **193** plus EDA (stoichiometric amounts of Cu)

Complex **193** (3.1 mg, 1 eq., 0.0017 mmol) was dissolved in CD_2Cl_2 (0.5 mL). EDA (3.7 μL , 2 eq., 0.0035 mmol) was added and the reaction followed by ^1H and ^{31}P NMR spectroscopy at room temperature. After 6 h no conversion to diethyl fumarate or diethyl maleate is observed. No changes are observed in the ^{31}P NMR spectrum and only very minor new peaks have appeared in the ^1H NMR spectrum. After 24 h two small peaks in the ^1H NMR have appeared at δ 6.2 and 6.8 ppm, diethyl maleate and diethyl fumarate, however most of the EDA remains. Two new phosphorous signals also appeared in the ^{31}P NMR spectrum at δ 42.21 and 41.55 ppm.

Oxidation of hydroquinone

To a solution of **193** (9 mg, 1 mol%, 0.005 mmol) in CH₂Cl₂ (2.5 mL) was added a solution of hydroquinone (55 mg, 1 eq., 0.5 mmol) in THF (1.5 mL). The resulting solution was subjected to one freeze-pump-thaw cycle and placed under an O₂ atmosphere. The reaction was followed by ¹H, ¹³C and ³¹P NMR spectroscopic analysis on 0.5 mL aliquots run without lock. No products were observed.

4.5.5 X-ray diffraction data

All crystals were crystallised in the solvents stated in Section 4.5.2 and mounted in inert oil. Diffraction data for **193**, **194** and **195** were collected at 110 K on a Bruker Smart Apex diffractometer with Mo-K_α radiation ($\lambda = 0.71073 \text{ \AA}$) using a SMART CCD camera. Diffractometer control, data collection and initial unit cell determination was performed using “SMART”.⁶⁵ Frame integration and unit-cell refinement was carried out with “SAINT+”.⁶⁶ Absorption corrections were applied by SADABS.⁶⁷ Structures were solved by “direct methods” using SHELXS-97 (Sheldrick, 1997)⁶⁸ and refined by full-matrix least squares using SHELXL-97 (Sheldrick, 1997).⁶⁹ All non-hydrogen atoms were refined anisotropically. Hydrogen atoms were placed using a “riding model” and included in the refinement at calculated positions, except for the alkene hydrogens in **194** and **195**, which were located by difference map.

ijf0829a (**193**): The crystals contained disordered solvents, presumably a mixture of dichloromethane and diethyl ether which could not be modelled as discrete atoms. Therefore the SQUEEZE algorithm was used to account for the solvent. The solvent void was measure to be 1469 Å³ and 776 electrons were attributed to the solvent. Since this is a due to mixture of solvents it is not possible to determine the overall formula, formula weight or density for the crystals. It is assumed that the oxygen ligands bound to the copper are water molecules but suitable locations for the hydrogens could not be determined and so these were omitted.

ijf0825m (**194**): The crystals contained a mixture of disordered solvents. Relative occupancy of each solvent was allowed to refine; overall occupancy was restrained to be 1.0. The solvents were modelled as an ether (79.4%) [with one terminal carbon disordered over two sites (C42 and C42a)] and a dichloromethane disordered over two sites (7.2% and 13.4%). All solvent atoms were modelled isotropically. Within the

solvents, C-C bonds were restrained to be 1.51 Å, C-O bonds to 1.425 Å and C-Cl to 1.728 Å.

ijf1015m (**195**): There is a small void in the model (volume 31 Å³). However, the largest peak in the difference map in the void is only 0.62 e/Å, so the space is assumed to be empty.

Table 3 Single crystal XRD data.

Compound reference	ijf0829a (193)	ijf0825m (194)	ijf1015m (195)
Chemical formula	C ₈₂ H ₆₄ Cu ₂ O ₄ P ₄ S ₄ •2(PF ₆)	C ₈₂ H ₆₄ Cl ₂ Cu ₄ O ₂ P ₄ S ₄ •2(PF ₆)•1.58(C ₄ H ₁₀ O)•0.41(CH ₂ Cl ₂)	C ₄₁ H ₃₂ Cl ₂ Cu ₂ OP ₂ S ₂
Formula Mass	1782.47	2117.11	864.71
Crystal system	Monoclinic	Triclinic	Monoclinic
<i>a</i> /Å	25.838(3)	12.0204(7)	29.431(3)
<i>b</i> /Å	25.365(3)	14.5437(9)	8.9496(10)
<i>c</i> /Å	14.7220(15)	15.1233(9)	16.2751(18)
<i>α</i> /°	90.00	71.942(1)	90.00
<i>β</i> /°	97.563(2)	71.271(1)	115.307(2)
<i>γ</i> /°	90.00	66.585(1)	90.00
Unit cell volume/Å ³	9564.7(17)	2246.5(2)	3875.4(7)
Temperature/K	110(2)	110(2)	110(2)
Space group	<i>P</i> 2(1)/ <i>c</i>	<i>P</i> $\bar{1}$	<i>C</i> 2/ <i>c</i>
No. of formula units per unit cell, <i>Z</i>	4	1	4
No. of reflections measured	16818	23138	18084
No. of independent reflections	16818	11056	4810
<i>R</i> _{int}	0.0000	0.0218	0.0640
Final <i>R</i> _I values (<i>I</i> > 2σ(<i>I</i>))	0.0828	0.0452	0.0423
Final <i>wR</i> (<i>F</i> ²) values (<i>I</i> > 2σ(<i>I</i>))	0.1993	0.1207	0.0954
Final <i>R</i> _I values (all data)	0.1422	0.0614	0.0880
Final <i>wR</i> (<i>F</i> ²) values (all data)	0.2117	0.1305	0.1134

4.6 References

- ¹ a) Alexakis, A.; Albrow, V.; Biswas, K.; d'Augustin, M.; Prieto, O.; Woodward, S. *Chem. Commun.* **2005**, 2843-2845. b) Alexakis, A.; Benhaim, C. *Eur. J. Org. Chem.* **2002**, 3221-3236.
- ² Zhu, L.; Li, G.; Luo, L.; Guo, P.; Lan, J.; You, J. *J. Org. Chem.* **2009**, *74*, 2200-2202.
- ³ Noh, D.; Chea, H.; Ju, J.; Yun, J. *Angew. Chem., Int. Ed.* **2009**, *48*, 6062-6064.
- ⁴ a) Burke, A. J.; Carreiro, E. d. P.; Chercheja, S.; Moura, N. M. M.; Ramalho, J. P. P.; Rodrigues, A. I.; dos Santos, C. I. M. *J. Organomet. Chem.* **2007**, *692*, 4863-4874. b) Eggers, F.; Luning, U. *Eur. J. Org. Chem.* **2009**, 2328-2341.
- ⁵ De Ornellas, S.; Storr, T. E.; Williams, T. J.; Baumann, C. G.; Fairlamb, I. J. S. *Curr. Org. Synth.* **2011**, *8*, 79-101.
- ⁶ a) Araki, H.; Tsuge, K.; Sasaki, Y.; Ishizaka, S.; Kitamura, N. *Inorg. Chem.* **2007**, *46*, 10032-10034. b) Araki, H.; Tsuge, K.; Sasaki, Y.; Ishizaka, S.; Kitamura, N. *Inorg. Hem.* **2005**, *44*, 9667-9675. c) Tsuboyama, A.; Kuge, K.; Furugori, M.; Okada, S.; Hoshino, M.; Ueno, K. *Inorg. Chem.* **2007**, *46*, 1992-2001. d) Ford, P. C.; Cariati, E.; Bourassa, J. *Chem. Rev.* **1999**, *99*, 3625-3647.
- ⁷ Zhao, H.; Qu, Z-R.; Ye, Q.; Abrahams, B. F.; Wang, Y-P.; Liu, Z-G.; Xue, Z.; Xiong, R-G.; You, X-Z. *Chem. Mater.* **2003**, *15*, 4166-4168.
- ⁸ a) Smith, D. W. *Annu. Rep. Prog. Chem., Sect. A: Inorg. Chem.* **1999**, *95*, 189-211. b) Xue, X.; Wang, X-S.; Xiong, R-G.; You, X-Z.; Abrahams, B. F.; Che, C-M.; Ju, H-X. *Angew. Chem., Int. Ed.* **2002**, *41*, 2944-2946.
- ⁹ Pearson, R. G. *J. Am. Chem. Soc.* **1963**, *85*, 3533-3539.
- ¹⁰ a) Zhang, Z.; Zhang, J.; Wu, T.; Bu, X.; Feng, P. *J. Am. Chem. Soc.* **2008**, *130*, 15238-15239. b) Fuhr, O.; Fernandez-Recio, L.; Fenske, D. *Eur. J. Inorg. Chem.* **2005**, 2306-2314.
- ¹¹ Saravanabharathi, D.; Nethji, M.; Samuelson, A. G. *Polyhedron* **2002**, *21*, 2793-2800.
- ¹² Sivasankar, C.; Sadhukhan, N.; Bera, J. K.; Samuelson, A. G. *New J. Chem.* **2007**, *31*, 385-393.
- ¹³ Poblet, J-M.; Benard, M. *Chem. Commun.* **1998**, 1179-1180.

-
- 14 a) Schmidbaur, H.; Graf, W.; Müller, G. *Angew. Chem., Int. Ed.* **1988**, *27*, 417-419. b) Schmidbaur, H. *Chem. Soc. Rev.* **1995**, 391-400. c) Pyykkö, P.; Li, J.; Runeberg, N. *Chem. Phys. Lett.* **1994**, *218*, 133-138.
- 15 a) Merz, Jr. K. M.; Hoffmann, R. *Inorg. Chem.* **1988**, *27*, 2120-2127. b) Kolmel, C.; Ahlrichs, R. *J. Phys. Chem.* **1990**, *94*, 5536-5542. c) Abraham, S. P.; Samuelson, A. G.; Chandrasekhar, J. *Inorg. Chem.* **1993**, *32*, 6107-6111.
- 16 Pyykkö, P. *Chem. Rev.* **1997**, *97*, 597-636.
- 17 Hallnemo, G.; Olsson, T.; Ullenius, C. *J. Organomet. Chem.* **1985**, *282*, 133-144.
- 18 Dias, H. V. R.; Lu, H-L.; Kim, H-J.; Polach, S. A.; Goh, T. K. H. H.; Browning, R. G.; Lovely, C. J. *Organometallics* **2002**, *21*, 1466-1473.
- 19 a) Perez, P. J.; Brookhart, M.; Templeton, J. L. *Organometallics*, **1993**, *12*, 261-262. b) Straub, B. F.; Eisentrager, F.; Hofmann, P. *Chem. Commun.* **1999**, 2507-2508.
- 20 Suzuki, T.; Noble, R. D.; Koval, C. A. *Inorg. Chem.* **1997**, *36*, 136-140.
- 21 Cucciolito, M. E.; Ruffo, F.; Vitagliano, A. *Tetrahedron Lett.* **1994**, *35*, 161-170.
- 22 Xie, Y-R.; Wang, X-S.; Zhao, H.; Zhang, J.; Weng, L-H.; Duan, C-Y.; Xiong, R-G.; You, X-Z.; Xue, Z-L. *Organometallics* **2003**, *22*, 4396.
- 23 a) Srinivasan, R. *J. Am. Chem. Soc.* **1964**, *86*, 3318. b) Franceschi, F.; Guardigli, M.; Solari, E.; Floriani, C.; Chiesi-Villa, A.; Rizzoli, C. *Inorg. Chem.* **1997**, *36*, 4099-4107.
- 24 Wang, X-S, Zhao, H.; Li, Y-H.; Xiong, R-G.; You, X-Z. *Topics in Catalysis* **2005**, *35*, 43-61 and references therein.
- 25 a) Rodriguez, F. I.; Esch, J. J.; Hall, A. E.; Binder, B. M.; Schaller, G. E.; Bleecker, A. B. *Science*, **1999**, *283*, 996-998. b) Bleecker, A. B. *Trends in Plant Science*, **1999**, *4*, 269-274.
- 26 Manchot, W.; Brandt, W. *Liebigs Ann. Chem.* **1909**, *370*, 286-296.
- 27 Van Den Hende, J. H.; Baird, W. C.; *J. Am. Chem. Soc.* **1963**, *85*, 1009-1010.
- 28 Baenziger, N. C.; Richards, G. F.; Doyle, J. R. *Inorg. Chem.* **1964**, *3*, 1529-1535.
- 29 Baenzinger, N. C.; Haight, H. L.; Doyle, J. R. *Inorg. Chem.* **1964**, *3*, 1535-1541.
- 30 Thompson, J. S.; Harlow, R. L.; Whitney, J. F. *J. Am. Chem. Soc.* **1983**, *105*, 3522-3527.
- 31 Allen, J. J.; Barron, A. R. *Dalton Trans.* **2009**, 878-890.

-
- 32 Bainbridge, M. J.; Lindsay Smith, J. R.; Walton, P. H. *Dalton Trans.* **2009**, 3143-3152.
- 33 Fianchini, M.; Dai, H.; Rasika Dias, H. V. *Chem. Commun.* **2009**, 6373-6375.
- 34 Hakansson, M.; Jagner, S.; Walther, D. *Organometallics* **1991**, *10*, 1317-1319.
- 35 Hakansson, M.; Brantin, K.; Jagner, S. *J. Organomet. Chem.* **2000**, *602*, 5-14.
- 36 Camus, A.; Marish, N.; Nardin, G.; Randaccio, L. *Inorg. Chim. Acta* **1977**, *23*, 131-144.
- 37 Bellott, B. J.; Girolami, G. S. *Organometallics* **2009**, *28*, 2046-2052.
- 38 Ye, Q.; Wang, X-S.; Zhao, H.; Xiong, R-G. *Chem. Soc. Rev.* **2005**, *34*, 208-225.
- 39 Zhang, J.; Xiong, R-G.; Chen, X-T.; Che, C-M.; Xue, Z.; You, X-Z. *Organometallics* **2001**, *20*, 4118-4121.
- 40 Searches of Scifinder database, Web of knowledge and CSD revealed no instances of Cu-dba or ba complexes (searched for copper complexes of (di)benzylidene acetone), 18th April 2011.
- 41 Kiyomori, A.; Marcoux, J-F.; Buchwald, S. L. *Tetrahedron Lett.* **1999**, *40*, 2657-2660.
- 42 Coles, S. J.; Faulds, P.; Hursthouse, M. B.; Kelly, D. G.; Toner, A. J. *Polyhedron* **2000**, *19*, 1271-1278.
- 43 Bennett, M. A.; Knrm, W. R.; Nyholm, R. S. *Inorg. Chem.* **1968**, *7*, 552-556.
- 44 Shapiro, N. D.; Toste, F. D. *P. Natl. Acad. Sci. USA* **2008**, *105*, 2779-2782.
- 45 Kaddouri, H.; Vicente, V.; Ouali, A.; Ouazzani, F.; Taillefer, M. *Angew. Chem., Int. Ed.* **2009**, *48*, 333-336.
- 46 Drinkel, E.; Briceño, A.; Dorta, R.; Dorta, R. *Organometallics* **2010**, *29*, 2503-2514.
- 47 No copper complexes were found containing both alkenes and phosphine sulfides. A search of the CSD revealed only Rh and Ir complexes where an alkene and phosphine sulfide were present. Accessed on 18th April 2011.
- 48 Room temperature is between 13-25 °C.
- 49 Anson, C. E.; Ponikiewski, L.; Rothenberger, A. *Z. Anorg. Allg. Chem.* **2006**, *632*, 2402-2404.
- 50 Liaw, B-J.; Lobena, T. S.; Lin, Y-W.; Wang, J-C.; Liu, C. W. *Inorg. Chem.* **2005**, *44*, 9921-9929.
- 51 Takemura, Y.; Nakajima, T.; Tanase, T. *Dalton Trans.* **2009**, 10231-10243.

-
- ⁵² a) van Albada, G. A.; Mutikainen, I.; Roubeau, O.; Turpeinen, U.; Reedijk, J. *Inorg. Chim. Acta* **2002**, *331*, 208-215. b) Balboa, S.; Carbello, R.; Castiñeiras, A.; González-Pérez, J. M.; Niclós-Gutiérrez, J. *Polyhedron*, **2008**, *27*, 2921-2930. c) Zheng, Y-Q.; Lin, J-L. *Z. Anorg. Allg. Chem.* **2002**, *628*, 203-208.
- ⁵³ Ainscough, E. W.; Bergen, H. A.; Brodie, A. M.; Brown, K. A. *J. Chem. Soc., Dalton Trans.* **1976**, 1949-1956.
- ⁵⁴ gNMR software package (version 5.1, P. H. M. Budzelaar, Department of Chemistry, University of Manitoba), see: <http://home.cc.umanitoba.ca/~budzelaar/gNMR/gNMR.html> (last accessed 11/05/2011).
- ⁵⁵ Chen, C. -S.; Yeh, W. -Y. *Chem. Commun.* **2010**, *46*, 3098-3100.
- ⁵⁶ Tanaka, H.; Yamada, K-i.; Kawazura, H. *J. Chem. Soc., Perkin Trans. II* **1978**, 231-235.
- ⁵⁷ a) Lebel, H.; Marcoux, J-F.; Molinaro, C.; Charette, A. B. *Chem. Rev.* **2003**, *103*, 977-1050. b) Beaufort, L.; Demonceau, A.; Noels, A. F. *Tetrahedron* **2005**, *61*, 9025-9030.
- ⁵⁸ García-López, J.; Yanez-Rodríguez, V.; Rocés, L.; García-Granda, S.; Martínez, A.; Gueara-García, A.; Castro, G. R.; Jiménez-Villacorta, F.; Iglesias, J.; López, Ortiz, F. *J. Am. Chem. Soc.* **2010**, *132*, 10665-10667.
- ⁵⁹ Fructos, M. R.; Belderrain, T. R.; Nicasio, M. C.; Nolan, S. P.; Kaur, H.; Díaz-Requejo, M. M.; Pérez, P. J. *J. Am. Chem. Soc.* **2004**, *126*, 10946-10847.
- ⁶⁰ a) Markó, I. E.; Giles, P. R.; Tsukazaki, M.; Brown, S. M.; Urch, C. J. *Science* **1996**, *274*, 2044-2046. b) Gamez, P.; Aubel, P. G.; Driessen, W. L.; Reedijk, J. *Chem. Soc. Rev.* **2001**, *30*, 376-385.
- ⁶¹ a) Sweeney, J. B. *Chem. Soc. Rev.* **2002**, *31*, 247-258. b) Evans, D. A.; Faul, M. M.; Bilodeau, M. T. *J. Am. Chem. Soc.* **1994**, *116*, 2742-2753. c) Li, Z.; Quan, R. W.; Jacobsen, E. N. *J. Am. Chem. Soc.* **1995**, *117*, 5889-5890. d) Dauban, P.; Dodd, R. H. *J. Org. Chem.* **1999**, *64*, 5304-5307.
- ⁶² Selected papers on S,C,S pincer ligands: a) Kuwabara, J.; Munezawa, G.; Okamoto, K.; Kanbara, T. *Dalton Trans.* **2010**, *39*, 6255-6261. b) Evans, D. R.; Huang, M.; Seganish, W. M.; Fettinger, J. C.; Williams, T. L. *Organometallics* **2002**, *21*, 893-900. c) Bergbreiter, D. E.; Osburn, P. L.; Liu, Y-S. *J. Am. Chem. Soc.* **1999**, *121*, 9531-9538. d) Morales-Morales, D.; Jensen, C. M. *The Chemistry*

-
- of Pincer Compounds* **2007**, Elsevier:Amsterdam. e) Singleton, J. T. *Tetrahedron* **2003**, *59*, 1837-1857.
- ⁶³ Kubas, G. J. *Inorg. Synth.* **1979**, *19*, 90-92.
- ⁶⁴ www.sigmaaldrich.com, accessed on 1st November 2010.
- ⁶⁵ "SMART" - control software Bruker SMART Apex X-ray Diffractometer. v5.625, Bruker-AXS GMBH, Karlsruhe, Germany.
- ⁶⁶ "SAINT+" - integration software for Bruker SMART detectors. v6.45, Bruker-AXS GMBH, Karlsruhe, Germany.
- ⁶⁷ "SADABS" - program for absorption correction. v2.10. Sheldrick, G. M. Bruker AXS Inc., Madison, Wisconsin, USA, 2007.
- ⁶⁸ "SHELXS-97" - program for structure solution. Sheldrick, G. M. University of Göttingen, Göttingen, Germany, 1997.
- ⁶⁹ "SHELXL-97" - program for the Refinement of Crystal Structures. Sheldrick, G. M. University of Göttingen, Göttingen, Germany, 1997.

Chapter 5: The photochemistry of monodbaTHIOPHOS

Introduction

During an investigation into the synthesis and reactivity of some novel phosphine and phosphine sulfide ligands, we came across the serendipitous discovery of a solid-state $[\pi 2s+\pi 2s]$ intermolecular photocycloaddition. This was unexpected though not unprecedented. A brief summary of solid-state reactions and general aspects of photochemistry, which aids the discussion of the results gathered, is given below.

5.1 Solid-state reactions

Solid-state reactions of organic compounds have been around since the beginning of synthetic organic chemistry. It is widely stated that organic synthesis started when Wöhler heated ammonium cyanate to give urea in 1828.¹ This would make the reaction the very first solid-state reaction as well. However, it is clear from his original paper that the urea was obtained by accident as Wöhler was actually trying to make ammonium cyanate itself.² It has since been recognised that ammonium cyanate can be transformed into urea both in the solid and solution state. Investigations into solid-state reactions have continued to the present day. By 2001 over twenty different reaction types had been identified, where solid-solid or gas-solid reactions are known (see Table 1 for examples).³

Table 1: Examples of reactions that can occur in the solid-state (taken from reference 3).

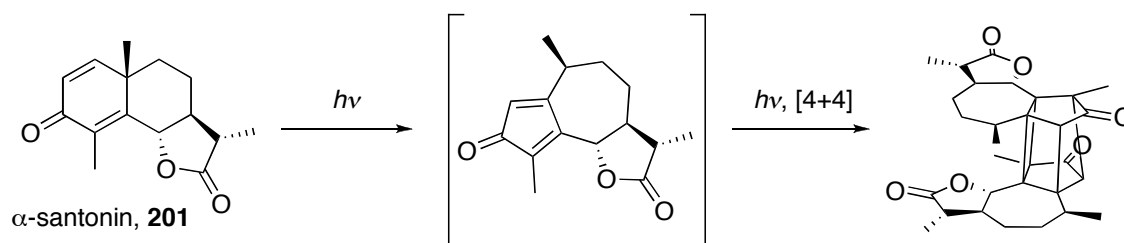
<i>Solid-state reaction types</i>	
1. Cycloadditions	13. Oxygenations
2. Cyclisations	14. Aromatic substitutions
3. Eliminations	15. Hydrogenations
4. Cascade reactions	16. Additions of $RR'NH$, H_2O ,
5. Rearrangements	17. Methylations
6. Inclusion reactions	18. Additions of halogens and HX
7. Condensation of carbonyls	19. Nitrations at N and C
8. Electron transfers	20. Diazotizations
9. Proton transfers	21. Azocoupling
10. Cycloreversions	22. C-C bond formation
11. Oxygen transfer	23. Sandmeyer reactions
12. Substitutions with RX	24. Carboxylations with CO_2

Recent investigations have highlighted the sustainability of these reactions. If the reactions run to completion then high atom efficiency results, which generates very little waste and avoids the need for the use of organic solvents and costly work-up procedures.^{3,4}

In a number of reactions the solid-state can be used to give different products to “normal” solution-based reactions. It should be pointed out that solid-state synthesis (solids interacting directly to form another solid product) is different from solvent-free synthesis (where neat reactants react in the absence of solvent via a fluid phase) and solid-phase synthesis (the reaction of molecules in a fluid phase with a solid, *e.g.* polymer supported peptide synthesis).⁴ In this investigation we are interested solely in solid-state synthesis.

5.2 Photochemistry

The photo-rearrangement of α -santonin, **201**, was one of the first organic photochemical reactions to be observed. It was initially reported in 1834, when Trommsdorff observed how crystals of α -santonin changed colour and burst on exposure to sunlight.⁵ Since then light has been used to effect a number of organic transformations both in the solution and in the solid state.



Scheme 1: Transformation of α -santonin in the solid-state.

A glance through a modern organic chemistry textbook brings up the following examples: *cis/trans* isomerisation of C=C bonds, polymerisation, cycloaddition, di- π -methane rearrangement (often referred to as the Zimmerman rearrangement), and the Norrish type I and type II reactions.⁶ More recently photochemical reactions have been investigated as “green” alternatives to thermal processes.⁷ The focus of this investigation is on the reactivity of alkene “C=C” bonds.

5.2.1 *E/Z* isomerisation of C=C bonds

It is well known that alkenes can undergo C=C bond isomerisation.⁶ For this to occur photochemically simple alkenes, such as 1,3-butadiene, need light of less than 200 nm. The addition of other functional groups (*e.g.* phenyl) in conjugation makes isomerisation viable at longer wavelengths (Woodward-Fieser rule). In many cases light of similar wavelengths promotes the isomerisation in both directions. As a result, full conversion cannot occur and after extended irradiation the photostationary state is reached (Figure 1).

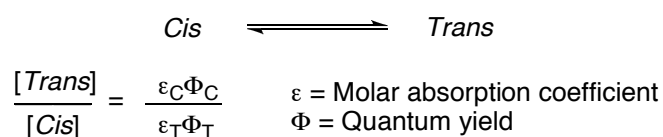
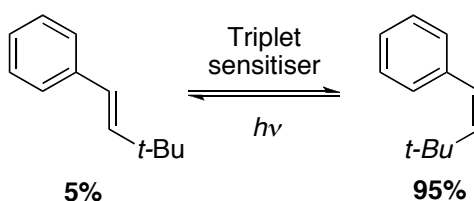


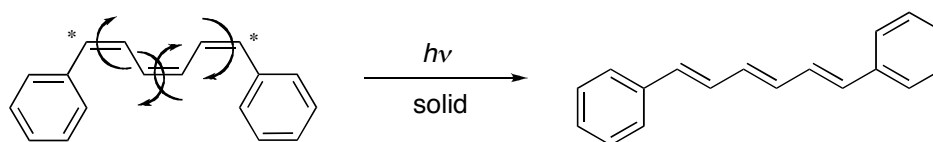
Figure 1: Photostationary state.

This is not the same equilibrium point as one would expect from thermodynamics. In thermal reactions sterics often play a part in determining the equilibrium point. One expects the equilibrium of alkenes with bulky substituents to lie toward the *trans* isomer. However, it is possible for the *cis*-isomer to be favoured under photochemical conditions where the product is determined by the exit from the S₁ (or T₁) states to S₀ (Scheme 2) *i.e.* under kinetic control.⁶



Scheme 2: *Trans/cis* isomerisation of a bulky alkene.

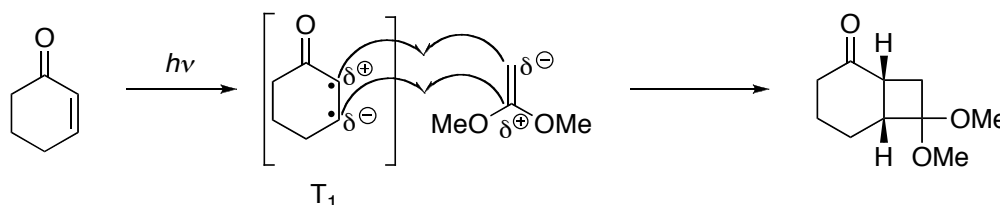
Despite being a relatively simple transformation, studies are still ongoing into the mechanism of alkene isomerisation both in the solution⁸ and solid-state.⁹ A number of mechanisms have been proposed, for example if you look at polyenes in the solid-state these include: the bicycle-pedal mechanism, which involves simultaneous rotation in the S₁ state about two polyene bonds (Scheme 3), and the hula-twist mechanism involving simultaneous rotation about a double bond and an adjacent essential single bond.¹⁰



Scheme 3: An example of a disrotatory double bicycle-pedal process in the S_1 stage of the *cis*-1,6-diphenyl-1,3,5-hexatriene to *trans*-1,6-diphenyl-1,3,5-hexatriene.

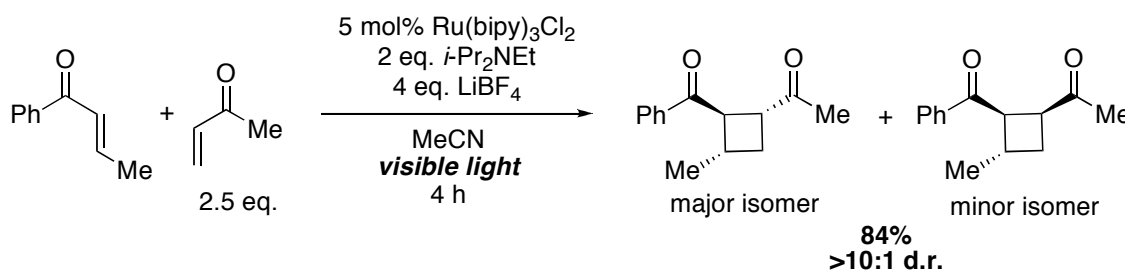
5.2.2 Cycloaddition

The most ubiquitous photochemical reactions are cycloaddition processes. Photochemical pericyclic reactions are typified by formal $[\pi 2s + \pi 2s]$ cycloadditions ($s =$ suprafacial), involving a concerted mechanism. However, often the mechanism is complex and involves both triplet states and/or biradicals.¹¹ The $[\pi 2s + \pi 2s]$ cycloaddition between an enone and an alkene is very efficient. These reactions can proceed from either the π , π^* or n , π^* states associated with the enone as the two states are close in energy. Electron-rich alkenes react more rapidly and with predictable regiochemistry (Scheme 4).^{6,12}



Scheme 4: Illustration of the cycloaddition reaction between an enone and an alkene.

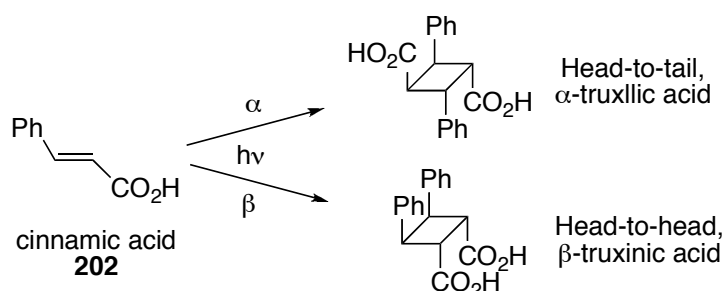
Often $[\pi 2s + \pi 2s]$ cycloadditions benefit from sensitizers (common photosensitizers include benzophenone) or photocatalysts to enable efficient intersystem crossing to and from the triplet state. Recent examples include the use of Ru complexes as photocatalysts (Scheme 5).¹³



Scheme 5: Ru(bipy)₃Cl₂ as a photocatalysis in a $[\pi 2s + \pi 2s]$ cycloaddition.

5.2.3 Photochemical solid-state reactions

By the 1920s the study of solid-state reactions was hampered by the lack of methods for analysis. It was the advent of X-ray crystallography that provided a method suited to the structural study of solids and solid-state reactions. Systematic research into solid-state reactions began in the 1960s with Schmidt and co-workers' investigation into the dimerisation of cinnamic acids (**202**).

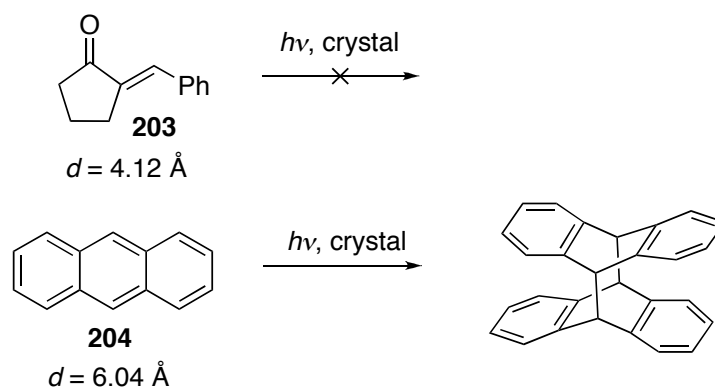


Scheme 6: Photochemical reactions of cinnamic acid.

Their results showed that the photochemical behaviour of these compounds did not correlate to the different ring substituents. Instead they saw differences in photochemical behaviour depending on crystal type, α or β (Scheme 6). Therefore Schmidt postulated that the photo-reactivity of the cinnamic acids was dependant on the crystal structure. He proposed the following topochemical¹⁴ rules for $[\pi 2s+\pi 2s]$ cycloaddition:

“...the stereochemistry of the dimer ($\bar{1}$ and m) is determined by the contact geometry [antiparallel (*i.e.* related by a crystallographic centre of symmetry) or parallel (*i.e.* related by a translational axis)] of nearest-neighbour double bonds, provided that the centre-to-centre distance d of these double bonds is of the order of 4 Å (experimentally observed limits $4.2 > d > 3.5$ Å).”¹⁶

The rules ensure that there is a good overlap between the p-orbitals of the double bond allowing the reaction to occur. These rules give a good indication of whether cycloaddition will occur, however there are numerous exceptions (Scheme 7). There are photostable crystals with double bonds less than 4.2 Å apart (*e.g.* **203**) and photoreactive crystals with larger double bond distances (*e.g.* anthracene, **204**, $d = 6.04$ Å) and unparallel bonds.¹⁵



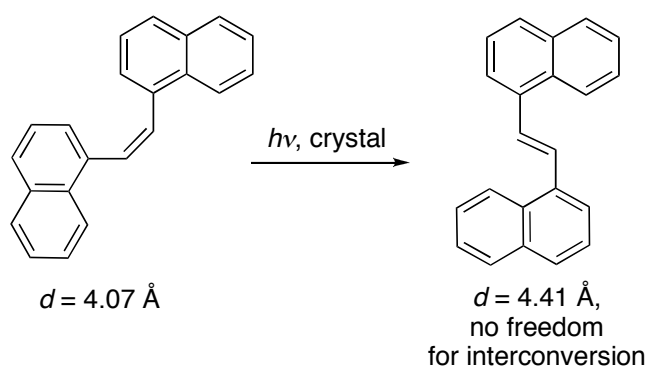
Scheme 7: Examples of adherence and breakdown of the topochemical rules.

A number of reasons were put forward to explain these exceptions. The main one favoured by Schmidt was that the formation of ‘topochemically forbidden’ dimers, which is due to defects in the crystal structure that bring the starting compound into the ‘correct’ geometry for cycloaddition.¹⁶ This view was backed up by the work of Thomas and Williams on anthracene.¹⁷ Cohen went further and introduced the concept of ‘reaction cavity’, which described the area that the starting molecules occupy.¹⁸ The topochemical principles can be interpreted to mean that reactions that occur with the minimum distortion to the surface of the reaction cavity will be favourable. Gavezzotti took this approach and updated it with the quantification of the free space around the reaction site by volume analysis using D_i maps, a three-dimensional measure of occupied space showing any holes or channels.¹⁹ Despite the above breakdowns, Schmidt’s topochemical rules still provide a good first indication of whether a reaction will occur.²⁰

By the 1990s developments in surface techniques such as AFM (Atomic Force Microscopy) had enabled scientists to observe the surface of crystals before and after irradiation. This led chemists to recognise that the crystal structure played a larger role than just aligning the double bonds at close distances. Indeed, the formation of microscopic face-selective features (up to nine different types)²¹ was observed, suggesting that long range molecular movements occurred that were governed by the crystal lattice. Kaupp highlighted the use of AFM, SNOM (scanning near-field optical microscopy) and SXM (scanning X-ray microscopy) in determining the mechanism of solid-solid reactions, as well as solid-gas reactions. By 2001 he had distinguished three distinct steps in the solid-state mechanisms:³

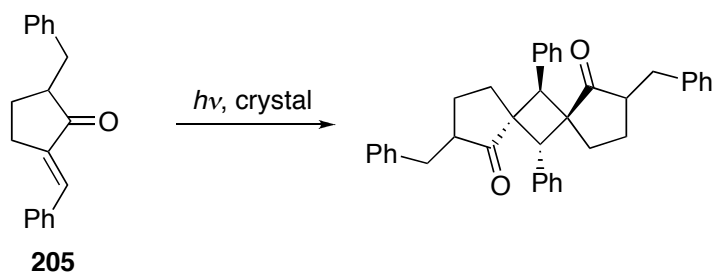
1. Phase rebuilding (initial continuous change)
2. Phase transformation (sudden change when product crystals are formed)
3. Crystal disintegration/detachment (fresh surface is created)

AFM will pick up changes in the surface for both steps 1 and 2. The failure of either of these steps will result in non-reactivity. Kaupp's mechanism explains why enone **203** does not react despite a short distance (4.12 Å). The two reacting molecules are heavily interlocked so cannot move out of the original lattice and then rebuild the solid phase. It also explains why *cis/trans* isomerisations around a C=C double bond can occur despite large molecular movements being necessary (an example is given Scheme 8).²¹ The long range migrations allow enough movement for the internal rotation of 180° that occurs.



Scheme 8: An example of *cis/trans* isomerisation in the solid-state.

Depending on the size of the phase transformation and the crystal disintegration, the crystals may break up. In these cases, grinding the crystals may lead to higher conversions. If the crystals do not disintegrate with the associated loss of crystallinity then the reaction can be referred to as a single-crystal to single-crystal (SCSC) process. In rare instances there is almost no change in the unit cell dimensions between the reactants and product. The reaction is said to be topotactic when there is <4% difference. It should be noted that this value is arbitrary. This is most likely to happen in intramolecular reactions, but has been seen in intermolecular reactions, *e.g.* in 2-benzyl-5-benzylidene-cyclopentanone, **205** (Scheme 9).²²



Scheme 9: An example of a topotactic reaction.

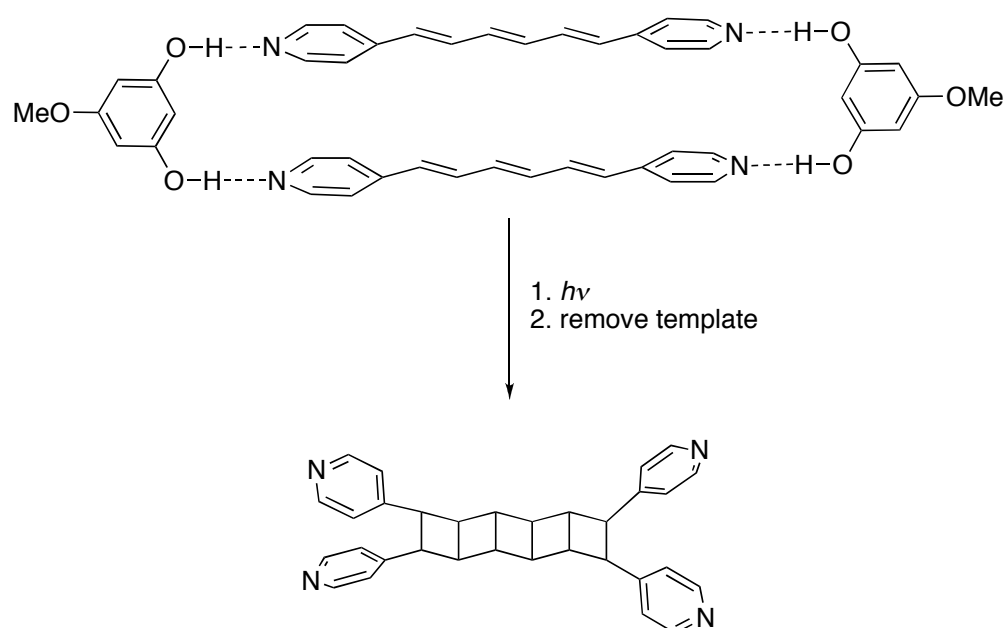
There is some disagreement in the literature over the exact designation of topotactic reactions. Kaupp maintains that true topotactic reactions are those where no long-range lattice movements are observed, *i.e.* there is no observable change to the surface crystal. In contrast, Enkelmann and co-workers differentiate between homogenous and heterogenous topotactic reactions.²³ Homogenous reactions are those that meet Kaupp's criteria and maintain the crystal throughout the reaction. In heterogeneous reactions a phase separation does occur, leading to the breakdown of the crystal. If the reactant and product crystal unit cell dimensions are less than 4% different it would still be correct to call them topotactic. Foxman and co-workers, meanwhile refer to both one-phase and two-phase topotactic reactions.²⁴ They describe a one-phase reaction as one in which "there is no change of space group, and only a single diffraction pattern is visible at any time during the process". Whilst a two-phase reaction is described as one where "the diffraction patterns of reactant and product are simultaneously visible". Overall, scientists working in the area agree that topotactic SCSC transformations are rare. One caveat to this discussion is the observation that instrumentation and data processing methodologies used have an impact on the designation of SCSC transformations, which may not relate directly to the reaction being observed.²⁵

Despite the advances made, the elucidation of solid-state reactions and their mechanisms is still on-going, even cinnamic acid has not yet given up all its secrets.²⁴ In the last 15 years solid-state NMR spectroscopy has begun to be used as a tool.²⁶ Solid-state NMR spectroscopy compliments the other major techniques used as it can provide information on polymorphs and other side reactions, as well as being used quantitatively.²⁷

The advances made in understanding the mechanism of solid-state reactions since Schmidt's work in the 1960s means that researchers are able to explain the reactivity

they observe. It has also allowed scientists to engineer solutions if the desired reactivity was not seen. Crystal engineering has become popular and each major publishing house has journals associated specifically with this area.²⁸ A number of different approaches have been utilised by crystal engineers to effect efficient $[\pi 2s+\pi 2s]$ cycloaddition reactions.²⁹ The most common are the use of hydrogen bonding,³⁰ metal-templating,³¹ π - π stacking³² and halogen bonding.³² This has enabled complex molecules such as ladderanes to be synthesised in high yield (Scheme 10).³⁰

Under the right conditions $[\pi 2s+\pi 2s]$ cycloadditions are reversible.³³ This makes them potential candidates for molecular switches,³⁴ and the storage of information.²³



Scheme 10: Methoxyresorcinol as a template for the synthesis of ladderanes.

5.3 Aims

The aim for this part of the project was to explore the photoreactivity of the ligands we have synthesised: dbaPHOS **127**, dbaTHIOPHOS **137**, monodbaTHIOPHOS **149** and monodbaPHOS **128**. The focus was on solid-state $[\pi 2s+\pi 2s]$ cycloaddition reactions.

5.4. Results and Discussion

During the course of our research into phosphino-alkene ligands, the phosphine sulfide variant, monodbaTHIOPHOS **149**, was prepared. The initial crystal structure obtained for monodbaTHIOPHOS was a mixture of the discrete compound **149** and the dimerised cycloadduct **206** in a 19:81 ratio as determined by atom occupancy (Figure 2a and b). The presence of the dimerised product was unexpected, though as the introduction section shows not unprecedented. It is worthy of note that the [2+2] reaction has occurred on the most hindered alkene (chemoselective).

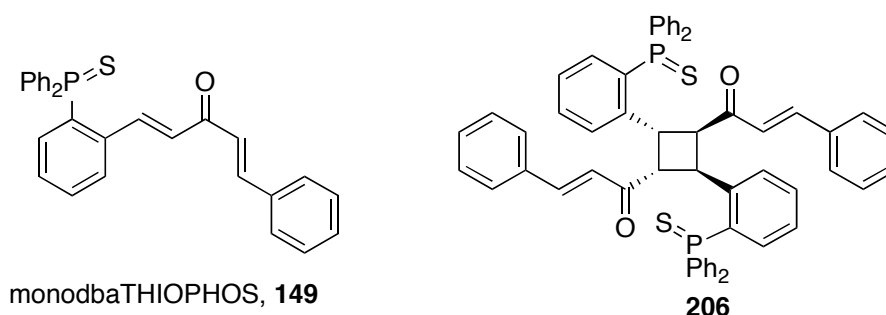


Figure 2a: Mixture of compounds in the initial X-ray single crystal structure determination of monodbaTHIOPHOS.

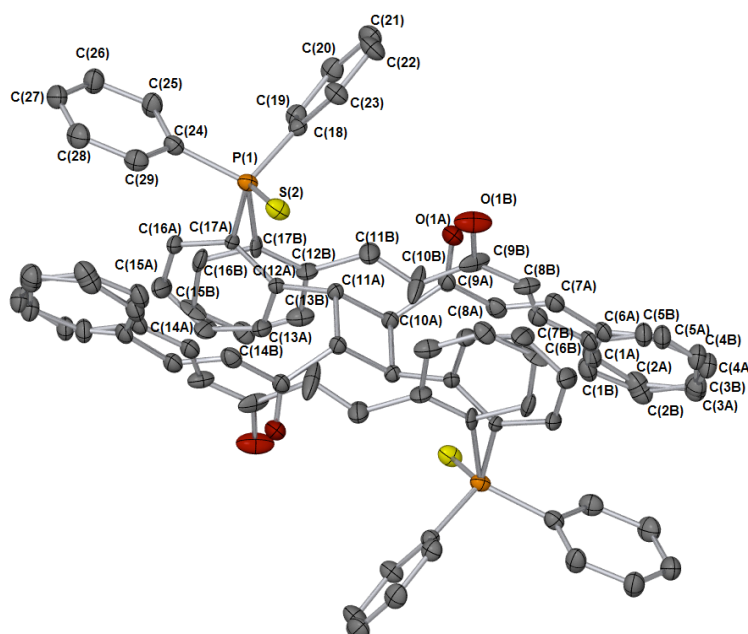
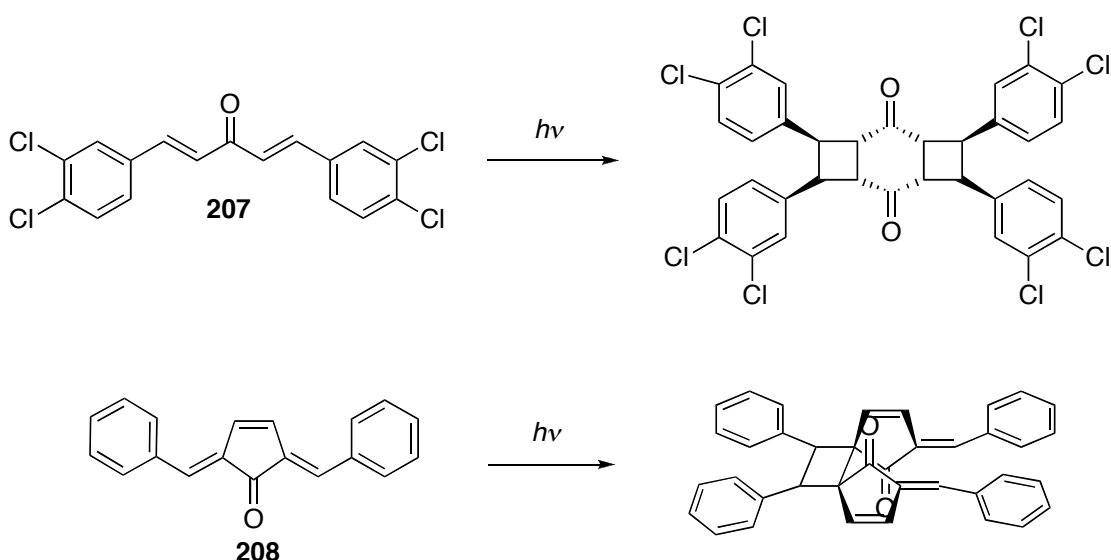


Figure 2b: X-ray crystal structure of monodbaTHIOPHOS **149, and **206**.** Ellipsoids shown at 50%. Hydrogen atoms removed for clarity.

The dbaPHOS family of ligands are based on dibenzylidene acetone (dba) and contain the 1,4-dien-3-one backbone. Dba has been shown to undergo intermolecular $[\pi 2s+\pi 2s]$ cycloaddition in the solution state.¹⁶ In isolation dba does not undergo photochemical $[\pi 2s+\pi 2s]$ cycloaddition in the solid state as the structure does not meet the required criteria. According to Schmidt's topochemical principles dba cannot undergo cycloaddition in the solid-state as the double bonds in adjacent molecules are all more than 4 Å apart. It should be noted that on irradiation single crystals of dba lose their diffracting properties.³⁵ However, the *bis*-(dichlorobenzylidene)acetones (e.g. **207**) tend to crystallise in cells where the *c* axis = 4 Å, controlling the distance between the molecules and are therefore able to undergo double cycloaddition to give the tricycle[6.2.0.0^{3,6}]decane system (Scheme 11).³⁶ It has also been shown that similar compounds such as 2,5-dibenzylidenecyclopent-3-ene-1-one, **208** (nearest double bonds 3.92 Å, but non-parallel) undergo $[\pi 2s+\pi 2s]$ cycloaddition (Scheme 11).³⁷



Scheme 11: Solid-state $[\pi 2s+\pi 2s]$ cycloadditions in dba-like compounds.

Dba has been shown to undergo photochemical cycloadditions when co-crystallised with additives such as UO_2Cl_2 and SnCl_4 .³⁸ These additives change the crystal packing of the dba molecules, therefore aligning the alkene bonds in an orientation that allows them to react.

The presence of the mixture of compounds in the crystal suggested that a photochemical $[\pi 2s+\pi 2s]$ reaction could be occurring in the solid-state. Further studies were conducted to answer the following questions:

- Does the [2+2] cycloaddition reaction occur in the solid or solution state?
- Is the reaction an example of a single-crystal to single-crystal reaction?
- Does the reaction go to full conversion?
- Do any of the other phosphino-alkene compounds exhibit photoreactivity?

5.4.1 Solution studies

During our work on the phosphino-alkene compounds and their phosphine sulfide variants, no observations had been made of any degradation of the compounds: dbaTHIOPHOS **137**, monodbaTHIOPHOS **149**, or monodbaPHOS **128**, on storing in solution in the presence of light. For example, NMR samples of monodbaTHIOPHOS **149** left for up to a week in the laboratory (exposed to fluorescent light and sunlight) showed no sign of any cycloaddition products. Dbaphos **127** was found to degrade when an O₂ free solution in C₆D₆ was stored in light for long periods (*ca.* 3 weeks); a mixture of unidentified products (20 peaks between 27.5-30 ppm in the ³¹P NMR) were observed.

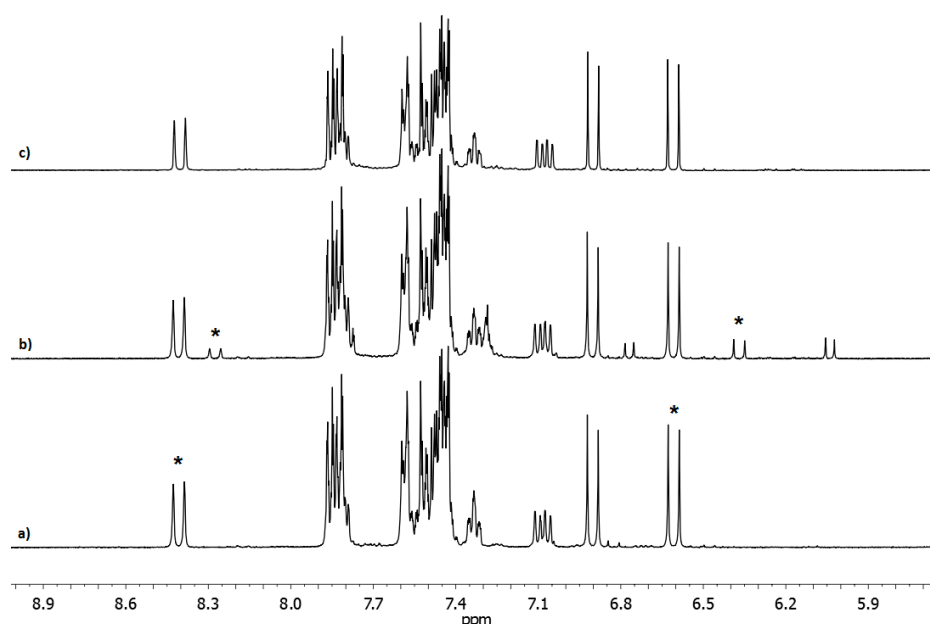
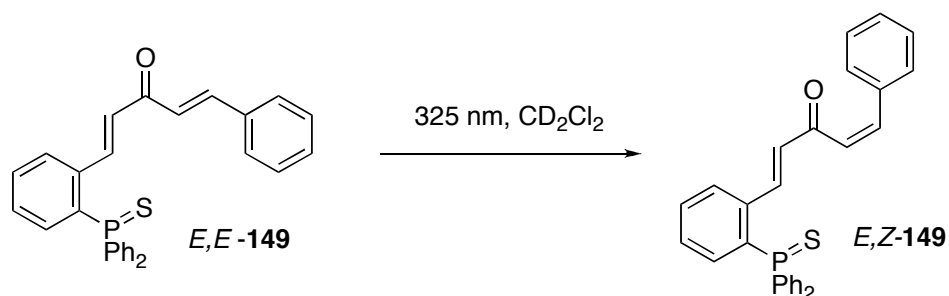


Figure 3: a) monodbaTHIOPHOS 149 before irradiation, b) after 10 h irradiation at 325 nm, c) after 48 h in the dark. * represents the alkenyl protons whose ¹³C peaks have C-P coupling.

Irradiation of monodbaTHIOPHOS, **149** in CD₂Cl₂ (0.07 and 0.25 M) using a 325 nm laser followed by *in-situ* NMR spectroscopy revealed that no [π2s+π2s] cycloaddition occurred even in a saturated solution (~0.25 M). Instead the sample underwent partial *trans-cis* isomerisation of one of the double bonds, shown by the reduction in the ³J_{HH} from 15.8 to 12.7 Hz. Once the sample was placed back in the dark for 48 h the

isomerisation reversed to give the original compound (Figure 3). ^1H - ^{13}C HSQC experiments reveal that the alkenyl protons exhibiting the change in coupling constant were associated with the alkenyl carbons without C-P coupling. Therefore it is the alkene furthest away from the phosphine sulfide that undergoes C=C isomerisation (Scheme 12).



Scheme 12: *Trans-cis* isomerisation on irradiation of monodbaTHIOPHOS 149 at 325 nm.

The weaker sample (0.07 M) gave the same product however, there was another set of peaks seen to grow in and then disappear as those indicated above appeared. The peaks were two doublets at 6.1 and 6.5 ppm with coupling constants of 12.3 and 16.2 Hz, respectively. It is unclear what these correspond to but it could be the isomerisation of the other double bond.

Overall, the evidence suggests that the $[\pi 2s + \pi 2s]$ cycloaddition is not a solution-phase photochemical reaction. As a result our attention turned to examining the solid-state photochemistry of monodbaTHIOPHOS.

5.4.2 Single crystal studies

Analysis of the crystal structures of dbaPHOS, dbaTHIOPHOS and monodbaTHIOPHOS revealed that monodbaTHIOPHOS met the criteria determined by Schmidt for solid-state photodimerisation (parallel C=C bonds and $<4.2 \text{ \AA}$ apart), one pair of double bonds are parallel and 3.575 \AA apart (Figure 5). It is therefore likely that the presence of cycloadduct **206** in the initial crystal structure of monodbaTHIOPHOS was the result of a $[\pi 2s + \pi 2s]$ cycloaddition, following the formation of the crystal. It can also be seen that due to the crystal packing, all the molecules in the crystal structure form close contacts with a partner molecule (Figure 4). Therefore, theoretically the $[\pi 2s + \pi 2s]$ cycloaddition would be able to go to 100% conversion.

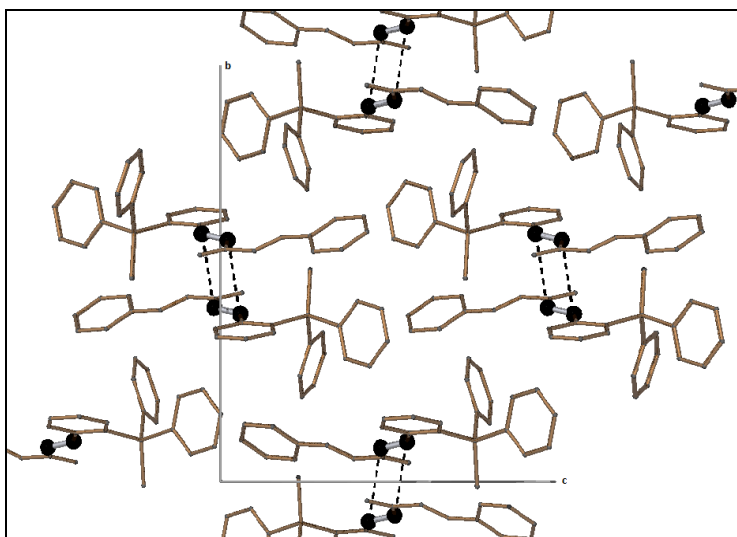


Figure 4: Crystal packing of monodbaTHIOPHOS viewed along the a axis of the unit cell. Black atoms indicate reacting alkene atoms, dashed lines indicate the shortest distance between alkenes (3.575 Å).

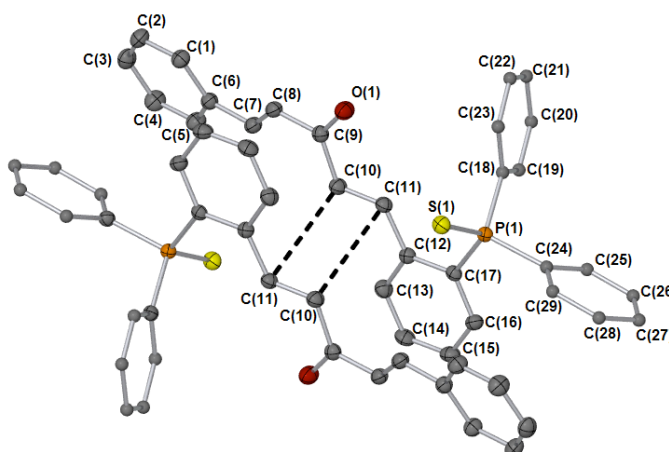


Figure 5: X-ray structure of monodbaTHIOPHOS showing close double bonds. Ellipsoids shown at 50%. Hydrogen atoms removed for clarity.

The crystal structures revealed that for dbaPHOS and dbaTHIOPHOS, the nearest double bonds were situated far further apart (6.308 Å and 7.602 Å, respectively). In both cases the double bonds are not parallel (Figure 6 and Figure 7), which would lead to poor orbital overlap. Therefore it is not expected that dbaPHOS **127** and dbaTHIOPHOS **137** will undergo photochemical $[\pi 2s + \pi 2s]$ cycloaddition in the solid state.

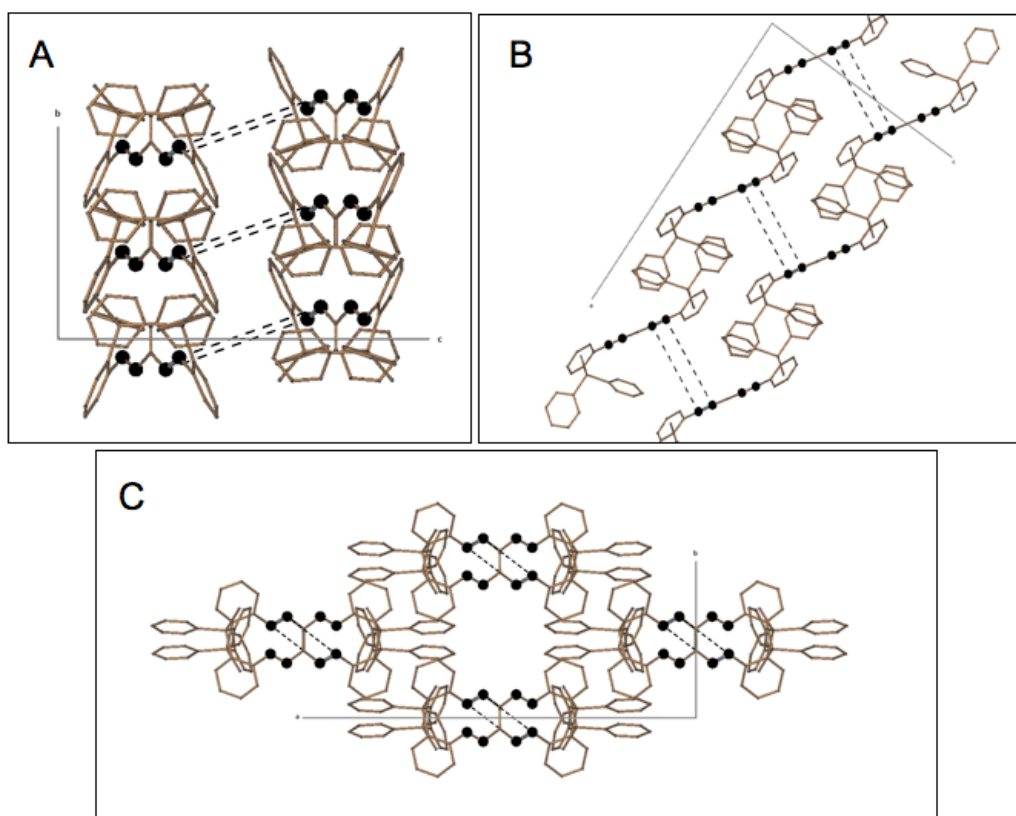


Figure 6: Crystal packing of dbaTHIOPHOS viewed along a) the *a* axis, b) the *b* axis and c) *c* axis. Black atoms indicate the alkene carbon atoms, dashed line indicates the shortest interaction (7.602 Å).

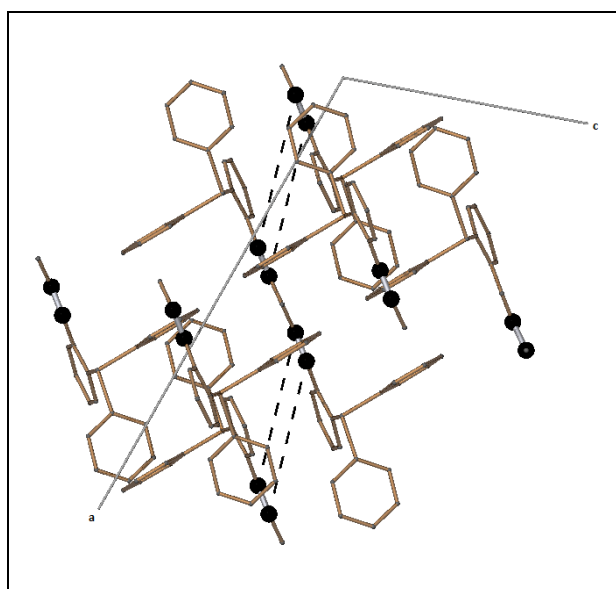
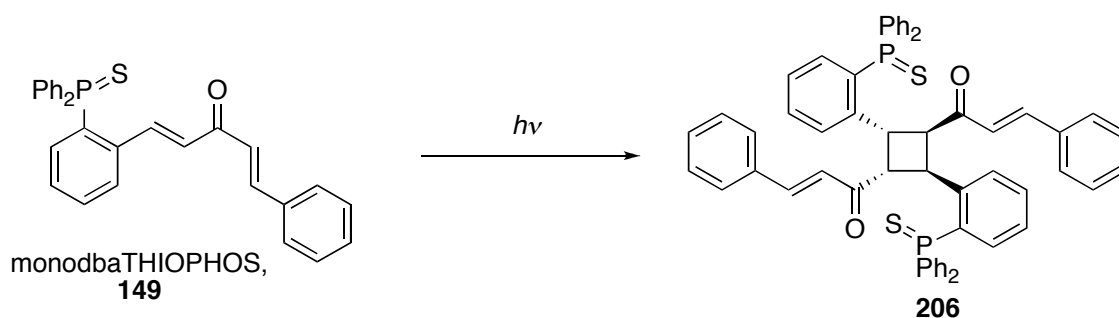


Figure 7: Crystal packing of dbaPHOS viewed along the *b* axis. Black atoms indicate the alkene carbon atoms, dashed line indicates the shortest interaction (6.308 Å).

Crystals of monodbaTHIOPHOS **149** were grown from a solution of the compound in CH_2Cl_2 layered with Et_2O and kept in the dark. The photocycloaddition was then

followed by single crystal X-ray diffraction. No reaction occurred on exposure of a single crystal to incandescent light for 2 h at 110K. After 48 h under fluorescent light at room temperature the reaction had reached a 31% conversion to the cycloadduct **206**. Fluorescent light is mostly comprised of light over 400 nm.³⁹ Solid-state UV-visible spectroscopy indicates that monodbaTHIOPHOS's λ_{max} is at 289 nm, and that the ligand has a long tail of absorbance across the visible region. Therefore the crystal is absorbing some radiation to enable excitation. Light of a wavelength that is absorbed in the tail-end of the absorption band has been previously shown to promote SCSC transformations.^{24, 23}



Scheme 13: Solid-state $[\pi 2s+\pi 2s]$ cycloaddition.

Unfortunately, after further irradiation the crystal was found to have disintegrated. This could be due to a number of reasons:

1. The X-ray diffraction data were collected at 110 K, so the movement of the crystal between room temperature and the cryostream would have resulted in thermal stress. Eventually, this could cause the crystal lattice to decompose.
2. The reaction in the solid-state may not be homogenous, *i.e.* the crystal may undergo a phase change as the $[\pi 2s+\pi 2s]$ cycloaddition occurs leading to the disintegration of the crystal. This is relatively common in these types of reactions, hence the rarity of SCSC transformations.²⁵
3. The crystal was moved into sunlight, which would have exposed it to higher energy light. In some cases, the exposure to non-tail end light (<400 nm) has been held responsible for crystal degradation as the reaction occurs too quickly or side reactions occur which disrupt the crystal lattice.^{21,40}

As a consequence of the above problems, a collaboration was initiated with Professor Paul Raithby (University of Bath). The single crystal X-ray diffraction experiments were repeated with *in-situ* irradiation of the crystal using UV LEDs (400 nm) whilst the

crystal is on the diffractometer.⁴¹ This ensures the thermal stress is kept to a minimum, as the crystal does not need to be removed from the cryostream. It also enables the reaction to be performed at different temperatures easily.

The cycloaddition was followed by single crystal XRD at 180 K. The majority of the conversion occurred in the first 4 h, after which the rate of reaction slowed down considerably reaching maximum conversion after 14 h (Table 2). The crystal was still intact and diffracting well, showing the reaction is a SCSC transformation at least up until 64% conversion. The unit cell parameters for the crystal at $t = 0$ and $t = 18$ h are very similar (Table 3); the largest difference is 1.5% for the a axis. This indicates the reaction could be topotactic, though it should be noted that we have not gone to 100% conversion. Attempts to probe the topotacticity of the reaction using AFM (in York) were unsuccessful. The crystals were too small to place flatly on the conductive surface to allow good tip contact in the AFM analysis.

Changing the temperature or using smaller crystals (to improve the penetration of light) did not lead to higher level of conversion than 70% (see Table 4 for temperature results). At higher temperatures the space around the double bonds is seen to increase (shown by the increase in offset see Table 5). This increase in space would allow more room for any isomerisation processes. After prolonged irradiation, the crystals were found to degrade. It is possible that the strain on the crystal above 70% conversion is large enough to break the crystal.

Table 2: Conversion of monodbaTHIOPHOS 149 on irradiation at 180 K.

Time, h	Excitation % (nearest whole %)
0	0
2	38
4	53
6	57
8	59
10	61
12	62
14	63
16	64
18	64

Table 3: Unit cell parameters, before irradiation and after 18 h.

Time, h	0 (149)	18 (149 and 206)
<i>a</i> , Å	9.5167(3)	9.3801(2)
<i>b</i> , Å	17.0830(4)	17.2580(2)
<i>c</i> , Å	14.5809(6)	14.7370(3)
α , °	90	90
β , °	101.961(3)	102.273(2)
γ , °	90	90

Table 4: Conversion of monodbaTHIOPHOS 149 on irradiation at different temperatures after 12-16 h.

Temperature, K	Excitation % ^a (nearest whole %)
298	decomposition (59) ^b
220	70
180	69
173	46
170	35
160	17
150	11
140 and below	negligible

^a after 12-16 h irradiation, ^b after 5 h, heavily disordered.

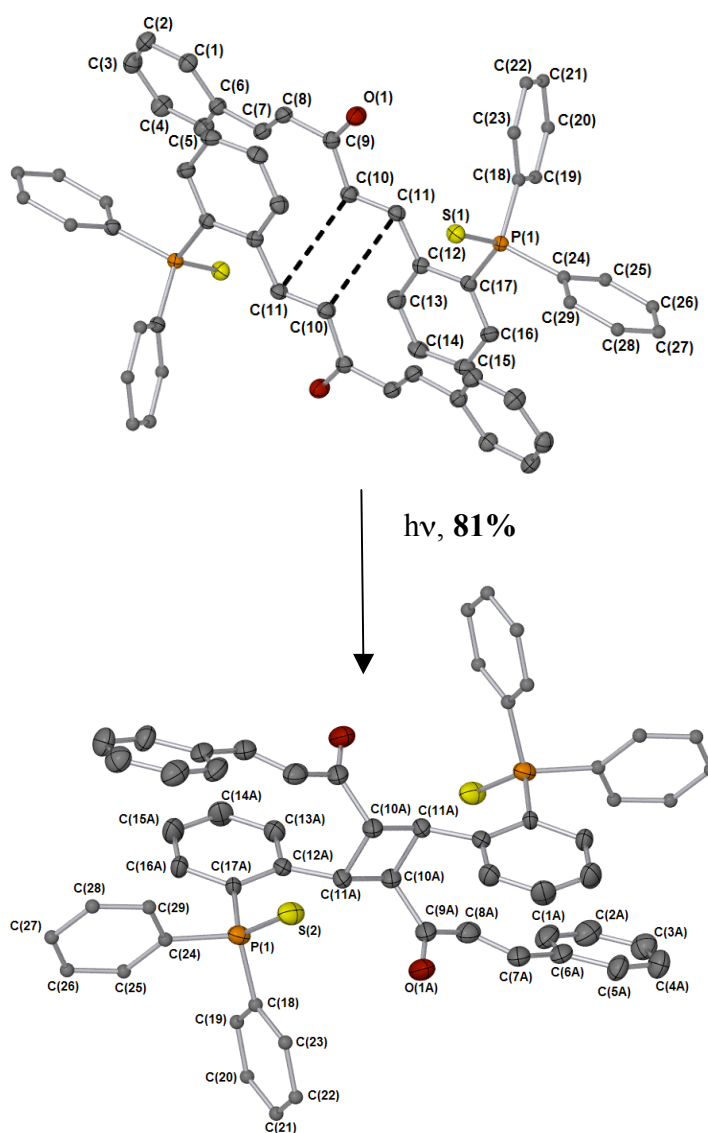
Table 5: Centroid-centroid and offset distances at different temperatures.

Temperature, K	Centroid-Centroid, ^a Å	Offset ^b , Å
220	3.689	1.655
180	3.718	1.604
173	3.679	1.549
170	3.643	1.362
160	3.612	1.358
150	3.604	1.339

^a calculated in the irradiated structure for each temperature, using the unexcited component (the centroid-centroid distance is taken as the distance between the mid-point of the C=C double bond), ^b offset of centroid positions between carbons of each C=C bond (the offset is calculated as the distance between the point when a perpendicular from one centroid is dropped to intersect with the vector generated through the other C=C bond, and the centroid position of the second C=C double bond).

In some cases it has been seen that different irradiation methods give different conversions.²⁰ Our initial crystal had a higher conversion of 81% (Scheme 14). Prior to the X-ray diffraction data being collected this crystal had been kept in an environment

shielded from direct light, over the winter holidays (*ca.* 3 weeks). As a result it would have had very little exposure to light allowing it to convert very slowly. This would mean that any stress building up in the crystal would have time to dissipate, so long as the crystal has a pathway to achieve this. The compound undergoes two different structural changes on irradiation, the $[\pi 2s+\pi 2s]$ cycloaddition and isomerisation around the single bond in the remaining enone from the *s-trans* to *s-cis* conformer. It is possible that the change in conformer allows the crystal to release some of the strain resulting from the $[\pi 2s+\pi 2s]$ cycloaddition.



Scheme 14: Solid-state $[\pi 2s+\pi 2s]$ cycloaddition of 149 to 206 depicted by crystal structures.

We anticipated that under the right conditions it would be possible to reach 100% conversion. The use of “2-photon” excitation to obtain full conversion in SCSC systems has been described in the literature.⁴² The two-photon excitation mentioned here refers to the simultaneous absorption of two photons by the compound, rather than two sequential one-photon absorption processes. For full conversion to be obtained two requirements of the light used for excitation need to be met; the crystal must only absorb a small amount of light, and the product must not absorb strongly at that wavelength. If these conditions are not met then the centre of the crystal does not get exposed to the light and thus cannot undergo excitation and reaction. In our system the product absorbs at lower wavelength than the starting material (300 nm ($\epsilon = 4218 \text{ mol}^{-1} \text{ dm}^3 \text{ cm}^{-1}$) compared to 306 nm ($\epsilon = 56471 \text{ mol}^{-1} \text{ dm}^3 \text{ cm}^{-1}$) in CH_2Cl_2). These two values are quite close, although the product is absorbing at a slightly lower λ_{max} , it has a much higher molar absorption coefficient suggesting that it would absorb a significant proportion of the photons. As the probability of a two-photon excitation is smaller than a one-photon excitation the light intensity remains almost constant in the bulk of the crystal. It was proposed that this would enable greater penetration of the light and therefore allow greater conversions to be reached.

Using a Nd:YAG laser pumped dye laser, 605 nm radiation was obtained and so single crystals of **149** irradiated. After 10 min of light of 0.5 mJ per pulse no change had occurred and the crystal was almost exactly the same as before ($R_f = 4.65\%$ before and 4.61% after). After 25 min of irradiation (10 mJ per pulse), 70% conversion of the crystal had been obtained, however the crystal had cracked into smaller pieces. It was hypothesised this could be due to irradiation approaching from one face of the crystal, leading to strain on the crystal packing causing disintegration. A single piece of the crystal was irradiated for a further 30 min, but no further conversion was obtained. Once again to obtain the diffraction data the crystal was being moved in and out of a cryostream and thus the degradation could be in part due to thermal stress, as well as the intense irradiation.

It had been seen that one removal from the cryostream and replacement had no effect on the crystal quality, therefore to reduce the thermal stress, the crystals were only placed in the cryostream for a unit cell determination, followed by irradiation at 10 mJ per pulse for 1 h, rotating the crystal 180° half way through. It was proposed that the longer

time, and the rotation would be enough to reach full conversion. However, degradation of the crystal still occurred suggesting it was due to irradiation and not thermal stress. A repeat of the experiment at 10 mJ per pulse, whilst rotating the crystal for 20 min gave only 26% conversion. There are two plausible explanations for the lower conversion:

1. The rotation of the crystal may not have been true causing the crystal to be in and out of the path of the laser.
2. In some cases it has been seen that dimerisation occurs at defect and dislocation sites leading to autocatalytic reactions.⁴³ The strain from irradiation from one side of the crystal could have increased the rate of the reaction by causing more defect sites. However, in these cases mixed product regioselectivities are often found which we do not observe.

Overall, the two-photon excitation did not appear to increase the amount of conversion. However, to be certain it would be preferable to do the irradiation *in-situ* as the goniometer head can rotate, and thermal stress will once again be minimised. It would also allow multiple temperatures to be studied. The rate of conversion is faster than with the one-photon excitation, as 70% conversion was obtained after just 25 min (75 μ s of irradiation). This could be due to the use of a laser as the light source. Taken together, the two-photon studies and the single X-ray crystallographic studies at Bath, suggest that the crystal lattice of **149** is confining the conversion to 70%. The observation with each technique of degradation of the crystal at some point, suggests that thermal stress is only one possible factor, and in some cases played no role in the degradation. It is therefore much more likely to be a result of the irradiation conditions, and rate of reaction.

5.4.3 Powder studies

Previous work detailed in the literature has shown SCSC reactions that do not go to 100% conversion, will go to completion upon grinding the crystals.^{30a, 44} On leaving a sample of **149** under ambient conditions the reaction went to 100% conversion after 2-3 months, as determined by ¹H NMR spectroscopy. Powder X-ray diffraction and solid-state NMR spectroscopic techniques allow reaction progress to be followed in the microcrystalline state. Powder X-ray diffraction gives basic information about the unit

cell dimensions, and solid-state reactions can be followed and any phase changes will be observed.^{1a} Solid-state NMR spectroscopy can also be utilised to give information about different polymorphs, and intermediates in the reaction.^{26, 27a} In collaboration with Dr. Hazel Sparkes (University of Durham), both powder X-ray diffraction and solid-state NMR spectroscopy were used to follow the photochemical [$\pi 2s + \pi 2s$] cycloaddition of monodbaTHIOPHOS **149**.

Samples for solid-state NMR spectroscopic analysis were obtained by irradiation of monodbaTHIOPHOS **149** using UV LEDs. Samples were taken before irradiation, and after 2.5, 5 and 43 h. The material was shaken every 30 min to ensure even irradiation. The ^{13}C CPMAS-NMR spectra clearly show the formation of the cyclobutane ring with the appearance of two peaks between 30 and 60 ppm (Figure 8). Although it is hard to unambiguously assign the peaks in the aromatic region, it is likely that the peaks at either side of the bulk of the aromatics are the C=C carbons. Interrupted decoupling measurements to remove the CH/CH₂ peaks, show these peaks are due to CH carbons. In the solution spectra the peaks corresponding to the alkene carbons are seen at either side of the bulk of the aromatics. It is also clear that the peak at 121.5 ppm disappears on irradiation, which suggests that the peak could be attributed to the C=C bond.

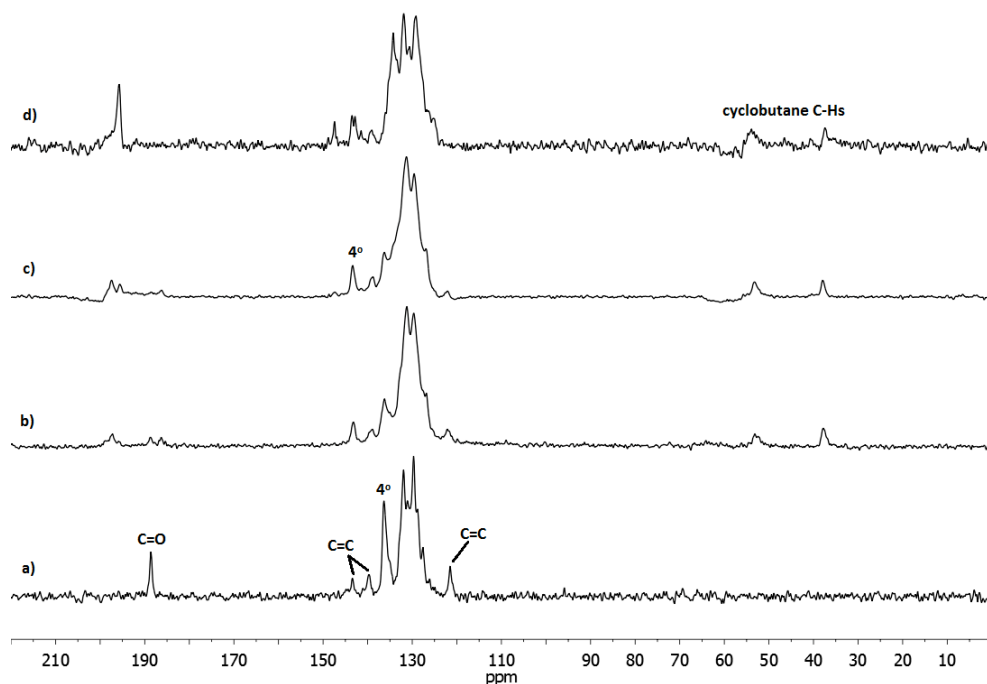


Figure 8: ^{13}C CPMAS-NMR spectra of a) monodbaTHIOPHOS **149**, b) after 2.5 h irradiation, c) after 5 h irradiation and d) after 43 h irradiation.

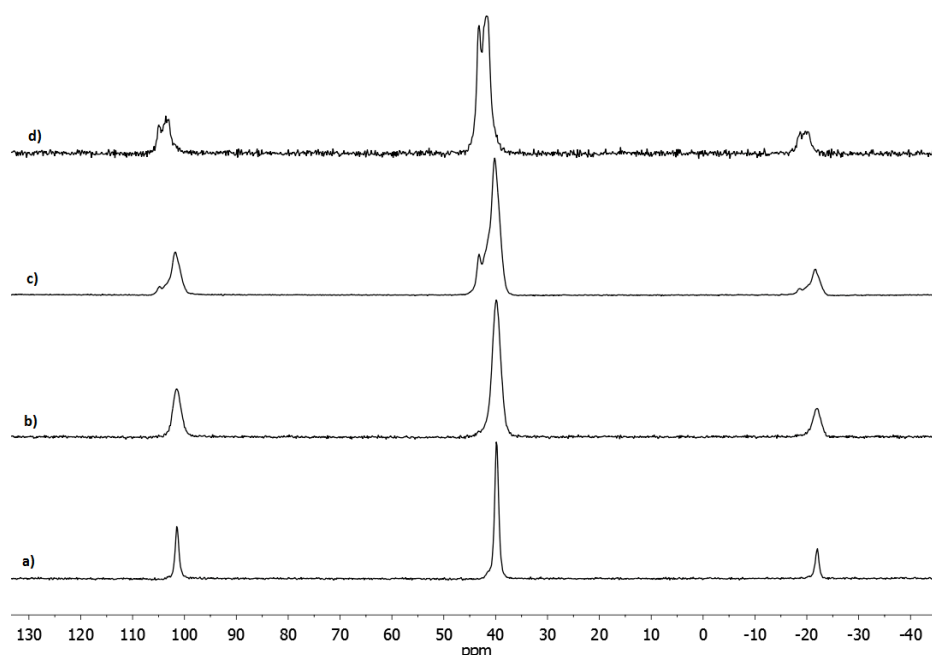
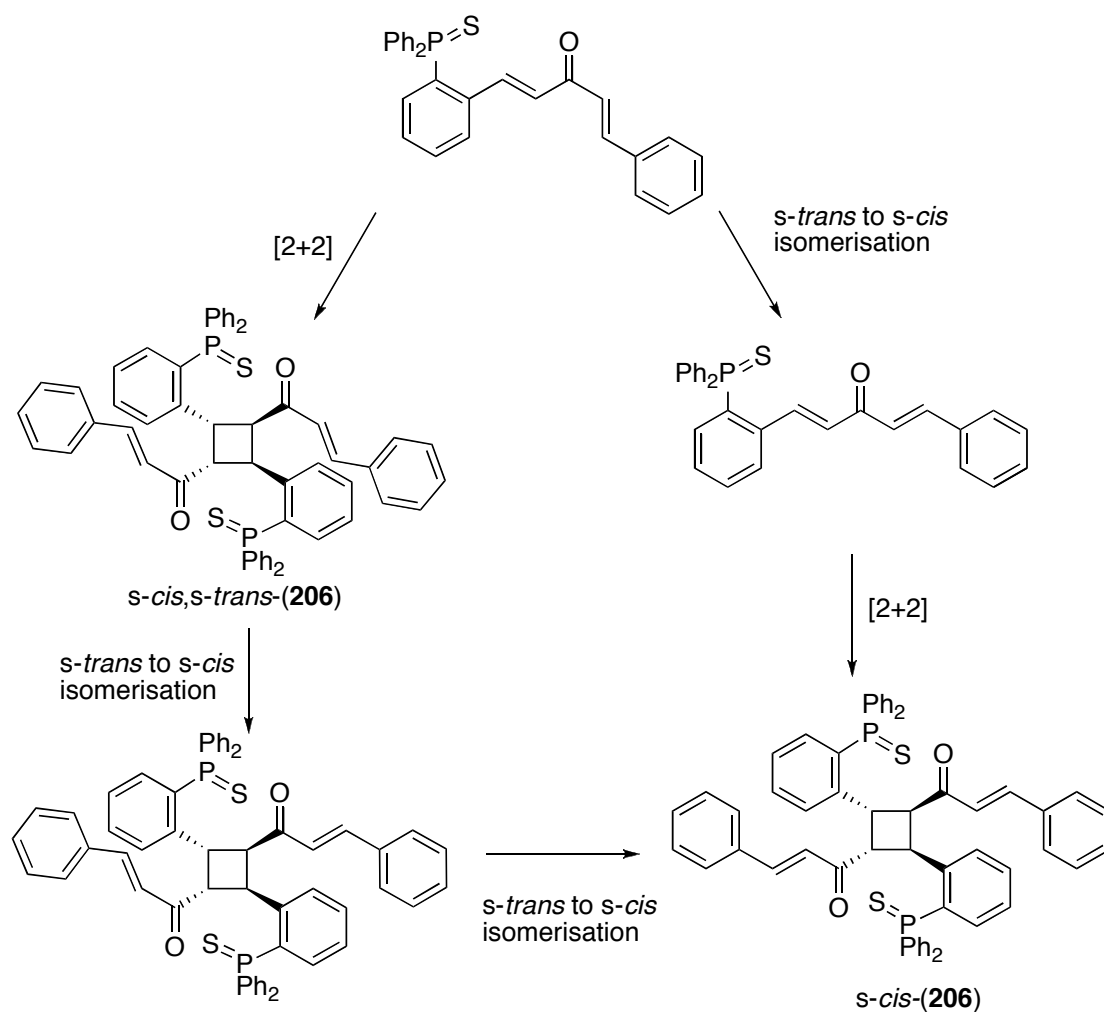


Figure 9: ^{31}P CPMAS-NMR spectra of a) monodbaTHIOPHOS 149, b) after 2.5 h irradiation, c) after 5 h irradiation and d) after 43 h irradiation.

The carbonyl peaks exhibited more complicated behaviour than you would expect from an ‘A to B’ reaction. The initial peak at 188 ppm is joined by two more (186 and 197 ppm) after 2.5 h irradiation. After 5 h the initial peak has disappeared and three other peaks are now present including the final carbonyl peak of the product (196 ppm). The number of peaks could indicate that we are observing a number of intermediates (Scheme 15), or that polymorphism is occurring.

The ^{31}P CPMAS-NMR spectroscopic analysis proved inconclusive. The non-irradiated material exhibits a peak at 39.7 ppm with spinning sidebands (Figure 9). On irradiation the peak broadened at first, before a new peak was observed at 43 ppm after 5 h irradiation. After 43 h the original peak had disappeared, however there were two peaks remaining, one sharp (43.1 ppm) and one broader (41.6 ppm). Deconvolution of the bandshape gives 32% at 43.1 ppm and 68% at 41.6 ppm, and closer inspection of the ^{31}P NMR spectrum shows that there are two singlets of similar intensities, one of which is partially obscured by another broad peak (Figure 10).



Scheme 15: Possible intermediates in the solid-state reaction.

It is unclear whether the observed spectrum is due to three separate products or two products, one of which has different phosphorus environments. Solution-state NMR spectroscopic analysis of the solid-state samples at 43 h confirmed that the reaction had reached 100% conversion, and the only product observed was **206**. Therefore it is likely that the different products are isomers that interchange in solution, *i.e.* the different conformers around the single bond in the enone (Figure 11). After 5 h 66% of the starting material had been converted to the cycloadduct **206**. This matches the results obtained from the single-crystal X-ray diffraction experiments which gave ~59% conversion after 5 h at 298 K.

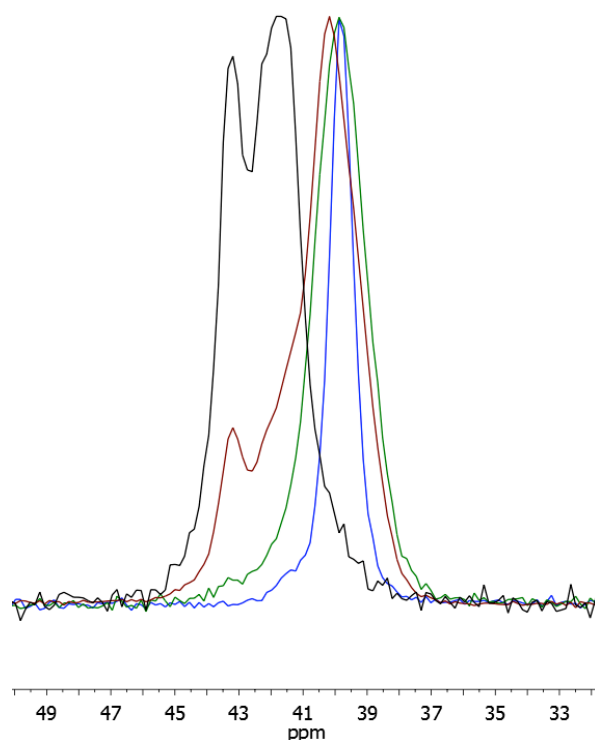


Figure 10: Overlay of ^{31}P CPMAS NMR.

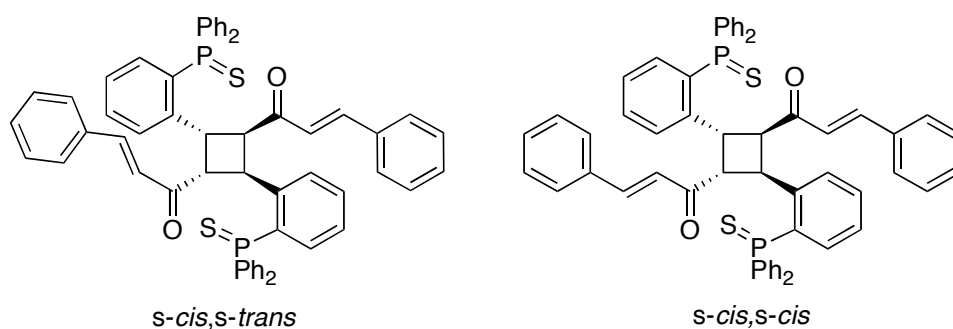


Figure 11: Conformers of the cycloadduct, **206**.

Single needle-like crystals of **206** were grown from CH_2Cl_2 layered with Et_2O . However, these crystals were unsuitable for X-ray diffraction and disintegrated on removal from the mother liquor. The observation of colourless needle crystals compared to the yellow blocks of the starting material could indicate that a different polymorph is formed on the recrystallisation of the cycloadduct **206**, from that formed during the SCSC reaction. This could be the limiting factor in the reaction reaching 100% conversion in the single-crystal.

The $[\pi 2s + \pi 2s]$ cycloaddition was also followed by powder X-ray diffraction, using the same irradiation source as for the solid-state NMR experiments. A simulation of the powder X-ray diffraction pattern from the crystal structures of monodbaTHIOPHOS **149** and the crystal at 81% conversion indicated that the changes in the powder diffraction pattern would be observable (see Appendix 6). This was found to be the case, see Figure 12. The simulated and observed diffraction patterns matched quite well, suggesting that the reaction does not undergo polymorphism in the powder samples. A sample of monodbaTHIOPHOS **149** was irradiated whilst being monitored by powder X-ray diffraction. The majority of the changes occurred in the first 10 h (Figure 13). The sample quality reduces on irradiation as shown by the broader peaks after 16 h and the lack of clear signals above 25° (Figure 12). This is unsurprising considering the observations from several of the single crystal experiments, which showed the breakdown of long-range order within the crystals upon irradiation.

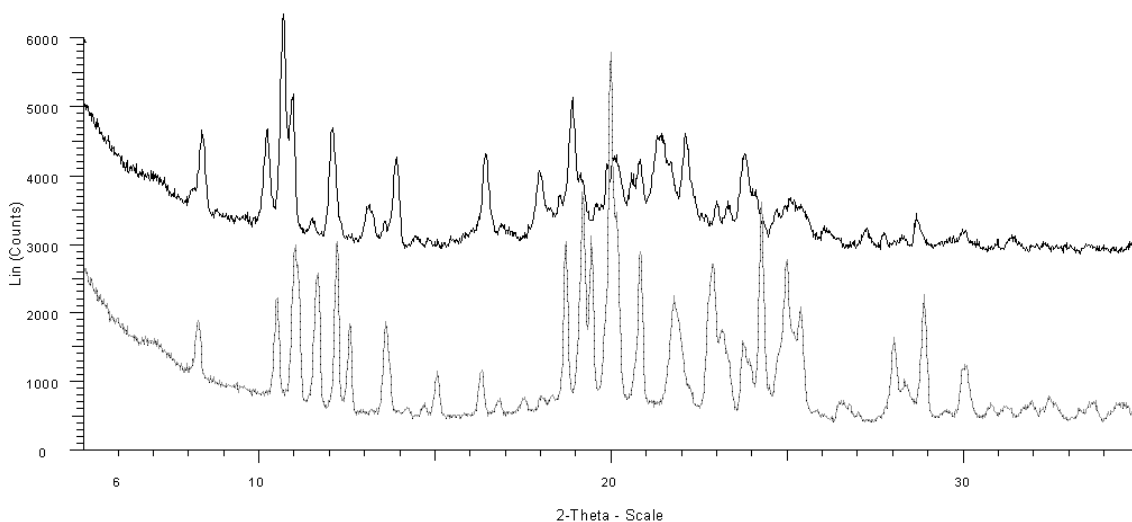


Figure 12: PXRD patterns monodbaTHIOPHOS **149 before irradiation (bottom) and after 16 h (top) (300 K).**

We wished to obtain information about the rate of the reaction and the effect of temperature. The biggest changes occurred in the first few hours of the reaction. The quality of the crystals meant that a 2θ scan from $0-35^\circ$ took ~ 20 min. To obtain more data along the time domain we focused on a smaller scan width of 2θ ($18.0-19.6^\circ$, ~ 3 min per scan), and repeated the experiment at 300 and 240 K (Figure 14-Figure 16). The change in the intensities of two peaks, $2\theta = 18.8$ and 19.4° , was normalised according to the following formula where: α = normalised intensity, I_t = intensity at a specified time, I_0 = intensity of monodbaTHIOPHOS **149**, I_∞ = intensity after 16 h.

$$\alpha = (I_t - I_0)/(I_\infty - I_0)$$

The normalised intensity, α , was plotted against time, to give an indication of the relative rate of reaction at each temperature.

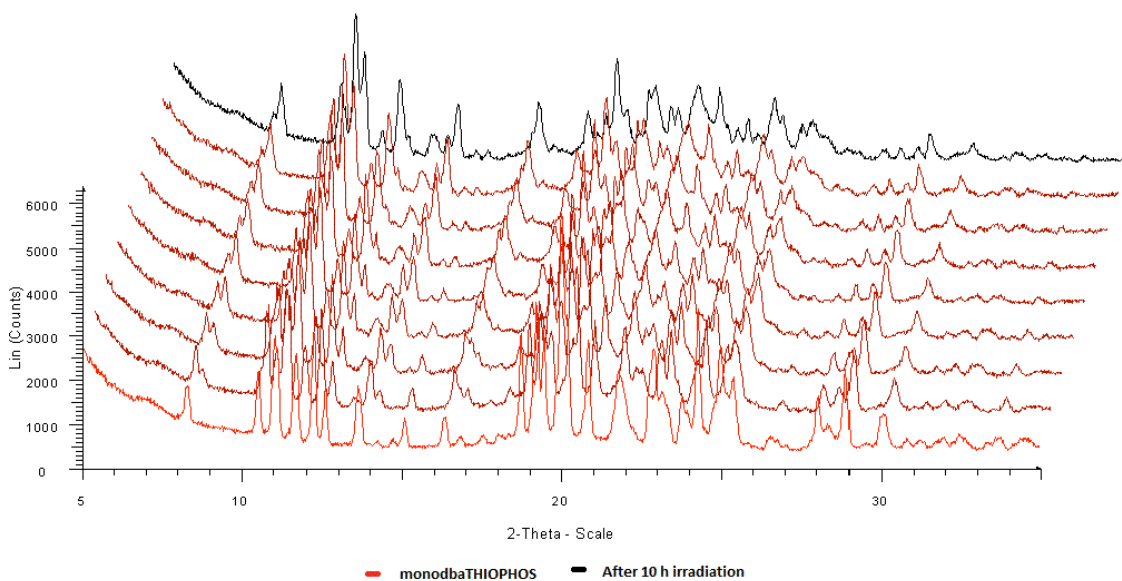


Figure 13: PXR D patterns of monodbaTHIOPHOS 149 on irradiation.

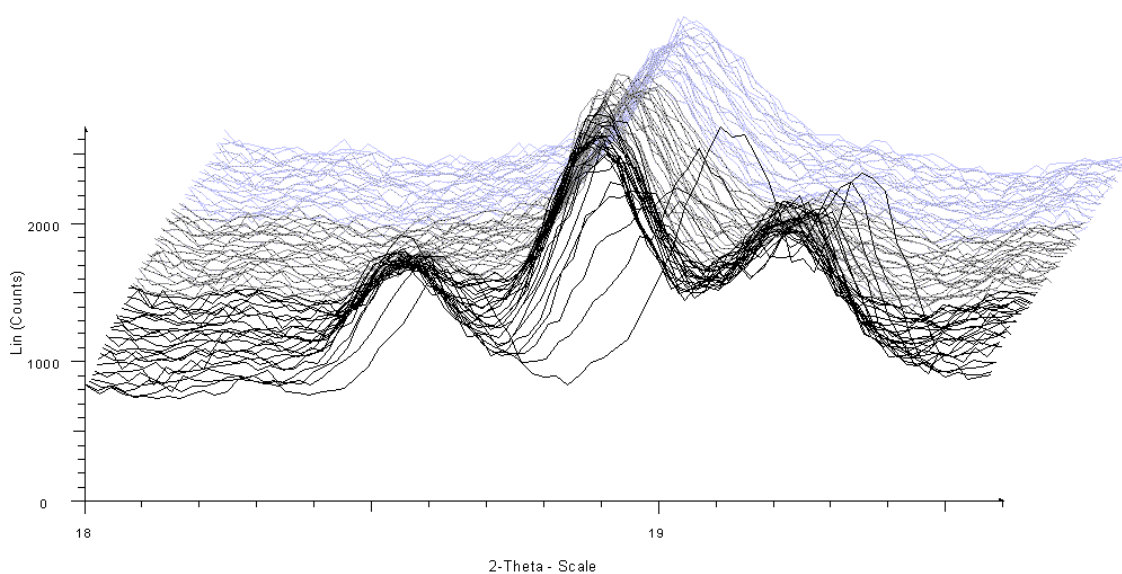


Figure 14: PXR D pattern for the 2θ range used for kinetics (300 K).

From the overall diffraction pattern between $18-19.6^\circ$ the reaction appears to take longer at lower temperatures (Figure 15 vs. Figure 16). This is certainly borne out by the normalised data for the peak at 18.8° . At 300 K, the change in intensity has stopped after 2.5 h, whilst at 240 K the change was almost 3.5 times slower taking 8.5 h to reach completion. However, when compared with the solid-state NMR spectroscopic data it is clear that the reaction had not reached completion after 2.5 h at 298 K. As well the data from the peak at 19.4° shows no change in rate on changing the temperature.

These results clearly indicate that care must be taken when following the reaction by powder X-ray diffraction. Only looking at a couple of peaks can give misleading information on what is happening in the bulk material. This is because each peak is associated with certain reflections, thus if they do not change much over the course of the reaction, or are changing independently of the reaction centre the information they give may not be directly relevant.

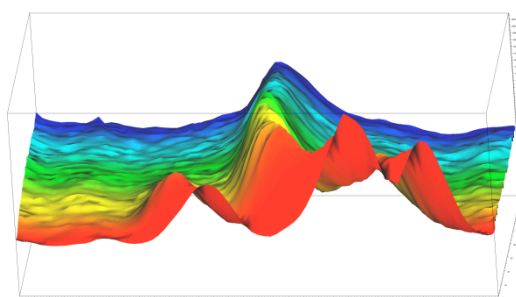


Figure 15: 300 K

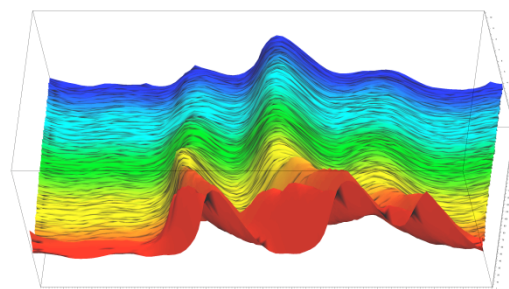


Figure 16: 240 K

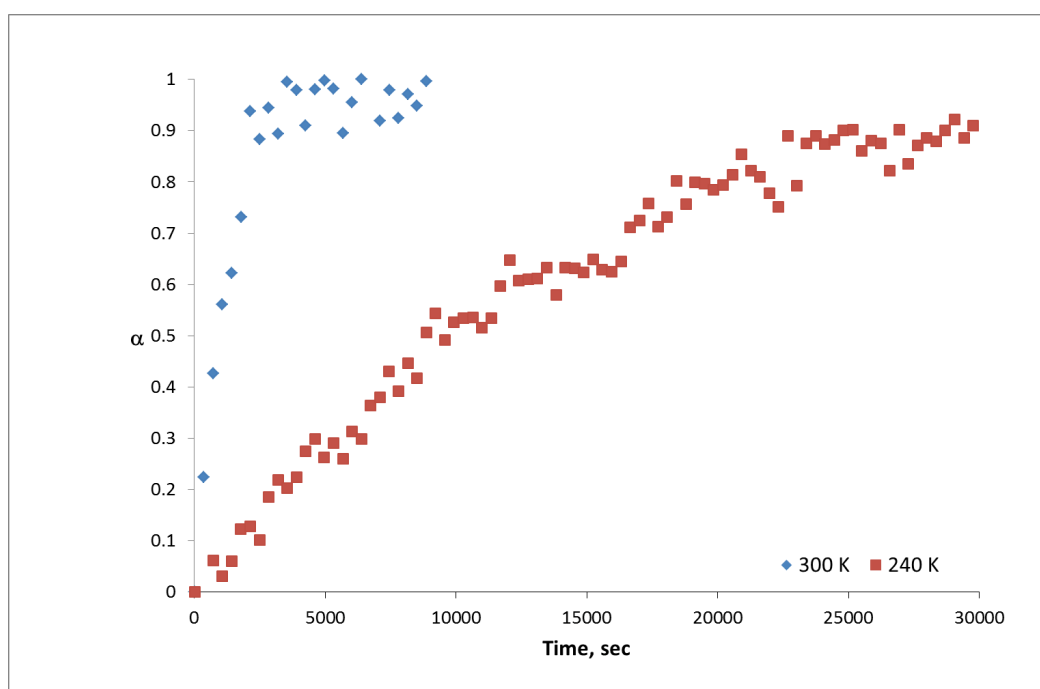


Figure 17: Plot of the normalised PXRD intensities for the peak at $2\theta = 18.8^\circ$ against time, at both 240 K and 300 K.

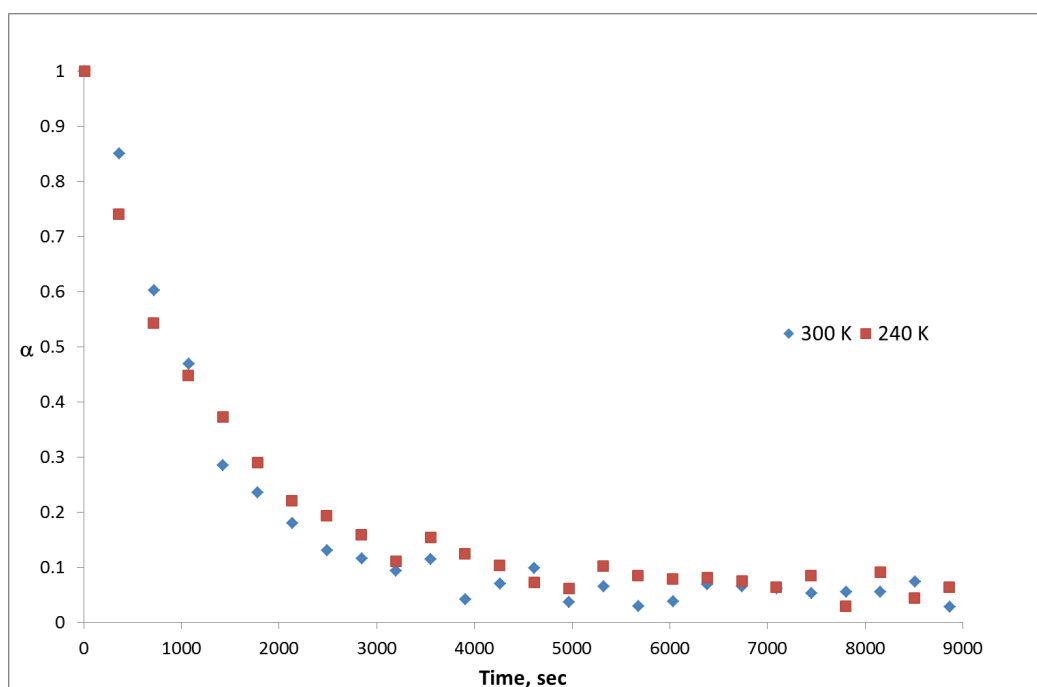


Figure 18: Plot of the normalised PXRD intensities for the peak at $2\theta = 19.4^\circ$ against time, at both 240 K and 300 K.

5.5 Summary

An unexpected photochemical $[\pi 2s + \pi 2s]$ cycloaddition of monodbaTHIOPHOS **149** to the cycloadduct **206** was observed. Further studies by single crystal X-ray diffraction showed that the reaction reached 70% conversion in the single crystal, when either UV light from LEDs (400 nm) or two-photon excitation methods were used. The reaction was found to be a topotactic SCSC transformation up to conversions up to 70%. After this point it is assumed that the crystal needs to disintegrate to reach higher conversions (Step 3 in Kaupp's general mechanism, see section 5.2.3). However, crystals exposed to low-level ambient light over a period of weeks show greater conversions (81%). We propose that 100% conversions would be reached, whilst retaining the crystal integrity, if low intensity tail-end radiation was used over extended periods of time. When the crystals are irradiated in the powder then 100% conversion is obtained within 2 days. The reaction was followed using both solid-state NMR and powder X-ray diffraction techniques. The solid-state NMR spectroscopic analysis revealed a number of intermediates in the reaction, presumably due to the isomerisation and cycloaddition processes that are occurring.

On a different note, the observation of a solid-state reaction and the subsequent investigation, has opened my eyes to a whole new area of chemistry. It is an area often

ignored by synthetic organic chemists despite the complementary activities that can be obtained.

5.6 Future Work

It is still unclear how the reaction progresses in the solid-state in particular with reference to the multiple carbonyl peaks observed by the solid-state NMR spectroscopic analysis. Further solid-state NMR experiments with ^{13}C labelled monodbaTHIOPHOS **149** (either the carbonyl or double bond carbons) could help elucidate the intermediates formed. If larger crystals can be grown, it is also possible that AFM experiments may reveal any long-range interactions that are occurring, giving a greater insight into the reaction mechanism. The results obtained so far suggest that the reaction kinetics and activation parameters of the SCSC transformation could be obtained.⁴⁵ Our studies so far show at least two processes are occurring in the crystal, namely the $[\pi 2s+\pi 2s]$ cycloaddition and the isomerisation around the enone single bond. Therefore we do not expect the reaction to be first-order (indeed treatment of the data as first order does not reveal a straight line for $\ln[\mathbf{149}]$ vs. time), but instead it is expected that more complicated kinetics will be observed. The kinetics will also be affected by the penetration of the light which may change over the course of the reaction, and the decrease in the number of molecules available as the reaction approaches 100% conversion.

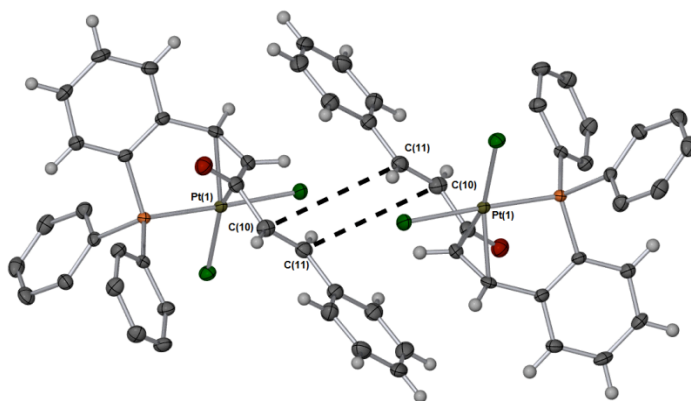


Figure 19: π - π stacking in $[\text{cis}\{-\{\text{PtCl}_2(\text{s-cis,s-trans-monodbaPHOS})\}\}]$ (177).

On a more general note, it appears that the bulky group on one-side of the dba backbone leads to crystal packing that places one of the double bonds close together, an observation that may be exploited in crystal engineering. This has also been seen in other compounds in our laboratory including the platinum(II) complex of monodbaPHOS, **177** (Figure 19).

Further work could investigate the reversibility of the cycloaddition, with the view to investigating molecular switches. In particular, the photochemistry of the metal complexes of monodbaTHIOPHOS **149** and monodbaPHOS **128** could be explored. It would also be interesting to see if other polymorphs of monodbaTHIOPHOS **149** formed and to investigate their photoreactivity. If the other double bond was also aligned for cycloaddition, it could lead to the formation of new polymers (Figure 20). It is possible the phosphine sulfides could then be used to coordinate metals to give different material applications, *e.g.* stabilise Pd nanoparticles for solid-supported catalysis.

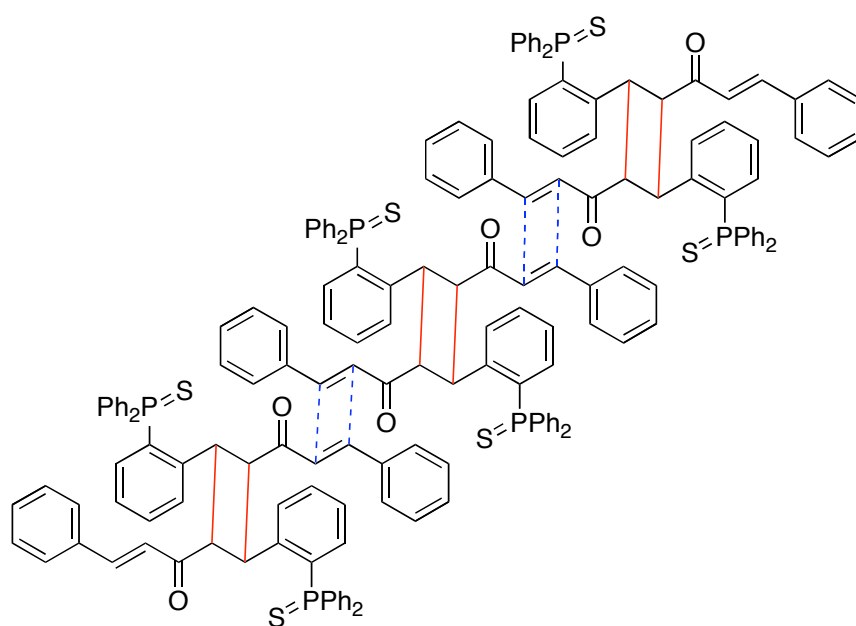


Figure 20: Hypothetical 2D polymer. Red lines indicate $[\pi2s+\pi2s]$ cycloaddition already observed.

5.7 Experimental

5.7.1 General information

NMR spectra were obtained in the solvent indicated, using a JEOL ECX400 or JEOL ECS400 spectrometer (400MHz for ^1H , 100 MHz for ^{13}C and 162 MHz for ^{31}P). Chemical shifts were referenced to the residual solvent of the deuterated solvent used (CHCl_3 $\delta = 7.26$ and 77.16 , CDHCl_2 $\delta = 5.31$ and 53.80 , ^1H and ^{13}C respectively). All ^{13}C NMR spectra were obtained with ^1H decoupling. ^{31}P NMR spectra were externally referenced to 85% H_3PO_4 , and obtained with ^1H decoupling. For ^{13}C NMR spectra the coupling constants are quoted to ± 1 Hz. For the ^1H NMR spectra the resolution varies from ± 0.15 to ± 0.5 Hz; the coupling constants have been quoted to ± 0.5 Hz in all cases for consistency. NMR spectra were processed using MestreNova software. Melting points were recorded using a Stuart digital SMP3 machine. IR spectroscopy was undertaken using a Jasco/MIRacle FT/IR-4100typeA spectrometer on the solid compounds, or KBr IR spectra were obtained on a spectrometer. The relative intensities of the peaks are denoted by (s) = strong, (m) = medium and (w) = weak, whilst (br) is used to describe broad peaks. MS spectra were measured using a Bruker Daltronics microTOF machine with electrospray ionisation (ESI) or on a Thermo LCQ using electrospray ionisation, with < 5 ppm error recorded for all HRMS samples. UV-visible spectra were recorded using a JASCO V-560 using quartz cells (1 cm path length). Solid-state UV-visible spectra were recorded using JASCO ISV-469 instrument. Elemental analysis was carried out on an Exeter Analytical CE-440 Elemental Analyser. Room temperature was between 13 - 25 $^\circ\text{C}$.

5.7.2. Synthesis

For the synthesis of MonodbaTHIOPHOS, **137**, see Chapter 2.6.2. Characterisation data is included below for convenience:

M.p. 199 - 200 $^\circ\text{C}$. ^1H NMR (400 MHz, CD_2Cl_2) δ 8.41 (dd, $^3J_{\text{HH}} = 16.0$ Hz, $J = 1.0$ Hz, 1H), 7.89-7.77 (m, 5H), 7.64-7.39 (m, 13H), 7.33 (apparent tdd, $J = 7.5$, 2.5, 1.0 Hz, 1H), 7.06 (dddd, $J_{\text{HP}} = 14.5$ Hz, $J_{\text{HH}} = 8.0$, 1.5, 0.5 Hz, 1H), 6.90 (d, $^3J_{\text{HH}} = 16.0$ Hz, 1H), 6.61 (d, $^3J_{\text{HH}} = 16.0$ Hz, 1H); ^{13}C NMR (100 MHz, CD_2Cl_2) δ 189.4, 143.0, 141.9

(d, $J_{CP} = 8$ Hz), 138.8 (d, $J_{CP} = 8$ Hz), 135.3, 134.0 (d, $^1J_{CP} = 83$ Hz), 133.4 (d, $J_{CP} = 11$ Hz), 132.7 (d, $J_{CP} = 11$ Hz), 132.4 (d, $J_{CP} = 3$ Hz), 132.3 (d, $^1J_{CP} = 85$ Hz), 132.2 (d, $J_{CP} = 3$ Hz), 130.7, 129.7 (d, $J_{CP} = 12$ Hz), 129.2, 129.2, 129.0 (d, $J_{CP} = 13$ Hz), 128.8 (d, $J_{CP} = 9$ Hz), 128.7, 123.4; ^{31}P NMR (162 MHz, CD_2Cl_2) δ 42.14 (s); HRMS (ESI) m/z 451.1285 $[\text{MH}]^+$ (calculated for $\text{C}_{29}\text{H}_{24}\text{OPS}$: 451.1280); LRMS (ESI) m/z (rel.%) 473 $[\text{MNa}]^+$ (20), 451 $[\text{MH}]^+$ (100), 346 (7); IR (ATR, ν cm^{-1}): 3057 (w), 1653 (m), 1593 (m), 1436 (m), 1331 (br, m), 1182 (br, m), 1096 (s), 984 (m), 764 (s), 749 (m), 708 (s), 689 (s), 636 (s); UV-vis (DCM) λ_{max} nm: 306 ($\epsilon = 4218$ $\text{mol}^{-1}\text{dm}^3\text{cm}^{-1}$); UV-Vis (solid) λ_{max} nm: 289 (br shoulder to 450); Anal. Calcd. for $\text{C}_{29}\text{H}_{23}\text{OPS}$ (450) C 77.31, H 5.15; Observed C 77.10, H 5.14.

Yellow block crystals suitable for X-ray crystallography were grown from a solution of **137** in CH_2Cl_2 layered with Et_2O in the dark (ijf0909m). An earlier crystal not grown in the dark was found to be 81% photo-dimer **206** (ijf0902). This crystal was exposed to stray external winter sunlight over 3 weeks.

[2+2] Intermolecular cycloaddition product, **206**

Compound **4** was left as a solid in a clear colourless glass flask for two months under ambient conditions (*i.e.* exposed to stray external sunlight and fluorescent light). The product was obtained as a white solid (>99% conversion to a single product determined by ^1H NMR spectroscopy). M.p. >225 $^\circ\text{C}_{(\text{dec.})}$. ^1H NMR (400 MHz, CDCl_3) δ 7.88-7.78 (m, 4H), 7.76-7.67 (m, 4H), 7.54-7.44 (m, 12H), 7.43-7.38 (m, 4H), 7.37-7.23 (m, 10H), 7.10 (d, $^3J_{\text{HH}} = 16.0$ Hz, 2H), 6.96-6.89 (m, 2H), 6.86 (d, $^3J_{\text{HH}} = 16.0$ Hz, 2H), 6.68 (ddd, $J_{\text{HP}} = 15.0$ Hz, $J_{\text{HH}} = 8.0, 1.0$ Hz, 2H), 5.44 (ddd, $J = \text{Hz}$, 2H), 4.34 (dd, $J = 10.5, 7.5$ Hz, 2H); ^{13}C NMR (100 MHz, CDCl_3) δ 196.9 (C=O), 142.9 (d, $J_{CP} = 9$ Hz, 4°), 142.1 (C=C), 135.3 (4°), 133.5 (d, $^1J_{CP} = 85$ Hz, ipso-C), 133.1 (d, $J_{CP} = 12$ Hz), 132.8 (d, $J_{CP} = 10$ Hz), 132.2 (d, $^1J_{CP} = 84$ Hz, ipso-C), 132.2 (d, $J_{CP} = 11$ Hz), 132.0 (d, $J_{CP} = 3$ Hz), 132.0 (d, $J_{CP} = 3$ Hz), 131.9 (d, $^1J_{CP} = 85$ Hz, ipso-C), 131.5 (d, $J_{CP} = 3$ Hz), 129.9, 129.7 (d, $J_{CP} = 10$ Hz), 128.8 (d, $J_{CP} = 13$ Hz), 128.70, 128.69, 128.6 (d, $J_P = 12$ Hz), 126.4 (d, $J_{CP} = 13$ Hz), 125.7 (C=C), 54.0 (cyclobutane), 39.9 (d, $J_{CP} = 7$ Hz, cyclobutane); ^{31}P NMR (162 MHz, CDCl_3) δ 43.19 (s); HRMS (ESI) m/z 901.2449 $[\text{MH}]^+$ (calculated for $\text{C}_{58}\text{H}_{47}\text{O}_2\text{P}_2\text{S}_2$: 901.2487); IR (KBr, ν cm^{-1}): 3055(m), 2919 (w), 1682 (m), 1650 (w), 1609 (s), 1575 (m), 1480 (w), 1448 (w), 1437 (s), 1329 (m), 1128

(w), 1099 (s), 1079 (m), 1067 (m), 770 (w), 748 (m), 712 (s), 691 (s), 636 (s), 614 (m), 532 (w), 516 (m); UV-vis (CH₂Cl₂) λ_{max} nm: 300 ($\epsilon = 56471 \text{ mol}^{-1} \text{ dm}^3 \text{ cm}^{-1}$).

Colourless needle crystals unsuitable for X-ray diffraction were obtained from CH₂Cl₂ layered with Et₂O.

5.7.3 Photochemistry experiments

5.7.3.1 Single crystal XRD experiments

Single X-ray diffraction data were collected at 110 K in the dark on an Oxford diffractometer or on a Bruker Smart Apex diffractometer with Mo-K α radiation ($\lambda = 0.71073 \text{ \AA}$) using a SMART CCD camera unless otherwise stated. Diffractometer control, data collection and initial unit cell determination was performed using “SMART”.⁴⁶ Frame integration and unit-cell refinement software was carried out with “SAINT+”.⁴⁷ Absorption corrections were applied by ADABS (v2.10, Sheldrick). Structures were solved by direct methods using SHELXS-97⁴⁸ and refined by full-matrix least squares using SHELXL-97. All non-hydrogen atoms were refined anisotropically. Hydrogen atoms were placed using a “riding model” and included in the refinement at calculated positions. Due to the disorder in the irradiated crystals restraints and constraints were applied, depending on the refinement requirements. The following possibilities were used: AFIX 66, ISOR, EADP, SADI.

The full diffraction dataset for a single crystal of monodbaTHIOPHOS **149** was obtained (ijf0909m). The crystal was then exposed to light from an incandescent bulb whilst at 110 K for 2 h. The full diffraction dataset was then collected again. The solution showed that no change had occurred. The crystal was then exposed to light from a fluorescent strip light for 48 h at room temperature. The diffraction data was then collected at 110 K and showed that 31% of the crystal had converted to the [2+2] photo-dimer **206** (ijf0911m). To see if the conversion could be increased the crystal was left in sunlight for 1 week. Unfortunately, the crystal was no longer of sufficient quality to diffract.

Table 6 Single crystal structures.

Compound reference	ijf0909m (149)	ijf0911m (149 and 206)	ijf0902 (149 and 206)
Chemical formula	C ₂₉ H ₂₃ OPS	C ₂₉ H ₂₃ OPS	0.81(C ₅₈ H ₄₆ O ₂ P ₂ S ₂) •0.38(C ₂₉ H ₂₃ OPS)
Formula Mass	450.50	450.50	901.03
Crystal system	Monoclinic	Monoclinic	Monoclinic
<i>a</i> /Å	9.4829(7)	9.3900(7)	9.39010(10)
<i>b</i> /Å	17.0177(13)	17.1409(14)	17.15340(10)
<i>c</i> /Å	14.5741(11)	14.6595(12)	14.8607(2)
α /°	90.00	90.00	90.00
β /°	101.8810(10)	102.038(2)	102.3283(10)
γ /°	90.00	90.00	90.00
Unit cell volume/Å ³	2301.5(3)	2307.6(3)	2338.45(4)
Temperature/K	110(2)	110(2)	120(2)
Space group	<i>P</i> 2(1)/ <i>n</i>	<i>P</i> 2(1)/ <i>n</i>	<i>P</i> 2(1)/ <i>n</i>
No. of formula units per unit cell, <i>Z</i>	4	4	2
No. of reflections measured	23431	23321	21056
No. of independent reflections	5718	5737	4254
<i>R</i> _{int}	0.0248	0.0259	0.0287
Final <i>R</i> _{<i>I</i>} values (<i>I</i> > 2σ(<i>I</i>))	0.0360	0.0421	0.0395
Final <i>wR</i> (<i>F</i> ²) values (<i>I</i> > 2σ(<i>I</i>))	0.0940	0.1043	0.0981
Final <i>R</i> _{<i>I</i>} values (all data)	0.0425	0.0548	0.0468
Final <i>wR</i> (<i>F</i> ²) values (all data)	0.0991	0.1126	0.1022

ijf0911: Mixture of monodbaTHIOPHOS, **149**, and [2+2] photo-dimer, **206**, with a refined ratio of 0.689:0.311(3). ADP of pairs of disordered atom constrained to be equal as follows: C1 C1A, C2 C2A, C3 C3A, C4 C4A, C5 C5A, C6 C6A, C12A C12, C13A C13, C14 C14A, C15A C15, C16A C16, C17A C17. Same distance restraint on C7-C6 & C7A-C6A; C7-C8 & C7A-C8A. Rigid bond restraint on C9-C8; C8A-C9A-C10A. Isotropic ADP restraint on C8A C7A C9 C9A C10A O1 O1A.

Follow-up experiments were carried out by Professor Paul Raithby at the University of Bath:

The data were collected on an Oxford Diffraction Gemini A Ultra CCD Diffractometer with Mo-Kα radiation ($\lambda = 0.71073 \text{ \AA}$) fitted with an Oxford Cryojet crystal cooling apparatus. The crystal of monodbaTHIOPHOS **149** was placed on the diffractometer at 180 K and between the data sets the crystal was irradiated for 2 h with 6 400 nm LEDs placed at a distance of 1 cm from the crystal.⁴⁹

A range of experiments, assessing the effect of temperature, were carried out. Crystals of monodbaTHIOPHOS **149** were irradiated for 12-16 h, at the required temperature, followed by collection of the diffraction data.

5.7.3.2 2-Photon irradiation experiments:

Non-resonant coherent two-photon absorption was achieved using the fundamental output of a single dye laser (Radiant Narrowscan, DCM/Rhodamine B) pumped by the second harmonic of a Nd:YAG laser (Continuum Surelite III) generating 5 ns pulses at 10 Hz, under the direction of Dr. Martin Cockett (University of York). The energy of the laser pre-amplifier was measured at 0.5 mJ per pulse (effectively 5 mW). With both preamplifier and amplifier on, the energy increased to between 10 and 13 mJ per pulse (*ca.* 100 to 130 mW).

Diffraction data were collected at 110 K on an Oxford Diffraction SuperNova diffractometer with Mo-K α radiation ($\lambda = 0.71073 \text{ \AA}$) using a EOS CCD camera. The crystal was cooled with an Oxford Instruments Cryojet. Diffractometer control, data collection, initial unit cell determination, frame integration and unit-cell refinement was carried out with “Crysalis”.⁵⁰ Empirical absorption correction using spherical harmonics, implemented in SCALE3 ABSPACK scaling algorithm.⁵¹ OLEX2⁵² was used for overall structure solution, refinement and preparation of computer graphics and publication data. Within OLEX2, the algorithms used for structure solution were “direct methods”, using the “A short history of SHELX (Sheldrick, 2007)/Bruker”. Refinement by full-matrix least-squares used the SHELXL-97⁵³ algorithm within OLEX2.⁵⁴ All non-hydrogen atoms were refined anisotropically. Hydrogen atoms were placed using a “riding model” and included in the refinement at calculated positions. Due to the disorder in the irradiated crystals, restraints and constraints were applied, depending on the refinement requirements. The following were used in those cases: AFIX 66, ISOR, EADP, SADI.

Experiment 1:

The full diffraction dataset of a single crystal of monodbaTHIOPHOS, **149**, was collected at 110 K (ijf1027). The crystal was then exposed at room temperature to 605 nm radiation at 0.5 mJ per pulse for 10 min. The diffraction data was then obtained at

110 K (ijf1028). No change was observed. The energy was then increased to 13 mJ pulse and the crystal exposed to 605 nm for 25 min. The XRD data was then collected (ijf1029); the data was not of high quality as the crystal split. A rough estimation of the percentage converted to the [2+2] photo-dimer **206** was 66%. As the crystal had split, the pieces were divided and one of the pieces was exposed to further irradiation at the higher output energies (605 nm, 15 min one side and then rotated 180° and exposed for a further 15 min). The XRD data was obtained and solved showing that 71% conversion to [2+2] photo-dimer **206** was recorded (ijf1030).

Experiment 2:

The unit cell of a single crystal of monodbaTHIOPHOS, **149**, was determined at 110 K ($a = 9.482(4)$, $b = 17.025(4)$, $c = 14.501(3)$; $\alpha = 90^\circ$, $\beta = 102.12(3)^\circ$, $\gamma = 90^\circ$). The crystal was irradiated at 605 nm at the higher output energies for 1 h, rotating the crystal 180° after 30 min. The crystal split and the remaining pieces were too small to diffract well enough for further data collection.

Experiment 3:

The unit cell of a single crystal of monodbaTHIOPHOS, **149**, was determined at 110 K ($a = 9.492(2)$, $b = 16.998(7)$, $c = 14.578(4)$; $\alpha = 90^\circ$, $\beta = 101.84(2)^\circ$, $\gamma = 90^\circ$). The crystal was then irradiated with 605 nm light at the higher output energies at ambient temperature for 20 min, whilst rotating on a mechanical stirrer (Citeno AQt9, F.H.P. Motors) at the lowest speed. The diffraction data were obtained at 110K and the crystal structure solved showing that 25% of the crystal had converted to the [2+2] photo-dimer **206** (ijf1038).

Table 7 2-Photon transformations

Compound reference	ijf1027	ijf1028	ijf1029	ijf1030	ijf1038
Chemical formula	C ₂₉ H ₂₃ OPS	C ₂₉ H ₂₃ OPS	C ₂₉ H ₂₃ OPS	C ₂₉ H ₂₃ OPS	C ₂₉ H ₂₃ OPS
Formula Mass	450.50	450.50	450.50	450.50	450.50
Crystal system					
<i>a</i> /Å	9.4598(10)	9.4904(3)	9.3365(5)	9.3733(3)	9.3833(3)
<i>b</i> /Å	16.9974(14)	17.0028(5)	17.1396(6)	17.2097(5)	17.1058(4)
<i>c</i> /Å	14.5643(13)	14.5622(4)	14.7354(13)	14.8077(5)	14.6168(3)
<i>α</i> /°	90.00	90.00	90.00	90.00	90.00
<i>β</i> /°	101.853(9)	101.951(3)	102.311(8)	102.379(3)	102.040(3)
<i>γ</i> /°	90.00	90.00	90.00	90.00	90.00
Unit cell volume/Å ³	2291.9(4)	2298.89(11)	2303.8(2)	2333.12(13)	2294.51(10)
Temperature/K	110.0	110.0	110.0	110.0	110.0
Space group	<i>P</i> 2 ₁ / <i>n</i>	<i>P</i> 2 ₁ / <i>n</i>	<i>P</i> 2 ₁ / <i>n</i>	<i>P</i> 2 ₁ / <i>n</i>	<i>P</i> 2 ₁ / <i>n</i>
No. of formula units per unit cell, <i>Z</i>	4	4	4	4	4
No. of reflections measured	7539	7096	4050	9725	9051
No. of independent reflections	4017	4020	3037	5517	5202
<i>R</i> _{int}	0.0225	0.0199	0.0229	0.0239	0.0257
Final <i>R</i> _{<i>I</i>} values (<i>I</i> > 2σ(<i>I</i>))	0.0379	0.0377	0.0639	0.0640	0.0600
Final <i>wR</i> (<i>F</i> ²) values (<i>I</i> > 2σ(<i>I</i>))	0.0826	0.0836	0.1349	0.1338	0.1346
Final <i>R</i> _{<i>I</i>} values (all data)	0.0465	0.0461	0.0850	0.0857	0.0836
Final <i>wR</i> (<i>F</i> ²) values (all data)	0.0887	0.0890	0.1485	0.1463	0.1517

ijf1029: The crystal contained a disordered mixture of monodbaTHIOPHOS, **149**, and [2+2] photo-dimer, **206**. The ratio of these compounds refined to 0.340:0.660(4). The ADP of the following pairs of atoms were constrained to be equal: O1 O1A, C1A C1, C2 C2A, C3A C3, C4A C4, C5A C5, C6A C6, C9A C9, C12A C12, C13A C13, C14A C14, C15A C15, C16A C16, C17A C17. The ADP of the following atoms were restrained to be isotropic C1 C1A C6 C6A C7 C7A C8 C8A O1 O1A. Rigid bond restraints were applied to C10-C11, C7-C8 & C7A-C8A. Two phenyl rings (C12-C17 & C12A-C17A) were constrained as regular hexagons with a C-C bond length of 1.39 Å.

ijf1030: The crystal contained a disordered mixture of monodbaTHIOPHOS, **149**, and [2+2] photo-dimer, **206**. The ratio of these compounds refined to 0.293:0.707(3). The ADP of the following pairs of atoms were constrained to be equal: O1 O1A, C1A C1, C2 C2A, C3A C3, C8a C8, C9A C9, C12A C12, C14A C14, C15A C15, C16A C16,

C17A C17. The ADP of the following atoms were restrained to be isotropic C11 C13 C13A. The bond lengths of C10-C11 & C10A-C11A were restrained to be equal. The bond lengths of C11-C12 & C11A-C12A were restrained to be equal. Two phenyl rings (C12-C17 & C12A-C17A) were constrained to be regular hexagons with a C-C bond length of 1.39 Å.

ijf1038: The crystal contained a disordered mixture of monodbaTHIOPHOS **149** and [2+2] photo-dimer **206**. The ratio of these compounds refined to 0.752:0.248(2) (occupancy). The ADP of the following pairs of atoms were constrained to be equal: O1 O1A, C1A C1, C2 C2A, C3A C3, C4A C4, C6A C6, C7 C7A, C8 C8A, C9A C9, C10, C10A, C11 C11A, C12A C12, C13A C13, C14A C14, C15A C15, C16A C16, C17A C17. The ADP of the following atoms were restrained to be isotropic C9 C9A. The bond lengths C10-C11 & C10A-C11A were restrained to be equal. The bond lengths C11-C12 & C11A-C12A were restrained to be equal. Two phenyl rings (C12-C17 & C12A-C17A) were constrained to be regular hexagons with a C-C bond length of 1.39 Å.

5.7.3.3 Powder XRD experiments:

This study was carried out in collaboration with Dr. Hazel Sparkes at the University of Durham:

Powder X-ray diffraction data were collected on Bruker D8 powder diffractometers using Cu K α radiation (1.5406 Å). Data were collected at 300 K ($2\theta = 0-35^\circ$) and at 240 and 300 K ($2\theta = 18-19.6^\circ$), using an Oxford Cryostream Pheonix to maintain the temperature over the run.

The samples for the PXRD experiments were prepared as follows. MonodbaTHIOPHOS **149** obtained by crystallisation from CH₂Cl₂:Et₂O (1:3, v/v) was ground to a fine powder using a pestle and mortar, and the material sieved (120 μm) onto a silicon disc coated in Vaseline. An initial PXRD scan was obtained in the dark. The sample was then irradiated using a Xenon lamp (Bentham 150W Xe lamp, model IL7), whilst recording the PXRD data.

5.7.3.4 Solid-state NMR experiments:

This study was carried out in collaboration with Dr. Hazel Sparkes at the University of Durham:

One batch of monodbaTHIOPHOS **149** (200 mg) was irradiated using a Xenon lamp (Bentham 150W Xe lamp, model IL7) and agitating the mixture every 30 min. After 2.5 h and 5 h samples (100 mg) were removed from the light for solid-state ^{13}C NMR spectroscopic analysis. A second batch was irradiated in the same manner for 43 h. The samples were submitted to the Durham Solid-State Research Service for analysis. The spectra were obtained on a Varian VNMRS spectrometer operating at 161.87 MHz (spin rate = 10000 Hz) for ^{31}P and 100.56 MHz (spin rate = 6800 Hz) for ^{13}C . A 4 mm probe was used for the ^{31}P measurements and a 6 mm probe for the ^{13}C . In the ^{13}C measurements the conditions used put a sideband over the ketone signal, so a TOSS sideband suppression experiment was used to reveal the ketone signal. Spectral referencing is with respect to 85% H_3PO_4 or neat trimethylsilane. All the spectra were obtained with a 120s recycle delay.

MonodbaTHIOPHOS 149: ^{13}C CPMAS NMR δ 188.6, 143.4, 139.7, 136.3, 131.9, 131.1, 129.7, 128.8, 127.6, 126.1, 121.5; Quaternary carbon environments were found by TPPM decoupling experiments δ 188.6 (C=O), 136.3, 132.4, 132.0, 129.6, 128.9; ^{31}P CPMAS NMR δ 39.82.

2.5 h: ^{13}C CPMAS NMR δ 197.2, 188.8, 186.3, 143.2, 138.9, 136.2, 131.2, 129.7, 126.8, 122.1, 54.2, 37.8; ^{31}P CPMAS NMR δ 39.86 (br, $\Delta V_{1/2} = 1.95$ ppm).

5 h: ^{13}C CPMAS NMR δ 197.4, 195.6, 186.2, 143.4, 138.8, 136.3, 131.3, 129.6, 126.9, 122.1, 53.2, 37.9; Quaternary carbon environments were found by TPPM decoupling experiments δ 197.4 (C=O), 195.7 (C=O), 188.9 (C=O), 186.1 (C=O), 143.4, 136.3, 134.2, 133.7, 131.7, 129.7; ^{31}P CPMAS NMR δ 43.19 (s), 40.18 (br s with a shoulder).

[2+2] Photo-dimer 206: ^{13}C CPMAS δ 195.7, 147.4, 143.5, 142.8, 141.5, 139.1, 134.3, 131.9, 130.6, 129.1, 125.1, 53.9, 37.4; Quaternary carbon environments were found by

TPPM decoupling experiments δ 195.6 (C=O), 147.5, 142.8, 134.3, 130.5, 129.4; ^{31}P CPMAS δ 43.22 (s), 41.76 (br s with a shoulder).

5.7.3.5 Solution state *in-situ* laser experiments:

This study was conducted with the assistance of Professor Simon Duckett and Mr. John Clarke (University of York). ^1H and ^{31}P NMR spectroscopy was carried out on a Bruker DRX 400 Advance fitted with an *in-situ* 325 nm cw 25 mW He-Cd laser as a light source.⁵⁵ Samples of monodbaTHIOPHOS, **149**, in CD_2Cl_2 (0.07 and \sim 0.25 M) were irradiated for 18 h at 298 K, whilst ^1H and ^{31}P NMR spectra were obtained every 20 minutes.

monodbaTHIOPHOS 149 (0.25 M): ^1H NMR (400 MHz, CD_2Cl_2) δ 8.43 (d, $J = 16.0$ Hz, 1H), 7.99-7.72 (m, 5H), 7.70-7.38 (m, 13H), 7.33 (apparent t, $J = 7.0$ Hz, 1H), 7.09 (dd, $J = 14.5, 8.0$ Hz, 1H), 6.92 (d, $J = 16.0$ Hz, 1H), 6.63 (d, $J = 16.0$ Hz, 1H); ^{31}P NMR (162 MHz, CD_2Cl_2) δ 41.11 (s).

10 h (0.25 M): ^1H NMR (400 MHz, CD_2Cl_2) δ 8.43 (d, $J = 16.0$ Hz, 1H), 8.30 (d, $J = 16.0$ Hz, 0.1H), 7.93-7.75 (m, 5.5H), 7.70-7.21 (m, 14.4H), 7.09 (dd, $J = 14.5, 8.0$ Hz, 1.1H), 6.92 (d, $J = 16.0$ Hz, 1H), 6.77 (d, $J = 12.5$ Hz, 0.1H), 6.63 (d, $J = 16.0$ Hz, 1H), 6.38 (d, $J = 16.0$ Hz, 0.1H), 6.05 (d, $J = 12.5$ Hz, 0.1H); ^{31}P NMR (162 MHz, CD_2Cl_2) δ 41.11 (s, 1P), 40.89 (s, 0.1P).

monodbaTHIOPHOS 149 (0.07 M): ^1H NMR (400 MHz, CD_2Cl_2) δ 8.39 (d, $J = 16.0$ Hz, 1H), 7.88-7.69 (m, 5H), 7.64-7.38 (m, 13H), 7.32 (ddd, $J = 7.5, 5.0, 1.5$ Hz, 1H), 7.06 (ddd, $J = 14.5, 8.0, 2.0$ Hz, 1H), 6.89 (d, $J = 16.0$ Hz, 1H), 6.60 (d, $J = 16.0$ Hz, 1H); ^{31}P NMR (162 MHz, CD_2Cl_2) δ 41.09 (s).

1h (0.07 M): ^1H NMR (400 MHz, CD_2Cl_2) δ 8.40 (d, $J = 16.0$ Hz, 1H), 7.90-7.75 (m, 5.9H), 7.62-7.38 (m, 16.3H), 7.37-7.20 (m, 2.8H), 7.13-6.99 (m, 1.3H), 6.89 (d, $J = 16.0$ Hz, 1H), 6.60 (d, $J = 16.0$ Hz, 1H), 6.52 (d, $J = 16.0$ Hz, 0.3H), 6.09 (d, $J = 12.0$ Hz, 0.3H); ^{31}P NMR (162 MHz, CD_2Cl_2) δ 41.13 (s, 0.3P), 41.09 (s, 1P).

15 h (0.07 M): ^1H NMR (400 MHz, CD_2Cl_2) δ 8.40 (d, $J = 16.0$ Hz, 1H), 8.27 (d, $J = 16.0$ Hz, 0.2H), 7.90-7.75 (m, 6H), 7.62-7.38 (m, 15H), 7.37-7.22 (m, 1.6H), 7.13-7.00 (m, 1.2H), 6.89 (d, $J = 16.0$ Hz, 1H), 6.76 (d, $J = 12.5$ Hz, 0.2H), 6.60 (d, $J = 16.0$ Hz, 1H), 6.36 (d, $J = 16.0$ Hz, 0.2H), 6.03 (d, $J = 12.5$ Hz, 0.2H); ^{31}P NMR (162 MHz, CD_2Cl_2) δ 41.09 (s, 1P), 40.87 (s, 0.2P).

5.8 References

- ¹ a) Dunitz, J. D.; Harris, K. D.; Johnston, R. L.; Kariuki, B. M.; MacLean, E. J.; Psallida, K.; Schweizer, W. B.; Tykwinski, R. R. *J. Am. Chem. Soc.* **1998**, *120*, 13274-13275. b) Cohen, P. S.; Cohen, S. M. *J. Chem. Edu.* **1996**, *73*, 883-886.
- ² Wöhler, F. *Ann. Phys.* **1828**, *88*, 253-256.
- ³ Kaupp, G.; Schmeyers, J.; Boy, J. *Chemosphere* **2001**, *43*, 55-61.
- ⁴ Cave, G. W. V.; Raston, C. L.; Scott, J. L. *Chem Commun.* **2001**, 2159-2169.
- ⁵ a) Natrajan, A.; Tsai, C. K.; Khan, S. I.; McCarren, P.; Houk, K. N.; Garcia-Garibay, M. A. *J. Am. Soc. Chem.* **2007**, *129*, 9846-9847. b) Trommsdorff, H. *Ann. Pharm.* **1834**, *11*, 190-207.
- ⁶ Anslyn, E. V.; Dougherty, D. A. *Modern Physical Organic Chemistry* **2006**, 935-1000, Sausalito: University Science Books.
- ⁷ Protti, S.; Dondi, D.; Fagnoni, M.; Albini, A. *Green Chem.* **2009**, *11*, 239-249.
- ⁸ a) Gorner, H.; Kuhn, H. J. *Advances in Photochemistry* **1995**, *19*, 1-117. b) Waldeck, D. H. *Chem. Rev.* **1991**, *91*, 415-436. c) Bushan, K. M.; Rao, G. V.; Soujanya, T.; Rao, V. J.; Saha, S.; Samanta, A. *J. Org. Chem.* **2001**, *66*, 681-688. d) Arai, T.; Tokumaru, K. *Chem. Rev.* **1993**, *93*, 23-39. e) Bao, J.; Weber, P. M. *J. Am. Chem. Soc.* **2011**, *133*, 4164-4167.
- ⁹ a) Natarajan, A.; Mague, J. T.; Venkatesan, K.; Arai, T.; Ramamurthy, V. *J. Org. Chem.* **2006**, *71*, 1055-1059. b) Kaupp, G. *Photochem. Photobiol.* **2002**, *76*, 590-595. c) Harada, J.; Ogawa, K. *J. Am. Chem. Soc.* **2001**, *123*, 10884-10888.
- ¹⁰ Saltiel, J.; Papadimitriou, D.; Krishna, T. S. R.; Huang, Z-N.; Krishnamoorthy, G.; Laohhasurayotin, S.; Clatk, R. J. *Angew. Chem., Int. Ed.* **2009**, *48*, 8082-8085.
- ¹¹ a) Schuster, D. I.; Lem, G.; Kaprinidis, N. A. *Chem. Rev.* **1993**, *93*, 3-22. b) Abe, M.; Terazawa, M.; Masuyama, A.; Hayashi, T. *Tetrahedron Lett.* **2006**, *47*, 2527-2530. c) Griesbeck, A. G.; Mauder, H.; Stratmueller, S. *Acc. Chem. Res.* **1994**, *27*, 70-75.
- ¹² Corey, E. J.; Bass, J. D.; LeManieu, R.; Mitra, R. B. *J. Am. Chem. Soc.* **1964**, *86*, 5570-5582.
- ¹³ a) Ischay, M. A.; Anzovino, M. E.; Du, J.; Yoon, T. P. *J. Am. Soc. Chem.* **2008**, *130*, 12886-12887. b) Chong, D.; Stewart, M.; Geiger, W. E. *J. Am. Chem. Soc.* **2009**, *131*, 7968-7969. c) Du, J.; Yoon, T. P. *J. Am. Chem. Soc.* **2009**, *131*, 14604-14605.

14 Topochemical is used here to describe reactions occurring under the control of the
crystal lattice, *i.e.* the organisation of the reactants controls the regio- and
stereochemistry of the products.

15 Kuapp, G. *Advances in Photochemistry* **1995**, *19*, 119-177.

16 Schmidt, G. M. J. *Pure Appl. Chem.*, **1971**, *27*, 647-678.

17 Thomas, J. M.; Williams, J. O. *Chem. Commun.* **1967**, 432-433.

18 Cohen, M. D. *Angew. Chem., Int. Ed.* **1975**, *14*, 386-393.

19 Gavezzotti, A. *J. Am. Chem. Soc.* **1983**, *105*, 5220-5225.

20 Mahon, M. F.; Raithby, P. R.; Sparkes, H. A. *CrystEngComm.* **2008**, *10*, 573-576.

21 a) Kaupp, G. *Int. J. Photoenergy*, 2001, *3*, 55-62. b) Kaupp, G. *Comprehensive
Supramolecular Chemistry* **1996**, *8*, 381-423.

22 a) Jones, W.; Nakanishi, H.; Theocharis, C. R.; and Thomas, J. M. *J. Chem. Soc.,
Chem. Comm.* **1980**, 610-611. b) Nakanishi, H.; Jones, W.; Thomas, J. M.;
Hursthouse, M. B.; Motevalli, M. *J. Chem. Soc., Chem. Comm.* **1980**, 611 -612.

23 Novak, K.; Enkelmann, V.; Wegne, G.; Wagener, K. B. *Angew. Chem., Int. Ed.*
1993, *32*, 1614-1616.

24 Abdelmoty, I.; Bucholz, V.; Di, L.; Guo, C.; Kowitz, K.; Enkelmann, V.; Wegner,
G.; Foxman, B. M. *Cryst. Growth Des.* **2005**, *5*, 2210-2217.

25 Halasz, I. *Cryst. Growth Des.* **2010**, *10*, 2817-2823.

26 Khan, M.; Brunklaus, G.; Enkelmann, V.; Spiess, H-W. *J. Am. Chem. Soc.* **2008**,
130, 1741-1748.

27 a) Nieuwendaal, R. C.; Bertmer, M.; Hayes, S. E. *J. Phys. Chem. B* **2008**, *112*,
12920-12926.

28 Examples include: *CrystEngComm*, RSC; *Crystal Growth and Design*, ACS; and
Crystal Engineering, Elsevier.

29 MacGillivray, L. R.; Papaefstathiou, G. S.; Friscic, T.; Hamilton, T. D.; Bucar, D-
K.; Chu, Q.; Varshney, D. B.; Georgiev, I. G. *Acc. Chem. Res.* **2008**, *41*, 280-291.

30 a) Peedikakkal, A. M. P.; Vittal, J. J. *Chem. Eur. J.* **2008**, *14*, 5329-5334. b)
Nagarathium, M.; Peedikakkal, A. M. P.; Vittal, J. J. *Chem. Commun.* **2008**,
5277-5288.

31 a) Toh, N. L.; Nagarathinam, M.; Vittal, J. J. *Angew. Chem., Int. Ed.* **2005**, *44*,
2237-2241. b) Barry, N. P. E.; Therrien, B. *Inorg. Chem. Comm.* **2009**, *12*, 465-
468.

- 32 Caronna, T.; Liantonio, R.; Logothetis, T. A.; Metrangolo, P.; Pilati, T.; Resnati, G. *J. Am. Chem. Soc.* **2004**, *126*, 4500-4501.
- 33 Akabori, S.; Habata, Y.; Nakazawa, M.; Yamada, Y.; Shindo, Y.; Sugimura, T.; Sato, S. *Bull. Chem. Soc. Jpn.* **1987**, *60*, 3453-3455.
- 34 Wu, L.; Jin, C.; Sun, X. *Biomacromolecules* **2011**, *12*, 235-241. For a general text on molecular switches see Feringa, B. L. *Molecular Switches* **2001**, Wiley-VCH:Weinheim
- 35 Turowska-Tyrk, I. *Chem. Phys.* **2003**, *288*, 241-247.
- 36 Green, B. S.; Schmidt, G. M. J. *Tetrahedron Lett.* **1970**, *11*, 4249-4252.
- 37 Desiraju, G. R.; Bernstein, J.; Kishan, K. V. R.; Sarma, J. A. R. P. *Tetrahedron Lett.* **1989**, *30*, 3029-3032.
- 38 Alcock, N. W.; de Meester, P.; Kemp, T. J. *J. Chem. Soc., Perkin Trans. II* **1979**, 921-926.
- 39 a) <http://tinyurl.com/3m58a8u>, last updated 4th September 2008, accessed on 9th May 2011. b) Srivastava, A.M.; Ronda, C. R. *The Electrochemical society Interface* **2003**, *12* (2), 48-51. c) Ultraviolet Radiation from Fluorescent Lamps NEMA, **1999**, LSD 7-1999, accessed at www.nema.org on 9th May 2011.
- 40 Enkelmann, V.; Wegner, G.; Novak, K.; Wagener, G. *J. Am. Chem. Soc.* **1993**, *115*, 10390-10391.
- 41 Brayshaw, S. K.; Knight, J. W.; Raithby, P. R.; Savarese, T. L.; Schiffers, S.; Teat, S. J.; Warren, J. E.; Warren, M. R. *J. Appl. Crystallogr.* **2010**, *43*, 337-340.
- 42 Harada, J.; Uekusa, H.; Ohashi, Y. *J. Am. Chem. Soc.* **1999**, *121*, 5809-5810.
- 43 a) Desvergne, J-P.; Thomas, J. M.; Williams, J. O.; Bouas-Laurent, H. *J. Chem. Soc., Perkin Trans. II* **1974**, 363-368. b) Ramdas, S.; Jones, W.; Thomas, J. M. *Chem. Phys. Lett.* **1978**, *57*, 468-470.
- 44 Kole, G. K.; Tan, G. K.; Vittal, J. J. *Org. Lett.* **2010**, *12*, 128-131.
- 45 References on solid-state kinetics: a) Khawam, A.; Flanagan, D. R. *J. Phys. Chem. B* **2006**, *110*, 17315-17328. b) Cao, D-K.; Sreevidya, T. V.; Botoshansky, M.; Golden, G.; Benedict, J. B.; Kaftory, M. *J. Phys. Chem. A* **2010**, *114*, 7377-7381. c) Feeder, N.; Honda, K. *Mol. Cryst. Liq. Cryst.* **1998**, *313*, 327-334.
- 46 Smart diffractometer control software (v5,625), Bruker-AXS, Bruker AXS GmbH, Karlsruhe, Germany.
- 47 Saint+ (v6.22) Bruker AXS, Bruker AXS GmbH, Karlsruhe, Germany.
- 48 Sheldrick, G. M. SHELXS-97, Program for solution of crystal structures,

-
- University of Göttingen, Germany, 1997.
- ⁴⁹ A similar (though not identical) process is described in reference 41.
- ⁵⁰ CrysAlisPro, Oxford Diffraction Ltd. Version 1.171.34.40
- ⁵¹ Empirical absorption correction using spherical harmonics, implemented in SCALE3 ABSPACK scaling algorithm within CrysAlisPro software, Oxford Diffraction Ltd. Version 1.171.34.40
- ⁵² Dolomanov, O.V.; Bourhis, L. J.; Gildea, R. J.; Howard, J. A. K.; Puschmann, H. OLEX2: a complete structure solution, refinement and analysis program. *J. Appl. Cryst.* **2009**, *42*, 339-341, using "SHELXS-97" - program for structure solution. Sheldrick, G. M. University of Göttingen, Göttingen, Germany, 1997.
- ⁵³ "SHELXL-97" - program for the Refinement of Crystal Structures. Sheldrick, G. M. University of Göttingen, Göttingen, Germany, 1997.
- ⁵⁴ "smtbx-flip" plug-in module to "Olex2" crystallography software, *J. Appl. Cryst.* **2009**, *42*, 339–341.
- ⁵⁵ Goddard, C. Photochemical substitution and bond activation reactions at cyclopentadienyl rhodium: synthetic and NMR studies. PhD Thesis, York, 2003.

Chapter 6: Conclusions

The overarching aim of this project was to prepare new ligand phosphine-alkene ligands. We were interested in phosphine-alkene ligands as they presented a relatively underdeveloped ligand target. Recent reports have established that these types of ligand show promise as ligands in transition metal catalysis.

Previous work within the Fairlamb group had explored dba as a tuneable alkene ligand for Pd-catalysis. In this project the dba backbone has been used as the framework for a series of multidentate phosphino-alkene and phosphine sulfide ligands. An advantage of using dba type ligands is that it is easily accessible by simple and straightforward synthetic routes. Ligands dbaPHOS, **127**, and dbaTHIOPHOS, **137**, have been prepared via a Horner-Wadsworth-Emmons reaction in excellent yields. Ligands monodbaPHOS, **128** and monodbaTHIOPHOS, **149** were synthesised via a Wittig reaction in good yields. As a result, the novel ligands are easily accessible for use by the rest of the scientific community.

Having met the first objective of the project-: to synthesise the phosphino-alkene ligands, attention turned to their coordination chemistry with common transition metals used by the catalysis community, Pd, Rh and Cu. A number of groups have been interested in the use of phosphino-alkene ligands in catalysis. However, often the discussion of their coordination chemistry goes little further than to determine the binding of the alkene, using either NMR spectroscopic analysis or a lone X-ray single-crystal structure determination. To complement this work we focused on the coordination chemistry of these ligands.

The Pt^{II}, Pd^{II}, Pd⁰ and Rh^I complexes of dbaPHOS were synthesised, and the ligands found to act as hemilabile flexible multidentate ligands. For the Pt^{II} and Pd^{II} complexes the ligand acts as a bidentate phosphine ligand, and a X-ray crystal structure was obtained for the *cis*-[PtCl₂(dbaPHOS)] complex (**163**). The crystal structure showed that dbaPHOS could be regarded as a wide bite angle ligand (106°). Further solution-state NMR spectroscopic analysis provides evidence for the synthesis of monomeric complexes with both *cis*- and *trans*-chelation of the phosphine depending on the conditions used. For example, *cis*-[PtCl₂(dbaPHOS)] (**163**) dissolved in DMSO and

then underwent associative isomerisation to the *trans* complex, **164**. Overtime a precipitate formed. We believe the initial *cis*- and *trans*-complexes are monomeric complexes, whilst the final precipitate is a dimer or higher order polymeric species. This was the first indication that the ligand could act as both a *cis* and *trans* chelating ligand.

Despite this success, the insolubility of some of the complexes meant it was difficult to know whether the bulk material was a monomer, dimer or polymer. Solid-state NMR spectroscopic analysis showed that both the Pt^{II} and Pd^{II} complexes had long-range order, suggesting that the material was not polymeric. These observations point to the first problems that may be encountered with these ligands in catalysis. One advantage to using Pd^{II}/Pt^{II} complexes directly in catalysis is that they are often more air stable than the Pd⁰/Pt⁰ complexes or the free ligand, making them easier to handle. However, if the complex does not dissolve or only partially dissolves then the true amount of palladium or platinum present will be unknown (in solution) and catalysis may fail.

The Pd⁰ and Pt⁰ complexes were also investigated, and [Pd⁰(dbaPHOS)] (**167**) successfully prepared. In comparison with the Pd^{II} complexes, [Pd⁰(dbaPHOS)] (**167**) was readily soluble in a variety of solvents including CH₂Cl₂, benzene and THF. NMR spectroscopic analysis showed that one alkene was coordinated to give a 3-coordinate Pd⁰ centre (16 electron). Once again it was unclear from the solution characterisation whether a monomeric or dimeric complex was formed. A single crystal structure was obtained which allowed the unambiguous conformation of a dimeric complex. The free and coordinated alkenes were exchanging, and using ³¹P-³¹P EXSY experiments the entropy, $\Delta S^\ddagger = -19.5 (\pm 11.1) \text{ J mol}^{-1} \text{ K}^{-1}$ and enthalpy, $\Delta H^\ddagger = 65.7 (\pm 3.4) \text{ kJ mol}^{-1}$, of exchange were determined. This indicated that the barrier to exchange was primarily enthalpic in origin, supporting an intramolecular exchange. The similarity in values observed to those in Cu dimer **193**, provides further support for the intramolecular exchange in a dimeric complex.

The aim for organic and organometallic chemists in designing any new ligand system is their use in catalysis. The stoichiometric addition of PhI to Pd⁰(dbaPHOS) (**167**) was carried out to examine the behaviour of the complex in the common first step of a large number of Pd catalysed reactions (*e.g.* cross-couplings). The soluble Pd^{II} complex **172** was formed. To our surprise only one signal was observed in the ³¹P NMR spectrum,

indicating the formation of the *trans*-phosphine complex. The single crystal X-ray structure of **172** provided unequivocal evidence for the *trans*-spanning nature of the dbaPHOS ligand **127**. This is an exciting discovery as interconverting *cis*- and *trans*-chelating bisphosphines are still relatively rare. Other ligands that can be *trans*-spanning include SPANPhos (**210**), XantPhos (**6**), TRANSPHOS (**209**), and the TRAP ligands (**212**) (Figure 1). The relatively low number of successful chiral *trans*-bisphosphine ligands indicates how rare and underdeveloped these ligands are, so far only the TRAP family of ligands have met with great success in asymmetric transformations. Preliminary studies in collaboration with Anny Jutand indicate that the dimer is in equilibrium with the monomer, which undergoes very rapid oxidative addition with PhI.

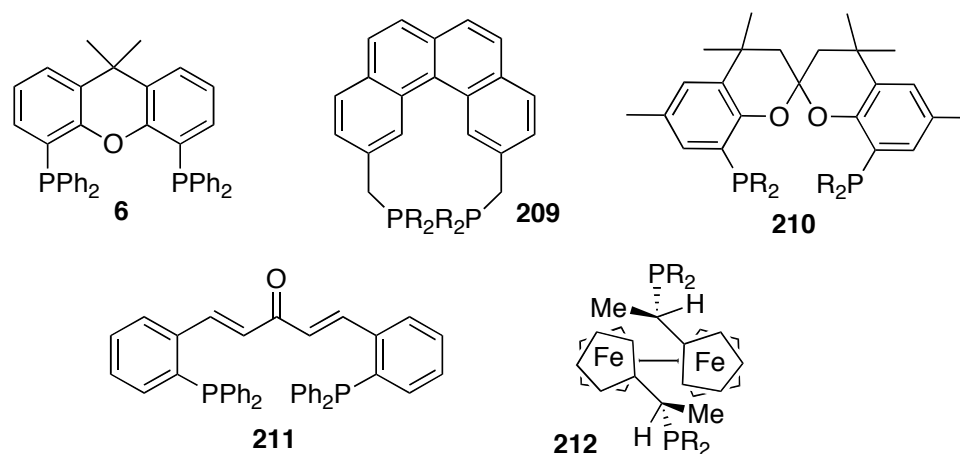


Figure 1: *Trans*-spanning ligands.

The next phase of the project would be to examine the complex in the other common steps of Pd-catalysed reactions, *e.g.* transmetallation and reductive elimination, and to screen the ligands in a variety of catalytic reactions. The Pd⁰ complex and the resulting Pd^{II} complex from oxidative addition are far more soluble than the other Pd^{II} complexes of dbaPHOS. This suggests that any preliminary catalytic experiments with palladium would be best conducted starting with a Pd⁰ species. The ability of the dbaPHOS to act as a *cis*- and *trans*-chelating ligand and its wide-bite angle, provide a starting point for catalytic screening. *Trans*-chelating ligands have been found to have applications in a number of transformations including amination reactions, whilst wide-bite angle ligands (100-120°) are often used in hydroformylation.

One potential problem for the ligand in catalysis is that the alkene could act as a substrate, for example in either Heck arylation or hydroformylation, leading to the

nature of the catalyst changing during the reaction. In reactions where the alkene is found to be essential, either due to coordination of the alkene stabilising intermediates or due to the rigidity they provide to the backbone, this would be detrimental. However, the dbaPHOS ligand could be viewed as a bidentate phosphine with a tethered alkene, and utilised as a reaction probe for observing catalytic intermediates. The monodbaPHOS could be utilised as a monophosphine variant.

Along with the phosphino-alkene ligands, the phosphine sulfide variants were also studied. The phosphine sulfide ligand, dbaTHIOPHOS, was found to be a viable ligand for Cu^I. Cationic and neutral Cu^I complexes of dbaTHIOPHOS were prepared. In the cationic complex, **193**, the alkenes were found to be hemilabile, with exchange occurring between the coordinated and free alkenes. Using variable temperature ¹H NMR spectroscopic analysis the exchange parameters were estimated to give enthalpy, $\Delta H^\ddagger = 56.0 \pm 6.4 \text{ kJ mol}^{-1}$, and entropy, $\Delta S^\ddagger = 0.43 \pm 6.9 \text{ J mol}^{-1} \text{ K}^{-1}$. As with the Pd⁰ complex **167**, the results supported intramolecular exchange of the alkenes, without the involvement of the solvent molecules. Crystal structures were obtained for three unique Cu^I complexes. Crystallisation of **193** gave crystals of an interesting ladder type complex, **194**, with four Cu^I atoms and two chloride ions, along with crystals on **193**. In all the structures obtained dbaTHIOPHOS acts as a bridging ligand between at least two Cu^I centres.

Complexes **193** and **195** were found to be catalytically active in the cyclopropanation of styrene at low catalyst loadings (1 mol%). High conversions were obtained (85-91%) and moderate diastereotopic ratios (*cis:trans* 30:70). These preliminary results show that phosphine-sulfides are viable ligands for catalytically active complexes, and their previous underutilisation should not lead to these ligands being ignored by the catalytic community. Further work is needed to optimise the ligand design for these reactions and determine their substrate scope. It would also be interesting to investigate related reactions such as arizindination and chiral variants.

In the development of the synthetic routes to these ligands a number of side reactions were observed and investigated. The observation of **138** in the microwave-assisted synthesis of **137** was at first quite puzzling. Further studies revealed that the side product arose from the favourable reduction of 2-hydroperoxytetrahydrofuran **144** (present in the THF due to storage conditions) to tetrahydrofuran-2-ol **145**, in the

microwave. The tetrahydrofuran-2-ol **145** then acts as a competing ‘masked’ aldehyde in the Horner-Wadsworth-Emmons reaction. This tale serves to act as a reminder that the reaction solvent is not always just an innocent medium for a reaction. In particular, the possibility of peroxides and lactones in THF (and ethereal solvents) should be taken into account when planning reaction conditions particularly if high temperatures or pressures are to be used.

The observation of a solid-state $[\pi 2s+\pi 2s]$ cycloaddition led to a detailed investigation into the photoreactivity of the ligands concentrating on monodbaTHIOPHOS **149**. Utilising a range of techniques available including single crystal X-ray diffraction, powder X-ray diffraction and solid-state NMR spectroscopic analysis, it was possible to monitor the reaction in both the single crystal form and the microcrystalline state. In the single crystal, 70% conversion to the cycloadduct **206** was obtained. Two structural changes had occurred; the $[\pi 2s+\pi 2s]$ cycloaddition and an isomerisation about the single bond of the remaining enone. The reaction could be considered topotactic as the change in unit cell parameters between the starting material and product was <4%. This was exciting as novel topotactic reactions are quite rare. Unfortunately attempts to push the conversion to 100% conversion in the single crystal failed. In the bulk material the reaction reached 100% conversion with retention of the regiocontrol seen in the single crystal experiments, as revealed by powder XRD with *in-situ* irradiation and by solid-state NMR spectroscopy. A number of intermediates were observed by the latter technique. This can be explained by considering that at least two structural changes are observed. The results from all the techniques indicate that for full conversion to be obtained movement has to occur within the crystal lattice in the later stages of the reaction. In the single crystal this manifests itself as crystal degradation after approximately 70% conversion. Only in the initial crystal were higher conversions to **206** seen (81%), whilst retaining structural integrity. This still points to the possibility of a fully SCSC reaction if the correct irradiation conditions can be found.

A number of other interesting findings were made in this project, which were not studied in further detail, in part, due to the inherent time restraints of the PhD program. Both the reactivity of the phosphine ligands to borane, and the apparent reduction of the double bonds of dbaTHIOPHOS **137** when treated with Raney® Nickel, in the absence of a known hydrogen donor, deserves further investigation. It is my opinion that each of these could serve as the basis of an undergraduate project. In particular, using

ReactIR™ in conjunction with the reactions with borane would provide a simple way to quickly gain some insight into the reaction, the products and the reaction mechanism.

Overall, this project has led to the successful synthesis of a new class of phosphino-alkene ligands and their phosphine sulfide variants. Extensive coordination studies show the ligands act as hemilabile multidentate ligands. Of particular note is the observation that dbaPHOS **127** can act as both a *cis* and *trans*-chelating bisphosphine ligand. The impact of this has not yet been fully studied in catalytic applications, but it is clearly set-up for exploitation.